

**Pulmonary delivery of mucoadhesive nanoparticles of an
antifungal agent using nebulizer or dry powder inhaler**

**Thesis submitted by
Mrs. Paramita Paul**

Doctor of Philosophy (Pharmacy)

**Department of Pharmaceutical Technology
Faculty of Engineering & Technology
Jadavpur University
Kolkata-700 032**

2018

JADAVPUR UNIVERSITY
KOLKATA-700032, INDIA

INDEX NO- 214/14/Ph

1. Title of the thesis: Pulmonary delivery of mucoadhesive nanoparticles of an antifungal agent using nebulizer or dry powder inhaler.

2. Name, Designation and Institution of the supervisor:

Prof. (Dr.) Biswajit Mukherjee, Professor, Department of Pharmaceutical Technology, Jadavpur University, Kolkata-700032, India.

3. List of Publications (related to thesis):

- i. **Paramita Paul**, Soma Sengupta, Biswajit Mukherjee, Tapan K Shaw, Raghuvir H. Gaonkar, Mita Chatterjee Debnath. Chitosan-coated nanoparticles enhanced lung pharmacokinetic profile of voriconazole upon pulmonary delivery in mice. **Nanomedicine (Lond)**. 2018; 13(5):501-520. (**Impact factor: 4.727**)
- ii. Pranab Jyoti Das[‡], **Paramita Paul**[‡], Biswajit Mukherjee, Bhaskar Mazumder, Laboni Mondal, Rinku Baishya, Mita Chatterjee Debnath, Kumar Saurav Dey. Pulmonary Delivery of Voriconazole Loaded Nanoparticles Providing A Prolonged Drug Level in Lungs- A Promise For Treating Fungal Infection. **Mol Pharm**. 2015; 12(8):2651-64. (**Impact Factor : 4.440**) ([‡]Equal contribution)

Other Publications:

- i. Tapan Kumar Shaw, Dipika Mandal, Goutam Dey, Murari Mohan Pal, **Paramita Paul**, Samrat Chakraborty, Kazi Asraf Ali, Biswajit Mukherjee, Amal Kumar Bandyopadhyay, Mahitosh Mandal. Successful Delivery of Docetaxel to Rat Brain using Experimentally Developed Nanoliposome: A Treatment Strategy for Brain Tumor. **Drug Deliv**. 2017;24(1):346-357. (**Impact Factor : 6.4**)
- ii. Biswajit Mukherjee, **Paramita Paul**, Ankan Choudhury, Sanchari Bhattacharya, Ruma Maji, Lopamudra Dutta. Variation of Pharmacokinetic Profiles of Some Antidiabetic Drugs from Nanostructured Formulations Administered Through Pulmonary Route. **Curr. Drug Metab**. 2016;17(3):271-8. (**Impact Factor : 2.659**)

- iii. R. Manasadeepa, **Paramita Paul**, Biswajit Mukherjee. Pressure sensitive mucoadhesive polymer based dental patches to treat periodontal diseases: an *in vitro* study. **Drug Deliv.** 2013; 20(6): 258–267. (**Impact Factor : 6.4**)
- iv. Sumit Basu, Biswajit Mukherjee, Samrat Roy Chowdhury, **Paramita Paul**, Rupak Choudhury, Ajeet Kumar, Laboni Mondal, Chowdhury Mobaswar Hossain, Ruma Maji. Colloidal gold-loaded, biodegradable, polymer-based stavudine nanoparticle uptake by macrophages: an in vitro study. **Int J Nanomedicine.** 2012;7:6049–6061. (**Impact Factor : 4.383**)

Book Chapters:

- i. Biswajit Mukherjee, **Paramita Paul**, Lopamudra Dutta, Samrat Chakraborty, Moumita Dhara, Laboni Mondal, Soma Sengupta.. Pulmonary administration of biodegradable drug nanocarriers for more efficacious treatment for fungal infections in lungs: insights based on recent findings. In: Grumezescu, A.M. (Ed.), Multifunctional system for combined delivery, Biosensing and diagnostic; Elsevier, Netherlands, 2017, pp. 261-280.
- ii. Biswajit Mukherjee, Niladri Shekhar Dey, Ruma Maji, Priyanka Bhowmik, Pranab Joyti Das, **Paramita Paul**. Current status and future scope for nanomaterials in drug delivery. In: Ali Demir Sezer (Ed.), Application of nanotechnology in drug delivery; In Tech. 2014 (ISBN no: 978-953-51-1628-8).
- iii. Biswajit Mukherjee, Shampa Ghosh, Laboni Mondal and **Paramita Paul**. Virus and Nanosized Viral Scaffolds as Drug Delivery Systems. In: Bhupinder Singh (Ed.), Medical Nanobiotechnology (Volume 5); Studium Press LLC, Texus, USA. 2014 (ISBN: 1-62699-055-7).

4. List of Patents:

1. Mukherjee Biswajit, Sengupta Soma, **Paul Paramita**. Process and carrier for targeting drugs/diagnostics of peripheral and central nervous system. Application No: 201731033454 A; Date 21.09.2017. (Published on 20.10.2017)

5. List of presentation in National/International Seminars

International:

- i. **Paramita Paul**, Biswajit Mukherjee. Pharmacokinetic study of Chitosan coated PLGA nanoparticles of an antifungal agent for better therapeutic effect in lung fungal infection. **International Conference** on “*Emerging Trends In Drug Discovery And Development*” 18-20th January, 2018. IIT-BHU, Varanasi. (**Poster**)
- ii. **Paramita Paul**, Biswajit Mukherjee, Mita Chatterjee Debnath. Radio imaging of chitosan coated nanoparticles of an antifungal agent for treatment of lung fungal infection: pulmonary retention and Biodistribution. **International Conference** on “*Current scenario in Pharmaceutical Technology and Healthcare: A move towards patient -centric approach*” 9th and 10th March, 2018. NSHM College of Pharmaceutical Technology and Department of Healthcare management NSHM Knowledge Campus, Kolkata- Group of Institutions. (**Oral**) (**1st Prize**)

National:

- i. **Paramita Paul**, Pranab Jyoti Das, Biswajit Mukherjee, Bhaskar Mazumder. Pulmonary Delivery of Biodegradable Nanoparticles containing to Provide Prolonged Drug Level in Lungs to Treat Lung Fungal Infection. **National Seminar** on “*Novel Pharmaceutical Technologies: Challenges and Opportunities*” held at Manipal University, Manipal 576 104, Karnataka, India, dated 15 November, 2015. (**Best poster Prize**)
- ii. **Paramita Paul**, Biswajit Mukherjee. Polymeric Nanoparticles of Antifungal Agent: Pulmonary Delivery Using Dry Powder Inhaler and In Vivo Study. **JU IAPST National Seminar 2016** on “*Drug and Diseases: Role of Pharmacists and Doctors*” at H.L. Roy building, Jadavpur University, Kolkata-700032, dated 16th January, 2016.
- iii. **Paramita Paul**, Biswajit Mukherjee. Chitosan coating on PLGA nanoparticles: a technology to enhance bioadhesion in murine lungs. One Day **National Symposium** on 'Nanotechnology From Materials to Medicines and Their Social Impact' March 25, 2017 Birla Industrial & Technological Museum, Kolkata.

CERTIFICATE FROM THE SUPERVISOR

This is to certify that the thesis entitled “**Pulmonary delivery of mucoadhesive nanoparticles of an antifungal agent using nebulizer or dry powder inhaler**” submitted by **Smt. Paramita Paul**, who got her name registered on 27.05.2014 for the award of **Ph.D. (Pharmacy)** degree of Jadavpur University is absolutely based upon her own work under the supervision of **Prof. (Dr.) Biswajit Mukherjee**, Professor, Department of Pharmaceutical Technology, Jadavpur University, Kolkata- 700032, India and that neither her thesis nor any part of the thesis has been submitted for any degree/diploma or any other academic award anywhere before.

.....
Signature of the Supervisor
and date with Official Seal

Prof. (Dr.) Biswajit Mukherjee

Professor, Division of Pharmaceutics

Department of Pharmaceutical Technology

Jadavpur University, Kolkata-32, India.

ACKNOWLEDGEMENTS

*I would like to express my deepest gratitude and sincere thanks to my mentor **Prof. Biswajit Mukherjee**, Professor and Ex-Head, Department of Pharmaceutical Technology, Jadavpur University, Kolkata- 32, India for his constant inspiration, encouragement and valuable advice at every phase of my research period in overcoming the challenges faced during the embryonic and mature stages of investigations. His sincerity, dedication and immense determination have infused the spirit of hard work in me. I am indebted to him and express my heartfelt reverence to him.*

*I sincerely acknowledge Department of Biotechnology (DBT), New Delhi and Department of Science and Technology Women Scientist Scheme (**DST WOS-A**), New Delhi, India [Sanction no. SR/WOS-A/LS-1356/2014, dated 28.07.2015] for providing me funding facilities.*

I take pleasure in expressing my deep respect Head, Department of Pharmaceutical Technology, Jadavpur University, Kolkata-32, India, Dr. Bholanath Karmakar, Principal Secretary, FET, Jadavpur University, Prof. Chiranjib Bhattacharjee, Dean, FET, Jadavpur University, Dr. Pradip Kumar Ghosh, Registrar, Jadavpur University, Mr. Gour Krishna Pattanayak, Finance Officer, Jadavpur University; Mr. Debasish Pal, Deputy Finance Officer; and Professor Suranjan Das, Vice Chancellor, Jadavpur University and Prof. Souvik Bhattacharya, Ex-Vice Chancellor for co-operation and assistance during the entire period of this research project.

*I thank the authority of **Jadavpur University** to provide all the necessary facility and space for working.*

Dr. Saikat Dewanjee, is gratefully acknowledged for providing permission and facility to conduct a part of my research work.

The support I received from other faculty members of this department specially Prof. Amalesh Samanta, Dr. Sanmay Karmakar, Prof. Tanmoy Bera and Dr. Bhaskar Majumdar from Dibrugarh University is thankfully acknowledged.

I take this opportunity to express my gratitude to Mr. Debabrata Karmakar, Dyutiman Chakraborty, Mritynjoy Mukherjee, Subrata Mondal and Research Section for their moral support during the entire period of my research work.

I would also like to thank Mr. Diptyodip Sarkar, and Arun Bandyopadhyay, IICB for Confocal Microscopy; Mr. Pratyush, Mr. Samrat, Ms Urmila CRNN for SEM, FESEM and TEM study, respectively; Dr. Jayati Sengupta, Mr. Chiranjib, IICB for Cryo-TEM and Mr. Muruganandan,

IICB for Atomic force Microscopy, Sudipto, Suman and Piu for particle size analysis whenever required.

I owe my sincere and heartfelt gratitude and regards to my beloved husband Dr. Tarun Kumar Dua for his encouragement, help at any level and inspiration towards completing my research work.

I express my heartiest thanks to my labmates specially Somadi, Biswadipda, Manasadeepadi, Falgunida, Miltuda, Masoomda, Bhabani, Tapanda, Samratda, Moumitadi, Labonidi, Sanchari, Dipikadi, Ashique, Iman, Leena, Lopamudra, Ruma, Niladrida, Tushidi, Meganadhan, Ajeet, Swapna, Elias, Ankan, Brahmachari, Rhitabrita, Vimal, Nobila, Somdyuti, Somdatta, Sourav, and all others. I also express my special thanks to Pranab from Dibrugarh University and Mr. Zewdu Yilma from Ehiopia for their moral support and co-operation.

I would like to thank Ranabir, Ritu, Niloy, Urmi, Swarnalata for extending their help and cooperation during the animal study without which it couldn't be possible to perform successfully.

I am truly blessed to have Arohi and my family: my parents in law, Bhai, Seuli who supported and encouraged me to continue my research work with their high co-operation.

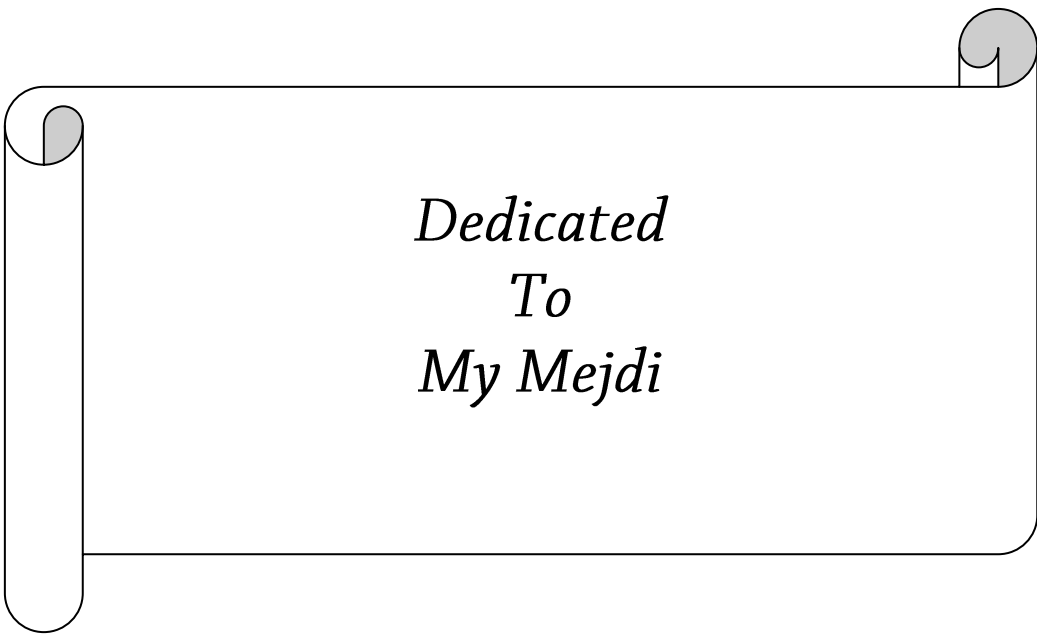
I cannot forget my loving and caring sisters without acknowledging them. In each and every hurdle and even in minute problems I got their advice, support, inspiration and way out.

I apologize all other unnamed who helped me in various ways to complete my research work.

Finally, I am grateful to almighty without whose blessings I couldn't have completed my research work.

Place: Jadavpur, Kolkata

(Paramita Paul)



*Dedicated
To
My Mejdī*

Table of Contents

Chapters	Chapter Name	Page No.
Chapter 1	Introduction	1-24
1.1	Anatomy of human lung	1-2
1.2	Lung fungal infections	3-5
1.3	Treatment of lung fungal infections	5-9
1.4	Nano-drug delivery systems under investigation, intended for the pulmonary lung fungal infections	10
1.5	Polymeric nanoparticles	10-11
1.6	Nanoparticles for the treatment of lung fungal infection	11-12
1.7	Mucoadhesive polymers	12-13
1.8	Theories of mucoadhesion	13
1.9	Why Pulmonary route?	13-17
1.10	Mechanism of deposition of the particles in the lung	17-19
1.11	Pulmonary drug delivery devices	19-23
1.12	Limitations of pulmonary route if any	24
Chapter 2	Literature review	25-35
Chapter 3	Objectives and plan of work	36-37
Chapter 4	Materials and equipments	38-45
4.1	List of Materials and chemicals used	38
4.1.1	Voriconazole	39-40
4.1.2	PLGA	40
4.1.3	Poly vinyl alcohol	41
4.1.4	Chitosan	42
4.1.5	Fluorescein isothiocyanate	42-43
4.1.6	Lactose mono hydrate	43
4.2	List of Instruments, equipments and devices used	44-45
4.3	Animals	45
4.4	Softwares	45
		46-56

Chapter 5	Methodology	
5.1	Determination of absorption maxima (λ_{max}) of Voriconazole	46
5.2	Development of calibration curve for Voriconazole in acetonitrile: water mixture (1:1)	46
5.3	Development of calibration curve for Voriconazole in phosphate buffer saline (PBS)	46
5.4	Fourier transform infrared (FTIR) spectroscopy	47
5.5	Preparation of non-coated PLGA nanoparticles containing voriconazole	47-48
5.6	Preparation of chitosan-coated PLGA nanoparticles containing voriconazole	48
5.7	Preparation of FITC containing nanoparticles	49
5.8	Drug loading (%) and entrapment efficiency (%)	49
5.9	Characterization of nanoparticles	50-51
5.9.1	Particle size distribution and zeta potential	50
5.9.2	Field emission scanning electron microscope (FESEM)	50
5.9.3	Cryogenic-transmission electron microscopy (Cryo-TEM)	50-51
5.9.4	Transmission electron microscopy (TEM)	51
5.9.5	Atomic force microscopy (AFM)	51
5.10	<i>In vitro</i> drug release and drug release kinetics study	51-52
5.11	Determination of mass median aerodynamic diameter (MMAD) and geometric standard deviation (GSD) using an eight-stage non-viable Anderson Cascade Impactor	52-53
5.12	<i>In vivo</i> deposition of nanoparticles in the lungs of mice using nose-only inhalation chamber and fabricated dry powder inhaler (DPI)	53
5.13	High performance liquid chromatography (HPLC)	54
5.14	Pharmacokinetics and lung lobe distribution study	55
5.15	Gamma scintigraphy	55
5.16	Biodistribution study	56
		57-77

Chapter 6	Results	
6.1	Determination of absorption maxima (λ_{max}) of Voriconazole	57-60
6.2	Preformulation study	60-61
6.2.1	Investigation of drug-excipients interaction	
6.3	Characterization of nanoparticles	62-66
6.3.1	Particle size distribution and zeta potential by dynamic light scattering (DLS) analysis	62
6.3.2	Determination of drug loading and entrapment efficiency	63
6.3.3	Surface morphology	63-66
6.4	<i>In vitro</i> drug release study	66-67
6.5	Drug release kinetics study	67-68
6.6	Determination of mass median aerodynamic diameter (MMAD) and geometric standard deviation (GSD) using an eight-stage nonviable Anderson cascade impactor	68-69
6.7	<i>In vivo</i> deposition of nanoparticles in the lungs of mice using nose-only inhalation chamber and fabricated dry powder inhaler (DPI)	69-71
6.8	High performance liquid chromatography (HPLC)	71-73
6.8.1	Calibration curve in plasma	71-72
6.8.2	Calibration curve in lung tissue	73
6.9	Pharmacokinetics and lung lobe distribution study	73-75
6.10	Gamma scintigraphy	75-76
6.11	Biodistribution	77
Chapter 7	Discussion	78-84
Chapter 8	Conclusion	85
Chapter 9	Summary	86-89
Chapter 10	References	90-105

Financial support from DST

Animal ethical clearance

**Paper presentation in national and international conferences/
seminars**

Published papers

List of Tables

Table No.	Description	Page No.
Table 1.1	Recommended treatment regimens for pulmonary fungal infections	7-9
Table 1.2	Comparative study pulmonary vs. other routes (iv, oral etc.)	14-16
Table 4.1	List of Materials and chemicals used	38
Table 4.2	List of Instruments, equipments and devices used	44-45
Table 4.3	Animals used in the study	45
Table 4.4	Softwares used in the study	45
Table 5.1	Formulation composition and process parameters for preparation of optimized formulations	49
Table 6.1	Result of linearity data of Voriconazole in acetonitrile water mixture (1:1)	57
Table 6.2	Result of linearity data of Voriconazole in simulated lung fluid (SLF)	58
Table 6.3	Result of linearity data of Voriconazole in phosphate buffer saline (PBS)	59
Table 6.4	Formulation characteristics such as %drug loading, encapsulation efficiency, average particle size and zeta potential values for the optimized PLGA formulation without chitosan coating (P5) and with chitosan coating (P6)	62
Table 6.5	Drug release kinetics of different formulations	68
Table 6.6	Result of linearity data of of voriconazole in acetonitrile–water–formic acid containing mice plasma	72
Table 6.7	Pharmacokinetic parameters for free drug voriconazole, optimized PLGA formulations without chitosan coating (P5) and with chitosan coating (P6) in Swiss albino mice after pulmonary administration	74
Table 6.8	Biodistribution study of ^{99m} Tc labeled voriconazole loaded PLGA nanoparticles and ^{99m} Tc labeled chitosan coated PLGA nanoparticles containing voriconazole in rats	77

List of Figures

Figure No.	Description	Page No.
Figure 1.1	Diagrammatic representation of lung morphology and anatomy showing structure of bronchioles	2
Figure 1.2	Classification of antifungals	6
Figure 1.3	Particles size dependant deposition in various parts of lungs.	18
Figure 1.4	Evolution of pulmonary delivery devices	19
Figure 1.5	Nebulizer and its components	20
Figure 1.6	Metered-dose inhaler and its components	21
Figure 1.7	Schematic diagram of some currently available dry powder inhalers and their components	23
Figure 5.1	Preparation of PLGA nanoparticles by multiple emulsion solvent evaporation method	47
Figure 5.2	Preparation of chitosan coated PLGA nanoparticles by multiple emulsion solvent evaporation method	48
Figure 5.3	Result from Cascade Impactor apparatus simulates the human respiratory system	52
Figure 6.1	Absorption maxima of voriconazole in acetonitrile water mixture (1:1) showing λ_{\max} at 255.0 nm	57
Figure 6.2	Calibration curve of voriconazole in acetonitrile: water mixture (1:1) showing R^2	58
Figure 6.3	Calibration curve of voriconazole in Simulated lung fluid, pH 7.4 (SLF)	59
Figure 6.4	Calibration curve of voriconazole in phosphate buffer saline, pH 7.4 (PBS)	60
Figure 6.5	FTIR spectroscopy studies of individual components, physical mixture, and nanoparticle formulations	61

Figure 6.6	Particle size distributions and zeta potential data. (A) Particle size distribution graph of non-coated PLGA nanoparticles; (B) Particle size distribution graph of chitosan-coated PLGA nanoparticles; (C) Zeta potential graph of non-coated PLGA nanoparticles; (D) Zeta potential graph of chitosan-coated PLGA nanoparticles	62
Figure 6.7	Field emission scanning electron microscopic images of non-coated PLGA nanoparticles and chitosan-coated PLGA nanoparticles. A) Formulation P1; (B) Formulation P2; (C) Formulation P3; (D) Formulation P4; (E) Formulation P5; (F) Formulation P6	64
Figure 6.8	Cryogenic transmission electron microscopic images of (A, B) non-coated PLGA nanoparticles (formulation P5) and (C, D) chitosan-coated PLGA nanoparticles (formulation P6)	65
Figure 6.9	Transmission electron microscopic image of (A) non-coated PLGA nanoparticles (Formulation P5) and (B) chitosan-coated PLGA nanoparticles (Formulation P6)	65
Figure 6.10	Atomic force microscopic image of (A) non-coated PLGA nanoparticles (Formulation P5) and (B) chitosan-coated PLGA nanoparticles (Formulation P6)	66
Figure 6.11	Release profiles of voriconazole from non-coated PLGA nanoparticles (P5) and chitosan-coated PLGA nanoparticles (P6) in (A) phosphate buffer saline (pH 7.4) and (B) simulated lung fluid (pH 7.4)	66-67
Figure 6.12	<i>In vitro</i> deposition of P5 and P6 from Andersen cascade impactor (data as mean \pm SD, n = 3)	69
Figure 6.13	Confocal laser scanning microscopic images of lungs treated with (A) non-coated PLGA nanoparticles (at 1 h, 8 h, and 24 h after pulmonary administration), and (B) chitosan-coated PLGA nanoparticles (at 1 h, 8 h, and 24 h after pulmonary administration)	70
Figure 6.14	CTCF values and integrated density quantification of FITC fluorescence staining in lungs tissue sections after pulmonary delivery of non-coated PLGA nanoparticles and chitosan-coated PLGA nanoparticles (data as mean \pm SD, n = 3) (*CTCF-Corrected total cell fluorescence)	71

Figure 6.15	Calibration curve of voriconazole in acetonitrile–water–formic acid containing mice plasma	72
Figure 6.16	Calibration curve of voriconazole in acetonitrile–water–formic acid containing mice lung homogenate	73
Figure 6.17	Distribution of voriconazole ($\mu\text{g/mL}$) in mice lung lobes at different time points up to 72 h after treatment with chitosan-coated nanoparticles in pulmonary route	75
Figure 6.18	Scintigraphy pictures of animals after receiving Tc-99m labeled PLGA nanoparticles containing voriconazole formulation and chitosan coated PLGA nanoparticles containing voriconazole by pulmonary route after 3 h and 6 h	76

List of abbreviations

%ID	%Injected Dose Per Gram of Organ
μg	Microgram
$^{99\text{m}}\text{Tc}$	$^{99\text{m}}$ Technetium
ABPA	Allergic Bronchopulmonary Aspergillosis
AFM	Atomic Force Microscopy
AFM	Atomic Force Microscopy
AmB	Amphotericin B
AUC	Area Under the Curve
AUMC	Area Under the First Moment Curve
CFC	Chlorofluorocarbons
CLSM	Confocal Laser Scanning Microscopy
CLSM	Confocal Laser Scanning Microscope
C_{max}	Peak Plasma Concentration
Cryo-TEM	Cryogenic Transmission Electron Microscopy
CS	Chitosan
CS	Chitosan
CTCF	Corrected Total Cell Fluorescence
Da	Daltons
D-AmB	Desoxycholate Amphotericin B
DCM	Dichloromethane
DLS	Dynamic Light Scattering
DMSA	Dimercaptosuccinic Acid
DPI	Dry Powders for Inhalation
DXM	Dexamethasone
ED%	Emitted Dose Percentage
EDTA	Ethylenediaminetetraacetic Acid
EPAS	Evaporative Precipitation into Aqueous Solution
FCZ	Fluconazole
FESEM	Field Emission Scanning Electron Microscope
FITC	Fluorescein Isothiocyanate
FPF	Fine Particle Fraction
FTIR	Fourier Transform Infrared
g	Gram
GSD	Geometric Standard Deviation
h	Hour
HFAs	Hydrofluoroalkanes
HPLC	High Performance Liquid Chromatography
i.v.	Intravenous
ID	Integrated Density
IFR	Inspiratory Flow Rate
IS	Internal Standard
ITZ	Itraconazole
L	Litre

LFI	Lung Fungal Infections
MDI	Metered Dose Inhalators
mg	Milligram
MIC	Minimum Inhibitory Concentration
min	Minutes
mL	Millilitre
MMAD	Mass Median Aerodynamic Diameter
MRT	Mean Residence Time
mw	Molecular Weight
nm	Nanometer
NPs	Nanoparticles
NPs	Nanoparticles
PBS	Phosphate Buffer Saline
PCS	Photon-Correlation Spectroscopy
PCZ	Posaconazole
PGA	Polyglutamic Acid
PLA	Poly-Lactic Acid
PLGA	Poly Lactic-Co-Glycolic Acid
pMDI	Pressurized Metered-Dose Inhaler
PVA	Poly(Vinyl Alcohol)
RF	Respirable Fraction
SC	Sodium Cholate
SEM	Scanning Electron Microscopy
SFL	Spray-Freezing into Liquid
SLF	Simulated Lung Fluid
SLNs	Solid Lipid Nanoparticles
SPC	Soybean Phosphatidylcholine
$T_{1/2}$	Half Life
TEM	Transmission Electron Microscopy
TOF-SIMS	Time-of-Flight Secondary Ion Mass Spectroscopy
TPP	Triphosphosphate
VRZ	Voriconazole
VRZ	Voriconazole
XPS	X-Ray Photoelectron Spectroscopy
λ_{\max}	Absorption Maxima
$\mu\text{g/mL}$	Microgram per Millilitre

Chapter 1

Introduction

1. Introduction

Globally, over 300 million people are affected with serious fungal infections and 25 million populations are at high threat of death or losing their sight. Approximation for the global burden of fungal diseases is based on population and disease demographics (age, gender, HIV infected, asthma etc.) (<https://www.gaffi.org/why/fungal-disease-frequency/>). Pulmonary fungal infections cover a broad spectrum related to a variety of fungal sources. They can particularly affect immune-compromised individuals (i.e. haematological, solid organ transplant or intensive care unit patients) and people residing in certain particular geographic areas. The infections of the persons due to their geographic location are referred to as endemic mycoses, whereas the persons having immune deficiency are found to develop opportunistic infections (Smith and Kauffman, 2012). Fungi may cause lung infection when fungus infected materials or fungal spores are inhaled. The incidence of pulmonary fungal infection has been increasing globally in the last few decades and it is one of the leading causes of death in developing countries (Erjavec *et al.*, 2009).

1.1 Anatomy of human lungs

The lungs, a pair of spongy organs located within the thoracic cavity, are the gaseous exchange centre of the human body, are surrounded by the chest wall and separated by the mediastinum from the heart and other organs (**Figure 1.1**). Both lungs have a central recession called the hilum at the root of the lung, where the blood vessels and bronchus enter into the organ (Gray and Standring, 2008). The right lung is normally larger and heavier than the left. The left lung is constituted with 2 lobes, namely superior and inferior lobes separated by an oblique fissure, while the right lung has three lobes, superior, middle and inferior lobes, divided by oblique and horizontal fissures (Sahasrabudhe *et al.*, 2013, Drake *et al.*, 2009).

Each lung lobe gets divide into broncho-pulmonary segments that are aerated by segmental/ tertiary bronchus (Arakawa *et al.*, 2000). The tube-like air pipe trachea acts as the passage for the air to the chest and neck; and it is divided in two main branches, bronchi, each of which enters into each lung. Outside the lungs, the pleura (a balloon-like structure), the covering membrane, protects the lungs (Lai-Fook, 2004), and at the same time it produces a lubricating fluid that causes smooth movement of lungs in the chest cavity. The airways branch approximately 20 times in the lungs. At each branch point, the airways become smaller and more

in number much like the branches of trees. The final branches of the bronchial tree are called atria that end in alveoli (Drake *et al.*, 2009).

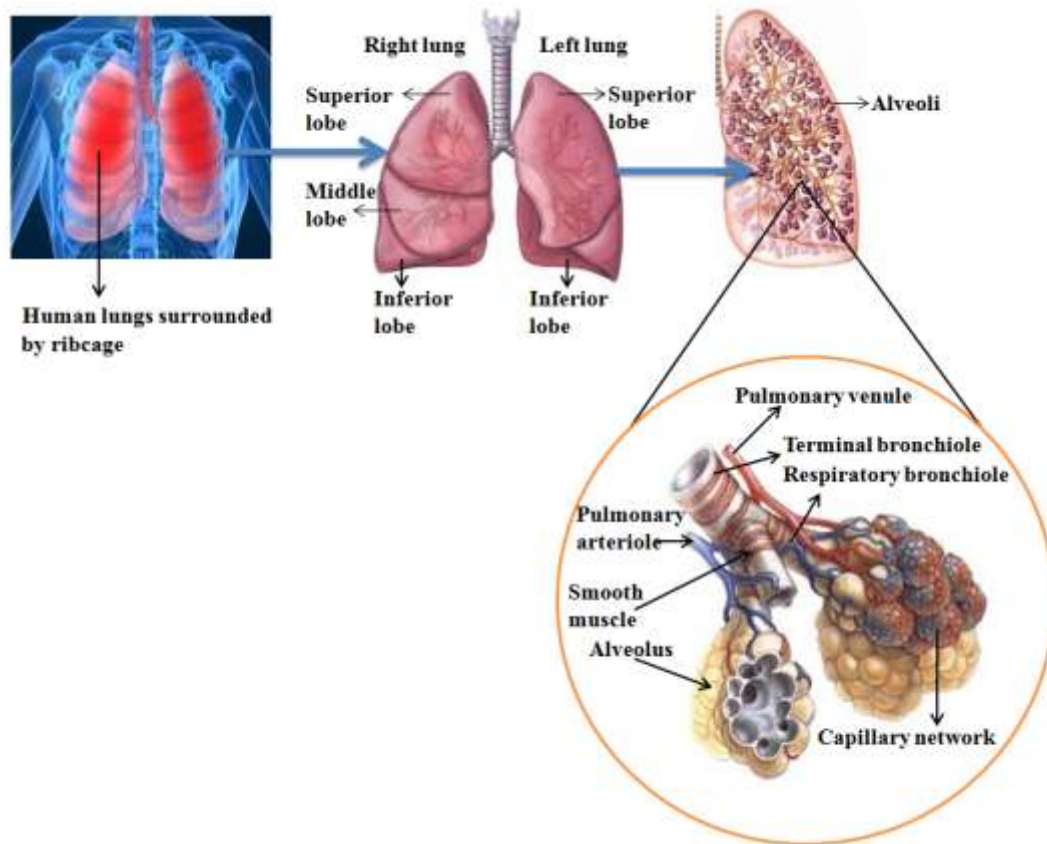


Figure 1.1: Diagrammatic representation of lung morphology and anatomy showing structure of bronchioles (Mukherjee *et al.*, 2017)

Alveoli resemble clusters of grapes under the microscope. There are about 300 million alveoli in each lung. The alveolar walls are extremely thin and fragile thus making them susceptible to irreversible damage. Alveoli are surrounded by “hair net” of capillaries. The blood in the capillaries is separated from the air in the alveoli only by the extremely thin alveolar and capillary walls. Each alveolus is made up type I and type II alveolar cells, alveolar macrophages (Koeppen, 2008). The inner layer of the alveolar epithelium is lined by the surfactant, synthesized by type II alveolar cells (Koeppen, 2008). Outside the bronchi, there is a lining of cells having tiny hairs called cilia. This part executes the first line of defense of lungs to fight against bacterial or viral infection.

1.2 Lung fungal infections

Lungs are susceptible to fungal infections as it is a primary passage of fungi causing deep mycosis. There are varieties of fungal infections such as histoplasmosis, sporotrichosis, blastomycosis, coccidioidomycosis, paracoccidioidomycosis, cryptococcosis, aspergillosis, candidiasis, pneumonia etc. that can cause severe pulmonary injury (Panda, 2004). They are described below:

1. Aspergillosis: In recent years, aspergillus infection in lungs is very predominant due to various factors such as random use of corticosteroids, various immunomodulating drugs, increasing immunosuppression by human immunodeficiency virus infection, and transplantation of solid organs and bone marrow (Thompson III and Patterson, 2008). Its pathological reactions can be manifested in humans in different ways, such as allergic bronchopulmonary aspergillosis (ABPA), allergic alveolitis, aspergilloma, invasive aspergillosis etc. (Addrizzo-Harris *et al.*, 1997; Patterson *et al.*, 2000; Greenberger, 2002; Denning *et al.*, 2003; Panda, 2004; Hope *et al.*, 2005; Zmeili and Soubani, 2007; Smith and Kauffman, 2012).

2. Fusariosis: Out of near about hundred species of *Fusarium*, only few of them such as *F. solani*, *F. moniliforme*, and *F. oxysporum* are the sources of about 90% of human fungal fusariosis infection. The symptoms of fusariosis are quite similar with aspergillus such as fever, chest pain, cough, dyspnoea and pleuritic (Torres and Kontoyiannis, 2011; Nucci and Anaissie, 2002).

3. Mucormycosis: Mucormycosis is a fungal infection caused by Mucorales. Among three genera such as *Rhizopus*, *Rhizomucor* and *Mucor* species accounts for up to 75% of mucormycosis (Kontoyiannis *et al.*, 2010). The infection occurs in upper airways in the form of granulomatous invasion and may gradually move forward into sinuses and/or brain tissue. The most common symptoms of mucormycosis are cough, chest pain, dyspnoea and haemoptysis (Smith and Kauffman, 2012; Roden *et al.*, 2005).

4. Scedosporiosis: *S. boydii* complex consisting *S. boydii*, *S. apiospermum*, *S. aurantiacum* and *S. prolificans* are very common fungi among *Scedosporium* species (Gilgado *et al.*, 2006). Haematopoietic cell transplant recipients, solid organ transplant recipients and patients suffering from haematological malignancies are prone to Scedosporiosis. *S. prolificans* is able to sporulate

in vivo, possibly causing greater risk of antifungal drug resistance. This phenomenon makes *S. prolificans* very unique from most other fungi (Rodriguez-Tudela *et al.*, 2009; Husain *et al.*, 2003).

5. Blastomycosis: *B. dermatitidis*, a dimorphic fungus, causes blastomycosis (Saccante and Woods, 2010). In case of acute pulmonary infection due to *B. dermatitidis*, patient may remain asymptomatic or may suffer from fever, dyspnoea, dry cough and mild chest pain (Smith and Kauffman, 2010). Chronic pulmonary blastomycosis may result in upper lobe cavitory lesions which may be looked similar to tuberculosis or histoplasmosis or mass-like lesions. The lesions may often look like a cancerous lesion (Smith and Kauffman, 2012, Limper *et al.*, 2011).

6. Cryptococcosis: *Cryptococcus neoformans* causes cryptococcosis. However, *Cryptococcus gattii* is also responsible for cryptococcosis. *Cryptococcus*, which remains in nature as encapsulated form, randomly produces a polysaccharide capsule while entering in the pulmonary region (Byrnes *et al.*, 2009; Limper *et al.*, 2011). Cryptococcosis is restricted to the lungs in immunocompetent host and it commonly exists in patients with chronic ailment of lungs. However, it may exhibit as dry cough, fever and dyspnoea which may lead to acute respiratory distress syndrome in case of immunocompromised patients (Pappas *et al.*, 2001; Chang *et al.*, 2006; Baddley *et al.*, 2008).

7. Coccidioidomycosis: Normally two species of coccidioidomycosis such as *C. immitis* and *C. posadasii* are most commonly found. In environment coccidioides which are present as mould form, are simply inhaled into alveoli. These moulds convert into spherules consisting of endospores in the lungs and after maturation these spherules split and discharge the endospores which cause coccidioidomycosis infection (Ampel, 2011; Smith and Kauffman, 2012). However, fever, dry cough, fatigue, dyspnoea and anterior chest pain may be manifested for Coccidioidomycosis. Acute pulmonary coccidioidomycosis can be different from community-acquired pneumonia due to limited response to antibacterial treatment as well as peripheral blood eosinophilia, hilar adenopathy, and existence of erythema nodosum and erythema multiforme (Valdivia *et al.*, 2006).

8. Histoplasmosis: *H. capsulatum*, which causes histoplasmosis, is found as a mould in nature and yeast inside tissues. Inhalation of *H. capsulatum* into alveoli causes infection in humans.

Pulmonary histoplasmosis may lead into acute self-limited pneumonia which may appear in the form of dry cough, mild chest discomfort, fever and fatigue. One of the exceptional difficulties of pulmonary histoplasmosis is the mediastinal fibrosis. Symptoms of this pulmonary histoplasmosis are cough, wheezing, dyspnoea and haemoptysis. But symptoms which persist for month may vary in case of chronic cavitory pulmonary histoplasmosis. Examples of such symptoms are fever, anorexia, fatigue, weight loss, haemoptysis and cough with purulent sputum etc. (Kauffman, 2007; Wheat *et al.*, 2004).

1.3 Treatment of lung fungal infections

The antifungal agents used in the treatment of fungal infection therapy are classified as below (**Figure 1.2**). In spite of several progresses made in this field, any vaccine for fungal infections is not yet available clinically. Several antifungal agents are currently available in the market for the treatment of pulmonary fungal infection. Among them, amphotericin B (AmB) had been the drug of choice for most cases of fungal infections. However, its usage is limited due to serious adverse effects, the most significant one being nephrotoxicity. Liposomal formulation of AmB is also developed and it greatly reduces nephrotoxicity, but still it encounters numerous drawbacks due to its non-targeted delivery via parenteral route. In addition, it gets rapidly cleared from the systemic circulation, for uptake by reticuloendothelial system, which cannot be overlooked (Bowden *et al.*, 2002; Moen *et al.*, 2009).

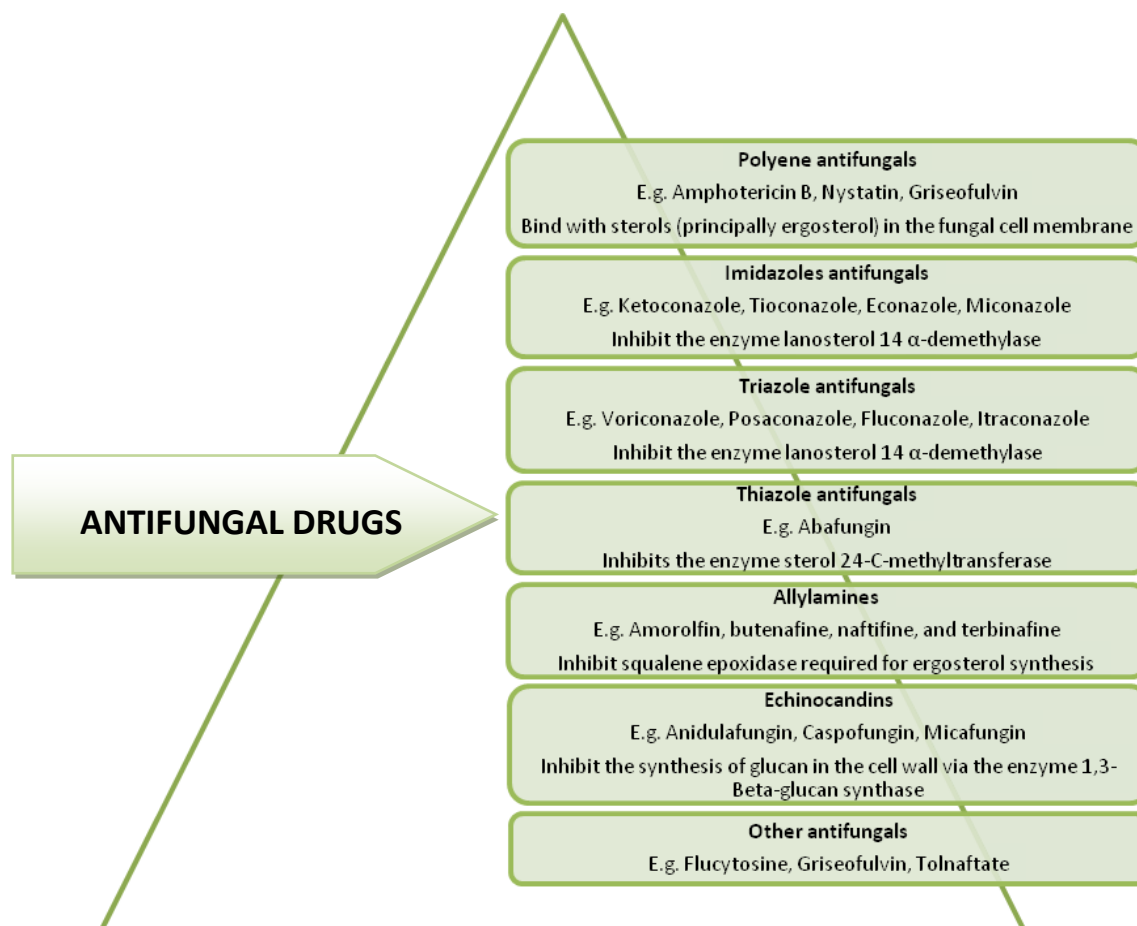


Figure 1.2: Classification of antifungals

Other chemotherapeutic agents found to be therapeutically effective for the treatment of pulmonary fungal infections include the newer second-generation triazole antifungals (voriconazole, posaconazole) and flucytosine. However, these drugs also suffer from several dose-dependent adverse effects such as hepatotoxicity, gastric disturbances, bone marrow suppression-characterized such as leukopenia, thrombocytopenia, and/or pancytopenia (Cook and Confer, 2011).

To overcome the various types of fungal infections, the favoured treatment, step-down therapy and second line therapy are summarized in **Table 1.1**.

Table 1.1: Recommended treatment regimens for pulmonary fungal infections

Fungal infection	Favoured treatment	Step-down therapy	Second line therapy	Reference
Aspergillosis	Voriconazole (VRZ), 4 mg/kg twice daily (<i>i.v.</i>) until stable.	VRZ, 200 mg, twice daily (oral), until lesions resolved.	Lipid amphotericin B (AmB); 5 mg/kg/day (<i>i.v.</i>), until stable, or posaconazole (PCZ), 400 mg, twice daily (oral). Echinocandins with/without VRZ	Walsh <i>et al.</i> , 2008; Limper <i>et al.</i> , 2011; Walsh <i>et al.</i> , 2007
Histoplasmosis	Drastic or immunocompromised: lipid AmB, 3–5 mg/kg/day (<i>i.v.</i>), until stable.	Itraconazole (ITZ), 200 mg, twice daily (oral), A loading dose of 200 mg three times a day (oral) for the first 3 days should be given for 6–12 months.	AmB-deoxycholate (D-AmB), 0.7-1 mg/kg/day (<i>i.v.</i>) until stable, then ITZ, 200 mg twice daily (oral), A loading dose of 200 mg total for the first 3 days should be given. for 6–12 months	Wheat <i>et al.</i> , 2007; Freifeld <i>et al.</i> , 2009
	Mild to moderate infection: ITZ, 200 mg twice daily (oral), A loading dose of 200 mg three times a day (oral) for the first 3 days should be given for 6–12 months	--	VRZ, 200 mg twice daily (oral), A loading dose of 400 mg twice daily (oral) for the first day should be given or fluconazole (FCZ), 800 mg every day (oral), for 6–12 months	
Mucormycosis	Lipid AmB, 5 mg/kg/day (<i>i.v.</i>), or higher doses until lesions resolved	PCZ 400 mg, twice daily (oral)	D-AmB, 1 mg/kg/day (<i>i.v.</i>), until lesions resolved (possible addition of echinocandin to AmB formulation)	Lewis <i>et al.</i> , 2010
Fusariosis	Lipid AmB, 5 mg/kg/day (<i>i.v.</i>), or VRZ, 4 mg/kg bid (<i>i.v.</i>), A loading	VRZ, 200 mg twice daily (oral), until lesions resolved	PCZ, 400 mg bid oral, PCZ can also be dosed as 200 mg 4 times a day (oral) as	Ho <i>et al.</i> , 2007; Lortholary <i>et al.</i> ,

	dose of 6 mg/kg twice daily iv for the first day should be given. or combination of lipid AmB, 5 mg/kg/day (<i>i.v.</i>), plus VRZ, 4 mg/kg twice daily (<i>i.v.</i>)		long as the patient is able to follow with frequent dosing.	2010; Raad <i>et al.</i> , 2006
Cryptococcosis	Drastic or with dissemination: lipid AmB, 3–5 mg/kg/day (<i>i.v.</i>) with flucytosine, 25 mg/kg, 4 times daily (oral), for about 15 to 30 days	FCZ, 400 mg every day (oral), for 8–10 weeks, then FCZ, 200 mg for 6–12 months	D-AmB, 0.7–1 mg/kg/day (<i>i.v.</i>) with flucytosine, 25 mg/kg 4 times a day (oral), for 2–4 weeks, followed by same step-down therapy.	Perfect <i>et al.</i> , 2010
Scedosporiosis	VRZ, 4 mg/kg twice daily (<i>i.v.</i>). A loading dose of 6 mg/kg twice daily (<i>i.v.</i>) for the first day should be given until stable	VRZ, 200 mg twice daily (oral), until lesions resolved	PCZ, 400 mg twice daily (oral), PCZ can also be dosed as 200 mg 4 times daily (oral) as long as the patient is able to comply with frequent dosing.	Troke <i>et al.</i> , 2008
Blastomycosis	Drastic or immunocompromised: lipid AmB, 3–5 mg/kg/day (<i>i.v.</i>) Mild to moderate infection: ITZ, 200 mg bid oral, A loading dose of 200 mg 3 times a day (oral) for the first 3 days should be given. for 6–12 months	ITZ, 200 mg bid oral, A loading dose of 200 mg 3 times a day (oral) for the first 3 days should be given for 6–12 months	D-AmB 0.7–1 mg/kg/day, until stable, then ITZ, 200 mg twice daily (oral), A loading dose of 200 mg 3 times a day (oral) for the first 3 days should be given. for 6–12 months VRZ, 200 mg bid oral, A loading dose of 400 mg twice daily (oral) for the first day should be given or FCZ, 800 mg every day (oral), for 6–12 months	Smith and Kauffman, 2010; Chapman <i>et al.</i> , 2008

Coccidioidomycosis	<p>Drastic or immunocompromised: lipid AmB, 3–5 mg/kg/day (<i>i.v.</i>), until stable.</p> <p>Mild to moderate infection: ITZ, 200 mg twice daily (oral), A loading dose of 200 mg three times a day (oral) for the first 3 days should be given or or FCZ, 400 mg every day (oral), for 6 months</p>	<p>ITZ, 200 mg bid oral, A loading dose of 200 mg 3 times a day (oral) for the first 3 days should be given. or FCZ, 400 mg every day (oral), for 12 months</p>	<p>D-AmB 0.7-1 mg/kg/day (<i>i.v.</i>), until stable, then ITZ, 200 mg bid oral, A loading dose of 200 mg 3 times a day (oral) for the first 3 days should be given or FCZ, 400 mg every day (oral), for 12 months.</p> <p>VRZ, 200 mg bid oral, A loading dose of 400 mg twice daily (oral) for the first day should be given. Or PCZ, 400 mg twice daily (oral), PCZ can also be dosed as 200 mg 4 times a day (oral) as long as the patient is able to comply with frequent dosing.</p>	Galgiani <i>et al.</i> , 2005; Smith and Kauffman, 2012
--------------------	-------------------------------------------------------------------------------------------------------------------------------------------------------------------------------------------------------------------------------------------------------------------------------------------------------	-----------------------------------------------------------------------------------------------------------------------------------------------------------------	--------------------------------------------------------------------------------------------------------------------------------------------------------------------------------------------------------------------------------------------------------------------------------------------------------------------------------------------------------------------------------------------------------------------------------------------------------------------------------------------	---------------------------------------------------------

1.4 Nano-drug delivery systems under investigation, intended for the pulmonary lung fungal infections

Influenced by the progress in nanomedicine, many researchers have showed innovation in formulation development with improved biopharmaceutical properties. The drugs which could not be administered for lung fungal infections directly can be delivered by pulmonary delivery system with a formulation of nanoscale size. Those inventions have opened a door in the treatment of pulmonary fungal infections. The present scenario demands the development of formulations which can directly deliver the desired dose of drug specifically to the site of action, thereby minimizing the dose related adverse effects of drug in other parts of the body. Nanotechnology in the field of drug delivery is emerging rapidly and holds great promise in the significant improvements in human health.

Nanotechnology offers a plethora of advantages over conventional therapy including smaller size, larger surface area, capability of surface modification, site specific targeting to increase local drug concentration, thereby reducing dose related side effects, potential to entrap both hydrophilic and hydrophobic drugs, and improved pharmacokinetic profile such as extended retention time, increased half-life of drugs etc. (Mittal *et al.*, 2018; ud Din *et al.*, 2017).

Nanoparticle-based system for pulmonary delivery may help to retain the particles at the desired site (lungs) for prolonged period of time, thus becoming more efficacious and less toxic as compared to conventional formulations (Mansour *et al.*, 2009; Watts and Williams, 2011).

1.5 Polymeric nanoparticles

A major part of nanotherapeutics includes the use of different types of polymers via different routes for pulmonary fungal infections. In many studies, polyvinyl alcohol and poly (lactide-co-glycolide) (PLGA) are used as sustained release agents because of their biocompatibility and minimal toxicity in both *in vitro* and *in vivo* (Salama *et al.*, 2009; Roberts *et al.*, 2013; Dailey *et al.*, 2006). Das *et al.* showed that voriconazole formulation with PLGA has a sustained effect on pulmonary fungal infections (Das *et al.*, 2015). However, these undissolved particles in the lungs may trigger pulmonary inflammation and fibrosis which is a serious concern. As these are foreign particles, they could be removed either by macrophage present in the lungs or mucociliary clearance (Tomashefski *et al.*, 1988). Therefore, *in vivo* safety and efficacy are still needed to be explored.

1.6 Nanoparticles for the treatment of lung fungal infection

Itraconazole has been strategically encapsulated into chitosan (CS)-based nanoparticles (NPs) using a modified ionic gelation method and to fabricate them as inhalable microparticles using spray drying technique. Different ratios of CS: tripolyphosphate (TPP) were used and is 55% encapsulation was found at 1:3 ratio of CS: TPP. *In vitro* inhalation parameters including fine particle fraction (FPF) and emitted dose percentage (ED%) were measured by a twin stage impinger (TSI). The data of *in vitro* deposition specify that processing of nanoparticles with mannitol and leucine could improve the aerosolization properties significantly (Jafarinejad *et al.*, 2012).

Amphotericin B was investigated as deoxycholate salt, liposomal or lipid complex form, PLGA–dimercaptosuccinic acid (DMSA) polymeric NPs loaded with deoxycholate amphotericin B (D-AmB) for sustained delivery of the drug found to reduce the number of AmB administrations with fewer undesirable effects and a favorable extended dosing interval required to treat mycosis intraperitoneally (Amaral *et al.*, 2009).

Later on AmB NPs was prepared through liquid antisolvent precipitation for oral administration. AmB nanoparticles exhibited 2.1 times faster dissolution rates and 13 times equilibrium solubility compared with the raw drug which could be of beneficial for aerosol delivery (Zu *et al.*, 2014).

The suitability of an aqueous solution of voriconazole solubilized with sulfobutyl ether- β -cyclodextrin for targeted drug delivery to the lungs via nebulization has been established (Tolman *et al.*, 2009a). Another interesting study depicts that PLGA nanoparticles containing voriconazole made porous using an effervescent mixture for improved pulmonary delivery for sustained drug release for over 15 days (Sinha *et al.*, 2013). Pulmonary deposition of the particles was studied using a customized inhalation chamber (Sinha & Mukherjee, 2012) for experimental mice. Porous particles had a lower mass median aerodynamic diameter (MMAD) and the highest initial drug deposition than nonporous particles. Voriconazole loaded PLGA NPs with improved drug loading were successfully delivered to murine lungs (Sinha *et al.*, 2013). Itraconazole dry powders for inhalation (DPI) composed of NPs using high-pressure homogenization with tocopherol polyethylene 1000 succinate as a stabilizer has been prepared and was embedded in carrier microparticles of mannitol and/or sodium taurocholate by spray

drying. It followed impaction studies using a multistage liquid impactor to determine the aerodynamic performance and FPF that is theoretically able to reach the lung (Duret *et al.*, 2012).

A recent study involved the development of PLGA NPs containing voriconazole, radiolabeling with technetium-99m to investigate the effect on their blood clearance, biodistribution, and *in vivo* gamma imaging. *In vivo* deposition of the drug in the lobes of the mice lung and accumulation in various major organs has been observed also. Drug accumulation was more pronounced in the lung in the case of administration of the NPs than that of the free drug following the inhalation route as assessed by gamma scintigraphy study (Das *et al.*, 2015).

Another recent study shows germination of inhaled fungal spores initiates infection causing severe pneumonia and even mortality. It has been observed that nebulized amphotericin B-polymethacrylic acid NPs prophylaxis prevents invasive aspergillosis. It was not toxic to lung epithelial cells or monocyte-derived macrophages *in vitro*, or in an *in vivo* transplant immunosuppression mouse model of life threatening invasive aspergillosis. Three days of nebulizer based prophylaxis delivered the NPs effectively to lung and prevented both fungal growth and lung inflammation (Shirkhani *et al.*, 2015).

Self-assembled amphotericin B-loaded polyglutamic acid NPs were prepared and characterized and *in vitro* potential against *Candida albicans* was determined. The biodegradable polyglutamic acid (PGA)-based formulation of AmB showed potent antimicrobial activity similar to that of Fungizone against *C. albicans*. Interestingly, AmB-bearing PGA NPs were found to inhibit biofilm formation to a considerable extent. In summary, AmB-PGA NPs showed highly attenuated toxicity when compared with Fungizone, while retaining equivalent active antifungal properties (Zia *et al.*, 2015).

1.7 Mucoadhesive polymers

Polymer is a generic term used to describe a very long molecule consisting of structural units and repeating units connected by covalent chemical bonds. The term is derived from the Greek word, 'poly' means many and 'meros' means parts. The good mucoadhesive properties are generally strongly exhibited when functional groups with hydrogen bond such as -OH, -COOH etc., are present in mucoadhesive polymers (Smart, 2005; Boddupalli et al. 2010). Thus

for selecting the mucoadhesive polymers, certain physicochemical features such as hydrophilicity, numerous hydrogen-bond forming groups, visco-elastic properties must be considered.

1.8 Theories of mucoadhesion

Mechanisms of polymer attachment to mucosal surfaces are not yet fully understood. However, certain theories of mucoadhesion have suggested that it might occur via physical entanglement (diffusion theory) and/or chemical interactions, such as electrostatic, hydrogen bonding, and van der Waals' interactions (adsorption and electronic theories). Five theories have been suggested to play a major role in mucoadhesion, namely, adsorption, diffusion, electronic, fracture, and wetting theories (Madsen *et al.* 1998). In the adsorption theory, primary and secondary chemical bonds of the covalent and non-covalent (electrostatic and van der Waals' forces, hydrogen, and hydrophobic bonds) types are formed upon initial contact between the mucus and the mucoadhesive polymer. Wetting theory explains the importance of contact angle and reduction of surface and interfacial energies to achieve good mucoadhesion. Though the diffusion theory elucidates how the degree of penetration helps the adhesion force of mucin and polymer, the penetration rate depends on the diffusion coefficient, flexibility and nature of the mucoadhesive chains, mobility and contact time. Fracture theory simply concerned the force required to separate two surfaces after adhesion is ascertained (Ahagon and Gent, 1975). Electronic theory defines the occurrence of adhesion by means of electron transfer between the mucus and the mucoadhesive system (Dodou *et al.*, 2005).

1.9 Why Pulmonary route?

In recent years, pulmonary drug delivery is an attractive route of administration of drugs due to various beneficial effects. In fact, the lungs are competent entry point for drugs to the bloodstream due to the huge surface area for absorption (about 100 m²), the very thin absorption membrane (0.1-0.2 μm), and outstanding blood flow (5 L/min) capability, which rapidly allocates molecules all over the body. Moreover, the lungs reveal fairly low local metabolic activity and in contrast to the oral route of drug administration, pulmonary inhalation is not subjected to first-pass metabolism (Goel *et al.*, 2013). The comparative study of drugs given via pulmonary comparison to other routes (*i.v.*, oral etc.) are given in **Table 1.2**.

Table 1.2: Comparative study pulmonary vs. other routes (*i.v.*, oral etc.) (Mukherjee *et al.*, 2017)

Drug	Dosage form	Route of administration	Conclusion	References
Amphotericin B	Liposome	Intrapulmonary	Targeted delivery of drugs may reduce systemic toxicity, improve treatment efficacy, but inhaled drugs may also interfere with pulmonary surfactant function.	Griese <i>et al.</i> , 1998
	Liposome (AmBisome) and non-liposomal (Fungizone) formulation	Nebulizer	Nebulization of either Fungizone or AmBisome leads to respirable aerosols and results in a substantial lung tissue concentration and low systemic exposure of AmB.	Ruijgrok <i>et al.</i> , 2000
	Nanoparticles	Intravenous	The approach was able to reduce the dosing frequency by 3-fold without causing renal or hepatic toxicity and avoid any increase in plasma lipid levels.	Amaral <i>et al.</i> , 2009
	Liposomes coated with <i>O</i> -palmitoyl mannan, and <i>O</i> -palmitoyl pullulan	Aerosol	The ligand anchored liposomal aerosols are very effective in rapid attainment of high-drug concentration in lungs and maintain the same over prolonged period of time.	Vyas <i>et al.</i> , 2009
	Liposome and lipid complex	Intravenous	Less nephro-toxicity in lipid formulations	Limper <i>et al.</i> , 2011
	Inhalation powder	Dry powder inhalation	Significant survival benefit and reductions in pulmonary fungal burden in model of invasive pulmonary aspergillosis.	Kirkpatrick <i>et al.</i> , 2012
Voriconazole	Infusion	Aerosol	An inhaled aqueous solution of voriconazole and sulfobutyl ether- β -cyclodextrin is capable of producing high lung tissue as well as plasma concentrations was observed following single and multiple inhaled doses in	Tolman <i>et al.</i> , 2009a

			pharmacokinetics study.	
	Aqueous solution	Aerosol	Inhaled voriconazole was well tolerated but signs of mild acute histiocytosis in lung tissue without other signs of inflammation was observed.	Tolman <i>et al.</i> , 2009b
	Nanoparticles	Pulmonary	Pulmonary deposition of the nanoparticles was studied using a customized inhalation chamber. Drug was detectable in lungs until 7 days and 5 days after administration, for porous and nonporous particles, respectively. Porous nanoparticles with lower MMADs showed better pulmonary deposition in deep lung regions and sustained presence in lungs than the nonporous particles.	Sinha <i>et al.</i> , 2013
	Solid Lipid Nanoparticles	Ophthalmic	The optimized formulation would offer shelf life of more than 2-year at room temperature. The resulting solid lipid nanoparticles seem to be promising approach for overcoming challenge caused by unsuccessful ocular delivery.	Khare <i>et al.</i> , 2016
Itraconazole (ITZ)	Nanostructured particles by Evaporative precipitation into aqueous solution (EPAS) and Spray-freezing into liquid (SFL)	Aerosolized with the nebulizer	The prolonged survival and limited systemic exposure with aerosolized delivery of EPAS and SFL-ITZ are encouraging.	Hoeben <i>et al.</i> , 2006

	Nanostructured particles by EPAS and SFL	Aerosolized with the nebulizer	An effective method of targeted delivery of ITZ to the deep lung for the treatment and prevention of acute fungal infections	McConville <i>et al.</i> , 2006
	Nanostructured particles by SFL formulation	aerosol	Aerosolized administration of SFL ITZ was effective as prophylaxis in improving survival in murine model of invasive pulmonary aspergillosis due to <i>A. fumigatus</i> . The survival benefit can be explained by the ability of aerosolized SFL ITZ to limit disease progression and angio-invasion, both of which were markedly reduced in comparison to mice that received control or ITZ oral solution by oral gavage.	Alvarez <i>et al.</i> , 2007
	Chitosan (CS) based polymeric micelles	Nebulizer	<i>In vitro</i> nebulization study of the ITZ loaded formulations showed that the stearic acid-CS based polymeric micelles had adequate capability as nanocarriers to deliver ITZ and can remain their stability during nebulization.	Moazeni <i>et al.</i> , 2012
Caspofungin	Caspofungin in 0.9% NaCl solutions 10 and 30 mg/mL	Aerosolized with disposable and reusable type of nebulizer	Two types of commercial nebulizing systems efficiently aerosolize the drug, the choice of which depends on whether a disposable or reusable type of jet nebulizer is most suitable for the particular patient care setting.	Wong-Beringer <i>et al.</i> , 2005
Pneumocandins	Aqueous solution for aerosol and solution in normal saline for i.p. administration	Aerosol	The pneumocandins are highly active against <i>Aspergillus</i> species and dramatic improvement in survival was found with aerosolized form.	Kurtz <i>et al.</i> , 1995

The various advantages of pulmonary drug delivery systems are listed as below (Banker and Rhodes, 2002; Feldmann and Merkel; 2015):

1. Delivery of drug in high concentrations directly to the disease site
2. Reduced dose is required for the desired pharmacological action that results in reduced risk of systemic side effects.
3. Quick onset of drug action resulting in rapid clinical response.
4. Bypass the barriers to therapeutic efficacy, such as poor gastrointestinal absorption and hepatic first-pass metabolism in the liver.
5. Much reduced hostile environment is present in the lungs than the oral route to most drugs, including proteins and peptides.

1.10 Mechanism of deposition of the particles in the lung

The respiratory deposition of inhaled drug particle in the lung is very complex and deposition is based on the many factors. Some of the influencing factors include breathing rate, lung volume, respiration volume, health of the subject, airway bifurcations leading to constant changing of hydrodynamic flow of fluid.

The deposition of particles in the different regions of the lungs depends on the particle size of the formulation (**Figure 1.3**). Based on the particle size, three different mechanisms of drug deposition are defined, namely impaction, sedimentation and diffusion/Brownian motion.

Impaction: In impaction, the aerosol particles pass through the oropharynx and upper respiratory passages at a high velocity. Due to the centrifugal force, the particles collide with the respiratory wall and are deposited in the oropharynx region. This mechanism is generally observed for DPI and metered dose inhalers (MDI), with particles sizes greater than 5 μm . In case of DPI, the inspiratory effort of the patient plays an important role in the deposition. If the force of inhalation is insufficient, the dry powder deposits in the upper airways, owing to the mass of the particles and the inertial forces. For MDI, despite of high speed of the generated aerosol, large particle sizes also lead to the deposition of the particles mostly in the upper respiratory tract region.

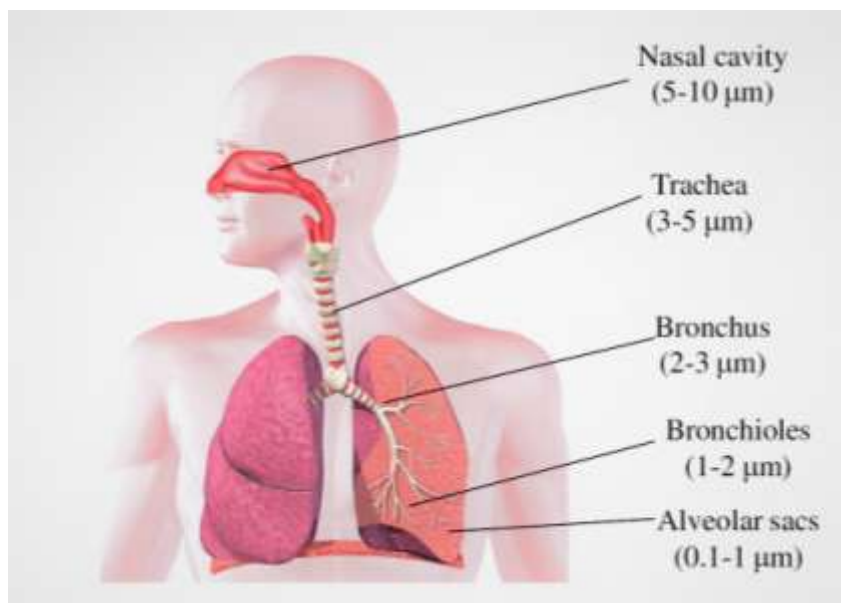


Figure 1.3: Particles size dependant deposition in various parts of lungs.

Sedimentation: Gravitational forces are predominantly responsible for the sedimentation of particles. Particles with sufficient mass and sizes between 1 to 5 μm deposit in the smaller airways and bronchioles, where they deposit slowly, for a sufficiently long time span. Therefore, sedimentation is also influenced by the breathing pattern. Slow breathing provides a sufficient time span for sedimentation.

Brownian motion: Apart from impaction and sedimentation, Brownian motion plays a major role in the deeper alveolar areas of the lungs. Brownian motion is the microscopic random motion of small particles due to the numerous random collisions by gas molecules. In the small airways where the distance is short and residence time is long, diffusion is an important mechanism for the deposition of small particles ($< 0.5 \mu\text{m}$). Macroscopically, we see the overall movement of particles from a higher concentration region (i.e., the center of air stream) to a lower concentration region (i.e., the airway wall).

Since it is caused by gas molecule collisions, the effectiveness of this mechanism increases as particle size decreases. Upon contact with the lung surfactant, the dissolution of drug in alveolar fluid is essential for diffusion. Additionally, the concentration gradient also influences the diffusion process. Particles smaller than 1 to 0.5 μm are deposited in the alveolar region, while most of the particles, owing to smaller sizes, are exhaled.

Apart from the mechanisms, parameters such as the particle size, particle morphology and geometry of the aerosol, along with surface properties play an important role in deposition phenomena. Furthermore, breathing frequency and the holding of breaths, humidity, air velocity and tidal volume also are vital factors influencing the deposition (<http://aerosol.ees.ufl.edu/respiratory/section04.html>; Patil and Sarasija, 2012).

1.11 Pulmonary drug delivery devices:

The development of modern inhalation devices can be broadly divided into two categories with various varieties (**Figure 1.4**) such as (i) Nebulizer and (ii) Compact portable inhaler.

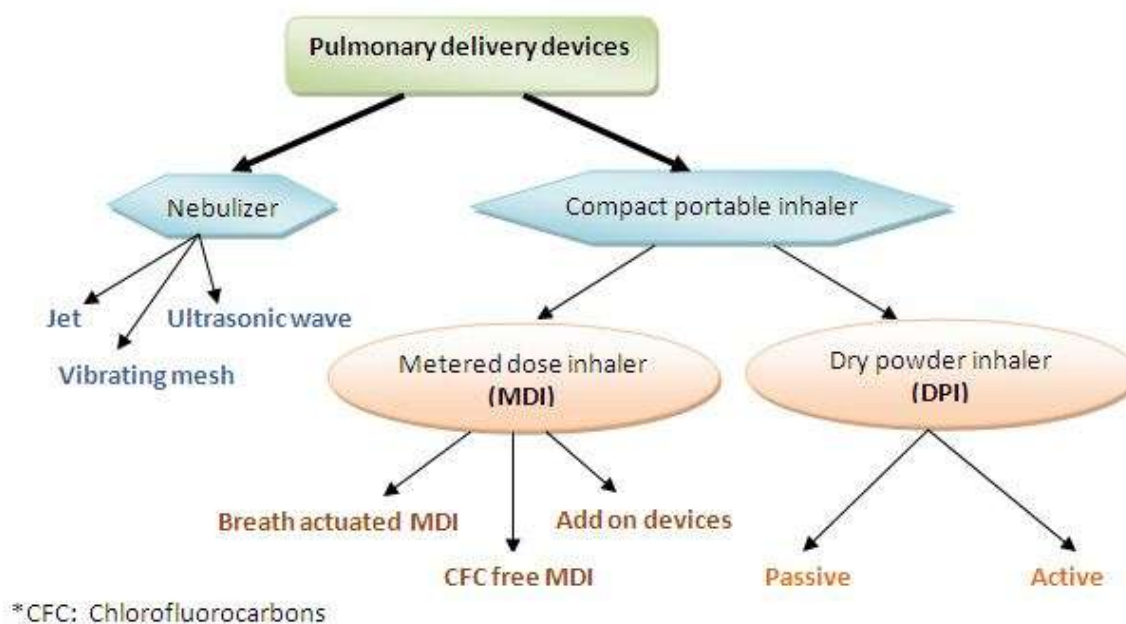


Figure 1.4: Evolution of pulmonary delivery devices (Mukherjee *et al.*, 2017)

Nebulizer:

Nebulizers have been used to treat respiratory diseases for many years. The working principle of jet nebulizer based on Bernoulli principle by which compressed gas (air or oxygen) is passed through a narrow orifice creating a low-pressure area at the adjacent liquid feed tube (**Figure 1.5**). This evacuates the solution with the drug being drawn up from the fluid reservoir

and shattered the gas stream through fine droplets. In an ultrasonic nebulizer, a piezoelectric crystal is used with a high vibrating frequency (usually 1-3 MHz) to generate a fountain of liquid in the mobilizing chamber.

The physical properties of pulmonary drug formulations may have an outcome based on particle size and nebulization rates. The viscosity, osmolarity, ionic strength, pH and surface tension may also affect the nebulization of some formulations.



Figure 1.5: Nebulizer and its components (Mukherjee *et al.*, 2017)

Constant output jet nebulizer can aerosolize most of the drug solution and provides a large dose with very little patient coordination skill. Treatment by using nebulizer can be time-consuming and also less effective, where there is 50% loss with a continuously operated nebulizer. On an average only 10% of the total dose loaded in a nebulizer is in reality deposited in the lungs (Giraud and Roche, 2002).

Recent technically advanced novel nebulizers have been developed to reduce drug wastage and improve delivery efficacy. In a nebulizer, the aerosol output is increased by directing auxiliary air entrained at the time of inspiration by enhanced delivery designs. Adaptive aerosol delivery monitors a patient's breathing pattern in the first three breaths and then targets the aerosol delivery into first 50% of inhalation of each time. This commits that the aerosol is

delivered to the patient during inspiration only, thereby eliminating loss during expiration that occurs with continuous output nebulizer (Borgstrom *et al.*, 1996; Ashurst *et al.*, 2000).

Compact portable inhaler

Metered –dose- inhaler:

It is a revolutionary invention of MDI that overcomes the problem of the hand-bulb nebulizer and serves portability to outpatients for the first time. This inhalation device is the most widely used aerosol delivery device today (**Figure 1.6**). MDI provides a drug aerosol driven by propellants, such as chlorofluorocarbons (CFC) and hydrofluoroalkanes (HFAs). MDI emits only a small portion of the drug dose to the lung. On average, only 10-20% of the delivered dose is deposited in the lung. The high velocity and large particle size of the spray cause around 50-80% of deposition of drug in the oropharyngeal region. Hand and mouth discoordination is another barrier in the optimal use of an MDI system.

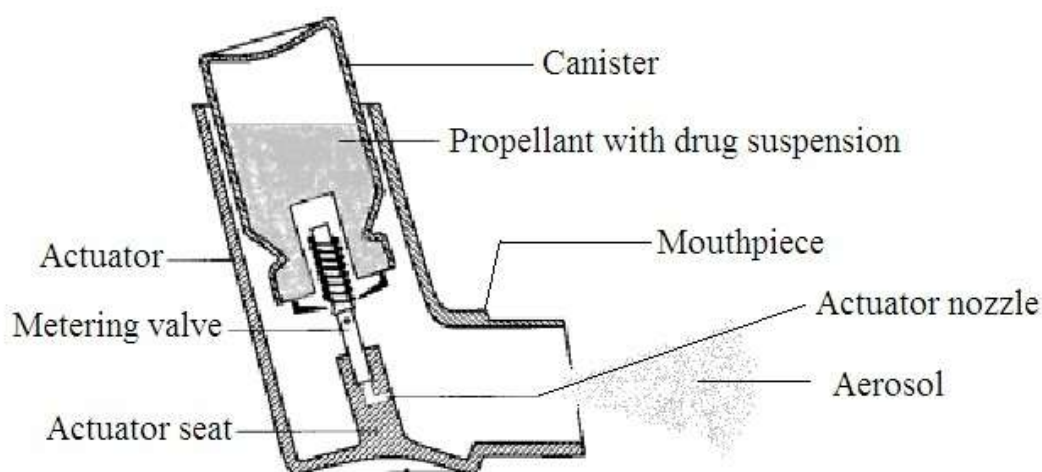


Figure 1.6: Metered-dose inhaler and its components (Mukherjee *et al.*, 2017)

The efficacy of an MDI device depends on a patient's breathing pattern, inspiratory flow rate (IFR) and hand and mouth co-ordination. Increased IFR results in a decrease in total pulmonary dose deposition and diffusion into the peripheral airway. Fast rate inhalation (>60 l.min⁻¹) results in a less peripheral deposition since deposition of the aerosol takes place by inertial impaction in the oropharyngeal region and the conducting airways. When aerosol is

inhaled slowly, drug deposition by gravitational sedimentation in the peripheral region of the lung is improved. Peripheral drug deposition has also been shown to improve with an increase in tidal volume and a decrease in respiratory frequency. As the inhaled volume is enhanced, aerosols are able to diffuse more into the lung-peripheral region. An increased breath-holding period on completion of inhalation enables particles which penetrate the periphery, to deposit in that region, instead of being exhaled during the expiratory phase. Thus, the best conditions for inhaling MDI aerosols include a starting volume equivalent to the functional residual capacity, actuation of the device at the start of inhalation, IFR of $<60 \text{ l min}^{-1}$ followed by a 10-s breath-hold at the end of inspiration (Norwood *et al.*, 1995).

Pressurized metered-dose inhalers:

The pressurized metered-dose inhaler (pMDI) is not available for all drugs or dosages, making it difficult for clinicians to prescribe the same type of device for diverse inhaled medications. This is exacerbated by the trend of many pharmaceutical companies not to release newer inhaled drugs as pMDIs. The design of the CFC-propellant pMDI requires initial and frequent priming of device. Failure to prime the device results in the administration of a substantially lower dose than that is prescribed. Unfortunately, frequent priming tends to waste drug to the atmosphere (Dalby and Suman, 2003).

Dry powder inhalers:

Interest in DPIs as an effective, efficient and environmentally friendly way of delivering drugs to the lung has accelerated in recent years. A fundamental difficulty with developing solid state aerosols or DPIs is managing both the ubiquitous and the transient forces contained in powder beds. Indeed, managing of such particulate forces, for example via particle engineering techniques, is now considered central to successful DPI formulation and production (**Figure 1.7**). In consequence, much attention is currently focused on producing “smart” formulations, where it may be possible to achieve excellent powder flow and low cohesive forces

Pharmaceutical scientists too frequently meet major obstacles when they engage in the world of DPI product design, because of the complications of this area resulting from the plethora of DPI device designs. There is tremendous variation in the methods used to store and meter powders and to generate the aerosol cloud. In case of DPI aerosol generation, there is a great deal of

variations between different types of device, in the fluid dynamic and electrostatic environment that the powder formulation experiences (Ashurst *et al.*, 2000).

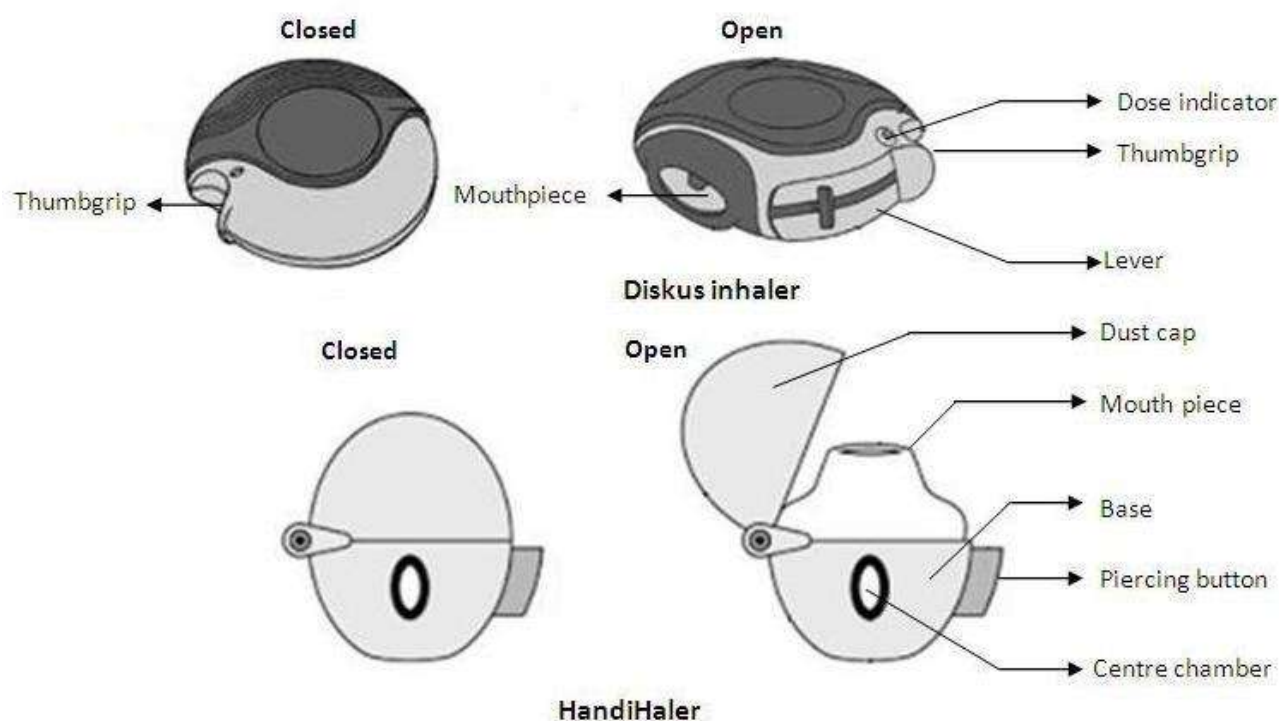


Figure 1.7: Schematic diagram of some currently available dry powder inhalers and their components (Mukherjee *et al.*, 2017)

The drug aerosol is created in a DPI by directing air through loose powder. Most drug particles from DPIs are too large to penetrate into the lungs as because of either large powder agglomerates or the presence of large carrier particles (e.g. lactose). Thus, dispersion of the powder into fine respirable particles depends on the creation of turbulent air flow that causes the aggregates to break up into particles small enough to be carried into the lower airways and also to separate carrier from the drug in the device chamber. Each DPI has a different air flow resistance that regulates the required inspiratory effort. The higher the resistance of the device, the more difficult it is to generate an inspiratory flow great enough to attain the maximum dose from the inhaler device. However, deposition in the lung tends to be augmented when using

high-resistance inhalers (Yu and Chien, 1997). However, an efficient and robust formulation technology can provide use of DPI products more acceptable (Begat *et al.*, 2004).

1.12 Limitations of pulmonary route if any

There are not only advantages but also some limitations of the pulmonary route of delivery. The limitations of the delivery of drugs to lungs (Sciarra and Cutie, 1990) are very important to design the effective pulmonary drug delivery systems. Some of them are mentioned below.

1. The oropharyngeal settlement may give local adverse effects.
2. Patients may face trouble using the delivery devices correctly.
3. Various aspects affect the reproducibility of drug delivery to the lungs, including physiological (respiratory scheme) and pharmaceutical (tool, formulation) variables. For the systemic delivery of drugs with a small therapeutic index, such deviations may be undesirable.
4. Drug absorption may be limited due to the barrier action of the mucus and the drug-mucus interactions.
5. Mucociliary clearance diminishes the retention time of drugs within the lungs which may affect the pharmacological efficacy of the slowly absorbed drugs.
6. The lungs are not easily reachable surface for drug delivery and complex delivery devices are required for targeted drug delivery in lungs.

Chapter 2

Literature review

2. Literature Review

Fungi are eukaryotic, achrrophyllus, saprobe and versatile group of living organisms that are widely found in environment. More than 250,000 species of fungi are found in our universe, out of which 300 are remarked as potential pathogens causing superficial to life threatening infections in humans as well as in a wide variety of animals (Brown *et al.*, 2012; Pal, 1997; Pal, 2004).

Lung fungal infections (LFI) are mostly affecting immunocompromised patients suffering from HIV/AIDS, cystic fibrosis, cancer, organ transplantation, burn, and prolonged use of antibiotic, corticosteroids and antineoplastic drugs (Pal, 1997, Cook and Confer, 2011). Pulmonary fungal infection is one of the leading causes of deaths in developing countries (Smith and Kauffman, 2012). The global occurrence of LFI in many regions of the world is not correctly documented due to insufficient diagnostic facilities (Pal, 2017). Endemic mycoses predominantly occur in specific climate zones whereas opportunistic infections is found in persons having immune deficiency (Lee and Lau, 2017; Smith and Kauffman, 2012). Respiratory tract is the prime portal of entry of most fungi resulting in pulmonary and systemic infections. Transmission can occur through inhalation of infectious spores, traumatic implantation of fungal cells, direct contact with infected persons/animals, and bite of animals (Pal, 2007; Pal, 2017).

AmB deoxycholate has been used as the firstline therapy for severe systemic fungal infections in the past few decades but its use has been limited for its associated adverse effects including nephrotoxicity and hemolytic anemia. Newer triazole antifungals such as itraconazole and fluconazole with limited spectrum of activity shows improved tolerability profiles, but their extensive use has led to the emergence of resistance among susceptible strains. Thus, newer antifungal agents with improved pharmacologic and resistance profiles are required with an extended spectrum of activity, better tolerability, and enhanced efficacy (Jeu *et al.*, 2003, Greer, 2003; Lat and Thompson, 2011).

Voriconazole (VRZ) is modified from fluconazole and acquires an improving potency and spectrum (Naithani and Kumar, 2005). It is the first available second-generation triazole group of antifungal agent from the 'azole' family, possesses broad-spectrum activity against resistant fungal species such as *Aspergillus*, *Candida*, *Scedosporium* and *Fusarium* (de Sa *et al.*,

2015; Chung *et al.*, 2015; Lin *et al.*, 2010). Antifungal effect of voriconazole exerts by altering the fungal cell membrane. Voriconazole blocks synthesis of ergosterol, an essential component of the membrane, by interacting with lanosterol 14- α demethylase (CYP51 or Erg11p), a cytochrome P-450 enzyme that is needed to convert lanosterol to ergosterol, affecting the integrity and function of the fungal membrane (Das *et al.*, 2015).

Various drug administration methods have been in research till date for delivering drug to the lungs (Kuzmov and Minko, 2015; Patil and Sarasija, 2012). Lung is becoming an attractive target due to its non-invasive nature, avoidance of “first-pass” metabolism, availability of huge surface area and plenty of blood supply for drug absorption for both local and systemic actions of therapeutics (Patil and Sarasija, 2012; Mansour *et al.*, 2009; Lee *et al.*, 2013). Local delivery of medications to the lungs is highly desirable, especially in patients with specific pulmonary diseases such as cystic fibrosis, asthma, chronic pulmonary infections, lung cancer, etc., where conventional therapy seems to be ineffective to maintain the desired drug concentration in the blood plasma for a prolonged time (Flume and Klepser, 2002; Codrons *et al.*, 2003; Gessler *et al.*, 2002; Gessler *et al.*, 2008).

For targeted drug delivery, nanocarriers are attractive choice in pharmaceutical research in the recent arena due to its various beneficial effects such as high stability, high carrier capacity by incorporating more drug molecules in the particle matrix, feasibility of incorporation of both hydrophilic and hydrophobic substances, and feasibility of variable routes of administration (including oral and inhalation) and most important is to provide controlled (sustained) drug release from the matrix (Smola *et al.*, 2008; Lee *et al.*, 2015; Gelperina *et al.*, 2005; Da Silva *et al.*, 2013; Das *et al.*, 2015). Nanoparticles are also known for their capability of sustaining drug in the pulmonary region (Zhao *et al.*, 2014; Liu *et al.*, 2008; Videira *et al.*, 2002; Sinha *et al.*, 2013).

Nanoparticles prepared with biodegradable and biocompatible polymers such as PLGA, Poly-lactic acid (PLA) and chitosan are (Makadia and Siegel, 2011) attractive choice to load the drug for delivering it to the pulmonary site of action. Among the various polymers used in the nanoparticles formulation, PLGA gained marked attention because of their biocompatibility and biodegradability, stability, non-toxicity (Lemoine *et al.*, 1996; Murakami *et al.*, 1999; Morales-Cruz *et al.*, 2012), and ability to have long systemic circulation by the colloidal particles made of

these FDA approved polymers (Murakami *et al* 1999). PLGA nanoparticles have been widely used in research in past few decades (Sahana *et al.*, 2010; Singh and Lillard, 2009; Ghosh *et al.*, 2017). Several works have been carried out on PLGA nanoparticles of other antifungal drugs particularly AmB (Venier-Julienne and Benoît, 1996; Van de Ven *et al.*, 2012; Italia *et al.*, 2011; Verma *et al.*, 2011; Nahar and Jain, 2009; Italia *et al.*, 2009; Amaral *et al.*, 2009; Yang *et al.*, 2018). Very few works has been done on the preparation of nanoparticles of PLGA containing the drug VRZ. Nanoparticles particularly solid lipid nanoparticles or lipid based nanoparticles were prepared using VRZ for ocular delivery (Füredi *et al.*, 2017; Khare *et al.*, 2016).

Several novel drug delivery systems were designed using VRZ as model drug. Salem *et al.*, 2016 have prepared porous voriconazole nanoagglomerates in a respirable range using the combination of edge activators (stearic acid and sodium deoxycholate) and diluted osmogenic polycationic polymer polyethyleneimine solution for enhancing the deposition and dissolution of voriconazole in the lung (Salem *et al.*, 2016). Another group of workers have prepared sustained-release voriconazole-containing thermogel that releases VRZ for 28 days (Cuming *et al.*, 2017).

Although the concept of preparing nanoparticles with PLGA polymer containing VRZ started long before (Peng *et al.*, 2008) and tested on candida infection, the researchers were trying to develop more effective formulation containing VRZ. Sinha *et al.*, 2013 have prepared porous and nonporous PLGA particles loaded with VRZ for effective delivery in the lung fungal infection (Sinha *et al.*, 2013). Later on Das *et al.* (2015) prepared PLGA nanoparticles of VRZ and found the *in vivo* localization of the formulations in live animal radio imaging and compared the data with the radio-labeled free VRZ (Das *et al.*, 2015).

Chitosan is a widely used material for preparing nanoparticles or as coating material on PLGA nanoparticles because of its recognized mucoadhesiveness, biodegradability, biocompatibility and ability to enhance the penetration of large molecules across mucosal surfaces (Chalikwar *et al.*, 2013; Kumar *et al.*, 2004). The advantages of modifying the surface of PLGA particles with a mucoadhesive polymer, such as CS, may cause the predominant variation or even inversion of zeta-potential, ability to promote cellular adhesion and retention of the drug delivery system at the target site (Yang *et al.*, 2009; Tahara *et al.*, 2010; Babu *et al.*, 2013). Moreover, a decreased burst effect in the release of the encapsulated drug and the possibility of conjugating ligand(s) for drug-targeting to the free amino groups of CS are the

added advantages (Chronopoulou *et al.*, 2013). The specific advantage of nanoparticles coated with CS for pulmonary delivery is the retention of the formulation in the pulmonary site of infection for a longer time period than that of CS-free nanoparticles providing effective treatment, curbing the phagocytic effects and thereby enhancing the longevity of the nanoparticles in the biological system (Parveen and Sahoo, 2011).

PLGA nanoparticles containing antifungal AmB were prepared earlier in 1996 by the solvent evaporation process. Blank nanoparticles, free AmB and drug loaded nanoparticles obtained were 130 ± 27 nm, $184\pm 64/ 997\pm 83$ nm and $168\pm 42/ 797\pm 100$ nm in diameter, respectively. When AmB was added in the organic phase, the final suspension showed two populations due to unbound drug. Free AmB was removed by addition of an adsorbent polymer, Amberlite XAD16, to the nanoparticle suspension and subsequently ultra-filtering the medium. The drug payload was between 0.7 and 1.3% (Venier-Julienne and Benoît, 1996).

PLGA nanoparticles were formulated by an emulsion-solvent evaporation method using polyvinyl alcohol (PVA) as a stabilizer generating negatively charged particles and heterogeneous size distribution for DNA delivery. Cationically modified PLGA nanoparticles or nanospheres were formulated by emulsion-diffusion-evaporation technique using PVA-CS blend with defined size and shape that can efficiently bind DNA. The nanospheres were characterized by atomic force microscopy (AFM), photon-correlation spectroscopy (PCS), and Fourier transform infrared spectroscopy (FTIR) and found that their size was around 200 nm. To understand the surface properties of nanospheres and their ability to condense negatively charged DNA, zeta potential and gel electrophoresis studies were also conducted and found that the charge on the nanospheres was adequate to effectively bind the negatively charged DNA electrostatically (Kumar *et al.*, 2004).

To understand the mechanism of adsorption of polyelectrolyte onto particles cationic PLGA nanoparticles were fabricated by adsorption of varying concentrations of a biodegradable polysaccharide, chitosan (0–2.4 g/L), using oil-in-water emulsion and solvent evaporation techniques. The particle diameter, zeta-potential, and chitosan adsorption of chitosan-coated PLGA nanoparticles confirmed the increase of polyelectrolyte adsorption. Five adsorption isotherm models (Langmuir, Freundlich, Halsey, Henderson, and Smith) were applied to the experimental data for understanding the adsorption mechanism. It was found that particle

diameter and adsorption of chitosan were found to increase with increasing concentration of chitosan during adsorption study. PLGA nanoparticles had a negative zeta-potential (-20 mV) prior to chitosan adsorption on the surface. The zeta-potential of chitosan-coated PLGA nanoparticles was positive and it increased with chitosan adsorbed until a maximum value ($+55$ mV) reached at approximately 0.4 – 0.6 g/L. It can be concluded that the cationic nature of chitosan, high surface energy and microporous non-uniform surface of PLGA nanoparticles could be the underlying reasons for adsorption of chitosan on PLGA nanoparticles (Guo and Gemeinhart, 2008).

Long-circulating nanoparticles were designed and formulated by optimizing the concentration of chitosan (CS) and polyethylene glycol (PEG). Paclitaxel loaded chitosan and polyethylene glycol coated PLGA (PLGA–CS–PEG) nanoparticles were formulated and characterized that could efficiently encapsulate hydrophobic drugs, and evade the phagocytic uptake by reducing opsonization by blood proteins resulting in an increased bioavailability of the drug. Cellular uptake efficiency and *in vitro* cytotoxicity of the experimental nanoparticles were assessed in different types of cancer cells such as retinoblastoma cells, breast cancer cells and pancreatic cancer cells. PLGA–CS–PEG nanoparticles showed dramatic prolongation in blood circulation and reduced macrophage uptake when compared to PLGA–CS and PLGA nanoparticles. Superior anti-proliferative effect and cell cycle inhibition were also found in case of PLGA–CS nanoparticles and PLGA–CS–PEG nanoparticles over PLGA nanoparticles and pure drug paclitaxel. Thus, a coating blend of PEG and chitosan may represent a significant step in the development of long-circulating tumor drug delivery (Parveen and Sahoo, 2011).

Positively and negatively charged PLGA nanoparticles were prepared using the natural polymers such as chitosan and alginate as coating materials, respectively. The oppositely charged nanoparticles when blended in different weight ratio resulted in a cohesive colloidal gel with stable 3D porous network due to the electrostatic forces between them. This colloidal gel may be molded to the desired shape. Scanning electron microscopic images of dried colloidal networks revealed an organized, 3D microporous structure. Viability tests of hUCMSCs seeded on the colloidal gels showed the insignificant cytotoxicity of the materials used in the formulation (Wang *et al.*, 2011).

Localized delivery can be achieved by incorporating of biomolecules within biodegradable nanoparticles followed by inclusion of such particulate nanocarriers into suitable porous scaffolds for accelerated bone regeneration. Freeze-dried porous chitosan–gelatin scaffolds were embedded with various amounts of PLGA nanoparticles and were subjected to physico-mechanical and biological characterizations. It has been found that incorporation of PLGA nanoparticles into porous crosslinked scaffolds changed the micro-architecture of the scaffolds, reduced the dissolution degree of the scaffolds, and increased the compressive modulus. The water uptake behavior of porous scaffolds containing PLGA nanoparticles significantly decreased (Nandagiri *et al.*, 2011).

Composite nanofibers composed of PLGA were prepared encapsulating chitosan/siRNA nanoparticles by electrospinning method. An optimized release profile had been achieved for prolonged and efficient gene silencing by acidic/alkaline hydrolysis and a bulk/surface degradation mechanism. Thermo-controlled AFM in situ imaging revealed the integrity of the encapsulated chitosan/siRNA polyplex. A triphasic release profile was obtained at pH 5.5 and pH 7.4. It was shown that a short alkaline pretreatment provided a homogeneous hydrolysis and consequently a nearly zero-order drug release profile. Further investigation confirmed the interesting release profile for siRNA transfection, where the encapsulated chitosan/siRNA NPs exhibited up to 50% EGFP gene silencing activity after 48 h post-transfection on H1299 cells (Chen *et al.*, 2012).

The surface of PLGA nanoparticles was modified by chitosan via amide bond formation mediated by carbodiimide to enhance the mucoadhesive potential of carrier system. Grafting of chitosan on PLGA surface and its improved mucoadhesive potential were confirmed by FTIR spectroscopy and in vitro mucoadhesion study, respectively. 2^3 factorial design was applied to fabricate self-assembled PLGA NPs containing chlorpromazine hydrochloride. Ex vivo permeation and histopathological study on sheep nasal mucosa disclosed safe mucoadhesion. The optimized formulation was found to be robust that can withstand to extreme conditions of temperature and relative humidity as supported by the accelerated stability testing (Chalikwar *et al.*, 2013).

One-step methodology for the development of formulation of chitosan coated PLGA nanoparticles containing dexamethasone (DXM) as a model drug was patented by a group of researchers. CS coating switched NPs zeta potential from negative to positive, without modifying particle size distribution. The nanoparticles were found to be spherical in shape with smooth surface found in SEM images. The uptake of fluorescent chitosan-coated PLGA NPs by hepatocytes (C3A) and fibroblasts (3T6) as well as the fate of internalized NPs were investigated by confocal microscopy. Chitosan-coating on the DXM loaded PLGA NPs permitted their uptake by cultured cells without inducing cytotoxicity (Chronopoulou *et al.*, 2013).

PLGA nanoparticles were modified with chitosan through physical adsorption and chemical binding methods in order to functionalize them for passive targeting and conjugation with targeting molecules. The surface charge of the nanoparticles changed from negative to positive after chitosan coating, making the drug carriers more affinity to cancer cells. Amine groups were presented on PLGA nanoparticle surface after the chitosan modification as confirmed by FTIR spectroscopy and X-ray photoelectron spectroscopy. It was found that the modified nanoparticles showed an initial burst release of drug followed by a moderate and sustained drug release profile (Wang *et al.*, 2013)

In a study a group of researchers compared mucoadhesion and cellular uptake efficiency of chitosan (CS) and chitosan oligosaccharide (COS) surface-modified polymer nanoparticles (NPs) for mucosal delivery of proteins. Surface-modified PLGA NPs were prepared by double emulsion solvent evaporation method loaded with bovine serum albumin and confirmed using physicochemical characterization methods such as particle size and zeta potential, FTIR analysis SEM, and TEM study. Both the surface modified PLGA NPs displayed a slow release of protein compared to PLGA NPs. Positively charged COS-PLGA NPs and CS-PLGA NPs exhibited enhanced mucoadhesion, compared to negatively charged PLGA NPs. All nanoformulations were found to be safe for cellular delivery when evaluated in A549 cells. Intracellular uptake behaviour of fluorescein isothiocyanate (FITC)-NPs was studied by confocal laser scanning microscopy and flow cytometry (Dyawanapelly *et al.*, 2016).

In a study Ludwig *et al.* prepared chitosan-coated PLGA nanoparticles containing AmB using single-emulsion solvent evaporation method and obtained nanoparticles that are spherical in shape with mean particle size of about 460 nm, positive zeta potential and 42% encapsulation efficiency. The nanoparticles were prepared to decrease the dose related toxicity. The antifungal efficacy of chitosan-coated PLGA nanoparticles containing AmB was determined in 20 strains of fungus isolates from patients suffering from varieties types of fungal infections such as bloodstream infections, urinary tract infection, vulvovaginal candidiasis etc. (Ludwig *et al.*, 2018).

The particle size analysis by dynamic light scattering gives a good indication on the actual size range and polydispersity of the self-assemblies (Laan and Denkova, 2017). Nanoparticles are used in many fields of research and technology and their proper characterization and analysis are important challenges in the present nanoscale metrology. Atomic force microscopy (AFM) is one of the most popular scanning probe microscopy methods among the methods available for surface characterization (Klapetek *et al.*, 2011). Individual particles as well as groups of particles can be resolved by the AFM, and unlike other microscopy techniques. Moreover, the AFM offers visualization and analysis in three dimensions (Rao *et al.*, 2007).

The size of the nanoparticles and their morphological state were measured by Field emission scanning electron microscope (FESEM). The external surface of nanoparticle samples can be measured by FESEM that provide the structural situation (Khanmohammadi *et al.*, 2015).

Transmission electron microscopy (TEM) is used for characterizing nanoparticles, it is an excellent tool since its resolution attains about 0.07 nm depending on thickness of the sample and accelerating voltage, but it is expensive and is operationally complex (Souza *et al.*, 2016).

Cryogenic transmission electron microscopy (cryo-TEM) for single particle analysis is a leading characterization method, which shows limited resolution due to poor alignment precision of noisy images captured under low electron exposure. The structural resolution of single particle reconstruction depends on particle size, shape, number, lamellarity and symmetry due to low signal-to-noise ratio (Hu *et al.*, 2008, Crawford *et al.* 2011). This method offers robust and powerful ways to visualize nanoparticles. This method involves imaging of the sample in a

frozen-hydrated state, allowing visualization of nanoparticles essentially as they exist in solution. Preparation of grid for cryo-TEM imaging can be performed with the sample in aqueous as well as in various organic and ionic solvents. Two-dimensional cryo-TEM provides a direct way to visualize the polydispersity within a nanoparticle preparation (Stewart, 2017). TEM, SEM or AFM are not appropriate techniques for determining the morphology of any soft-matter species. It is very important to know that TEM analysis is performed using the drying method where a drop of the sample is dried onto a grid by evaporation of the solvent from the sample, which can result in deformation or even complete destruction of the particles. In case of cryo-TEM, the sample is instantly vitrified i.e. rapidly frozen on the grid impairing any changes of the morphology of the particles (Laan and Denkova, 2017).

Increasing attention has been given to the potential of pulmonary route as an alternative for non-invasive delivery of therapeutic agents to the systemic circulation as well as local infection in lung. In a study by Liu and his coworkers, novel nebulizer-compatible solid lipid nanoparticles (SLNs) for pulmonary drug delivery of insulin were developed by reverse micelle-double emulsion method. The influences of the amount of sodium cholate (SC) and soybean phosphatidylcholine (SPC) on the deposition properties of the nanoparticles were also investigated. Under optimal environment, the entrapment delivery, respirable fraction (RF) and nebulization efficiency of SLNs were found to reach at 96.53, 82.11 and 63.28%, respectively. The SLN were found to remain stable during the process of nebulization. Fasting plasma glucose level was reduced to 39.41% and insulin level was increased to approximately 170 microIU/ml 4h after pulmonary administration of 20 IU/kg SLNs. Fluorescent SLNs were successfully and evenly distributed in the lung alveoli. Thus, it can be concluded from their study that SLNs could be used as a potential carrier for pulmonary delivery of insulin by improving both *in vitro* and *in vivo* stability as well as prolonging hypoglycemic effect, which resulted in improved bioavailability (Liu *et al.*, 2008).

In another study, nanoparticles were microencapsulated by spray drying using mannitol as carrier, resulting in a dry powder with aerodynamic properties suitable for lung delivery. Hybrid chitosan/hyaluronic acid nanoparticles were developed by ionotropic gelation and characterized for their physicochemical properties, being further studied by solid nuclear magnetic resonance. Confocal laser scanning microscopy (CLSM) and X-ray photoelectron

spectroscopy (XPS) in combination with time-of-flight secondary ion mass spectroscopy (TOF-SIMS) were conducted to investigate the nanoparticles distribution within the carrier matrix. In summary it was concluded that the developed delivery system holds great potential for lung delivery of macromolecules (Al-Qadi *et al.*, 2011).

A group of researchers illustrated a strategy to encapsulate itraconazole into CS -based nanoparticles using a modified ionic gelation method. Further, they fabricated them as inhalable microparticles using spray drying technique using different ratios of CS:TPP prepared at pH 1.2, using higher ratios of TPP with respect to CS. When the amount of TPP was increased up to 4 times higher than CS it resulted in the production of large particles. Below the ratio of 1:3, the particle sizes ranged from 190 to 240 nm. The prepared nanoparticles were characterized by TEM analysis for morphology. Microparticles were prepared with 2.5, 10 and 20% of lactose and mannitol with or without 10% of leucine, with respect to nanoparticle weights by co-spray drying of nanoparticles. *In vitro* inhalation parameters including fine particle fraction (FPF) and emitted dose percentage (ED%) were measured by a twin stage impinge. The *in vitro* deposition data indicated that processing of nanoparticles with mannitol and leucine could improve the aerosolization characteristics of the drug significantly (Jafarinejad *et al.*, 2012).

Biodistribution of amikacin solid lipid nanoparticles (SLNs) after pulmonary delivery was investigated to increase the drug concentration in the lungs for the treatment of cystic fibrosis lung infections and also providing a new method for clinical application of amikacin. Amikacin was labeled with ^{99m}Tc and was loaded in cholesterol SLNs. The radiolabelled SLNs and free drug were administered through pulmonary and *i.v.* routes to male rats for qualitative localization and quantitative biodistribution studies. Results showed that pulmonary delivery of SLNs of amikacin by microsyringe caused higher drug concentration in lungs than kidneys while *i.v.* administration of free drug caused the reverse conditions. Thus, it can be concluded that pulmonary delivery of SLNs may improve patients' compliance by reducing the side-effects of drug in kidneys and drug dosing intervals also increased due to the sustained drug release from SLNs (Varshosaz *et al.* 2013).

Mangal and coworkers have recently reviewed the challenges and opportunities of nanoparticle containing chemotherapeutic agents for pulmonary delivery for the treatment of lung cancers, since systemic chemotherapy has very limited efficacy as well as severe systemic

side-effects. Moreover, it attributed to the distribution of anticancer drugs to non-targeted sites. Inhalation routes permit the delivery of drugs directly to the lungs providing high local concentrations that may enhance the anti-tumor effect while reducing systemic side-effects. Promoting the deposition of anticancer drugs in tumorous cells and minimizing access to healthy lung cells further augmented the efficacy and reduced the risk of local toxicities caused by inhaled chemotherapy. Sustained release and tumor localization characteristics made nanoparticle formulations a promising candidate for the inhaled delivery of chemotherapeutic agents against lung cancers. However, the physiology of respiratory tracts and lung clearance mechanisms present key barriers for the effective deposition and retention of inhaled nanoparticle formulations in the lungs. Thus the development of novel formulations to maximize lung deposition and to minimize pulmonary clearance of inhaled nanoparticles is in the research arena (Mangal *et al.*, 2017).

There are so many methods are available for preparing nanoparticles with the polymers like PLGA, chitosan etc. Here multiple emulsion solvent evaporation method has been employed for preparing both non-coated and chitosan coated PLGA nanoparticles. The plan of this research was to develop mucoadhesive nanoparticles using a simple, unique technique. In this method, incorporation of chitosan coating was done simultaneously during the process of development of multiple emulsion and no additional step for coating was required. Furthermore, time of lyophilization was also same as it was required for non-coated formulation. Thus, this simple process of chitosan coating on nanoparticles could be highly beneficial for the industrial production point of view.

The present study aimed to prepare mucoadhesive nanoparticles containing voriconazole for pulmonary delivery in order to treat lung fungal infection and to overcome the deficiencies in this field of research. The particles were coated with the mucoadhesive polymer chitosan and rendered them mucoadhesiveness to increase the residence time in the lung when delivered by pulmonary route using dry powder inhaler. Moreover, the blood residence time also increased as measured from its *in vivo* pharmacokinetic study.

Chapter 3

Objectives and plan of work

3. Objectives

Effective delivery of drugs to the pulmonary site of infection has been a challenging task because of rapid removal of drug due to high blood flow turnover in the tissue. The existing conventional drug delivery systems have been inefficient in selectively attaining drug in therapeutic concentration in lungs. Although the fungal infection may reduce, but the spores remain dormant, and causes recurrence of fungal infection, if medicaments are not continued, which is also difficult because of the high toxicity of available all antifungal drugs for systemic use. In such context, the investigation of nano-encapsulated drug formulations has been intensified over the past few years. Voriconazole, the active substance of VFEND, is reported to possess excellent antifungal activity against a wide range of fungal infections such as *aspergillosis*, *candidiasis*, *coccidioidomycosis*, *histoplasmosis*, *penicilliosis*, and infections by *Scedosporium* or *Fusarium* etc.

In the present study, effort has been made to develop a mucoadhesive nanoparticles containing antifungal drug voriconazole with a special attention to lung as a delivery site by dry powder inhaler and nebulizer for drug action for a prolonged period of time. In this study mucoadhesive nanoparticles will be prepared by using different types of biodegradable polymers such as PLGA, chitosan etc. by the modified multiple emulsion solvent evaporation method. The experimental NPs is supposed to deliver the drug for a prolonged period to maintain the persistent local concentration of drug in lung, which is not possible by other routes of drug administration due to rapid blood turn over in lung. Here, we will investigate both qualitatively and quantitatively the potential of our developed formulation to deliver drug in the pulmonary site of infection as well as in plasma *in vivo*. Various critical formulation and process parameters will be optimized in order to keep the size of the final formulation within ≤ 500 nm along with the satisfactory physicochemical properties. The hypothesis of this work is that the experimental formulation carrying voriconazole will reach in therapeutic concentration and lead to sustained drug release in the infection site of lung and plasma as compared to the uncoated PLGA nanoparticles and free drug voriconazole. Thus, the overall aim is to develop an optimized method of preparation of chitosan coated mucoadhesive, biocompatible drug nanocarrier system with a reasonable drug payload for efficient treatment of recurrent lung fungal infection, with an improved blood residence time and better efficacy for the treatment of fungal infection in lung, which are still lacking in the presently available nanomedicine.

Plan of work:

- A. Preformulation study
 - i. FTIR study
 - ii. Analytical method development by UV-Vis spectrophotometer and High-performance liquid chromatography (HPLC)
 - iii. Preparation of Standard curve
- B. Development and optimization of nanoparticles formulation
 - i. Preparation of non-coated PLGA nanoparticles with or without voriconazole
 - ii. Preparation of CS-coated PLGA nanoparticles with or without voriconazole
 - iii. Preparation of FITC containing nanoparticles both coated and non-coated
- C. Physicochemical characterization
 - i. Determination of particle size and size distribution
 - ii. Determination of zeta potential or surface charge
 - iii. Determination of particle morphology
 - iv. Determination of drug loading and entrapment efficiency
- D. *In vitro* drug release and drug release kinetics study
- E. Determination of mass median aerodynamic diameter by eight stage Andersen Cascade Impactor
- F. *In vivo* deposition of nanoparticles in the lungs of mice using nose-only inhalation chamber and fabricated dry powder inhaler (DPI)
- G. Pharmacokinetic studies of chitosan coated PLGA nanoparticles, PLGA nanoparticles and free voriconazole
- H. Study on distribution of drug in different lung lobes by validated HPLC method
- I. Gamma scintigraphy study
- J. Biodistribution study

Chapter 4

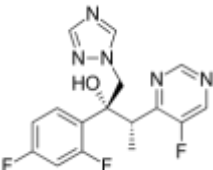
Materials and equipments

4. Materials and equipments

Table 4.1: List of Materials and chemicals used

Name of the chemical	Manufactured by (Company, city, Country)
0.45 µm syringe filter	Chromatography syringe filter, Cole-Parmer, Mumbai, India
Acetone	E. Merck (India) Ltd., Mumbai, Maharashtra, India
Acetonitrile for HPLC	Merck Life Sc. Pvt. Ltd., Mumbai, Maharashtra, India
Carbon coated Copper grid	300#, Ted Pella Inc., CA, USA
Chitosan	Himedia Lab. Pvt. Ltd., Mumbai, Maharashtra, India
Dichloromethane (DCM)	E. Merck (India) Ltd., Mumbai, Maharashtra, India.
Disodium hydrogen orthophosphate	Process Chemical Industries, Kolkata, W.B., India
Ethylenediaminetetraacetic acid (EDTA)	Himedia Lab. Pvt. Ltd., Mumbai, Maharashtra, India
Fluorescein 5-isothiocyanate (FITC)	Himedia Lab. Pvt. Ltd., Mumbai, Maharashtra, India
Fluconazole (FCZ) (gift sample)	Regional Drugs Testing Laboratory, Guwahati, India.
Formic acid	Merck Life Sc. Pvt. Ltd., Mumbai, Maharashtra, India
Hydrochloric acid	Merck Life Sc. Pvt. Ltd., Mumbai, Maharashtra, India
Lactose monohydrate	Himedia Lab. Pvt. Ltd., Mumbai, Maharashtra, India
Methanol for HPLC	Spectrochem Pvt. Ltd., Mumbai, Maharashtra, India
Milli-Q water	Millipore Corp., Billerica, MA, USA
Muscovite ruby mica sheet for AFM	ASTM V1 grade ruby mica, Micafab, Chennai, India
Poly-lactic-co-glycolic acid (MW 50,000-75,000; lactide to glycolide ratio 85:15)	Sigma-Aldrich Chemicals Pvt. Ltd., Bangalore, Karnataka, India.
Polyvinyl alcohol (PVA, MW 1,25,000)	S.D. fine-chem. Ltd., Mumbai, Maharashtra, India.
Potassium hydrogen phosphate	Process Chemical Industries, Kolkata, W.B., India
Sodium Chloride	Merck Life Sc. Pvt. Ltd., Mumbai, Maharashtra, India
Sodium hydroxide pellets	Merck Life Sc. Pvt. Ltd., Mumbai, Maharashtra, India
Voriconazole (VRZ) (gift sample)	Dr. Reddy's Laboratories Ltd., Hyderabad, India.
Water for HPLC	Merck Life Sc. Pvt. Ltd., Mumbai, Maharashtra, India

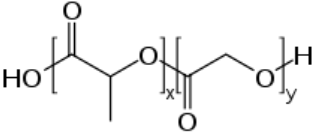
Drug Profile:**4.1.1 Voriconazole**

Brand Name	Vfend
Synonyms	<ul style="list-style-type: none"> • (2<i>R</i>,3<i>S</i>)-2-(2,4-difluorophenyl)-3-(5-fluoro-4-pyrimidinyl)-1-(1<i>H</i>-1,2,4-triazol-1-yl)-2-butanol • (R-(R*,s*))-alpha-(2,4-difluorophenyl)-5-fluoro-beta-methyl-alpha-(1<i>H</i>-1,2,4-triazol-1-ylmethyl)-4-pyrimidineethanol • Voriconazol • Voriconazolium • VCZ
Chemical Name	(2 <i>R</i> ,3 <i>S</i>)-2-(2,4-Difluorophenyl)-3-(5-fluoropyrimidin-4-yl)-1-(1 <i>H</i> -1,2,4-triazol-1-yl)butan-2-ol
Molecular Weight	349.317 g/mol
Empirical formula	C ₁₆ H ₁₄ F ₃ N ₅ O
Structural formula	 <p>The image shows the chemical structure of Voriconazole. It consists of a central chiral carbon atom bonded to a hydroxyl group (HO), a 1,2,4-triazole ring, a 5-fluoropyrimidin-4-yl ring, and a 2,4-difluorophenyl ring. The stereochemistry is indicated with a wedge bond to the hydroxyl group and a dashed bond to the 1,2,4-triazole ring.</p>
Physicochemical Profile	
Description	White to light-colored solid powder
Solubility	<p>Voriconazole has a low aqueous solubility (9.78e-02 g/L), its maximum solubility being in acidic conditions (2.7mg/ml at pH 1.2)</p> <p>Soluble in Acetone, Acetonitrile, Dimethyl sulfoxide, Methanol, Dichloromethane</p>
Melting Point	127-130 °C
Dissociation Constant	0.42 μM
Pharmaceutical Profile	
Ultraviolet spectrum	Absorption maxima 256 nm
Dosage form available	Vfend [oral suspension (200mg/5mL); Injection, powder for reconstitution (200mg); tablets(50mg, 200mg)]
Dosage and administration	6 mg/kg IV q12hr for first 24 hours, then 4 mg/kg IV q12hr or 200 mg PO q12hr
Side effects	Visual disturbances, fever, rash, vomiting, nausea, diarrhea, headache, sepsis, peripheral edema, abdominal pain, and respiratory disorder.
Pharmacokinetics	
Bioavailability	Oral bioavailability 96%
Elimination half life (hr)	Approx. 6 h
Volume of distribution (L)	2-4.6 L/kg

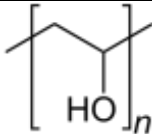
Protein Binding	58%
Metabolism	Hepatic cytochrome P450 (CYP) isoenzymes, CYP2C19, CYP2C9 and CYP3A4
Excretion	80% by urine
Storage	Room temperature

Excipients profile:

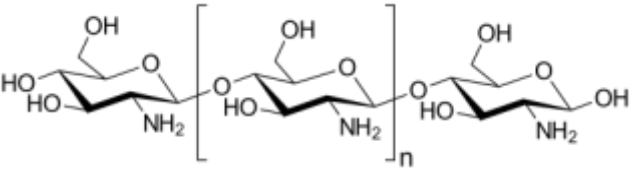
4.1.2 Poly(lactic-*co*-glycolic acid) (PLGA)

Chemical Name	Poly(lactic-<i>co</i>-glycolic acid)
Chemical formula	$[C_3H_4O_2]_x[C_2H_2O_2]_y$
CAS number	26780-50-7
Grade	lactide:glycolide 85:15
Structural formula	
Molecular weight	50,000-75,000
Physicochemical Profile	
Description	amorphous
Solubility	Soluble in tetrahydrofuran, acetone, ethyl acetate and chlorinated solvents like dichloromethane, chloroform etc
Melting Point	40-60 °C
Transition Temperature	45-50 °C
Viscosity	0.55-0.75 dL/g, 0.1 % (w/v) in chloroform(25 °C)
Storage	Store at 4-8°C
Safety	FDA approved, biodegradable, bio compatible and non-toxic
Functional category	Biodegradable polymer
Applications	Biocompatible devices such as sutures, tissue scaffolds, and drug delivery vehicles

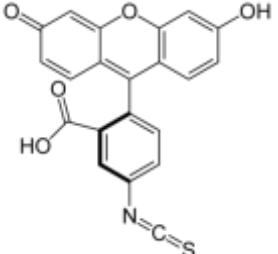
4.1.3 Polyvinyl alcohol (PVA)

Synonyms	PVOH; Poly(Ethenol), Ethenol, homopolymer; PVA; PVAI; Polyviol; Vinol; Alvyll; Alcotex; Covol; Gelvatol; Lemol; Mowiol; Mowiflex, Alcotex, Elvanol, Gelvatol, Lemol, Mowiol, Nelfilcon A, Polyviol und Rhodoviol
Trade name	PVOH Polymers; Gohsenol; Kuraray Poval; Mowiol; Selvol; Polyviol; Sinopac
Chemical name	VINYL ALCOHOL; Ethenol; POLYVINYL ALCOHOL; Hydroxyethene; Hydroxyethylene; Ethenol,
Chemical formula	$[\text{CH}_2\text{CH}(\text{OH})]_n$
Structural formula	
Molecular weight	85,000-124,000
Physicochemical Profile	
Solubility	Soluble in water
Melting point	230 °C and 180–190 °C for the fully hydrolyzed and partially hydrolyzed grades, respectively
Description	white (colorless) and odorless powder
Synthesis	<p>PVA instead is prepared by first polymerizing vinyl acetate, and the resulting polyvinyl acetate is converted to the PVA.</p> <p>The conversion of the polyesters is usually conducted by base-catalyzed trans-esterification with ethanol:</p> $[\text{CH}_2\text{CH}(\text{OAc})]_n + \text{C}_2\text{H}_5\text{OH} \rightarrow [\text{CH}_2\text{CH}(\text{OH})]_n + \text{C}_2\text{H}_5\text{OAc}$
Storage	To be kept in a tightly closed container and stored in a cool, dry, ventilated area
Safety	PVA is nontoxic. It biodegrades slowly, and solutions containing up to 5% PVA are nontoxic to fish
Functional category	Excellent film forming, emulsifying and adhesive
Applications	Emulsion polymerization aid; Injection moulding of soluble containers for active release of detergents and agrichemicals; Paper adhesive with boric acid in spiral tube winding and solid board production; Thickener, modifier, in polyvinyl acetate glues; Textile sizing agent; Paper coatings, release liner

4.1.4 Chitosan

Synonyms	Poliglusam; Deacetylchitin; Poly-(D)glucosamine; BC; Chitopearl; Chitopharm; Flonac; Kytex
Chemical name	Chitosan; Poliglusam; Deacetylchitin; Chicol; Flonac C; Flonac N
Chemical formula	$C_{56}H_{103}N_9O_{39}$
Structural formula	
Molecular weight	1526.464 g/mol
Physicochemical Profile	
Solubility	Insoluble in water and organic solvent, soluble in dilute aqueous acidic solution (pH<6.5) using <i>formic</i> , <i>acetic</i> and <i>propionic</i> acids
Synthesis	Chitosan is produced commercially by deacetylation of chitin, which is the structural element in the exoskeleton of crustaceans (such as crabs and shrimp) and cell walls of fungi
Safety	chitosan has low oral toxicity and local tolerance potential supporting use in non-parenteral formulations
Functional category	Polymer
Applications	Development of hydrogel, nanomaterials, bioadhesives, and edible coatings.

4.1.5 Fluorescein isothiocyanate (FITC)

Synonyms	FITC
Chemical name	Fluorescein isothiocyanate
Chemical formula	$C_{21}H_{11}NO_5S$
Structural formula	
Molecular weight	389.382 g/mol
Physicochemical Profile	
Solubility	Ethanol
Melting point	359.5 °C
Description	FITC has excitation and emission spectrum peak wavelengths of

	approximately 495 nm/519 nm, ^[1] giving it a green color.
Stability and storage	The FITC is light-sensitive, and should be stored dry and in the dark at 2 °C to 8 °C
Functional category	Fluorochromes
Applications	Flow cytometry.

4.1.6 Lactose mono hydrate

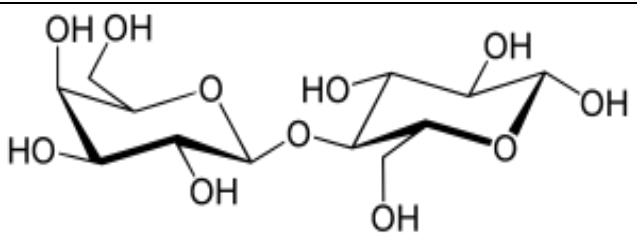
Synonyms	Milk sugar; 4- <i>O</i> -β-D-galactopyranosyl-D-glucose
Chemical name	β-D-galactopyranosyl-(1→4)-D-glucose
Chemical formula	C ₁₂ H ₂₂ O ₁₁
Structural formula	
Molecular weight	342.30 g/mol
Physicochemical Profile	
Solubility	Soluble in water (19.5 g/100 mL)
Melting point	202.8 °C
Description	White to yellowish, finely crystallized powder
Synthesis	Lactose is a disaccharide derived from the condensation of galactose and glucose, which form a β-1→4 glycosidic linkage
Storage	Stored at 15-25 °C
Functional category	Filler
Applications	Filler-binder or diluent in tablets and capsules

Table 4.2: List of Instruments, equipments and devices used

Name of the instrument	Manufacturer (Model no., Company, City, Country)
Atomic force Microscopy (AFM)	Dimension Icon, Bruker, Karlsruhe, Germany
Bath Sonicator	TRANS-O-SONIC, Mumbai, India
Cold centrifuge	Sigma Lab Centrifuge 3K30, Merrington Hall Farm, Shrewsbury, UK
Confocal laser scanning microscope (CLSM)	CLSM 510; Carl Zeiss, Jena, Germany
Cryo TEM	Tecnai G2 Polara, D357 Twin, FEI Company, Eindhoven, Netherland
Differential Scanning Calorimetry	Differential scanning calorimeter, Jade DSC, Perkin Elmer, Japan
Distillation apparatus	Sicco, Kolkata, India
Eight-stage non-viable Andersen Cascade Impactor	Model 20-800, Thermo Fischer Scientific, Waltham, Massachusetts, USA
FESEM	JEOL JSM-7600F, Tokyo, Japan
Freeze dryer	Laboratory Freeze Dryer, Instrumentation India, Kolkata, India
FTIR Spectroscopy	Alpha E, Bruker Alpha, Ettlingen, Germany
Gamma scintillation counter	Electronic Corporation of India, Model LV4755, Hyderabad, India
High Speed Homogenizer	IKA Laboratory Equipment, Model T10B, Ultra- Turrax, Staufen, Germany
HPLC column	Agilent C18 column (4.6 mm × 250 mm, 5 μm) (Thermo Scientific™ Hypersil GOLD™, Waltham, MA, USA
Incubator shaker	Shaking incubator, KMC 8480SL, vision scientific co., Yuseong-Gu, Daejeon-Si, Korea
Magnetic Stirrer	Remi Equipments, Mumbai, India
Particle size analyzer/ Malvern Zetasizer	Malvern Zetasizer, Nano-ZS 90, Malvern Instruments, Malvern, UK
pH meter	Mettler Toledo, GmbL, Switzerland

Refrigerated centrifuge	Z 32 HK, Hermle refrigerated centrifuge, Wehingen, Deutschland
Rotary vacuum evaporator	Superfit, Rotavac, model- PBU-6, Mumbai, India
RP-HPLC system	Dionex Ultimate 3000 RP-HPLC system (Dionex, Idstein, Germany)
TEM	JEM 2100; JEOL, Tokyo, Japan
Ultra-freezer	So-Low, Environmental Equipment, Ohio, USA
UV-VIS Spectrophotometer	Advanced Microprocessor UV-VIS Single Beam, Intech-295, AP, India
Weighing balance	Sartorius, GD103 and GE8121, Gottingen, Germany

Table 4.3: Animals used in the study

Animals	Source
Swiss Albino mice	M/s. Chakraborty Enterprise, 3/1D, Girish Vidyaratna Lane, Narikeldanga, Kolkata-700 011, West Bengal 1443/PO/Bt/S/11/CPCSEA
	Saha Enterprise, 386/2, Nilachal Birati, Kolkata – 700 051, West Bengal 1828/Po/Bt/S/15/CPCSEA
Sprague–Dawley Rats	Indian Institute of Chemical Biology, 4, Raja S.C. Mullick Road, Jadavpur, Calcutta - 700 032, West Bengal 147/GO/ReBi/S/99/CPCSEA

Table 4.4: Softwares used in the study

Softwares used	Source
GraphPad Prism™ (version 5.0) software	California, USA
Kinetica software version 5.0	Thermo Scientific, Waltham, MA USA
ImageJ	Maryland, USA,
WinNonlin Pro	Pharsight Corp, Mountain View, CA

Chapter 5

Methodology

5. Methodology

5.1 Determination of absorption maxima (λ_{\max}) of Voriconazole

Absorption maxima of voriconazole were measured in three different media, such as phosphate buffer saline (PBS), pH 7.4; simulated lung fluid (SLF), pH 7.4; and in a mixture of acetonitrile: water (1:1). Briefly, 10 mg of drug was accurately weighed on a digital balance (Sartorius, Göttingen, Germany) and dissolved in 10 ml PBS in a volumetric flask to produce a 1000 $\mu\text{g/ml}$ solution. This solution was diluted 100 times with the same media to produce of 10 $\mu\text{g/ml}$ solution concentration. This drug solution was scanned in the wavelength from 200 nm to 400 nm using PBS as blank solvent. The same process was repeated using a mixture of acetonitrile: water (1:1) and SLF as solvents. PBS and SLF was used as medium for drug release study and acetonitrile-water mixture was taken as medium for drug loading study.

5.2 Development of calibration curve for Voriconazole in acetonitrile: water mixture (1:1)

Accurately 10 mg of drug was weighed using a digital balance and taken in a volumetric flask of 10 ml capacity. The previously prepared mixture of acetonitrile and water in the ratio of 1:1 was added into the volumetric flask up to 10 ml mark. The flask was shaken well for proper dissolution of drug. This solution was 100 times diluted with the same media to prepare stock solution of Voriconazole having concentration of 10 $\mu\text{g/ml}$. From the stock solution of drug 5 solutions of different concentrations were prepared. Absorbance of the above solutions was determined against acetonitrile:water (1:1) as blank at a wavelength of 255 nm.

5.3 Development of calibration curve for Voriconazole in PBS and SLF

About 10 mg of drug was accurately weighed using a digital balance and taken in a volumetric flask of 10 ml capacity. The previously prepared PBS, pH 7.4 (Martin *et al.*, 2006) or SLF, pH 7.4 (Marques *et al.*, 2011) was added into the volumetric flask up to 10 ml mark. The flask was shaken well for proper dissolution of drug. This solution was 100 times diluted with the same media to prepare stock solution of voriconazole having concentration of 10 $\mu\text{g/ml}$ in respective media. From the stock solution of drug 5 solutions of different concentrations were prepared. Absorbance of the above solutions was determined against PBS or SLF as blank at a wavelength of 255 nm.

5.4 Fourier transform infrared (FTIR) spectroscopy

In FTIR spectroscopic study, voriconazole and all the individual excipients such as PLGA, PVA, chitosan and their physical mixtures, and lyophilized formulations were scanned in an inert atmosphere over a wave number range of 4000-400 cm^{-1} in FTIR spectrophotometer (Alpha E, Bruker Alpha, Ettlingen, Germany).

5.5 Preparation of non-coated PLGA nanoparticles containing voriconazole

Multiple emulsion solvent evaporation technique was employed for the preparation of both non-coated PLGA nanoparticles (**Figure 5.1**) and chitosan-coated PLGA nanoparticles (**Figure 5.2**), with some modifications (Pattnaik *et al.*, 2012). Briefly, non-coated nanoparticles were prepared by solubilizing approximately 250 mg of PLGA in 4 mL of organic phase containing DCM and acetone (4:1, w/w ratio). Aqueous PVA solutions, 1.5% (w/v) and 2.5% (w/v), were prepared previously.

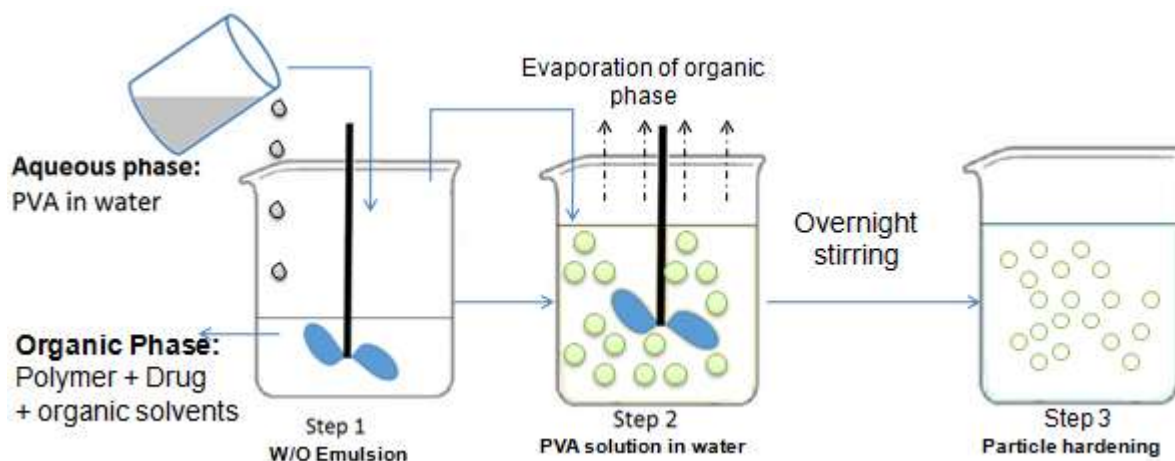


Figure 5.1: Preparation of PLGA nanoparticles by multiple emulsion solvent evaporation method

The organic polymeric solution containing voriconazole was emulsified quickly with drop-wise gradual addition of 1.5 mL of 2.5% PVA solution, and continuous homogenization for 4 min using a high speed homogenizer at 20,000 rpm (IKA Laboratory Equipment, Model T10B, Ultra-Turrax, Staufen, Germany). The water-in-oil emulsion (primary emulsion) was quickly added to 75 mL of 1.5% PVA solution and homogenized for about 8 min at 20,000 rpm to get secondary emulsion. The emulsion thus obtained was kept in a bath-sonicator for 10 to 15 min to

break the large globules and then stirred on a magnetic stirrer overnight without heating for complete removal of organic solvents used to dissolve the polymer. The organic phase was allowed to diffuse out and evaporated to get homogenous nanoparticles. While nanoparticles were hardening, the particles suspension was kept on a bath sonicator (Trans-O-sonic, Mumbai, India) for about 45 min to break the agglomerates, if any. Then the particles were separated by centrifugation at 3000 rpm and 16000 rpm in a refrigerated centrifuge (Hermle refrigerated centrifuge, Wehingen, Deutschland) and washed twice with double distilled water to remove the excess of PVA and kept in petridish in an ultra-freezer (So-Low, Environmental Equipment, Ohio, USA). After that, the frozen sample was lyophilized in a freeze dryer (Laboratory Freeze Dryer, Instrumentation India, Kolkata, India).

5.6 Preparation of chitosan-coated PLGA nanoparticles containing voriconazole

Chitosan-coated PLGA nanoparticles of voriconazole was prepared using the above-mentioned method with the modification in the following steps. Required amount of chitosan (**Table 5.1**) was dissolved in 1.5% (w/v) PVA solution with pH adjusted at 3.0 using 0.1M HCl solution. The primary emulsion was homogenized in 75 mL of the chitosan in 1.5% PVA solution for 8 min to get multiple emulsion followed by adjustment of pH from 3.0 to 9.0 by addition of NaOH solution. The various composition of the nanoparticle batches are also mentioned in **Table 5.1**.

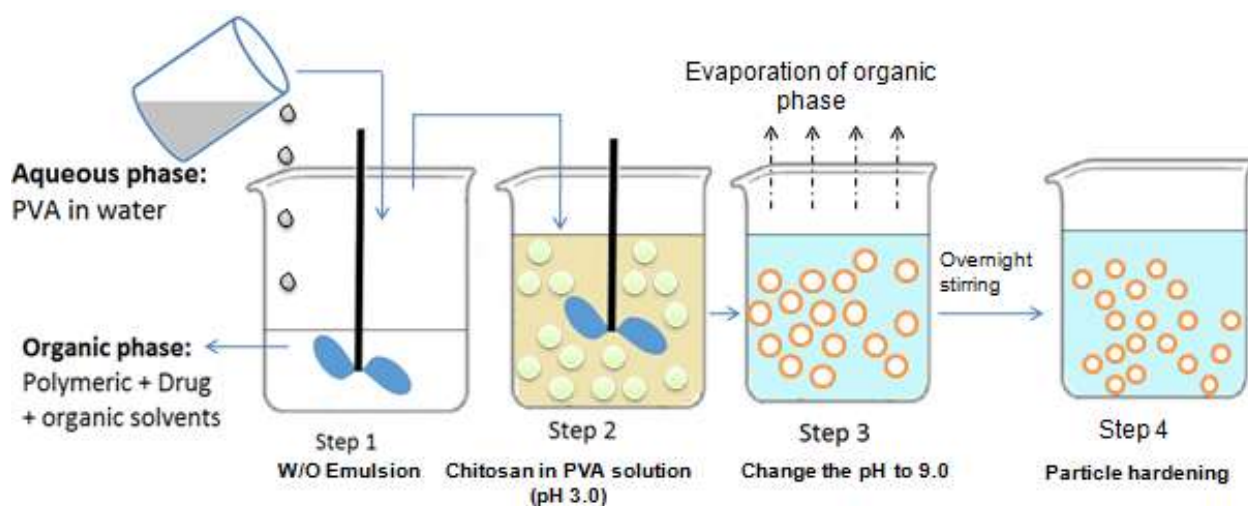


Figure 5.2: Preparation of chitosan coated PLGA nanoparticles by multiple emulsion solvent evaporation method

Table 5.1: Formulation composition and process parameters for preparation of optimized formulations

Code	Drug: PLGA: Chitosan (mg:mg:mg)	Homogenization speed (RPM)	Stabilizer [#]	Sonication time (min)
P-Blank	0: 100: 0	20000	PVA*	10
PC-Blank	0: 100: 80	20000	PVA	10
P1	100: 108: 0	16000	PVA	10
P2	101:108: 80	16000	PVA	10
P3	100: 107: 40	16000	PVA	10
P4	100: 105: 20	16000	PVA	10
P5	250: 254: 0	20000	PVA	15
P6	250: 257: 100	20000	PVA	15
P7	250: 254: 0	25000	PVA	10
P5-FITC	250: 254: 0	20000	PVA	15
P6-FITC	250: 257: 100	20000	PVA	15

*PVA, polyvinyl alcohol; [#]Stabilizer: 2.5% and 1.5% aqueous PVA solution

5.7 Preparation of FITC containing nanoparticles

The FITC containing non-coated and chitosan-coated nanoparticles were prepared using the same processes described above except the incorporation of 100 μ L of FITC solution into the organic phase containing polymer and drug before homogenization. FITC solution (0.4% w/v) was prepared in absolute alcohol.

5.8 Drug loading (%) and entrapment efficiency (%)

For the determination of %drug loading, 2 mg of lyophilized NPs (accurately weighed) was solubilized in 2 mL of acetonitrile and water (50:50 v/v). The formed solution was kept for maximum 4 h in an incubator shaker (Somax Incubator Shaker; Shenjhen Pango Electronic Co. Ltd., Shenzhen, China) and then centrifuged at 16,000 rpm for 15 min in a refrigerated centrifuge and the supernatant was suitably diluted with the same solvent mixture and analyzed spectrophotometrically at the corresponding λ_{\max} of 255 nm using nanoparticles (without drug) in the same solvent mixture as blank (Sinha *et al.*, 2013).

Drug loading was determined as follows (Maji *et al.*, 2014; Seju *et al.*, 2011):

$$\text{Drug loading (actual) (\%)} = \frac{\text{Amount of drug in nanoparticles}}{\text{Amount of nanoparticles obtained}} \times 100$$

Drug entrapment efficiency was calculated as follows (Das *et al.*, 2015; Ochiuz *et al.*, 2016):

$$\text{Drug entrapment efficiency (\%)} = \frac{\text{Drug loading (actual) (\%)}}{\text{Drug loading (theoretical) (\%)}} \times 100$$

5.9 Characterization of nanoparticles

5.9.1 Particle size distribution and zeta potential

The average particle size and zeta potential values of all the experimental formulations were measured using Malvern Zetasizer Nano-ZS 90 (Malvern Instruments, Malvern, UK) utilizing dynamic light scattering technique (Satapathy *et al.*, 2016). A weighed quantity of the experimental sample was dispersed in Milli-Q water (Millipore Corp., Billerica, MA, USA) followed by sonicating and vortexing before placing it in the cuvette for particle size and zeta potential measurement (Das *et al.*, 2015; Maji *et al.*, 2014).

5.9.2 Field emission scanning electron microscope (FESEM)

Particle morphology was assessed by FESEM (JEOL JSM-7600F, Tokyo, Japan). The lyophilized particles were placed on a carbon tabs mounted on SEM specimen stubs. The specimen stubs were coated with gold of 4 nm thickness by ion sputtering device (Au5 Quorum, Q150TES) and was operated at 15-20 kV accelerating voltage.

5.9.3 Cryogenic-transmission electron microscopy (Cryo-TEM)

Carbon coated copper grid (300#) (Ted Pella Inc., USA) was glow-discharged (Pelco easiglow, Ted Pella Inc., CA, USA) for 30 s to remove dust particles or contamination if any (Shaw *et al.*, 2017; Helvig *et al.*, 2015). Chitosan-coated PLGA nanoparticles and non-coated PLGA nanoparticles were dispersed in doubled distilled water and the dispersion was spread on glow-discharged grid and plunge-frozen in liquid ethane using Vitrobot (Vitrobot Mark IV, FEI, Eindhoven, Netherlands). Grids were transferred to a cryoholder containing liquid ethane in

liquid nitrogen and the samples on the grids were visualized in Tecnai G2 Polara (D357 Twin, FEI Company, Eindhoven, Netherland) equipped with 300 kV field emission gun (FEG). Images were collected at 82600 \times magnification with an underfocus of 4.5 μm . Images were captured on a BM-Eagle 4 k \times 4 k charged coupled device camera (FEI Company, Eindhoven, Netherlands) unbinned with a final pixel size of 1.89 \AA .

5.9.4 Transmission electron microscopy (TEM)

For TEM measurements, 10 μL of lyophilized nanoparticles in water were carefully placed on a 300-mesh carbon-coated copper TEM grid (Ted Pella Inc., Redding, CA, USA). The excess solution on the grid was removed using a piece of fine-filter paper, and the samples were allowed to air-dry for 10 h prior to imaging the particles under TEM (JEM 2100; JEOL, Tokyo, Japan) (Roy *et al.*, 2014).

5.9.5 Atomic force microscopy (AFM)

The samples were dispersed in Milli-Q water using brief vortexing and sonication. One drop of sample was placed in a glass slide and dried in a vacuum dryer. The morphology and particle size were analyzed by AFM (Dimension Icon, Bruker, Karlsruhe, Germany) under ambient conditions by mode PeakForce QNM (Quantitative NanoMechanical mapping) using silicon nitride probe having a resonance frequency 150-350 kHz and a force constant 0.4 N/m.

5.10 *In vitro* drug release and drug release kinetics study

In vitro drug release study was carried out in PBS, pH 7.4 (Parikh and Dalwadi, 2014; Zhang *et al.*, 2016) and in SLF, pH 7.4, respectively, (Das *et al.*, 2015; Parikh and Dalwadi, 2014) for 8 days. The studies were performed with non-coated and chitosan-coated nanoparticles. Briefly, nanoparticles were weighed (triplicate for each type of formulation) accurately 2 mg and taken in 2 mL microcentrifuge tube. Drug release media (2 mL) was added in each tube and shaken briefly and the time was considered as zero. The tubes were kept in an incubator shaker at 37 $^{\circ}\text{C}$ with shaking (20 rpm). Samples were taken at predetermined time points and centrifuged at 16000 rpm for 10 min. The supernatant (2 mL) was withdrawn and 2 mL fresh media was added and the tubes were kept in shaker incubator for next time point (Das *et al.* 2015; Maji *et al.*, 2014). The supernatant was analysed by UV-Vis spectroscopy with proper dilution (if required), at 255 nm. The drug release data were plotted as cumulative

percentage of drug released against time (h) for both non-coated and coated PLGA nanoparticles (Ochiuz *et al.*, 2016).

In order to predict and correlate the behavior of the *in vitro* voriconazole release from both the non-coated and coated nanoparticles studied, suitable mathematical models were used. Thus, the experimental data obtained from *in vitro* drug release experiments of voriconazole-loaded non-coated and chitosan-coated nanoparticles were investigated using five conventional models: zero-order, first-order, Higuchi, Hixson–Crowell and Korsmeyer-Peppas models (Pattnaik *et al.*, 2012; Dash *et al.*, 2010).

5.11 Determination of mass median aerodynamic diameter (MMAD) and geometric standard deviation (GSD) using an eight-stage non-viable Anderson cascade impactor

The cascade impactor device is designed as a replacement for the human respiratory tract to collect and separate particulate matter according to its aerodynamic size, shape, density and all other physical properties (**Figure 5.3**).

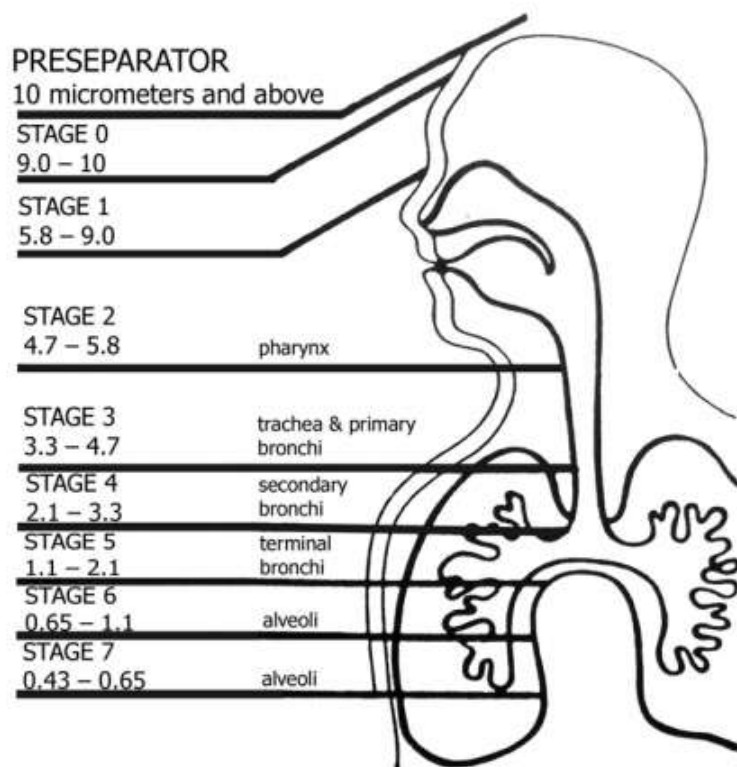


Figure 5.3: Result from Cascade Impactor apparatus simulates the human respiratory system (<https://tisch-env.com/wp-content/uploads/2015/06/TE-20-800-Non-viable-Cascade-Impactor.pdf>)

MMAD is defined as the average diameter under which 50% of the particles remain. This study was performed to determine MMAD and GSD. Weighed amount of nanoparticle was blended with micronized lactose (1:3 w/w) ratio and introduced into an eight-stage non-viable Anderson cascade impactor (Model 20-800, Thermo Fischer Scientific, Waltham, Massachusetts, USA). After that, the plates were accumulated and weighed. MMAD and GSD were calculated from the deposited particles using the MMAD calculator for Anderson apparatus at a flow rate of 28.3 L/min (Sinha *et al.*, 2013).

5.12 *In vivo* deposition of nanoparticles in the lungs of mice using nose-only inhalation chamber and fabricated dry powder inhaler (DPI)

The experimental animals were divided into two groups for three time points study (1 h, 8 h and 24 h) and each group had three animals. FITC loaded nanoparticles of each type were weighed (50 mg) and mixed with 150 mg of microfine lactose. The powder blend was placed inside the fluidization chamber and dosed in the nose-only inhalation chamber all at once. After the completion of dosing, the animals were sacrificed at the pre-designated time points (1 h, 8 h and 24 h) and lungs were removed, washed, and fixed with formalin solution, and embedded in paraffin blocks by the conventional method (Sinha *et al.*, 2013). The tissue sections were observed under a confocal laser scanning microscope (CLSM) (LSM 510; Carl Zeiss, Jena, Germany) at an excitation wavelength of 494 nm and emission wavelength of 521 nm to observe the distribution of FITC tagged nanoparticles and images were captured at suitable magnification. The images were finally analysed and total fluorescence intensity of each lung tissue was determined (integrated density, ID) using ImageJ software (Rasband WS, ImageJ, U. S. National Institutes of Health, Bethesda, Maryland, USA, <http://imagej.nih.gov/ij/>, 1997–2015). The background was obtained by measuring the fluorescence intensity of the regions out of the tissues. The corrected total cell fluorescence (CTCF) was then determined by subtracting the background from the integrated density ($CTCF = ID - (\text{Area of selected cell} \times \text{Mean fluorescence of background readings})$) (Stefančíková *et al.*, 2014).

5.13 High performance liquid chromatography (HPLC)

The concentration of voriconazole in blood at different time points after the pulmonary administration was measured by Dionex Ultimate 3000 RP-HPLC system (Dionex, Idstein, Germany), equipped with an Agilent C18 column (4.6 mm × 250 mm, 5 μm) (Thermo Scientific™ Hypersil GOLD™, Waltham, MA, USA). The injection volume was 20 μL. The mobile phase for the chromatographic separation composed of acetonitrile–water–formic acid (60:40:0.05) (v/v/v) was filtered before using it isocratically at room temperature at a flow rate of 1 mL/min, and voriconazole was detected by UV detector at 254 nm (Das *et al.*, 2015).

For calibration curve, pooled plasma was thawed at room temperature, plasma (90 μL), internal standard solution (fluconazole) (10 μL), calibrator solution (10 μL) and acetonitrile (890 μL) were pipetted into respective microcentrifuge tubes and capped. The tubes were vortexed for 20 minutes and the centrifuged for 10 min at 10,000 rpm. The supernatant was filtered through 0.45 μm syringe filter (chromatography syringe filter, Cole-Parmer, Mumbai, India) and transferred to a microcentrifuge tube. The samples (20 μL in each case) were injected into the system. Peak height measurements were analyzed to obtain the ratio of voriconazole versus fluconazole (internal standard). The ratios of voriconazole versus fluconazole were used to establish a calibration curve and to quantify voriconazole from the calibration curve. Test samples or controls were prepared by transferring 90 μL of test or control plasma into a respective microcentrifuge tubes, 10 μL of internal standard solution was then added to each tube followed by 900 μL of acetonitrile. The tubes were capped and processed in the same manner as calibrators.

The different lung lobes were thawed and the lung tissues were homogenized separately with the addition of normal saline (1:4, tissue:normal saline) for 2 min. To the lung homogenate (90 μL), 400 μL of acetonitrile was added, followed by vortexing for 20 min. Internal standard fluconazole 10 μL (2500 μg/mL) was then mixed with it. The samples were then centrifuged in a cold centrifuge at 4°C at 10000 rpm for 10 min. The supernatant was then filtered through 0.45 μm syringe filter and the filtrate was injected (20 μL) into the column. The drug content was calculated from the calibration curve developed in the same way within the concentration range 0.1562 to 10.00 μg/mL.

5.14 Pharmacokinetics and lung lobe distribution study

All the animal studies were approved by Institutional Animal Ethics Committee (IAEC), Jadavpur University. The studies were performed in male Swiss albino mice weighing about 20–25 g. The mice were fasted overnight before experimentation and were accessed to water ad libitum.

Free drug voriconazole, coated and non-coated PLGA nanoparticles (50 mg) mixed with microfine lactose monohydrate (150 mg) were administered to mice through the pulmonary route using nose-only inhalation chamber and dry powder inhaler (Sinha and Mukherjee, 2012). After complete dosing (taken as zero time), blood samples and lungs were collected at 1, 3, 6, 24, 48 h post inhalation. Lung lobes were collected separately and marked as left lobe, cranial lobe, middle lobe, accessory lobe, and caudal lobe and were stored at -80°C until further use.

At each time point, blood (~1 ml) from three mice from each group was collected *via* terminal cardiac puncture following deep anesthesia using chloroform. Ethylenediaminetetraacetic acid (EDTA) (2 mg) was added to each tube, as an anticoagulant. The blood sample was mixed with EDTA and centrifuged at 5000 rpm for 5 min at 4°C for separation of plasma. Plasma sample was stored at -20°C until analyzed.

The voriconazole plasma concentration–time data were analyzed by standard non-compartmental methods using the program WinNonlin Pro (Pharsight Corp, Mountain View, CA) (Reddy and Murthy, 2004; Ma *et al.*, 2012; Kan *et al.*, 2014; Kudgus *et al.*, 2014).

5.15 Gamma scintigraphy

Gamma imaging was performed for mice after administering Technetium-99m (Tc-99m) labeled PLGA nanoparticles containing voriconazole formulation (Tc-99m-P5) and chitosan coated PLGA nanoparticles containing voriconazole (Tc-99m-P6). They had 200 microcurie of radioactivity and administered through pulmonary route. The animals were anesthetized by ketamine hydrochloride prior to imaging. Mice were fixed on a wooden board and imaging was performed on a planar gamma camera (GE Infinia Gamma Camera equipped with Xeleris Workstation, GE, Cleveland, OH, USA) at 3 h and 6 h after administration.

5.16 Biodistribution study

The biodistribution of the radiolabeled nanoparticles was investigated in male Sprague Dawley rats weighing between 250-300 g. Tc-99m-P5 and Tc-99m-P6 were administered as previously for gamma scintigraphy. Rats were sacrificed at 3 and 6 h post-injection, the organs and tissues (heart, lung, liver, kidneys, spleen, stomach, intestine, muscle *etc.*) were collected and then weighed after washing them with normal saline and drying briefly by blotting paper (wherever applicable), and the corresponding radioactivity was measured using well-type γ -scintillation counter along with an injection standard. The results were expressed as percent injected dose/g of tissue/ organ (%ID).

Chapter 6

Results

6. Results

6.1 Determination of absorption maxima (λ_{\max}) of Voriconazole

The absorption maxima for voriconazole was found to be 255.0 nm in all media such as acetonitrile-water mixture, PBS or SLF (**Figure 6.1**). Thus, this value was selected for further analysis.

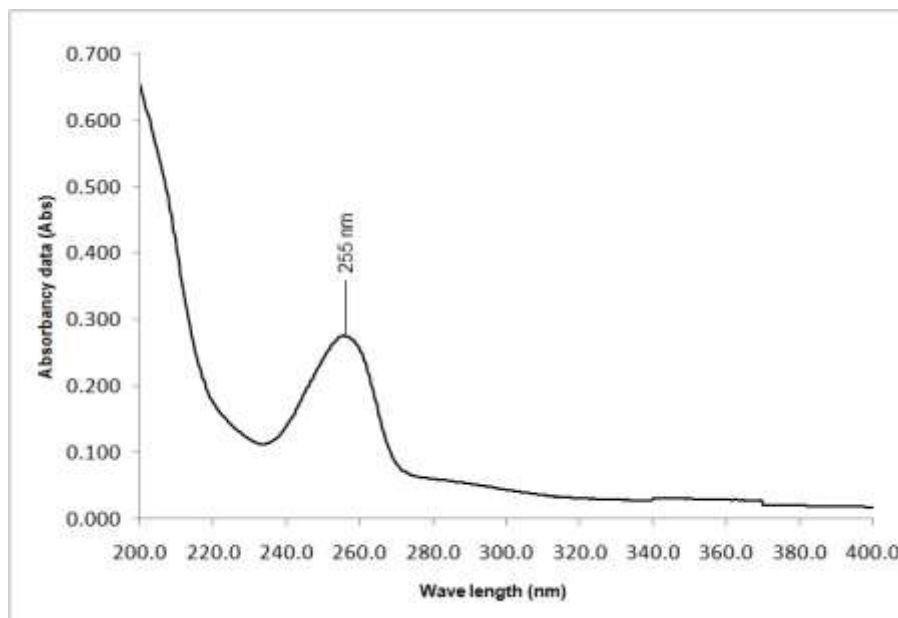


Figure 6.1: Absorption maxima of voriconazole in acetonitrile water mixture (1:1) showing λ_{\max} at 255.0 nm

The absorbance and standard deviation of voriconazole in acetonitrile water mixture (1:1) are given in **Table 6.1**. From the plot of Absorbance on Y-axis vs. concentration on X-axis (**Figure 6.2**), the correlation coefficient (R^2) value was found to be 0.998.

Table 6.1: Result of linearity data of Voriconazole in acetonitrile water mixture (1:1)

Concentration ($\mu\text{g/ml}$)	Absorbance ($n=3$)	
	Absorbance	Standard deviation (SD)
0	0	0
2	0.047	0.002
5	0.127	0.018
10	0.242	0.040
15	0.337	0.002
20	0.449	0.016
25	0.559	0.020
30	0.674	0.027
40	0.890	0.019

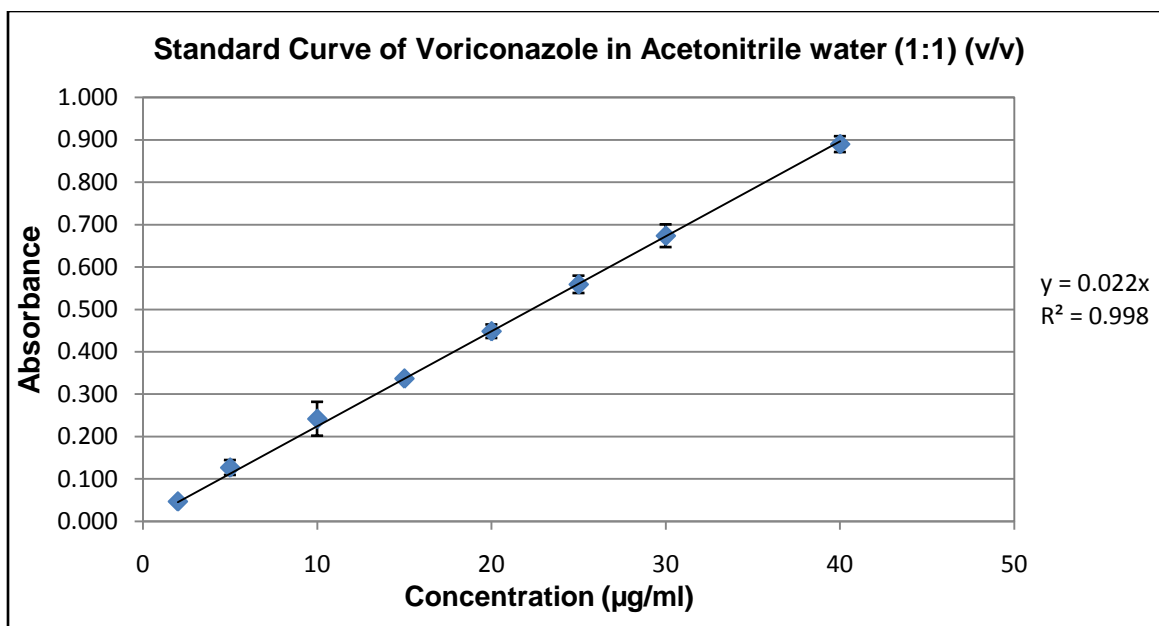


Figure 6.2: Calibration curve of Voriconazole in acetonitrile:water mixture (1:1) showing R^2 value

The absorbance values and standard deviation of voriconazole in SLF are given in **Table 6.2**. From the plot of Absorbance on Y-axis vs. concentration on X-axis (**Figure 6.3**), the correlation coefficient (R^2) value was found to be 0.995

Table 6.2: Result of linearity data of Voriconazole in simulated lung fluid (SLF)

Concentration (µg/ml)	Absorbance ($n=3$)	
	Absorbance	Standard deviation (SD)
0	0	0
2	0.056	0.005
4	0.1	0.004
6	0.165	0.001
8	0.219	0.004
10	0.233	0.009
15	0.337	0.006
20	0.474	0.004
25	0.597	0.012

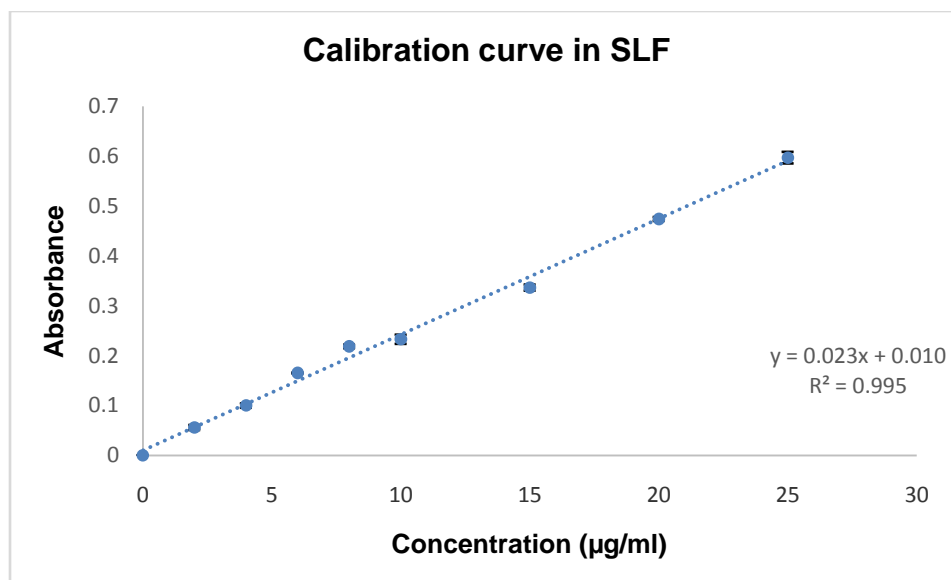


Figure 6.3: Calibration curve of Voriconazole in simulated lung fluid, pH 7.4 (SLF)

The absorbance values and standard deviation of voriconazole in PBS are given in **Table 6.3**. From the plot of absorbance on Y-axis vs. concentration on X-axis (**Figure 6.4**), the correlation coefficient (R^2) value was found to be 0.998.

Table 6.3: Result of linearity data of Voriconazole in phosphate buffer saline (PBS)

Concentration (µg/ml)	Absorbance (n=3)	
	Absorbance	Standard deviation (SD)
0	0	0
1	0.042	0.002
2	0.055	0.001
4	0.112	0.001
6	0.144	0.002
10	0.248	0.001
15	0.358	0.001
20	0.456	0.002
25	0.596	0.002
30	0.720	0.001

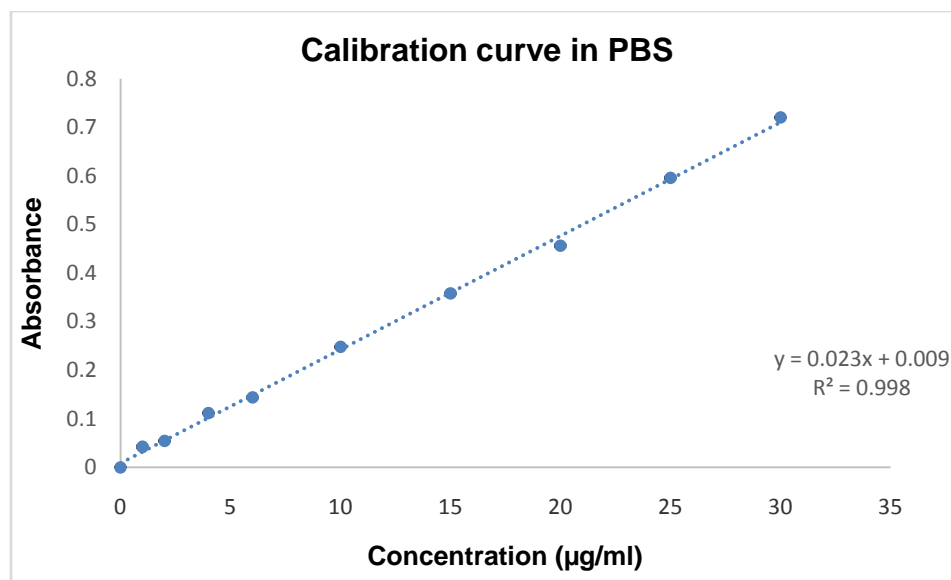


Figure 6.4: Calibration curve of Voriconazole in phosphate buffer saline, pH 7.4 (PBS)

6.2 Preformulation study

6.2.1 Investigation of drug-excipients interaction

Figure 6.5 shows the FTIR spectra of voriconazole, each of the excipients, mixture of voriconazole with PLGA, PVA and/or chitosan and a mixture of the polymers, respectively. The FTIR spectra of pure voriconazole, mixture of drug with the polymers and the lyophilized formulations with or without drug show that the characteristic peaks (C-N, C-F, and C-C stretching bands at 3190.86–3117.54, 1498.31–1452.41, and 1586.96–1452.41 cm^{-1} , respectively) of the drug were present (Das *et al.*, 2015; Kumirska *et al.*, 2010).

The shifting of the following peaks of chitosan while in the physical mixture with the drug and the polymers from 652 to 657 cm^{-1} and 605 to 606 cm^{-1} might be due to medium intensity stretching of C-H and C-H bending and ring puckering, C-H deformation and O-H bending (out of plane), respectively, from 1697 to 1693 cm^{-1} for C=O stretching and from 1082 to 1086 cm^{-1} for C-N medium intensity stretching and C-O stretching (Shaw *et al.*, 2017). In the FTIR spectrum of PLGA, sharp peaks at 3589.45 – 3643.84 cm^{-1} for –OH (free) and of 2995.43–2946.79 cm^{-1} for C-H stretching were observed as the typical bands of PLGA. The ester C-O stretching band of PLGA was observed at 1748.61 cm^{-1} . The main bands appearing in that spectrum were due to stretching vibrations of OH groups in the range from 3750 cm^{-1} to 2900 cm^{-1} , which were overlapped to the stretching vibration of N-H; and C–H bond in –CH₂ (2918

cm^{-1}) and $-\text{CH}_3$ (2852 cm^{-1}) groups, respectively. In the FTIR spectrum of chitosan, the band located near 1146 cm^{-1} is related to asymmetric vibrations of CO in the oxygen bridge resulting from deacetylation of chitosan. The small peak at $\sim 890 \text{ cm}^{-1}$ corresponds to wagging of the saccharide structure of chitosan (Darder *et al.* 2003; Paluszkiewicz *et al.*, 2011; Yuan *et al.*, 2010; Silva *et al.*, 2012). Thus, from this it can be concluded that there is no chemical interaction seen between the drug and the excipients.

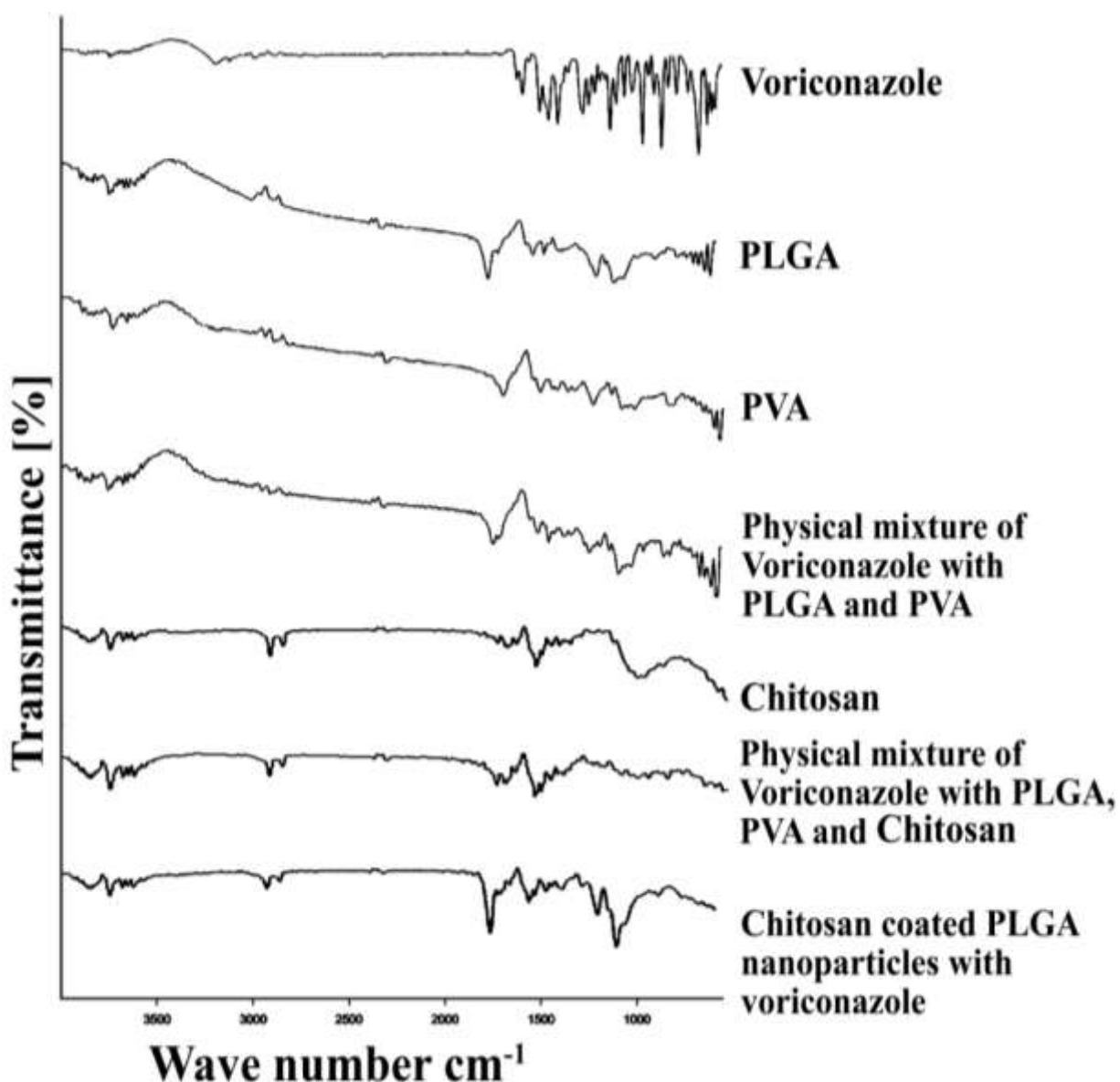


Figure 6.5: FTIR spectroscopy studies of individual components, physical mixture, and nanoparticle formulations

6.3 Characterization of nanoparticles

6.3.1 Particle size distribution and zeta potential by dynamic light scattering (DLS) analysis

The average particle size and zeta potential values of the experimental formulations are given in **Table 6.4**. The data (**Figure 6.6**) revealed that most of the particles had an average particle size of 154.6 nm and 277 nm with zeta potential value of -14.8 mV and +39.1 mV for non-coated and coated nanoparticles, respectively.

Table 6.4: Formulation characteristics such as % drug loading, encapsulation efficiency, average particle size and zeta potential values for the optimized PLGA formulation without chitosan coating (P5) and with chitosan coating (P6)

Formulation code	% Drug loading	% Encapsulation efficiency	Average particle size (nm)	Zeta potential (mV)
P5	35.62±0.135	71.24	154.6	-14.8
P6	28.57±3.704	68.57	277	31.9

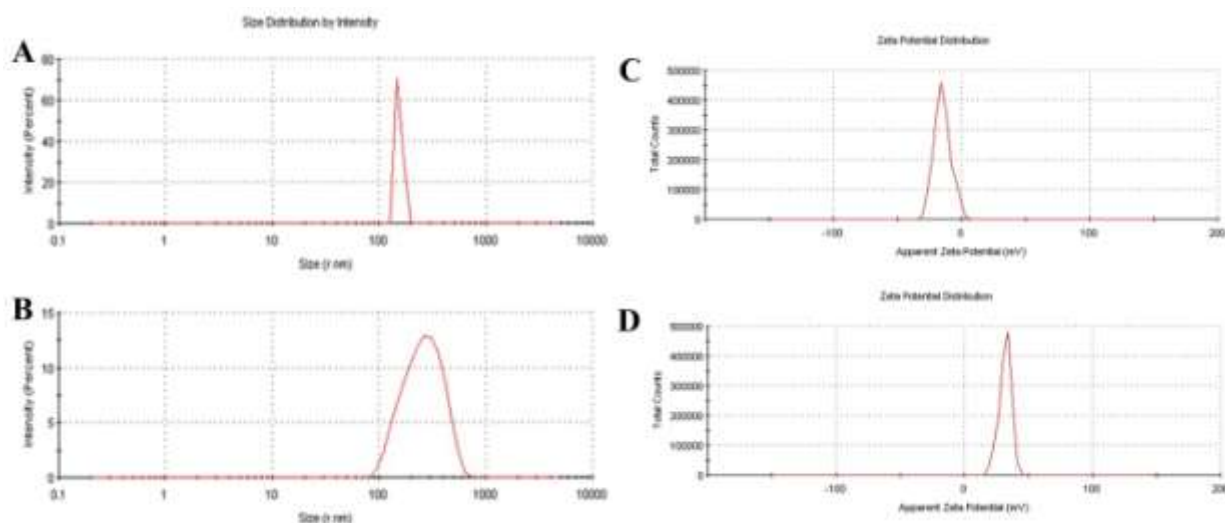


Figure 6.6: Particle size distributions and zeta potential data. (A) Particle size distribution graph of non-coated PLGA nanoparticles; (B) Particle size distribution graph of chitosan-coated PLGA nanoparticles; (C) Zeta potential graph of non-coated PLGA nanoparticles; (D) Zeta potential graph of chitosan-coated PLGA nanoparticles

6.3.2 Determination of drug loading and entrapment efficiency

The drug loading values were expressed by the quantity of voriconazole encapsulated in the formulations and the drug entrapment efficiency was associated with the percentage of voriconazole encapsulated with respect to theoretical voriconazole loading in a particular formulation (Das *et al.*, 2015; Shaw *et al.*, 2017). The percentage values of drug loading of non-coated and coated nanoparticles were $35.62 \pm 0.135\%$ and $28.57 \pm 3.704\%$ with the drug loading efficiency values of 71.24% and 68.57%, respectively (**Table 6.4**).

6.3.3 Surface morphology

FESEM images revealed that experimental formulations were spherical in shape (**Figure 6.7**). **Figure 6.7(A-D)** shows particles were in submicron range. Thus the later experiments were performed with the optimised non-coated formulation (P5) and chitosan coated formulation (P6). In formulations P5, most of the particles were below 500 nm (**Figure 6.7E**) in size and the particles of the formulation P6 (**Figure 6.7F**) were little bit larger than those of non-coated formulation.

But the surface coating was not distinguished properly by FESEM data. The surface coating of chitosan onto the PLGA nanoparticles were confirmed by Cryo-TEM images (**Figure 6.8A-B**) and TEM image (**Figure 6.9A-D**). The particles of non-coated formulation were smooth in surface (**Figure 6.8A-B**). The AFM images of non-coated (P5) and coated (P6) nanoparticles have been shown in **Figure 6.10A** and **Figure 6.10B**, respectively. AFM image shows that the particles of both the formulations were purely spherical in shape and the surface was coated in case of chitosan coated nanoparticles. Amount of chitosan coated in the formulation was determined by subtracting the weight of uncoated lyophilized drug loaded nanoparticles from the weight of chitosan coated lyophilized drug loaded nanoparticles, and the amount of chitosan was determined to be $13.89 \pm 1.94\%$ of the uncoated lyophilized drug loaded nanoparticles. The size of nanoparticles was in nano-grade. The sphere-like particles were 150-300 nm in diameter.

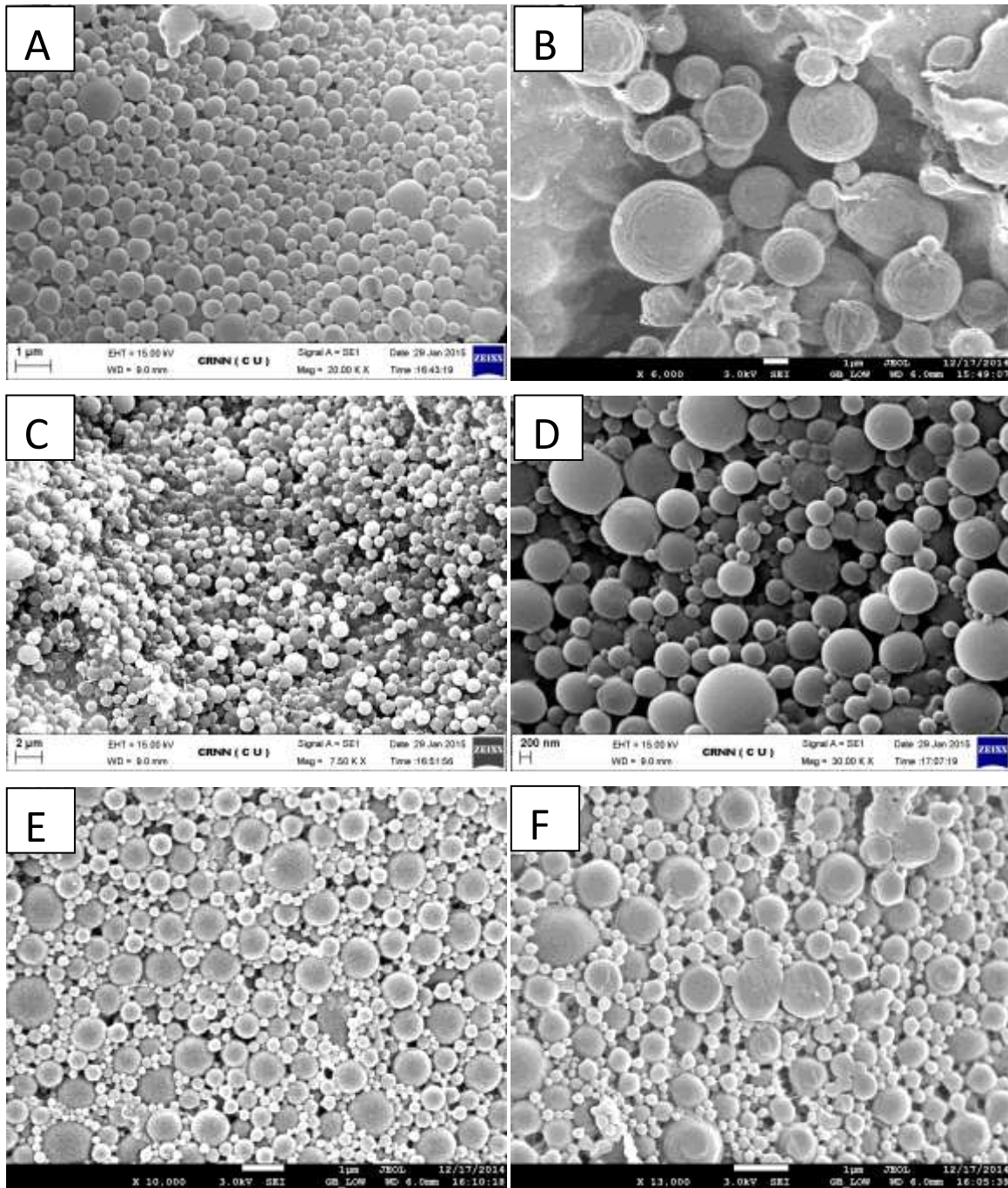


Figure 6.7: Field Emission Scanning Electron Microscopic images of non-coated PLGA nanoparticles and chitosan-coated PLGA nanoparticles. **(A)** Formulation P1; **(B)** Formulation P2; **(C)** Formulation P3; **(D)** Formulation P4; **(E)** Formulation P5; **(F)** Formulation P6

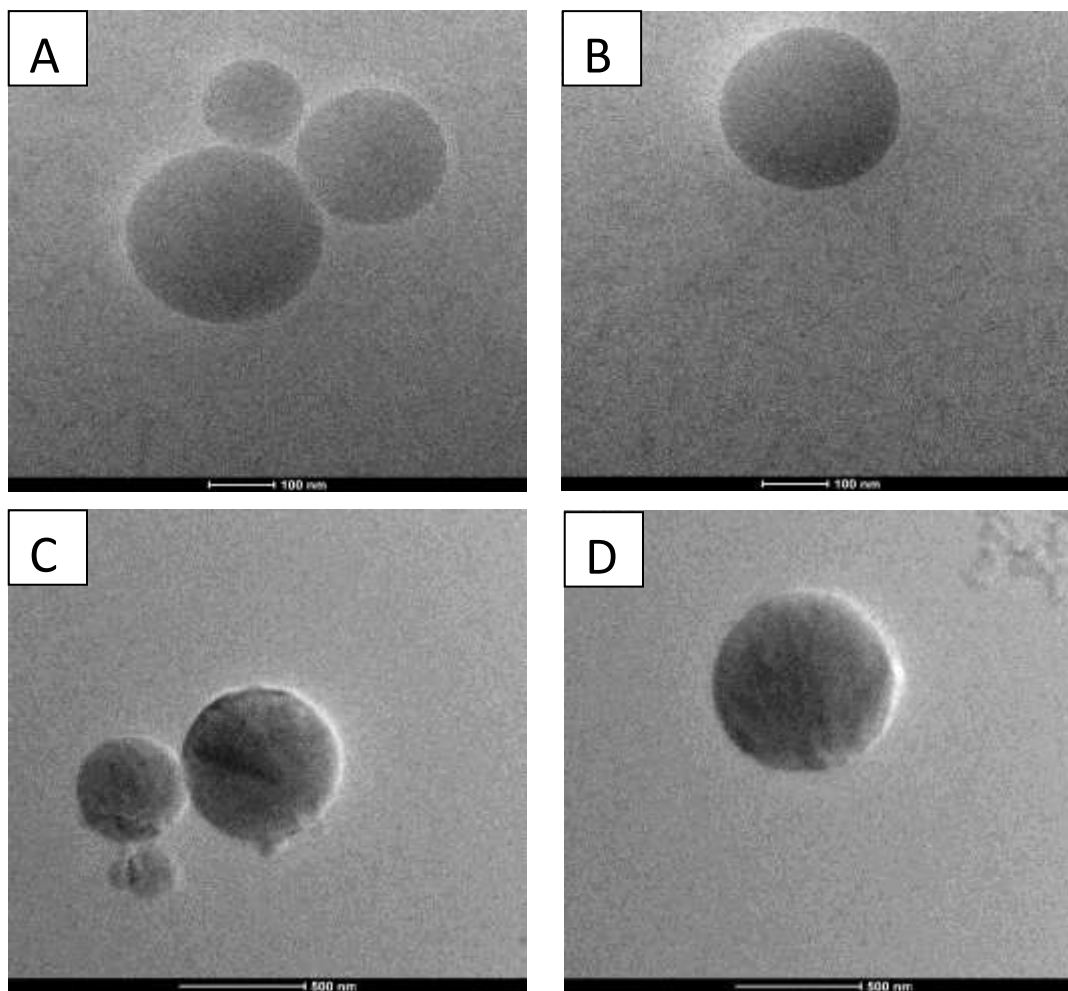


Figure 6.8: Cryogenic Transmission Electron Microscopic images of (A, B) non-coated PLGA nanoparticles (formulation P5) and (C, D) chitosan-coated PLGA nanoparticles (formulation P6)

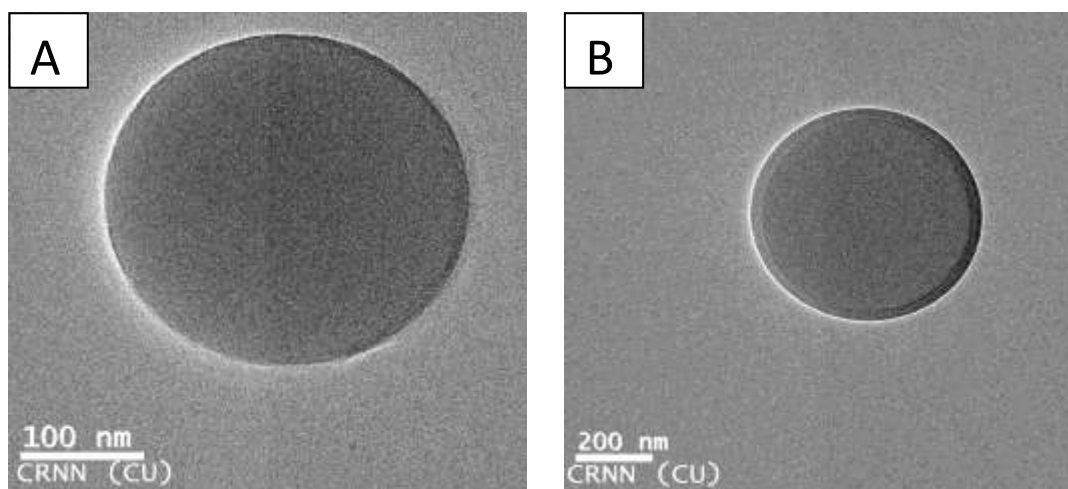


Figure 6.9: Transmission Electron Microscopic image of (A) non-coated PLGA nanoparticles (Formulation P5) and (B) chitosan-coated PLGA nanoparticles (Formulation P6)

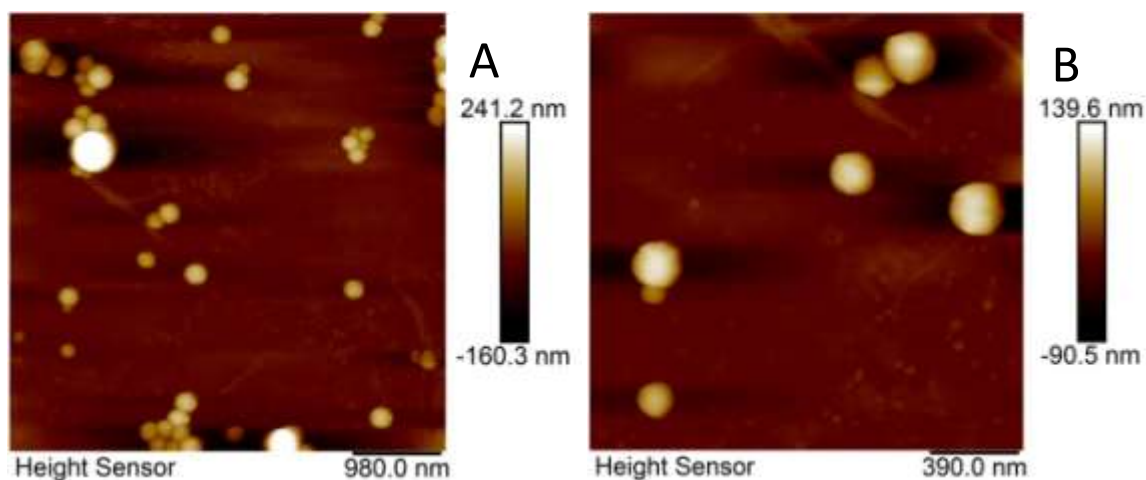
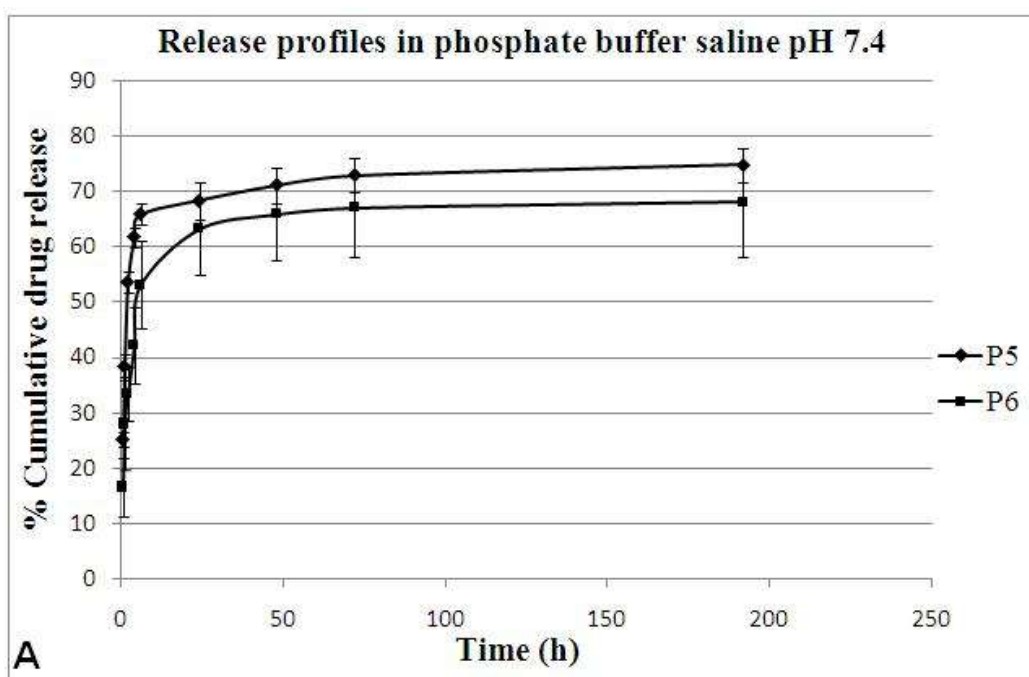


Figure 6.10: Atomic force microscopic image of (A) non-coated PLGA nanoparticles (Formulation P5) and (B) chitosan-coated PLGA nanoparticles (Formulation P6)

6.4 *In vitro* drug release study

Both the experimental formulations had more or less similar drug release pattern in phosphate buffer saline (PBS), pH 7.4 up to 21 days (**Figure 6.11A**). The drug released from the experimental formulations initially at a faster rate up to 24 h and then at a slower rate in a sustained manner up to 8 days (After 8 days no significant increase in the percentage cumulative drug release was seen).



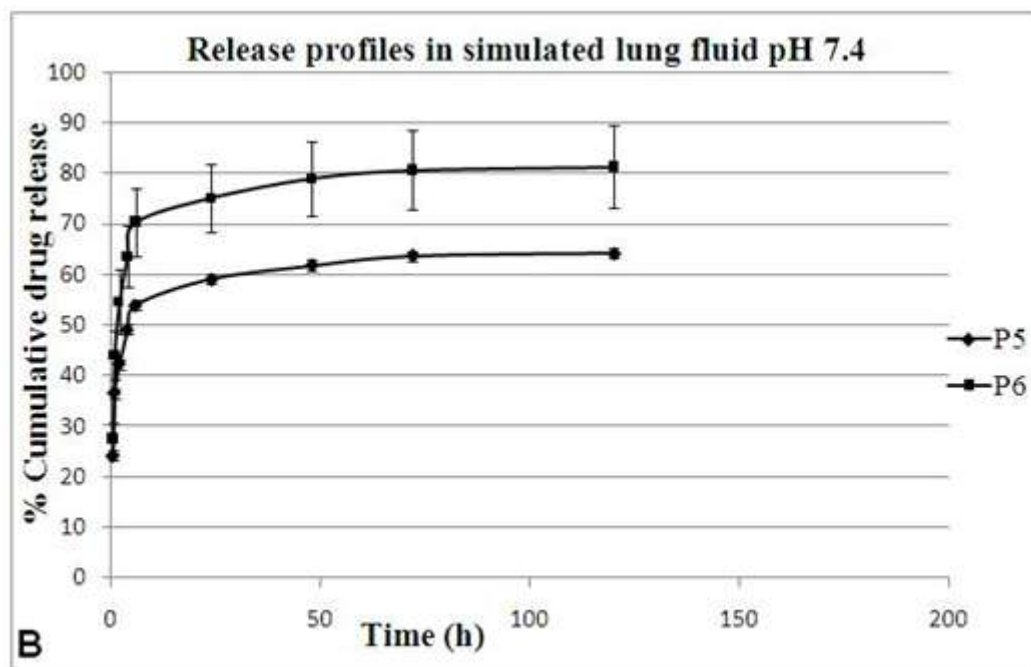


Figure 6.11: Release profiles of voriconazole from non-coated PLGA nanoparticles (P5) and chitosan-coated PLGA nanoparticles (P6) in (A) phosphate buffer saline (pH 7.4) and (B) simulated lung fluid (pH 7.4)

It shows that at first 30 min about 25% of the drug released from the optimized uncoated nanoparticles, whereas the data for the optimized chitosan coated nanoparticles was less (16%). The drug released in a similar sustained manner after 24 h of release from both the formulation. After 8 days, 74.76% and 68.12% of drug released from P5 and P6, respectively in PBS. A distinct difference was observed for drug released in simulated lung fluid, pH 7.4 (**Figure 6.11B**). For non-coated nanoparticles, 54% of drug was released at 6 h, but in chitosan coated nanoparticles drug released 70% and at day 5, drug release values were 64% and 81% from non-coated and coated nanoparticles, respectively.

6.5 Drug release kinetics study

The drug release kinetic revealed that the drug release followed the Korsmeyer–Peppas kinetic model ($R^2 = 0.719$ and 0.896 for P5 and P6 in PBS; and 0.835 and 0.801 for P5 and P6 in SLF, respectively) (**Table 6.5**). The release of drug from the particles followed non-Fickian diffusion kinetics, as depicted from the release component value.

Table 6.5: Drug release kinetics of different formulations

<i>In vitro</i> Release Kinetics Model	Phosphate buffer saline, pH 7.4		Simulated lung fluid, pH 7.4	
	Formulation P5	Formulation P6	Formulation P5	Formulation P6
Zero order	$y = 0.055x + 56.27$ $R^2 = 0.307$	$y = 0.232x + 39.40$ $R^2 = 0.482$	$Y = 0.236x + 43.27$ $R^2 = 0.509$	$Y = 0.321x + 55.83$ $R^2 = 0.485$
First order	$y = -0.001x + 1.647$ $R^2 = 0.417$	$y = -0.002x + 1.766$ $R^2 = 0.597$	$Y = 0.002x + 1.745$ $R^2 = 0.591$	$Y = -0.004x + 1.617$ $R^2 = 0.653$
Higuchi	$y = 2.77x + 46.26$ $R^2 = 0.513$	$y = 4.038x + 29.70$ $R^2 = 0.721$	$Y = 3.113x + 37.12$ $R^2 = 0.695$	$Y = 4.25x + 47.39$ $R^2 = 0.669$
Korsmeyer-Peppas	$y = 0.150x + 1.605$ $R^2 = 0.719$ $n = 0.150$	$y = 0.195x + 1.479$ $R^2 = 0.896$ $n = 0.195$	$Y = 0.150x + 1.545$ $R^2 = 0.835$ $n = 0.150$	$Y = 0.164x + 1.643$ $R^2 = 0.801$ $n = 0.164$
Hixon-Crowell	$y = -0.004x + 3.562$ $R^2 = 0.381$	$y = -0.006x + 3.895$ $R^2 = 0.558$	$Y = -0.005x + 3.826$ $R^2 = 0.564$	$Y = -0.010x + 3.485$ $R^2 = 0.598$

6.6 Determination of mass median aerodynamic diameter (MMAD) and geometric standard deviation (GSD) using an eight-stage nonviable Anderson cascade impactor

Cascade impactor scenario of the non-coated (P5) and chitosan-coated (P6) PLGA nanoparticles are shown in **Figure 6.12**. P5 and P6 had the highest particle retention in stage 5 and lowest particle deposition at stage 8 of the impactor. The particles were deposited less than 10% in stage 0-2, 6-7. Stage 3 and stage 4 showed particle deposition above 10% but below 20%; whereas only stage 5 showed particle deposition above 20%. MMAD and GSD of P5 (non-coated) and P6 (chitosan-coated) were calculated to be 2.46 μm and 2.15 (for P5), and 2.8 μm and 3.04 (for P6), respectively.

Particle size below 5 μm was considered as fine fraction (Mitchell and Roberts, 2013). Fine powder fraction of non-coated (P5) and chitosan coated (P6) nanoparticles from cascade impactor device were 0.6676 and 0.5747, respectively. Emitted dose percent of non-coated (P5) and chitosan coated (P6) nanoparticles were calculated excluding the total loss during the delivery to cascade impactor device. The values were 11.67% and 9.96%, respectively.

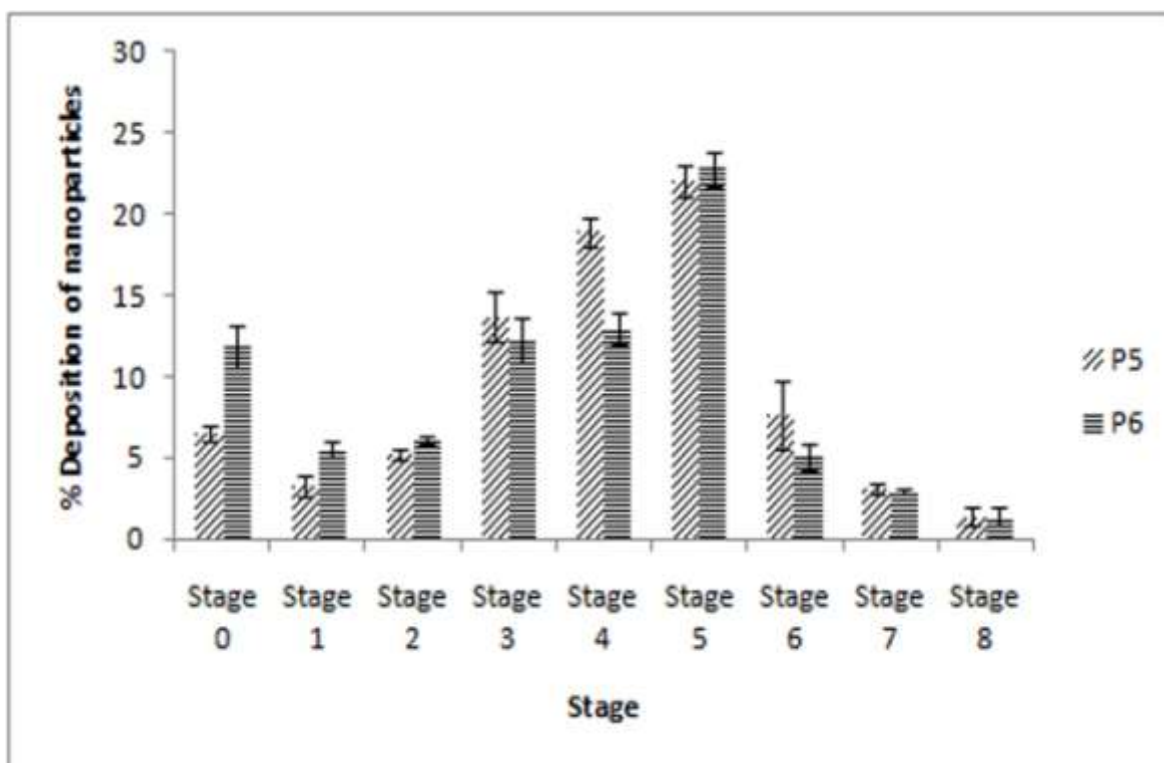


Figure 6.12: *In vitro* deposition of P5 and P6 from Anderson cascade impactor (data as mean \pm SD, n = 3)

6.7 *In vivo* deposition of nanoparticles in the lungs of mice using nose-only inhalation chamber and fabricated dry powder inhaler (DPI)

In vivo deposition of FITC nanoparticles coated and non-coated types in the lungs have been confirmed by confocal images taken at 1 h, 8 h and 24 h during the experiment. **Figure 6.13 (A-B)** revealed that NPs penetrated into the lung tissue cell membrane and were distributed uniformly in the alveoli. In addition, the green fluorescent intensity in the cells augmented with time.

In order to investigate the influence of the chitosan coating on nanoparticles on the nanoparticle deposition in the lung tissues, we calculated the corrected total cell fluorescence (CTCF) values for non-coated and chitosan coated PLGA nanoparticles at different time points of 1 h, 8 h, 24 h. The CTCF values have been summarized in **Figure 6.14**. CTCF values of both the formulations at different time points (1 h, 8 h, and 24 h) showed that CTCF value decreased with time in case of non-coated nanoparticles whereas the value increased gradually with time for chitosan coated nanoparticles.

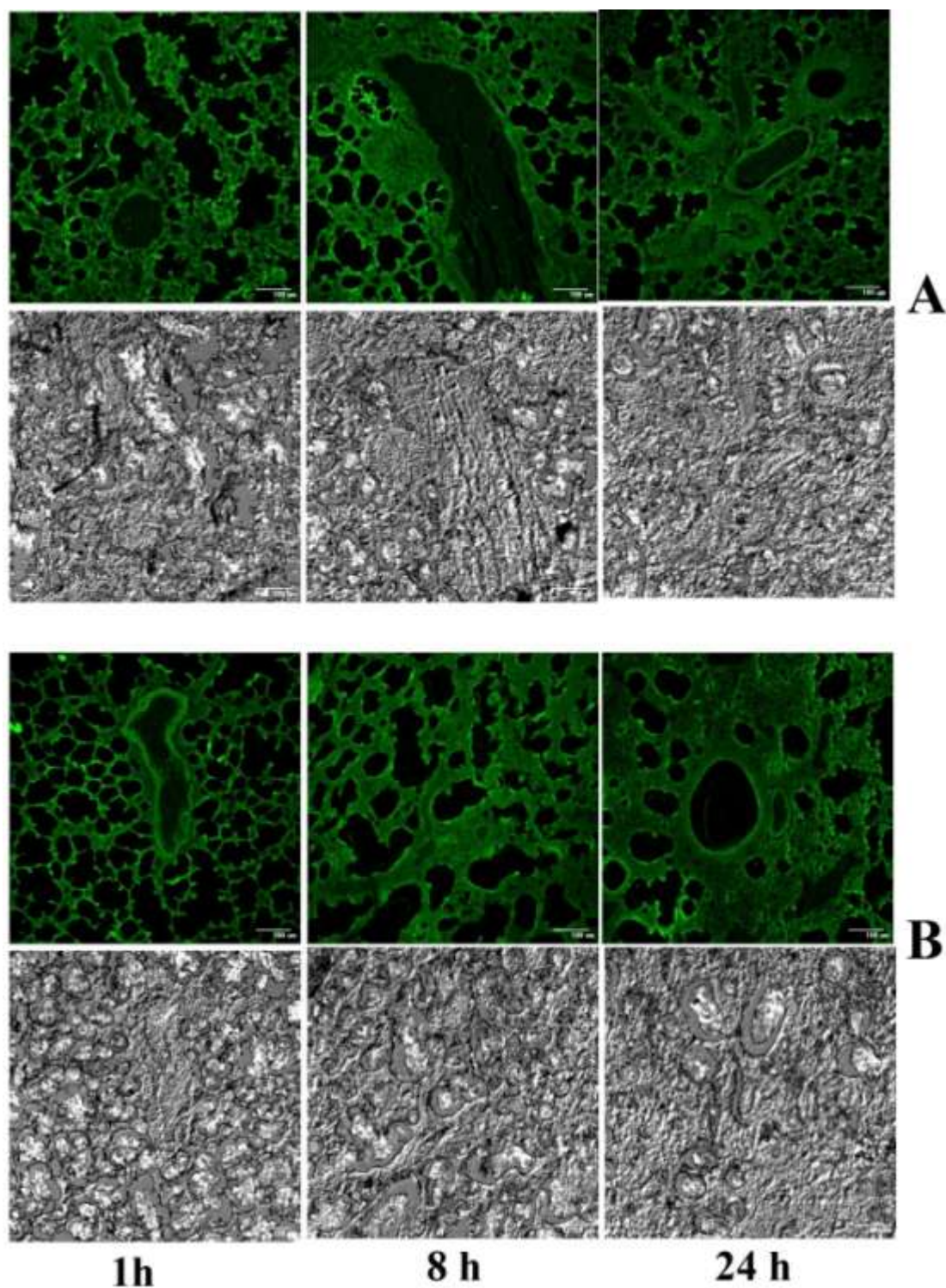


Figure 6.13: Confocal laser scanning microscopic images of lungs treated with (A) non-coated PLGA nanoparticles (at 1 h, 8 h, and 24 h after pulmonary administration), and (B) chitosan-coated PLGA nanoparticles (at 1 h, 8 h, and 24 h after pulmonary administration)

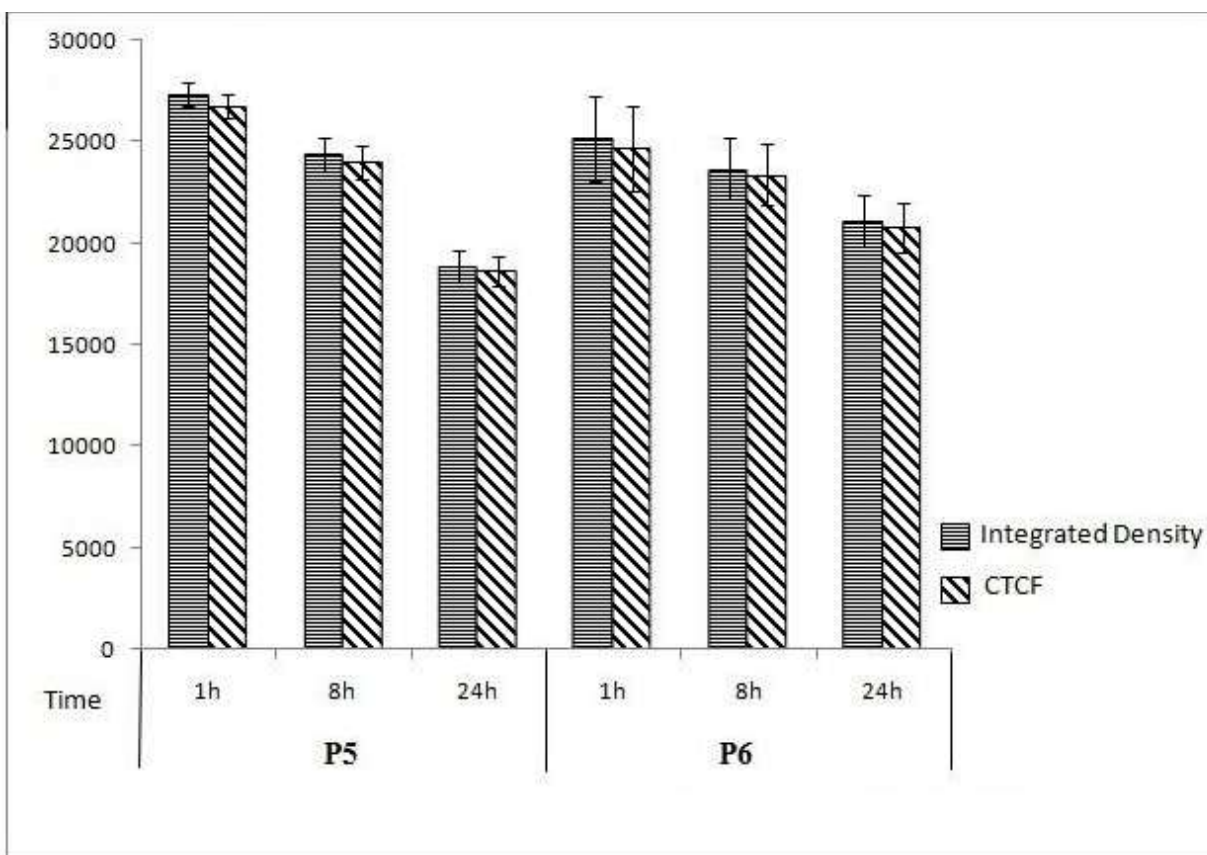


Figure 6.14: CTCF values and integrated density quantification of FITC fluorescence staining in lungs tissue sections after pulmonary delivery of non-coated PLGA nanoparticles and chitosan-coated PLGA nanoparticles (data as mean \pm SD, n = 3) (*CTCF-Corrected total cell fluorescence)

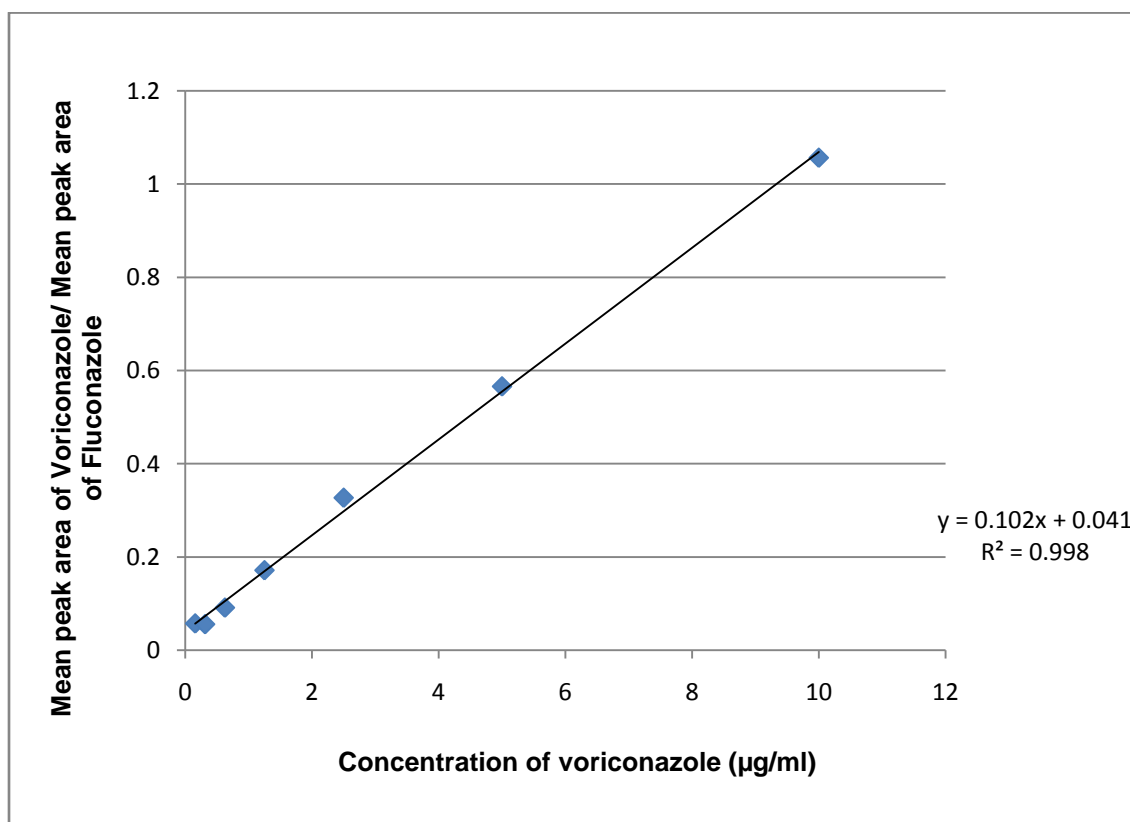
6.8 High performance liquid chromatography (HPLC)

6.8.1 Calibration curve in plasma

To measure the drug content in plasma a calibration curve in HPLC was developed in the concentration range 0.1562 to 10.00 $\mu\text{g/mL}$ (**Table 6.6**). The linearity was found to be good (correlation coefficient 'R' = 0.998) (**Figure 6.15**).

Table 6.6: Result of linearity data of of Voriconazole in acetonitrile–water–formic acid containing mice plasma (n=3)

Concentration ($\mu\text{g/ml}$)	Mean peak area of Voriconazole	Mean peak area of Fluconazole	Mean peak area of Voriconazole/ Mean peak area of Fluconazole
0.15625	0.139	2.4184	0.057476
0.3125	0.1416	2.5334	0.055893
0.625	0.2044	2.236	0.091413
1.25	0.4172	2.4302	0.171673
2.5	0.7398	2.2605	0.327273
5	0.9626	1.7	0.566235
10	2.0871	1.9748	1.056867

**Figure 6.15:** Calibration curve of voriconazole in acetonitrile–water–formic acid containing mice plasma

6.8.2 Calibration curve in lung tissue

To measure the drug content in plasma a calibration curve in HPLC was developed in the concentration range 0.1562 to 10.00 $\mu\text{g/mL}$. The linearity was found to be good (correlation coefficient 'R' = 0.992) (**Figure 6.16**).

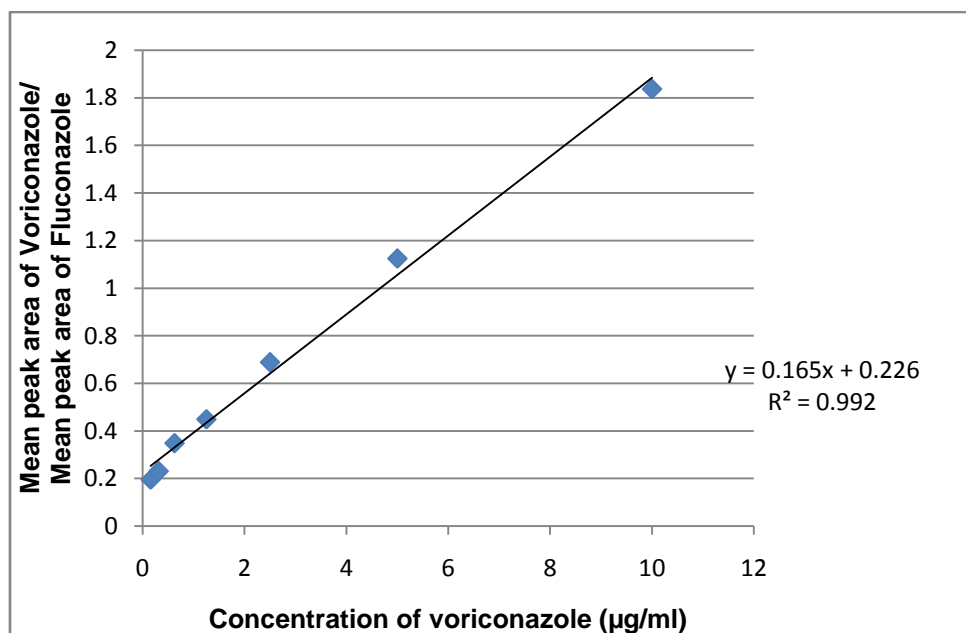


Figure 6.16: Calibration curve of voriconazole in mice lung homogenate

6.9 Pharmacokinetics and lung lobe distribution study

Different pharmacokinetic parameters after pulmonary administration of free voriconazole, non-coated and chitosan-coated nanoparticles have been listed in **Table 6.7**. Voriconazole levels in blood and lungs were located after single dose administration of nanoparticles containing voriconazole given through pulmonary route. Drug level was observed at six different time points up to 72 h. Both the nanoparticles showed sustained drug release profile for up to 72 h in comparison to the free voriconazole (Das *et al.*, 2015). Our formulation showed to maintain the plasma concentration of voriconazole above minimum inhibitory concentration (MIC ~ 0.5 mg/liter) (Jeans *et al.*, 2012) required for effective treatment of lung fungal infection.

Table 6.7: Pharmacokinetic parameters for free drug voriconazole, optimized PLGA formulations without chitosan coating (P5) and with chitosan coating (P6) in Swiss albino mice after pulmonary administration

Parameter	Plasma kinetics			Lung kinetics		
	Free VRZ [#]	PLGA NPs ^{\$}	CS [¥] -coated PLGA NPs	Free VRZ	PLGA NPs	CS-coated PLGA NPs
C_{max} (µg/mL)	15.33±1.16	29.69±2.87	22.15±2.10*	12.03±0.47	19.62±6.76	14.33±4.37
T_{max} (h)	1	6	3	1	24	24
AUC (µg/µL*h)	0.25±0.01	1.87±0.09	8.92±2.93	0.07±0.01	1.81±0.67	4.49±0.54**
AUMC (µg/µL*(h) ²)	4.08±0.30	126.78±20.92	4799.7±891.61*	0.57±0.14	134.94±23.05	1341.55±469.26*
MRT (h)	15.95±0.41	67.73±7.38	537.97±97.92*	7.84±0.94	74.60±15.36	298.49±83.65*
t_{1/2} (h)	10.01±0.36	45.55±7.92	372.8±132.48	5.37±0.77	48.28±13.25	204.10±64.12*

Note: [#]VRZ, Voriconazole; ^{\$}NPs, nanoparticles; [¥]CS, chitosan; Values represent mean ± SD (n=3); Statistical significance evaluations (using two-tailed unpaired t-test) represented by asterisks compared to PLGA nanoparticles (*P <0.05 at 95 % confidence interval; ** P <0.01 at 99 % confidence interval)

The maximum concentration of voriconazole in plasma was achieved 3 h before for chitosan-coated nanoparticles compared to the non-coated one. But the free drug was found to be maximum in 1 h in both plasma and lung (**Table 6.7**).

Whereas, the concentration to achieve maximum concentration in lung was same for both the formulations. The concentration of drug was found to be relatively more in plasma as a result of the higher perfusion rate in lung due to more denser capillary network present in the pulmonary region (Sangwan *et al.*, 2001; Townsley, 2012). The mean residence time (MRT) and the half life (t_{1/2}) of voriconazole were found to increase in both plasma and lung for chitosan-coated nanoparticles as compared to the non-coated nanoparticles and free drug.

From **Figure 6.17** it is evident that left lung lobe had the highest voriconazole concentration, while, distribution of drug in the middle lobe was found to have the lowest value during the entire study duration (i.e., 72 h). Drug concentration was detected in all the lobes of lung above MIC level (0.5 µg/mL) within 24 h.

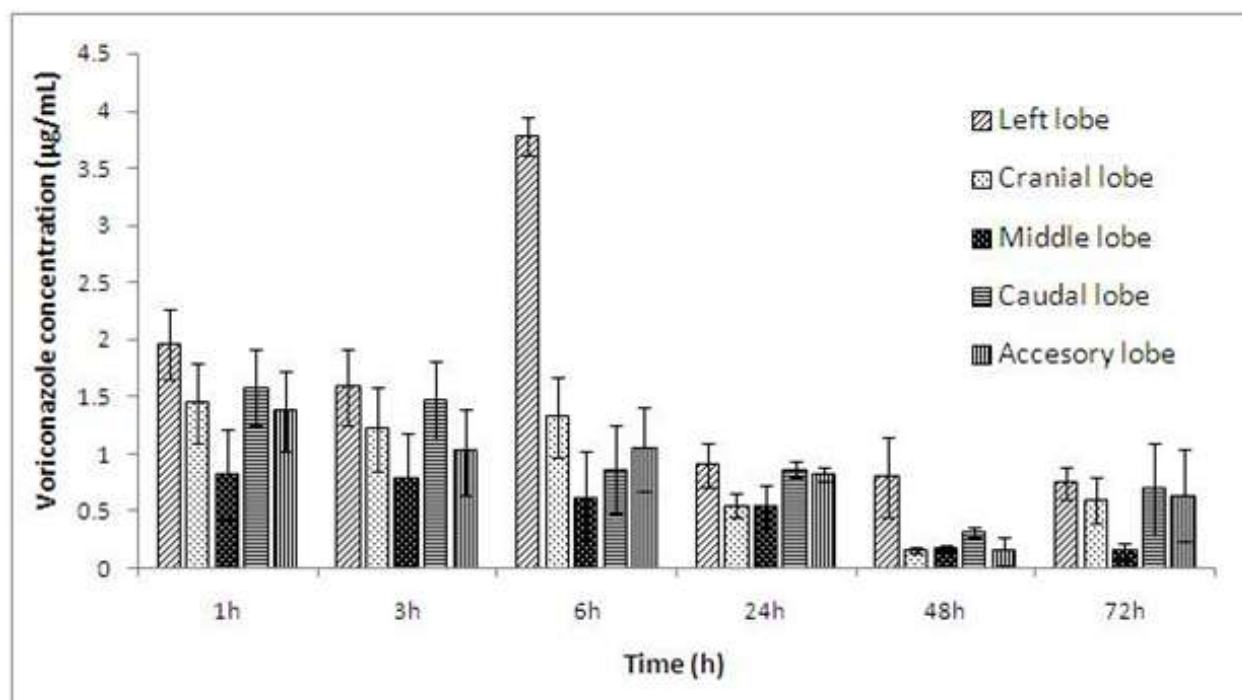


Figure 6.17: Distribution of voriconazole ($\mu\text{g/mL}$) in mice lung lobes at different time points up to 72 h after treatment with chitosan-coated nanoparticles in pulmonary route

6.10 Gamma scintigraphy

The non-coated and chitosan coated nanoparticles containing voriconazole were radiolabeled with Tc-99m with more than 95 percent efficiency. **Figure 6.18** shows gamma scintigraphy pictures of animals which received Tc-99m-P5 and Tc-99m-P6 by pulmonary delivery method.

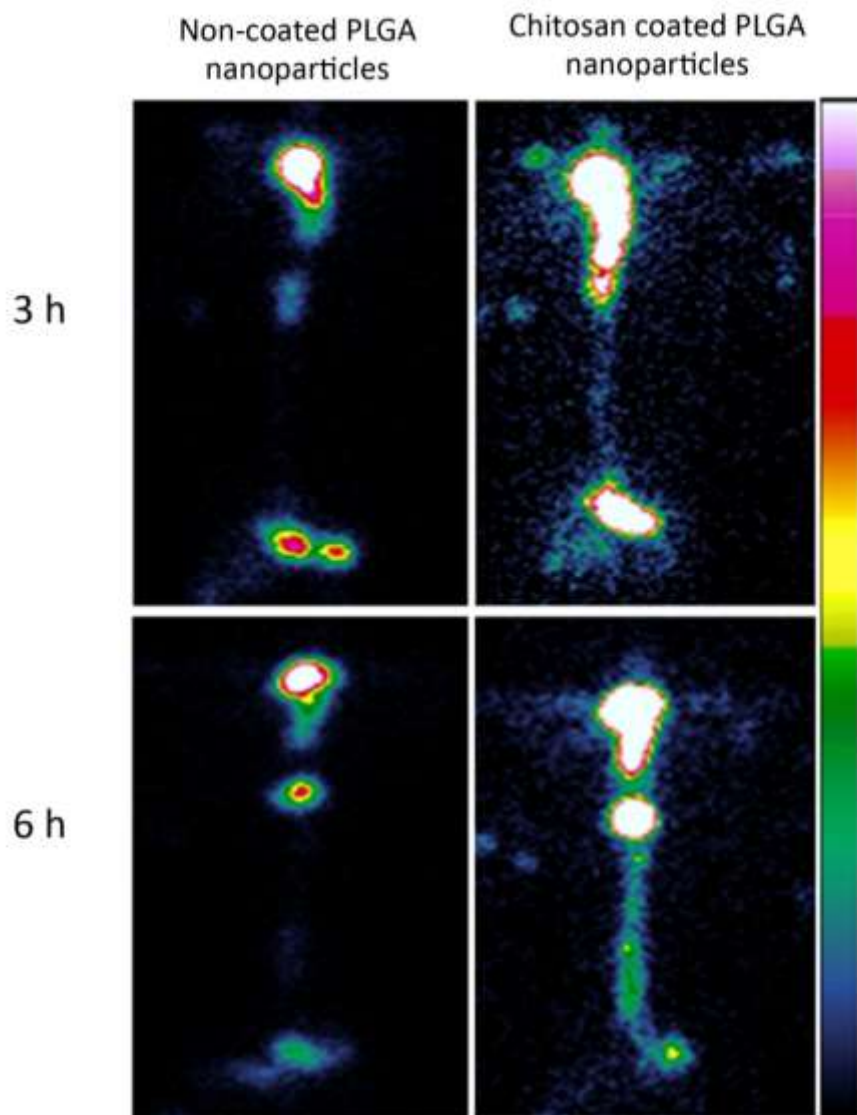


Figure 6.18: Scintigraphy pictures of animals after receiving Tc-99m labeled PLGA nanoparticles containing voriconazole formulation and chitosan coated PLGA nanoparticles containing voriconazole by pulmonary route after 3 h and 6 h

Tc-99m-P6 was found to be predominantly more in lungs and urinary bladder at 3 h after its pulmonary administration. Interestingly, at 6 h after its administration, it was found to accumulate more in liver and simultaneously there was a sustentative decrease in urinary bladder. This suggests its urinary clearance decreased remarkably along with eventual hepatic accumulation. Similar phenomenon was observed in animals after pulmonary administration of Tc-99m-P5 at 3h and 6 h. However, markedly low signal was detected in lungs indicating lower amount of retention of Tc-99m-P5 in lungs than Tc-99m-P6.

6.11 Biodistribution

Biodistribution of the radiolabeled non-coated PLGA nanoparticles (P5) and radiolabeled chitosan coated PLGA nanoparticle containing voriconazole (P6) was investigated in rats at 3 h and 6 h after injection. For chitosan coated PLGA nanoparticles, hepatic accumulation was higher (35 % injected dose (ID) per gram of organ (% ID/g)) at 6 h than that (31.25% ID/g) at 3 h (Table 6.8). Predominant accumulation was also observed in lungs and spleen (5.11% ID/g and 4.28% ID/g respectively at 3 h and 3.93% ID/g and 3.55% ID/g, respectively at 6 h). This can also be justified for the targeting and retention of the chitosan coated voriconazole containing nanoparticles to lungs. Uptake of drug in heart and muscle was not prominent. Urinary excretion was predominant at 6 h compared to at 3 h in both type of formulations.

Table 6.8: Biodistribution study of ^{99m}Tc labeled voriconazole loaded PLGA nanoparticles and ^{99m}Tc labeled chitosan coated PLGA nanoparticles containing voriconazole in rats

Organ/Tissue	Non coated PLGA NPs		Chitosan coated PLGA NPs	
	3h	6h	3h	6h
Heart	0.42 ± 0.16 ^a	0.35 ± 0.11 ^a	0.51 ± 0.13 ^a	0.45 ± 0.16 ^a
Blood	0.72 ± 0.11	0.61 ± 0.19	0.98 ± 0.21	0.85 ± 0.21
Liver	25.16 ± 1.29	31.21 ± 1.95	31.25 ± 1.26	35 ± 1.15
Lungs	3.45 ± 0.31	2.91 ± 0.65	5.11 ± 0.96	3.93 ± 0.41
Spleen	3.61 ± 0.22	2.55 ± 0.29	4.28 ± 0.51	3.55 ± 0.61
Muscle	0.09 ± 0.01	0.07 ± 0.02	0.08 ± 0.01	0.07 ± 0.02
Kidney	3.91 ± 0.51	4.11 ± 0.15	3.26 ± 0.19	5.39 ± 1.20
Stomach	0.92 ± 0.26	1.25 ± 0.16	0.72 ± 0.19	1.10 ± 0.51
Intestine	4.51 ± 0.15	5.10 ± 1.92	3.96 ± 1.15	4.12 ± 1.10
Urine	16.26 ± 1.25	21 ± 2.25	21.25 ± 1.15	25.29 ± 2.15

^a each data indicates % injected dose (ID) per gram of organ ± SD (n=6)

Chapter 7

Discussion

7. Discussion

The present investigation was aimed to develop chitosan coated biodegradable polymer based nanoparticles for pulmonary delivery of voriconazole to treat fungal infections in lungs which are one of the major killer diseases in immunocompromised patients. Here, PLGA, a US-FDA approved biodegradable polymer was used in the formulation of both coated and noncoated formulations. Further, *in vitro* characterization, *in vivo* pharmacokinetic evaluation and biodistribution study of the developed formulations have been reported here and compared with the non-coated one. Before the formulation and development and process optimization study, a preformulation study is performed to select the suitable excipients for the drug to formulate drug delivery system. Initially we have investigated drug to excipients interaction by FTIR spectroscopy. Data reveal that all the typical bands of PLGA and voriconazole were present in the FTIR spectrum of their physical mixture. Further, the presence of the characteristic peaks of drug and the excipients in the formulations was observed. This suggests that there was no chemical interaction between the drug and the excipients used in this study. However, shifting of some peaks was also observed. The probable reason might be due to the physical interactions by formation of weak physical bonds such as van der Waals force of attraction, H-bonding, or dipole–dipole interaction between the various functional groups of voriconazole, PLGA, chitosan and PVA molecules. The physical interaction might be responsible for the formation of spherical structure of the nanoparticles and sustained drug release from them. Presence of drug peak in the lyophilized formulations, suggests that some drug molecules were present on the surface.

Voriconazole was present in DCM along with the PLGA in the primary emulsion (W/O). This primary emulsion was further emulsified in the 1.5% PVA solution to prepare W/O/W emulsion. Initially the pH of the PVA solution for preparation of secondary emulsion was brought down to pH 3.0 to solubilize Chitosan and during this process some of the voriconazole molecules leached from the DCM solution to the aqueous media and at this low pH voriconazole remained dissolved along with the Chitosan in this aqueous PVA media. However, for coating purpose when the pH was raised to pH 9.0, there might be co-precipitation of Chitosan along with the drug on the surface of the nanoparticles. Presence of this drug molecule on the surface might have been detected by FTIR study.

Various process parameters were changed to optimize the formulation such as, drug to polymers ratio, homogenization speed, Sonication time etc. Drug-polymer ratio was varied to initially optimize the drug loading and particle size of the experimental non-coated nanoparticles and drug polymer ratio (1:1) was established to be the best for this purpose. After that chitosan, in increasing concentration (9.09%, 16.67% and 28.57%) was used for the surface coating purpose. The ratio of drug: PLGA: chitosan was optimized as 1:1:0.4 for the purpose of development of chitosan coated nanoparticles. In this method, incorporation of chitosan coating was done simultaneously during the process of development of multiple emulsion and no additional step for coating was required. Further, time of lyophilization was also same as it was required for non-coated formulation. Thus, this simple process of chitosan coating on nanoparticle could be highly beneficial for the industrial production point of view. However, due to chitosan coating the drug loading was found to decrease as compared to the non-coated formulation. This might be due to the dissolution of some drug molecules which escape from the formulation due to acidic pH (pH 3.0) as voriconazole has high solubility in acidic pH (1.2) (Buchanan *et al.*, 2007). As we have mentioned earlier the coating was developed by co-precipitation of the drug along with the polymer, there must be a loss of drug owing to the precipitation of the drug at higher pH. Drug loading efficiencies in both the type of formulations were more or less similar. However, the overall value (approx. 70%) was less than the expected. It might be due to the incomplete removal of the whole product from the small containers and the homogenizer. There was a little variation of % drug loading efficiency due to chitosan coating and that may be due to the use of much less quantity of material for preparation of nanoparticles.

There are several investigations proposing PLGA/chitosan nanoparticles available in the literature. Yang *et al.*, 2008 and Babu *et al.*, 2017 have prepared chitosan coated nanoparticles by multistep method. Initially they have prepared PLGA nanoparticles and lyophilized them. In the next step the lyophilized nanoparticles were coated with chitosan. Both of them used PLGA variety 50:50 with variable drug loading (Yang *et al.*, 2009; Babu *et al.*, 2017). Babu *et al.*, 2017 had 6.5% drug loading (Babu *et al.*, 2017). On the other hand Yang *et al.*, 2008 had drug loading of about 3.5% (Yang *et al.*, 2009). In another study Taetz *et al.*, 2009 wanted to deliver antisense 20-Omethyl-RNA (2OMR) using chitosan coated PLGA nanoparticles where the variety of PLGA used was 70:30. Initially they mix PLGA-EA solution with chitosan containing PVA solution for 1 h and this mixture was homogenized at 13500 rpm for 15 min. But no data related

to drug loading was reported (Taetz *et al.*, 2009). In our study we used PLGA (85:15) and chitosan to develop chitosan coated PLGA nanoparticles. This is a single step method where formation of nanoparticles and coating of chitosan was done simultaneously. Our method is similar to the method described by Taetz *et al.*, 2009. However instead of mixing PLGA-EA solution with aqueous chitosan containing 2.5%PVA for 1 h (Taetz *et al.*, 2009), we added primary emulsion (PLGA-DCM-Acetone in 2.5% aqueous PVA) to chitosan dissolved in 1.5% PVA solution at pH3 just before the preparation of secondary emulsion. This improves the drug loading about 5 times more than the other two reported methods.

Five different methods, namely Dynamic light scattering (DLS), FESEM, TEM, Cryo-TEM, and AFM were adopted in order to accurately know the particle size, particle size distribution, surface morphology and surface coating by chitosan on the PLGA nanoparticles containing voriconazole in lyophilized as well as hydrated states. Sizes of lyophilized particles observed using FESEM were smaller than those detected by DLS. The difference in size may be because of the DLS method which measures the average hydrodynamic diameter of nanoparticles in aqueous suspension where the particles might swell and increase in size (Yu *et al.*, 2010). Size analysis data by DLS (**Figure 6.6**) show that the average size (Z-average) of non-coated nanoparticles (154.6 nm) (**Figure 6.6A**) and that of chitosan coated nanoparticles (277 nm) (**Figure 6.6B**) were well below 300 nm. The range of obtained particle size has been reported to distribute throughout the lungs (i.e. from the upper lobe to lower lobe region) by pulmonary delivery (<https://tisch-env.com/wp-content/uploads/2015/06/TE-20-800-Non-viable-Cascade-Impactor.pdf>). Lyophilized PLGA nanoparticles and chitosan coated nanoparticles were free flowing in nature. In pulmonary drug delivery flowability of powder is predominantly important for distribution of nanoparticles by DPI/nebulizer to the lungs. More is the flowability of the powder, more is its distribution and deposition in various parts of lungs. Presence of chitosan can help the nanoparticulate powder to adhere to the alveoli and not to be phagocytosed quickly (Parveen and Sahoo, 2011).

Maximum deposition of particles from P5 and P6 were observed at stage 5 (1.1–2.1 μm diameter) of cascade impactor apparatus (**Figure 5.3**, **Figure 6.12**). Data obtained upon deposition of particles on different stages of cascade impactor showed that particle size obtained in P5 and P6 are relevant (150-300 nm) for deposition in trachea, primary and secondary

bronchi, and alveolar region for deep lung penetration (Mitchell and Roberts, 2013). Higher deposition from chitosan coated particles (P6) at stage 0 (9.0–10 μm) to stage 2 (4.7–5.8 μm) and at stage 5 (1.1–2.1 μm), are also suitable for deposition in the pharynx and terminal bronchial area, respectively, of the pulmonary tract (Mitchell and Roberts, 2013). The zeta potential of a particle is the overall charge that particles acquire in a particular medium and at particular temperature (Averineni *et al.*, 2012). The physical stability of particles can also be predicted from their zeta potential value. Zeta potential value above +30 mV and/or below -30 mV indicates that the particles are having good colloidal stability (Dey *et al.*, 2016). Zeta potential values in between +30 and -30 mV suggest that the precipitation of particles in a suspension is more as the zeta potential value changes more towards zero (Tuan *et al.*, 2015). Thus, the non-coated nanoparticles (surface charge -14.8 mV) (**Figure 6.6C**) may settle down faster than the chitosan coated nanoparticles (surface charge +31.9 mV (**Figure 6.6D**), while in suspension. Presence of terminal carboxyl group in the PLGA polymer provided negative surface charge in the non coated nanoparticles (Sun *et al.*, 2015), while positive surface charge of the coated nanoparticles was due to the presence of amino group of chitosan (Ing *et al.*, 2012). In case of non-coated nanoparticles they should be stored in a lyophilized form and should be reconstituted just before use to prevent faster precipitation.

FESEM images (**Figure 6.7 E,F**) of the experimental nanoparticles show that all the particles belonged to P5 and P6 had smooth surface. This data along with the findings of AFM (**Figure 6.10**) and Cryo-TEM (**Figure 6.8**) suggest that the particles were spherical and submicron size with a heterogeneous distribution where particles size varied from 150 to 300 nm.

Further, their characterization by Cryo-TEM reveals that the obtained nanoparticles were coated (**Figure 6.8 C,D**). The analysis by Cryo-TEM is a method for the amplification of selected basic structural questions rather than for regular quality control issues (Laan and Denkova, 2017). TEM analysis (**Figure 6.9**) of chitosan-coated nanoparticles shows that the additional polymer (chitosan) was uniformly deposited (as a coat) on to the surface of PLGA nanoparticles.

In vitro drug release data for PLGA nanoparticles and chitosan-coated PLGA nanoparticles containing voriconazole show that voriconazole released in a sustained manner with a predominant burst release (about 35-45%) initially within 1 h in simulated lung fluid

(SLF), pH 7.4 and phosphate buffer saline (PBS), pH 7.4 (**Figure 6.11**). Burst release of coated formulation found to be more in SLF than PBS. Burst release decreased in case of same formulation when studied in PBS. This might be due to the presence of several salts such as magnesium chloride, potassium chloride, sodium acetate, sodium sulfate, sodium citrate etc. in the SLF and those salts might have enhanced the drug dissolution faster in case of chitosan coated formulation as compared to the non-coated PLGA formulation. Drug release kinetic data show that drug release from the nanoparticles might follow a complex mechanism of diffusion as well as erosion as the data were best supported by Korsmeyer–Peppas kinetic model.

In vivo uptake of FITC nanoparticles containing drug in the alveoli of both the lungs was found to remain almost similar with the duration (24 h) of the study in case of coated nanoparticles. However, for non coated nanoparticles the initial uptake was found to be more but with the duration the value decreased. Possibly this could be due to the mucoadhesive effect of the coated particles which retained longer time in the lungs as compared to the non coated one.

The pharmacokinetic data reveal that the C_{\max} was found to be greater for non-coated nanoparticles in both the plasma and lung. This could be due to the slow drug release. Further, CS is a hydrophilic polymer and voriconazole has little solubility in water. Hence, diffusion of hydrophobic voriconazole through chitosan might have taken longer time as compared to PLGA nanoparticle. T_{\max} values of voriconazole of P5 and P6 for lung pharmacokinetics were same. However, those values varied in plasma kinetics. T_{\max} value for chitosan coated formulation in plasma kinetics was 3 h which was half of that value for non coated formulation.

Chitosan coating increased the AUC and AUMC 4.77 times and 38 times in plasma and 2.49 times and 10 times in lungs, respectively. The enhanced AUC and AUMC values suggest that the availability of drug from the formulation was more for chitosan coated formulation. This might be due to the slower release and predominantly longer retention time (MRT) of drug in plasma and lung tissue from the chitosan coated formulation.

Several reasons may be given for improved bioavailability of voriconazole after pulmonary administration of chitosan-coated nanoparticles. Bioadhesion, conferred by chitosan, is probably responsible for the enhancement of drug pharmacokinetic profile in both blood and lung. The bioadhesion is achieved through different mechanisms such as electrostatic interaction, hydrogen bond, covalent linkage or van der Waals forces (Parveen and Sahoo, 2011;

Dyawanapelly *et al.*, 2016). Bioadhesion results in increased residence time at the lung epithelial cells and thus enhances the drug absorption due to the close intimacy of nanoparticles with the epithelial cells. Moreover, avoidance of hepatic “first-pass” metabolism contributes to improve bioavailability of the nanoparticles. The improved AUC values for the coated particles also guarantee for the prolonged drug release from the nanoformulations in a slow and sustained manner. A marked increase in MRT of voriconazole in case of chitosan-coated nanoparticles was noticed as compared to the voriconazole in PLGA nanoparticles and free voriconazole. This is because of the more residence time of the nanoparticles in the lung due to chitosan coating. The slow release of voriconazole from the nanoparticles due to more biodegradation time of the nanoparticles prepared with biocompatible and biodegradable polymer PLGA also increases the pharmacokinetic parameters in comparison with the free voriconazole (**Table 6.7**). In this study drug level in lung tissue as well as plasma was measured. Due to the localized nature of lung fungal infections, to measure concentration of voriconazole in different lobe is more meaningful especially for chitosan coated PLGA nanoparticulate formulation due to its better pharmacokinetic profile.

The micron-sized foreign bodies primarily have clearance by phagocytosis by resident alveolar macrophages. Inhaled nanosized particles generally are not recognized by macrophages and might instead be internalized by traversing the alveolar epithelium consisting of cuboidal alveolar type II epithelial (ATII) cells and flattened alveolar type I epithelial (ATI) cells (Thorley *et al.*, 2014). The ATI cells are the primary target of inhaled nanoparticles mediated through clathrin- and caveolin-mediated endocytic pathways important in *trans*-epithelial transport, receptor recycling, and cellular signaling. Whereas, secretory ATII cells synthesize and release pulmonary surfactant which helps reducing the surface tension at the air–liquid interface and contains surfactant proteins A–D, which act as opsonins to promote clearance (Thorley *et al.*, 2014). In case of chitosan coated particles due to the mucoadhesive nature of chitosan, the clearance through A-D cell surfactant protein might be distinctly hindered compared to the non-coated particles. This might have held prolonged retention time of P6 formulation in the alveoli resulting in remarkably longer AUC and AUMC values of the drug in lungs. This is an important requirement for treating the lung fungal infection.

As far as toxicity is concerned, study shows that PLGA nanoparticles without the tamoxifen citrate failed to show any toxicity to viable cells and exhibited viability of 99.11% in MCF7 cell line (Maji *et al.*, 2014). Another study revealed that chitosan coated PLGA nanoparticles showed less toxicity in lung fibroblasts than in cancer cells and interestingly it showed negligible toxicity in normal human bronchial epithelial cells at equivalent drug concentrations used in cancer cells (Babu *et al.*, 2017). Dyawanapelly *et al.*, 2016 found that none of the PLGA nanoparticles or chitosan coated PLGA nanoparticles exhibit cytotoxicity to A549 cells as compared to 1% Triton X-100 as positive control (100% cytotoxic) even at much higher concentrations of 20 mg/mL (Dyawanapelly *et al.*, 2016). Trif and co-workers (2015) found that PLGA and chitosan-PLGA nanoparticles were not cytotoxic at concentrations up to 2500 µg/mL in Madin-Darby bovine kidney and human colorectal adenocarcinoma cells (Trif *et al.*, 2015). Parveen and Sahoo, 2011 showed that void nanoparticles of PLGA and PLGA-chitosan showed no considerable toxicity of 5 days of incubation study in different cell lines used (Parveen and Sahoo, 2011). Chronopoulou *et al.*, 2013 concluded that chitosan coating of DXM loaded PLGA NPs without inducing cytotoxicity permit their uptake by cultured 3T6 and C3A cells (Chronopoulou *et al.*, 2013).

In vivo evaluation of experimentally developed chitosan coated nanoparticles was achieved by gamma scintigraphic imaging of the particles deposited in the lung. Imaging provides information on the amount and localization of Tc-99m-P5 and Tc-99m-P6 deposited in lungs after their administration through pulmonary route. The comparatively more deposition and retention of the nanoformulations was seen in case of chitosan coated formulation in spite of more elimination of chitosan coated formulation from the mice with respect to the non-coated formulation. The non-adhered particles might have eliminated and Tc-99m-P6 was found to eliminate more as compared to Tc-99m-P5. More water affinity of chitosan polymer might have eliminated the non-adhered chitosan coated formulation more and faster in the excretory organ. On the other hand the mucoadhesive nature of the polymer chitosan might overcome the problem of low retaintability of the formulation in lungs and thus helped promoting more and longer retention of the sustained release formulation. With the time (at 3 h and 6 h) there were eventual enhancement of hepatic accumulation of Tc-99m-P6 and Tc-99m-P5 and a simultaneous decrease of them in urinary bladder. It suggests that nanoparticles deposited in the lungs preferentially eliminated through liver.

Chapter 8

Conclusion

8. Conclusion

Lung fungal infection has been increasing the death burden day by day. Treatment with potent antifungals does not warrant complete cure with conventional methods. The present work has provided an optimized method for the development of nanoscale size chitosan coated PLGA nanoparticulate drug delivery system containing voriconazole for successful delivery and treatment of fungal infection in lung. The outcome of the present investigation proposes a novel formulation of TNPs, prepared by a multiple emulsion solvent evaporation technique. The method provided stable optimized nanoparticles after a profound understanding of the inherent relationship between formulation variables and the desired responses. The anticipated range of particle size, zeta potential, drug loading, encapsulation efficiency, are found in desired range. Morphological studies demonstrated smooth and spherical shape of the nanoparticles without any aggregation. The drug release profile showed initial burst release followed by sustained drug release. The confocal images of lung tissue showed an adequate distribution of the fluorescent NPs throughout the tissue. Pharmacokinetic studies performed following pulmonary administration in healthy Swiss Albino mice displayed enhanced systemic bioavailability with much higher MRT value. Further studies presented on the present thesis indicate that the administration of inhalable chitosan coated PLGA nanoparticles led to predominantly prolonged retention of the NPs in the lung as well as in plasma as compared to the PLGA nanoparticles and free voriconazole. We believe that this improvement was caused by the enhancement of mucoadhesion effect owing to the surface coating using chitosan and sustained drug release was obtained due to the presence of both the PLGA and chitosan. Experimental nanoparticles intended for pulmonary delivery may have considerable pharmaceutical potential in the treatment of lung fungal infection.

Chapter 9

Summary

9. Summary

Various drug administration methods have been in research till date for delivering drug to the lungs. Local delivery of medications to the lungs is highly desirable, especially in patients with specific pulmonary diseases such as cystic fibrosis, chronic pulmonary infections, lung cancer, asthma, etc., where conventional therapy seems to be ineffective to maintain the desired drug concentration in lung for a prolonged period of time. PLGA nanoparticles have been widely used in research in the past few decades and are also known for their capability of sustaining drug in the pulmonary region. The advantages of modifying the surface of PLGA particles with a mucoadhesive polymer, such as chitosan, may include the predominant variation or even inversion of zeta-potential, ability to promote cellular adhesion and retention of the drug delivery system at the target site. The specific advantage of nanoparticles coated with chitosan for pulmonary delivery is the retention of the formulation in the pulmonary site of infection for a longer time period than that of chitosan-free nanoparticles providing effective treatment, curbing the phagocytic effects and thereby enhancing the longevity of the nanoparticles in the biological system.

Voriconazole, the first available second-generation triazole group of antifungal agent from the 'azole' family, possesses broad-spectrum activity against resistant fungal species such as *Aspergillus*, *Candida*, *Scedosporium* and *Fusarium*. Antifungal effect of voriconazole exerts by altering the fungal cell membrane by blocking synthesis of ergosterol that converts lanosterol to ergosterol, affecting the integrity and function of the fungal membrane.

The objective of the present study was to prepare, characterize and deliver mucoadhesive PLGA nanoparticles containing an antifungal drug (voriconazole) by pulmonary route to treat lung fungal infection. The *in vivo* deposition, pharmacokinetics and biodistribution of the drug was detected and compared with the non-coated PLGA nanoparticles.

In this study mucoadhesive nanoparticles have been prepared by using different types of biodegradable polymers such as PLGA and chitosan by multiple emulsion solvent evaporation method. Various critical formulation and process parameters were optimized in order to keep the size of the final formulation within ≤ 500 nm along with the satisfactory physicochemical properties. Here, we have investigated both qualitatively and quantitatively the potential of our

developed formulations to deliver drug in the pulmonary site of infection as well as in plasma *in vivo*.

Initially the drug-excipient interaction study was conducted by FTIR spectroscopy and the data showed that there was no chemical interaction between the excipients namely, PLGA, PVA and chitosan used for the preparation of nanoparticles and the drug, voriconazole. By selecting specific conditions and process parameters, we had prepared a numbers of voriconazole loaded PLGA nanoparticles (P5) and chitosan coated voriconazole loaded PLGA nanoparticles (P6). Based on their physicochemical characterization data namely data of FTIR spectroscopy, drug loading and drug encapsulation efficiency, P5 (voriconazole loaded PLGA nanoparticles) and P6 (chitosan coated voriconazole loaded PLGA nanoparticles) were selected for further *in vitro* characterization and *in vivo* study and reported here.

The Malvern particle size analyzer data showed that particle size of P5 and P6 were 154.6 nm and 277 nm, respectively. The surface charges of P5 and P6 were found to be -14.8 mV and 31.9 mV, respectively. Presence of terminal carboxyl group in the PLGA polymer provided negative surface charge in the uncoated nanoparticles, while positive surface charge of the coated nanoparticles was due to the presence of amino group of chitosan. The drug loading of P5 and P6 formulations were 35.62% and 28.57% with the drug encapsulation efficiency of 71.24% and 68.57%, respectively. The particle size and size distribution analysis were further substantiated by FESEM, AFM and Cryo-TEM study. FESEM images revealed that experimental formulations were spherical in shape with smooth surface. In non-coated formulations, most of the particles were below 500 nm in size and the particles of the coated nanoparticle formulation were little bit larger than those of the non-coated formulation. But the surface coating was not distinguished properly by FESEM data. The surface coating of chitosan onto the PLGA nanoparticles were confirmed by Cryo-TEM and TEM images. AFM image showed that the particles of both the formulations were purely spherical in shape and the surface was coated with chitosan was smooth.

Both the experimental formulations had more or less similar drug release pattern in phosphate buffer saline, pH 7.4 (PBS) up to 8 days. The drug released from the experimental formulations initially at a faster rate up to 24 h and then at a slower rate in a sustained manner up

to 8 days. After 8 d, 74.76% and 68.12% of drug released from formulations, P5 and P6, respectively in PBS. A distinct difference was observed for drug released in simulated lung fluid, pH 7.4. After 5 d, drug release values were 64% and 81% from P5 and P6, respectively.

Maximum deposition of particles from formulations, P5 and P6, were observed at stage 5 (1.1–2.1 μm diameter) of cascade impactor apparatus. Data obtained upon deposition of particles on different stages of cascade impactor showed that particle size obtained in P5 and P6 are relevant (150–300 nm) for deposition in trachea, primary and secondary bronchi, and alveolar region for deep lung penetration. Higher deposition from chitosan coated particles (P6) at stage 0 (9.0–10 μm) to stage 2 (4.7–5.8 μm) and at stage 5 (1.1–2.1 μm), are also suitable for deposition in the pharynx and terminal bronchial area, respectively, of the pulmonary tract.

In vivo deposition at 1 h, 8 h and 24 h after pulmonary administration of FITC containing coated and non-coated formulations in the lungs have been confirmed by confocal images. The result revealed that nanoparticles penetrated into the lung tissue cell membrane and were distributed uniformly in the alveoli. In addition, the green fluorescent intensity in the cells augmented with time as measured by ImageJ analysis. For both the formulations at different time points (1 h, 8 h, and 24 h), the corrected total cell fluorescence (CTCF) value decreased with time in case of non-coated nanoparticles whereas the value increased gradually with time for chitosan coated nanoparticles.

Voriconazole levels in blood and lungs were determined at six different time points up to 72 h after single dose administration of both types of nanoparticles containing voriconazole as well as free drug given through pulmonary route and different pharmacokinetic parameters were found out. Both the nanoparticles showed sustained drug release profile for up to 72 h in comparison to the free voriconazole. Our formulation showed to maintain the plasma concentration of voriconazole above minimum inhibitory concentration (MIC) required for effective treatment of lung fungal infection. The mean residence time (MRT) and the half life ($t_{1/2}$) of voriconazole were found to increase in both plasma and lung for chitosan-coated nanoparticles as compared to the non-coated nanoparticles and free drug. Study shows that left lung lobe had the highest voriconazole concentration, while, distribution of drug in the middle lobe was found to have the lowest value during the entire study duration (i.e., 72 h).

The formulation P5 and P6 containing voriconazole were radiolabeled with Tc-99m with more than 95% efficiency. Gamma scintigraphy pictures of animals which received Tc-99m-P5 and Tc-99m-P6 by pulmonary route showed that Tc-99m-P6 accumulated predominantly more in lungs and urinary bladder at 3 h after its pulmonary administration. Interestingly, at 6 h after its administration, it was found to accumulate more in liver and simultaneously there was a decrease in urinary bladder. Similar phenomenon was observed in animals after pulmonary administration of Tc-99m-P5 at 3 h and 6 h with a lesser signal than P6.

The experimentally developed nanoparticles have thus been found to be an emerging way to deliver the drug in the lung and this could be a successful strategy to treat lung fungal infection using voriconazole.

Chapter 10

References

10. References

- Addrizzo-Harris DJ, Harkin TJ, McGuinness G, Naidich DP, Rom WN. Pulmonary aspergilloma and AIDS: a comparison of HIV infected and HIV-negative individuals. *Chest*. 1997;111:612-618.
- Ahagon A, Gent AN. Effect of interfacial bonding on the strength of adhesion. *J. Polym. Sci. Polym. Phys.* 1975;13:1285-1300.
- Al-Qadi S, Grenha A, Remuñán-López C. Microspheres loaded with polysaccharide nanoparticles for pulmonary delivery: Preparation, structure and surface analysis. *Carbohydrate polymers*. 2011;86(1):25-34.
- Alvarez CA, Wiederhold NP, McConville JT, Peters JI, Najvar LK, Graybill JR, *et al.* Aerosolized nanostructured itraconazole as prophylaxis against invasive pulmonary aspergillosis. *Journal of infection*. 2007;55(1):68-74.
- Amaral AC, Bocca AL, Ribeiro AM, Nunes J, Peixoto DL, Simioni AR, *et al.* Amphotericin B in poly(lactic-co-glycolic acid) (PLGA) and dimercaptosuccinic acid (DMSA) nanoparticles against paracoccidioidomycosis. *The Journal of antimicrobial chemotherapy*. 2009;63:526-533.
- Ampel NM. Coccidioidomycosis. In: Kauffman CA, Pappas PG, Sobel JD, Dismukes WE. (Eds.), *Essentials of Clinical Mycology*. Springer, New York, 2011; pp. 349-366.
- Arakawa H, Niimi H, Kurihara Y, Nakajima Y, Webb WR. Expiratory high-resolution CT: diagnostic value in diffuse lung diseases. *American Journal of Roentgenology*. 2000;175(6):1537-1543.
- Ashurst II, Malton A, Prime D, Sumbly B. Latest advances in the development of dry powder inhalers. *Pharmaceutical Science & Technology Today*. 2000;3:246-256.
- Averineni RK, Shavi GV, Gurram AK, Deshpande PB, Arumugam K, Maliyakkal N, *et al.* PLGA 50:50 nanoparticles of paclitaxel: Development, in vitro anti-tumor activity in BT - 549 cells and in vivo evaluation. *Bulletin of Material Science*. 2012;35(3):319-326.
- Babu A, Amreddy N, Muralidharan R, Pathuri G, Gali H, Chen A, *et al.* Chemodrug delivery using integrin-targeted PLGA-Chitosan nanoparticle for lung cancer therapy. *Scientific Reports*. 2017;7(1):14674.
- Babu A, Templeton AK, Munshi A, Ramesh R. Nanoparticle-based drug delivery for therapy of lung cancer: progress and challenges. *Journal of Nanomaterials*. 2013;2013:1-11.
- Baddley JW, Perfect JR, Oster RA, Larsen RA, Pankey GA, Henderson H, Haas DW, Kauffman CA, Patel R, Zaas AK, Pappas PG. Pulmonary cryptococcosis in patients without HIV infection: factors associated with disseminated disease. *European Journal of Clinical Microbiology & Infectious Diseases*. 2008;27:937-943.

- Banker GS, Rhodes TR. *Modern Pharmaceutics*, Marcel Dekker, New York, 2002; pp. 529-586.
- Begat P, Morton DAV, Staniforth JN, Price R. The cohesive adhesive balances in dry-powder inhaler formulations II: influence on fine particle delivery characteristics. *Pharm. Res.* 2004;21:1826-1833.
- Boddupalli BM, Mohammed ZN, Nath RA, Banji D. Mucoadhesive drug delivery system: An overview. *Journal of advanced pharmaceutical technology & research.* 2010;1(4):381-387.
- Borgstrom L, Derom E, Stahl E, Wahlin-Boll E, Pauwels R. The inhalation device influences lung deposition and bronchodilating effect of terbutaline. *Am. J. Respir. Crit. Care Med.* 1996;153:1636-1640.
- Bowden R, Chandrasekar P, White MH, Li X, Pietrelli L, Gurwith M, van Burik JA, Laverdiere M, Safrin S, Wingard JR. A double-blind, randomized, controlled trial of amphotericin B colloidal dispersion versus amphotericin B for treatment of invasive aspergillosis in immunocompromised patients. *Clin. Infect. Dis.* 2002;35:359-366.
- Brown GD, Denning DW, Gow NA, Levitz SM, Netea MG, White TC. Hidden killers: human fungal infections. *Sci. Transl. Med.* 2012;4(165):165rv13.
- Buchanan CM, Buchanan NL, Edgar KJ, Ramsey MG. Solubility and dissolution studies of antifungal drug: hydroxybutenyl- β -cyclodextrin complexes. *Cellulose.* 2007;14(1):35-47.
- Byrnes EJ III, Bildfell RJ, Frank SA, Mitchell TG, Marr KA, Heitman J. Molecular evidence that the range of the Vancouver Island outbreak of *Cryptococcus gattii* infection has expanded into the Pacific northwest in the United States. *J. Infect. Dis.* 2009;199:1081-1086.
- Chalikwar SS, Mene BS, Pardeshi CV, Belgamwar VS, Surana SJ. Self-assembled, chitosan grafted PLGA nanoparticles for intranasal delivery: Design, development and ex vivo characterization. *Polymer-Plastics Technology and Engineering.* 2013;52(4):368-80.
- Chang, WC, Tzao C, Hsu HH, Lee SC, Huang KL, Tung HJ, Chen CY. Pulmonary cryptococcosis: comparison of clinical and radiographic characteristics in immunocompetent and immunocompromised patients. *Chest.* 2006;129:333-340.
- Chapman SW, Dismukes WE, Proia LA, Bradsher RW, Pappas PG, Threlkeld MG, Kauffman CA. Clinical practice guidelines for the management of blastomycosis: 2008 update by the Infectious Diseases Society of America. *Clin. Infect. Dis.* 2008;46:1801:1812.
- Chen M, Gao S, Dong M, Song J, Yang C, Howard KA, Kjemis J, Besenbacher F. Chitosan/siRNA nanoparticles encapsulated in PLGA nanofibers for siRNA delivery. *ACS nano.* 2012;6(6):4835-44.
- Chronopoulou L, Massimi M, Giardi MF, Cametti C, Devirgiliis LC, Dentini M, Palocci C. Chitosan-coated PLGA nanoparticles: a sustained drug release strategy for cell cultures. *Colloids Surf. B. Biointerfaces.* 2013;103:310-317.

- Chung H, Lee H, Han H, An H, Lim KS, Lee YJ, *et al.* A pharmacokinetic comparison of two voriconazole formulations and the effect of CYP2C19 polymorphism on their pharmacokinetic profiles. *Drug Des. Devel. Ther.* 2015;9:2609-2616.
- Codrons V, Vanderbist F, Verbeeck RK, Arras M, Lison D, Pr at V, Vanbever R. Systemic delivery of parathyroid hormone (1-34) using inhalation dry powders in rats. *J. Pharm. Sci.* 2003;92:938-950.
- Cook S, Confer J. Assessment and treatment of fungal lung infections. *US Pharm.* 2011;36(7):HS-17–HS-24.
- Crawford R, Dogdas B, Keough E, Haas RM, Wepukhulu W, Krotzer S, *et al.* Analysis of lipid nanoparticles by Cryo-EM for characterizing siRNA delivery vehicles. *International journal of pharmaceutics.* 2011;403(1-2):237-44.
- Cuming RS, Abarca EM, Duran S, Wooldridge AA, Stewart AJ, Ravis W, *et al.* Development of a sustained-release voriconazole-containing thermogel for subconjunctival injection in horses. *Investigative ophthalmology & visual science.* 2017;58(5):2746-54.
- Da Silva AL, Santos R, Xisto D, Alonso SV, Morales MM, Rocco PRM. Nanoparticle-based therapy for respiratory diseases. *An. Acad. Bras. Cienc.* 2013;85(1):137-146.
- Dailey LA, Jekel N, Fink L, Gessler T, Schmehl T, Wittmar M, Kissel T, Seeger W. Investigation of the proinflammatory potential of biodegradable nanoparticle drug delivery systems in the lung. *Toxicol. Appl. Pharmacol.* 2006;215:100-108.
- Dalby R, Suman J. Inhalation therapy: technological milestones in asthma treatment. *Adv. Drug Deliv. Rev.* 2003;55:779-791.
- Darder M, Colilla M, Ruiz-hitzky E. Biopolymer-clay nanocomposites based on chitosan intercalated in montmorillonite. *Chem. Mater.* 2003;15:3774-3780.
- Das PJ, Paul P, Mukherjee B, Mazumder B, Mondal L, Baishya R, Debnath MC, Dey KS. Pulmonary delivery of voriconazole loaded nanoparticles providing a prolonged drug level in lungs- a promise for treating fungal infection. *Mol. Pharm.* 2015;12(8):2651-2664.
- Dash S, Murthy PN, Nath L, Chowdhury P. Kinetic modeling on drug release from controlled drug delivery systems. *Acta Pol. Pharm.* 2010;67(3):217-223.
- de Sa FA, Taveira SF, Gelfuso GM, Lima EM, Gratieri T. Liposomal voriconazole (VOR) formulation for improved ocular delivery. *Colloids Surf. B Biointerfaces.* 2015;133:331-338.
- Denning DW, Riniotis K, Dobrashian R, Sambatakou H. Chronic cavitary and fibrosing pulmonary and pleural aspergillosis: case series, proposed nomenclature change, and review. *Clin. Infect. Dis.* 2003;37:S265-S280.

- Dey NS, Mukherjee B, Maji R, Satapathy BS. Development of linker-conjugated nanosize lipid vesicles: a strategy for cell selective treatment in breast cancer. *Curr. Cancer Drug Targets*. 2016;16(4):357-372.
- Dodou D, Breedveld P, Wieringa P. Mucoadhesives in the gastrointestinal tract: revisiting the literature for novel applications. *Eur. J. Pharm. Biopharm*. 2005;60:1-16.
- Drake R, Vogl AW, Mitchell AW. *Gray's Anatomy for Students E-Book*. Elsevier Health Sciences; 2009.
- Duret C, Wauthoz N, Sebti T, Vanderbist F, Amighi K. New inhalation-optimized itraconazole nanoparticle-based dry powders for the treatment of invasive pulmonary aspergillosis. *Int. J. Nanomedicine*. 2012;7:5475-5489.
- Dyawanapelly S, Koli U, Dharamdasani V, Jain R, Dandekar P. Improved mucoadhesion and cell uptake of chitosan and chitosan oligosaccharide surface-modified polymer nanoparticles for mucosal delivery of proteins. *Drug Deliv. Transl. Res.* 2016;6(4):365-79.
- Erjavec Z, Kluin Nelemans H, Verweij PE. Trends in invasive fungal infections, with emphasis on invasive aspergillosis. *Clin. Microbiol. Infect*. 2009;15:625-633.
- Feldmann DP, Merkel OM. The advantages of pulmonary delivery of therapeutic siRNA. *Therapeutic delivery*. 2015;6(4):407-9.
- Flume P, Klepser ME. The rationale for aerosolized antibiotics. *Pharmacother*. 2002;22:71-79.
- Freifeld A, Proia L, Andes D, Baddour LM, Blair J, Spellberg B, Arnold S, Lentnek A, Wheat LJ. Voriconazole use for endemic fungal infections. *Antimicrob. Agents Chemother*. 2009;53:1648-1651.
- Füredi P, Pápay ZE, Kovács K, Kiss BD, Ludányi K, Antal I, Klebovich I. Development and characterization of the voriconazole loaded lipid-based nanoparticles. *Journal of pharmaceutical and biomedical analysis*. 2017;132:184-9.
- Galgiani JN, Ampel NM, Blair JE, Catanzaro A, Johnson RH, Stevens DA, Williams PL. Coccidioidomycosis. *Clin. Infect. Dis*. 2005;41:1217-1223.
- Gelperina S, Kisich K, Iseman MD, Heifets L. The potential advantages of nanoparticle drug delivery systems in chemotherapy of tuberculosis. *Am. J. Respir. Crit. Care. Med*. 2005;172(12):1487-1490.
- Gessler T, Schmehl T, Olschewski H, Grimminger F, Seeger W. Aerosolized vasodilators in pulmonary hypertension. *J. Aerosol Med*. 2002;15:117-122.
- Gessler T, Seeger W, Schmehl T. Inhaled prostanoids in the therapy of pulmonary hypertension. *J. Aerosol Med. Pulm. Drug Deliv*. 2008;21(1):1-12.

- Ghosh S, Mondal L, Chakraborty S, Mukherjee B. Early stage HIV management and reduction of stavudine-induced hepatotoxicity in rats by experimentally developed biodegradable nanoparticles. *AAPS PharmSciTech*. 2017;18(3):697-709.
- Gilgado F, Cano J, Gené J, Serena C, Guarro J. Different virulence of the species of the *Pseudallescheria boydii* complex. *Med. Mycol*. 2009;47:371-374.
- Giraud V, Roche N. Misuse of corticosteroid metered-dose inhaler is associated with decreased asthma stability. *Eur. Respir. J*. 2002;19(2):246-251.
- Goel A, Baboota S, Sahni JK, Ali J. Exploring targeted pulmonary delivery for treatment of lung cancer. *Int. J. Pharm. Investig*. 2013;3:8-14.
- Gray H and Standring S. *Gray's anatomy: the anatomical basis of clinical practice*. Churchill Livingstone. London, UK, 2008.
- Greenberger PA. Allergic bronchopulmonary aspergillosis. *J. Allergy Clin. Immunol*. 2002;110:685-692.
- Greer ND. Voriconazole: the newest triazole antifungal agent. *Proceedings (Baylor University Medical Center)*. 2003;16(2):241-248.
- Griese M, Schams A, Lohmeier KP. Amphotericin B and pulmonary surfactant. *European journal of medical research*. 1998;3(8):383-6.
- Guo C, Gemeinhart RA. Understanding the adsorption mechanism of chitosan onto poly (lactide-co-glycolide) particles. *European Journal of Pharmaceutics and Biopharmaceutics*. 2008;70(2):597-604.
- Helvig S, Azmi IDM, Moghimi SM, Yaghmur A. Recent advances in cryo-TEM imaging of soft lipid nanoparticles. *AIMS Biophysics*. 2015;2(2):116-130.
- Ho DY, Lee JD, Rosso F, Montoya J G. Treating disseminated fusariosis: amphotericin B, voriconazole, or both? *Mycoses*. 2007;50:227-231.
- Hoeben BJ, Burgess DS, McConville JT, Najvar LK, Talbert RL, Peters JI, *et al*. In vivo efficacy of aerosolized nanostructured itraconazole formulations for prevention of invasive pulmonary aspergillosis. *Antimicrobial agents and chemotherapy*. 2006;50(4):1552-4.
- Hope WW, Walsh TJ, Denning DW. The invasive and saprophytic syndromes due to *Aspergillus* spp. *Med. Mycol*. 2005;43:S207-S238.
- <http://aerosol.ees.ufl.edu/respiratory/section04.html>
- <https://tisch-env.com/wp-content/uploads/2015/06/TE-20-800-Non-viable-Cascade-Impactor.pdf>
(date 16th May 2017)
- <https://www.gaffi.org/why/fungal-disease-frequency/>

- Hu M, Qian L, Briñas RP, Lyman ES, Kuznetsova L, Hainfeld JF. Gold nanoparticle–protein arrays improve resolution for cryo-electron microscopy. *Journal of structural biology*. 2008;161(1):83-91.
- Husain S, Alexander BD, Munoz P, Avery RK, Houston S, Pruett T, Jacobs R, Dominguez EA, Tollemar JG, Baumgarten K, Yu CM, Wagener MM, Linden P, Kusne S, Singh N. Opportunistic mycelia fungi in organ transplant recipients: emerging importance of non-*Aspergillus* mycelial fungi. *Clin. Infect. Dis*. 2003;37:221-229.
- Ing LY, Zin NM, Sarwar A, Katas H. Antifungal activity of chitosan nanoparticles and correlation with their physical properties. *Int. J. Biomater*. 2012;2012:632698.
- Italia JL, Sharp A, Carter KC, Warn P, Kumar MR. Peroral amphotericin B polymer nanoparticles lead to comparable or superior *in vivo* antifungal activity to that of intravenous Ambisome® or Fungizone™. *PLoS One*. 2011;6(10):e25744.
- Italia JL, Yahya MM, Singh D, Kumar MR. Biodegradable nanoparticles improve oral bioavailability of amphotericin B and show reduced nephrotoxicity compared to intravenous Fungizone®. *Pharmaceutical research*. 2009;26(6):1324-31.
- Jafarinejad S, Gilani K, Moazeni E, Ghazi-Khansari M, Najafabadi AR, Mohajel N. Development of chitosan-based nanoparticles for pulmonary delivery of itraconazole as dry powder formulation. *Powder Technol*. 2012;222:65-70.
- Jeans AR, Howard SJ, Al-Nakeeb Z, Goodwin J, Gregson L, Warn PA, Hope WW. Combination of voriconazole and anidulafungin for treatment of triazole-resistant *aspergillusfumigatus* in an *in vitro* model of invasive pulmonary aspergillosis. *Antimicrob Agents Chemother*. 2012;56(10):5180-5185.
- Jeu L, Piacenti FJ, Lyakhovetskiy AG, Fung HB. Voriconazole. *Clinical therapeutics*. 2003;25(5):1321-81.
- Kan SL, Li J, Liu JP, He HL, Zhang WZ. Evaluation of pharmacokinetics and pharmacodynamics relationships for salvianolic acid B micro-porous osmotic pump pellets in angina pectoris rabbit. *AJPS*. 2014;9(3):137-145.
- Kauffman CA. Histoplasmosis: clinical and laboratory update. *Clin. Microbiol. Rev*. 2007;20:115-132.
- Khanmohammadi M, Elmizadeh H, Ghasemi K. Investigation of Size and Morphology of Chitosan Nanoparticles Used in Drug Delivery System Employing Chemometric Technique. *Iranian Journal of Pharmaceutical Research : IJPR*. 2015;14(3):665-675.
- Khare A, Singh I, Pawar P, Grover K. Design and evaluation of voriconazole loaded solid lipid nanoparticles for ophthalmic application. *Journal of drug delivery*. 2016;2016: 6590361.

- Kirkpatrick WR, Najvar LK, Vallor AC, Wiederhold NP, Bocanegra R, Pfeiffer J, *et al.* Prophylactic efficacy of single dose pulmonary administration of amphotericin B inhalation powder in a guinea pig model of invasive pulmonary aspergillosis. *Journal of antimicrobial chemotherapy.* 2012;67(4):970-6.
- Klapetek P, Valtr M, Nečas D, Salyk O, Dzik P. Atomic force microscopy analysis of nanoparticles in non-ideal conditions. *Nanoscale Research Letters.* 2011;6(1):514.
- Koepfen BM, Stanton BA. *Berne and Levy Physiology.* 2008;6:338-340.
- Kontoyiannis DP, Marr KA, Park BJ, Alexander BD, Anaissie EJ, Walsh TJ, *et al.* Prospective surveillance for invasive fungal infections in hematopoietic stem cell transplant recipients, 2001-2006: overview of the Transplant. Associated Infection Surveillance Network (TRANSNET) database. *Clin. Infect. Dis.* 2010;50:1091-1100.
- Kudgus RA, Walden CA, McGovern RM, Reid JM, Robertson JD, Mukherjee P. Tuning pharmacokinetics and biodistribution of a targeted drug delivery system through incorporation of a passive targeting component. *Sci. Rep.* 2014;4:1-6.
- Kumar MR, Bakowsky U, Lehr CM. Preparation and characterization of cationic PLGA nanospheres as DNA carriers. *Biomaterials.* 2004;25(10):1771-7.
- Kumirska J, Czerwicka M, Kaczyński Z, Bychowska A, Brzozowski K, Thöming J, Stepnowski P. Application of spectroscopic methods for structural analysis of chitin and chitosan. *Mar. Drugs.* 2010;8(5):1567-1636.
- Kurtz MB, Bernard EM, Edwards FF, Marrinan JA, Dropinski J, Douglas CM, Armstrong D. Aerosol and parenteral pneumocandins are effective in a rat model of pulmonary aspergillosis. *Antimicrobial agents and chemotherapy.* 1995;39(8):1784-9.
- Kuzmov A, Minko T. Nanotechnology approaches for inhalation treatment of lung diseases. *J. Control. Release.* 2015;219:500-518.
- Laan AC, Denkova AG. Cryogenic transmission electron microscopy: the technique of choice for the characterization of polymeric nanocarriers. *EJNMMI Res.* 2017;7(1):44.
- Lai-Fook SJ. Pleural mechanics and fluid exchange. *Physiol. Rev.* 2004;84:385-410.
- Lat A, Thompson III GR. Update on the optimal use of voriconazole for invasive fungal infections. *Infection and drug resistance.* 2011;4:43-53.
- Lee C, Choi JS, Kim I, Oh KT, Lee ES, Park ES, Lee KC, Youn YS. Long-acting inhalable chitosan-coated (polylactic-co-glycolic acid) nanoparticles containing hydrophobically modified exendin-4 for treating type 2 diabetes. *Int. J. Nanomedicine.* 2013;8:2975-2983.
- Lee PP, Lau YL. Cellular and Molecular Defects Underlying Invasive Fungal Infections—Revelations from Endemic Mycoses. *Frontiers in immunology.* 2017;8:735.

- Lee WH, Loo CY, Traini D, Young PM. Inhalation of nanoparticle-based drug for lung cancer treatment: Advantages and challenges. *AJPS*. 2015;10(6):481-489.
- Lemoine D, Francois C, Kedzierewicz F, Preat V, Hoffman M, Maincent P. Stability study of nanoparticles of poly (ϵ -caprolactone), poly (d, l-lactide) and poly (d, l-lactide-co-glycolide). *Biomaterials*. 1996;17(22):2191-7.
- Lewis RE, Albert ND, Liao G, Hou J, Prince RA, Kontoyiannis DP. Comparative pharmacodynamics of amphotericin B lipid complex and liposomal amphotericin B in a murine model of pulmonary mucormycosis. *Antimicrob. Agents Chemother*. 2010;54:1298-1304.
- Limper AH, Knox KS, Sarosi GA, Ampel NM, Bennett J.E, Catanzaro A, *et al*. An official american thoracic society statement: treatment of fungal infections in adult pulmonary and critical care patients. *Am. J. Respir. Crit. Care Med*. 2011;183:96-128.
- Lin SC, Lin SW, Chen JM, Kuo CH. Using sweeping-micellar electrokinetic chromatography to determine voriconazole in patient plasma. *Talanta*. 2010;82(2):653-659.
- Liu J, Gong T, Fu H, Wang C, Wang X, Chen Q, Zhang Q, He Q, Zhang Z. Solid lipid nanoparticles for pulmonary delivery of insulin. *Int. J. Pharm*. 2008;356(1-2):333-344.
- Lortholary O, Obenga G, Biswas P, Caillot D, Chachaty E, Bienvenu AL, *et al*. International retrospective analysis of 73 cases of invasive fusariosis treated with voriconazole. *Antimicrob. Agents Chemother*. 2010;54:4446-4450.
- Ludwig DB, de Camargo LE, Khalil NM, Auler ME, Mainardes RM. Antifungal activity of chitosan-coated poly (lactic-co-glycolic) acid nanoparticles containing amphotericin B. *Mycopathologia*. 2018:1-0.
- Ma W, Lu S, Pan P, Sadatmousavi P, Yuan Y, Chen P. Pharmacokinetics of peptide mediated delivery of anticancer drug ellipticine. *Plos One*. 2012;7(8):1-6.
- Madsen F, Eberth K, Smart J. A rheological examination of the mucoadhesive/mucus interaction: the effect of mucoadhesive type and concentration. *J. Control. Release*. 1998;50:167-178.
- Maji R, Dey NS, Satapathy BS, Mukherjee B, Mondal S. Preparation and characterization of tamoxifen citrate loaded nanoparticles for breast cancer therapy. *Int. J. Nanomedicine*. 2014;9:3107-3118.
- Makadia HK, Siegel SJ. Poly lactic-co-glycolic acid (PLGA) as biodegradable controlled drug delivery carrier. *Polymers*. 2011;3(3):1377-1397.
- Mangal S, Gao W, Li T, Zhou QT. Pulmonary delivery of nanoparticle chemotherapy for the treatment of lung cancers: challenges and opportunities. *Acta Pharmacologica Sinica*. 2017;38(6):782.

- Mansour HM, Rhee YS, Wu X. Nanomedicine in pulmonary delivery. *Int. J. Nanomedicine*. 2009;4:299-319.
- Marques MRC, Loebenberg R, Almukainzi M. Simulated Biological Fluids with Possible Application in Dissolution Testing. *Dissolution Technol*. 2011;18:15-28.
- Martin NC, Pirie AA, Ford LV, Callaghan CL, McTurk K, Lucy D, Scrimger DG. The use of phosphate buffered saline for the recovery of cells and spermatozoa from swabs. *Science & Justice*. 2006;46:179-184.
- McConville JT, Overhoff KA, Sinswat P, Vaughn JM, Frei BL, Burgess DS, *et al*. Targeted high lung concentrations of itraconazole using nebulized dispersions in a murine model. *Pharmaceutical research*. 2006;23(5):901-11.
- Mitchell JP, Roberts DL. Current approaches to APSD measurements of OIPs based on inertial impaction. In: Tougas, T. P., Jolyon P. Mitchell, J. P. and Lyapustina, S. A. (Eds.), *Good Cascade Impactor Practices, AIM and EDA for Orally Inhaled Products*. Springer, Boston, MA, 2013; pp. 15-55.
- Mittal R, Patel AP, Jhaveri VM, Samantha Kay SI, Debs LH, Parrish JM, Pan DR, Nguyen D, Mittal J, Jayant RD. Recent Advancements in Nanoparticle Based Drug Delivery for Gastrointestinal Disorders. *Expert opinion on drug delivery*. 2018;15(3):301-318.
- Moazeni E, Gilani K, Najafabadi AR, reza Rouini M, Mohajel N, Amini M, Barghi MA. Preparation and evaluation of inhalable itraconazole chitosan based polymeric micelles. *DARU Journal of Pharmaceutical Sciences*. 2012;20(1):85.
- Moen MD, Lyseng-Williamson KA, Scott LJ. Liposomal amphotericin B. *Drugs*. 2009;69(3):361-392.
- Morales-Cruz M, Flores-Fernández GM, Morales-Cruz M, Orellano EA, Rodriguez-Martinez JA, Ruiz M, Griebenow K. Two-step nanoprecipitation for the production of protein-loaded PLGA nanospheres. *Results in pharma sciences*. 2012;2:79-85.
- Mukherjee B, Paul P, Dutta L, Chakraborty S, Dhara M, Mondal L, Sengupta S. Pulmonary administration of biodegradable drug nanocarriers for more efficacious treatment for fungal infections in lungs: insights based on recent findings. In: Grumezescu, A.M. (Ed.), *Multifunctional system for combined delivery, Biosensing and diagnostic*; Elsevier, Netherlands, 2017, pp. 261-280.
- Murakami H, Kobayashi M, Takeuchi H, Kawashima Y. Preparation of poly (DL-lactide-co-glycolide) nanoparticles by modified spontaneous emulsification solvent diffusion method. *International journal of pharmaceutics*. 1999;187(2):143-52.

- Nahar M, Jain NK. Preparation, characterization and evaluation of targeting potential of amphotericin B-loaded engineered PLGA nanoparticles. *Pharmaceutical research*. 2009;26(12):2588.
- Naithani R, Kumar R. Voriconazole. *Indian Pediatr*. 2005;42:1207-1212.
- Nandagiri VK, Gentile P, Chiono V, Tonda-Turo C, Matsiko A, Ramtoola Z, *et al*. Incorporation of PLGA nanoparticles into porous chitosan–gelatin scaffolds: influence on the physical properties and cell behavior. *Journal of the mechanical behavior of biomedical materials*. 2011;4(7):1318-27.
- Norwood DL, Prime D, Downey BP, Creasey J, Sethi SK, Haywood P. Analysis of polycyclic aromatic hydrocarbons in metered dose inhaler drug formulations by isotope dilution gas chromatography/ mass spectrometry. *J. Pharm. Biomed. Anal*. 1995;13:293-304.
- Nucci M, Anaissie E. Cutaneous infection by *Fusarium* species in healthy and immunocompromised hosts: implications for diagnosis and management. *Clin. Infect. Dis*. 2002;35:909-920.
- Ochiuz L, Grigoras C, Popa M, Stoleriu I, Munteanu C, Timofte D, Profire L, Grigoras AG. Alendronate-loaded modified drug delivery lipid particles intended for improved oral and topical administration. *Molecules*. 2016;21(7):pii: E858.
- Pal M. Efficacy of Narayan stain for morphological studies of moulds, yeasts and algae. *Revista iberoamericana De micologia*. 2004;21:219.
- Pal M. Morbidity and mortality due to fungal infections. *J. Appl. Microbiol. Biochem*. 2017;1:1–3.
- Pal M. Use of Pal’s sunflower seed medium for an early diagnosis of cryptococcosis. *The Antiseptic*. 1997;95:175.
- Paluszkiwicz C, Stodolak E, Hasik M, Blazewicz M. FT-IR study of montmorillonite–chitosan nanocomposite materials. *Spectrochim. Acta A Mol. Biomol. Spectrosc*. 2011;79:784-788.
- Panda BN. Fungal infections of lungs: the emerging scenario. *Indian J. Tuberc*. 2004;51:63-69.
- Pappas PG, Perfect JR, Cloud GA, Larsen RA, Pankey GA, Lancaster DJ, *et al*. Cryptococcosis in human immunodeficiency virus-negative patients in the era of effective azole therapy. *Clin. Infect. Dis*. 2001;33:690-699.
- Parikh R, Dalwadi S. Preparation and characterization of controlled release poly-ε-caprolactonemicroparticles of isoniazid for drug delivery through pulmonary route. *Powder Technol*. 2014;264:158-165.
- Parveen S, Sahoo SK. Long circulating chitosan/PEG blended PLGA nanoparticle for tumor drug delivery. *Eur. J Pharmacol*. 2011;670(2-3):372-383.

- Patil JS, Sarasija S. Pulmonary drug delivery strategies: A concise, systematic review. *Lung India*. 2012;29(1):44-49.
- Patterson TF, Kirkpatrick WR, White M, Hiemenz JW, Wingard JR, Dupont B. Invasive aspergillosis. Disease spectrum, treatment practices, and outcomes. I3 Aspergillus Study Group. *Medicine (Baltimore)*. 2000;79:250-260.
- Pattnaik G, Sinha B, Mukherjee B, Ghosh S, Basak S, Mondal S, Bera T. Submicron-size biodegradable polymer-based didanosine particles for treating HIV at early stage: an in vitro study. *J. Microencapsul.* 2012;29(7):666-676.
- Peng HS, Liu XJ, Lv GX, Sun B, Kong QF, Zhai DX, *et al.* Voriconazole into PLGA nanoparticles: Improving agglomeration and antifungal efficacy. *International journal of pharmaceutics*. 2008;352(1-2):29-35.
- Perfect JR, Dismukes WE, Dromer F, Goldman DL, Graybill JR, Hamill RJ, *et al.* Clinical practice guidelines for the management of cryptococcal disease: 2010 update by the Infectious Diseases Society of America. *Clin. Infect. Dis.* 2010;50:291-322.
- Raad II, Hachem RY, Herbrecht R, Graybill JR, Hare R, Corcoran G, Kontoyiannis DP. Posaconazole as salvage treatment for invasive fusariosis in patients with underlying hematologic malignancy and other conditions. *Clin. Infect. Dis.* 2006;42:1398-1403.
- Rao A, Schoenenberger M, Gnecco E, Glatzel T, Meyer E, Brändlin D, Scandella L. Characterization of nanoparticles using atomic force microscopy. In *Journal of Physics: Conference Series 2007 (Vol. 61, No. 1, p. 971)*. IOP Publishing.
- Rasband WS, ImageJ, U. S. National Institutes of Health, Bethesda, Maryland, USA, <http://imagej.nih.gov/ij/>, 1997–2015
- Reddy LH, Murthy RS. Pharmacokinetics and biodistribution studies of doxorubicin loaded poly(butyl cyanoacrylate) nanoparticles synthesized by two different techniques. *Biomed Pap. Med. Fac. Univ. Palacky Olomouc Czech Repub.* 2004;148(2):161-166.
- Roberts RA, Shen T, Allen IC, Hasan W, DeSimone JM, Ting JP. Analysis of the murine immune response to pulmonary delivery of precisely fabricated nano-and microscale particles. *PloS one*. 2013;8:e62115.
- Roden MM, Zaoutis TE, Buchanan WL, Knudsen TA, Sarkisova TA, Schaufele RL, Sein M, Sein T, Chiou CC, Chu JH, Kontoyiannis DP, Walsh TJ. Epidemiology and outcome of zygomycosis: a review of 929 reported cases. *Clin. Infect. Dis.* 2005;41:634-653.
- Rodriguez-Tudela JL, Berenguer J, Guarro J, Kantarcioglu AS, Horre R, de Hoog GS, Cuenca-Estrella M. Epidemiology and outcome of *Scedosporium prolificans* infection: a review of 162 cases. *Med. Mycol.* 2009;47:359-370.

- Roy P, Das S, Auddy RG, Mukherjee, A. Engineered andrographolide nanosystems for smart recovery in hepatotoxic conditions. *Int. J. Nanomedicine*. 2014;9:4723-4735.
- Ruijgrok EJ, Vulto AG, Van Etten EW. Aerosol delivery of amphotericin B desoxycholate (Fungizone) and liposomal amphotericin B (AmBisome): aerosol characteristics and in-vivo amphotericin B deposition in rats. *J. Pharm. Pharmacol.* 2000;52, 619-627.
- Saccente M, Woods GL. Clinical and laboratory update on blastomycosis. *Clin. Microbiol. Rev.* 2010;23:367-381.
- Sahana B, Santra K, Basu S, Mukherjee B. Development of biodegradable polymer based tamoxifen citrate loaded nanoparticles and effect of some manufacturing process parameters on them: a physicochemical and *in-vitro* evaluation. *Int. J. Nanomedicine*. 2010;5:621-630.
- Sahasrabudhe N, Gosney JR, Hasleton P. The normal lung: histology, embryology, development, aging and function, in: Hasleton, P., Flieder, D.B. (Eds.), *Spencer's Pathology of the Lung*. Cambridge University Press, Cambridge, 2013; pp.1-40.
- Salama RO, Traini D, Chan HK, Sung A, Ammit AJ, Young PM. Preparation and evaluation of controlled release microparticles for respiratory protein therapy. *J. Pharm. Sci.* 2009;98(8):2709-2717.
- Salem HF, Kharshoum RM, Abdel Hakim LF, Abdelrahim ME. Edge activators and a polycationic polymer enhance the formulation of porous voriconazole nanoagglomerate for the use as a dry powder inhaler. *Journal of liposome research*. 2016;26(4):324-35.
- Sangwan S, Agosti JM, Bauer LA, Otulana BA, Morishige RJ, Cipolla DC, Blanchard JD, Smaldone GC. Aerosolized protein delivery in asthma: Gamma camera analysis of regional deposition and perfusion. *J. Aerosol Med.* 2001;14:185-195.
- Satapathy BS, Mukherjee B, Baishya R, Debnath MC, Dey NS, Maji R. Lipid nanocarrier-based transport of docetaxel across the blood brain barrier. *RSC Adv.* 2016;6(88):85261-85274.
- Sciarra JJ, Cutie AJ. Pharmaceutical Aerosols. In: Lachman L, Lieberman HA, Kanig JL (Eds.), *The Theory and Practice of Industrial Pharmacy*. 3rd ed., Varghese Publishing House, Bombay, 1990; pp. 589-618.
- Seju U, Kumar A, Sawant KK. Development and evaluation of olanzapine-loaded PLGA nanoparticles for nose-to-brain delivery: *in vitro* and *in vivo* studies. *Acta Biomater.* 2011;(12):4169-4176.
- Shaw TK, Mandal D, Dey G, Pal MM, Paul P, Chakraborty S, *et al.* Successful delivery of docetaxel to rat brain using experimentally developed nanoliposome: a treatment strategy for brain tumor. *Drug Deliv.* 2017;24(1):346-357.

- Shirkhani K, Teo I, Armstrong-James D, Shaunak S. Nebulised amphotericin B-polymethacrylic acid nanoparticles prophylaxis prevents invasive aspergillosis. *Nanomedicine*. 2015;11:1217-1226.
- Silva SML, Braga CRC, Fook MVL, Raposo CMO, Carvalho LH, Canedo EL. Analysis of Chitosan/Clay Nanocomposites. In: Theophile, T (Eds.), *Infrared Spectroscopy - Materials Science, Engineering and Technology*. InTech, Croatia, 2012; pp. 43-62.
- Singh R, Lillard JW Jr. Nanoparticle-based targeted drug delivery. *Exp Mol. Pathol.* 2009;86(3):215-223.
- Sinha B, Mukherjee B, Pattnaik G. Poly-lactide-co-glycolide nanoparticles containing voriconazole for pulmonary delivery: in vitro and in vivo study. *Nanomedicine*. 2013;9:94-104.
- Sinha B, Mukherjee B. Development of an inhalation chamber and a dry powder inhaler device for administration of pulmonary medication in animal model. *Drug Dev. Ind. Pharm.* 2012;38:171-179.
- Smart JD. The basics and underlying mechanisms of mucoadhesion. *Adv. Drug Deliv. Rev.* 2005;57:1556-1568.
- Smith JA, Kauffman CA. Blastomycosis. *Proc. Am. Thorac. Soc.* 2010;7:173-180.
- Smith JA, Kauffman CA. Pulmonary fungal infections. *Respirology*. 2012;17:913-926.
- Smola M, Vandamme T, Sokolowski A. Nanocarriers as pulmonary drug delivery systems to treat and to diagnose respiratory and non respiratory diseases. *Int. J. Nanomedicine*. 2008;3(1):1-19.
- Souza TG, Ciminelli VS, Mohallem ND. A comparison of TEM and DLS methods to characterize size distribution of ceramic nanoparticles. In *Journal of Physics: Conference Series* 2016 Jul (Vol. 733, No. 1, p. 012039). IOP Publishing.
- Stefančíková L, Porcel E, Eustache P, Li S, Salado D, Marco S, *et al.* Cell localisation of gadolinium-based nanoparticles and related radiosensitising efficacy in glioblastoma cells. *Cancer Nanotechnol.* 2014;5(1):6.
- Stewart PL. Cryo-electron microscopy and cryo-electron tomography of nanoparticles. *Wiley Interdisciplinary Reviews: Nanomedicine and Nanobiotechnology*. 2017;9(2).
- Sun SB, Liu P, Shao FM, Miao QL. Formulation and evaluation of PLGA nanoparticles loaded capecitabine for prostate cancer. *Int. J. Clin. Exp. Med.* 2015;8(10):19670-19681.
- Taetz S, Nafee N, Beisner J, Piotrowska K, Baldes C, Murdter TE, Huwer H, Schneider M, Schaefer UF, Klotz U, Lehr CM. The influence of chitosan content in cationic chitosan/PLGA nanoparticles on the delivery efficiency of antisense 2'-O-methyl-RNA

- directed against telomerase in lung cancer cells. *Eur. J. Pharm. Biopharm.* 2009;72(2):358-369.
- Tahara K, Yamamoto H, Hirashima N, Kawashima Y. Chitosan-modified poly(d,l-lactide-co-glycolide) nanospheres for improving siRNA delivery and gene-silencing effects. *Eur. J. Pharm. Biopharm.* 2010;74(3):421-426.
- Thompson III GR, Patterson TF. Pulmonary Aspergillosis. *Semin. Respir. Crit. Care Med.* 2008;28:103-110.
- Thorley AJ, Ruenaroengsak P, Potter TE, Tetley TD. Critical Determinants of Uptake and Translocation of Nanoparticles by the Human Pulmonary Alveolar Epithelium. *ACS Nano.* 2014;8(11):11778-11789.
- Tolman JA, Nelson NA, Son YJ, Bosselmann S, Wiederhold NP, Peters JI, *et al.* Characterization and pharmacokinetic analysis of aerosolized aqueous Voriconazole solution. *Eur. J. Pharm. Biopharm.* 2009a;72:199-205.
- Tolman JA, Wiederhold NP, McConville JT, Najvar LK, Bocanegra R, Peters JI, *et al.* Inhaled voriconazole for prevention of invasive pulmonary aspergillosis. *Antimicrobial agents and chemotherapy.* 2009b;53(6):2613-5.
- Tomashefski JF, Cohen AM, Doershuk CF. Longterm histopathologic follow-up of bronchial arteries after therapeutic embolization with polyvinyl alcohol (Ivalon) in patients with cystic fibrosis. *Hum. Pathol.* 1988;19:555-561.
- Torres HA, Kontoyiannis DP. Hyalohyphomycoses (hyaline molds). In: Kauffman, C.A., Pappas, P.G., Sobel, J.D. et al. (Eds.), *Essentials of Clinical Mycology*. 2nd ed. Springer, New York, 2011; pp. 281-304.
- Townsley MI. Structure and composition of pulmonary arteries, capillaries and veins. *Compr. Physiol.* 2012;2:675-709.
- Trif M, Florian PE, Roseanu A, Moisei M, Craciunescu O, Astete CE, Sabliov CM. Cytotoxicity and intracellular fate of PLGA and chitosan-coated PLGA nanoparticles in Madin-Darby bovine kidney (MDBK) and human colorectal adenocarcinoma (Colo 205) cells. *J. Biomed. Mater. Res. A.* 2015;103(11):3599-611.
- Troke P, Aguirrebengoa K, Arteaga C, Ellis D, Heath CH, Lutsar I, *et al.* Treatment of scedosporiosis with voriconazole: clinical experience with 107 patients. *Antimicrob. Agents Chemother.* 2008;52:1743-1750.
- Tuan TQ, Hao PV, Quynh LM, Luong N H, Hai NH. Preparation and Properties of Silver Nanoparticles by Heat-combined Electrochemical Method. *VNU J. Sci. Math. Phys.* 2015;31(2):36-44.

- ud Din F, Aman W, Ullah I, Qureshi OS, Mustapha O, Shafique S, Zeb A. Effective use of nanocarriers as drug delivery systems for the treatment of selected tumors. *Int. J. Nanomedicine*. 2017;12:7291.
- Valdivia L, Nix D, Wright M, Lindberg E, Fagan T, Lieberman D, *et al*. Coccidioidomycosis as a common cause of community-acquired pneumonia. *Emerg. Infect. Dis*. 2006;12:958-962.
- Van de Ven H, Paulussen C, Feijens PB, Matheeußen A, Rombaut P, *et al*. PLGA nanoparticles and nanosuspensions with amphotericin B: potent in vitro and in vivo alternatives to Fungizone and AmBisome. *Journal of controlled release*. 2012;161(3):795-803.
- Varshosaz J, Ghaffari S, Mirshojaei SF, Jafarian A, Atyabi F, Kobarfard F, Azarmi S. Biodistribution of amikacin solid lipid nanoparticles after pulmonary delivery. *BioMed research international*. 2013;2013.
- Venier-Julienne MC, Benoit JP. Preparation, purification and morphology of polymeric nanoparticles as drug carriers. *Pharmaceutica Acta Helvetiae*. 1996;71(2):121-8.
- Verma RK, Pandya S, Misra A. Loading and release of amphotericin-B from biodegradable poly (lactic-co-glycolic acid) nanoparticles. *Journal of biomedical nanotechnology*. 2011;7(1):118-20.
- Videira MA, Botelho MF, Santos AC, Gouveia LF, de Lima JJ, Almeida AJ. Lymphatic uptake of pulmonary delivered radiolabelled solid lipid nanoparticles. *J. Drug Target*. 2002;10(8):607-613.
- Vyas SP, Khatri K, Goyal AK. Functionalized nanocarrier (s) to image and target fungi infected immune cells. *Medical mycology*. 2009;47(Supplement_1):S362-8.
- Walsh TJ, Anaissie EJ, Denning DW, Herbrecht R, Kontoyiannis DP, Marr KA, *et al*. Treatment of aspergillosis: clinical practice guidelines of the Infectious Diseases Society of America. *Clin. Infect. Dis*. 2008;46:327-360.
- Walsh TJ, Raad I, Patterson TF, Chandrasekar P, Donowitz GR, Graybill R, *et al*. Treatment of invasive aspergillosis with posaconazole in patients who are refractory to or intolerant of conventional therapy: an externally controlled trial. *Clin. Infect. Dis*. 2007;44:2-12.
- Wang Q, Jamal S, Detamore MS, Berkland C. PLGA-chitosan/PLGA-alginate nanoparticle blends as biodegradable colloidal gels for seeding human umbilical cord mesenchymal stem cells. *Journal of biomedical materials research Part A*. 2011;96(3):520-7.
- Wang Y, Li P, Kong L. Chitosan-modified PLGA nanoparticles with versatile surface for improved drug delivery. *Aaps Pharmscitech*. 2013;14(2):585-92.
- Watts AB, Williams III RO. Nanoparticles for pulmonary delivery. In: *Controlled pulmonary drug delivery*. Springer New York. 2011; pp. 335-366.

- Wheat LJ, Conces D, Allen SD, Blue-Hnidy D, Loyd J. Pulmonary histoplasmosis syndromes: recognition, diagnosis, and management. *Semin. Respir. Crit. Care Med.* 2004;25:129-144.
- Wheat LJ, Freifeld AG, Kleiman MB, Baddley JW, McKinsey DS, Loyd JE, Kauffman CA. Clinical practice guidelines for the management of patients with histoplasmosis: 2007 update by the Infectious Diseases Society of America. *Clin. Infect. Dis.* 2007;45:807-825.
- Wong-Beringer A, Lambros MP, Beringer PM, Johnson DL. Suitability of caspofungin for aerosol delivery: physicochemical profiling and nebulizer choice. *Chest.* 2005;128(5):3711-6.
- Yang M, Xie S, Adhikari VP, Dong Y, Du Y, Li D. The synergistic fungicidal effect of low-frequency and low-intensity ultrasound with amphotericin B-loaded nanoparticles on *C. albicans* in vitro. *International journal of pharmaceutics.* 2018;542(1-2):232-41.
- Yang R, Yang SG, Shim WS, Cui F, Cheng G, Kim IW, *et al.* Lung-specific delivery of paclitaxel by chitosan-modified PLGA nanoparticles via transient formation of microaggregates. *J. Pharm. Sci.* 2009;98(3):970-984.
- Yu DH, Lu Q, Xie J, Fang C, Chen HZ. Peptide-conjugated biodegradable nanoparticles as a carrier to target paclitaxel to tumor neovasculature. *Biomaterials.* 2010;31(8):2278-2292.
- Yu J, Chien YW. Pulmonary drug delivery: physiologic and mechanistic aspects. *Crit. Rev. Ther. Drug Carrier Syst.* 1997;14:395-453.
- Yuan Q, Shah J, Hein S, Misra RD. Controlled and extended drug release behavior of chitosan-based nanoparticle carrier. *Acta Biomaterialia.* 2010;6:1140-1148.
- Zhang L, Li Y, Zhang Y, Zhu C. Sustained release of isoniazid from polylactide microspheres prepared using solid/oil drug loading method for tuberculosis treatment. *Sci China Life Sci.* 2016;59(7):724-731.
- Zhao K, Zhang Y, Zhang X, Shi C, Wang X, Wang X, Jin Z, Cui S. Chitosan-coated poly(lactic-co-glycolic) acid nanoparticles as an efficient delivery system for Newcastle disease virus DNA vaccine. *Int. J. Nanomedicine.* 2014;9(1):4609-4619.
- Zia Q, Khan AA, Swaleha Z, Owais M. Self-assembled amphotericin B-loaded polyglutamic acid nanoparticles: preparation, characterization and in vitro potential against *Candida albicans*. *Int. J. Nanomedicine.* 2015;10:1769-1790.
- Zmeili OS, Soubani AO. Pulmonary aspergillosis: a clinical update. *QJM.* 2007;100:317-334.
- Zu Y, Sun W, Zhao X, Wang W, Li Y, Ge Y, Liu Y, Wang K. Preparation and characterization of amorphous amphotericin B nanoparticles for oral administration through liquid antisolvent precipitation. *Eur. J. Pharm. Sci.* 2014;53:109-117.

No.SR/WOS-A/LS-1356/2014 (G)
Government of India
Ministry of Science & Technology
Department of Science & Technology

Technology Bhavan
New Mehrauli Road
New Delhi-110 016
Dated 28.07.2015

ORDER

Sub: Financial approval of the project under Women Scientist Scheme A (WOS-A) entitled "Pulmonary delivery of mucoadhesive nanoparticles of an antifungal agent using dry powder inhaler."

PI Ms. Paramita Paul, Department of Pharmaceutical Technology, Jadavpur University, Kolkata-700032, WB.

Sanction of the President is hereby accorded to the above mentioned project at a total cost of ₹ 25,96,000/- (Rupees Twenty Five Lac Ninety Six Thousand only) with a break up of ₹ 5,00,000/- under 'Capital head' and ₹ 20,96,000/- under 'General head' for a duration of Three years. The items of expenditure for which the total allocation of ₹ 25,96,000/- has been approved for Three years are given below:

Sl. No.	Heads	1 st Year	2 nd Year	3 rd Year	Total
A.	Non-Recurring (Capital Items)				
	Equipments: Cold centrifuge, HPLC Column	5,00,000/-	-----	-----	5,00,000/-
B.	Recurring(General)				
	Fellowship for M.Pharma@₹40,000/-	4,80,000/-	4,80,000/-	4,80,000/-	14,40,000/-
	Consumables	1,00,000/-	1,00,000/-	1,00,000/-	3,00,000/-
	Contingencies	20,000/-	20,000/-	20,000/-	60,000/-
	Travel	20,000/-	20,000/-	20,000/-	60,000/-
C.	Overhead	80,000/-	78,000/-	78,000/-	2,36,000/-
D.	Total of Recurring Grant (B+C)	7,00,000/-	6,98,000/-	6,98,000/-	20,96,000/-
E.	GRAND TOTAL (A+D)	12,00,000/-	6,98,000/-	6,98,000/-	25,96,000/-

2. Overhead expenses are meant for the host institute towards the cost for providing infrastructure Facilities and benefits to the staff engaged in the project, etc.

3. Sanction of the grant is subject to the conditions as detailed in website www.online-wosa.gov.in.

4. The sanction of the President is also accorded to the payment of ₹ 5,00,000/- (Rupees Five Lac only) under 'Grants for Creation of Capital Assets' and ₹ 7,00,000/- (Rupees Seven Lac only) under 'Grant-in-aid General' to the Registrar, Jadavpur University, Kolkata-700032, WB being the first installment of the grant for the year 2015-2016 for implementation of the said research project.

C ontd..p/- 2

Dr. Biswajit Mukherjee

M.Pharm., Ph.D., F.I.C., F.I.C.S.

Associate Professor in Pharmaceutics

Coordinator, GMP Model Cell (Pharmacy)

Joint Coordinator,

Centre for Advance Research in Pharmaceutical Sciences,

Jadavpur University, Kolkata

Former DAAD Fellow (Germany) and E-guest Scientist,

German Cancer Research Center (DFG)

Heidelberg, Germany

Indo-Hungarian Education Exchange Fellow,

Budapest, Hungary

Former Fellow Scientist, School of Pharmacy,

University of London, London, U.K.

Ex. Biotechnology Overseas Associate,

Department of Biotechnology

(Government of India) and Worked in DFG

Heidelberg, Germany



Department of Pharmaceutical Technology

JADAVPUR UNIVERSITY

Kolkata - 700 032, India

Phone: +91-33-2474 8677 / 2474 8698 ext. 2306

Res: +91-33-2427 8028

Fax: +91-33-2474 8677 / 8286 (C)

E-mail: biswajit@yahoo.com

To,

Ms. Soumitra Saha

c/o Prof. Biswajit Mukherjee

Dept. of Pharmaceutical Technology

Jadavpur University Kolkata - 82, W.B.

Project title: Pulmonary delivery of mucoadhesive nanoparticles

of an anti-fungal agent using nebulizer or dry powder inhaler

Ref No.: *AEC/PHARM/1406/2014*

Date: *18.12.2014*

Dear Sir/Madam,

As per the meeting of Animal Ethics Committee (AEC), Jadavpur University, held on 09/12/2014, I am pleased to inform you that the AEC, Jadavpur University, has approved your project for fresh /renewal applied to the respective funding agencies. However, you are requested to abide by the following guidelines-

- 1) All the animal experiments should be conducted strictly following the guidelines of CPCSEA (Govt. of India) and the UGC, New Delhi.
- 2) Animals are to be purchased from registered breeders only and record should be maintained and required to be submitted to the convenor, AEC, Jadavpur University.
- 3) Details of animals housed and sacrifice of animals being carried out should be given to the AEC time to time.

Furthermore, you are requested to submit the project no. to the AEC once the project is sanctioned. Moreover, you are requested to note further that the expenditure regarding maintenance of the animals has to be made from your project only. Special attention should be provided to prohibit any unlawful cruelty to the animals.

Thanking you

Yours sincerely,

(Dr. Biswajit Mukherjee)

Professor (Dr) Biswajit Mukherjee

Department of Pharmaceutical Technology

Jadavpur University

Kolkata - 700032, India



Dr. Biswajit Mukherjee

Convenor

Animal Ethics Committee

JADAVPUR UNIVERSITY

Kolkata-700 032



Institutional Animal Ethics Committee (IAEC)

Department of Pharmaceutical Technology

Jadavpur University

Kolkata-700032

RefNo: AEC/PHARM/1701/11/2017

This is to certify that Project title **“Pulmonary Delivery of Mucoadhesive Nanoparticles of an Antifungal Agent using Dry Powder Inhaler”** has been approved by the IAEC

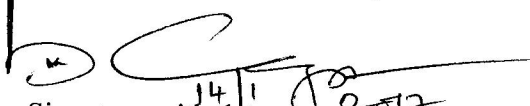
Prof. (Dr.) Biswajit Mukherjee

Dr. Kuladip Jana


Name of the Chairman/ Member Secretary IAEC:

Name of the CPSCEA nominee

Chairman/Member Secretary of IAEC


Signature with date 14/11/2017

CPSCEA nominee


Signature with date 14/11/17

Chairman
Institutional Animal Ethics Committee
Jadavpur University
Kolkata-700032

ETDDD
2018

International Conference on Emerging Trends in Drug Discovery and Development

January 18-20, 2018

Organized by :

Department of Pharmaceutical Engineering & Technology, IIT(BHU), Varanasi-221005 (UP), India

Certificate of Participation

Certified that

Prof./Dr./Mr./Ms.

Paramita Paul

has attended the conference.

He/She ~~chaired a technical session / delivered an invited lecture /~~
presented poster.

Prof. Sushil Kumar Singh
Organizing Chairman

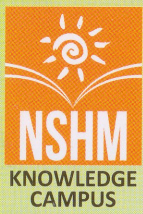
भारतीय
प्रौद्योगिकी
संस्थान
काशी हिन्दू विश्वविद्यालय



INDIAN
INSTITUTE OF
TECHNOLOGY
BANARAS HINDU UNIVERSITY

Dr. Sairam K.
Organizing Secretary

Certificate



INTERNATIONAL CONFERENCE
ON
CURRENT SCENARIO IN PHARMACEUTICAL TECHNOLOGY & HEALTHCARE:
A MOVE TOWARDS PATIENT-CENTRIC APPROACH



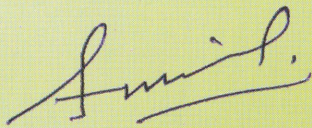
KOLKATA – MARCH 9 & 10, 2018

ORGANIZED BY :

NSHM COLLEGE OF PHARMACEUTICAL TECHNOLOGY & DEPARTMENT OF HEALTHCARE MANAGEMENT
NSHM KNOWLEDGE CAMPUS, KOLKATA – GROUP OF INSTITUTIONS

CERTIFICATE

This is to certify that Smt. Paromita Paul has presented ~~Poster~~ / Oral paper in the International Conference on "Current Scenario in Pharmaceutical Technology & Healthcare : A Move Towards Patient-Centric Approach" organized by **NSHM** College of Pharmaceutical Technology & Department of Healthcare Management, **NSHM** Knowledge Campus, Kolkata-Group of Institutions on 9th and 10th March 2018 at Science City Auditorium and Institute campus, Kolkata.


Conference Chairman



Manipal College of Pharmaceutical Sciences

Manipal University, Manipal 576 104.



Certificate

This is to certify that

MR/MS *Paramita Paul*

has participated / presented poster in the National Seminar on

"Novel Pharmaceutical Technologies: Challenges and Opportunities" held on 15 November 2015
in Manipal College of Pharmaceutical Sciences, Manipal University, Manipal.

Dr N Udupa
Convener

Dr C Mallikarjuna Rao
Organizing Secretary

Dr M Sreenivasa Reddy
Coordinator

JU IAPST National Seminar on
Drug and Diseases: Role of Pharmacists and Doctors

16th January, 2016

Certificate

This Certificate is awarded to Ms./ Mr./ Dr./ Prof. Paramita Paul.

for participation as Delegate / ~~Resource Person~~ / ~~Chairing a Session~~ / Presenting a Paper (Research/~~Review~~).

B Mukherjee
16/01/2016

Prof. Biswajit Mukherjee
Organizing Secretary

Anup Pal
16.01.2016

Mr. Anup Pal
Hon. Secretary, IAPST

Kuotsu
16/1/16

Dr. Ketousetuo Kuotsu
Chairperson, Scientific Committee

Dewanjee
16/1/2016

Dr. Saikat Dewanjee
Chairperson, Scientific Committee

Banasri Hazra
16/01/2016

Prof. Banasri Hazra
Chairperson, Scientific Committee

Jointly Organized by:



The Centre for Advance Research in Pharmaceutical
Sciences, Department of Pharmaceutical Technology,
Jadavpur University, Kolkata



Indian Association of Pharmaceutical
Scientists and Technologists,
Kolkata

CIRE

CENTRE FOR INTERDISCIPLINARY RESEARCH AND EDUCATION

404B, Jodhpur Park, Kolkata – 700068

25th March, 2017

CERTIFICATE OF PARTICIPATION

This is to certify that

Paramita Paul

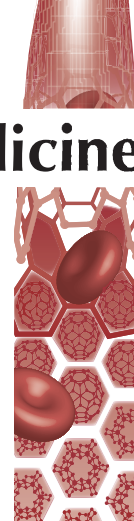
*has contributed through Lecture / Oral Presentation / Poster Presentation / Participation to the success
of the One Day National Symposium on Nanotechnology:
From Materials to Medicine and their Social Impact held on 25th March, 2017
at Birla Industrial and Technological Museum, Kolkata.*

PSarkar

Prof Sanjib Sarkar

President, CIRE

Publications



Chitosan-coated nanoparticles enhanced lung pharmacokinetic profile of voriconazole upon pulmonary delivery in mice

Paramita Paul¹, Soma Sengupta¹, Biswajit Mukherjee^{*1}, Tapan K Shaw^{1,2}, Raghuvir H Gaonkar³ & Mita Chatterjee Debnath³

¹Department of Pharmaceutical Technology, Jadavpur University, Kolkata 700032, West Bengal, India

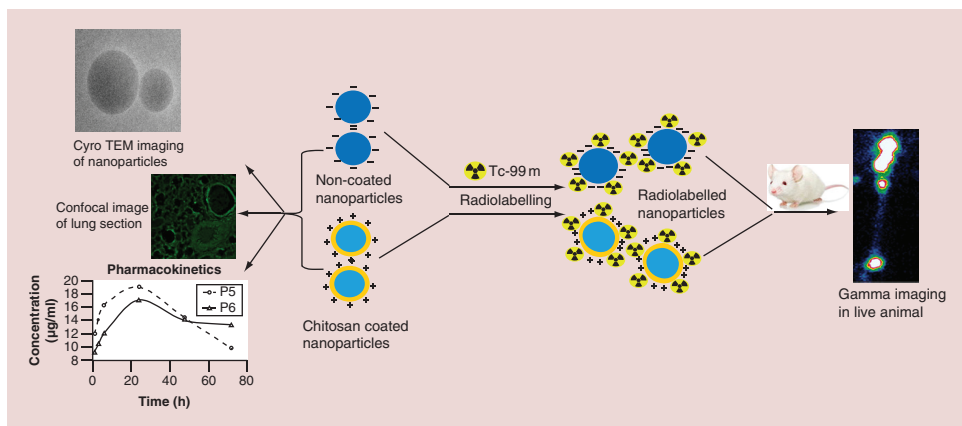
²NSHM College of Pharmaceutical Technology, NSHM Knowledge Campus, 124, B. L. Saha Road, Kolkata 700053, West Bengal, India

³Infectious Diseases & Immunology Division, CSIR Indian Institute of Chemical Biology, Kolkata 700032, India

* Author for correspondence: biswajit.mukherjee@jadavpuruniversity.in; biswajit55@yahoo.com

Aim: Chitosan-coated poly(lactic-co-glycolic acid) nanoparticles of voriconazole (VChNP) were developed to increase residence time and provide sustained drug release locally to treat recurrent lung-fungal infection. **Materials & methods:** VChNP has been developed using a simple, unique technique and characterized. Pharmacokinetics, lung deposition with time and gamma imaging were conducted with optimized formulations. **Results:** The deposition of fluorescein isothiocyanate-labeled VChNP in lung was confirmed by confocal microscopy. Gamma-scintigraphic images showed that Tc-99m-labeled VChNP had better pulmonary retention for longer period than that of noncoated formulation. Drastic improvement in pharmacokinetic profile of VChNP than noncoated formulation was observed. **Conclusion:** Thus, VChNP may be useful for effective pulmonary delivery with improved bioavailability. Such chitosan-coated nanoparticles may open up a new avenue for efficacious treatment of lung-fungal infection.

Graphical abstract:



First draft submitted: 20 September 2017; Accepted for publication: 19 December 2017; Published online: 31 January 2018

Keywords: aerodynamic diameter • chitosan-coated nanoparticles • gamma imaging • lung deposition • mucoadhesive • pharmacokinetics • voriconazole

Various drug administration methods have been in research till date for delivering drug to the lungs [1,2]. Lung is becoming an attractive target due to its noninvasive nature, avoidance of 'first-pass' metabolism, availability of huge surface area and plenty of blood supply for drug absorption for both local and systemic actions of therapeutics [2–4]. Local delivery of medications to the lungs is highly desirable, especially in patients with specific pulmonary diseases such as cystic fibrosis, asthma, chronic pulmonary infections, lung cancer, etc., where conventional therapy seems

to be ineffective to maintain the desired drug concentration in the blood plasma for a prolonged time [5–8]. For targeted drug delivery, nanocarriers are attractive choice in pharmaceutical research in the recent arena due to its various beneficial effects such as high stability, high carrier capacity by incorporating more drug molecules in the particle matrix, feasibility of incorporation of both hydrophilic and hydrophobic substances, and feasibility of variable routes of administration (including oral and inhalation) and most important is to provide controlled (sustained) drug release from the matrix [9–13]. Nanoparticles are also known for their capability of sustaining drug in the pulmonary region [14–17].

Nanoparticles prepared with biodegradable and biocompatible polymers such as polylactic-*co*-glycolic acid (PLGA), polylactic acid and chitosan, are [18] attractive choice to load the drug for delivering it to the pulmonary site of action. PLGA nanoparticles have been widely used in research in past few decades [19–21]. The advantages of modifying the surface of PLGA particles with a mucoadhesive polymer, such as chitosan, may cause the predominant variation or even inversion of zeta potential, ability to promote cellular adhesion and retention of the drug delivery system at the target site [22–24]. Moreover, a decreased burst effect in the release of the encapsulated drug, and the possibility of conjugating ligand(s) for drug-targeting to the free amino groups of chitosan are the added advantages [25]. The specific advantage of nanoparticles coated with chitosan for pulmonary delivery is the retention of the formulation in the pulmonary site of infection for a longer time period than that of chitosan-free nanoparticles providing effective treatment, curbing the phagocytic effects and thereby enhancing the longevity of the nanoparticles in the biological system [26].

Voriconazole, the first available second-generation triazole group of antifungal agent from the ‘azole’ family, possesses broad-spectrum activity against resistant fungal species such as *Aspergillus*, *Candida*, *Scedosporium* and *Fusarium* [27–29]. Antifungal effect of voriconazole exerts by altering the fungal cell membrane. Voriconazole blocks synthesis of ergosterol, an essential component of the membrane, by interacting with lanosterol 14- α demethylase (CYP51 or Erg11p), a CYP-450 enzyme that is needed to convert lanosterol to ergosterol, affecting the integrity and function of the fungal membrane. The objective of the present study was to prepare, characterize and deliver mucoadhesive PLGA nanoparticles containing antifungal drug voriconazole to treat fungal infection, especially in lungs.

Materials & methods

Materials

Voriconazole (gift sample) was obtained from Dr Reddy’s Laboratories Ltd., Hyderabad, India. Fluconazole was kindly donated by Regional Drugs Testing Laboratory, Guwahati, India. PLGA (MW 50,000–75,000; lactide to glycolide ratio 85:15) was procured from Sigma-Aldrich Chemicals Pvt. Ltd., Bangalore, India. Polyvinyl alcohol (PVA, MW 125,000) was obtained from S.D. Fine-Chem. Ltd., Mumbai, India. Chitosan, fluorescein isothiocyanate (FITC) and lactose monohydrate were purchased from HiMedia Lab. Pvt. Ltd., Mumbai, India. Acetone, acetonitrile and dichloromethane (DCM) were acquired from E. Merck (India) Ltd., Mumbai, India. Disodium hydrogen orthophosphate and potassium hydrogen phosphate were obtained from Process Chemical Industries, Kolkata, India. All other chemicals used were of analytical grade.

Animals

Swiss Albino mice weighing 20–25 g of either sex were used for pharmacokinetics study and *in vivo* lung deposition study. The entire experimental protocol was approved by Animal Ethics Committee, Jadavpur University and procedures followed were in accordance with the Committee for the Purpose of Control and Supervision of Experiments on Animals guidelines, with necessary care. The animals were fed with a standard diet [30] and water *ad libitum*.

Preformulation study by Fourier transform infrared spectroscopy

In Fourier transform infrared (FTIR) spectroscopic study, voriconazole and all the individual excipients such as PLGA, PVA, chitosan and their physical mixtures, and lyophilized formulations were scanned in an inert atmosphere over a wave number range of 4000–400 cm^{-1} in FTIR spectrophotometer (Alpha E, Bruker Alpha, Ettlingen, Germany).

Table 1. Formulation composition and process parameters for preparation of optimized formulations.

Code	Drug:PLGA:chitosan (mg:mg:mg)	Homogenization speed (rpm)	Stabilizer [†]	Sonication time (min)
P-Blank	0:100:0	20,000	PVA	10
PC-Blank	0:100:80	20,000	PVA	10
P1	100:108:0	16,000	PVA	10
P2	101:108:80	16,000	PVA	10
P3	100:107:40	16,000	PVA	10
P4	100:105:20	16,000	PVA	10
P5	250:254:0	20,000	PVA	15
P6	250:257:100	20,000	PVA	15
P7	250:254:0	25,000	PVA	10
P5-FITC	250:254:0	20,000	PVA	15
P6-FITC	250:257:100	20,000	PVA	15

[†]Stabilizer: 2.5 and 1.5% aqueous PVA solution.

FITC: Fluorescein isothiocyanate; PC: PLGA-chitosan; PC-Blank: PLGA-chitosan blank nanoparticles; PLGA: Polylactic-co-glycolic acid; PVA: Polyvinyl alcohol.

Preparation of noncoated PLGA nanoparticles containing voriconazole

Multiple emulsion solvent evaporation technique was employed for the preparation of both chitosan-coated PLGA nanoparticles and noncoated PLGA nanoparticles, with some modifications [31]. Briefly, noncoated nanoparticles were prepared by solubilizing approximately 250 mg of PLGA in 4 ml of organic phase containing DCM and acetone (4:1, w/w ratio). Aqueous PVA solutions, 1.5% (w/v) and 2.5% (w/v), were prepared previously. The organic polymeric solution containing voriconazole was emulsified quickly with dropwise gradual addition of 1.5 ml of 2.5% PVA solution, and continuous homogenization for 4 min using a high-speed homogenizer at 20,000 rpm (IKA Laboratory Equipment, Model T10B, Ultra-Turrax, Staufen, Germany). The water-in-oil emulsion (primary emulsion) was quickly added to 75 ml of 1.5% PVA solution and homogenized for about 8 min at 20,000 rpm to get secondary emulsion. The emulsion thus obtained was kept in a bath sonicator for 10–15 min to break the large globules and then stirred on a magnetic stirrer overnight without heating for complete removal of organic solvents used to dissolve the polymer. The organic phase was allowed to diffuse out and evaporated to get homogenous nanoparticles. While nanoparticles were hardening, the particles suspension was kept on a bath sonicator (Trans-O-sonic, Mumbai, India) for about 45 min to break the agglomerates, if any. Then, the particles were separated by centrifugation at 3000 rpm and 16,000 rpm in a refrigerated centrifuge (Hermle refrigerated centrifuge, Wehingen, Deutschland) and washed twice with double distilled water to remove the excess of PVA and kept in Petridish in an ultrafreezer (So-Low, Environmental Equipment, OH, USA). After that, the frozen sample was lyophilized in a freeze dryer (Laboratory Freeze Dryer, Instrumentation India, Kolkata, India).

Preparation of chitosan-coated PLGA nanoparticles containing voriconazole

Chitosan-coated PLGA nanoparticles of voriconazole (VChNP) was prepared using the above-mentioned method with the modification in the following steps. Required amount of chitosan (Table 1) was dissolved in 1.5% (w/v) PVA solution with pH adjusted at 3.0 using 0.1 M HCl solution. The primary emulsion was homogenized in 75 ml of the chitosan in 1.5% PVA solution for 8 min to get multiple emulsion followed by adjustment of pH from 3.0 to 9.0 by addition of NaOH solution. The various composition of the nanoparticle batches are also mentioned in Table 1.

Preparation of FITC containing nanoparticles

The FITC containing noncoated and chitosan-coated nanoparticles were prepared using the same processes described above except the incorporation of 100 µl of FITC solution into the organic phase containing polymer and drug before homogenization. FITC solution (0.4% w/v) was prepared in absolute alcohol.

Drug loading (%) & entrapment efficiency (%)

For the determination of % drug loading, 2 mg of lyophilized nanoparticles (NPs) (accurately weighed) was solubilized in 2 ml of acetonitrile and water (50:50 v/v). The formed solution was kept for maximum 4 h in an incubator shaker (Somax Incubator Shaker; Shenjhen Pango Electronic Co. Ltd., Shenzhen, China) and then

centrifuged at 16,000 rpm for 15 min in a refrigerated centrifuge and the supernatant was suitably diluted with the same solvent mixture and analyzed spectrophotometrically at the corresponding λ_{\max} of 255 nm using nanoparticles (without drug) in the same solvent mixture as blank [17].

Drug loading was determined as follows [32,33]:

$$\text{Drug loading (actual) (\%)} = \text{Amount of drug in nanoparticles} \times 100 / \text{Amount of nanoparticles obtained};$$

Drug entrapment efficiency was calculated as follows [13,34]:

$$\text{Drug entrapment efficiency (\%)} = \text{Drug loading (actual) (\%)} \times 100 / \text{Drug loading (theoretical) (\%)}.$$

Characterization of nanoparticles

Particle size distribution & zeta potential

The average particle size and zeta potential values of all the experimental formulations were measured using Malvern Zetasizer Nano-ZS 90 (Malvern Instruments, Malvern, UK) utilizing dynamic light scattering (DLS) technique [35]. A weighed quantity of the experimental sample was dispersed in Milli-Q water (Millipore Corp., MA, USA), followed by sonicating and vortexing before placing it in the cuvette for particle size and zeta potential measurement [13,32].

Cryogenic-transmission electron microscopy

Carbon-coated copper grid (300#; Ted Pella Inc., CA, USA) was glow-discharged (Pelco easiglow, Ted Pella Inc.) for 30 s to remove dust particles or contamination if any [36,37]. Chitosan-coated PLGA nanoparticles and noncoated PLGA nanoparticles were dispersed in doubled distilled water and the dispersion was spread on glow-discharged grid and plunge-frozen in liquid ethane using Vitrobot (Vitrobot Mark IV, FEI Company, Eindhoven, the Netherlands). Grids were transferred to a cryoholder containing liquid ethane in liquid nitrogen and the samples on the grids were visualized in Tecnai G2 Polara (D357 Twin, FEI Company) equipped with 300 kV field emission gun. Images were collected at 82,600 \times magnification with an underfocus of 4.5 μm . Images were captured on a BM-Eagle 4 k \times 4 k charged coupled device camera (FEI Company), unbinned with a final pixel size of 1.89 \AA .

Transmission electron microscopy

For transmission electron microscopy (TEM) measurements, 10 μl of lyophilized nanoparticles in water was carefully placed on a 300-mesh carbon-coated copper TEM grid (Ted Pella Inc.). The excess solution on the grid was removed using a piece of fine-filter paper, and the samples were allowed to air dry for 10 h prior to imaging the particles under TEM (JEM 2100; JEOL, Tokyo, Japan) [38].

Field emission scanning electron microscope

Particle morphology was assessed by field emission scanning electron microscope (FESEM; JEOL JSM-7600F, Tokyo, Japan). The lyophilized particles were placed on a carbon tabs mounted on SEM specimen stubs. The specimen stubs were coated with gold of 4-nm thickness by ion sputtering device (Au5 Quorum, Q150TES) and were operated at 15–20 kV accelerating voltage.

Atomic force microscopy

The samples were dispersed in Milli-Q water using brief vortexing and sonication. One drop of sample was placed in a glass slide and dried in a vacuum dryer. The morphology and particle size were analyzed by atomic force microscopy (AFM; Dimension Icon, Bruker, Karlsruhe, Germany) under ambient conditions by mode PeakForce QNM (Quantitative NanoMechanical mapping) using silicon nitride probe having a resonance frequency 150–350 kHz and a force constant 0.4 N/m.

In vitro drug release & drug release kinetics study

In vitro drug release study was carried out in phosphate-buffered saline (PBS), pH 7.4 [39,40] and in simulated lung fluid (SLF), pH 7.4, respectively [13,39], for 8 days. The studies were performed with noncoated and chitosan-coated nanoparticles. Briefly, nanoparticles were weighed (triplicate for each type of formulation) accurately 2 mg and

taken in 2 ml microcentrifuge tube. Drug release media (2 ml) were added in each tube and shaken briefly and the time was considered as zero. The tubes were kept in an incubator shaker at 37°C with shaking (20 rpm). Samples were taken at predetermined time points and centrifuged at 16,000 rpm for 10 min. The supernatant (2 ml) was withdrawn and 2 ml fresh media were added and the tubes were kept in shaker incubator for next time point [13,32]. The supernatant was analyzed by UV-Vis spectroscopy with proper dilution (if required), at 255 nm. The drug release data were plotted as cumulative percentage of drug released against time (h) for both noncoated and coated PLGA nanoparticles [34].

In order to predict and correlate the behavior of the *in vitro* voriconazole release from both the noncoated and coated nanoparticles studied, suitable mathematical models were used. Thus, the experimental data obtained from *in vitro* drug release experiments of voriconazole-loaded noncoated and chitosan-coated nanoparticles were investigated using five conventional models: zero-order, first-order, Higuchi, Hixson-Crowell and Korsmeyer-Peppas models [31,41].

Determination of mass median aerodynamic diameter & geometric standard deviation using an eight-stage nonviable Andersen cascade impactor

Mass median aerodynamic diameter (MMAD) is defined as the average diameter under which 50% of the particles remain. This study was performed to determine MMAD and geometric standard deviation (GSD). Weighed amount of nanoparticle was blended with micronized lactose (1:3 w/w) ratio and introduced into an eight-stage nonviable Andersen cascade impactor (model 20–800, Thermo Fischer Scientific, MA, USA). After that, the plates were accumulated and weighed. MMAD and GSD were calculated from the deposited particles using the MMAD calculator for Andersen apparatus at a flow rate of 28.3 l/min [17].

In vivo deposition of nanoparticles in the lungs of mice using nose-only inhalation chamber & fabricated dry powder inhaler

The experimental animals were divided into two groups for three time points study (1, 8 and 24 h) and each group had three animals. FITC-loaded nanoparticles of each type were weighed (50 mg) and mixed with 150 mg of microfine lactose. The powder blend was placed inside the fluidization chamber and dosed in the nose-only inhalation chamber all at once. After the completion of dosing, the animals were sacrificed at the predesignated time points (1, 8 and 24 h) and lungs were removed, washed and fixed with formalin solution, and embedded in paraffin blocks by the conventional method [17]. The tissue sections were observed under a confocal laser scanning microscope (LSM 510; Carl Zeiss, Jena, Germany) at an excitation wavelength of 494 nm and emission wavelength of 521 nm to observe the distribution of FITC-tagged nanoparticles and images were captured at suitable magnification. The images were finally analyzed and total fluorescence intensity of each lung tissue was determined (integrated density, ID) using ImageJ software [42]. The background was obtained by measuring the fluorescence intensity of the regions out of the tissues. The corrected total cell fluorescence (CTCF) was then determined by subtracting the background from the ID [CTCF = ID - (area of selected cell x mean fluorescence of background readings)] [43].

High performance liquid chromatography

The concentration of voriconazole in blood at different time points after the pulmonary administration was measured by Dionex Ultimate 3000 RP-HPLC system (Dionex, Idstein, Germany), equipped with an Agilent C18 column (4.6 mm × 250 mm, 5 μm; Thermo Scientific™ Hypersil GOLD™, MA, USA). The injection volume was 20 μl. The mobile phase for the chromatographic separation composed of acetonitrile–water–formic acid (60:40:0.05; v/v/v) was filtered before using it isocratically at room temperature at a flow rate of 1 ml/min, and voriconazole was detected by UV detector at 254 nm [13].

For calibration curve, pooled plasma was thawed at room temperature, plasma (90 μl); internal standard solution (fluconazole; 10 μl), calibrator solution (10 μl) and acetonitrile (890 μl) were pipetted into respective microcentrifuge tubes and capped. The tubes were vortexed for 20 min and then centrifuged for 10 min at 10,000 rpm. The supernatant was filtered through 0.45-μm syringe filter (chromatography syringe filter, Cole-Parmer, Mumbai, India) and transferred to a microcentrifuge tube. The samples (20 μl in each case) were injected into the system. Peak height measurements were analyzed to obtain the ratio of voriconazole versus fluconazole (internal standard). The ratios of voriconazole to fluconazole were used to establish a calibration curve and to quantify voriconazole from the calibration curve. Test samples or controls were prepared by transferring 90 μl of

test or control plasma into a respective microcentrifuge tubes, 10 μl of internal standard solution was then added to each tube followed by 900 μl of acetonitrile. The tubes were capped and processed in the same manner as calibrators.

The different lung lobes were thawed and the lung tissues were homogenized separately with the addition of normal saline (1:4, tissue:normal saline) for 2 min. To the lung homogenate (90 μl), 400 μl of acetonitrile was added, followed by vortexing for 20 min. Internal standard fluconazole 10 μl (2500 $\mu\text{g}/\text{ml}$) was then mixed with it. The samples were then centrifuged in a cold centrifuge at 4°C at 10,000 rpm for 10 min. The supernatant was then filtered through 0.45- μm syringe filter and the filtrate was injected (20 μl) into the column. The drug content was calculated from the calibration curve developed in the same way within the concentration range of 0.1562–10.00 $\mu\text{g}/\text{ml}$.

Pharmacokinetics & lung lobe distribution study

All the animal studies were approved by Animal Ethics Committee, Jadavpur University. The studies were performed in male Swiss Albino mice weighing about 20–25 g. The mice were fasted overnight before experimentation and were accessed to water *ad libitum*.

Free drug voriconazole, coated and noncoated PLGA nanoparticles (50 mg) mixed with microfine lactose monohydrate (150 mg) were administered to mice through the pulmonary route using nose-only inhalation chamber and dry powder inhaler (DPI) [44]. After complete dosing (taken as zero time), blood samples and lungs were collected at 1, 3, 6, 24 and 48 h post inhalation. Lung lobes were collected separately and marked as left lobe, cranial lobe, middle lobe, accessory lobe and caudal lobe and were stored at -80°C until further use.

At each time point, blood (~1 ml) from three mice from each group was collected via terminal cardiac puncture following deep anesthesia using chloroform. EDTA (2 mg) was added to each tube, as an anticoagulant. The blood sample was mixed with EDTA and centrifuged at 5000 rpm for 5 min at 4°C for separation of plasma. Plasma sample was stored at -20°C until analyzed.

The voriconazole plasma concentration–time data were analyzed by standard noncompartmental methods using the program WinNonlin Pro (Pharsight Corp, CA, USA) [45–48].

Gamma scintigraphy

Gamma imaging was performed for mice after administering Technetium-99m (Tc-99m)-labeled PLGA nanoparticles containing voriconazole formulation (Tc-99m-VNP) and chitosan-coated PLGA nanoparticles containing voriconazole (Tc-99m-VChNP). They had 200 microcurie of radioactivity and administered through pulmonary route. The animals were anesthetized by ketamine hydrochloride prior to imaging. Mice were fixed on a wooden board and imaging was performed on a planar gamma camera (GE Infinia Gamma Camera equipped with Xeleris Workstation; GE, OH, USA) at 3 and 6 h after administration.

Results

Preformulation study

Investigation of drug-excipients interaction

Figure 1 shows the FTIR spectra of voriconazole, each of the excipients, mixture of voriconazole with PLGA, PVA and/or chitosan and a mixture of the polymers, respectively. The FTIR spectra of pure voriconazole, mixture of drug with the polymers and the lyophilized formulations with or without drug show that the characteristic peaks (C–N, C–F and C–C stretching bands at 3190.86–3117.54, 1498.31–1452.41 and 1586.96–1452.41 cm^{-1} , respectively) of the drug were present [13,49].

The shifting of the following peaks of chitosan while in the physical mixture with the drug and the polymers from 652 to 657 cm^{-1} and 605 to 606 cm^{-1} might be due to medium intensity stretching of C–H and C–H bending and ring puckering, C–H deformation and O–H bending (out of plane), respectively, from 1697 to 1693 cm^{-1} for C=O stretching and from 1082 to 1086 cm^{-1} for C–N medium intensity stretching and C–O stretching [36]. In the FTIR spectrum of PLGA, sharp peaks at 3589.45–3643.84 cm^{-1} for –OH (free) and of 2995.43–2946.79 cm^{-1} for C–H stretching were observed as the typical bands of PLGA. The ester C–O stretching band of PLGA was observed at 1748.61 cm^{-1} . The main bands appearing in that spectrum were due to stretching vibrations of OH groups in the range from 3750 to 2900 cm^{-1} , which were overlapped to the stretching vibration of N–H; and C–H bond in –CH₂ (2918 cm^{-1}) and –CH₃ (2852 cm^{-1}) groups, respectively. In the FTIR spectrum of chitosan, the band located near 1146 cm^{-1} is related to asymmetric vibrations of CO in the oxygen bridge resulting from

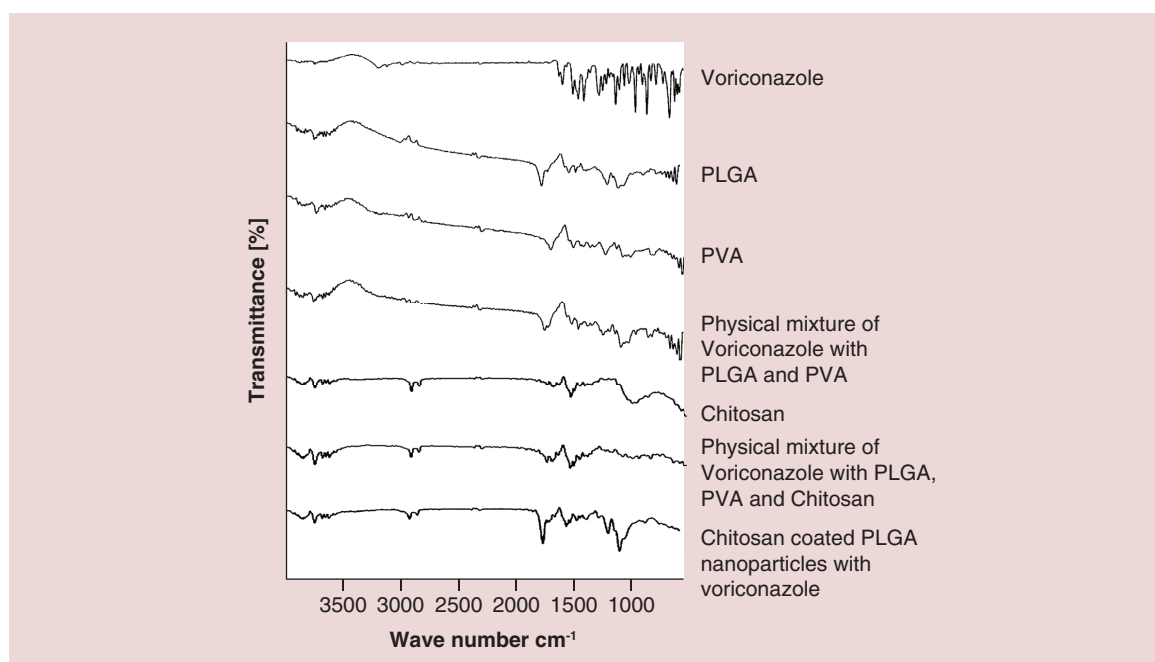


Figure 1. Fourier transform infrared spectroscopy studies of individual components, physical mixture and nanoparticle formulations. PLGA: Polylactic-co-glycolic acid; PVA: Polyvinyl alcohol.

Table 2. Formulation characteristics such as percent drug loading, percent encapsulation efficiency, average particle size and zeta potential values for the optimized polylactic-co-glycolic acid formulation without chitosan coating (P5) and with chitosan coating (P6).

Formulation code	Drug loading (%)	Encapsulation efficiency (%)	Average particle size (nm)	Zeta potential (mV)
P5	35.62 ± 0.135	71.24	154.6	-14.8
P6	28.57 ± 3.704	68.57	277	31.9

deacetylation of chitosan. The small peak at approximately 890 cm^{-1} corresponds to wagging of the saccharide structure of chitosan [50–53]. Thus, from this it can be concluded that there is no chemical interaction seen between the drug and the excipients.

Characterization of nanoparticles

Particle size distribution & zeta potential by DLS analysis

The average particle size and zeta potential values of the experimental formulations are given in Table 2. The data (Supplementary Figure 1) revealed that most of the particles had an average particle size of 154.6 and 277 nm with zeta potential value of -14.8 and +39.1 mV for noncoated and coated nanoparticles, respectively.

Determination of drug loading & entrapment efficiency

The drug loading values were expressed by the quantity of voriconazole encapsulated in the formulations and the drug entrapment efficiency was associated with the percentage of voriconazole encapsulated with respect to theoretical voriconazole loading in a particular formulation [13,36]. The percentage values of drug loading of noncoated and coated nanoparticles were 35.62 ± 0.135% and 28.57 ± 3.704% with the drug-loading efficiency values of 71.24 and 68.57%, respectively (Table 2).

Surface morphology

FESEM images revealed that experimental formulations were spherical in shape. In noncoated formulations, most of the particles were below 500 nm (Figure 2D) in size and the particles of the coated nanoparticle formulation (Figure 2E) were little bit larger than those of noncoated formulation. But the surface coating was not distinguished

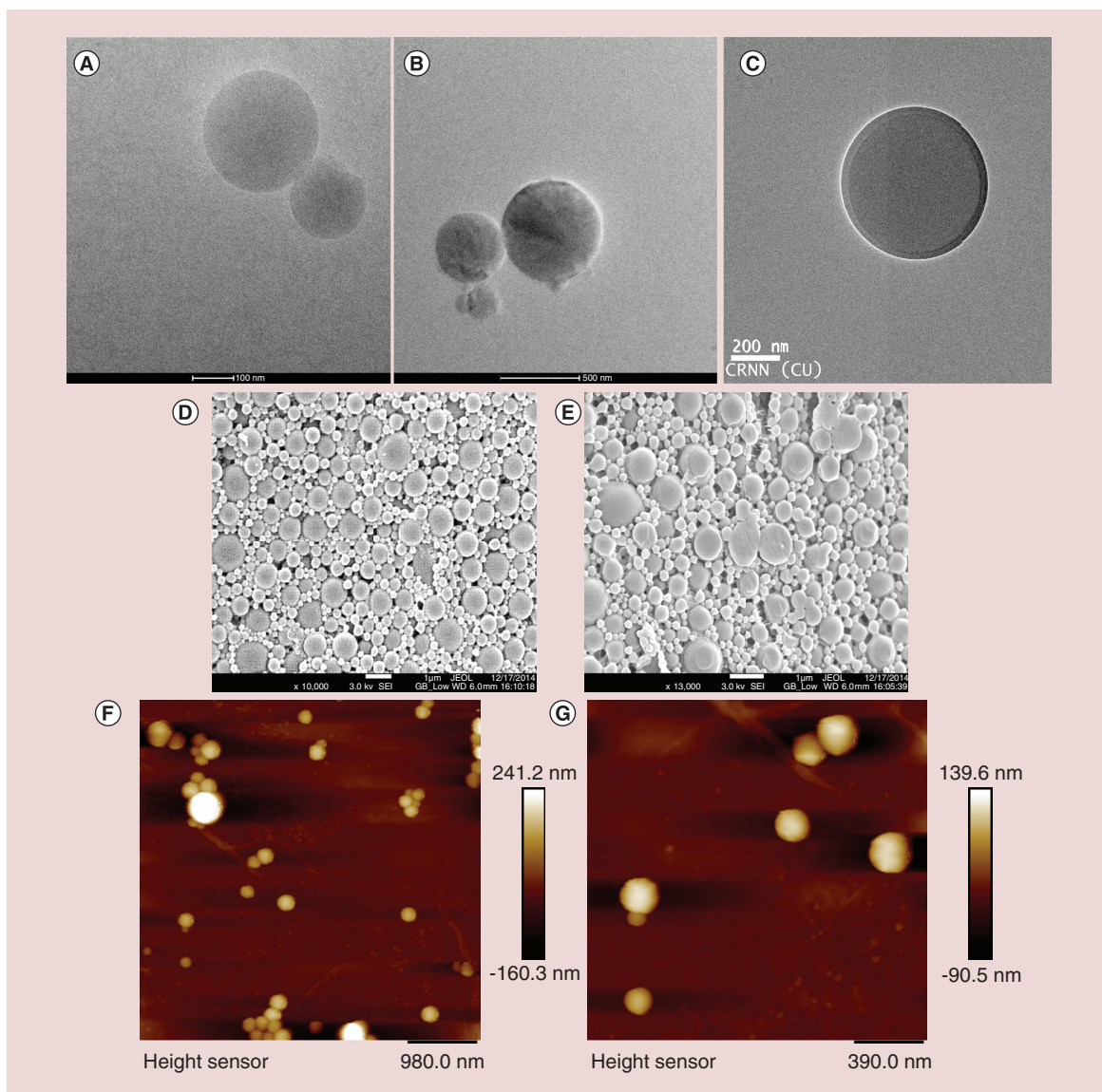


Figure 2. Morphology of the experimental nanoparticles. Cryogenic transmission electron microscopic images of (A) noncoated PLGA nanoparticles and (B) chitosan-coated PLGA nanoparticles; (C) transmission electron microscopic image of chitosan-coated PLGA nanoparticles; Field Emission scanning electron microscopic images of (D) noncoated PLGA nanoparticles and (E) chitosan-coated PLGA nanoparticles; atomic force microscopic images of (F) noncoated PLGA nanoparticles and (G) chitosan-coated PLGA nanoparticles. PLGA: Polylactic-co-glycolic acid.

properly by FESEM data. The surface coating of chitosan onto the PLGA nanoparticles was confirmed by cryogenic (cryo)-TEM images (Figure 2B) and TEM image (Figure 2C). The particles of noncoated formulation were smooth in surface (Figure 2A). The AFM images of noncoated (P5) and coated (P6) nanoparticles have been shown in Figure 2F and G. AFM image shows that the particles of both the formulations were purely spherical in shape and the surface was coated in case of chitosan-coated nanoparticles. Amount of chitosan coated in the formulation was determined by subtracting the weight of uncoated lyophilized drug-loaded nanoparticles from the weight of chitosan-coated lyophilized drug-loaded nanoparticles, and the amount of chitosan was determined to be $13.89 \pm 1.94\%$ of the uncoated lyophilized drug-loaded nanoparticles. The size of nanoparticles was in nanograde. The sphere-like particles were 150–300 nm in diameter.

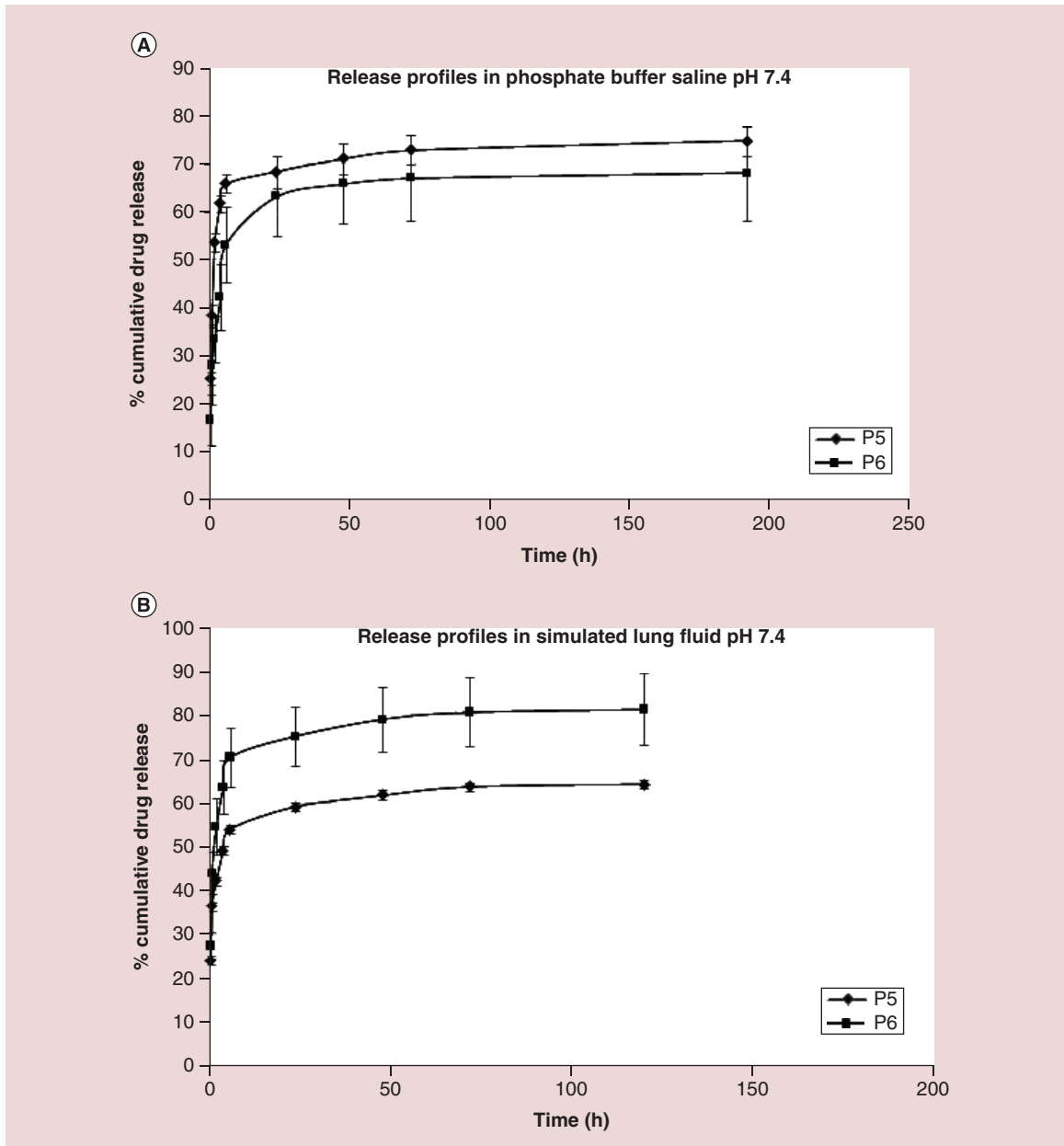


Figure 3. Release of voriconazole from the experimental nanoparticles in different drug release media. Release profiles of voriconazole from noncoated PLGA nanoparticles (P5) and chitosan-coated PLGA nanoparticles (P6) in (A) phosphate-buffered saline (pH 7.4) and (B) simulated lung fluid (pH 7.4). PLGA: Polylactic-co-glycolic acid.

In vitro drug release study

Both the experimental formulations had more or less similar drug release pattern in PBS, pH 7.4 up to 21 days (Figure 3A). The drug released from the experimental formulations initially at a faster rate up to 24 h and then at a slower rate in a sustained manner up to 8 days (after 8 days, no significant increase in the percentage cumulative drug release was seen). It shows that at first 30 min about 25% of the drug released from the optimized uncoated nanoparticles, whereas the data for the optimized chitosan-coated nanoparticles were less (16%). The drug released in a similar sustained manner after 24 h of release from both the formulations. After 8 days, 74.76 and 68.12% of drug released from P5 and P6, respectively, in PBS.

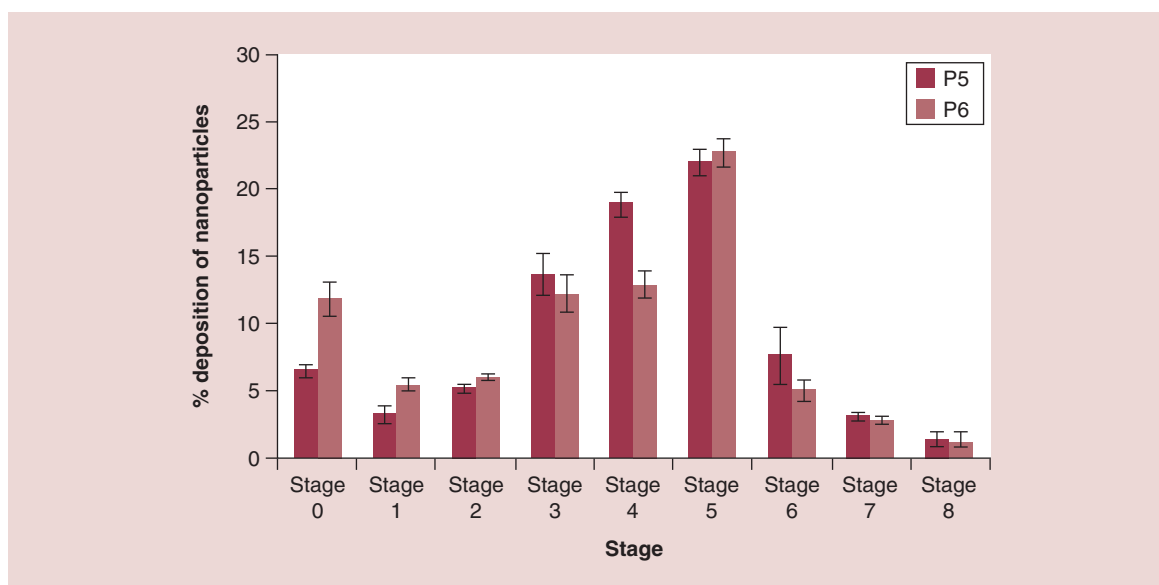


Figure 4. *In vitro* deposition of nanoparticles analyzed by cascade impactor. *In vitro* deposition of noncoated PLGA nanoparticles (P5) and chitosan-coated PLGA nanoparticles (P6) from Andersen cascade impactor (data as mean \pm SD, $n = 3$).

PLGA: Polylactic-co-glycolic acid; SD: standard deviation.

A distinct difference was observed for drug released in SLF, pH 7.4 (Figure 3B). For noncoated nanoparticles, 54% of drug was released at 6 h, but in chitosan-coated nanoparticles drug released 70% and at day 5, drug release values were 64 and 81% from noncoated and coated nanoparticles, respectively.

Drug release kinetics study

The drug release kinetic revealed that the drug release followed the Korsmeyer–Peppas kinetic model ($R^2 = 0.719$ and 0.896 for P5 and P6 in PBS; and 0.835 and 0.801 for P5 and P6 in SLF, respectively; Supplementary Table 1). The release of drug from the particles followed non-Fickian diffusion kinetics, as depicted from the release component value.

Determination of MMAD & GSD using an eight-stage nonviable Andersen cascade impactor

Cascade impactor scenario of the noncoated (P5) and chitosan-coated (P6) PLGA nanoparticles are shown in Figure 4. P5 and P6 had the highest particle retention in stage 5 and lowest particle deposition at stage 8 of the impactor. The particles were deposited less than 10% in stages 0–2, 6–7. Stages 3 and 4 showed particle deposition above 10% but below 20%; whereas only stage 5 showed particle deposition above 20%. MMAD and GSD of P5 (noncoated) and P6 (chitosan-coated) were calculated to be $2.46 \mu\text{m}$ and 2.15 (for P5), and $2.8 \mu\text{m}$ and 3.04 (for P6), respectively.

Particle size below $5 \mu\text{m}$ was considered as fine fraction [54]. Fine powder fraction of noncoated (P5) and chitosan-coated (P6) nanoparticles from cascade impactor device were 0.6676 and 0.5747 , respectively. Emitted dose percent of noncoated (P5) and chitosan-coated (P6) nanoparticles were calculated excluding the total loss during the delivery to cascade impactor device. The values were 11.67 and 9.96% , respectively.

In vivo deposition of nanoparticles in the lungs of mice using nose-only inhalation chamber & fabricated DPI

In vivo deposition of FITC nanoparticles coated and noncoated types in the lungs have been confirmed by confocal images taken at 1, 8 and 24 h during the experiment. Figure 5A and B revealed that NPs penetrated into the lung tissue cell membrane and were distributed uniformly in the alveoli. In addition, the green fluorescent intensity in the cells augmented with time. In order to investigate, the influence of the chitosan coating on nanoparticles on the nanoparticle deposition in the lung tissues, we calculated the CTCF values for noncoated and chitosan-coated PLGA nanoparticles at different time points of 1, 8 and 24 h.

The CTCF values have been summarized in Figure 6A. CTCF values of both the formulations at different time

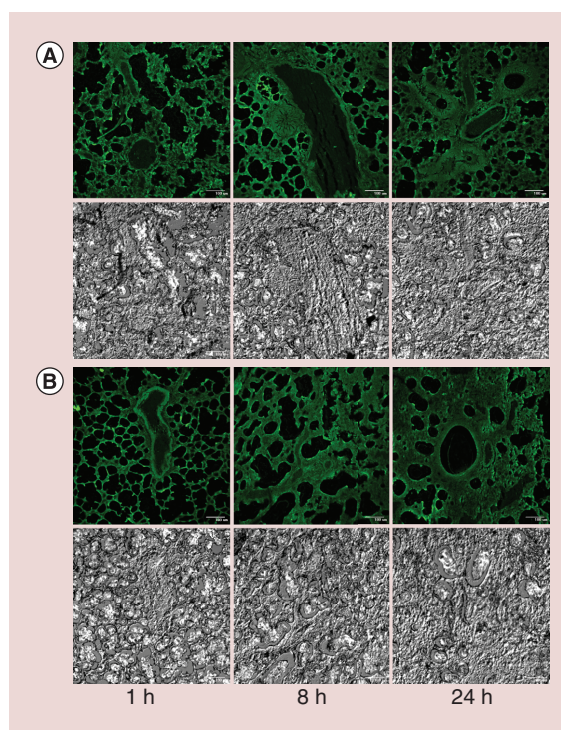


Figure 5. Confocal microscopic images of lung tissue section of mice treated with the experimental nanoparticles. Confocal laser scanning microscopic images of lungs treated with (A) noncoated PLGA nanoparticles (P5) (at 1, 8 and 24 h after pulmonary administration), and (B) chitosan-coated PLGA nanoparticles (P6) (at 1, 8 and 24 h after pulmonary administration). PLGA: Poly(lactic-co-glycolic acid).

Table 3. Pharmacokinetic parameters for free drug voriconazole, optimized poly(lactic-co-glycolic acid) formulations without chitosan coating (P5) and with chitosan coating (P6) in Swiss albino mice after pulmonary administration.

Parameter	Plasma kinetics			Lung kinetics		
	Free voriconazole	PLGA nanoparticles	CS-coated PLGA nanoparticles	Free voriconazole	PLGA nanoparticles	CS-coated PLGA nanoparticles
C_{max} ($\mu\text{g/ml}$)	15.33 ± 1.16	29.69 ± 2.87	$22.15 \pm 2.10^*$	12.03 ± 0.47	19.62 ± 6.76	14.33 ± 4.37
T_{max} (h)	1	6	3	1	24	24
AUC ($\mu\text{g}/\mu\text{l} \cdot \text{h}$)	0.25 ± 0.01	1.87 ± 0.09	8.92 ± 2.93	0.07 ± 0.01	1.81 ± 0.67	$4.49 \pm 0.54^{**}$
AUMC ($\mu\text{g}/\mu\text{l} \cdot (\text{h})^2$)	4.08 ± 0.30	126.78 ± 20.92	$4799.7 \pm 891.61^*$	0.57 ± 0.14	134.94 ± 23.05	$1341.55 \pm 469.26^*$
MRT (h)	15.95 ± 0.41	67.73 ± 7.38	$537.97 \pm 97.92^*$	7.84 ± 0.94	74.60 ± 15.36	$298.49 \pm 83.65^*$
$t_{1/2}$ (h)	10.01 ± 0.36	45.55 ± 7.92	372.8 ± 132.48	5.37 ± 0.77	48.28 ± 13.258	$204.10 \pm 64.125^*$

CS: chitosan; Values represent mean \pm SD (n = 3); Statistical significance evaluations (using two-tailed unpaired t-test) represented by asterisks compared with PLGA nanoparticles.
 $^*p < 0.05$ at 95% CI.
 $^{**}p < 0.01$ at 99% CI.
AUC: Area under the curve; AUMC: Area under the first moment curve; CS: Chitosan; MRT: Mean residence time; PLGA: Poly(lactic-co-glycolic acid); SD: Standard deviation; $t_{1/2}$: Half-life.

points (1, 8 and 24 h) showed that CTCF value decreased with time in case of noncoated nanoparticles, whereas the value increased gradually with time for chitosan-coated nanoparticles.

Pharmacokinetics & lung lobe distribution study

Different pharmacokinetic parameters after pulmonary administration of free voriconazole, noncoated and chitosan-coated nanoparticles have been listed in Table 3. Voriconazole levels in blood and lungs were located after single-dose administration of nanoparticles containing voriconazole given through pulmonary route. Drug level was observed at six different time points up to 72 h. Both the nanoparticles showed sustained drug release profile for up to 72 h in comparison to the free voriconazole [13]. Our formulation showed to maintain the plasma concentration of voriconazole above minimum inhibitory concentration (~ 0.5 mg/l) [55] required for effective treatment of lung-fungal infection (LFI).

The maximum concentration of voriconazole in plasma was achieved 3 h before for chitosan-coated nanoparticles compared with the noncoated one. But the free drug was found to be maximum in 1 h in both the plasma and lung (Table 3). Whereas the time required to achieve maximum concentration in lung was same for both the formulations.

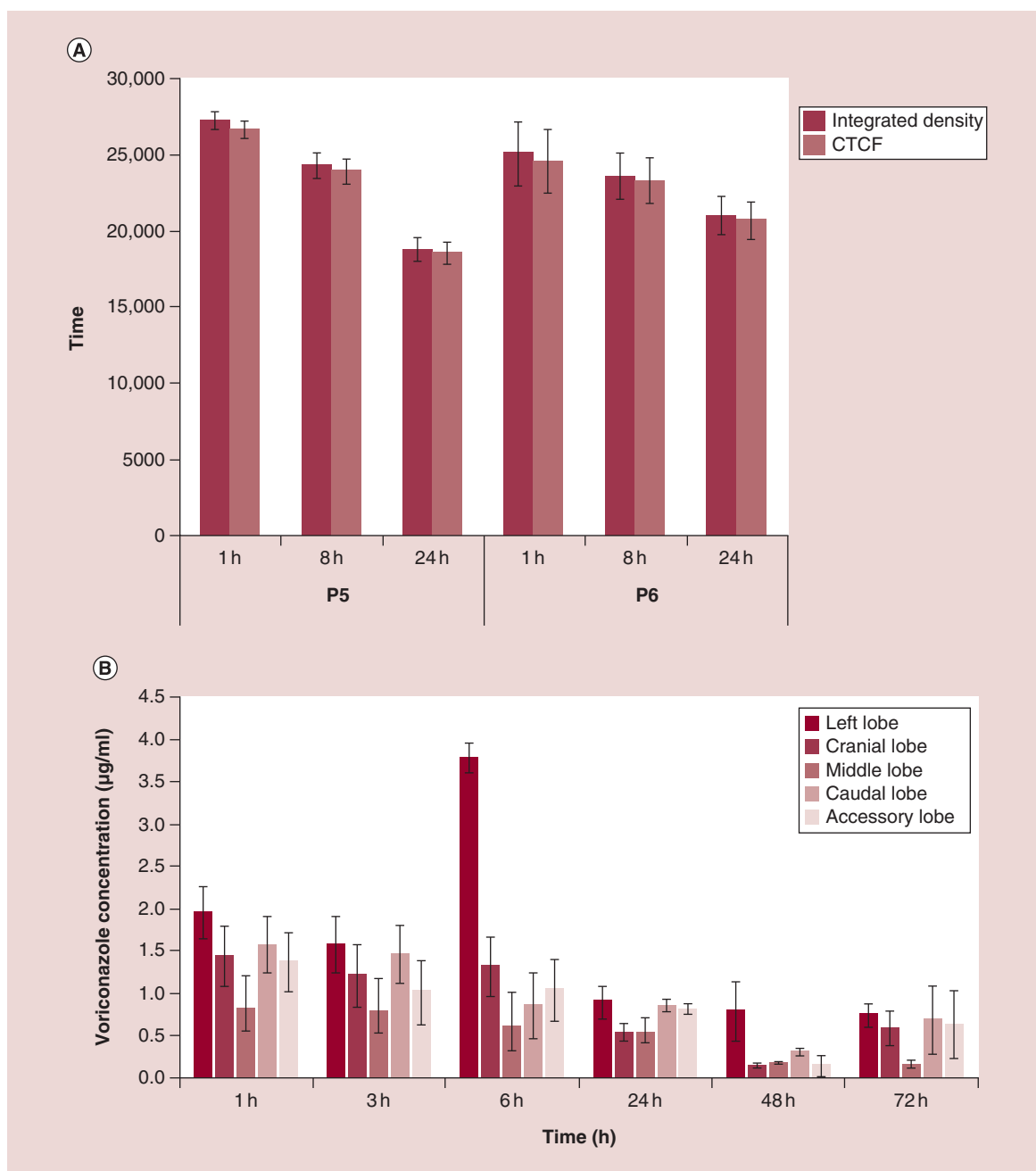


Figure 6. Quantification of fluorescence from lung sections of the experimental animals and distribution of voriconazole in different lobes of lungs of the experimental mice treated with developed nanoparticles. (A) CTCF values and integrated density quantification of FITC fluorescence staining in lung tissue sections after pulmonary delivery of noncoated PLGA nanoparticles and chitosan-coated PLGA nanoparticles (data as mean \pm SD, $n = 3$); (B) Distribution of voriconazole ($\mu\text{g/ml}$) in mice lung lobes at different time points up to 72 h after treatment with noncoated and chitosan-coated nanoparticles in pulmonary route. CTCF: Corrected total cell fluorescence; FITC: Fluorescein isothiocyanate; PLGA: Polylactic-co-glycolic acid; SD: Standard deviation.

The concentration of drug was found to be relatively more in plasma as a result of the higher perfusion rate in lung due to more denser capillary network present in the pulmonary region [56,57]. The mean residence time (MRT) and the half-life ($t_{1/2}$) of voriconazole were found to increase in both the plasma and lung for chitosan-coated nanoparticles as compared with the noncoated nanoparticles and free drug.

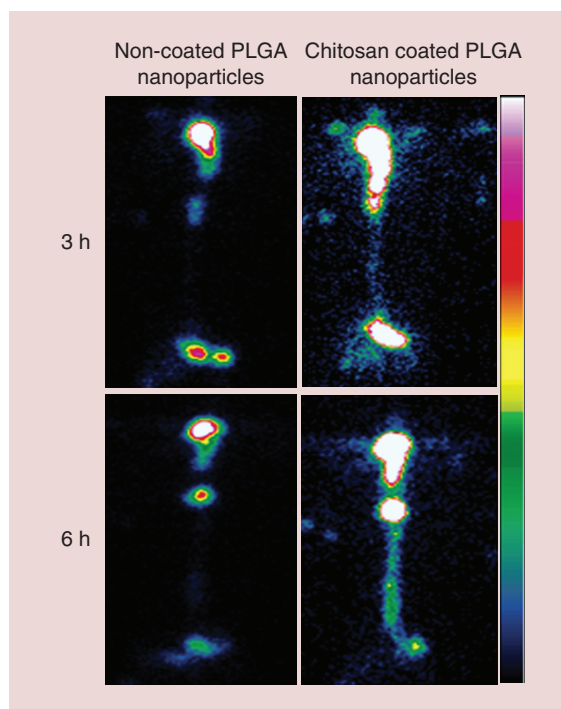


Figure 7. Gamma scintigraphic images of mice treated with Technetium-labelled experimental nanoparticles. Scintigraphy pictures of animals after receiving Tc-99m-labelled poly(lactic-co-glycolic acid) nanoparticles containing voriconazole formulation (P5) and chitosan-coated poly(lactic-co-glycolic acid) nanoparticles containing voriconazole (P6) by pulmonary route after 3 and 6 h.

From Figure 6B, it is evident that left lung lobe had the highest voriconazole concentration, while distribution of drug in the middle lobe was found to have the lowest value during the entire study duration (i.e., 72 h). Drug concentration was detected in all the lobes of lung above minimum inhibitory concentration level (0.5 µg/ml) within 24 h.

Gamma scintigraphy

The noncoated and chitosan-coated nanoparticles containing voriconazole were radiolabeled with Tc-99m with more than 95% efficiency. Figure 7 shows gamma scintigraphy pictures of animals which received Tc-99m-VNP and Tc-99m-VChNP by the pulmonary delivery method. Tc-99m-VChNP was found to be predominantly more in lungs and urinary bladder at 3 h after its pulmonary administration. Interestingly, at 6 h after its administration, it was found to accumulate more in liver and simultaneously there was a substantive decrease in urinary bladder. This suggests its urinary clearance decreased remarkably along with eventual hepatic accumulation. Similar phenomenon was observed in animals after pulmonary administration of Tc-99m-VNP at 3 and 6 h. However, markedly low signal was detected in lungs indicating lower amount of retention of Tc-99m-VNP in lungs than Tc-99m-VChNP.

Discussion

In this study, we have developed chitosan-coated, US-FDA-approved biodegradable polymer (PLGA)-based nanoparticles for pulmonary delivery of voriconazole to treat fungal infections in lungs, which is one of the major killer diseases in immunocompromised patients. Furthermore, its *in vitro* characterization and pharmacokinetic evaluation have been reported here. Initially, we have investigated drug to excipients interaction by FTIR spectroscopy. Data reveal that all the typical bands of PLGA and voriconazole were present in the FTIR spectrum of their physical mixture. Furthermore, the presence of the characteristic peaks of drug and the excipients in the formulations were observed. This suggests that there was no chemical interaction between the drug and the excipients used in this study. However, shifting of some peaks was also observed. The probable reason might be due to the physical interactions by formation of weak physical bonds such as van der Waals force of attraction, H-bonding or dipole–dipole interaction between the various functional groups of voriconazole, PLGA, chitosan and PVA molecules. The physical interaction might be responsible for the formation of spherical structure of the nanoparticles and sustained drug release from them. Presence of drug peak in the lyophilized formulations suggests that some drug molecules were present on the surface.

Voriconazole was present in DCM along with the PLGA in the primary emulsion (W/O). This primary emulsion was further emulsified in the 1.5% PVA solution to prepare W/O/W emulsion. Initially, the pH of the PVA solution for preparation of secondary emulsion was brought down to pH 3.0 to solubilize chitosan and during this process some of the voriconazole molecules leached from the DCM solution to the aqueous media and at this low pH voriconazole remained dissolved along with the chitosan in this aqueous PVA media. However, for coating purpose, when the pH was raised to pH 9.0, there might be coprecipitation of chitosan along with the drug on the surface of the nanoparticles. Presence of this drug molecule on the surface might have been detected by the FTIR study.

Drug–polymer ratio was varied to initially optimize the drug loading and particle size of the experimental noncoated nanoparticles and drug–polymer ratio (1:1) was established to be the best for this purpose. The ratio of drug:PLGA:chitosan was optimized as 1:1:0.4 for the purpose of development of chitosan-coated nanoparticles. In this method, incorporation of chitosan coating was done simultaneously during the process of development of multiple emulsion and no additional step for coating was required. Furthermore, time of lyophilization was also same as it was required for noncoated formulation. Thus, this simple process of chitosan coating on nanoparticle could be highly beneficial for the industrial production point of view. However, due to chitosan coating, the drug loading was found to decrease as compared with the noncoated formulation. This might be due to the dissolution of some drug molecules, which escape from the formulation due to acidic pH (pH 3.0) as voriconazole has high solubility in acidic pH (1.2) [58,59]. As we have mentioned earlier, the coating was developed by coprecipitation of the drug along with the polymer, there must be a loss of drug owing to the precipitation of the drug at higher pH. Drug-loading efficiencies in both the types of formulations were more or less similar. However, the overall value (~70%) was less than the expected. It might be due to the incomplete removal of the whole product from the small containers and the homogenizer. There was a little variation of % drug-loading efficiency due to chitosan coating and that may be due to the use of much less quantity of material for preparation of nanoparticles.

There are several investigations proposing PLGA/chitosan nanoparticles available in the literature. Yang *et al.* and Babu *et al.* have prepared chitosan-coated nanoparticles by the multistep method. Initially, they have prepared PLGA nanoparticles and lyophilized them. In the next step, the lyophilized nanoparticles were coated with chitosan. Both of them used PLGA variety 50:50 with variable drug loading [60,61]. Babu *et al.* had 6.5% drug loading [61]. On the other hand, Yang *et al.* had drug loading of about 3.5% [60]. In another study, Taetz *et al.* wanted to deliver antisense 20-Omethyl-RNA using chitosan-coated PLGA nanoparticles where the variety of PLGA used was 70:30. Initially, they mix PLGA-ethyl acetate (EA) solution with chitosan containing PVA solution for 1 h and this mixture was homogenized at 13,500 rpm for 15 min. But no data related to drug loading were reported [62]. In our study, we used PLGA (85:15) and chitosan to develop chitosan-coated PLGA nanoparticles. This is a single-step method where formation of nanoparticles and coating of chitosan were done simultaneously. Our method is similar to the method described by Taetz *et al.* However, instead of mixing PLGA-EA solution with aqueous chitosan containing 2.5% PVA for 1 h [62], we added primary emulsion (PLGA-DCM-acetone in 2.5% aqueous PVA) to chitosan dissolved in 1.5% PVA solution at pH 3.0 just before the preparation of secondary emulsion. This improves the drug loading about five-times more than the other two reported methods.

Four different methods, namely, DLS, FESEM, AFM and Cryo-TEM were adopted in order to accurately know the particle size, particle size distribution, surface morphology and surface coating by chitosan on the PLGA nanoparticles containing voriconazole in lyophilized as well as hydrated states. Sizes of lyophilized particles observed using FESEM were smaller than those detected by DLS. The difference in size may be because of the DLS method, which measures the average hydrodynamic diameter of nanoparticles in aqueous suspension where the particles might swell and increase in size [63]. Size analysis data by DLS (Supplementary Figure 1) show that the average size (Z-average) of noncoated nanoparticles (154.6 nm; Supplementary Figure 1A) and that of chitosan-coated nanoparticles (277 nm; Supplementary Figure 1B) were well below 300 nm. The range of obtained particle size has been reported to distribute throughout the lungs (i.e., from the upper lobe to lower lobe region) by pulmonary delivery [64]. Lyophilized PLGA nanoparticles and chitosan-coated nanoparticles were free flowing in nature. In pulmonary drug delivery, flowability of powder is predominantly important for distribution of nanoparticles by DPI/nebulizer to the lungs. More is the flowability of the powder, more is its distribution and deposition in various parts of lungs. Presence of chitosan can help the nanoparticulate powder to adhere to the alveoli and not to be phagocytosed quickly [26].

Maximum deposition of particles from P5 and P6 were observed at stage 5 (1.1–2.1 μm diameter) of cascade impactor apparatus (Figure 4). Data obtained upon deposition of particles on different stages of cascade impactor showed that particle size obtained in P5 and P6 is relevant (150–300 nm) for deposition in trachea, primary and

secondary bronchi, and alveolar region for deep lung penetration [54]. Higher deposition from chitosan-coated particles (P6) at stage 0 (9.0–10 μm) to stage 2 (4.7–5.8 μm) and at stage 5 (1.1–2.1 μm) is also suitable for deposition in the pharynx and terminal bronchial area, respectively, of the pulmonary tract [54]. The zeta potential of a particle is the overall charge that particles acquire in a particular medium and at particular temperature [65]. The physical stability of particles can also be predicted from their zeta potential value. Zeta potential value above +30 mV and/or below -30 mV indicates that the particles are having good colloidal stability [30]. Zeta potential values in between +30 and -30 mV suggest that the precipitation of particles in a suspension is more as the zeta potential value changes more toward zero [66]. Thus, the noncoated nanoparticles (surface charge -14.8 mV; Supplementary Figure 1C) may settle down faster than the chitosan-coated nanoparticles (surface charge +31.9 mV; Supplementary Figure 1D), while in suspension. Presence of terminal carboxyl group in the PLGA polymer provided negative surface charge in the noncoated nanoparticles [67], while positive surface charge of the coated nanoparticles was due to the presence of amino group of chitosan [68]. In case of noncoated nanoparticles, they should be stored in a lyophilized form and should be reconstituted just before use to prevent faster precipitation.

FESEM images (Figure 2D & E) of the experimental nanoparticles show that all the particles belonged to P5 and P6 had smooth surface. This data along with the findings of AFM (Figure 2F & G) and cryo-TEM (Figure 2A & B) suggest that the particles were spherical and submicron size with a heterogenous distribution where particles size varied from 150 to 300 nm.

Furthermore, their characterization by cryo-TEM reveals that the obtained nanoparticles were coated (Figure 2D). The analysis by cryo-TEM is a method for the amplification of selected basic structural questions rather than for regular quality control issues [69]. TEM analysis (Figure 2C) of chitosan-coated nanoparticles show that the additional polymer (chitosan) was uniformly deposited (as a coat) on to the surface of PLGA nanoparticles.

In vitro drug release data for PLGA nanoparticles and chitosan-coated PLGA nanoparticles containing voriconazole show that voriconazole released in a sustained manner with a predominant burst release (about 35–45%) initially within 1 h in SLF, pH 7.4 and PBS, pH 7.4 (Figure 3). Burst release of coated formulation found to be more in SLF than PBS. Burst release decreased in case of same formulation when studied in PBS. This might be due to the presence of several salts such as magnesium chloride, potassium chloride, sodium acetate, sodium sulfate, sodium citrate, etc., in the SLF and those salts might have enhanced the drug dissolution faster in case of chitosan-coated formulation as compared with the noncoated PLGA formulation. Drug release kinetic data show that drug release from the nanoparticles might follow a complex mechanism of diffusion as well as erosion as the data were best supported by the Korsmeyer–Peppas kinetic model.

In vivo uptake of FITC nanoparticles containing drug in the alveoli of both the lungs was found to remain almost similar with the duration (24 h) of the study in case of coated nanoparticles. However, for noncoated nanoparticles, the initial uptake was found to be more but with the duration the value decreased. Possibly, this could be due to the mucoadhesive effect of the coated particles that retained longer time in the lungs as compared with the noncoated one.

The pharmacokinetic data reveal that the C_{max} was found to be greater for noncoated nanoparticles in both the plasma and lung. This could be due to the slow drug release. Furthermore, chitosan is a hydrophilic polymer and voriconazole has little solubility in water. Hence, diffusion of hydrophobic voriconazole through chitosan might have taken longer time as compared with PLGA nanoparticle. T_{max} values of voriconazole of P5 and P6 for lung pharmacokinetics were same. However, those values varied in plasma kinetics. T_{max} value for chitosan-coated formulation in plasma kinetics was 3 h, which was half of that value for noncoated formulation.

Chitosan coating increased the AUC and AUMC 4.77-times and 38-times in plasma and 2.49-times and 10-times in lungs, respectively. The enhanced AUC and AUMC values suggest that the availability of drug from the formulation was more for chitosan-coated formulation. This might be due to the slower release and predominantly longer MRT of drug in plasma and lung tissue from the chitosan-coated formulation.

Several reasons may be given for improved bioavailability of voriconazole after pulmonary administration of chitosan-coated nanoparticles. Bioadhesion, conferred by chitosan, is probably responsible for the enhancement of drug pharmacokinetic profile in both the blood and lung. The bioadhesion is achieved through different mechanisms such as electrostatic interaction, hydrogen bond, covalent linkage or van der Waals forces [26,70]. Bioadhesion results in increased residence time at the lung epithelial cells and thus enhances the drug absorption due to the close intimacy of nanoparticles with the epithelial cells. Moreover, avoidance of hepatic 'first-pass' metabolism contributes to improve bioavailability of the nanoparticles. The improved AUC values for the coated particles also guarantee for the prolonged drug release from the nanoformulations in a slow and sustained manner.

A marked increase in MRT of voriconazole in case of chitosan-coated nanoparticles was noticed as compared with the voriconazole in PLGA nanoparticles and free voriconazole. This is because of the more residence time of the nanoparticles in the lung due to chitosan coating. The slow release of voriconazole from the nanoparticles due to more biodegradation time of the nanoparticles prepared with biocompatible and biodegradable polymer PLGA also increases the pharmacokinetic parameters in comparison with the free voriconazole (Table 3). In this study, drug level in lung tissue as well as plasma was measured. Due to the localized nature of LFIs, to measure concentration of voriconazole in different lobe is more meaningful, especially for chitosan-coated PLGA nanoparticulate formulation due to its better pharmacokinetic profile.

The micron-sized foreign bodies primarily have clearance by phagocytosis by resident alveolar macrophages. Inhaled nanosized particles generally are not recognized by macrophages and might instead be internalized by traversing the alveolar epithelium consisting of cuboidal alveolar type II epithelial cells and flattened alveolar type I epithelial cells [71]. The alveolar type I epithelial cells are the primary target of inhaled nanoparticles mediated through clathrin- and caveolin-mediated endocytic pathways important in *trans*-epithelial transport, receptor recycling and cellular signaling. Whereas secretory alveolar type II cells synthesize and release pulmonary surfactant that helps reducing the surface tension at the air–liquid interface and contains surfactant proteins A–D, which act as opsonins to promote clearance [71]. In case of chitosan-coated particles due to the mucoadhesive nature of chitosan, the clearance through A–D cell surfactant protein might be distinctly hindered compared with the noncoated particles. This might have held prolonged retention time of P6 formulation in the alveoli resulting in remarkably longer AUC and AUMC values of the drug in lungs. This is an important requirement for treating the LFI.

As far as toxicity is concerned, study shows that PLGA nanoparticles without the tamoxifen citrate failed to show any toxicity to viable cells and exhibited viability of 99.11% in MCF7 cell line [32]. Another study revealed that chitosan-coated PLGA nanoparticles showed less toxicity in lung fibroblasts than in cancer cells and interestingly it showed negligible toxicity in normal human bronchial epithelial cells at equivalent drug concentrations used in cancer cells [61]. Dyawanapelly *et al.* found that none of the PLGA nanoparticles or chitosan-coated PLGA nanoparticles exhibit cytotoxicity to A549 cells as compared with 1% Triton X-100 as positive control (100% cytotoxic) even at much higher concentrations of 20 mg/ml [70]. Trif *et al.* found that PLGA and chitosan-PLGA nanoparticles were not cytotoxic at concentrations up to 2500 µg/ml in Madin–Darby bovine kidney and human colorectal adenocarcinoma cells [72]. Parveen and Sahoo showed that void nanoparticles of PLGA and PLGA-chitosan showed no considerable toxicity of 5 days of incubation study in different cell lines used [26]. Chronopoulou *et al.* concluded that chitosan coating of dexamethasone-loaded PLGA NPs without inducing cytotoxicity permit their uptake by cultured 3T6 and C3A cells [25].

In vivo evaluation of experimentally developed chitosan-coated nanoparticles was achieved by gamma scintigraphic imaging of the particles deposited in the lung. Imaging provides information on the amount and localization of Tc-99m-VNP and Tc-99m-VChNP deposited in lungs after their administration through pulmonary route. The comparatively more deposition and retention of the nanoformulations was seen in case of chitosan-coated formulation in spite of more elimination of chitosan-coated formulation from the mice with respect to the noncoated formulation. The nonadhered particles might have eliminated and Tc-99m-VChNP was found to eliminate more as compared with Tc-99m-VNP. More water affinity of chitosan polymer might have eliminated the nonadhered chitosan-coated formulation more and faster in the excretory organ. On the other hand, the mucoadhesive nature of the polymer chitosan might overcome the problem of low retainability of the formulation in lungs and thus helped promoting more and longer retention of the sustained release formulation. With the time (at 3 and 6 h), there were eventual enhancement of hepatic accumulation of Tc-99m-VChNP and Tc-99m-VNP and a simultaneous decrease of them in urinary bladder. It suggests that nanoparticles deposited in the lungs preferentially eliminated through liver.

Conclusion

Studies presented on the current article indicate that the administration of inhalable chitosan-coated PLGA nanoparticles led to predominantly prolonged retention of the nanoparticles in the lung as well as in plasma. We believe that this improvement was caused by the enhancement of mucoadhesion effect owing to the surface coating using chitosan and sustained release effect of PLGA and chitosan. Further studies are warranted in the area. Experimental nanoparticles intended for pulmonary delivery may have considerable pharmaceutical potential in the treatment of LFI.

Summary points

Background

- Local delivery of medications to the lungs is highly desirable, especially in patients with specific pulmonary diseases such as cystic fibrosis, asthma, chronic pulmonary infections or lung cancer.
- Current therapies are insufficient to prevent recurrent fungal infection in lungs.
- The aim of the present investigation was to develop, characterize and evaluate chitosan-coated poly(lactic-co-glycolic acid) (PLGA) nanoparticles containing voriconazole intended for pulmonary delivery of medication to lungs for treating lung-fungal infections.

Methods

- The novelty relies on the simple and reproducible preparation method for chitosan-coated biodegradable polymer-based nanoparticles with uniform coating.
- Physicochemical *in vitro* and *in vivo* characterizations of the developed nanoformulations using advanced scientific methods have been performed to get extensive understanding of the developed formulation.

Results & conclusion

- Nanoparticles reached in deep lung tissue and delivered drug for both local and systemic actions by promoting cellular adhesion and retention of the delivery system at the target site.
- Deposition of FITC-containing chitosan-coated nanoparticles in lung and the lung alveoli has been confirmed by confocal images up to 24 h.
- Pharmacokinetics study showed that chitosan coating onto PLGA nanoparticles promoted to release drug in lungs from where it was transferred to systemic circulation having advantage of highly vascularized system and increased *in vivo* residence time in comparison to the PLGA nanoparticles.
- Gamma scintigraphic imaging showed that more retention of chitosan-coated nanoparticles in lungs as compared with noncoated formulation was achieved.
- Nanoparticles maintained prolonged drug level in lungs and the distribution of drug from the chitosan-coated formulation in five different lobes of lung up to 72 h showed that drug was above minimum inhibitory concentration level, thus, it was obviously beneficial to kill the fungal spores that generally remain dormant and survive in case of conventional treatment and causes recurrence of the disease.
- Therefore, chitosan coating on PLGA nanoparticles is promising for bioavailability improvement for effective pulmonary delivery and may be for efficacious treatment of fungal infection in lung.

Acknowledgements

The authors are thankful to S Dewanjee and TK Dua for HPLC analysis and assisting in animal study. The authors are indebted to J Sengupta and C Biswas for Cryo-TEM analysis, SN Bhattacharyya and D Sarkar for confocal microscopy at CSIR-IICB, Kolkata. The authors also acknowledge WBPCB for the Cascade Impactor Facility and Centre for Research in Nanoscience and Nanotechnology, University of Calcutta for FE-SEM analysis.

Financial & competing interests disclosure

This work is supported by Women Scientist (WOS-A), Department of Science & Technology (DST), Govt. of India (sanction no. SR/WOS-A/LS-1356/2014, dated 28.07.2015). The authors have no other relevant affiliations or financial involvement with any organization or entity with a financial interest in or financial conflict with the subject matter or materials discussed in the manuscript apart from those disclosed.

No writing assistance was utilized in the production of this manuscript.

Ethical conduct of research

The experimental protocol of the study was approved by the Institutional Animal Ethics Committee of Jadavpur University, Kolkata. Animal care was in accordance with the Committee for the Purpose of Control and Supervision of Experiments on Animals guidelines.

References

Papers of special note have been highlighted as: ● of interest; ●● of considerable interest

1. Kuzmov A, Minko T. Nanotechnology approaches for inhalation treatment of lung diseases. *J. Control. Release* 219, 500–518 (2015).
2. Patil JS, Sarasija S. Pulmonary drug delivery strategies: a concise, systematic review. *Lung India* 29(1), 44–49 (2012).
3. Mansour HM, Rhee YS, Wu X. Nanomedicine in pulmonary delivery. *Int. J. Nanomedicine* 4, 299–319 (2009).

4. Lee C, Choi JS, Kim I *et al.* Long-acting inhalable chitosan-coated (polylactic-co-glycolic acid) nanoparticles containing hydrophobically modified exendin-4 for treating type 2 diabetes. *Int. J. Nanomedicine* 8, 2975–2983 (2013).
5. Flume P, Klepser ME. The rationale for aerosolized antibiotics. *Pharmacotherapy* 22, 71–79 (2002).
6. Codrons V, Vanderbist F, Verbeeck RK *et al.* Systemic delivery of parathyroid hormone (1–34) using inhalation dry powders in rats. *J. Pharm. Sci.* 92, 938–950 (2003).
7. Gessler T, Schmehl T, Olschewski H, Grimminger F, Seeger W. Aerosolized vasodilators in pulmonary hypertension. *J. Aerosol. Med.* 15, 117–122 (2002).
8. Gessler T, Seeger W, Schmehl T. Inhaled prostanoids in the therapy of pulmonary hypertension. *J. Aerosol. Med. Pulm. Drug Deliv.* 21(1), 1–12 (2008).
9. Smola M, Vandamme T, Sokolowski A. Nanocarriers as pulmonary drug delivery systems to treat and to diagnose respiratory and non respiratory diseases. *Int. J. Nanomedicine* 3(1), 1–19 (2008).
10. Lee WH, Loo CY, Traini D, Young PM. Inhalation of nanoparticle-based drug for lung cancer treatment: advantages and challenges. *AJPS* 10(6), 481–489 (2015).
11. Gelperina S, Kisich K, Iseman MD, Heifets L. The potential advantages of nanoparticle drug delivery systems in chemotherapy of tuberculosis. *Am. J. Respir. Crit. Care Med.* 172(12), 1487–1490 (2005).
12. Da Silva AL, Santos R, Xisto D, Alonso SV, Morales MM, Rocco PRM. Nanoparticle-based therapy for respiratory diseases. *An. Acad. Bras. Cienc.* 85(1), 137–146 (2013).
13. Das PJ, Paul P, Mukherjee B *et al.* Pulmonary delivery of voriconazole loaded nanoparticles providing a prolonged drug level in lungs- a promise for treating fungal infection. *Mol. Pharm.* 12(8), 2651–2664 (2015).
- **Describes the development of HPLC method and preparation of polylactic-co-glycolic acid nanoparticles to enhance particles retention in lung over free drug as shown in gamma imaging.**
14. Zhao K, Zhang Y, Zhang X *et al.* Chitosan-coated poly(lactic-co-glycolic) acid nanoparticles as an efficient delivery system for Newcastle disease virus DNA vaccine. *Int. J. Nanomedicine* 9(1), 4609–4619 (2014).
15. Liu J, Gong T, Fu H *et al.* Solid lipid nanoparticles for pulmonary delivery of insulin. *Int. J. Pharm.* 356(1–2), 333–344 (2008).
16. Videira MA, Botelho MF, Santos AC, Gouveia LF, de Lima JJ, Almeida AJ. Lymphatic uptake of pulmonary delivered radiolabelled solid lipid nanoparticles. *J. Drug Target.* 10(8), 607–613 (2002).
17. Sinha B, Pattnaik G, Mukherjee B. Poly-lactide-co-glycolide nanoparticle containing voriconazole for pulmonary delivery: *in vitro* and *in vivo* study. *Nanomedicine* 9(1), 94–104 (2013).
18. Makadia HK, Siegel SJ. Poly lactic-co-glycolic acid (PLGA) as biodegradable controlled drug delivery carrier. *Polymers* 3(3), 1377–1397 (2011).
19. Sahana B, Santra K, Basu S, Mukherjee B. Development of biodegradable polymer based tamoxifen citrate loaded nanoparticles and effect of some manufacturing process parameters on them: a physicochemical and *in-vitro* evaluation. *Int. J. Nanomedicine* 5, 621–630 (2010).
20. Singh R, Lillard JW Jr. Nanoparticle-based targeted drug delivery. *Exp. Mol. Pathol.* 86(3), 215–223 (2009).
21. Ghosh S, Mondal L, Chakraborty S, Mukherjee B. Early stage HIV management and reduction of stavudine-induced hepatotoxicity in rats by experimentally developed biodegradable nanoparticles. *AAPS PharmSciTech.* 18(3), 697–709 (2017).
22. Yang R, Yang SG, Shim WS *et al.* Lung-specific delivery of paclitaxel by chitosan-modified PLGA nanoparticles via transient formation of microaggregates. *J. Pharm. Sci.* 98(3), 970–984 (2009).
23. Tahara K, Yamamoto H, Hirashima N, Kawashima Y. Chitosan-modified poly(d,l-lactide-co-glycolide) nanospheres for improving siRNA delivery and gene-silencing effects. *Eur. J. Pharm. Biopharm.* 74(3), 421–426 (2010).
24. Babu A, Templeton AK, Munshi A, Ramesh R. Nanoparticle-based drug delivery for therapy of lung cancer: progress and challenges. *J. Nanomater.* 2013, 1–11 (2013).
25. Chronopoulou L, Massimi M, Giardi MF *et al.* Chitosan-coated PLGA nanoparticles: a sustained drug release strategy for cell cultures. *Colloids Surf. B Biointerfaces* 103, 310–317 (2013).
26. Parveen S, Sahoo SK. Long circulating chitosan/PEG blended PLGA nanoparticle for tumor drug delivery. *Eur. J. Pharmacol.* 670(2–3), 372–383 (2011).
27. de Sa FA, Taveira SF, Gelfuso GM, Lima EM, Gratieri T. Liposomal voriconazole (VOR) formulation for improved ocular delivery. *Colloids Surf. B Biointerfaces* 133, 331–338 (2015).
28. Chung H, Lee H, Han HK *et al.* A pharmacokinetic comparison of two voriconazole formulations and the effect of CYP2C19 polymorphism on their pharmacokinetic profiles. *Drug Des. Devel. Ther.* 9, 2609–2616 (2015).
29. Lin SC, Lin SW, Chen JM, Kuo CH. Using sweeping-micellar electrokinetic chromatography to determine voriconazole in patient plasma. *Talanta* 82(2), 653–659 (2010).
30. Dey NS, Mukherjee B, Maji R, Satapathy BS. Development of linker-conjugated nanosize lipid vesicles: a strategy for cell selective treatment in breast cancer. *Curr. Cancer Drug Targets* 16(4), 357–372 (2016).

31. Pattnaik G, Sinha B, Mukherjee B *et al.* Submicron-size biodegradable polymer-based didanosine particles for treating HIV at early stage: an *in vitro* study. *J. Microencapsul.* 29(7), 666–676 (2012).
32. Maji R, Dey NS, Satapathy BS, Mukherjee B, Mondal S. Preparation and characterization of tamoxifen citrate loaded nanoparticles for breast cancer therapy. *Int. J. Nanomedicine* 9, 3107–3118 (2014).
33. Seju U, Kumar A, Sawant KK. Development and evaluation of olanzapine-loaded PLGA nanoparticles for nose-to-brain delivery: *in vitro* and *in vivo* studies. *Acta Biomater.* 7(12), 4169–4176 (2011).
34. Ochiuz L, Grigoras C, Popa M *et al.* Alendronate-loaded modified drug delivery lipid particles intended for improved oral and topical administration. *Molecules* 21(7), pii:E858 (2016).
35. Satapathy BS, Mukherjee B, Baishya R, Debnath MC, Dey NS, Maji R. Lipid nanocarrier-based transport of docetaxel across the blood brain barrier. *RSC Adv.* 6(88), 85261–85274 (2016).
36. Shaw TK, Mandal D, Dey G *et al.* Successful delivery of docetaxel to rat brain using experimentally developed nanoliposome: a treatment strategy for brain tumor. *Drug Deliv.* 24(1), 346–357 (2017).
37. Helvig S, Azmi IDM, Moghimi SM, Yaghmur A. Recent advances in cryo-TEM imaging of soft lipid nanoparticles. *AIMS Biophysics* 2(2), 116–130 (2015).
38. Roy P, Das S, Auddy RG, Mukherjee A. Engineered andrographolide nanosystems for smart recovery in hepatotoxic conditions. *Int. J. Nanomedicine* 9, 4723–4735 (2014).
39. Parikh R, Dalwadi S. Preparation and characterization of controlled release poly-ε-caprolactone microparticles of isoniazid for drug delivery through pulmonary route. *Powder Technol.* 264, 158–165 (2014).
40. Zhang L, Li Y, Zhang Y, Zhu C. Sustained release of isoniazid from polylactide microspheres prepared using solid/oil drug loading method for tuberculosis treatment. *Sci. China Life Sci.* 59(7), 724–731 (2016).
41. Dash S, Murthy PN, Nath L, Chowdhury P. Kinetic modeling on drug release from controlled drug delivery systems. *Acta Pol. Pharm.* 67(3), 217–223 (2010).
- **Describes the release kinetics model.**
42. Rasband WS. ImageJ. US National Institutes of Health, MD, USA (1997–2015). <http://imagej.nih.gov/ij/>
43. Stefančíková L, Porcel E, Eustache P *et al.* Cell localisation of gadolinium-based nanoparticles and related radiosensitising efficacy in glioblastoma cells. *Cancer Nanotechnol.* 5(1), 6 (2014).
- **Describes the method for quantification of fluorescence of fluorescein isothiocyanate in nanoparticles in the lung tissue section.**
44. Sinha B, Mukherjee B. Development of an inhalation chamber and a dry powder inhaler device for administration of pulmonary medication in animal model. *Drug Dev. Ind. Pharm.* 38, 171–179 (2012).
- **Designed a nose-only inhalation chamber for delivering the nanoparticles to mice using dry powder inhaler.**
45. Reddy LH, Murthy RS. Pharmacokinetics and biodistribution studies of doxorubicin loaded poly(butyl cyanoacrylate) nanoparticles synthesized by two different techniques. *Biomed. Pap. Med. Fac. Univ. Palacky Olomouc. Czech Repub.* 148(2), 161–166 (2004).
46. Ma W, Lu S, Pan P, Sadatmousavi P, Yuan Y, Chen P. Pharmacokinetics of peptide mediated delivery of anticancer drug ellipticine. *PLoS ONE* 7(8), e43684 (2012).
47. Kan SL, Li J, Liu JP, He HL, Zhang WZ. Evaluation of pharmacokinetics and pharmacodynamics relationships for salvianolic acid B micro-porous osmotic pump pellets in angina pectoris rabbit. *AJPS* 9(3), 137–145 (2014).
48. Kudgus RA, Walden CA, McGovern RM, Reid JM, Robertson JD, Mukherjee P. Tuning pharmacokinetics and biodistribution of a targeted drug delivery system through incorporation of a passive targeting component. *Sci. Rep.* 4, 1–6 (2014).
49. Kumirska J, Czerwicka M, Kaczyński Z *et al.* Application of spectroscopic methods for structural analysis of chitin and chitosan. *Mar. Drugs* 8(5), 1567–1636 (2010).
50. Darder M, Colilla M, Ruiz-hitzky E. Biopolymer-clay nanocomposites based on chitosan intercalated in montmorillonite. *Chem. Mater.* 15, 3774–3780 (2003).
51. Paluszkiwicz C, Stodolak E, Hasik M, Blazewicz M. FT-IR study of montmorillonite–chitosan nanocomposite materials. *Spectrochim. Acta A Mol. Biomol. Spectrosc.* 79, 784–788 (2011).
52. Yuan Q, Shah J, Hein S, Misra RD. Controlled and extended drug release behavior of chitosan-based nanoparticle carrier. *Acta Biomater.* 6, 1140–1148 (2010).
53. Silva SML, Braga CRC, Fook MVL, Raposo CMO, Carvalho LH, Canedo EL. Application of Infrared Spectroscopy to Analysis of Chitosan/Clay Nanocomposites. In: *Infrared Spectroscopy- Materials Science, Engineering and Technology*. Theophile T (Ed.). InTech, Rijeka, Croatia, 43–62 (2012).
54. Mitchell JP, Roberts DL. Current approaches to APSD measurements of OIPs based on inertial impaction. In: *Good Cascade Impactor Practices, AIM and EDA for Orally Inhaled Products*. Tougas TP, Mitchell JP, Lyapustina SA (Eds). Springer, MA, USA, 15–55 (2013).
55. Jeans AR, Howard SJ, Al-Nakeeb Z *et al.* Combination of voriconazole and anidulafungin for treatment of triazole-resistant aspergillus fumigatus in an *in vitro* model of invasive pulmonary aspergillosis. *Antimicrob. Agents Chemother.* 56(10), 5180–5185 (2012).

56. Sangwan S, Agosti JM, Bauer LA *et al.* Aerosolized protein delivery in asthma: gamma camera analysis of regional deposition and perfusion. *J. Aerosol Med.* 14, 185–195 (2001).
57. Townsley MI. Structure and composition of pulmonary arteries, capillaries and veins. *Compr. Physiol.* 2, 675–709 (2012).
58. Buchanan Charles Michael, Buchanan Norma Lindsey, Lambert Juanelle Little. WO 2007047253 A2 (2007).
59. European Medicines Agency. VFEND scientific discussion. www.ema.europa.eu/docs/en_GB/document_library/EPAR_-_Scientific_Discussion_-_Variation/human/000387/WC500049757.pdf
60. Yang R, Yang SG, Shim WS *et al.* Lung-specific delivery of paclitaxel by chitosan-modified PLGA nanoparticles via transient formation of microaggregates. *J. Pharm. Sci.* 98(3), 970–984 (2009).
61. Babu A, Amreddy N, Muralidharan R *et al.* Chemodrug delivery using integrin-targeted PLGA-Chitosan nanoparticle for lung cancer therapy. *Sci. Rep.* 7(1), 14674 (2017).
62. Taetz S, Nafee N, Beisner J *et al.* The influence of chitosan content in cationic chitosan/PLGA nanoparticles on the delivery efficiency of antisense 2'-O-methyl-RNA directed against telomerase in lung cancer cells. *Eur. J. Pharm. Biopharm.* 72(2), 358–369 (2009).
63. Yu DH, Lu Q, Xie J, Fang C, Chen HZ. Peptide-conjugated biodegradable nanoparticles as a carrier to target paclitaxel to tumor neovasculature. *Biomaterials* 31(8), 2278–2292 (2010).
64. Tisch Environmental, Inc. Model 20–800 Ambient Cascade Impactor (non-viable). Operations manual. <https://tisch-env.com/wp-content/uploads/2015/06/TE-20--800-Non-viable-Cascade-Impactor.pdf>
65. Averineni RK, Shavi GV, Gurram AK *et al.* PLGA 50:50 nanoparticles of paclitaxel: development, *in vitro* anti-tumor activity in BT - 549 cells and *in vivo* evaluation. *Bull. Mater. Sci.* 35(3), 319–326 (2012).
66. Tuan TQ, Hao PV, Quynh LM, Luong NH, Hai NH. Preparation and properties of silver nanoparticles by heat-combined electrochemical method. *VNU J. Sci. Math. Phys.* 31(2), 36–44 (2015).
67. Sun SB, Liu P, Shao FM, Miao QL. Formulation and evaluation of PLGA nanoparticles loaded capecitabine for prostate cancer. *Int. J. Clin. Exp. Med.* 8(10), 19670–19681 (2015).
68. Ing LY, Zin NM, Sarwar A, Katas H. Antifungal activity of chitosan nanoparticles and correlation with their physical properties. *Int. J. Biomater.* 2012, 632698 (2012).
69. Laan AC, Denkova AG. Cryogenic transmission electron microscopy: the technique of choice for the characterization of polymeric nanocarriers. *EJNMMI Res.* 7(1), 44 (2017).
70. Dyawanapelly S, Koli U, Dharamdasani V, Jain R, Dandekar P. Improved mucoadhesion and cell uptake of chitosan and chitosan oligosaccharide surface-modified polymer nanoparticles for mucosal delivery of proteins. *Drug Deliv. Transl. Res.* 6(4), 365–379 (2016).
71. Thorley AJ, Ruenraroengsak P, Potter TE, Tetley TD. Critical determinants of uptake and translocation of nanoparticles by the human pulmonary alveolar epithelium. *ACS Nano* 8(11), 11778–11789 (2014).
72. Trif M, Florian PE, Roseanu A *et al.* Cytotoxicity and intracellular fate of PLGA and chitosan-coated PLGA nanoparticles in Madin-Darby bovine kidney (MDBK) and human colorectal adenocarcinoma (Colo 205) cells. *J. Biomed. Mater. Res. A* 103(11), 3599–3611 (2015).

Pulmonary Delivery of Voriconazole Loaded Nanoparticles Providing a Prolonged Drug Level in Lungs: A Promise for Treating Fungal Infection

Pranab Jyoti Das,^{†,‡} Paramita Paul,^{§,‡} Biswajit Mukherjee,^{*,§} Bhaskar Mazumder,[†] Laboni Mondal,[§] Rinku Baishya,^{||} Mita Chatterjee Debnath,^{||} and Kumar Saurav Dey[⊥]

[†]Department of Pharmaceutical Sciences, Dibrugarh University, Dibrugarh, Assam-786004, India

[§]Department of Pharmaceutical Technology, Jadavpur University, Kolkata-700032, West Bengal, India

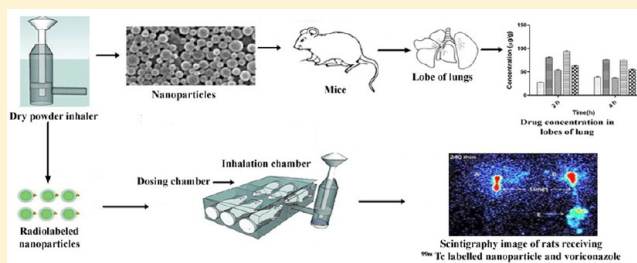
^{||}Infectious and Immunology Division, CSIR-Indian Institute of Chemical Biology, Kolkata-700032, India

[⊥]Guwahati Biotech Park, Technology Complex, Indian Institute of Technology, Guwahati-781039, India

Supporting Information

ABSTRACT: Current therapies are insufficient to prevent recurrent fungal infection especially in the lower part of the lung. A careful and systematic understanding of the properties of nanoparticles plays a significant role in the design, development, optimization, and *in vivo* performances of the nanoparticles. In the present study, PLGA nanoparticles containing the antifungal drug voriconazole was prepared and two best formulations were selected for further characterization and *in vivo* studies. The nanoparticles and the free drug were radiolabeled with technetium-99m with 90% labeling efficiency, and the radiolabeled particles were administered to investigate the effect on their blood clearance, biodistribution, and *in vivo* gamma imaging. *In vivo* deposition of the drug in the lobes of the lung was studied by LC–MS/MS study. The particles were found to be spherical and had an average hydrodynamic diameter of 300 nm with a smooth surface. The radiolabeled particles and the free drug were found to accumulate in various major organs. Drug accumulation was more pronounced in the lung in the case of administration of the nanoparticles than that of the free drug. The free drug was found to be excreted more rapidly than the nanoparticle containing drug following the inhalation route as assessed by gamma scintigraphy study. Thus, the study reveals that pulmonary administration of nanoparticles containing voriconazole could be a better therapeutic choice even as compared to the iv route of administration of the free drug and/or the drug loaded nanoparticles.

KEYWORDS: biodistribution, clearance, gamma imaging, lungs, nanoparticles, pulmonary drug delivery, radiolabeling



1. INTRODUCTION

Voriconazole [(2*R*,3*S*)-2-(2,4-difluorophenyl)-3-(5-fluoro-4-pyrimidinyl)-1-(1*H*-1,2,4-triazol-1-yl)-2-butanol] is an antifungal drug that is derived by modification of fluconazole molecule, having one triazole moiety replaced by a fluoropyrimidine ring and a methyl group added to the propanol backbone.¹ Voriconazole is the first line available second-generation triazole with potent activity against a broad spectrum of clinically significant fungal pathogens, including *Aspergillus*, *Candida*, *Cryptococcus*, and some less common molds. Voriconazole primarily acts by inhibiting fungal cytochrome P450-dependent 14 α -sterol demethylase, an essential enzyme in ergosterol biosynthesis.²

Invasive fungal infection occurs in both immunocompetent and immunocompromised patients.³ Patients with malignancy, HIV, hematologic disease, and conditions requiring immunosuppressive medications have contributed to an escalation of respiratory fungal infections. Fungal infection may be endemic or opportunistic. Many available antifungal treatments are often

limited by concerns about efficacy, safety, drug interaction, and/or cost. Although some liposomal formulations of amphotericin B are developed, these formulations suffer from some problems such as use of lipids in the formulations (lipid peroxidation and stability) and increased toxicity due to nontargeted delivery through the parenteral route.⁴ Moreover, their rapid clearance from circulation due to uptake by the reticuloendothelial system, primarily in the liver, cannot be ignored. Treatment becomes difficult if fungal infection occurs in the lower respiratory tract or deep in the lung, as sustained availability of therapeutic quantities of drug at the site of infection is often inadequate because of rapid removal of drug due to high blood flow turnover in the tissue. Delivery of drug

Special Issue: Advances in Respiratory and Nasal Drug Delivery

Received: January 21, 2015

Revised: April 24, 2015

Accepted: May 5, 2015

Published: May 5, 2015

Table 1. Composition, % Yield, Drug Loading (%), Size Distribution, and Zeta Potential Values of the Experimental Nanoparticle Formulations

formulation code	drug polymer ratio (w/w)	stabilizer used	DCM ^a :acetone (v/v)	homogenization speed (RPM)	% yield	drug loading (%) ± SD (n = 3)	av particle diam (Z-av) (nm)	zeta potential (mV)
FP1	1:10	PVA ^b	4:1	20000	71	2.91 ± 0.09	300	-10.5
FP2	1:10	PVA	4:1	15000	56	2.57 ± 0.22	303.5	-8.10

^aDichloromethane. ^bPolyvinyl alcohol.

directly to the site of action in the case of pulmonary infection can reduce the drug level in the whole blood significantly while the desired therapeutic concentration at the site of infection is maintained. Developing a nanoparticle-based system and delivering it to the lungs may help to retain the particle in lungs over a prolonged period of time and reduce the toxicity compared to the parenteral route. Biodegradability, biocompatibility, mechanical strength, and processing ease are the prime requirements of a polymer matrix for nanoparticle preparation.⁵ Among the various classes of synthetic polymers, poly lactic-co-glycolic acid (PLGA) has a wide range of applicability for controlled drug delivery system.⁶ The lactide/glycolide polymer chains are cleaved by hydrolysis into natural metabolites (lactic acid and glycolic acid) and are washed out from the biosystem by the citric acid cycle.⁷

In the present study, a PLGA based nanosize sustained release delivery system of voriconazole was developed and evaluated to treat fungal infection in lungs. The hypothesis of the present study is that “since the drug is a well-known antifungal agent, if it releases from a formulation and is available at a desirable concentration at the infected tissue site, it would certainly exert its action”. So the prime concern of the study was not to investigate antifungal testing of the drug in the formulation but to understand and ensure that the antifungal drug would be available at an effective concentration at the site of action (lungs) for a prolonged period of time when administered through the pulmonary route.

2. EXPERIMENTAL SECTION

2.1. Materials. Voriconazole (gift sample) was obtained from Dr. Reddy's Laboratories Ltd., Hyderabad, India. Fluconazole was obtained from Regional Drugs Testing Laboratory, Guwahati, India. PLGA (molecular weight (MW) 50,000–75,000; lactide to glycolide ratio 85:15) was purchased from Sigma-Aldrich Chemicals Pvt. Ltd., Bangalore, Karnataka, India. Poly(vinyl alcohol) (PVA, MW 1,25,000) was procured from S. D. Fine-Chem. Ltd., Mumbai, Maharashtra, India. Lactose monohydrate was purchased from Himedia Lab. Pvt. Ltd., Mumbai, Maharashtra, India. Acetone and dichloromethane (DCM) were obtained from E. Merck (India) Ltd., Mumbai, Maharashtra, India. Potassium hydrogen phosphate and disodium hydrogen orthophosphate were procured from Process Chemical Industries, Kolkata, West Bengal, India. All the other chemicals used in this study were of analytical grade.

2.2. Animals. Swiss albino mice weighing 20–25 g of either sex at a ratio of 1:1 were used for gamma scintigraphy and *in vivo* deposition study. Sprague–Dawley rats of either sex (male:female ratio 1:1) (body weight 250 to 300 g) were selected for the blood clearance and biodistribution studies. The experimental protocols were approved by the Jadavpur University and Dibrugarh University Animal Ethics Committees, and procedures followed were in accordance with the Committee's guidelines, with necessary care. The animals were

kept in individual cages and fed with a standard diet⁸ and water *ad libitum*.

2.3. Preformulation Study. Preformulation study was carried out to detect any interaction between voriconazole and the excipients. Different techniques such as Fourier transform infrared spectroscopy (FTIR), infrared spectroscopy, differential scanning calorimetry (DSC), thermogravimetric analysis, X-ray diffraction study, etc. are available to detect drug–excipient interaction. In the present study, we initially used FTIR spectroscopy to determine the drug–excipient interaction (if any) at the level of their functional groups. Chemical interaction (if any) between the drug and the excipients was further verified by DSC analysis of the drug, the individual excipients, their physical mixture with or without the drug; and the formulations with or without the drug.

2.3.1. FTIR Spectroscopy. In the FTIR spectroscopic study, pure drug voriconazole, PLGA, PVA, the physical mixture of voriconazole with the excipients, and the lyophilized formulations with or without drug were scanned over a wavenumber range of 4000–400 cm⁻¹ in an inert atmosphere in an FTIR spectrophotometer (Alpha, Bruker, Ettlingen, Germany).

2.3.2. DSC Study. In the DSC study, physicochemical compatibility between voriconazole and the polymers was evaluated using a differential scanning calorimeter (Jade DSC, PerkinElmer, Tokyo, Japan). In the DSC study, accurately weighed samples were hermetically sealed in flat bottom aluminum pans and heated over a temperature range from 40 to 220 °C at a constantly increasing rate of 20 °C/min in an atmosphere of nitrogen gas environment with a flow rate of 20 mL/min.

2.4. Preparation of Voriconazole Loaded PLGA Nanoparticles. Several formulations were prepared by varying voriconazole to polymer ratio (1:10, 1:5 or 1:2.5), stabilizer (PVA or poloxamer), homogenization speed (15000 or 20000 rpm), using solvent(s) in different ratios (DCM:acetone, 1:0, 4:1, 1:4, or 0:1), and the solvent removal process (namely, using rotary vacuum evaporator or overnight stirring on a magnetic stirrer) (Table 1), and the best two formulations (FP1 and FP2) based on % yield, % drug loading, particle size, drug release pattern, etc. were selected. Out of the two formulations, FP1, further showed good drug loading capacity and a smaller range of particle size. Hence, FP1 was finally selected for further *in vitro* and *in vivo* characterizations.

Voriconazole nanoparticles were prepared by a modified multiple emulsion solvent evaporation technique.⁹ Initially blank nanoparticles (without drug) were prepared without adding the drug. Briefly, 250 mg of PLGA was solubilized in 3 mL of DCM. 1.5% (w/v) and 2.5% (w/v) aqueous PVA solutions were prepared by slowly adding the required amount of PVA in double distilled water (DDW) and heating lightly on a magnetic stirrer with a heating facility (IMLH magnetic stirrer, Remi Equipment, Mumbai, India). The organic polymeric solution was emulsified with dropwise gradual

addition of 0.5 mL of 2.5% PVA solution, homogenized for 5 min using a high speed homogenizer (Ultra-Turrax, model T10B, IKA Laboratory Equipment, Staufen, Germany). This primary emulsion (water-in-oil) was quickly poured dropwise into 75 mL of PVA (1.5% w/v) solution and homogenized for 8 min to get a multiple emulsion of water-in-oil-in-water (w/o/w) type. This w/o/w emulsion was kept in a bath sonicator for 10 min to break the large globules and then stirred overnight on a magnetic stirrer to remove the organic solvents completely.¹⁰ Rotary vacuum evaporator (Rotovac, model PBU-6, Superfit Continental Pvt. Ltd., Mumbai, India) was also used for removal of organic solvents for some preparations. It was run for 30 min at 130 rpm at 40 °C. Thus, DCM was allowed to diffuse out and evaporate to get homogeneous nanoparticles. When the nanoparticles started hardening, the particle suspension was kept on a bath-type sonicator (50 Hz) (model ULAC-14, Trans-O-Sonic, Mumbai, India) for 45 min to break the agglomerate if any. Then the particles were separated by centrifugation at 3000 and 15000 rpm in a cooling centrifuge (3K30 Sigma Lab Centrifuge, Merrington Hall Farm, Shrewsbury, U.K.) and washed twice with DDW to remove the excess of PVA and free drug and kept in a Petri dish in an ultrafreezer (Ultra-Low Freezer, model no C85-S, So-Low Environmental Equipment, Cincinnati, OH, USA). Then the preparation was lyophilized (without any cryoprotectant) in a freeze-dryer (laboratory freeze-dryer, Instrumentation India, Kolkata, India) for 8 h. The same experimental procedure was followed for the preparation of voriconazole loaded PLGA nanoparticles. Here the drug was added to the organic polymeric solution after complete dissolution of the polymer.

2.5. Characterization of Nanoparticles. **2.5.1. Percent-age of Yield (% Yield).** The lyophilized nanoparticles were weighed, and the percentage yield of respective formulations was calculated by using the following formula:¹¹

$$\% \text{ yield} = \frac{\text{weight of nanoparticles obtained}}{\text{total weight of drug and polymers used}} \times 100$$

2.5.2. Particle Size Distribution and Zeta Potential. Particle size distribution and zeta potential of all the experimental formulations were measured using a Malvern Zetasizer Nano-ZS 90 (Malvern Instruments, Malvern, U.K.). A weighed quantity of the experimental sample was dispersed in Milli-Q water (Milli-Q, Merck Millipore, Billerica, MA, USA) by vortexing and then sonicated and placed in a cuvette for size and zeta potential measurement.

2.5.3. Drug Loading Study. A drug loading study was performed to find out the amount of drug that had been actually encapsulated in the nanoparticles. In this study a mixture of acetonitrile and DDW in a 1:1 ratio was prepared and used as the solvent system. An amount of 2 mg of nanoparticles was weighed accurately and taken in a micro-centrifuge tube, 2 mL of the solvent mixture was added, and the tube was closed tightly and kept in an incubator shaker (Somax Incubator Shaker; Shenzhen Pango Electronic Co. Ltd., Shenzhen, China) for 4 h. The drug was extracted in the solvent mixture, and the amount of drug present was quantified using a UV-vis spectrophotometer (advanced microprocessor UV-vis single beam, Intech-295, AP, India) at 255 nm. Drug loading was determined as follows:¹²

drug loading (actual) (%)

$$= \frac{\text{amount of drug in nanoparticles}}{\text{amount of nanoparticles obtained}} \times 100$$

2.5.4. Scanning Electron Microscopy (SEM). Particle morphology was assessed by SEM (Jeol JSM-6360, Japan). The lyophilized particles were placed on a carbon tab mounted on an SEM specimen stub. The specimen stub was coated with palladium before observation, which was carried out at 20 kV accelerating voltage.

2.5.5. Transmission Electron Microscopy (TEM). Samples for TEM were prepared by dispersing approximately 1 mg of lyophilized formulation (FP1) in 600 μL of Milli-Q water in a microcentrifuge tube and placing one drop of the sample on a copper grid. The sample was then allowed to dry in air, and finally the dried sample was analyzed using a transmission electron microscope (FEI, Tecnai G2 Spirit Bio Twin, Czech Republic) at about 210–240 V and 50–60 Hz frequency.

2.5.6. Atomic Force Microscopy (AFM). 10 μL of the sample (as mentioned in an earlier paragraph) was deposited onto a freshly cleaved muscovite ruby mica sheet (ASTM V1 grade ruby mica, Micafab, Chennai, India) and placed for 15–30 min. Although mica sheets are strongly negative, the mica surface was chemically altered using 3-aminopropyltriethoxysilane to create positive charge at the surface. This helps bind negatively charged materials (such as nanoparticles in this case) on the mica surface. After 15 min, the sample was dried using a vacuum dryer. The sample was gently washed from time to time with 0.5 mL of Milli-Q water to remove the molecules that were not firmly attached to the mica, and the sample was dried as mentioned above.

Acoustic mode AFM was performed using a Pico plus 5500 ILM AFM (Agilent Technologies, Santa Clara, CA, USA) by a piezo scanner with a maximum range of 9 μm . Microfabricated silicon cantilevers of 225 μm in length with a nominal spring force constant of 21–98 N/m were used from Nanosensors, Soquel, CA, USA. Cantilever oscillation frequency was tuned to resonance frequency (150–350 kHz). The images (512 by 512 pixels) were captured with a scan area of 2.0 \times 2.0 μm at the scan speed rate of 0.5 lines/s. Images were analyzed with the help of PicoView 1.12 version software (Agilent Technologies, Santa Clara, CA, USA).¹³

2.6. In Vitro Assessment. **2.6.1. In Vitro Drug Release Study.** For studying the drug release at various time intervals (mentioned below), an accurately weighed amount of voriconazole loaded nanoparticles (5 mg) from each of the formulations was taken separately in pre-labeled microcentrifuge tubes (2 mL) in triplicate for each time point. The nanoparticles in each of the tubes were suspended in 2 mL of simulated lung fluid (SLF, pH 7.4)¹⁴/phosphate buffer saline (PBS, pH 7.4). The tubes were incubated at 37 °C (with gentle shaking) using an incubator shaker after brief vortexing for the specific time period of 15 days. The pre-labeled respective tubes were taken out at their respective time points, i.e., 3 h and 1, 3, 5, 7, 10, and 15 days, and centrifuged at 5000 rpm for 15 min. The supernatant was separated out and analyzed by UV-vis spectroscopy. The drug release data were plotted as cumulative percentage drug release against time for different formulations.¹⁵

2.6.2. Drug Release Kinetics Study. Data obtained from the *in vitro* drug release study were plotted in different release kinetic models such as zero-order, first-order, Higuchi,

Korsmeyer–Peppas, and Hixson–Crowell kinetic models. Coefficients of determination (R^2), rate constants for zero-order kinetics (K_0), first-order kinetics (K_1), the Higuchi model (K_H), the Hixson–Crowell model (K_{HC}), and the release component (n) for the Korsmeyer–Peppas model were determined (by putting the data in the corresponding plots)¹⁶ to understand drug release kinetics.

2.7. In Vivo Investigation. 2.7.1. Radiolabeling of Voriconazole and Voriconazole Loaded PLGA Nanoparticles.

The radiolabeling of voriconazole and voriconazole loaded nanoparticles with technetium-99m (^{99m}Tc) was done by reduction with stannous chloride (SnCl_2) dihydrate as per the reported method^{17,18} with some modifications. Briefly, 2 mg of voriconazole was dissolved in 1 mL of ethanol (pH adjusted to 4.0), and voriconazole loaded nanoparticle (equivalent to 2 mg of voriconazole; pH 4.0) was dispersed in 1 mL of nitrogen purged water. Aqueous ^{99m}Tc -pertechnetate ($^{99m}\text{TcO}_4^-$) (74–148 MBq) was added to them, followed by the addition of freshly prepared stannous chloride dihydrate solution (20 μL containing 20 μg of SnCl_2). They were then incubated for 15 min at room temperature. The radiolabeled efficiencies were then analyzed by ascending thin layer chromatography (TLC) using 2.5 cm \times 10 cm silica gel strips (Merck, Darmstadt, Germany) as the stationary phase and acetone as a mobile phase. The quantitative analysis of the chromatograms was performed by cutting the strips into 1 cm pieces and counting them in a well-type gamma scintillation counter (Electronic Corporation of India, model LV4755, Hyderabad, India) at 140 keV. The contaminants were identified as reduced/hydrolyzed (R/H) technetium, colloids of tin hydroxides, and free $^{99m}\text{TcO}_4^-$. The free pertechnetate (TcO_4^-) which moved with the solvent front ($R_f = 0.9$) was estimated as 15–20% of the total radioactivity added.

2.7.2. Blood Clearance of Radiolabeled Nanoparticles in Rats. All the animal experiments were approved by the Institutional Animal Ethics Committee, Jadavpur University, Kolkata. Sprague–Dawley rats of either sex (male:female ratio 1:1) (body weight 250 to 300 g) were selected for the blood clearance study. The animals were anesthetized (ketamine 30–50 mg/kg intramuscular), and the femoral vein of each animal was cannulated for blood sampling. A volume of 0.2 mL of the ^{99m}Tc -labeled complexes of voriconazole loaded nanoparticles was intravenously injected. The blood samples were collected starting from 2 min to 4 h, weighed, and analyzed for radioactivity in a gamma ray spectrometer considering the volume of blood as 7.3% of the total body weight.

2.7.3. Biodistribution Study in Rats. The biodistribution of the radiolabeled nanoparticles was investigated in male Sprague–Dawley rats weighing between 250 and 300 g. All animals were well hydrated by the intraperitoneal administration (2 mL) of normal saline (0.9% NaCl (w/v) in water) for 1 h. Then after a gap of 1 h, ^{99m}Tc -chelates of free voriconazole or ^{99m}Tc labeled voriconazole loaded PLGA nanoparticles in a total volume 0.03 mL in each case (8–12 MBq/kg) were injected in each rat through the tail vein. The rats were sacrificed at 0.5 and 4 h postinjection, the organs and tissues (heart, lung, liver, kidneys, spleen, stomach, intestine, muscle, etc.) were collected and then weighed after being washed with normal saline and dried briefly by blotting paper (wherever applicable), and the corresponding radioactivity was measured using a well-type gamma scintillation counter along with an injection standard. The results were expressed as percent injected dose/g of organ/tissue.

2.7.4. Gamma Scintigraphy. *In vivo* evaluation and comparison of the radiolabeled nanoparticles and the radiolabeled free drug were achieved by gamma scintigraphic imaging of both types of particles deposited in lungs. For gamma imaging studies, male and female (ratio 1:1) Swiss albino mice weighing 20–25 g were used. The animals were subjected to dosing once using fabricated and validated dosing chamber and dry powder inhaler (DPI),¹⁹ as mentioned below, and then anesthetized by intramuscular injection of 1 mL of ketamine hydrochloride, and they were fixed on a board in the posterior position. Imaging was performed at different time intervals to 4 h (30 min, 60 min, and 4 h) using a planar gamma camera (GE Infinia Gamma Camera equipped with Xeleris Workstation, GE, Cleveland, OH, USA). Imaging provided direct information on the amount (qualitatively) and location of the nanoparticles and free drug deposited in the lungs after the administration.

2.7.5. In Vivo Deposition of Voriconazole Loaded PLGA Nanoparticles Using Fabricated Dry Powder Inhaler (DPI) and Inhalation Chamber. *In vivo* deposition of voriconazole in different lobes of lungs was studied using previously fabricated and validated inhalation chamber and DPI. Briefly, the DPI consisted of a sample holder with a tube for pumping out the dry powder, which was then transported through a connecting tube and delivered at the dosing chamber region of the inhalation chamber. The inhalation chamber is a rectangular chamber that can hold up to six animals, fabricated in such a way that the noses of the animals are exposed in the dosing chamber. The animals were divided into two groups for two time point study (2 and 4 h), and each group had six animals. Voriconazole nanoparticles (50 mg) were weighed and mixed with 150 mg of microfine lactose. The powder blend was placed inside the fluidization chamber and dosed in the inhalation chamber once. After the completion of dosing, the animals were sacrificed at the designated time points, lungs were removed, and different lobes were separated and marked as left lobe, cranial lobe, middle lobe, accessory lobe, and caudal lobe. They were stored at -80°C until further use. The lung tissue lobes were thawed and homogenized separately with the addition of 1 mL of normal saline for 3 min, followed by vortexing for 30 s and addition of 500 μL of 0.02 M borate buffer (pH 9.0). Again after vortexing for 30 s, 500 μL of ethyl acetate was added, followed by brief vortexing. Internal standard fluconazole 10 μL (4 $\mu\text{g}/\text{mL}$) was then mixed with it. The samples were placed in an aluminum heating block at room temperature and dried under nitrogen stream for 60 min. The samples were redispersed in 200 μL of mobile phase, centrifuged at 15000 rpm for 3 min, and transferred to HPLC vial after filtration for LC–MS quantification. The drug content was calculated from the calibration curve developed in the same way within the concentration range 45.30 to 961.92 ng/mL.

2.7.6. Chromatographic and Mass Spectroscopic Analysis. The liquid chromatography tandem mass spectrometry (LC–MS/MS) (Agilent 6410 Triple Quad MS-MS, Baltimore, MD, USA) was used for quantification of voriconazole from the different lobes of lungs. The mobile phase for the chromatographic separation was composed of acetonitrile–water–formic acid (60:40:0.05 v/v/v). The mobile phase was filtered before being used, and it was delivered at a flow rate of 0.4 mL/min. The analyte was monitored using a mass spectrometer equipped with a double quadrupole and an electrospray ionization interface, operated in a positive mode. The analysis

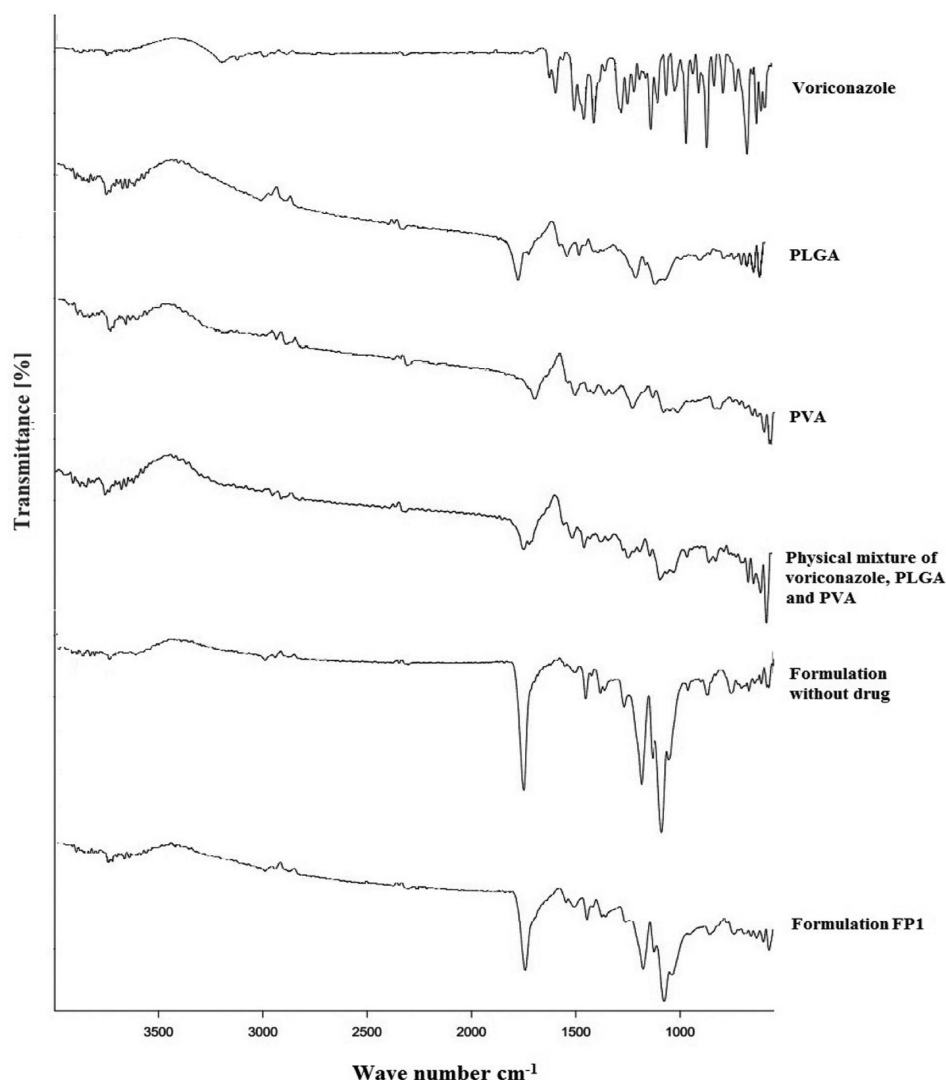


Figure 1. Fourier transform infrared (FTIR) spectra of (A) voriconazole; (B) poly lactic-*co*-glycolic acid (PLGA); (C) poly(vinyl alcohol) (PVA); (D) physical mixture of voriconazole, PLGA, and PVA; (E) formulation without drug; (F) formulation FP1.

was carried out at 40 °C with a sample injection volume of 20 μL .

2.8. Statistical Analysis. Mean values and standard deviations of the various sets of data were performed using SPSS 16.0 software. The number of replicas considered for calculation for each set of data has been mentioned under the relevant data sets in tables and figures.

3. RESULTS

3.1. Preformulation Study. *3.1.1. FTIR Spectroscopic Analysis.* Among the various preformulation studies, investigation of interaction between drug and the excipients in a formulation provides information about the stability of the drug in the formulation, the drug release pattern, and the lag time of drug release from the formulation.²⁰ Among the available analytical methods, FTIR spectroscopy provides a distinct idea regarding interaction among the different functional groups present in the drug and the excipients.²¹ In the present study, when the FTIR spectra of voriconazole, PLGA, PVA, physical mixture of voriconazole, PLGA, and PVA, formulation without drug, and formulation with drug (FP1) were compared, no positional shifting of characteristic peaks of voriconazole was

detected (Figure 1). Voriconazole used in the formulation was of pure grade, and the FTIR spectrum revealed that the peaks of C–N, C–F, and C–C stretching bands of the drug were at 3190.86–3117.54 cm^{-1} , 1498.31–1452.41 cm^{-1} , and 1586.96–1452.41 cm^{-1} , respectively, which match with our earlier observations.²² In the FTIR spectrum of PLGA, the peaks, at 3564.81 cm^{-1} for OH and at 2995.43–2946.79 cm^{-1} for C–H stretching bands, were observed, showing the presence of the characteristic peaks of PLGA. The typical ester C–O stretching band of PLGA was observed at 1748.61 cm^{-1} . All the characteristic peaks of PLGA and voriconazole appeared in the FTIR spectrum of their physical mixture. For PVA, OH and H are the predominant reactive groups. The FTIR spectrum of PVA revealed the peaks at 2943.94 cm^{-1} for CH_2 asymmetric stretching. The peak observed at 1088.36 cm^{-1} is attributed to the presence of terminal polyvinyl groups, while 1705.29 cm^{-1} indicates the carbonyl (C=O) stretching band.²³ Therefore, physical interactions existing between the functional groups of voriconazole and the excipients and among the excipients resulted in minor shifting of the peaks. Formation of a weak hydrogen bond, interaction due to van der Waals force, or dipole–dipole interaction among those functional groups might be responsible for the physical interactions. The presence of the

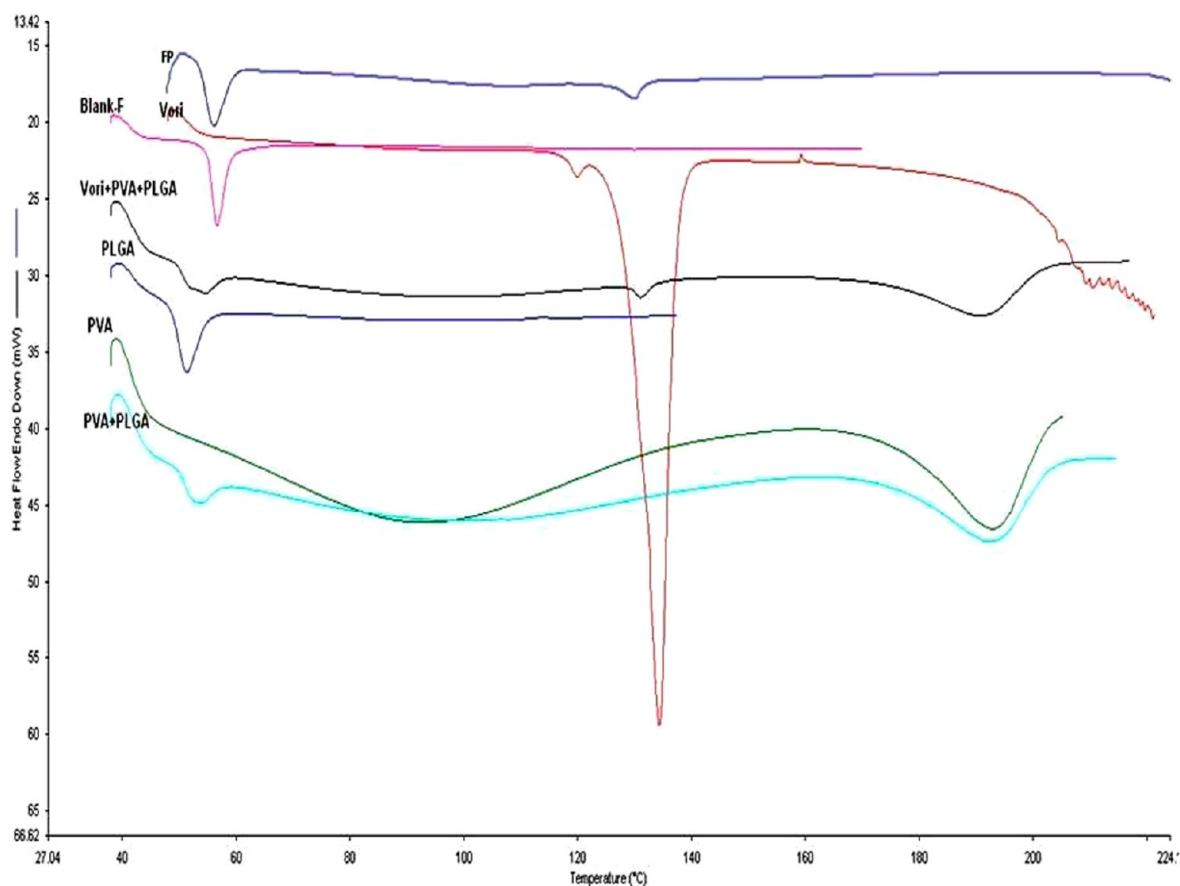


Figure 2. Differential scanning calorimetry thermograms of voriconazole (Vori); PLGA; PVA; and their physical blends (Vori+PVA+PLGA, PVA+PLGA); formulation without drug (Blank-F); and formulation with drug (FP).

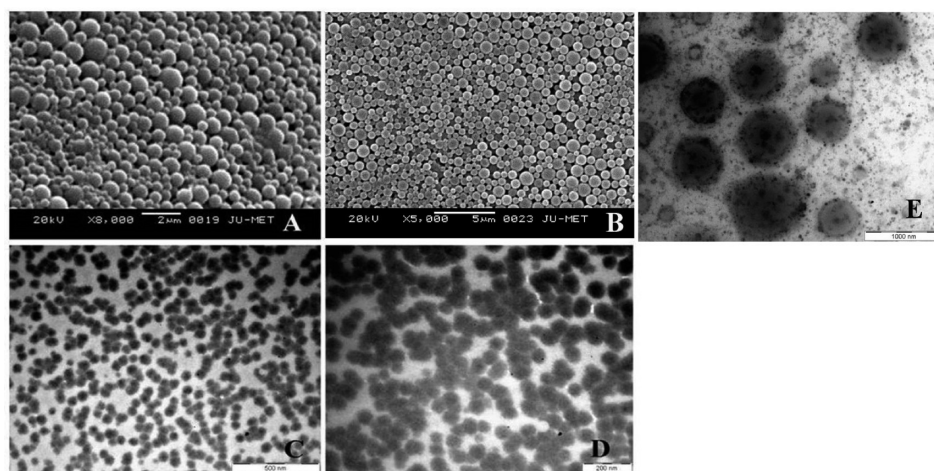


Figure 3. Scanning electron microscopic images of (A) formulation FP1 at 8000 \times ; (B) formulation FP2 at 5000 \times . Transmission electron microscopy photographs of formulation FP1 (C, E) of formulation FP2 (D), showing entrapped drug particles in the nanoparticles.

characteristic peaks of the drug and the excipients suggests that there was no chemical interaction. Such physical interactions might have been responsible for the sustained release of the drug from the formulations and might provide a spherical structure of the nanoparticles.²⁴ The characteristic peaks of PLGA were also present in the FTIR spectra of the formulations with and without the drug. However, no drug peak was observed for PLGA nanoparticles, indicating complete encapsulation of the drug.

3.1.2. DSC Analysis. The DSC thermograms (Figure 2) obtained for the pure drug, formulations with (FP) or without drug (Blank-F), polymers, and the physical mixtures of drug–polymers have been compared. The DSC thermograms show a broad endotherm at 134.29 °C for voriconazole and at 51.33 °C for PLGA. In the physical mixture, the endothermic peak of voriconazole and that of PLGA were in those respective positions. This implies the nonreactive nature of PLGA with voriconazole. Since PVA was removed by washing the

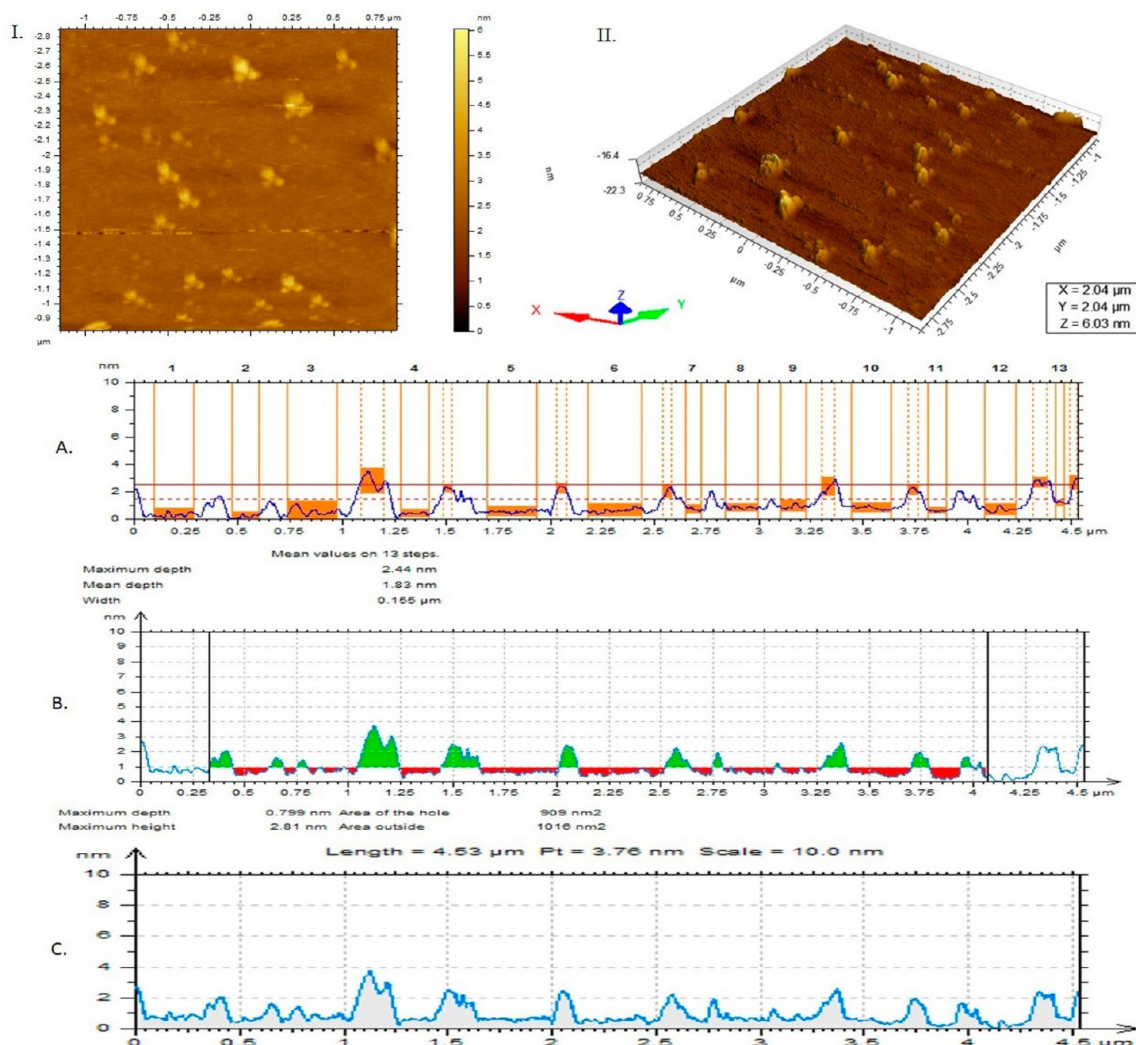


Figure 4. Atomic force microscopy images of nanoparticles formulation FP1 obtained 20 min after the deposition on mica support. (I) Topography flattened and (II) 3D view; (A) step height measurement; (B) surface of a hole or peak; (C) profile curve.

nanoparticles three times during the centrifugal separation process, the formulations with or without the drug have shown the absence of PVA.

3.2. Characterization of Experimental Nanoparticles.

3.2.1. Particle Size and Zeta Potential. Different PLGA nanoparticle formulations containing voriconazole were prepared by a multiple emulsification–solvent evaporation method by altering their composition and different process parameters. Most of the prepared formulations had their particle size diameter (Z average) less than 1000 nm. Out of those formulations, the two best formulations in terms of drug loading and other physicochemical properties have been reported here. Formulation FP1 had an average particle size of 300 nm, which was close to that of FP2 (303.5 nm). Zeta potential values of both formulations were found to be negative, and the values were 10.5 and 8.10 for FP1 and FP2, respectively (Table 1).

3.2.2. Drug Loading and % Yield. The drug loading values were expressed by the quantity of voriconazole encapsulated per unit quantity of the formulations.²⁵ The various composition and the process parameters of the experimental

formulations with their respective drug loading are shown in Table 1.

The reported two formulations were prepared keeping the same drug to polymer ratio of 1:10 (w/w) using the stabilizer PVA but were homogenized at different RPM. These result in a formation of particles with 2.91% and 2.57% drug loading and a yield of 71% and 56% for formulations FP1 and FP2 respectively.

3.2.3. SEM and TEM Analysis. The nanoparticles were found to be spherical and had a smooth surface as seen in SEM and TEM images (Figure 3). The photographs revealed that the particles loaded with voriconazole were of submicron size. TEM photograph (Figure 3E) shows the entrapment of drug particles inside the polymeric nanoparticles (formulation FP1), as seen in darker spots.

3.2.4. AFM Analysis. In the AFM images, the flattened topography and the three-dimensional view of PLGA nanoparticles on mica support as well as step height measurement, surface of a hole or peak, and the profile curve of FP1 are shown in Figure 4. Data revealed that the PLGA nanoparticles had an average width of 155 nm, a mean depth of 1.83 nm (Figure 4A), and a tendency to agglomerate.

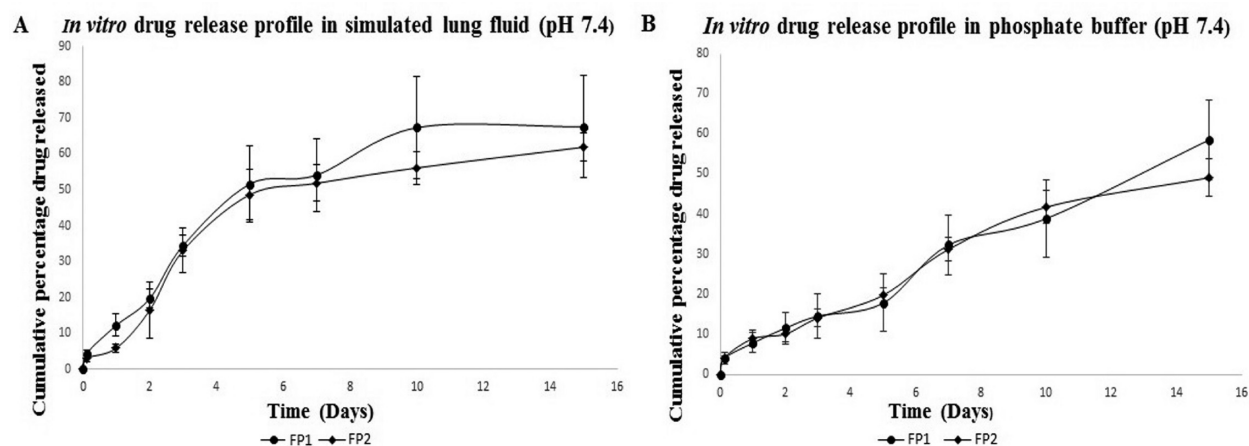


Figure 5. *In vitro* drug release profile. (A) Cumulative percent drug released (% CDR) vs time (days) in simulated lung fluid (pH 7.4) and (B) % CDR vs time (days) in phosphate buffer (pH 7.4) from various nanoparticle formulations at different time points (data as mean \pm SD, $n = 3$).

Table 2. Data of Drug Release Kinetics of the Experimental Nanoparticles

	simulated lung fluid		phosphate buffer saline	
	FP1	FP2	FP1	FP2
zero order	$y = 0.199x + 11.622$ $R^2 = 0.835^a$ $K_0 = 0.199^b$	$y = 0.183x + 9.635$ $R^2 = 0.811$ $K_0 = 0.183$	$y = 0.155x + 2.862$ $R^2 = 0.987$ $K_0 = 0.155$	$y = 0.138x + 4.093$ $R^2 = 0.967$ $K_0 = 0.138$
first order	$y = -0.002x + 1.953$ $R^2 = 0.898$ $K_1 = -0.0006^c$	$y = -0.0013x + 1.958$ $R^2 = 0.87$ $K_1 = -0.0005$	$y = -0.001x + 1.999$ $R^2 = 0.977$ $K_1 = -0.0004$	$y = -0.001x + 1.988$ $R^2 = 0.982$ $K_1 = -0.0003$
Higuchi kinetics	$y = 4.126x - 2.327$ $R^2 = 0.952$ $K_H = 4.126^d$	$y = 3.799x - 3.262$ $R^2 = 0.929$ $K_H = 3.799$	$y = 2.904x - 5.249$ $R^2 = 0.920$ $K_H = 2.904$	$y = 2.654x - 3.726$ $R^2 = 0.948$ $K_H = 2.654$
Korsmeyer–Peppas kinetics	$y = 0.626x + 0.312$ $R^2 = 0.971$ $n = 0.626^e$	$y = 0.722x + 0.044$ $R^2 = 0.921$ $n = 0.722$	$y = 0.551x + 0.225$ $R^2 = 0.927$ $n = 0.551$	$y = 0.527x + 0.268$ $R^2 = 0.928$ $n = 0.527$
Hixson–Crowell kinetics	$y = -0.004x + 4.465$ $R^2 = 0.879^f$ $K_{HC} = -0.004$	$y = -0.004x + 4.491$ $R^2 = 0.854$ $K_{HC} = -0.004$	$y = -0.003x + 4.623$ $R^2 = 0.984$ $K_{HC} = -0.003$	$y = -0.003x + 4.592$ $R^2 = 0.978$ $K_{HC} = -0.003$

^aCoefficient of determination. ^bZero order rate constant ($\text{mg mL}^{-1} \text{h}^{-1}$). ^cFirst order rate constant (h^{-1}). ^dHiguchi rate constant ($\text{h}^{-1/2}$). ^eRelease exponent. ^fHixson–Crowell rate constant ($\text{mg}^{1/3} \text{mm}^{-1} \text{h}^{-1}$).

3.3. *In Vitro* Assessment. 3.3.1. *In Vitro* Drug Release.

FP1 and FP2 had more or less similar drug release pattern in SLF up to 7 days (Figure 5A). After that, there was a sudden jump of drug release which occurred from FP1 in 10 days, and in 15 days about 67% and 62% drug was released from formulations FP1 and FP2 respectively. Likewise, steady mimicking drug release patterns were observed from formulations FP1 and FP2, and in 15 days drug release was about 58% and 49% respectively from them in PBS (Figure 5B).

3.3.2. Drug Release Kinetics. Drug release profiles of FP1 and FP2 in PBS were much more linear as compared to those in SLF. Amounts of drug release of FP1 and FP2 in SLF at different time points were found to be generally more (except a few cases where the values were marginally less) than those in PBS at the respective time points. The R^2 values and rate constants/release exponent values determined from the data of drug release following different kinetic models²⁶ are given in Table 2. More linearity (by assessing R^2 values) was detected in the Korsmeyer–Peppas plot ($R^2 = 0.970, 0.921$ for FP1, FP2, respectively) followed by Higuchi's ($R^2 = 0.952, 0.928$ for FP1, FP2, respectively) in SLF. The drug release exponent (n value)

in Korsmeyer–Peppas plot was found to be between 0.45 and 0.89, suggesting anomalous diffusion of the drug from the matrix-type nanoparticles.²⁷ Drug release profiles of FP1 and FP2 in PBS were found to be best fitted in Hixson–Crowell kinetics ($R^2 = 0.984, 0.978$ for FP1, FP2, respectively). However, FP1 had more linearity toward zero-order kinetics ($R^2 = 0.987$), and FP2 had a tendency to follow first-order ($R^2 = 0.982$) kinetics.

3.4. *In Vivo* Investigation. 3.4.1. Radiolabeling. The radiolabeling efficiency as determined by instant thin layer chromatography (ITLC) was about 90% (in both cases). The radiolabeled nanoparticles remained at the origin of the TLC sheets, and free TcO_4^- was moved to the solvent front at a R_f value of 0.9. The amount of free TcO_4^- was about 10%.

3.4.2. Blood Clearance. The serum elimination of the radiolabeled nanoparticles is shown in Figure 6. The decline in the percentage of injected dose in blood was observed over the increasing duration after injection.

3.4.3. Biodistribution. Biodistribution of the radiolabeled free drug and radiolabeled nanoparticles containing voriconazole was investigated in rats at 30 min and 4 h after injection. Hepatic accumulation was higher (37.37% injected dose (ID)

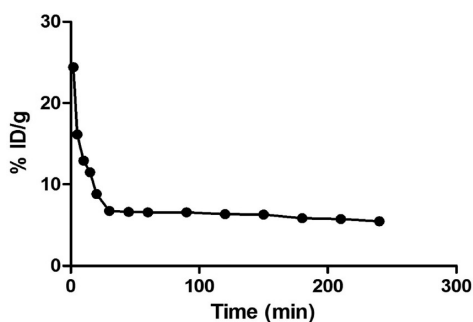


Figure 6. Blood clearance of radiolabeled nanoparticles at different time points.

per gram of organ (% ID/g)) at 30 min than that (28.08% ID/g) at 4 h (Table 3). Predominant accumulation was also observed in lungs and spleen (5.65% ID/g and 5.98% ID/g respectively at 30 min and 3.46% ID/g and 4.83% ID/g respectively at 4 h). This can also be justified for the targeting of the voriconazole loaded nanoparticles to lungs. Uptake of the drug in heart was not prominent. Urinary excretion was predominant at 4 h compared to at 30 min in the case of the free drug. About 50–70% less urinary excretion of drug loaded nanoparticles was seen in 30 min to 4 h.

3.4.4. Gamma Scintigraphy. Figure 7 shows the gamma scintigraphy pictures of mice which received ^{99m}Tc labeled nanoparticles containing drug and ^{99m}Tc labeled free drug by the pulmonary route. The pictures were taken after 0.5 h, 1 h, and 4 h of administration of the nanoparticles/free drug. The figures confirm that nanoparticles remained longer in lungs with respect to the free drug after pulmonary administration.

3.4.5. In Vivo Deposition. The concentration of voriconazole in the different lobes of lungs was assessed. The drug was found to be available more in the accessory lobe followed by the cranial, caudal, middle, and last left lobes, respectively, after 2 h of administration (Figure 8). The drug concentration reduced at 4 h in all the lobes except the left lobe, where the drug concentration increased 40% of its value at 2 h.

4. DISCUSSION

Effects of formulation variables such as the drug to polymer ratio, stabilizer concentrations, solvent variation, types of stabilizer, homogenizing speeds, etc. were investigated to develop formulation. These parameters were found to affect

% yield, drug loading, particle size, zeta potential, drug release, etc. of the particles (please see the Supporting Information). When we enhanced the polymer content in drug to polymer ratio, the drug loading increased. This could be due to the hydrophobic nature of the drug. Different solvent compositions (DCM and acetone) were used in the formulation development stage. We found that the solvent ratio 4:1 of DCM to acetone (by volume) resulted in an increased drug loading compared to the other solvent ratios. The solvent composition might favor more drug partitioning than the other solvent compositions studied. This caused higher drug loading. Solvent removal process plays an important role in the *in vitro* properties of the particles. We used a rotary vacuum evaporator followed by overnight stirring on a magnetic stirrer and only the overnight stirring on a magnetic stirrer. Particle size was found to reduce in case of the first process. Initial quick evaporation of solvent might prevent the small clusters of smaller particles to aggregate to form larger particles. However, the drug loading was reduced. When all other parameters remained constant, the homogenizing speed was optimized and it showed that, at 20,000 rpm, maximum drug loading and the smallest size of the particles were obtained. At higher and lower speeds, drug loading (decreased) as well as the particle size (increased) were altered. Lower homogenizing speed might produce insufficient force to form the desired decreased particle size, whereas higher speed could produce smaller particles which upon the solvent evaporation process might aggregate in small numbers to form larger particles. Finally, based on the physicochemical characterizations, we have selected the best two formulations and reported here the findings related to them.

4.1. Preformulation Study. **4.1.1. FTIR and DSC.** Drug–excipient(s) interaction is an important preformulation study as it indicates whether the drug is compatible with the excipients used in a particular formulation.²⁸ In the present investigation, the interaction study was done using FTIR and DSC to confirm any interaction between voriconazole and the polymers, PLGA and PVA. The data of FTIR spectroscopy and DSC reveal that there was no chemical interaction, although minor shifting of some peaks in FTIR spectra was found possibly due to the formation of physical bond(s) such as weak H-bond, van der Waals force of attraction, dipole–dipole interaction, etc., which might be responsible for sustained drug release and formation of nanoparticles. Further, in the case of the drug loaded formulations, absence of drug peak in the FTIR spectra and presence of drug peak in DSC thermogram reveal that drug was

Table 3. Biodistribution Study of ^{99m}Tc Labeled Voriconazole Loaded PLGA Nanoparticles and ^{99m}Tc -Chelate of Free Voriconazole in Rats

organ/tissue	voriconazole loaded PLGA nanoparticles		free voriconazole	
	30 min	240 min	30 min	240 min
heart	0.45 ± 0.06 ^a	0.39 ± 0.12 ^a	0.36 ± 0.05 ^a	0.32 ± 0.07 ^a
blood	1.30 ± 0.11	0.88 ± 0.18	0.95 ± 0.13	0.73 ± 0.11
liver	37.37 ± 1.20	28.09 ± 2.19	41.06 ± 1.23	32.04 ± 1.01
lungs	5.65 ± 0.50	3.46 ± 0.49	3.05 ± 0.06	2.19 ± 0.07
spleen	5.98 ± 1.38	4.83 ± 0.63	4.02 ± 0.07	3.75 ± 0.06
muscle	0.08 ± 0.01	0.07 ± 0.02	0.13 ± 0.02	0.11 ± 0.03
kidney	2.65 ± 0.30	3.45 ± 0.35	4.44 ± 1.05	5.75 ± 0.94
stomach	0.88 ± 0.12	1.64 ± 0.40	1.11 ± 0.12	1.94 ± 0.22
intestine	2.12 ± 0.22	3.20 ± 0.21	1.18 ± 0.09	2.57 ± 0.65
urine	3.67 ± 0.43	15.14 ± 2.11	7.89 ± 0.08	26.54 ± 0.15

^aEach data indicates % injected dose (ID) per gram of organ/tissue ± SD ($n = 6$).

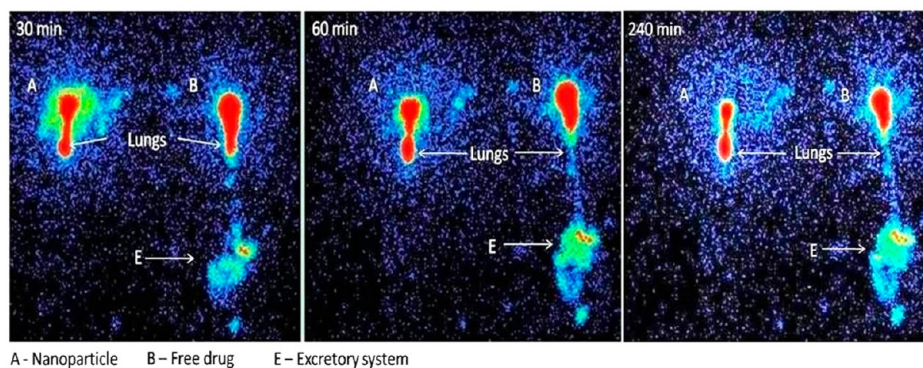


Figure 7. Scintigraphy pictures of animals which received ^{99m}Tc labeled nanoparticles and free drug by pulmonary route after 0.5 h, 1 h, and 4 h.

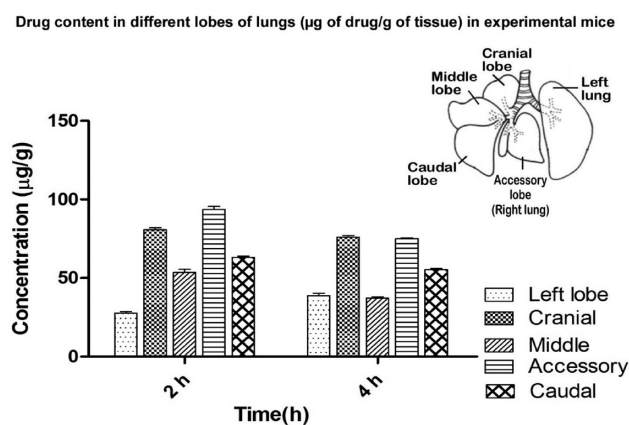


Figure 8. Voriconazole concentration in different lobes of lung.

completely encapsulated and no free drug was available on the particle surface.

4.2. Characterization of Nanoparticles. **4.2.1. Particle Size and Zeta Potential.** Particle size, in particular, plays a crucial role in the distribution of nanoparticles in lungs when administered by the pulmonary route. A report suggests that the aerodynamic diameter of the particles in the range of 0.43–0.65 μm was capable of distributing nanoparticles in alveoli of deep lung tissue.²⁹ Particle size equally plays a key role in the biodistribution of nanoparticles.³⁰ Particles with a hydrodynamic diameter less than 5.5 nm (which is the cutoff size for renal excretion) are rapidly excreted in the urine.³¹ Since the particle sizes of the developed nanoparticles were much higher than the above-mentioned size, they might have escaped size dependent rapid clearance through urine.

The PDI values were found to be nearly 1 (data not shown), which suggests that polymer chains approached uniform chain length.³² The surface charge (zeta potential) of nanoparticles has a significant impact on their biodistribution and pharmacokinetic profiles. Positively charged particles are filtered more rapidly than the negatively charged particles in the basement membrane of glomerulus, mainly consisting of negatively charged polysaccharide glycosaminoglycans.³³ Since the experimental particles had negative zeta potentials, they were devoid of the charge dependent rapid clearance problem through kidneys. The zeta potential values were found to be negative for all the formulations, and the negative values might be due to the dissociation of hydrogen ion from carboxyl group ($-\text{COOH}$) of the PLGA chain.³⁴

4.2.2. % Yield. Alteration of homogenizing speed was found to vary % yield marginally within an approximate range of 60–70%. As a whole, little less % yield was due to the recovery problem of the sticky PLGA polymeric mass adherence to the homogenizer and use of smaller quantities of formulation ingredients. However, the formulation prepared in a large quantity will automatically improve the yield value, by minimizing the loss.

4.2.3. Drug Loading. % drug loading was found to be less in FP2 formulation as compared to FP1. Enhancing the speed of homogenization might help, effectively improving drug retention in the particles.³⁵ Further, higher homogenizing speed enhanced a greater intensive shear force, quicker solvent evaporation, and faster water diffusion in the oil phase, resulting in a decrease in drug partitioning and/or drug permeability from the lipid layer to the aqueous media.³⁶

4.2.4. SEM, TEM, and AFM. The surface morphology of the particles of FP1, as assessed by SEM, has shown that the particles were spherical in shape and homogeneously distributed in the nanoscale range. They had smooth surface also. TEM image suggests that drug was distributed in particulate form throughout the nanoparticle bodies.³⁷

AFM data was applied for imaging the PLGA nanoparticle surface and to measure the size of the particles absorbed onto a mica sheet. The greater abundance of the smaller particles on the lower end of the 3D structure was observed. AFM images showed that no reorganization occurred in the surface structure of nanoparticles due to the presence of the therapeutically active agent. Drug particles were completely covered by the polymeric surface, and the particles fused or aggregated in small clusters of size less than 155 nm in width. A very high dilution reduced the numbers of nanoparticles on the mica surface. Since mica is hydrophilic, traces of solvent even after drying could cause agglomeration of nanoparticles.

4.3. In Vitro Assessment. **4.3.1. Drug Release in SLF and PBS.** *In vitro* drug release was studied in SLF (mimicking lung fluid) and in PBS (mimicking blood serum). Our objective was, first, to investigate whether drug release from the same formulation differs due to a variation of the drug release media and, second, to get drug release data in PBS that would also provide an idea of drug release from the formulation when injected into blood. The release of voriconazole from FP1 and FP2 was studied in SLF and PBS, of which the former is considered to be the more relevant medium for *in vivo* condition.³⁸ Physicochemical characteristics of drug and formulation such as particle size, shape, surface charge, etc., manufacturing parameters such as formulation composition,

homogenizing speed, method of preparation, etc., and even the different release media contribute to drug release behavior.³⁹ A comparison of Figure 5A and Figure 5B shows a crucial role of drug release medium on drug release from a formulation. Since SLF and PBS contained high amounts and varieties of salts, these excess amounts of salts in the release medium might obviously affect the swelling behavior of PLGA and retard drug diffusion from the particles, limiting its incorporation in water.⁴⁰ Further, PBS mediated alteration in drug diffusion might retard drug release comparatively more slowly and steadily.

4.3.2. Drug Release Kinetics. Drug release data were fitted to different kinetic models (Table 2) to identify the possible drug release mechanism(s). Drug release kinetics in SLF showed that FP1 and FP2 followed the Korsmeyer–Peppas model and they had also a good amount of linearity toward Higuchi kinetics. This suggests that a coupling of diffusion and erosion mechanism, so-called anomalous diffusion or non-Fickian diffusion (based on n values), was involved in controlling drug release from the nanoparticles. In contrast, drug release of FP1 and FP2 in PBS followed Hixson–Crowell kinetics, suggesting that drug release was limited by the drug particle dissolution rate.

4.4. In Vivo Investigation. **4.4.1. Radiolabeling.** In the present study, voriconazole and its nanoparticle formulation (FP1) were labeled with ^{99m}Tc having significant radiolabeling efficiency. The mechanism of this radiolabeling process involves the reduction of TcO_4^- from its existing heptavalent oxidation state to a lower valence state by SnCl_2 . SnCl_2 is essential for good radiolabeling efficiency.⁴¹ This is a well-known radiolabeling process for the labeling of drug as well as the formulations presented in many studies.⁴²

After conducting preliminary trials, pH adjusted for reduced ^{99m}Tc to obtain high labeling efficiency (about 90%) was optimized to 4.0. The amount of SnCl_2 used for reducing the TcO_4^- performs a major role in the radiolabeling process since higher amount results in formation of undesirable radiocolloids whereas a lower amount of SnCl_2 causes poor labeling efficiency. In the present investigation, 20 μg of SnCl_2 was found to be optimum for high labeling efficiency with a low amount of free and R/H pertechnetate. Incubation time at room temperature in which maximum percentage of labeling occurred has been optimized as 15 min after the addition of $^{99m}\text{TcO}_4^-$ to the preparation containing voriconazole or voriconazole nanoparticles. For optimizing the above parameters, quality control tests were performed by TLC using ITLC strips.⁴³

4.4.2. Blood Clearance. The blood clearance graph had two phases in it. The first phase had a comparatively rapid clearance of the nanoparticles within 30 min, which might occur due to the quick biodistribution of the nanoparticles. In the second phase, slow and steady clearance of nanoparticles was observed until 240 min. This suggests that the nanoparticles were eventually bound to plasma protein, delaying their plasma clearance.

4.4.3. Biodistribution. Generally, the biodistribution of nanoparticles implies the nanoparticle mass in tissues at various time points. Biodistribution of nanoparticles is dependent on their physicochemical properties (such as size, surface charge, etc.).⁴⁴ Free drug and the nanoparticles were found to distribute into tissues within 30 min. The residence time of nanoparticles in blood was found to be more compared to the free drug. Predominantly faster clearance of free drug from the

body compared to nanoparticles, as supported by the urinary excretion data (Table 3) and their tissue accumulation data in liver, kidneys, and to some extent stomach, could be responsible for that. Among the organs tested, the liver showed maximum accumulation of free drug/nanoparticles (FP1) at 30 min after administration. After 4 h, both the free drug and nanoparticle concentrations started decreasing, indicating their hepatic elimination from the body. Although the hepatic elimination was found to be less for nanoparticles, both the free drug and the nanoparticles were well excreted by the liver. Hepatic drug metabolizing enzymes, hepatic macrophages, and Kupffer cells are known to play a significant role in such hepatic clearance.⁴⁵ Data further suggest that nanoparticle delivery directly to the target tissue (such as lungs in this case) could be more fruitful to avoid their significant loss due to processes of major systemic clearances.⁴⁶

Spleen uptake of the formulation was higher as compared to free drug and decreased with time. Thus, spleen-mediated elimination of free drug and nanoparticles should not be ignored.

A higher amount of accumulation of voriconazole in kidneys and predominantly faster urinary excretion of the free drug suggest that nanoparticles would remain in the body for a longer period of time than the free drug.⁴⁷ Lungs have shown a predominant uptake of nanoparticles (about 1.5 times more) than the free drug. Slower and much less distribution of nanoparticles in the muscles might be due to a much larger volume of the tissue. Heart muscles had marginally higher nanoparticle distribution as compared to the free drug. However, distribution patterns were more or less similar. Complicated muscular structure and very active functional role might take part in the role of less distribution of both the free drug and the nanoparticle in heart tissues.

4.4.4. Gamma Scintigraphy. When radiolabeled drug (free drug) and radiolabeled nanoparticles containing drug were administered to two different groups of mice through the pulmonary route using a dry powder inhaler, the distribution of nanoparticles and free drug in lungs was predominant at 30 min after their administration. The images taken at 60 and 240 min show that accumulation of radioactivity in kidneys became progressively prominent in the case of the animals treated with the free drug, suggesting the genitourinary tract as a major excretory pathway of radiolabeled voriconazole. However, labeled nanoparticles were not observed in the excretory organ even after 240 min. Nanoparticles may have poorer plasma protein absorption as compared to the free drug, ultimately leading to less clearance of drug through urine. However, the amount of nanoparticles in lungs became less, which could be due to the biodistribution of nanoparticles in other organs. Further, the data indicate a better retention of nanoparticles in the lungs after 4 h as compared to the free drug, following the pulmonary/inhalation route. Retention of the nanoparticles in the deeper tissues of the lungs is very complex. The presence of varieties of proteins and lipids in the alveolar lining and the tight junctions at the epithelial cell acts as a barrier for the particles to be transported. Hence, they are retained in the tissue for a longer time and are not easily phagocytosed by the alveolar macrophages, whereas, in the case of the free drug deposited in the lungs, they might translocate to the pulmonary epithelial cells and interstitial cells, which ultimately could transport the drug to the blood, causing clearance of the drug from the lungs.

4.4.5. In Vivo Deposition. Voriconazole levels in the different lobes of the lungs of the experimental animals following pulmonary administration suggest that the drug levels in the different parts of lungs were not the same at any time point after the administration. Size-dependent distribution of nanoparticles in different lobes of lung⁴⁸ and a rapid turnover of blood supply⁴⁹ might be the cause of such variation of drug levels. Further, a nonsteady blood level of the drug could be detrimental as the fungal spores in lungs may survive and even the drug level may not be sufficient to kill the active fungi.^{50,51} The findings undoubtedly suggest why fungal diseases in lungs are extremely difficult to be managed therapeutically. Thus, an alternative route such as pulmonary drug delivery or lung targeting of the drug may be a better prospective approach to treating pulmonary fungal diseases.

5. CONCLUSIONS

Physicochemical characteristics and *in vitro* and *in vivo* distribution of the developed voriconazole loaded nanoparticles have shown that they were therapeutically more efficacious for delivery of the drug in different lobes of lungs, as compared to the iv route of delivery. The nanoparticles were subsequently radiolabeled with ^{99m}Tc. Administration of radiolabeled PLGA nanoparticles containing voriconazole leads to prolonged retention of particles in lungs with enhanced biodistribution when compared to voriconazole alone. This study also reveals that voriconazole encapsulated PLGA nanoparticles are a better drug delivery system to deliver drug in deep lung tissue in high concentration for a prolonged period of time and are assumed to provide greater antifungal effect in fungal infections.

■ ASSOCIATED CONTENT

● Supporting Information

At the beginning, various formulation variables such as the drug to polymer ratio, stabilizer concentrations, solvent variation, types of stabilizers, homogenizing speeds, etc., which affect % yield, drug loading, particle size, and zeta potential, were investigated and optimized to develop and screen the formulations. Please see the Supporting Information for the data table. The Supporting Information is available free of charge on the ACS Publications website at DOI: 10.1021/acs.molpharmaceut.5b00064.

■ AUTHOR INFORMATION

Corresponding Author

*Division of Pharmaceutics, Department of Pharmaceutical Technology, Jadavpur University, Kolkata-700032, India. Tel: +91-33-2457 2588. Fax: +91-33-2414 6677. E-mail: biswajit55@yahoo.com.

Author Contributions

‡P.J.D. and P.P. contributed equally.

Notes

The authors declare no competing financial interest.

■ ACKNOWLEDGMENTS

This work is supported by Department of Biotechnology (DBT), Govt. of India (Sanction No. BT/259/NE/TBP/2011 dated April 23, 2012). The authors are thankful to T. Muruganandan and Dr. Arun Bandyopadhyay of Indian Institute of Chemical Biology for conducting the AFM study.

■ ABBREVIATIONS USED

PLGA, poly lactic-co-glycolic acid; MW, molecular weight; PVA, poly(vinyl alcohol); DCM, dichloromethane; FTIR, Fourier transform infrared spectroscopy; DSC, differential scanning calorimetry; DDW, double distilled water; w/o/w, water-in-oil-in-water; SEM, scanning electron microscopy; TEM, transmission electron microscopy; AFM, atomic force microscopy; SLF, simulated lung fluid; PBS, phosphate buffer saline; R^2 , coefficients of determination; ^{99m}Tc, technetium-99m; ^{99m}TcO₄⁻, ^{99m}Tc-pertechnetate; TcO₄⁻, pertechnetate; TLC, thin layer chromatography; LC-MS/MS, liquid chromatography tandem mass spectrometry; ITLC, instant thin layer chromatography

■ REFERENCES

- (1) Heeres, J.; Meerpoel, L.; Lewi, P. Conazoles. *Molecules* **2010**, *15*, 4129–4188.
- (2) Ghannoum, M. A.; Rice, L. B. Antifungal Agents: Mode of Action, Mechanisms of Resistance, And Correlation of These Mechanisms with Bacterial Resistance. *Clin. Microbiol. Rev.* **1999**, *12*, 501–517.
- (3) Cook, S.; Confer, J. Assessment And Treatment of Fungal Lung Infections. *U.S. Pharm.* **2011**, *36*, HS-17–HS-24.
- (4) Moen, M. D.; Lyseng-Williamson, K. A.; Scott, L. J.; Liposomal Amphotericin, B. A Review of Its Use As Empirical Therapy in Febrile Neutropenia And in the Treatment of Invasive Fungal Infections. *Drugs* **2009**, *69*, 361–392.
- (5) Keum, C. G.; Noh, Y. W.; Baek, J. S.; Lim, J. H.; Hwang, C. J.; Na, Y. G.; Shin, S. C.; Cho, C. W. Practical Preparation Procedures for Docetaxel-Loaded Nanoparticles using Poly(lactic Acid-Co-Glycolic Acid). *Int. J. Nanomed.* **2011**, *6*, 2225–2234.
- (6) Makadia, H. K.; Siegel, S. J. Poly Lactic-co-Glycolic Acid (PLGA) As Biodegradable Controlled Drug Delivery Carrier. *Polymers (Basel)* **2011**, *3*, 1377–1397.
- (7) Dinarvand, R.; Sepehri, N.; Manoochehri, S.; Rouhani, H.; Atyabi, F. Polylactide-Co-Glycolide Nanoparticles for Controlled Delivery of Anticancer Agents. *Int. J. Nanomed.* **2011**, *6*, 877–895.
- (8) Clarke, H. E.; Coates, M. E.; Eva, J. K.; Ford, D. J.; Milner, C. K.; O'donoghue, P. N.; Scott, P. P.; Ward, R. J. Dietary Standards for Laboratory Animals: Report of the Laboratory Animals Centre Diets Advisory Committee. *Lab. Anim.* **1977**, *11*, 1–28.
- (9) Maji, R.; Dey, N. S.; Satapathy, B. S.; Mukherjee, B.; Mondal, S. Preparation And Characterization of Tamoxifen Citrate Loaded Nanoparticles for Breast Cancer Therapy. *Int. J. Nanomed.* **2014**, *9*, 3107–3118.
- (10) Davda, J.; Labhasetwar, V. Characterization of Nanoparticle Uptake by Endothelial Cells. *Int. J. Pharm.* **2002**, *233*, 51–59.
- (11) Jithan, A. V.; Madhavi, K.; Madhavi, M.; Prabhakar, K. Preparation And Characterization of Albumin Nanoparticles Encapsulating Curcumin Intended for the Treatment of Breast Cancer. *Int. J. Pharm. Invest.* **2011**, *1*, 119–125.
- (12) Snehalatha, M.; Venugopal, K.; Saha, R. N. Ethoposide Loaded PLGA And PCL Nanoparticles I: Preparation And Effect of Formulation Variable. *Drug Delivery* **2008**, *15*, 267–275.
- (13) Ghosh, A.; Sarkar, S.; Mandal, A. K.; Das, N. Neuroprotective Role of Nanoencapsulated Quercetin in Combating Ischemia-Perfusion Induced Neuronal Damage in Young And Aged Rats. *PLoS One* **2013**, *8*, 1–12.
- (14) Marques, M. R. C.; Loebenberg, R.; Almukainzi, M. Simulated Biological Fluids with Possible Application in Dissolution Testing. *Dissolution Technol.* **2011**, 15–28.
- (15) Ranjan, A. P.; Mukerjee, A.; Helson, L.; Vishwanatha, J. K. Scale Up, Optimization And Stability Analysis of Curcumin C3 Complex-Loaded Nanoparticles for Cancer Therapy. *J. Nanobiotechnol.* **2012**, *10*, 1–18.

- (16) Dash, S.; Murthy, P. N.; Nath, L.; Chowdhury, P. Kinetic Modeling on Drug Release from Controlled Drug Delivery Systems. *Acta Pol. Pharm.* **2010**, *67*, 217–223.
- (17) Babbar, A.; Kashyap, R.; Chauhan, U. P. A. Convenient Method for the Preparation of ^{99m}Tc -Labelled Pentavalent DMSA And Its Evaluation As a Tumour Imaging Agent. *J. Nucl. Biol. Med.* **1991**, *35*, 100–104.
- (18) Halder, K. K.; Mandal, B.; Debnath, M. C.; Bera, H.; Ghosh, L. K.; Gupta, B. K. Chloramphenicol-Incorporated Poly(lactide-Co-Glycolide) (PLGA) Nanoparticles: Formulation, Characterization, Technetium-99m Labeling And Biodistribution Studies. *J. Drug Targeting* **2008**, *16*, 311–320.
- (19) Sinha, B.; Mukherjee, B. Development of an Inhalation Chamber And a Dry Powder Inhaler Device for Administration of Pulmonary Medication in Animal Model. *Drug Dev. Ind. Pharm.* **2012**, *38*, 171–179.
- (20) Bharate, S. S.; Bharate, S. B.; Bajaj, A. N. Interactions And Incompatibilities of Pharmaceutical Excipients with Active Pharmaceutical Ingredients: A Comprehensive Review. *J. Excipients Food Chem.* **2010**, *1*, 3–26.
- (21) Cunha-Filho, M. S.; Martínez-Pacheco, R.; Landín, M. Compatibility of the Antitumoral Beta-Lapachone with Different Solid Dosage Forms Excipients. *J. Pharm. Biomed. Anal.* **2007**, *45*, 590–598.
- (22) Sinha, B.; Mukherjee, B.; Pattnaik, G. Poly-Lactide-Co-Glycolide Nanoparticles Containing Voriconazole for Pulmonary Delivery: *In-Vitro* And *In-Vivo* Study. *Nanomedicine* **2013**, *9*, 94–104.
- (23) Doustgani, A.; Vasheghani-Farahani, E.; Soleimani, M.; Hashemi-Najafabadi, S. Preparation And Characterization of Aligned And Random Nanofibrous Nanocomposite Scaffolds of Poly (Vinyl Alcohol), Poly (ϵ -Caprolactone) And Nanohydroxyapatite. *Int. J. Nanosci. Nanotechnol.* **2011**, *7*, 127–132.
- (24) Sahana, B.; Santra, K.; Basu, S.; Mukherjee, B. Development of Biodegradable Polymer Based Tamoxifen Citrate Loaded Nanoparticles And Effect of Some Manufacturing Process Parameters on Them: A Physicochemical And *In-Vitro* Evaluation. *Int. J. Nanomed.* **2010**, *5*, 1–10.
- (25) Basu, S.; Mukherjee, B.; Chowdhury, S. R.; Paul, P.; Choudhury, R.; Kumar, A.; Mondal, L.; Hossain, C. M.; Maji, R. Colloidal Gold-Loaded, Biodegradable, Polymer-Based Stavudine Nanoparticle Uptake by Macrophages: An *In-Vitro* Study. *Int. J. Nanomed.* **2012**, *7*, 6049–6061.
- (26) Manasadeepa, R.; Paul, P.; Mukherjee, B. Pressure-Sensitive Mucoadhesive Polymer-Based Dental Patches to Treat Periodontal Diseases: An *In-Vitro* Study. *Drug Delivery* **2013**, *20*, 258–267.
- (27) Pattnaik, G.; Sinha, B.; Mukherjee, B.; Ghosh, S.; Basak, S.; Mondal, S.; Bera, T. Submicron-size Biodegradable Polymer-based Didanosine Particles for Treating HIV at Early Stage: an *In vitro* Study. *J. Microencapsulation* **2012**, *29*, 666–676.
- (28) Fathima, N.; Mamatha, T.; Qureshi, H. K.; Anitha, N.; Venkateswara Rao, J. Drug-Excipient Interaction And Its Importance in Dosage Form Development. *J. Appl. Pharm. Sci.* **2011**, *1*, 66–71.
- (29) Courrier, H. M.; Butz, N.; Vandamme, T. F. Pulmonary Drug Delivery Systems: Recent Developments And Prospects. *Crit. Rev. Ther. Drug Carrier Syst.* **2002**, *19*, 425–498.
- (30) He, C.; Hu, Y.; Yin, L.; Tang, C.; Yin, C. Effects of Particle Size And Surface Charge on Cellular Uptake And Biodistribution of Polymeric Nanoparticles. *Biomaterials* **2010**, *31*, 3657–3666.
- (31) Choi, H. S.; Liu, W.; Misra, P.; Tanaka, E.; Zimmer, J. P.; Ipe, B. I.; Bawendi, M. G.; Frangioni, J. V. Renal Clearance of Quantum Dots. *Nat. Biotechnol.* **2007**, *25*, 1165–1170.
- (32) Atkins, P.; Paula, J. D. *Atkins' Physical Chemistry*, 9th ed.; Oxford University Press: Oxford, 2010.
- (33) Haraldsson, B.; Nyström, J.; Deen, W. M. Properties of the Glomerular Barrier And Mechanisms of Proteinuria. *Physiol. Rev.* **2008**, *88*, 451–487.
- (34) Kim, H. W.; Chung, C. W.; Kim, Y. B.; Rhee, Y. H. Preparation And Hydrolytic Degradation of Semi-Interpenetrating Networks of Poly(3-Hydroxyundecenoate) And Poly(Lactide-Co-Glycolide). *Int. J. Biol. Macromol.* **2005**, *37*, 221–226.
- (35) Mehrotra, A.; Pandit, J. K. Critical Process Parameters Evaluation of Modified Nanoprecipitation Method on Lomustine Nanoparticles And Cytostatic Activity Study on L132 Human Cancer Cell Line. *J. Nanomed. Nanotechnol.* **2012**, *3*, 1–8.
- (36) Zeini, D.; Khoshkenar, P.; Rabiee, M. The Influence of Formulation And Process Parameters on the Morphology, Size And Release Profile of L-Dopa-Loaded Poly Lactic-Co-Glycolic Acid (PLGA) Microspheres. *Open Conf. Proc. J.* **2012**, *3*, 1–7.
- (37) Rudra, A.; Manasadeepa, R.; Ghosh, M. K.; Ghosh, S.; Mukherjee, B. Doxorubicin-Loaded Phosphatidylethanolamine-Conjugated Nanoliposomes: *In Vitro* Characterization And Their Accumulation in Liver, Kidneys, And Lungs in Rats. *Int. J. Nanomed.* **2010**, *5*, 811–823.
- (38) Nafee, N.; Husari, A.; Maurer, C. K.; Lu, C.; de Rossi, C.; Steinbach, A.; Hartmann, R. W.; Lehr, C. M.; Schneider, M. Antibiotic Free Nanotherapeutics: Ultra-Small, Mucus Penetrating Solid Lipid Nanoparticles Enhance the Pulmonary Delivery And Anti-Virulence Efficacy of Novel Quorum Sensing Inhibitors. *J. Controlled Release* **2014**, *192*, 131–140.
- (39) Mukherjee, B.; Santra, K.; Pattnaik, G.; Ghosh, S. Preparation, Characterization And *In-Vitro* Evaluation of Sustained Release Protein-Loaded Nanoparticles Based on Biodegradable Polymers. *Int. J. Nanomed.* **2008**, *3*, 487–496.
- (40) Nazemi, K.; Moztarzadeh, F.; Jalali, N.; Asgari, S.; Mozafari, M. Synthesis And Characterization of Poly(Lactic-Co-Glycolic) Acid Nanoparticles-Loaded Chitosan/Bioactive Glass Scaffolds As a Localized Delivery System in The Bone Defects. *Biomed. Res. Int.* **2014**, *2014*, 1–9.
- (41) Spies, H.; Pietzsch, H. J. Stannous Chloride in the preparation of ^{99}Tc Pharmaceuticals. In *Technetium-99m Pharmaceuticals: preparation and quality control in Nuclear Medicine*; Zolle, I., Ed.; Springer: Berlin, 2007; pp 59–66.
- (42) Reddy, L. H.; Sharma, R. K.; Murthy, R. S. Enhanced Tumour Uptake of Doxorubicin Loaded Poly (Butyl Cyanoacrylate) Nanoparticles in Mice Bearing Dalton's Lymphoma Tumour. *J. Drug Targeting* **2004**, *12*, 443–451.
- (43) Mishra, P.; Babbar, A.; Chauhan, U. P. A Rapid Instant Thin Layer Chromatographic Procedure for Determining Radiochemical Purity of ^{99}Tc -IDA Agents. *Nucl. Med. Commun.* **1991**, *12*, 467–469.
- (44) Li, M.; Panagi, Z.; Avgoustakis, K.; Reineke, J. Physiologically Based Pharmacokinetic Modeling of PLGA Nanoparticles with Varied mPEG Content. *Int. J. Nanomed.* **2012**, *7*, 1345–1356.
- (45) Mukherjee, B.; Mondal, L.; Chakraborty, S.; Paul, P.; Choudhury, A.; Bhattacharya, S.; Hossain, C. M. Size Dependant Variations in Systemic Activity of Lipid Based Vesicular Drug Carriers. *Curr. Pharm. Biotechnol.* **2015**, *16*, 380–391.
- (46) Labiris, N. R.; Dolovich, M. B. Pulmonary Drug Delivery. Part II: The Role of Inhalant Delivery Devices And Drug Formulations in Therapeutic Effectiveness of Aerosolized Medications. *Br. J. Clin. Pharmacol.* **2003**, *56*, 600–612.
- (47) Snehalatha, M.; Kolachina, V.; Saha, R. N.; Babbar, A. K.; Sharma, N.; Sharma, R. K. Enhanced Tumor Uptake, Biodistribution And Pharmacokinetics of Etoposide Loaded Nanoparticles in Dalton's Lymphoma Tumor Bearing Mice. *J. Pharm. Bioallied Sci.* **2013**, *5*, 290–297.
- (48) Heyder, J.; Gebhart, J.; Rudolf, G.; Stahlhofen, W. Deposition of Particles in the Human Respiratory Tract in the Size Range 0.005–15 μm . *J. Aerosol Sci.* **1986**, *17*, 811–825.
- (49) Lombry, C.; Bosquillon, C.; Preat, V.; Vanbever, R. Confocal Imaging of Rat Lungs Following Intratracheal Delivery of Dry Powders or Solutions of Fluorescent Probes. *J. Controlled Release* **2002**, *83*, 331–341.
- (50) Kontoyiannis, D. P.; Lewis, R. E. How I Treat Mucormycosis. *Blood* **2011**, *118*, 1216–1224.

(51) Badiie, P.; Hashemizadeh, Z. Opportunistic Invasive Fungal Infections: Diagnosis & Clinical Management. *Indian J. Med. Res.* **2014**, *139*, 195–204.



Successful delivery of docetaxel to rat brain using experimentally developed nanoliposome: a treatment strategy for brain tumor

Tapan Kumar Shaw, Dipika Mandal, Goutam Dey, Murari Mohan Pal, Paramita Paul, Samrat Chakraborty, Kazi Asraf Ali, Biswajit Mukherjee, Amal Kumar Bandyopadhyay & Mahitosh Mandal

To cite this article: Tapan Kumar Shaw, Dipika Mandal, Goutam Dey, Murari Mohan Pal, Paramita Paul, Samrat Chakraborty, Kazi Asraf Ali, Biswajit Mukherjee, Amal Kumar Bandyopadhyay & Mahitosh Mandal (2017) Successful delivery of docetaxel to rat brain using experimentally developed nanoliposome: a treatment strategy for brain tumor, Drug Delivery, 24:1, 346-357, DOI: [10.1080/10717544.2016.1253798](https://doi.org/10.1080/10717544.2016.1253798)

To link to this article: <http://dx.doi.org/10.1080/10717544.2016.1253798>



© 2017 The Author(s). Published by Informa UK Limited, trading as Taylor & Francis Group.



[View supplementary material](#)



Published online: 06 Feb 2017.



[Submit your article to this journal](#)



Article views: 803



[View related articles](#)



[View Crossmark data](#)



[Citing articles: 2](#) [View citing articles](#)

RESEARCH ARTICLE

Successful delivery of docetaxel to rat brain using experimentally developed nanoliposome: a treatment strategy for brain tumor

Tapan Kumar Shaw¹, Dipika Mandal¹, Goutam Dey², Murari Mohan Pal¹, Paramita Paul¹, Samrat Chakraborty¹, Kazi Asraf Ali³, Biswajit Mukherjee¹, Amal Kumar Bandyopadhyay¹, and Mahitosh Mandal²

¹Department of Pharmaceutical Technology, Jadavpur University, Kolkata, West Bengal, India, ²School of Medical Science and Technology, Indian Institute of Technology Kharagpur, Kharagpur, West Bengal, India, and ³Dr. B. C. Roy College of Pharmacy and Allied Health Sciences, Dr. Meghnad Saha Sarani, Bidhan Nagar, Durgapur, West Bengal, India

Abstract

Docetaxel (DTX) is found to be very effective against glioma cell *in vitro*. However, *in vivo* passage of DTX through BBB is extremely difficult due to the physicochemical and pharmacological characteristics of the drug. No existing formulation is successful in this aspect. Hence, in this study, effort was made to send DTX through blood–brain barrier (BBB) to brain to treat diseases such as solid tumor of brain (glioma) by developing DTX-loaded nanoliposomes. Primarily drug-excipients interaction was evaluated by FTIR spectroscopy. The DTX-loaded nanoliposomes (L-DTX) were prepared by lipid layer hydration technique and characterized physicochemically. *In vitro* cellular uptake in C6 glioma cells was investigated. FTIR data show that the selected drug and excipients were chemically compatible. The unilamellar vesicle size was less than 50 nm with smooth surface. Drug released slowly from L-DTX *in vitro* in a sustained manner. The pharmacokinetic data shows more extended action of DTX from L-DTX in experimental rats than the free-drug and Taxotere[®]. DTX from L-DTX enhanced 100% drug concentration in brain as compared with Taxotere[®] in 4 h. Thus, nanoliposomes as vehicle may be an encouraging strategy to treat glioma with DTX.

Introduction

Astrocytoma (commonly known as glioma) is most prevalent among three different types of brain tumors, namely astrocytomas, oligodendrogliomas and oligoastrocytomas, in adults. This aggressive malignant form of cancer accounts for ~45–50% of all primary tumors resulting in death of patients within a couple of years (Guo et al., 2011; Nance et al., 2014). The characteristic features such as lack of sharp border, infiltration ability of the tumor cells in the brain of glioma as well as their wide distribution restrict their treatments by surgery and radiotherapy (Guo et al., 2011). Further, due to the strategic location of the blood–brain barrier (BBB) that allows a selective transport of drugs into the brain, chemotherapy becomes an auxiliary treatment for malignant glioma. In the last few decades, many drugs have been or being explored for the treatment of glioma. Most of them including docetaxel (DTX) are large hydrophobic molecules, which are unable to

Keywords

Blood–brain barrier, nanoliposomes of Docetaxel, glioma, C6 cells, brain distribution

History

Received 4 August 2016
Revised 23 October 2016
Accepted 23 October 2016

cross the BBB easily (Asperen et al., 1997) and may become an effective candidate for efflux by various efflux pumps governed by BBB as well as tumor cells (Beaulieu et al., 1997).

Docetaxel (DTX) is a complex diterpene alkaloid, isolated from the bark of *Texas baccata*, congener of paclitaxel. It has an efficient antineoplastic effect against a wide spectrum of solid tumors, such as ovarian, breast and lung cancer. It is found to be effective in the treatment of glioma *in vitro* but its *in vivo* efficacy is highly compromised due to its poor aqueous solubility and high molecular weight (Banks, 2009; Liu et al., 2011; Tan et al., 2012). Therefore, suitable design and development of appropriate vehicle for the transport of therapeutic payload is of prime importance in order to develop an effective therapy against glioma. In this context colloidal drug carrier especially nanoliposomes have gained significant interest among the researchers around the globe. (Jain, 2012; Zhang & Zhang, 2013; Hao et al, 2015; Sonali et al., 2016a; Sonali et al., 2016b; Sonali et al., 2016c).

Liposomes, the small spherical vesicle with single or multiple lipid bilayers, made from natural and/or synthetic lipids have been widely exploited due to their unique characteristics such as high biocompatibility, biodegradability, and non-immunogenicity (Laouini et al., 2012; Akbarzadeh et al., 2013). They usually improve biodistribution and pharmacokinetic profile of the therapeutic payload by sustained drug release from the formulation and

Address of correspondence: Biswajit Mukherjee, Department of Pharmaceutical Technology, Jadavpur University, Kolkata – 700032, West Bengal, India. Tel: +91-33-24146677. Fax: +91-33-24146677. E-mail: biswajit55@yahoo.com

This is an Open Access article distributed under the terms of the Creative Commons Attribution License (<http://creativecommons.org/licenses/by/4.0/>), which permits unrestricted use, distribution, and reproduction in any medium, provided the original work is properly cited.

minimizing the toxicity of the chemotherapeutics by their selective accumulation in the target area (Chang & Yeh, 2012; Akbarzadeh et al., 2013). Moreover, liposomes are able to accommodate both hydrophilic (in the aqueous core) drug and hydrophobic (in the lipidic bilayers) drug. Thus a liposomal drug delivery system can be used to increase the solubility of hydrophobic drugs and can protect them from metabolism in the body fluid (Allen & Moase, 1996; Irache et al., 2011; Akbarzadeh et al., 2013). However, optimized size of liposomal formulation is a critical aspect in order to develop efficient therapeutics against glioma. It has been reported in the literature that a nanosize (<200 nm) drug carrier can exploit the advantages of leaky vasculature associated with primary brain cancer for transport of therapeutic payload within the tumor easily through a common mechanism known as enhanced permeability and retention effect (EPR) (Kobayashi et al., 2014).

The marketed formulation of DTX (Taxotere[®]) contains a solubilizing vehicle which consists of 50:50 mixtures of tween 80 and dehydrated ethanol; and tween 80 is responsible for certain adverse effects such as severe hypersensitivity reactions, anaphylaxis, hyperlipidemia, abnormal lipoprotein patterns, and aggregation of erythrocytes (Tije et al., 2003). Further, infusion of DTX for a prolong period of time may sometimes cause cumulative fluid retention, and peripheral neuropathy (Sanchez-Moreno et al., 2012).

Administration of DTX requires a long infusion period (typically 3–24 h) and patients are generally required to be admitted in hospitals overnight resulting additional inconvenience. Therefore, incorporation of DTX into liposomal formulation results in a sustained release formulation, which could be administered easily through intravenous route and also use of tween 80 can be avoided, resulting improve patient compliance and better therapeutic outcome. Innovations of the present study focused on the development of nanosize (<100 nm) homogeneously distributed liposomes containing DTX using common materials with a simple technology. The developed formulation was able to cross blood brain barrier successfully to provide adequate concentration of drug in brain for a longer period by releasing the drug in a sustained manner. Comparable to the commercial formulation containing tween 80, further our formulation was devoid of tween 80 related toxicity.

Few similar recent important investigations (Hao et al., 2015, Sonali et al., 2016b, Sonali et al., 2016c) also developed nanoformulations with receptor targeting agents. However, they were constituted with absolutely different constituents such as D- α -tocopheryl polyethylene glycol 1000 succinate (TPGS), poly-lactic-co-glycolic acid (PLGA). Further, Sonali et al. (2016c) developed micelles. Hao et al. (2015) developed multifunctional nanoparticles and Sonali et al. (2016b) developed theranostic liposomes.

Advantages of our studies over those studies are that we have developed simple nanosize liposome with very common constituents such as phospholipid and cholesterol without any receptor targeting agent, using a very simple technology. Our formulations were much smaller than the size of the liposomes and nanoparticles reported in those studies. However, our formulations were little larger than the micelles, but well below 100 nm in size. Further, it provided much slower drug release

with a more sustaining effect as compared to the above three formulations. Moreover, IC₅₀ value of our formulation was considerably lower and the formulations were internalized well by the C6 glioma cells. The major disadvantage of the targeted delivery is the saturation of the receptor by the targeting agent. Our formulation is also devoid of such problem, and thus would deliver the drug more effectively for a prolonged period of time across the BBB to the brain.

Therefore, the objective of the present study was to develop nanoliposomal formulation of DTX and to establish its successful delivery in the brain. This may be beneficial for the treatment of brain cancer such a glioma.

Materials and methods

DTX was obtained as gift sample from Fresenius-Kabi Oncology Ltd. (Kalyani, West Bengal, India). Cholesterol (CHL) and chloroform were purchased from Merck (Mumbai, India) and soya-L- α -lecithin (SPC), fluorescein isothiocyanate (Isomer I) (FITC), Dulbecco's Modified Eagle's Medium (DMEM) containing 10% fetal bovine serum (FBS) and antibiotics (10,000 U/L penicillin and 10 mg/L streptomycin) were purchased from HiMedia Laboratories Pvt. Ltd (Mumbai, India). NaHCO₃ was purchased from Invitrogen Corporation (Carlsbad, CA), butylated hydroxy toluene (BHT) was purchased from Qualigens Fine Chemicals (Mumbai, India). 4',6-Diamidino-2-phenylindole (DAPI) and tetrazolium dye 3-(4,5-dimers dimethylthiazol-2-yl)-2,5-diphenyltetrazolium bromide (MTT) were purchased from Sigma-Aldrich (St. Louis, MO). C6 glioma cells of rats were purchased from National Center for Cell Science (Pune, India). Marketed formulation of DTX (Taxotere[®] injection 20 mg vial) was purchased from M/s Adeline, Kolkata, India (batch no. 4F170A, invoice no. 31375). All other chemicals and reagents used were of analytical grade.

Experimental animals

Male Sprague-Dawley rats of body weight 160 ± 20 g were used for this study. Animals were obtained from animal house, Department of Pharmaceutical Technology, Jadavpur University, Kolkata, India. The animals were acclimatized to the laboratory condition at 22 ± 1 °C and humidity of $60 \pm 10\%$ for 7 days prior to the actual experiment and they had free access to water and food (Dey et al., 2016). The animals were maintained at 12 h dark/light circle. The animal experiments were conducted with the prior approval of the Institutional Animal Ethical Committee (IAEC), Jadavpur University, Kolkata, by strictly following the guidelines of the IAEC. The animals were deprived of food for 12 h with a free access of water before administration of different formulations.

Drug-excipients interaction study

In the present study, we have investigated the drug-excipients interaction by Fourier transform infrared (FTIR) spectroscopy (Dey et al., 2016). The pure components of the experimental formulations (i.e. DTX, CHL and SPC, a mixture of CHL, SPC and a mixture of drug with CHL, SPC), the optimized formulation containing DTX (L-DTX) and formulation without DTX (B-DTX) (both the formulations were in the lyophilized forms) were mixed separately, with infrared

Table 1. Formulation composition, % yield, drug loading and loading efficiency of different formulations.

Formulation code	DTX:SPC:CHL (by weight)	Yields %*	% of drug loading*	Loading efficiency %*
NL1	1:5:5	42.03 ± 4.19	2.6 ± 0.45	28.61 ± 5.05
NL2	1:10:5	69.21 ± 4.75	5.48 ± 0.5	87.81 ± 7.82
NL3	1:15:5	49.89 ± 2.86	1.86 ± 0.5	70.26 ± 11.04

*Data show mean ± standard deviation of three different formulations or three different experiments in triplicate (where applicable).

grade potassium bromide (KBr) in a ratio of 1:100. Pellets were prepared using KBr press at a pressure of 5.5 metric ton. The pellets were then scanned using FTIR spectrophotometer (Jasco, FTIR 4200, Japan).

Preparation of nanoliposomes (NLs)

DTX loaded NLs (L-DTX) were prepared by lipid layer hydration method as reported earlier (Dey et al., 2016). Requisite weights of different components of NLs such as SPC, CHL, DTX (Table 1) were taken into a 250 mL round bottom flask and were dissolved in 10 mL chloroform. The resultant mixture was mixed by gently-shaking the content in a rotary vacuum evaporator (Rotavap, model: PBU-6, Superfit Continental Pvt. Ltd., Mumbai, India) fitted with an A3S aspirator (Eyela, Tokyo Rikakikai Co. Ltd., Taguig City, Philippines) and circulating water bath (at 4 °C) (Spac-N Service, Kolkata, India) and the chloroform was evaporated at 40 °C in the water bath. It was then kept overnight in a vacuum desiccator. The thin film thus obtained was hydrated in PBS (pH,7.4) for 60 min at 60 °C at 160 rpm and sonicated at about 30 ± 3 KHz using a sonicator (Trans-o-Sonic, Mumbai, India) for 60 min. It was then preserved overnight at 4 °C. The suspension was centrifuged in a cold centrifuge (3K30 Sigma Lab Centrifuge, Merrington Hall Farm, Shrewsbury, UK) at 16 000, rpm at 4 °C for 60 min to obtain the liposomes and collected in a petridish; and freeze-dried using a laboratory freeze-drier (Laboratory-Freeze Dryer, Instrumentation India Ltd., Kolkata, India) for getting a dried mass of the sample.

NLs without DTX (B-DTX) were prepared by the same method without the addition of DTX during preparation. Fluorescent NLs containing DTX (F-DTX) for cellular uptake study were prepared by the same method of L-DTX preparation except that addition of 100 µL of 0.4% (w/v) FITC, as a fluorescent marker, dissolved in a mixture of chloroform and ethanol (3:1 v/v) (Sinha et al., 2013) during the initial mixing of the components in chloroform.

Vesicle characterization

DLS study

The average vesicle size, polydispersity index (PDI) and zeta potential of L-DTX were determined by dynamic light scattering (DLS) technology in a Zetasizer Nano ZS90 (Malvern Instruments, Malvern, UK) at 25 °C using a standard method of analysis (Dey et al., 2016).

Surface morphology study by field emission scanning electron microscopy (FESEM)

FESEM of optimized NLs was done by using electron microscope (Model-JSM-6700F; JEOL, Tokyo, Japan).

Lyophilized formulation was spread on to a carbon tape over a stub and a platinum coating of about 5 nm was applied at an accelerating voltage of 10 kV and 10 mA current with the help of a platinum coater (JEOL, Tokyo, Japan).

Cryogenic-transmission electron microscopy (Cryo-TEM) study

Further, morphology, rigidity and lamellarity were confirmed by Cryo-TEM as reported earlier and images were captured on a BM-Eagle 4 k × 4 k CCD camera (FEI Company, Eindhoven, The Netherlands) and the final pixel size was 1.89 Å (Helvig et al., 2015; Dey et al., 2016).

Yield percentage

Yield of each formulation batch was determined to know the amount of NLs obtained with respect to the total amount of raw materials used for the formulation. The completely dried formulation was weighed after a batch run and percentage yield was then determined by the following equation:

$$\text{Percentage yield} = \frac{\text{Amount of NLs obtained}}{\text{Total amount of components in the formulation}} \times 100$$

Percentage of drug loading and loading efficiency percentage

Requisite quantity of NLs (2 mg) was lysed by sonication followed by vortex in acetonitrile (HPLC grade) and DTX was separated out by centrifugation at 10 000, rpm for 10 min. The absorbance of supernatant was measured at 230 nm in an ultraviolet-visible spectrophotometer (Advanced Microprocessor UV-Visible single beam, Intech 295, Andhra Pradesh, India). The same procedure was repeated for formulation without drug (B-DTX) to get absorbance to nullify the effect of excipients on DTX absorbance readings by subtracting the readings of the absorbance of B-DTX from those of L-DTX. The percentage drug loading and loading efficiency were calculated from following equations as mentioned earlier (Dey et al., 2016).

$$\text{Percentage of drug loading} = \frac{\text{Amount of DTX in NLs}}{\text{Amount of NLs taken}} \times 100$$

$$\text{Percentage loading efficiency} = \frac{\text{Practical loading \%}}{\text{Theoretical loading \%}} \times 100$$

In vitro drug release and drug release kinetic study

Comparative *in vitro* drug release behavior of the optimized formulation (L-DTX) with the marketed formulation

(Taxotere[®]) and free-drug suspension, consisted of 2 mg/mL of DTX in a mixture of 520 mg of tween 80 and 13% ethanol (Dou et al., 2014) was investigated by dialysis method (Dey et al., 2016). Briefly, phosphate-buffer saline pH 7.4 (PBS), 50 ml containing 0.5% (w/v) sodium lauryl sulfate (SLS) (Hu et al., 2012) was taken as drug release media in a borosilicate glass beaker of 100 ml capacity. Accurately weighed (5 mg) formulation (lyophilized) and an equivalent amount of free-drug suspension; and Taxotere[®]; were reconstituted with 1 mL drug release media and poured into a dialysis bag (molecular weight cut-off 12–14 kDa). The bag containing formulations was made and immersed centrally into the release media in a glass beaker (100 ml) with the help of a glass rod. The beaker was placed on a magnetic stirrer and maintained the content of the beaker for a rotation of 300 rpm using a magnetic bead. At different predetermined time intervals for 48 h, drug release medium (1 mL) was withdrawn and replaced with 1 mL fresh drug release media. The absorbance of the samples was measured in a spectrophotometer at λ_{max} of 229 nm. The different concentrations were calculated from the calibration curve of DTX in PBS containing 0.5% SLS.

To understand *in vitro* DTX release kinetics from L-DTX formulation, the drug release data was analyzed by different release kinetic models such as zero-order, first-order, Higuchi kinetics, Korsmeyer–Peppas model and Hixon–Crowell model for the highest correlation coefficient value (R^2) (Pattnaik et al., 2012).

In vitro cell viability assay

Cell viability assay in rat C6 glioma cells was performed to monitor growth inhibitory potential or cytotoxicity of different formulations of DTX such as, L-DTX, B-DTX, Taxotere[®] and free DTX solution, by MTT assay (Barth, 1998; Dey et al., 2015). These cells were grown in DMEM containing 10% FBS, NaHCO₃ and antibiotics (10 000 U/L penicillin and 10 mg/L streptomycin). C6 cells were maintained in T-25 culture flask at 37 °C in CO₂-incubator (Heraeus Hera Cell, Burladingen, Germany). Briefly the method is as follows:

C6 glioma cells (2.5×10^3 cells in 100 μ l incomplete media/per well (media without FBS) were placed in 96-well plate and kept overnight in CO₂-incubator. Then, the cells were treated with various concentrations of different DTX formulations (equivalent to 5–150 nM drug). After 48 h of treatment, incomplete media was discarded and 100 μ l of MTT solution (1 mg/ml) was added in each well and kept in the incubator for 4 h. After incubation, MTT solution was discarded and 100 μ l DMSO was added in each well to dissolve insoluble formazan dye produced by mitochondrial reductase enzyme of viable cells. Then, plates were put on shaker for 10 min and optical density (O.D.) was measured at 560 nm by plate reader (Biorad, Hercules, CA). Antiproliferative effect was evaluated by measuring the percentage of cell viability as given below:

$$\begin{aligned} & \% \text{ of cell viability} \\ &= \frac{\text{O.D. at 560 nm of the sample of treated cells}}{\text{O.D. at 560 nm of the sample of untreated cells}} \times 100 \end{aligned}$$

Cellular uptake studies in C6 rat glioma cells

Cellular uptake study was performed to evaluate cellular localization of DTX-loaded fluorescent liposome in C6 rat glioma cell line (Venkatesan et al., 2011). In brief, C6 cells were seeded (3×10^4) and grown on poly-L-lysine coated cover slips. Then, cells were treated with F-DTX (FITC-L-DTX) suspension in water for injection (WFI) at an equivalent DTX concentration of 7.5 nM for 0.5 and 6 h in serum free DMEM medium. After the time dependent treatment, medium was discarded and cover slips were carefully washed with PBS. Treated cells were then fixed with 4% paraformaldehyde solution for 5 min. After fixation, the cells were washed with PBS and stained with DAPI. Cover slips were dried for overnight and mounted on glass slide using DPX (dibutylphthalate polystyrene xylene). Fluorescence images (20 \times magnification) were taken using a fluorescence microscope (Carl Zeiss, Oberkochen, Germany) to evaluate localization of nanoliposomes. Further, the quantification of amount of DTX uptake was done using flow cytometry analysis as follows: C6 rat glioma cells were grown in 60 mm petri dish. After 70% confluency, complete DMEM medium was removed and incomplete DMEM media was added. Then, cells were treated with F-DTX for 0.5 and 6 h. After treatment, cells were collected by trypsin treatment. Cells were then fixed in chilled ethanol and kept in -20°C overnight. Next day, samples were centrifuged to collect the cells and resuspended in sterile PBS. Samples were then subjected to flow cytometric analysis (FACS Canto II[™] cell sorter, BD Biosciences, San Jose, CA) using FACS Diva software (BD Biosciences) to measure cellular uptake of liposomes (Baishya et al., 2016).

In vivo plasma and brain pharmacokinetic (PK) study

In vivo plasma and brain pharmacokinetics of the different preparation of DTX were investigated to know the comparative distribution of DTX in the plasma and brain from L-DTX, Taxotere[®], the marketed DTX formulation (Taxotere[®]) and free-drug suspension, consisted of 2 mg/mL of DTX in WFI (Dou et al., 2014; Dey et al., 2016).

The animals were divided into four groups. One group of animals was treated with L-DTX dispersed in WFI, second group with Taxotere[®] and third group with free-drug suspension in WFI at an equivalent dose of 10 mg/kg body weight of rats of DTX intravenously through tail vein (Venishetty et al., 2013; Dey et al., 2016) and the fourth group of animals was treated as control group. At a time interval of 0.25 h, 0.5 h, 1 h, 2 h, 4 h, 8 h of dosing, about 1.0 mL blood was collected into a microcentrifuge tube containing EDTA solution from the heart of each animal by terminal cardiac puncture following deep anesthesia using chloroform. The plasma was separated out by centrifugation at 5000 rpm for 6 min. The plasma was then stored at -80°C until analysis. The brain portion was separated and stored in -80°C until further analysis by tandem liquid chromatography-mass spectroscopy (LC-MS/MS) (Kuppens et al., 2005; Venishetty et al., 2013).

Sample analysis by LC-MS/MS

Working stock of DTX was prepared by serial dilution in HPLC grade methanol. Calibration control (CC) and quality

control (QC) samples were prepared by spiking the working stocks in blank plasma. CC, QC and pharmacokinetic (PK) study samples were extracted by protein precipitation technique. Plasma sample (100 μ l) was precipitated with 300 μ l ice cold acetonitrile containing 500 ng/ml paclitaxel as internal standard (IS), vortex-mixed for 10 min, centrifuged at 4000 rpm at 15 °C for 15 min. Supernatant (100 μ l) was mixed with 100 μ l water and loaded into LC-MS/MS (LC: Shimadzu Model 20AC, MS: AB-SCIEX, Model: API4000, Software: Analyst 1.6) (Hou et al., 2004). Analytes were eluted using YMC Triat C18 column (2.1 \times 30 mm, 5 μ) and gradient elution technique of two mobile phases (mobile phase A: 0.1% formic acid in water and mobile phase B: 0.1% formic acid in 80:20 acetonitrile/water), with injection volume: 20 μ l, flow rate 0.8 ml/min and total run time 3.5 min. Brain samples were weighed and four times water was added, homogenized and analyzed by LC-MS/MS following the above-mentioned technique. Quantified DTX concentrations were plotted and different PK parameters such as maximum blood concentration (C_{max}), area under the concentration–time curve from time of injection ($t=0$) to a determined time point, i.e. AUC_{0-t} , time taken for C_{max} to drop in half-life ($t_{1/2}$), clearance (CL), steady state volume of distribution (V_{ss}), mean residence time (MRT) of DTX were calculated using NCA toolbox of Phoenix-WinNonlin software (Certara, Princeton, NJ) (Kuppens et al., 2005). The intake of DTX from all the investigating formulations into the brain was assessed from the plasma to brain value (plasma/brain value) of DTX (Kemper et al., 2004; Venishetty et al., 2013).

Statistical analysis

All the experiments were performed in triplicate in order to check the reproducibility and all the data were expressed as mean \pm standard deviation. Statistical calculations were performed using one-way ANOVA followed by the Tukey *post hoc* test using Origin Pro 8 (OriginLab, Northampton, MA, USA). Differences were considered statistically significant when the probability value (p) was less than 0.05 at 95% confidence level.

Results

Drug-excipients interaction study

Drug-excipients interaction (if any) was investigated using FTIR spectroscopy to assess the type of interaction among the various functional groups of the drug and the excipients of a formulation (Figure 1A–G). When the FTIR spectra of the excipients (namely, CHL, SPC) and the pure drug (DTX) were compared with their physical mixtures, it was found that the characteristic bands of all the excipients and the drug were present in their physical mixtures. The C=C asymmetric stretch of medium intensity bending vibration and C=O variable weak intensity out of plane bending vibration (at 721 cm^{-1}), strong intensity C=O stretching vibration (at 1741 cm^{-1}) and medium intensity bending vibration of $-CH_3$ deformation (at 1379 cm^{-1}) of SPC were present in the physical mixture. Similarly, the characteristics bands of CHL were observed in the spectra of physical mixture and in the spectra of cholesterol alone. For example, strong intensity

stretching vibration of C–OH group (at 1057 cm^{-1}) and medium intensity bending vibration of $-CH_3$, $-CH_2$, $-CH$ deformations (at 1465 cm^{-1}) indicate the presence of CHL in the physical mixture of CHL, SPC and DTX and that of SPC and CHL. Further, in case of DTX, medium intensity out of plane bending vibration C=C (at 800 cm^{-1}) and C–O stretching bands were observed in the spectrum of physical mixture and the spectrum of drug alone. This suggests that there is no chemical interaction seen between the drug and the excipients.

In the FTIR spectra of L-DTX and B-DTX, minor shifts of few characteristic bands of SPC from 1739 to 1743 cm^{-1} and from 1378 to 1381 cm^{-1} were observed. Again, for CHL, a shift of characteristic bands from 1465 to 1466 cm^{-1} , from 1060 to 1063 cm^{-1} in L-DTX were observed. In case of DTX, the characteristic peak at wave number 800 cm^{-1} was retained by the formulation with reduction of band intensity, suggesting that there was no chemical interaction between the drug and the excipients. Further, minor shifts of some bands in case of SPC and CHL in the formulation might be due to some physical interactions. After the selection of drug and the excipients, various formulations were prepared and the best optimized formulation (NL2) was selected and reported here.

Vesicles characterization

The data from Malvern particle size analyzer revealed that the 100 percentage vesicles of NL2 had an average particle size 45.9 ± 12.3 nm (Figure 2A) with a PDI of 0.27 ± 0.04 and zeta potential was found to be -56.8 ± 8.7 mV (Figure 2B and Supplementary Table 1A). Further, FESEM image revealed that L-DTX had smooth surface and were homogeneously distributed having size less than 50 nm (Figure 2C). From Cryo-TEM images, it was further confirmed that the vesicles were unilamellar with the intact lamellarity and were in the nanometer range (Figure 2D).

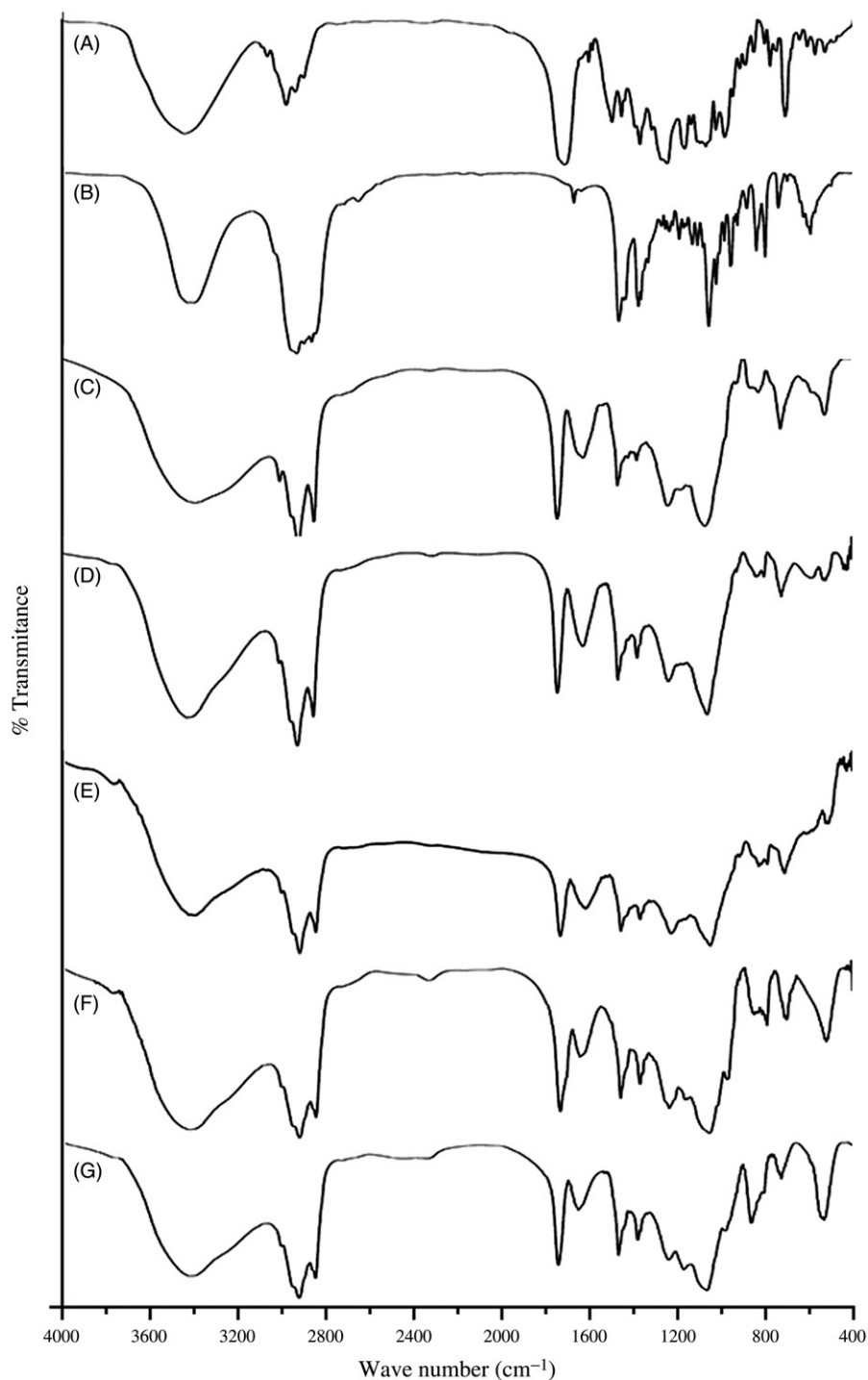
Percentage of drug loading, drug loading efficiency percentage and yield

The percentage of drug loading of NL2 was $5.48 \pm 0.5\%$ with a drug loading efficiency percentage $87.81 \pm 7.82\%$ and product yield, $69.21 \pm 4.75\%$ (Table 1).

In vitro drug release and drug release kinetic study

The comparative *in vitro* release of DTX from the experimental formulation (L-DTX), Taxotere[®] and free-drug solution was done by dialysis method and the result was expressed as cumulative drug release percentage against time in hour (h) (Figure 3A). It shows that $38.3 \pm 2.6\%$ of drug was released at the end of 48 h, whereas the release of DTX from Taxotere[®] was very fast in comparison to L-DTX. More than 95% of DTX released within 8 h. The release of DTX from free-drug solution was at a lower rate than Taxotere[®] but quicker than L-DTX. More than 83% DTX released within 24 h. Thus the experimental formulation possessed a slower rate of release of DTX than Taxotere[®] and free drug solution. However, the drug released from L-DTX formulation initially at a faster rate up to 12 h and then at a slower rate in a sustained manner.

Figure 1. FTIR spectral data of (A) DTX, (B) CHL and (C) SPC, (D) a mixture of CHL, SPC and (E) a mixture of drug with CHL, SPC, (F) the optimized formulation with DTX (L-DTX) and (G) formulation without DTX (B-DTX).



The drug release kinetic revealed that the release was occurring by the Korsmeyer–Peppas kinetic ($R^2=0.955$) (Supplementary Table 2A). The release of the drug from the vesicles followed non-Fickian diffusion kinetics, as depicted from the release component value ($n=0.848$).

In vitro cell viability assay

In vitro cell viability or anti-proliferative effect of free DTX, L-DTX, B-DTX and Taxotere[®], was evaluated in C6 glioma cells of rats using MTT assay method. The plot of % cell viability against dose (nM) shows that as the concentration of

formulation of DTX (L-DTX) increased, the death rate of cells increased. L-DTX-mediated cellular death was found to be more compared to the cells treated with free-drug solution and Taxotere[®], respectively. The half maximal inhibitory concentration (IC_{50}) value of L-DTX significantly decreased in comparison to others. IC_{50} values of DTX from L-DTX was found at 9.5 ± 0.8 nM which is significantly very less in comparison to free-DTX (IC_{50} value, 70.8 ± 0.1 nM) and Taxotere[®] (IC_{50} value, 86.5 ± 0.3 nM). The data also reveal that there was no effect of the excipients used in the formulation on the cytotoxicity of DTX as the cell death from blank formulation (B-DTX) was insignificant (Figure 3B).

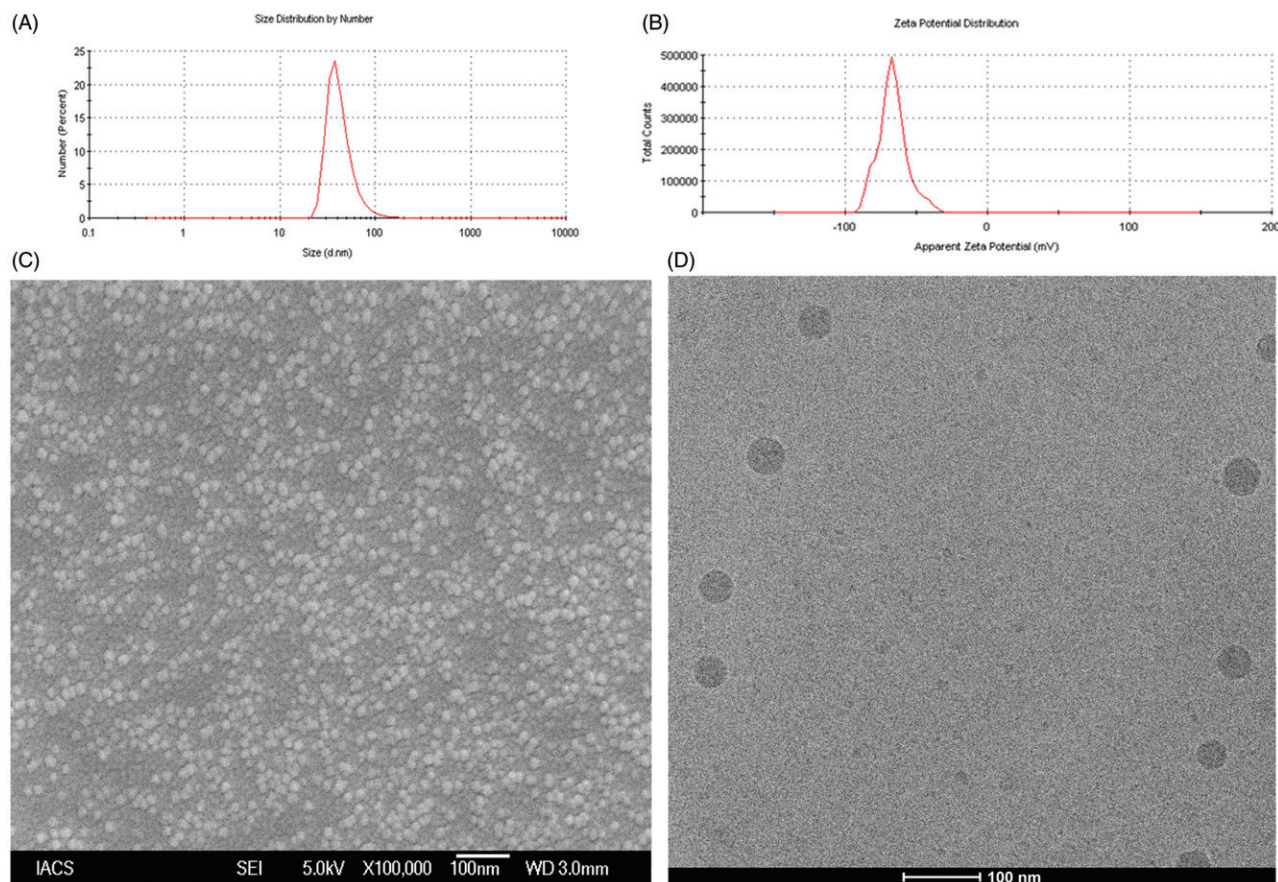


Figure 2. (A) Particle size distribution (B) Zeta potential value (C) Field emission scanning electron microscopic image at a magnifications of (70 000 \times) and (D) Cryo-TEM image of the experimental formulation (L-DTX).

Cellular uptake studies in C6 rat glioma cells

To ascertain whether the prepared NLs can permeate into the cell or not, we have performed *in vitro* cellular uptake study in C6 glioma cells by fluorescent microscopy using F-DTX formulation. The images reveal that the formulation was internalized into the cells through the cell membrane and distributed at the cytoplasm. As the time of dosing increased, the amount of uptake of NLs also increased (Figure 3C). This was further substantiated by the flow cytometry study (Figure 3D), data shows about 18%, and about 23% enhancement of uptake in terms of FITC incorporated liposomes in cells at 0.5 h (Figure 3D-II) and 6 h (Figure 3D-III) of treatments, respectively, in comparison to untreated cells (Figure 3D-I).

In vivo plasma and brain pharmacokinetic (PK) study

The pharmacokinetic data of DTX from the experimental formulations in plasma and brain were investigated in Sprague-Dawley rats. A dose of 10 mg/kg body weight of rats of DTX was administered by intravenous route and different PK parameters of DTX were calculated (Table 2).

The mean plasma concentrations of DTX from L-DTX at the different time points were comparatively higher than those of the free DTX-treated rats up to 6 h (Figure 4A). However, the plasma concentration of DTX could not be detected below the lower limit of quantification (2 ng/mL) after 6 h for the free-drug, but for L-DTX, the drug was

detected up to 8 h. The plasma concentration of DTX from L-DTX was 5.44-fold higher than that of free drug at the end of 8 h, indicating more circulation of DTX in the blood of the experimental rats.

When we compared Taxotere[®] with L-DTX, concentrations of DTX in plasma at the different time points of post-dosing did not significantly vary. The plasma $t_{1/2}$ value of DTX from L-DTX was higher than those of the free-drug and Taxotere[®]-treated rats by 2.43 folds and 2.21 folds, respectively. MRT value of DTX was considerably higher for L-DTX than free-drug and Taxotere[®] by about 66% and 42%, respectively. Further, there was a decrease of clearance and increase of AUC of DTX by 27.3% and 37.5%, respectively, in L-DTX-treated rats in comparison to free-drug-treated group of animals.

DTX level in brain was 4.4-fold higher in L-DTX-treated rats than the free-drug-treated rats at 1 h (Figure 4B). After 1 h the drug concentration in brain could not be quantified for free-drug-treated animals although DTX concentration for L-DTX-treated animals was measured up to 4 h. The drug level in brain from L-DTX was little lower than that from Taxotere[®] up to 2 h, but DTX concentration became predominantly more in L-DTX-treated animals at 4 h than Taxotere[®]-treated rats.

We have also calculated the plasma/brain value of DTX from the different groups of animals at the different time points up to 4 h of study. There was 4.07-fold increase of plasma/brain value of DTX for L-DTX with respect to the

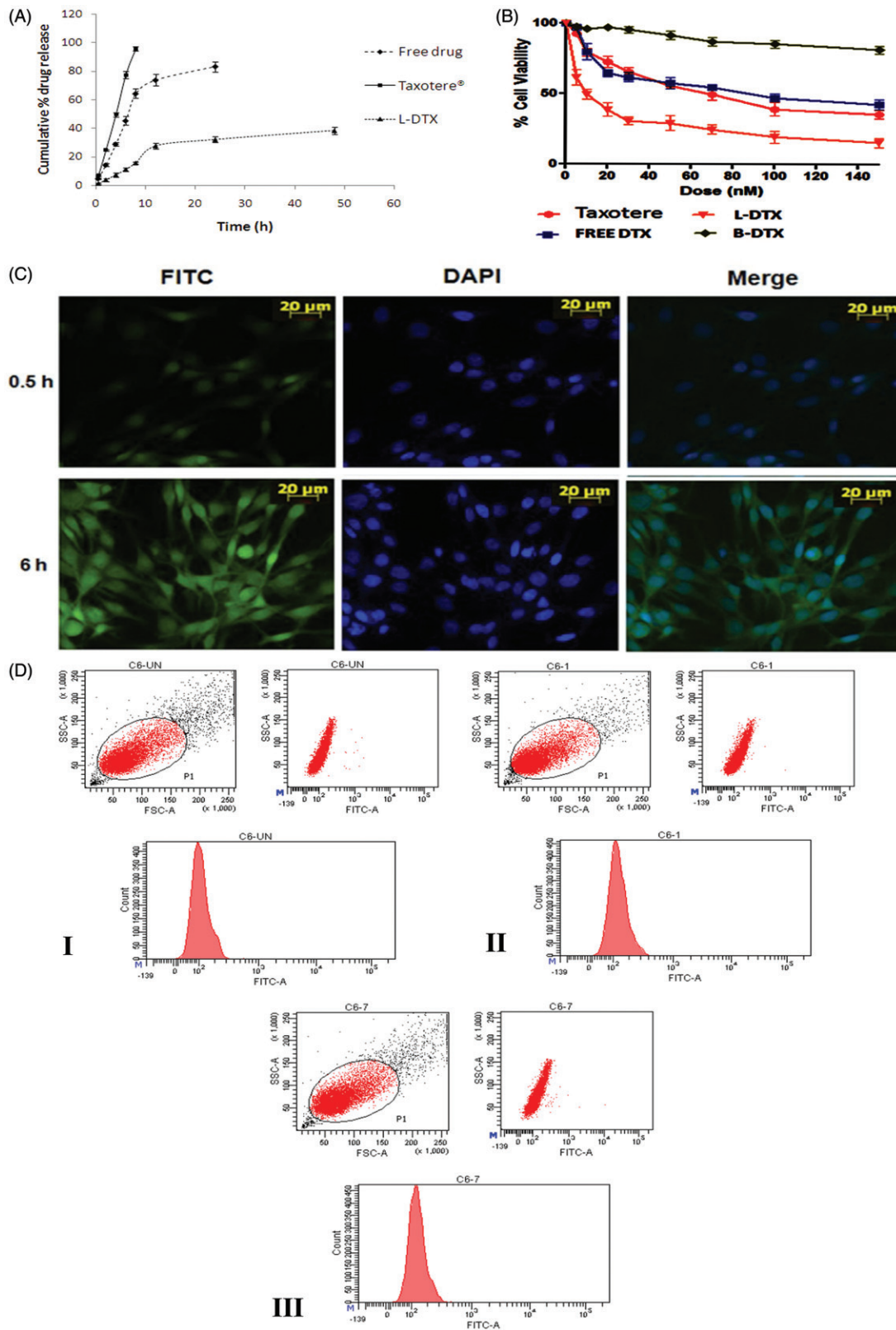


Figure 3: (A) *In vitro* release profile of DTX from the experimental formulation (L-DTX), marketed formulation (Taxotere[®]) and free-DTX solution in phosphate buffer, pH 7.4. Data show mean \pm standard deviation of three different experiments in triplicate. (B) Cell viability study by MTT assay of blank formulation (B-DTX), L-DTX (formulation with DTX), marketed preparation (Taxotere[®]) and free-drug (DTX) in C6 glioma cells of rats. Data show mean \pm standard deviation of three different experiments. (C) Cellular localization study of FITC-L-DTX (F-DTX) at different time points by fluorescence microscopy in C6 glioma cells of rats and (D) Flow cytometric measurement of C6 glioma cells of rats incubated with F-DTX at 0.5 h and 6 h of treatments, indicating about 18%, and about 23% enhancement of uptake in terms of FITC incorporated liposomes in cells at 0.5 h (Figure 3D-II) and 6 h (Figure 3D-III) of treatments, respectively, in comparison to untreated cells (Figure 3D-I).

Table 2. Pharmacokinetic parameters and plasma to brain values in different groups of rats treated with DTX-loaded liposome (L-DTX), marketed formulation of DTX (Taxotere[®]) and free-drug (DTX), administered intravenously at a dose of 10 mg/kg of average body weight of the rats.

Formulation	* $t_{1/2}$ (h)	** C_{max} (ng/ml)	# $AUC_{0 \rightarrow t}$ (ng.h/ml)	## $AUMC_{0 \rightarrow t}$ (ng.h ² /ml)	S MRT (h)	$^+$ CL (L/h)	$^{++}$ V_{ss} (L)	Mean plasma/brain value at different time interval in hour	
L-DTX	1.97 ± 0.02 ^{*,€}	1508.4 ± 33.9	2061.04 ± 88.19 [†]	3630.19 ± 255.81 ^{†,€}	1.76 ± 0.13 ^{†,€}	4.85 ± 0.26 [†]	8.55 ± 0.49 ^{†,€}	0.5	0.016 ± 0.001
								1.0	0.058 ± 0.005 [†]
								2.0	0.059 ± 0.008
								4.0	0.072 ± 0.017
Taxotere [®]	0.89 ± 0.05 [€]	1725.2 ± 179.1 [‡]	2192.57 ± 168.80 [‡]	2726.41 ± 431.27 ^{€,‡}	1.24 ± 0.08 [€]	4.56 ± 0.22 [‡]	5.67 ± 0.29 ^{‡,€}	0.5	0.019 ± 0.003
								1.0	0.063 ± 0.001 [‡]
								2.0	0.049 ± 0.005
								4.0	0.035 ± 0.0038
Free drug	0.81 ± 0.04 [†]	1308.1 ± 54.7 [‡]	1499.25 ± 68.73 ^{†,‡}	1587.77 ± 206.70 ^{†,‡}	1.06 ± 0.08 [†]	6.67 ± 0.30 ^{†,‡}	7.06 ± 0.17 ^{†,‡}	0.5	×××
								1.0	0.0143 ± 0.002 ^{†,‡}
								2.0	×××
								4.0	×××

Values represent mean ± standard deviation ($n = 3$); Statistical calculations were performed using one-way ANOVA followed by the Tukey *post hoc* test using Origin Pro 8 (OriginLab, Northampton, MA). Differences were considered statistically significant when the probability value (p) is less than 0.05 at 95% confidence level.

* $t_{1/2}$, half-life.

** C_{max} , maximum blood concentration.

$AUC_{0 \rightarrow t}$, area under the concentration-time curve from time of injection ($t = 0$) to a determined time point.

$AUMC$, area under the first moment curve.

S MRT, mean residence time.

$^+$ CL, clearance.

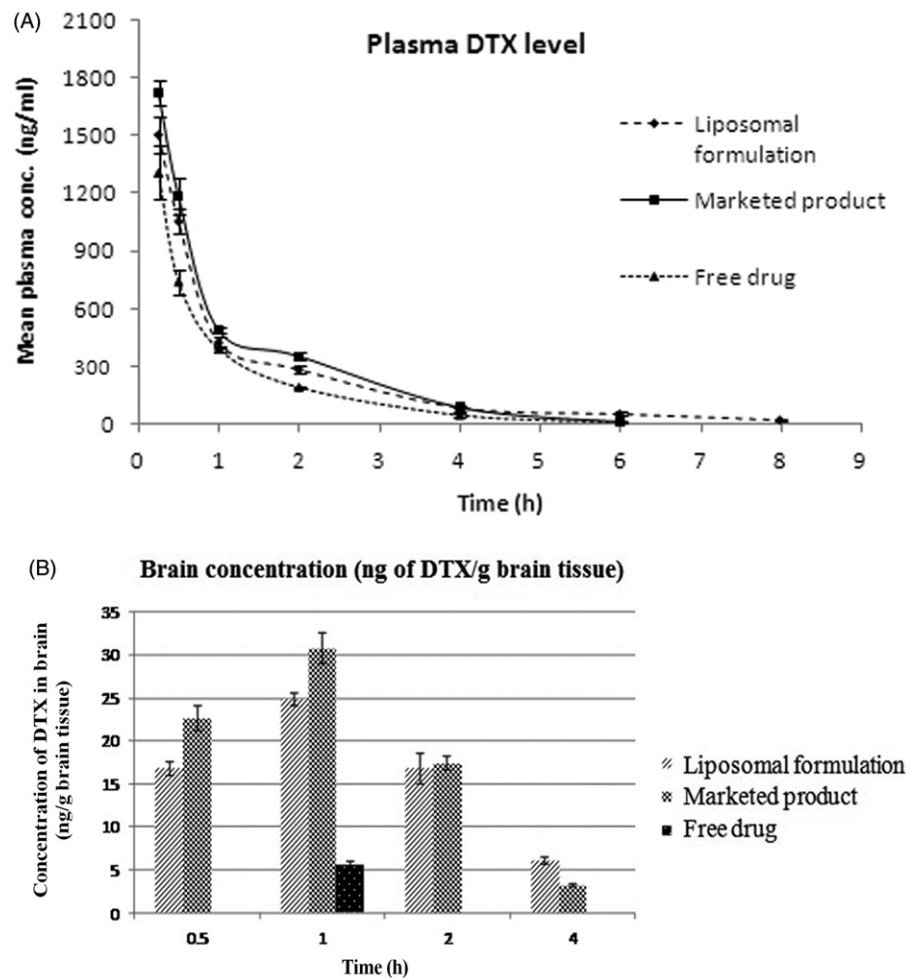
$^{++}$ V_{ss} , steady state volume of distribution.

[†]Denotes comparison made between L-DTX and free drug.

[€]Denotes comparison made between L-DTX and Taxotere[®].

[‡]Denotes comparison made between Taxotere[®] and free drug.

Figure 4: (A) Plasma level of DTX in rats after intravenous administration of L-DTX, free drug and Taxotere[®]. (B) Concentration of DTX in brain after intravenous administration of nanoliposomal formulation containing DTX (L-DTX), marketed formulation (Taxotere[®]) and free drug to rats at a dose of 10 mg/kg of DTX. Note: Data show mean ± standard deviation ($n = 3$).



free-drug-treated animals at 1 h. The values of plasma/brain of DTX for L-DTX and Taxotere[®] were 0.0159 vs. 0.0190 at 0.5 h, 0.0583 vs. 0.0628 at 1 h, 0.0589 vs. 0.0487 at 2 h, respectively. At 4 h, the value from L-DTX was predominantly higher than that of Taxotere[®] (Table 2).

Discussion

NLs were prepared by lipid layer hydration technique, and the drug and the excipients were taken at the ratio (by weight) of DTX, SPC, CHL varied from 1:5:5 (NL1) to 1:10:5 (NL2) to 1:15:5 (NL3) (w/w/w) (Table 1) to get optimized formulation in terms of better product yield, percentage of drug loading and drug loading efficiency percentage. The percentage of drug loading and percentage loading efficiency study revealed that $5.48 \pm 0.5 \mu\text{g}$ of drug per mg of the formulation with a loading efficiency of $87.81 \pm 7.82\%$ was achieved in case of NL2 formulation. So, a ratio of 1:10:5 of DTX:SPC:CHL was considered as an optimized formulation in this work. Hence, it has been considered for further physicochemical characterization and different *in vitro* and *in vivo* pharmacokinetic studies.

DTX is an approved drug to tumor of brain in combination therapy, but its entry to the brain is prevented by BBB due to its different physicochemical and pharmacological factors (Chen et al., 2004; van Rooy et al., 2011). We have tried to deliver DTX by incorporating it into the liposomes, based on the hypothesis that the nanosize of the vesicle may help to deliver DTX and the use of nanoliposomes may overcome the solubility problem of DTX and reported toxicity of Taxotere[®], the marketed formulation (Yang et al., 2007; Yousefi et al., 2009; Costantino & Boraschi, 2012). In this work we have formulated nanoliposomes of DTX using SPC as lipid component, and CHL as a stabilizer of lipid membranes.

Drug-excipients interaction was studied by FTIR spectroscopy. FTIR spectra showed that the characteristic peaks of drug, SPC and CHL were present in the physical mixture of the excipients and drug; and in the formulation. The characteristic peak of DTX existed in the formulation suggests that drug was encapsulated in the bilayer.

The FESEM images of the optimized formulation show that the obtained vesicles were within 50 nm in size and had smooth surface, and they were homogeneously distributed. Further, their characterization by Cryo-TEM reveals that the obtained NLs were of unilamellar spherical vesicle with intact lamellarity.

The particle size analysis data by DLS method show that the NLs were in the nanometer range with a very narrow size distribution as indicated by the PDI value. Further, PDI value of a colloidal system gives an indication of particle size distribution and also the physical stability of the system. For drug delivery aspects by intravenous injection or intravenous infusion, it is preferred that the particle should be of same size in the formulation. The PDI value of 0.1–0.25 indicates that the liposomal vesicles are uniformly distributed having appreciable physical stability and PDI value more than 0.5 indicates poor uniformity of the vesicles in the formulation (Dey et al., 2016). In this study, we obtained nanoliposomes having PDI value 0.27 ± 0.04 ,

indicating that the prepared liposomes were mostly distributed homogeneously.

The physical stability of the vesicles can also be predicted from the value of zeta potential. A zeta potential value above +30 mV and/or below –30 mV indicates that the vesicles of liposomes are good as per stability of the colloidal system is concerned (MacLachlan, 2007; Dey et al., 2016). In this work we got vesicles having zeta potential 56.8 ± 8.7 mV, suggesting that L-DTX vesicles had good colloidal stability. The presence of terminal carboxyl group in the lipids could be liable for this negative charge in the NLs.

In vitro drug release profile of the optimized formulation shows that the release of DTX from the experimental formulation (L-DTX) was found to occur faster initially (up to 12 h) and then at a slower rate in a sustained manner in comparison to free-drug and marketed product.

The pattern of drug release from the formulation was best fitted with the Korsmeyer–Peppas kinetics, which clearly demonstrates the involvement of anomalous diffusion which is controlled by more than one parameter. In case of the Korsmeyer–Peppas model, the fraction of drug release with time is considered and represented as $M_t/M_\infty = Kt^n$, where M_t/M_∞ is a fraction of drug released at time t and n is the drug release exponent. The drug release mechanism is governed by the value of “ n ”. When $n \leq 0.45$, the drug release is considered to follow the Fickian diffusion mechanism and it is non-Fickian when $n = 0.45–0.89$ (Pattnaik et al., 2012). When $n = 0.89$, drug release follows Case II (relaxational) transport, and if $n > 0.89$, it undergoes super case II transport mechanism of drug release (Pattnaik et al., 2012). The value of “ n ” was 0.848 in our study. Hence, the drug release occurred by non-Fickian diffusion or anomalous diffusion mechanism for L-DTX.

The MTT assay data for antitumor activity assessment in C6 rat glioma cells reveal that at each dosing interval the death rate was always higher for L-DTX as compared to Taxotere[®] and free-drug, suggesting that better antitumor efficacy of the experimental nanoliposomal vesicles of DTX (L-DTX) was seen at a comparatively low dose and the IC₅₀ value of L-DTX was significantly decreased ($p < 0.05$) as compared to Taxotere[®] and free drug-treated C6 cells. For B-DTX formulation (without drug), the decrease in cell viability of the cultured cell population was not notably significant, suggesting that the excipients of the formulation had no predominant impact on the death rate and these excipients are safe for glioma treatment.

For cellular uptake of NLs, C6 glioma cell line was used. FITC-NLs were used to visualize localization of the vesicles in the cells by its green fluorescence. In order to discriminate the localization of the vesicles into the nucleus, cells were stained with DAPI, as a nucleus staining color substance (blue fluorescence). The fluorescence microscopy images and the flow cytometry quantification of the internalized FITC incorporated liposomes disclosed that our nanoliposomal formulation predominantly concentrated in a time-dependent manner in the cytoplasmic part of the cells.

Pharmacokinetic profiles of DTX in plasma and brain were evaluated after its intravenous dosing in rats at a dose of 10 mg/kg. Pharmacokinetic studies reveal that the plasma concentrations of DTX were higher for the experimental

formulation at each investigational time point in comparison to free-drug. There was a rapid decrease of the plasma level up to first 2 h, which might be due to the rapid distribution of drug in the other tissues. Our formulation sustained the release of the drug at least up to 8 h (period of study) while the marketed product and the free-drug treatments showed detectable blood level of the drug up to 6 h only. There was a significant difference ($p < 0.05$) in AUC values among the various groups of animals treated with free-drug, Taxotere[®] and the experimental formulation. The AUC values of L-DTX and Taxotere[®]-treated rats were significantly higher ($p < 0.05$) than that of the free-drug treated rats, whereas there was non-significant difference ($p > 0.05$) of AUC value between L-DTX and Taxotere[®].

The plasma/brain values at 1 h among the free-drug, Taxotere[®] and L-DTX were significantly different ($p < 0.05$), but upon the Tukey *post hoc* test, there was no significant difference in value between our formulation and Taxotere[®] ($p > 0.05$). Amount of drug was not detectable at 0.5 h in brain tissues from the animals treated with free-drug. However, at 1 h only, DTX was detected in the same groups of animals. The DTX concentration in brain was observed from L-DTX and Taxotere[®] at all the time points studied.

In L-DTX-treated rats, the plasma/brain values were more than those of the marketed formulation at 2 h and 4 h of the study. Thus the experimental formulation crossed through the BBB better into the brain compartment than the free-drug. L-DTX was found to maintain 100% more drug concentration in brain at 4 h as compared to the marketed formulation. The size ranges of nanocarriers should be from 40 nm to 200 nm, for a successful brain delivery of a drug (Jain, 2012; Masserini, 2013; Mukherjee et al., 2015; Sonali et al., 2016a; Shilo et al., 2015). The vesicle size in this work was below 50 nm, hence the experimental formulation might improve the drug delivery by virtue of its nanosize (Sonali et al., 2016a; Shilo et al., 2015; Jain, 2012; Masserini, 2013; Mukherjee et al., 2015) and highly lipidic in nature. The decrease of brain concentration of the drug with time was held faster for Taxotere[®] than L-DTX. The MRT value of DTX from L-DTX was significantly elevated ($p < 0.05$) than free drug and Taxotere[®]-treated groups of rats (Table 2). Thus, the MRT values indicate that L-DTX was available in plasma more than the marketed formulation, suggesting longer sustaining effect of the drug from L-DTX.

A comparable drug level in brain from the experimental formulation with respect to the tween 80 containing commercial formulation suggests that the use of nanoliposome may avoid tween 80-related side-effects.

Conclusion

DTX-incorporated nanoliposomes may help us to avoid the use of tween 80, and thus escape tween 80 containing formulation related side-effects. Due to the sustained release of the drug from the vesicles, nanoliposomes of DTX may be used for depot preparation. Predominant uptake of L-DTX in the rat glioma cells showed the successful entry of the drug in the cells. The nanosize of the prepared vesicles was found to cross the BBB successfully *in vivo*. The experimentally

developed nanoliposomes are thus found to be an emerging way to deliver the drug in the brain and this could be a successful strategy to treat brain cancer using DTX.

Declaration of interest

The authors confirm that this article content has no conflicts of interest. The work was supported by Dr. V. Ravichandran Endowment Fund, Department of Pharmaceutical Technology, Jadavpur University (grant number CARPS/RF/04/12).

References

- Akbarzadeh A, Rezaei-Sadabady R, Davaran S, et al. (2013). Liposome: classification, preparation, and applications. *Nanoscale Res Lett* 8:102.
- Allen TM, Moase EH. (1996). Therapeutic opportunities for targeted liposomal drug delivery. *Adv Drug Deliv Rev* 21:117–33.
- Asperen JA, Mayer U, Tellingens OV, et al. (1997). The functional role of p-glycoprotein in the blood–brain barrier. *J Pharm Sci* 86:881–4.
- Baishya R, Nayak DK, Sinha S. (2016). Ursolic acid loaded PLGA nanoparticles: *in vitro* and *in vivo* evaluation to explore tumor targeting ability on B16F10 melanoma cell lines. *Pharm Res* 33: 2691–703.
- Banks WA. (2009). Characteristics of compounds that cross the blood–brain barrier. *BMC Neurol* 9:S3.
- Barth RF. (1998). Rat brain tumor models in experimental neuro-oncology: the 9L, C6, T9, F98, RG2 (D74), RT-2 and CNS-1 gliomas. *J Neurooncol* 36:91–102.
- Beaulieu E, Demeule M, Ghitescu L, et al. (1997). P-glycoprotein is strongly expressed in the luminal membranes of the endothelium of blood vessels in the brain. *Biochem J* 326:539–44.
- Chang HI, Yeh MK. (2012). Clinical development of liposome-based drugs: formulation, characterization, and therapeutic efficacy. *Int J Nanomedicine* 7:49–60.
- Chen Y, Dalwadi G, Benson HA. (2004). Drug delivery across the blood–brain barrier. *Curr Drug Deliv* 1:361–76.
- Costantino L, Boraschi D. (2012). Is there a clinical future for polymeric nanoparticles as brain–targeting drug delivery agents? *Drug Discov Today* 17:367–78.
- Dey G, Bharti R, Dhanarajan G, et al. (2015). Marine lipopeptide Iturin A inhibits Akt mediated GSK3 β and FoxO3a signaling and triggers apoptosis in breast cancer. *Sci Rep* 5:10316.
- Dey NS, Mukherjee B, Maji R, et al. (2016). Development of linker-conjugated nanosize lipid vesicles: a strategy for cell selective treatment in breast cancer. *Curr Cancer Drug Targets* 16:357–72.
- Dou J, Zhanga H, Liub X, et al. (2014). Preparation and evaluation *in vitro* and *in vivo* of docetaxel loaded mixed micelles for oral administration. *Colloids Surf B Biointerfaces* 114:20–7.
- Guo J, Gao X, Su L, et al. (2011). Aptamer-functionalized PEG-PLGA nanoparticles for enhanced anti-glioma drug delivery. *Biomaterials* 32:8010–20.
- Hao Y, Wang L, Zhao Y, et al. (2015). Targeted imaging and chemophototherapy of brain cancer by a multifunctional drug delivery system. *Macromol Biosci* 15:1571–85.
- Helvig S, Azmi IDM, Moghimi SM, et al. (2015). Recent advances in cryo-TEM imaging of soft lipid nanoparticles. *AIMS Biophysics* 2:116–30.
- Hou W, Watters JW, McLeod HL. (2004). Simple and rapid docetaxel assay in plasma by protein precipitation and high-performance liquid chromatography-tandem mass spectrometry. *J Chromatogr B Analyt Technol Biomed Life Sci* 804:263–7.
- Hu K, Cao S, Hu F, et al. (2012). Enhanced oral bioavailability of docetaxel by lecithin nanoparticles: preparation, *in vitro*, and *in vivo* evaluation. *Int J Nanomedicine* 7:3537–45.
- Irache JM, Esparza I, Gamazo C, et al. (2011). Nanomedicine: novel approaches in human and veterinary therapeutics. *Vet Parasitol* 180: 47–71.
- Jain KK. (2012). Nanobiotechnology-based strategies for crossing the blood–brain barrier. *Nanomedicine (Lond)* 7:1225–33.
- Kemper EM, Verheij M, Boogerd W, et al. (2004). Improved penetration of docetaxel into the brain by co-administration of inhibitors of P-glycoprotein. *Eur J Cancer* 40:1269–74.

- Kobayashi H, Watanabe R, Choyke PL. (2014). Improving conventional enhanced permeability and retention (EPR) effects; what is the appropriate target? *Theranostics* 4:81–9.
- Kuppens IE, van Maanen MJ, Rosing H, et al. (2005). Quantitative analysis of docetaxel in human plasma using liquid chromatography coupled with tandem mass spectrometry. *Biomed Chromatogr* 19: 355–61.
- Laouini A, Jaafar-Maalej C, Limayem-Blouza I, et al. (2012). Preparation, characterization and applications of liposomes: state of the art. *J Colloid Sci Biotechnol* 1:147–68.
- Liu Z, Liu D, Wang L, et al. (2011). Docetaxel-loaded pluronic P123 polymeric micelles: *in vitro* and *in vivo* evaluation. *Int J Mol Sci* 12: 1684–96.
- MacLachlan I. (2007). Liposomal formulations for nucleic acid delivery. In: Stanley T. Crooke, ed. *Antisense drug technology: principles: strategies, and applications*. Taylor and Francis Group, LLC: London, 2007; 253–54.
- Masserini M. (2013). Nanoparticles for brain drug delivery. *ISRN Biochem* 2013:1–18.
- Mukherjee B, Mondal L, Chakraborty S, et al. (2015). Size dependent variations of phospholipid based vesicular drug carriers in systemic drug activity. *Curr Pharm Biotechnol* 16:380–91.
- Nance E, Zhang C, Shih TY, et al. (2014). Brain-penetrating nanoparticles improve paclitaxel efficacy in malignant glioma following local administration. *ACS Nano* 8:10655–64.
- Pattnaik G, Sinha B, Mukherjee B, et al. (2012). Submicron-size biodegradable polymer-based didanosine particles for treating HIV at early stage: an *in vitro* study. *Microencapsulation* 29:666–76.
- Sanchez-Moreno P, Boulaiz H, Ortega-Vinuesa JL, et al. (2012). Novel drug delivery system based on docetaxel-loaded nanocapsules as a therapeutic strategy against breast cancer cells. *Int J Mol Sci* 13: 4906–19.
- Shilo M, Sharon A, Baranes K, et al (2015). The effect of nanoparticle size on the probability to cross the blood-brain barrier: an *in-vitro* endothelial cell model. *J Nanobiotechnology* 13:1–7.
- Sinha B, Mukherjee B, Pattnaik G. (2013). Poly-lactide-co-glycolide nanoparticles containing voriconazole for pulmonary delivery: *in vitro* and *in vivo* study. *Nanomedicine* 9:94–104.
- Sonali S, Singh RP, Singh N, et al. (2016a). Transferrin liposomes of docetaxel for brain targeted cancer applications: formulation and brain theranostics. *Drug Deliv* 23:1261–71.
- Sonali S, Agrawal P, Singh RP, et al. (2016c). Transferrin receptor targeted vitamin E TPGS micelles for brain cancer therapy: preparation, characterization and brain distribution in rats. *Drug Deliv* 23:1788–98.
- Sonali S, Singh RP, Sharma G, et al. (2016b). RGD-TPGS decorated theranostic liposomes for brain targeted delivery. *Colloids Surf B Biointerfaces* 147:129–41.
- Tan Q, Liu X, Fu X, et al. (2012). Current development in nanoformulations of docetaxel. *Expert Opin Drug Deliv* 9:975–90.
- Tije AJ, ten Verweij J, Loos WJ, et al. (2003). Pharmacological effects of formulation vehicles : implications for cancer chemotherapy. *Clin Pharmacokinet* 42:665–85.
- van Rooy I, Cakir-Tascioglu S, Hennink WE, et al. (2011). *In vivo* methods to study uptake of nanoparticles into the brain. *Pharm Res* 28:456–71.
- Venishetty VK, Komuravelli R, Kuncha M, et al. (2013). Increased brain uptake of docetaxel and ketoconazole loaded folate-grafted solid lipid nanoparticles. *Nanomedicine* 9:111–21.
- Venkatesan P, Puvvada N, Dash R, et al. (2011). The potential of celecoxib-loaded hydroxyapatite-chitosan nanocomposite for the treatment of colon cancer. *Biomaterials* 32:3794–806.
- Yang T, Cui FD, Choi MK, et al. (2007). Enhanced solubility and stability of PEGylated liposomal paclitaxel: *in vitro* and *in vivo* evaluation. *Int J Pharm* 338:317–26.
- Yousefi A, Esmaeili F, Rahimian S, et al. (2009). Preparation and *in vitro* evaluation of a pegylated nano-liposomal formulation containing docetaxel. *Sci Pharm* 77:453–64.
- Zhang L, Zhang N. (2013). How nanotechnology can enhance docetaxel therapy. *Int J Nanomedicine* 8:2927–41.

Supplementary material available online

Variation of Pharmacokinetic Profiles of Some Antidiabetic Drugs from Nanostructured Formulations Administered Through Pulmonary Route

Biswajit Mukherjee*, Paramita Paul, Ankan Choudhury, Sanchari Bhattacharya, Ruma Maji and Lopamudra Dutta

Department of Pharmaceutical Technology, Jadavpur University, Kolkata-700032, West Bengal, India

Abstract: Background: Diabetes is a chronic disease that occurs when the pancreas does not produce enough insulin, or when the body cannot effectively use the insulin it produces. WHO projects that diabetes death will be doubled between 2005 and 2030, where 347 million people worldwide had diabetes as per the report of 2013. The increase in the prevalence of diabetes is due to three influences - lifestyle, ethnicity, and age.

Methods: The present review summarizes the pharmacokinetic parameters and challenges in the field of nanoparticles and nanoliposomes of insulin and other antidiabetic drugs given through pulmonary route to treat diabetes effectively.

Results: Current challenges in diabetes management include optimizing the use of the already available therapies to ensure adequate glycemic condition, blood pressure, lipid control and to reduce complications. At present, several pieces of research have been focusing on new management options for diabetes. Among these options, the use of nanomedicine is becoming an eye catching and most promising one. Currently, nanoparticles and nanoliposomes are thrust areas of research to treat any deadly disease like diabetes. These drug delivery systems ultimately result in longer circulation half-lives, improved drug pharmacokinetics, and reduced side effects of therapeutically active substances that may be insulin and non-insulin.

Conclusions: Thus, the pulmonary route is the most promising alternative route of drug delivery since it is non-invasive and lungs have a large surface area, richly supplied by the capillary network, for absorption of drugs.

Keywords: Antidiabetics, diabetes, insulin, nanoliposomes, nanoparticles, pulmonary.



Biswajit Mukherjee

INTRODUCTION

Diabetes mellitus is caused by the insufficient production of insulin in pancreatic islet cells, leading to an increase in blood glucose level or hyperglycemia. Diabetes mellitus has been classified as insulin-dependent diabetes (type 1) and non-insulin-dependent diabetes (type 2) [1].

As on today, the subcutaneous route has widely been the primary mode for insulin delivery. Nevertheless, clinical studies showed that a significant percentage of patients had failed to attain this long-term glycemic control with this treatment [2, 3]. Few well-recognized reasons for this failure are the poor patient compliance due to the fear of injection and the other physiological reasons such as pain, discomfort *etc.* [4]. Several novel approaches like supersonic injectors, infusion pumps, sharp needles, pens *etc.* have been developed to increase the compatibility of diabetic patients. Oral delivery is the most convenient and acceptable route but the antidiabetic drugs specially insulin is degraded by intestinal enzymes and is not absorbed intact across the gastrointestinal mucosa [5].

The pulmonary delivery route for antidiabetic medication has shown a huge hope and expectation and is receiving a lot of scholastic interests. Few main reasons behind it are the non-invasive nature of the method, providing a large area for absorption (75-150 m²) [6-9], avoidance of hepatic first-pass metabolism, enhanced solubility of the drug in alveolar fluid and rapid onset of action due to the presence of a very thin (0.1-0.2 μm) monolayer epithelial diffusion path [1, 10] from the airspaces into the blood in the alveoli [10-12]. Additionally, the alveolar environment has limited degradative activity by enzymes in both the extra and intracellular compartments as compared to gastrointestinal tract

(GIT) [1, 9, 10, 13], thus making it an attractive path for delivering peptides and protein-based therapeutics including insulin [14].

Despite many advantages of the pulmonary route, a frequent and long-term inhalation is necessary to achieve satisfactory efficacy because the therapeutic effects of most of the protein drugs are short [15].

The objective of pharmaceutical formulations is the transformation of drug compounds into active products with the desired therapeutic effect. Accordingly, a delivery system that allows the long-term release of drugs after a single inhalation is required. In this context, nanoformulations developed for pulmonary delivery of drugs have numerous benefits. The alveolar delivery ensures efficient and uniform distribution of drug. The lung environment and alveolar surface enhance the solubility of the drug, more so than its intrinsic aqueous solubility. Moreover, alveolar retention mimics sustained release pattern and hence decreases dosing frequency. These features decrease the dose related side-effects, enhance cellular internalization of drugs and improve patient compliance [10, 16]. Thus, the pulmonary route of delivery of insulin or other peptides and protein brings special attention to the drug delivery researchers.

There are numerous applications for nanotechnology but the branch involving treatment, diagnosis, monitoring and control of physiological systems is broadly termed as "nanomedicine" by the National Institutes of Health (Bethesda, MD, USA) [17]. The two main types of nanomedicine products currently in clinical trials are: diagnostic agents and drug delivery devices [18]. Over the past few decades, research efforts have been focused on developing nanoformulations such as nanoparticles, liposomes, nanoemulsions, dendrimers *etc.* to ensure efficient delivery of drugs to the target tissues. Insulin nanoliposomes are one of the recent approaches in the controlled release aerosol preparation. Intratracheal delivery of insulin liposomes has shown to produce the desired insulin effect [19].

In this review article, we will mainly focus on the various approaches taken to deliver conventional antidiabetic drugs in the

*Address correspondence to this author at the Division of Pharmaceutics, Department of Pharmaceutical Technology, Jadavpur University, Kolkata-700032, India; Tel: +91-33-2457 2588; Fax: +91-33-2414 6677; E-mail: biswajit55@yahoo.com

nanoformulations via the pulmonary route and their advantages or limitations over the concurrent traditional therapies from the pharmacokinetic viewpoint.

Respiratory System: The respiratory area and the conducting airways are two important regions of the human respiratory system. The first region includes respiratory bronchioles, alveolar ducts, and alveolar sacs; and the later comprises of nasal cavity, associated sinuses, nasopharynx, oropharynx, larynx, trachea, bronchi, and bronchioles. A major portion (90%) of drug particles are removed in the upper airways as it has a higher filtering capacity. In the wall of the conducting airways, mucus containing the glycosylated protein called mucin forms a gel-like covering and has a ciliary action which washes drug molecules away. The main components of lungs are bronchi, alveoli, small air passage, lymph tissues and blood vessels of which bronchi are further divided into bronchioles and alveoli (approx 300 million). The maximum transepithelial (i.e., through the blood-gas barrier) drug transport uses the smaller airways and alveolar spaces which comprise more than 95% of lung's surface area and are directly connected with systemic circulation through dense capillary network [20, 21], making them ideal for non-invasive drug administration. The various advantages and disadvantages are listed in Table 1.

Significance of Delivery of Drug Nanocarriers by Pulmonary Route

Pulmonary route of drug delivery via nanocarriers offers well maintained systemic as well as local delivery of drugs in various ways such as using dry powder inhaler (DPI), nebulizers etc. It is also a convenient method for delivery of protein/peptide drug molecules encapsulated in those nanocarriers for treating respiratory as well as non-respiratory diseases [23]. Nanomedicine imparts more specificity to the treatments compared to the other modes of drug delivery, resulting in higher bioavailability and minimum dose related toxicity. The common nanocarriers used for this purpose are described below [22, 23]:

- **Liposome:** It is a phospholipid vesicle composed of one or more concentric phospholipid bilayer(s) encapsulating an aqueous core and is often helpful for achieving sustained systemic release of drugs and efficient encapsulation of both hydrophilic and hydrophobic drugs [22].
- **Nanoparticles:** Nanoparticles are colloidal particles where the drug molecules are either encapsulated or dissolved or entrapped or attached chemically to the main matrix. Nanoparticles provide some advantages which include sustained release of drugs, minimal risk of adverse effects, increased patient compliance etc. [22].

- **Polymeric Micelles:** Micelles in nanoscale range (10-400 nm) are promising carriers for various drug molecules for pulmonary administration. Drugs are incorporated in the core of these structures. Such formulations often result in a better stability, prolonged *in vivo* retention time and enhanced capability of drug action on the target organs [23].

Pulmonary Deposition of Inhaled Nanocarriers

The mass median aerodynamic diameter (MMAD) of nanoparticles, along with the breathing pattern determine the deposition of the particles in the lungs [9, 10, 12]. The aerodynamic diameter of a particle is the combined function of its shape, size and density of the particle given by the formula [24]:

$$d_{aer} = \sqrt{\frac{\rho}{\rho_o \chi}} d_g$$

Where, d_{aer} is the aerodynamic diameter, d_g is the geometric diameter, χ is the shape factor and $\frac{\rho}{\rho_o}$ is the specific gravity of the particle.

The particles deposit along the pulmonary pathway by inertial impact, interception, sedimentation, and diffusion [24, 25]. The alveolar deposition is a bimodal phenomenon in which two types of particles (in terms of their size ranges) are involved. One kind involves particles between 1000 nm and 5000 nm and another one involves particles below 100 nm [9]. Only the two aforementioned size ranges penetrate deeper into the central and distal tracts of the lungs [12, 26] through sedimentation and diffusion. The highest alveolar diffusion occurs for particles below 100 nm [7] as shown in Fig. (1). Though the size ranges are not always consensual and pulmonary delivery of nanoparticles for therapeutic purposes may supersede such limits. Depending on their size and shape, the particles usually deposit by following the fundamental mechanisms as mentioned below.

Impaction: Impaction is the physical phenomenon by which the particles of an aerosol tend to follow a trajectory movement due to inertia while travelling through the airways of the respiratory tract. This mainly happens in the first 10 bronchial generations, where the velocity of the air is high and the flow pattern is turbulent. The particles >5000 nm impact inertially in the nasopharyngeal region and are swallowed [10]. Particles above 100 nm and below 1000 nm are either deposited in the inert tracheobronchial region or are exhaled out [7, 16], especially if the drug is given through dry powder inhalers (DPI) or metered-dose inhalers (MDI).

Table 1. Advantages and limitations of pulmonary drug delivery

Advantages	Limitations	References
<ul style="list-style-type: none"> • Non-invasive in nature • Less toxic/ negligible side effects • Requires less and infrequent dosage • Quick onset of action • Avoids gastro intestinal tract related problems like gastric irritation, low bioavailability, protein binding, enzymatic degradation, etc. • Avoids first pass metabolism • High bioavailability • Minimum exposure to other vital organs. • Suitable for long-term treatments in asthma, diabetes etc. 	<ul style="list-style-type: none"> • Less stable <i>in vivo</i> • Difficulty in transportation through the alveolar cells for certain types of molecules. • Pulmonary irritation and toxicity. • Poor drug retention. 	[1, 9, 12, 22]

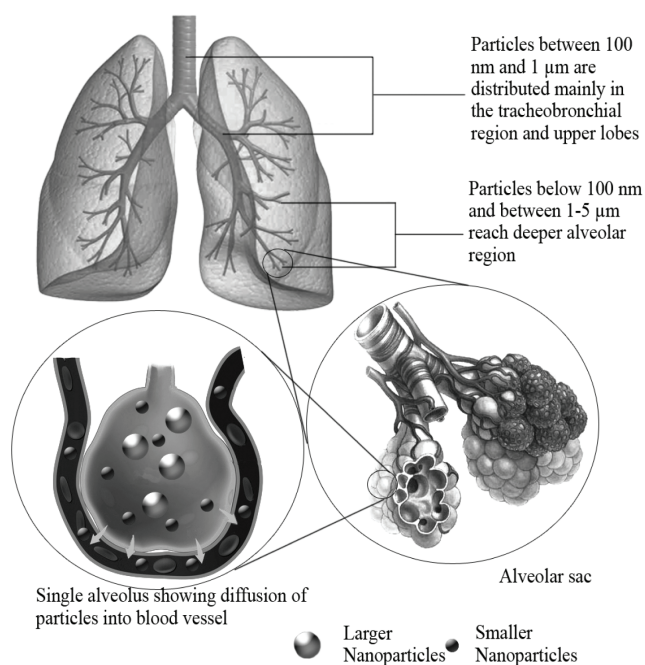


Fig. (1). Distribution and absorption of formulations in the respiratory system on the basis of the sizes of the inhaled particles.

Interception: Interception occurs mainly in the case of fibers. Due to their elongated shape, they are deposited on the wall of the airways as soon as they come in contact with it.

Sedimentation: Sedimentation is the physical phenomenon by which particles having sufficient mass are deposited due to gravity when they remain in the airways for a sufficient period of time. This occurs predominantly in the last 5 bronchial generations, where the air velocity is slow with a long residence time.

Diffusion: This occurs mainly for the particles below 100 nm where the clouds of nanoparticles remain suspended in the alveolar spaces in a fluidic motion. This phenomenon is guided by the concentration and/or pressure gradient, which facilitates the flow of the particles into the alveolar sacs for further absorption into the capillary network.

Besides, size and other factors such as composition, surface charges etc. are also crucial. Polymeric nanoparticles of 400 nm diameter [27] and lipid nanoparticles of 300 nm diameter [28] produced alveolar deposition in the magnitude of 75% and 45% respectively of the initial dose delivered. Nanoparticle aggregates with an aerodynamic diameter between 1 and 5 μm may enhance alveolar deposition provided they segregate on contact with the alveolar fluid [29].

Pharmacokinetics of Inhaled Nanocarriers Containing Antidiabetic Drugs

Hypoglycemic agents, be it insulin or other oral anti-diabetic agents, act primarily when they reach the systemic circulation. They mainly sensitize various receptors on the cell membrane either by acting as secretagogues for insulin or by improving insulin resistance [30, 31]. Hence rapid absorption of an antidiabetic drug through alveolar surface and subsequent rapid onset of action with a longer residence time in the systemic circulation ensure efficient hypoglycemic action of that agent from a nanoformulation delivered through pulmonary route. However, residence time of a formulation in blood depends on the combined effect of bypassing the hepatic portal system and sustained drug-releasing capability of a nanocarrier [32]. Drug permeability through alveolar epithelium is

found to be predominantly more than that of other noninvasive routes. As an example, the bioavailability of insulin administered via pulmonary route has been reported to be 20-100 times greater than that of other noninvasive routes. The reason may be the higher permeability of the drug through the alveolar epithelium and less volume of local fluid, resulting in high concentrations of drug near the bloodstream [23, 33]. Out of the three main types of alveolar cells, other than the Type I and Type II pneumocytes, macrophages are mainly responsible for the immunogenic phagocytotic response to foreign substances such as drug nanocarriers [34]. Particles between 300-500 nm are more susceptible to phagocytosis [35], but small particles (<260 nm) [7] are capable of escaping phagocytosis [10, 36]. Particles with size around 100 nm are widely considered as desirable for the purpose of delivering drugs [11, 37]. Though anything below 1000 nm is considered as the nanoparticle, but all submicron sizes are not considered for pulmonary delivery due to safety concerns [11]. Inconsistent or uncontrolled dosing of inhalable nanoparticles induces inflammatory responses, epithelial damage in lungs, and extrapulmonary effects, such as oxidative stress or increased blood clotting, as well [9, 36, 38, 39]. But these studies mostly relied on inorganic nanoparticles of very high doses. Generally, these threats do not correspond entirely to the homogenized and metered dosage of polymeric or lipid nanoparticles used in the therapeutic purpose, with care taken during their administration [40].

Alveolar Absorption

Drug absorption through alveolar epithelium is very high due to its large surface area and all lipophilic and non-ionised molecules are readily permeated through it into the circulation [12]. The alveolar epithelium is composed of specialized cells with apparent structural polarity and the cells are permeable to water, gases and lipophilic molecules [9]. Hydrophilic molecules have a mean half-life value of about an hour whereas the similar size lipophilic molecules have half-lives less than a minute [41] in the alveoli. Many molecules undergo parallel transportation via the transcellular and paracellular pathways [42], with tight junctions between Type I pneumocytes allowing diffusion of molecules only below 0.6 nm diameter. Besides, macromolecules above 40 kDa are absorbed very slowly over several hours but smaller peptides such as insulin (5.8 kDa) reach the circulation within minutes [43]. This inverse relation is more strongly demonstrated for proteins and peptides as they are primarily absorbed through the paracellular pathways where size/molecular weight acts as a major barrier [9]. Still there are many instances where proteins and peptides of higher molecular weight crossed transcellular barrier through receptor-mediated transcytosis and non-specific pinocytosis [12]. Peptides and similar molecules can be absorbed by active transport using a high-affinity peptide transporter (PEPT-2) present in alveolar Type II cells and in capillary endothelium [8, 44]. This possibility is further enforced by the presence of the protein Caveolin in alveolar Type I cells and endothelial cells of the lung. Clathrin (another adjuvant protein) in alveolar Type I and II pneumocytes also attribute to active transportation and absorption of protein through the alveolar pinocytosis [45]. Transcellular passive diffusion occurs only for the lipophilic molecules [4]. Since most of the antidiabetic drugs have low lipophilicity, they are absorbed mainly through the paracellular pathway into the system [4]. However, drug encapsulation within a hydrophobic scaffold and a large area for absorption in the alveoli compensate for this problem [7, 16, 46].

Clearance from the Lungs

The mucociliary escalator mechanism causes a major obstacle for nanoparticles deposited in the airways against penetration into alveolar region [47] by decreasing pulmonary retention and enhancing elimination of nanoparticles [12]. The cells secreting mucous exist in the region from the trachea to the terminal bronchiole. This

mucous creates a blockade for many particles to reach the alveolar site of action [48]. Drug particles held in this mucus layer are removed by the mucociliary clearance mechanism where the constantly beating cilia push the entrapped drug back towards the pharynx [49]. The alveolar Type II cells synthesize lung surfactants that are primarily made of phospholipids (mainly dipalmitoylphosphatidylcholine), cholesterol and surfactant-associated proteins [50]. Insoluble or poorly soluble particles in the mucus and the surfactant are not readily absorbed [9]. Since the nanocarrier scaffolds are mostly hydrophobic, they undergo dissolution in both intracellular and extracellular fluids including mucus.

Hydrophobic nanocarriers allow hydrophilic hypoglycemic molecules to be absorbed by passive diffusion across the alveolar epithelium [7]. However, the level and duration of retention and elimination of such nanoparticles vary with the nature of the nanoparticles [9] and physiological condition of lungs [12]. For instance, the thickness of the mucus layer increases from 2 to 30 μm in healthy lungs whereas even more than 250 μm in cases of cystic fibrosis and other obstructive airway diseases [51]. The nuisance of mucociliary and alveolar clearance can be controlled by keeping the particle diameter around 100 nm as seen by an experiment by Möller *et al.* (2008) [38] using $^{99\text{m}}\text{Tc}$ labeled carbon nanoparticles. In this experiment the mucociliary clearance resulted in elimination of just 25% of the deposited nanoparticles after 1 day, while clearance from the periphery of lungs is only about 3% of the deposited nanoparticles as explored by a radioactive probe. Pharmacokinetic (PK) data gathered after administering Cyclosporine-A loaded liposome in mice showed that the liposome was retained 16.9 times longer than the free Cyclosporine-A in healthy lungs and 7.5 times longer than the lungs with inflamed epithelial lining and increased mucociliary build-up, upon the administration of the same formulation [52].

Although phagocytosis is the predominant mechanism in the clearance of solid particles from pulmonary passages, the percentage of nanoparticles present in macrophages after inhalation has been found to decrease [9]. This may be due to a certain inefficiency of macrophages in recognition and elimination of particles below a certain size [33, 53]. As mentioned earlier, particles below 260 nm undergo less phagocytosis [7, 54, 55] and below 70 nm are not recognized by macrophages [7]. This may be attributed to the absence or reduced promotion of the chemotactic signal from the smaller nanoparticles [36]. This further ensures the important role played by endocytosis in epithelial translocation of nanoparticles at the cellular level. There are several existing transcellular endocytotic pathways such as pinocytosis, adsorptive endocytosis (nonspecific binding to receptors) and receptor-mediated endocytosis exhibited by both the types of alveolar pneumocytes [45, 56]. The abundance of Caveolin 1 protein in alveolar type I pneumocytes and in the pulmonary capillary endothelium may establish the possibility of Caveolin-mediated endocytosis as an important pathway in epithelial translocation of nanoparticles [51, 57]. The hypothesis has been further supported by an experiment by Brandenberger *et al.* (2010) where inhibition of Caveolin and Clathrin-mediated endocytosis by methyl- β -cyclodextrin resulted in a significant reduction in uptake of gold nanoparticles by human alveolar epithelial cells and inhibition was more attenuated when the nanoparticles were coated with polyethylene glycol (PEG) [58]. These factors are often helpful in delivering peptides and peptidomimetic molecules such as insulin [59], exendin-4 [15] etc. in the form of nanoparticles for inducing hypoglycemia through pulmonary routes.

In vivo Fate of Insulin and non-Insulin Nanoformulations: A Pharmacokinetic View

Once the nanoparticles cross the physiological barrier and enter the systemic circulation, nature of the drug molecules governs their ultimate fate. Antidiabetic formulations can be divided broadly into

two classes- insulin and non-insulin agents (oral hypoglycemic agents) [60].

Insulin

Insulin is probably the most studied antidiabetic drug for developing nanoformulations to deliver through pulmonary routes [9]. Insulin is generally used for patients suffering from diabetes mellitus type 1, the subtype of the disease which is caused by the lack of insulin secretions by β cells of islets of Langerhans in the pancreas. Insulin is a dipeptide molecule where the two polypeptidic chains of 21 and 30 amino acids long respectively are joined by two disulfide linkages [1]. Insulin has gathered so much interest solely for being a peptide but unfit for oral administration due to its degradation by the proteolytic/peptidolytic enzymes (pepsin in stomach; trypsin, chymotrypsin, and carboxypeptidases in the duodenum) of the gastro-intestinal tract [61, 62]. Parenteral administration, in particular subcutaneous route, is accepted widely and unanimously for insulin delivery [1]. But there are problems such as patient non-compliance due to painful injections and episodes of acute hypoglycemia due to inconsistent and careless dosing since the delivery route is irreversible [63, 64]. Transdermal route acts as a popular alternative as a non-invasive parenteral delivery route but the peptidic (ionized) nature, molecular weight and size of insulin make it a poor candidate for transdermal absorption and hence, even though it reduces the pain problem, it produces incomplete and inconvenient results [1]. This led to further investigation with other routes among which pulmonary route has become a very prominent choice [14] and has been in use since 1925 [9, 14, 65]. This even culminated in a pulmonary antidiabetic product called Exubera® which came to the market in 2006 after the approval of the United States Food and Drug Administration and European Medical Agency, but was withdrawn in 2007. The product was developed by Nektar/Pfizer as a dry powder formulation [1, 9, 14]. Another aerosol-based product for the delivery of insulin was developed jointly by Aradigm and Novo Nordisk but was discontinued from 2008 while it was in Phase III trials [9].

Many experimental formulations have been developed for pulmonary delivery of insulin through nanocarriers. The main goal for such delivery is to allow the nano-encapsulated insulin molecules to enter the systemic circulation through a non-invasive route and release insulin through a gradual biodegradation of the polymeric scaffold [10]. Insulin molecules in the blood bind with the insulin receptors present on the cell membrane and initiate a phosphorylation reaction on the Insulin Receptor Substrate 1 (IRS1) [66]. Phosphorylated IRS1 then initiates the activation of phosphoinositol-3-kinase (PI3K) which in turn converts phosphatidylinositol 4,5-bisphosphate (PIP2) into phosphatidylinositol 3,4,5-triphosphate (PIP3). This reaction activates the protein kinase B which functions bimodally [67] by upregulating glycogen synthesis through inactivation of glycogen synthase kinase, and results in migration of glucose transporter-4 (GLUT4) towards the plasma membrane [68]. This migration of GLUT4 causes increased uptake of free glucose from the blood into the cells. Glucose then either undergoes glycolysis or gets stored as glycogen in the cells [68]. But these physiological reactions require a steady blood insulin content of 8–11 $\mu\text{IU/mL}$ (57–79 pmol/L) [69]. The product Exubera® had to be withdrawn [9] because the Pfizer found it to be commercially non-feasible even though it produced patient comfort and convenience and showed similar postprandial glycemic control and similar values of glycated haemoglobin (HbA1c) to that of subcutaneous insulin injections [70]. The main reason is that it was a short-term insulin formulation and failed to maintain the required physiological insulin level for a longer duration, which again necessitates further injection of long-term insulin [71]. Strategies were taken to prolong the duration of action by modification of the structure of the insulin molecules by attaching biodegradable molecules such as PEG to it (PEGylation). PEGylated insulin were delivered via pulmonary routes in rats and dogs and it was seen that PEGylated insulin were

systemically absorbed from the lungs [12, 72]. The extent of absorption was decreased following PEGylation on multi-protein sites as well as the use of large PEGs (5–12 kDa). In the circulation, PEGylated proteins maintain a sustained plasma level of insulin as they would do when injected subcutaneously at regular intervals. PEGylation also protects peptides from local proteolysis in the lungs and thereby increases the systemic absorption of the intact molecule from the alveoli [48, 73, 74].

As mentioned before, nanocarriers address the problem of degradation of proteins or peptides by nano-encapsulation which enables the drug to remain in the circulation for a longer time and drug release remains sustained for such longer duration. They also protect the encapsulated material from phagocytosis and enzymatic degradation. Bi *et al.* (2008) encapsulated insulin into liposomal carriers to increase drug retention time and control the drug release in the lungs [75]. Nanoliposomes with an average diameter of 295 nm and an encapsulation efficiency of 43% were administered through intratracheal instillation in diabetic rats, causing a decrease in systemic levels of glucose for 12 h after its administration [75]. It resulted in successful hypoglycemic effect with low blood glucose level for a prolonged period and a relative pharmacological bioavailability as high as 38.38% in the group of 8 IU/kg dosage. These data were compared against the results shown by the traditional subcutaneous insulin injection and naked insulin solution given through pulmonary route. Another study by Chono *et al.* (2009) showed that liposome of dipalmitoylphosphatidylcholine containing insulin reduced serum glucose to a greater extent than insulin solution when both were administered via intratracheal routes to the experimental rats [76]. This study also showed the relationship between the size of liposomes and their macrophagic uptake. Liposomes of mean diameter 100 nm showed elevated serum insulin level and those of 1000 nm size were preferentially retained by alveolar macrophages. A parallel *in vitro* study in the same experiment using Calu-3 cell cultures showed that liposomal encapsulation enhanced absorption of insulin through the opening of the tight junctions of alveolar cells. Insulin encapsulated lecithin nanoparticles of an average diameter 300 nm not only produced a deposition of 45% of the delivered dose in the alveolar level but also retained the primary, secondary and tertiary polypeptide structures of the insulin molecule [28]. Liu *et al.* (1993) studied the effects of oligomerization and liposomal entrapment on pulmonary insulin. Pulmonary absorption was investigated in rats using an intratracheal instillation method. Their study confirmed that the intratracheal administration of insulin liposomes led to the facilitated pulmonary uptake of insulin and enhanced the hypoglycemic effect [77]. Liu *et al.* (2008) also produced solid lipid nanoparticles of phosphatidylcholine having an average diameter of 115 nm, which showed a prolonged hypoglycemic effect in diabetic mice by lowering the plasma glucose level to 39% within 8 h and elevating insulin level to 170 μ IU/ml within 4 h of pulmonary administration of the nanoparticles containing weight equivalent in insulin of about 20 IU/kg of formulation [78]. The nanoparticles continued the hypoglycemic effect up to 12 h and the basal glucose level returned only after 24 h. The formulation achieved a mean residence time (MRT) approximately 7.7 h.

Poly(lactide-co-glycolic acid) (PLGA) nanosphere of 400 nm loaded with insulin was administered to guinea pig through nebulization for 20 minutes and recorded a significant alveolar deposition (75%) and a considerable reduction in blood glucose level with a prolonged effect over 48 h as compared to aqueous native insulin solution [27]. In a follow-up study, the same research group later modified the PLGA nanoparticles with chitosan but this time with a different peptide calcitonin (a calcitonin analogue) so as to utilize the properties of the coating to adhere the particles for a longer period in the mucociliary environment of the lungs in guinea pigs [79]. This strategy was used by Lee *et al.* (2013) for antidiabetic action in delivering a palmitic acid derivative of exendin-4 (ex-

enatide), a glucagon-like peptide (GLP) receptor agonist which decreased the release of plasma glucagon [15]. The retention of the particles in lungs over 72 h with a sustained release prolonged the hypoglycemic action for over 4 days in mice. Huang *et al.* (2009) developed nanoparticles of insulin using low molecular weight chitosan, of an average diameter of approximately 400 nm and an encapsulation efficiency of 95.5% which gave a characteristic release profile of insulin beginning with a burst effect followed by prolonged release for 24 h. The nanoparticles demonstrated a hypoglycemic effect similar to subcutaneous insulin injection but prolonged in time in diabetic mice [80]. The biphasic release of insulin, also seen by Kawashima *et al.* (1999), can mimic the actions of available insulin mixtures of short and long duration of action [27]. Yamamoto *et al.* (2007) produced PLGA nanoparticles which showed an *in vitro* and *in vivo* alveolar deposition of approximately 45% (w/w) of emitted dose and a more prolonged pharmacological effect (over 12 h) compared to the solutions of insulin administered via pulmonary and *i.v.* routes [81]. In another study, chitosan nanoparticles (average diameter 380–450 nm) were produced with [46] and without lipid coating [82] obtained by ionic gelation with triphosphate ion. The resultant nanoparticles had encapsulation efficiency between 65 and 81%. A rapid release of insulin from nanoparticles without lipid coating was observed while the formulations with the lipid coating showed a prolonged release of insulin [46, 82]. Poly(*n*-butyl cyanoacrylate) (PBCA)/dextran nanoparticles with an average diameter of 255 nm showed that insulin release (*in vitro*) had a biphasic characteristic of an initial burst effect followed by prolonged release of insulin, while *in vivo* studies showed a more prolonged therapeutic effect when compared with insulin solution administered via lungs [83]. Further, there was insulin bioavailability of 57% from the nanoparticles as compared to the subcutaneous injection of insulin solution [83]. The minimum blood glucose concentration reached 46.9%, 30.4% and 13.6% respectively of the initial level after pulmonary delivery of 5, 10 and 20 IU Kg⁻¹ insulin-loaded nanoparticles to normal rats. The time to reach the minimum blood glucose level (T_{min}) was 4, 4 and 8 h for three doses, respectively.

Non-Insulin

The non-insulin antidiabetics include the classical oral antidiabetics and the peptide analogues which act primarily in diabetes mellitus type 2 where the insulin secretion is normal, but the cells become desensitized to insulin. The predominant classes of oral antidiabetics include biguanides, sulfonylureas, thiazolidinediones and α -glucosidase inhibitors [84]. The peptide analogues include incretin mimetic insulin secretagogues such as glucagon-like peptide-1 (GLP-1) and gastric inhibitory peptide analogues [85]. These molecules have warranted far fewer attentions than insulin in terms of pulmonary delivery, but there have been some noteworthy works involving such drugs. These drugs act mainly via subsidiary pathways that help insulin secretion or that manipulate glucose metabolism in the body through enzymatic inhibition/upregulation. Since all these drugs have poor lipophilicity, encapsulation in a nanolipoidal or polymeric scaffold enhances their absorption through the highly lipophilic cellular membranes [4]. Pulmonary route can be a highly preferable route as it provides a very large surface for the absorption of drug, something that may compensate for the poor penetration factor as it is seen in the highly folded epithelium of the intestine where larger surface area of the cell overcomes the difference in partitioning between the cell membrane and the extracellular fluid [4].

Sulfonylureas act as insulin secretagogues by inhibiting the K⁺ ATP channel in the β cells of the pancreas, thereby stopping the K⁺ efflux and leading to subsequent depolarization of the cells which initiate a Ca²⁺ influx and a protein activation cascade. This ends in exocytosis of insulin-loaded vesicles and hence increases plasma insulin level [86]. Non-sulfonyl urea insulin secretagogues include

meglitinide and repaglinide, which follow the same mechanism but differ in their binding site with the sulfonylureas [87]. They are fast, but short-acting insulinotropic drugs which have been employed in chitosan-alginate nanocomplexes for inhalation purpose [88]. In this study they used repaglinide as the hypoglycemic agent and prepared nanocomplexes of sizes in the 300-400 nm range and utilized the mucoadhesive properties of chitosan-alginate gel to achieve a gradual sustained hypoglycemic effect which lowered the blood glucose level to 47% within 8 h and up to 38% in 24 h post-treatment [88].

Biguanides, such as metformin and phenformin, and thiazolidinediones, such as pioglitazone and rosiglitazone [86], act by reducing insulin resistance in diabetes mellitus type 2 (DMT2). The biguanides are usually the first-line drugs given in DMT2 though their mechanisms are not fully understood. Metformin decreases hyperglycemia primarily by suppressing hepatic gluconeogenesis and may decrease insulin resistance by activation of AMP-activated protein kinase (AMPK) [89]. The thiazolidinediones are dependent on the presence of insulin for activity, but they themselves do not affect insulin secretion. The thiazolidinediones are highly selective and potent agonist for the peroxisome proliferator activated receptor-gamma (PPAR- γ). Activation of PPAR- γ regulates the transcription of insulin-responsive genes involved in the control production, transport, and utilization of glucose through increased production of GLUT 1 and GLUT 4 receptors [84].

Peptide analogues include GLP-1 and GLP-1 agonist such as exenatide (Ex4), which bind with the GLP receptors to inhibit the release of glucagon and increase the release of insulin, thus lowering blood glucose level. They have been extensively investigated through strategies such as PEGylation and nano-encapsulation for administration via pulmonary route. Both the strategies resulted in nanoscale formulations capable of protecting them from the proteolytic enzymes of the alveolar epithelium and mucociliary passage [12,48]. PEGylated versions of GLP-1 were studied for pulmonary delivery in diabetic rats where GLP-1 was conjugated with PEG (molecular weight 1, 2, or 5 kDa) [90]. The PEG-2000 conjugate had the greatest hypoglycemic response as the PEGylation of GLP-1 prolonged the half-life of GLP-1 and decreased renal clearance rate [90]. Although the study showed that the half-life directly depended on the length of the PEG chain, but the length was inversely related to the rate of absorption and biological activity of the peptide [90]. This may be due to larger PEG chains which might effectively prevent proteolysis of the peptide molecules and hence increased their bioavailability. Another study investigated Ex4 in type 2 diabetic mice [91] where Ex4 was conjugated with PEG (molecular weight 1, 2, or 5 kDa) showing prolonged half-life and hypoglycemia. Ex4 was also studied in nanoparticle formulation in its palmitic acid derivative form. The mucoadhesive nature of chitosan-coated PLGA nanoparticles ensured that the drug was released over three days *in vitro* and produced hypoglycemia over four days in mice. The above-mentioned findings may encourage formulation scientists to explore new strategies to receive more success in the field in near future.

CONCLUSION

The review highlights that the pulmonary drug delivery is a highly prospective field of drug administration in the near future. Pulmonary drug delivery also offers a huge opportunity for systemic administration of antidiabetic drug molecules such as insulin or non-insulin agents. The large surface area, good vascularization, solute exchange capacity and ultra-thin membranes of alveolar epithelia are unique features that facilitate pulmonary drug delivery. Further large lung surface area and thin alveolar epithelium permit rapid drug absorption and the first-pass metabolism can be avoided, too.

Pulmonary drug delivery depends upon several factors including particle size, shape, density, charge and pH of delivery entity,

velocity of entry, quality of aerosol deposition, character of alveoli, binding characteristics of aerosol on the alveolar surface, quality of alveolar capillary bed and its subsequent vascular tree. Those parameters ultimately reflect the pharmacokinetic modulation of the administered therapeutic agent using the pulmonary route. However, the defense mechanism of lungs against foreign particle should not be ignored. The defense can be by either mucosal clearance or degradation by macrophages and enzymes. The lung can also develop immunological reactions against unwanted entities such as viruses. As per the safety concern, depending on the size of the nanocarriers it is possible to escape the phagocytosis by delivering the nanoparticles generally of small sizes (i.e. <260 nm) to the lungs. However, particles > 5000 nm to 3 μ m are generally phagocytosed by macrophages. The large particles (i.e. >5000 nm) are not suitable for the pulmonary delivery as they tend to deposit in the nasopharyngeal region and are swallowed. The particles above 100 nm and below 1000 nm also have a tendency to get deposited in the tracheobronchial region or exhaled. Again, particles having a size below 100 nm reach the lungs efficiently and show the highest alveolar diffusion. From the different experimental studies it was observed that antidiabetic drug such as insulin can be easily encapsulated to the nanostructured systems for pulmonary delivery which gave results similar or sometimes better than the conventional delivery routes such as subcutaneous injection. Evidence shows that this strategy improves the therapeutic efficacy and reduces the systemic toxicity of the drug by improving its pharmacokinetic profile.

It is expected that the continued research interest in the pulmonary route of administration will lead to more breakthroughs in several areas of formulation and device designs for pulmonary drug delivery, resulting in an improved patients' acceptance and compliance.

CONFLICT OF INTEREST

The authors confirm that this article content has no conflicts of interest.

ACKNOWLEDGEMENTS

All the authors contributed in writing of the manuscript. All the authors jointly developed the structure and arguments for the paper. Biswajit Mukherjee made critical revisions and approved final version. All authors reviewed and approved the final manuscript.

REFERENCES

- [1] Elçioglu, H.K.; Sezer A.D. Nanoparticle Insulin Drug Delivery — Applications and New Aspects. *Application of Nanotechnology in Drug Delivery*, INTECH publishing: Croatia, **2014**.
- [2] Petitti, D.B.; Klingensmith, G.J.; Bell, R.A.; Andrews, J.S.; Dabelea, D.; Imperatore, G.; Marcovina, S.; Pihoker, C.; Standiford, D.; Waitzfelder, B.; Mayer-Davis, E. Glycemic control in youth with diabetes: the SEARCH for diabetes in Youth Study. *J. Pediatr.*, **2009**, *155*, 668-672.
- [3] Mortensen, H.B.; Robertson, K.J.; Aanstoot, H.J.; Danne, T.; Holl, R.W.; Hougaard, P.; Atchison, J.A.; Chiarelli, F.; Daneman, D.; Dinesen, B.; Dorchy, H.; Garandeau, P.; Greene, S.; Hoey, H.; Kaprio, E.A.; Kocova, M.; Martul, P.; Matsuura, N.; Schoenle, E.J.; Søvik, O.; Swift, P.G.; Tsou, R.M.; Vanelli, M.; Aman, J. Insulin management and metabolic control of type 1 diabetes mellitus in childhood and adolescence in 18 countries. Hvidore Study Group on Childhood Diabetes. *Diabet. Med.*, **1998**, *15*, 752-759.
- [4] Gundogdu, E.; Yurdasiper, A. Drug transport mechanism of oral antidiabetic nanomedicines. *Int. J. Endocrinol. Metab.*, **2014**, *12*, e8984.
- [5] Pandey, S.; Choudhary, A.; Patel, B.; Mahalaxmi, R.; Devmurari, V.; Jivani, N.P. Pulmonary delivery as a route for insulin. *Int. J. Pharm. Tech. Res.*, **2009**, *1*, 1190-1197.
- [6] Iazzetti, G.; Rigutti, E. *Atlas of Anatomy*. Taj Books: Surrey, UK, **2005**.
- [7] Yang, W.; Peters, J.; Williams, R.R. Inhaled nanoparticles - a current review. *Int. J. Pharm.*, **2008**, *356*, 239-247.

- [8] Groneberg, D.; Fischer, A.; Chung, K.; Daniel, H. Molecular mechanisms of pulmonary peptidomimetic drug and peptide transport. *Am. J. Respir. Cell Mol. Biol.*, **2004**, *30*, 251-260.
- [9] Andrade, F.; Videira, M.; Ferreira, D.; Sarmiento, B. Nanocarriers for Pulmonary Administration of Peptides and Therapeutic Proteins. *Nanomedicine*, **2011**, *6*, 123-141.
- [10] Sung, J.C.; Pulliam, B.L.; Edwards, D.A. Nanoparticles for drug delivery to the lungs. *Trends Biotechnol.*, **2007**, *25*, 563-570.
- [11] Mansour, H.M.; Rhee, Y.; Wu, X. Nanomedicine in pulmonary delivery. *Int. J. Nanomedicine*, **2009**, *4*, 299-319.
- [12] Loira-Pastoriza, C.; Todoroff, J.; Vanbever, R. Delivery strategies for sustained drug release in the lungs. *Adv. Drug Deliv. Rev.*, **2014**, *75*, 81-91.
- [13] Cryan, S.; Sivadas, N.; GarciaContreras, L. *In vivo* animal models for drug delivery across the lung mucosal barrier. *Adv. Drug Deliv. Rev.*, **2007**, *59*, 1133-1151.
- [14] Henkin, R.I. Inhaled insulin-Intrapulmonary, intranasal and other routes of administration: Mechanisms of action. *Nutrition*, **2010**, *26*, 33-39.
- [15] Lee, C.; Choi, J.S.; Kim, I.; Oh, K.T.; Lee, E.S.; Park, E.S.; Lee, K.C.; Youn, Y.S. Long-acting inhalable chitosan-coated poly(lactic-co-glycolic acid) nanoparticles containing a hydrophobically modified exendin-4 for treating type 2 diabetes. *Int. J. Nanomedicine*, **2013**, *8*, 2975-2983.
- [16] Bailey, M.M.; Berkland, C.J. Nanoparticle formulations in pulmonary drug delivery. *Med. Res. Rev.*, **2009**, *29*, 196-212.
- [17] Park, J.H.; Lee, S.; Kim, J.H.; Park, K.; Kim, K.; Kwon, I.C. Polymeric nanomedicine for cancer therapy. *Prog. Polym. Sci.*, **2008**, *33*, 113-137.
- [18] Resnik, D.B.; Tinkle, S.S. Ethical issues in clinical trials involving nanomedicine. *Contemp. Clin. Trials*, **2007**, *28*, 433-441.
- [19] Huang, Y.Y.; Wang, C.H. Pulmonary delivery of insulin by liposomal carriers. *J. Control. Release*, **2006**, *113*, 9-14.
- [20] Patil, J.S.; Sarasija, S. Pulmonary drug delivery strategies: A concise, systematic review, *Lung India*, **2012**, *29*, 44-49.
- [21] Paranjpe, M.; Müller-Goymann, C.C. Nanoparticle-mediated pulmonary drug delivery: a review, *Int. J. Mol. Sci.*, **2014**, *15*, 5852-5873.
- [22] Chaturvedi, N.P.; Solanki, H. Pulmonary drug delivery system: review *Int. J. App. Pharm.*, **2013**, *5*, 7-10.
- [23] Smola, M.; Vandamme, T.; Sokolowski, A. Nanocarriers as pulmonary drug delivery systems to treat and to diagnose respiratory and non respiratory diseases. *Int. J. Nanomedicine*, **2008**, *3*, 1-19.
- [24] Hinds, W.C. Ed. *Aerosol technology: properties, behavior, and measurement of airborne particles*, 2nd ed, Wiley: New York, **1999**.
- [25] Crowder, T.; Rosati, J.; Schroeter, J.; Hickey, A.; Martonen, T. Fundamental effects of particle morphology on lung delivery: predictions of Stokes' law and the particular relevance to dry powder inhaler formulation and development. *Pharm. Res.*, **2002**, *19*, 239-245.
- [26] Usmani, O.S.; Biddiscombe, M.F.; Barnes, P.J. Regional lung deposition and bronchodilator response as a function of beta2-agonist particle size. *Am. J. Respir. Crit. Care Med.*, **2005**, *172*, 1497-1504.
- [27] Kawashima, Y.; Yamamoto, H.; Takeuchi, H.; Fujioka, S.; Hino, T. Pulmonary delivery of insulin with nebulized DL-lactide/glycolide copolymer (PLGA) nanospheres to prolong hypoglycemic effect. *J. Control. Release*, **1999**, *62*, 279-287.
- [28] Nyambura, B.; Kellaway, I.; Taylor, K. Insulin nanoparticles: stability and aerosolization from pressurized metered dose inhalers. *Int. J. Pharm.*, **2009**, *375*, 114-122.
- [29] Grenha, A.; CarriónRecio, D.; TeijeiroOsorio, D.; Seijo, B.; RemuñánLópez, C. Eds. *Nano and Microparticulate Carriers for Pulmonary Drug Delivery*. American Scientific Publishers: Valencia, CA, USA, **2008**.
- [30] Rodbard, H.W.; Jellinger, P.S.; Davidson, J.A. Statement by an American association of clinical endocrinologists/American college of endocrinology consensus panel on type 2 diabetes mellitus: an algorithm for glycemic control. *Endocr. Pract.*, **2009**, *15*, 540-559.
- [31] Ramesan, R.M.; Sharma, C.P. Challenges and advances in nanoparticles based oral insulin delivery. *Expert Rev. Med. Devices*, **2009**, *6*, 665-676.
- [32] Mosser, D.M.; Edwards, J.P. Exploring the full spectrum of macrophage activation. *Nat. Rev. Immunol.*, **2008**, *8*, 958-69.
- [33] Tomoda, K.; Ohkoshi, T.; Nakajima, T.; Makino, K. Preparation and properties of inhalable nanocomposite particles: effects of the size, weight ratio of the primary nanoparticles in nanocomposite particles and temperature at a spray dryer inlet upon properties of nanocomposite particles. *Colloids Surf. B Biointerfaces*, **2008**, *64*, 70-76.
- [34] Lambrecht, B. N. Alveolar Macrophage in the Driver's Seat. *Immunity*, **2006**, *24*, 366-368.
- [35] Chono, S.; Tanino, T.; Seki, T.; Morimoto, K. Influence of particle size on drug delivery to rat alveolar macrophages following pulmonary administration of ciprofloxacin incorporated into liposomes. *J. Drug Target.*, **2006**, *14*, 557-566.
- [36] Oberdörster, G.; Oberdörster, E.; Oberdörster, J. Nanotoxicology: an emerging discipline evolving from studies of ultrafine particles. *Environ. Health Perspect.*, **2005**, *113*, 823-839.
- [37] Shekunov, B. Nanoparticle technology for drug delivery - From nanoparticles to cutting-edge delivery strategies - Part I. *I drugs.*, **2005**, *8*, 399-401.
- [38] Möller, W.; Felten, K.; Sommerer, K. Deposition, retention, and translocation of ultrafine particles from the central airways and lung periphery. *Am. J. Respir. Crit. Care Med.*, **2008**, *177*, 426-432.
- [39] Renwick, L.; Brown, D.; Clouter, A.; Donaldson, K. Increased inflammation and altered macrophage chemotactic responses caused by two ultrafine particle types. *Occup. Environ. Med.*, **2004**, *61*, 442-447.
- [40] Chang, C. The immune effects of naturally occurring and synthetic nanoparticles. *J. Autoimmun.*, **2010**, *34*, J234-J246.
- [41] Patton, J.S.; Fishburn, C.S.; Weers, J.G. The lungs as a portal of entry for systemic drug delivery. *Proc. Am. Thorac. Soc.*, **2004**, *1*, 338-344.
- [42] Pezron, I.; Mitra, R.; Pal, D.; Mitra, A. Insulin aggregation and asymmetric transport across human bronchial epithelial cell monolayers (Calu3). *J. Pharm. Sci.*, **2002**, *91*, 1135-1146.
- [43] Patton, J.S.; Byron, P.R. Inhaling medicines: delivering drugs to the body through the lungs. *Nat. Rev. Drug Discov.*, **2007**, *6*, 67-74.
- [44] Islam, N.; Gladki, E. Dry powder inhalers (DPIs) - a review of device reliability and innovation. *Int. J. Pharm.*, **2008**, *360*, 1-11.
- [45] Kim, K.; Malik, A. Protein transport across the lung epithelial barrier. *Am. J. Physiol. Lung Cell. Mol. Physiol.*, **2003**, *284*, L247-L259.
- [46] Grenha, A.; Remuñán-López, C.; Carvalho, E.; Seijo, B. Microspheres containing lipid/chitosan nanoparticles complexes for pulmonary delivery of therapeutic proteins. *Eur. J. Pharm. Biopharm.*, **2008**, *69*, 83-93.
- [47] Beck-Broichsitter, M.; Merkel, O.M.; Kissel, T. Controlled pulmonary drug and gene delivery using polymeric nano-carriers. *J. Control. Release*, **2012**, *161*, 214-224.
- [48] Muralidharan, P.; Mallory, E.; Malapit, M.; Hayes, D.; Mansour, H. M. Inhalable PEGylated Phospholipid Nanocarriers and PEGylated Therapeutics for Respiratory Delivery as Aerosolized Colloidal Dispersions and Dry Powder Inhalers. *Pharmaceutics*, **2014**, *6*, 333-353.
- [49] Har-el, Y.; Fiegel, J.; Dawson, M.; Hanes, J. Chapter 16: Gene Delivery to the Lung. In *Pharmaceutical Inhalation Aerosol Technology*; Hickey, A.J., Ed.; Marcel Dekker Inc.: New York, NY, USA, Vol. 134, pp. 498-505, **2004**.
- [50] Hills, B. A. An alternative view of the role(s) of surfactant and the alveolar model. *J. Appl. Physiol.*, **1999**, *87*, 1567-1583.
- [51] Roy, I.; Vij, N. Nanodelivery in airway diseases: challenges and therapeutic applications. *Nanomedicine*, **2010**, *6*, 237-244.
- [52] Arppe, J.; Vidgren, M.; Waldrep, J.C. Pulmonary pharmacokinetics of cyclosporin a liposomes. *Int. J. Pharm.*, **1998**, *161*, 205-214.
- [53] SemmlerBehnke, M.; Takenaka, S.; Fertsch, S. Efficient elimination of inhaled nanoparticles from the alveolar region: Evidence for interstitial uptake and subsequent reentrainment onto airways epithelium. *Environ. Health Perspect.*, **2007**, *115*, 728-733.
- [54] Dailey, L.; Jekel, N.; Fink, L. Investigation of the proinflammatory potential of biodegradable nanoparticle drug delivery systems in the lung. *Toxicol. Appl. Pharmacol.* **2006**, *215*, 100-108.
- [55] Azarmi, S.; Roa, W.; Löbenberg, R. Targeted delivery of nanoparticles for the treatment of lung diseases. *Adv. Drug Deliv. Rev.*, **2008**, *60*, 863-875.
- [56] Hartig, S.; Greene, R.; Dasgupta, J. Multifunctional nanoparticulate polyelectrolyte complexes. *Pharm. Res.*, **2007**, *24*, 2353-2369.

- [57] Kathuria, H.; Cao, Y.; Ramirez, M.; Williams, M. Transcription of the caveolin1 gene is differentially regulated in lung type I epithelial and endothelial cell lines. A role for ETS proteins in epithelial cell expression. *J. Biol. Chem.*, **2004**, *279*, 30028-30036.
- [58] Brandenberger, C.; Mühlfeld, C.; Ali, Z. Quantitative evaluation of cellular uptake and trafficking of plain and polyethylene glycol-coated gold nanoparticles. *Small*, **2010**, *6*, 1669-1678.
- [59] Lassmann-Vague, V.; Raccach, D. Alternatives routes of insulin delivery. *Diabetes Metab.*, **2006**, *32*, 513-522.
- [60] Moses, R.G. Combination therapy for patients with type 2 diabetes: repaglinide in combination with metformin. *Expert Rev. Endocrinol. Metab.*, **2010**, *5*, 331-342.
- [61] Damge, C.; Reis, C.P.; Maincent, P. Nanoparticle strategies for the oral delivery of insulin. *Expert Opin. Drug Deliv.*, **2008**, *5*, 45-68.
- [62] Card, J.W.; Magnuson, B.A. A review of the efficacy and safety of nanoparticle-based oral insulin delivery systems. *Am. J. Physiol. Gastrointest. Liver. Physiol.*, **2011**, *301*, G956-G967.
- [63] Hermansen, K.; Rønnemaa, T.; Petersen, A.H.; Bellaire, S.; Adamson, U. Intensive therapy with inhaled insulin via the AERx® insulin diabetes management system: A 12-week proof-of-concept trial in patients with type 2 diabetes. *Diabetes Care*, **2004**, *27*, 162-167.
- [64] Rolla, A.R.; Rakek, R.E. Practical approaches to insulin therapy for type 2 diabetes mellitus with premixed insulin analogues. *Clin. Ther.*, **2005**, *27*, 1113-1125.
- [65] Gänsölen, M. About inhalation of insulin. *Klin Wochenschr*, **1925**, *4*, 71.
- [66] Sun, X.J.; Rothenberg, P.; Kahn, C.R.; Backer, J.M.; Araki, E.; Wilden, P.A.; Cahill, D.A.; Goldstein, B.J.; White, M.F. Structure of the insulin receptor substrate IRS-1 defines a unique signal transduction protein. *Nature*, **1991**, *352*, 73-77.
- [67] Fang, X.; Yu, S.X.; Lu, Y.; Bast, R.C.; Woodgett, J.R.; Mills, G.B. Phosphorylation and inactivation of glycogen synthase kinase 3 by protein kinase A. *Proc. Natl. Acad. Sci. USA*, **2000**, *97*, 11960-11965.
- [68] McManus, E.J.; Sakamoto, K.; Armit, L.; Ronaldson, L.; Shpiro, N.; Marquez, R.; Alessi, D.R. Role that phosphorylation of GSK3 plays in insulin and Wnt signalling defined by knocking analysis. *EMBO J.*, **2005**, *24*, 1571-1583.
- [69] Iwase, H.; Kobayashi, M.; Nakajima, M.; Takatori, T. The ratio of insulin to C-peptide can be used to make a forensic diagnosis of exogenous insulin overdosage. *Forensic Sci. Int.*, **2001**, *115*, 123-127.
- [70] Wolzt, M.; De La Peña, A.; Berclaz, P.; Tibaldi, F.; Gates, J.; Muchmore, D. Air inhaled insulin versus subcutaneous insulin: pharmacokinetics, glucodynamics, and pulmonary function in asthma. *Diabetes Care*, **2008**, *31*, 735-740.
- [71] Karathanasis, E.; Bhavane, R.; Annapragada, A. Glucosensing pulmonary delivery of human insulin to the systemic circulation of rats. *Int. J. Nanomedicine*, **2007**, *2*, 501-513.
- [72] Leach, C.; Kuo, M.; Bueche, B.; Fishburn, S.; Viegas, T.; Bossard, M.; Guo, L.; Bentley, M.; Hobbs, C.; Cherrington, A. Modifying the pulmonary absorption and retention of proteins through PEGylation. *Respir. Drug Deliv. IX*, **2004**, *1*, 69-78.
- [73] Lee, K.C.; Chae, S.Y.; Kim, T.H.; Lee, S.; Lee, E.S.; Youn, Y.S. Intrapulmonary potential of polyethylene glycol-modified glucagon-like peptide-1s as a type 2 anti-diabetic agent. *Regul. Pept.*, **2009**, *152*, 101-107.
- [74] Insulin inhalation—Pfizer/Nektar therapeutics: Hmr 4006, inhaled peg-insulin—Nektar, PEGylated insulin—Nektar. *Drugs RD*, **2004**, *5*, 166-170.
- [75] Bi, R.; Shao, W.; Wang, Q.; Zhang, N. Spray freeze dried dry powder inhalation of insulin loaded liposomes for enhanced pulmonary delivery. *J. Drug Target.*, **2008**, *16*, 639-648.
- [76] Chono, S.; Fukuchi, R.; Seki, T.; Morimoto, K. Aerosolized liposomes with dipalmitoylphosphatidylcholine enhance pulmonary insulin delivery. *J. Control. Release*, **2009**, *137*, 104-109.
- [77] Liu, F.Y.; Shao, Z.; Kildsig, D.O.; Mitra, A.K. Pulmonary delivery of free and liposomal insulin. *Pharm. Res.*, **1993**, *10*, 228-232.
- [78] Liu, J.; Gong, T.; Fu, H. Solid lipid nanoparticles for pulmonary delivery of insulin. *Int. J. Pharm.*, **2008**, *356*, 333-344.
- [79] Yamamoto, H.; Kuno, Y.; Sugimoto, S.; Takeuchi, H.; Kawashima, Y. Surface modified PLGA nanosphere with chitosan improved pulmonary delivery of calcitonin by mucoadhesion and opening of the intercellular tight junctions. *J. Control. Release*, **2005**, *102*, 373-381.
- [80] Huang, X.; Du, Y.; Yuan, H.; Hu, F. Preparation and pharmacodynamics of low molecular weight Chitosan nanoparticles containing insulin. *Carbohydr. Polym.*, **2009**, *76*, 368-373.
- [81] Yamamoto, H.; Hoshina, W.; Kurashima, H. Engineering of poly(DL-lactic-co-glycolic acid) nanocomposite particles for dry powder inhalation dosage forms of insulin with the sprayfluidized bed granulating system. *Adv. Powder Technol.*, **2007**, *18*, 215-228.
- [82] Grenha, A.; Seijo, B.; Remunan-Lopez, C. Microencapsulated chitosan nanoparticles for lung protein delivery. *Eur. J. Pharm. Sci.*, **2005**, *25*, 427-437.
- [83] Zhang, Q.; Shen, Z.; Nagai, T. Prolonged hypoglycemic effect of insulin loaded polybutylcyanoacrylate nanoparticles after pulmonary administration to normal rats. *Int. J. Pharm.*, **2001**, *218*, 75-80.
- [84] DeRuitter, J. *Overview of the Antidiabetic Agents*. Endocrine Pharmacotherapy Module, Spring, **2003**.
- [85] Reddy, V.S.; Sahay, R.K.; Bhadada, S.K.; Agrawal J.K.; Agrawal, N.K. Newer Oral Antidiabetic Agents. *J. Indian Acad. Clin. Med.*, **2000**, *1*, 245-251.
- [86] Agabegi, E.D.; Agabegi, S.S. *Step-Up to Medicine (Step-Up Series)*. Lippincott Williams & Wilkins: Hagerstown, MD, **2008**.
- [87] Rendell, M. Advances in diabetes for the millennium: drug therapy of type 2 diabetes. *MedGenMed*, **2004**, *6*, 9.
- [88] Elmowafy, E.; Osman, R.; El-Shamy, A.H.; Awad, G.A. Nano-complexes of an insulinotropic drug: optimization, microparticle formation, and antidiabetic activity in rats. *Int. J. Nanomedicine*, **2014**, *9*, 4449-4465.
- [89] Zhou, G.; Myers, R.; Li, Y.; Chen, Y.; Shen, X.; Fenyk-Melody, J.; Wu, M.; Ventre, J.; Doebber, T.; Fujii, N.; Musi, N.; Hirshman, M.; Goodyear, L.; Moller, D. Role of AMP-activated protein kinase in mechanism of metformin action. *J. Clin. Invest.*, **2001**, *108*, 1167-1174.
- [90] Youn, Y.S.; Jeon, J.E.; Chae, S.Y.; Lee, S.; Lee, K.C. PEGylation improves the hypoglycaemic efficacy of intranasally administered glucagon-like peptide-1 in type 2 diabetic db/dbmice. *Diabetes Obes. Metab.*, **2008**, *10*, 343-346.
- [91] Kim, T.H.; Park, C. W.; Kim, H.Y.; Chi, M.H.; Lee, S.K.; Song, Y. M.; Jiang, H.H.; Lim, S.M.; Youn, Y.S.; Lee, K.C. Low molecular weight (1 kDa) polyethylene glycol conjugation markedly enhances the hypoglycemic effects of intranasally administered exendin-4 in type 2 diabetic db/dbmice. *Biol. Pharm. Bull.*, **2012**, *35*, 1076-1083.

ORIGINAL ARTICLE

Pressure-sensitive mucoadhesive polymer-based dental patches to treat periodontal diseases: an *in vitro* study

R. Manasadeepa, Paramita Paul, and Biswajit Mukherjee

Department of Pharmaceutical Technology, Jadavpur University, Kolkata, West Bengal, India

Abstract

Local drug delivery for periodontal diseases is still a challenge due to very short residence time, involuntary swallowing and salivary wash-out. Present study is, therefore, an attempt to develop pressure-sensitive adhesive polymers-based mucoadhesive dental patches to ensure satisfactory prolonged release of drugs, to treat periodontal diseases locally. Polymers such as duro-tak[®] 387-2516 and duro-tak[®] 387, ethylcellulose, polyvinylpyrrolidone, polyvinyl alcohol along with drugs amoxicillin trihydrate and diclofenac sodium were used to develop the experimental patches. The patches were characterized for mass variation, thickness, area, moisture-content and moisture-uptake, folding endurance, structural integrity in simulated saliva, bioadhesive strength, surface pH, scanning electron microscopy, cellular morphology, *in vitro* drug release and temperature-dependant stability study as per ICH guideline. Incorporation of release enhancers in the patches improved drug release. Drugs released in a sustained manner due to the formation of physical bonds between the polymers (as assessed by FTIR study) which might alter the length of drug diffusion pathways. The formulation F3 with tween 80 as release enhancer provided best drug release profile over the period of 8 h, thus it could be a successful attempt for the management of oral pathogens and dental pain.

Keywords

Bioadhesive strength, dental pain management, mucoadhesive, periodontal diseases, pressure-sensitive adhesives, release enhancers

History

Received 16 April 2013
Accepted 5 July 2013
Published online 19 July 2013

Introduction

In the oral cavity, periodontal region is a suitable environment for the growth of many bacteria (Paster et al., 2001). When the bacterial plaques affect the gum, it is termed as gingivitis and when they spread into the deeper tissues, it is called as periodontal infection (Bascones & Figuera, 2004). The oral mucoadhesive drug delivery systems are now becoming more and more popular due to ease of drug administration (Gandhi & Robinson, 1994; Hearnden et al., 2012), by-passing hepatic “first-pass” metabolism (Hoogstraate et al., 1996; Morales & McConville, 2011), increase residence time (Ahuja et al., 2006; Andrews et al., 2009) and high drug flux at the site of action for localized function (Nafee et al., 2003; Puratchikody et al., 2011). Many scientific studies have confirmed that the earlier procedures adopted for the treatment of periodontal diseases cause bleeding, bacteremia, development of infective endocarditis, etc. A prolonged systemic therapy with antibiotics has been proved to enhance the risk of endocarditis and immune suppression (Tong & Rothwell, 2000; Lockhart et al., 2009). The topical anti-inflammatory and analgesic formulations (sprays, gels, paints, etc.) are failed to produce the satisfactory therapeutic effect due to quick wash-out by salivary secretion (Nafee et al., 2004). It is, therefore,

desirable to develop formulations which remain attached to the oral mucosa, and release the depot drug(s) slowly from them for a prolonged period of time (Nafee et al., 2003). Amoxicillin trihydrate is widely used in dental practice to treat periodontal diseases and bacterial infections (Bascones & Figuera, 2004; Herrera et al., 2008). Amoxicillin trihydrate is a β -lactam antibiotic, used to treat both Gram positive and Gram negative bacteria (Mukherjee et al., 2009). Diclofenac sodium is used as an analgesic, anti-inflammatory agent (Özgüney et al., 2006). The present study was intended to develop a matrix-type oral mucoadhesive patch with an appropriate adhesive property to the oral mucosa, tooth and gum, using a blend of pressure-sensitive adhesives (PSA) (duro-tak[®] 387-2516 and duro-tak[®] 387-2051) along with the model drug(s), (amoxicillin trihydrate and diclofenac sodium) to provide prolonged local drug action.

Materials and methods

Diclofenac sodium and amoxicillin trihydrate were obtained as gift sample from Micro Labs Ltd., Hosur, India and Dey's Medical Stores (Manufacturing) Ltd., Kolkata, India, respectively. Duro-tak[®] 387-2516 and duro-tak[®] 387-2051 (National Starch and Chemical Company, Bridgewater, NJ), polyvinylpyrrolidone (PVP) (Loba Chemie Pvt Ltd, Mumbai, India), polyvinyl alcohol (PVA) (molecular weight 125,000 Dalton), tween 80 and ethyl cellulose (EC) (SD Fine-Chem. Ltd., Mumbai, India), dibutyl phthalate (DBP), polyethylene glycol (PEG) 400 and PEG 6000 (E. Merck, Mumbai, India), and

Address for correspondence: Biswajit Mukherjee, Department of Pharmaceutical Technology, Jadavpur University, Kolkata-700032, West Bengal, India. Tel: +91 33 2414 6677. Fax: +91 33 2414 6677. Email: biswajit55@yahoo.com

glycerol (Qualigens Fine Chemicals, Mumbai, India) were procured. All the other chemicals used were of analytical grade.

Drug-excipients interaction

Drug-excipients interaction was carried out using Fourier transform infrared (FTIR) spectrometer (Magna IR 750 series II, Jasco, FTIR 4200, Japan). FTIR-spectra for pure drug(s), excipients, physical mixture of drug(s) with excipients, formulation without drug and formulations with drug(s) were obtained by scanning over the region of 4000 cm^{-1} to 400 cm^{-1} using KBr pellet technique (Rudra et al., 2010).

Preparation of the backing membrane

A weighed amount of PVA (6% w/v) was mixed with a requisite volume of warm, glass distilled water by constant stirring at 60°C till it formed a homogeneous solution (Mukherjee et al., 2006). The homogeneous solution (3 mL each) was then poured onto the covered bottom end (wrapped with aluminium foil) of glass molds (2.55 cm inner diameter hollow glass cylinder of 2 cm height). The molds were kept at 60°C for 8 h in an oven (Damodharan et al., 2010) to form smooth, uniform and transparent backing membrane (Figure 1).

Preparation of protective membrane

Blend of EC and PVP (in different ratios of 1:1, 1:2 and 2:1) was dissolved in chloroform along with 1% v/v DBP

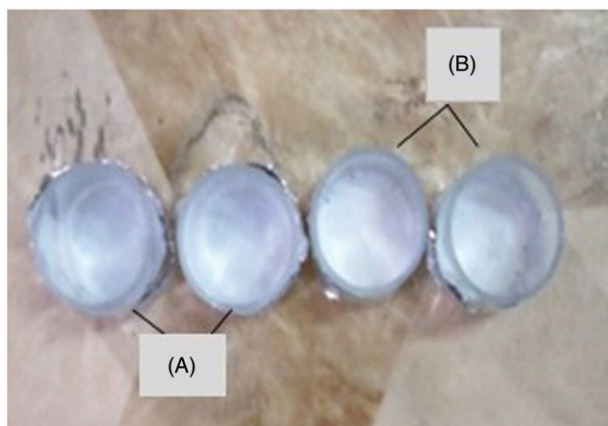


Figure 1. Dental patches containing (A) backing membrane, (B) backing membrane along with protective membrane.

(Gupta & Mukherjee, 2003) and 1% v/v glycerol as plasticizers to get a homogenous mixture. The homogenous solution (2 mL each) was then poured over the previously prepared backing membrane remained in mold and dried at 60°C for 6 h in an oven. Among those protective membranes prepared at various ratios, the membrane with EC: PVP ratio 2:1 was found to form a film with smooth surface (Figure 1).

Casting of drug matrix over the protective membrane

Various combination ratios of liquid polymers duro-tak[®] 387-2516 and duro-tak[®] 387-2051 were used initially to develop formulations for screening. The blend with 4:5 ratio (by volume) was chosen best (based on tackiness and drug release pattern) for further development of patches. The liquid polymers were measured and a homogeneous mixture was made using a magnetic stirrer (Mukherjee et al., 2006). To the above mixture, a release enhancer (when required) such as PEG 400 (1% v/v)/tween 80 (1% v/v)/PEG 6000 (1% w/v)/glycerol (1% v/v) (Siegel et al., 1981) was added along with the required quantities of drug(s) (Table 1). The entire dispersion (2 mL for each patch) was then casted on the EC-PVP protective membrane. The prepared matrix patches were dried at room temperature for 24 h, resulting in a flat, uniform medicated matrix patch.

In vitro characterization of the patches

From the different formulations, F4 and F5 were rejected due to more stickiness, and F1, F2 and F3 were selected for physicochemical characterization.

Determination of average mass uniformity and patch thickness

Randomly selected twenty patches from each type were directly weighed on a digital balance (Sartorius, GD-103, Goettingen, Germany) and average mass was calculated. Deviations of mass of individual patch from the mean value were determined.

Thickness of backing membrane, protective membrane and of the whole patch (adhesive matrix with the drug(s) plus the backing membrane and the protective membrane) was measured at five different randomly selected points of 20 patches using digital calipers (Digmatic Massschieber, CD-6"CSX, Mitutoyo Corp., Japan) and average thicknesses were determined (Mukherjee et al., 2006) (Table 2).

Table 1. Composition of different formulations.

Formulation No.	Ratio of mucoadhesive polymers ^a (Duro-Tak [®] 387-2516: Duro-Tak [®] 387-2051)	Amount of release enhancer	Weight of drug(s)
F1	4:5	–	A ^c – 6 mg and D ^d – 4 mg
F2	4:5	1% PEG ^b 400(v/v)	A – 6 mg and D – 4 mg
F3	4:5	1% tween 80(v/v)	A – 6 mg and D – 4 mg
F4	4:5	1% PEG 6000(w/v)	A – 6 mg and D – 4 mg
F5	4:5	1% glycerol(v/v)	A – 6 mg and D – 4 mg

^aPolymers are taken in ratio by volume.

^bPolyethylene glycol.

^cAmoxicillin trihydrate.

^dDiclofenac sodium.

Table 2. Physical characterization of different experimental formulations.

Physical characteristics (unit)	Formulation F1 (Avg ^a ± SD ^b)	Formulation F2 (Avg ± SD)	Formulation F3 (Avg ± SD)
Mass variation ^c (g)	0.39 ± 0.08	0.52 ± 0.06	0.58 ± 0.02
Whole patch thickness ^c (mm)	0.59 ± 0.02	0.54 ± 0.03	0.56 ± 0.03
Diameter of the patch ^c (cm)	2.40 ± 0.03	2.36 ± 0.03	2.43 ± 0.03
Area of the patch ^c (cm ²)	4.38 ± 0.12	4.53 ± 0.11	4.64 ± 0.14
Moisture content ^d (weight %)	1.18 ± 0.59	1.09 ± 0.17	0.79 ± 0.22
Moisture absorption ^d (weight %)	10.30 ± 2.18	10.46 ± 2.31	10.21 ± 2.07
Folding endurance ^d	91 ± 3.05	114 ± 5.29	92.3 ± 4.50
Bioadhesive strength ^c (kg/mm ²)	12.28 ± 0.10	11.65 ± 0.45	11.55 ± 0.36
Surface pH ^c	6.09 ± 0.13	6.58 ± 0.28	6.45 ± 0.21

^aAverage.^bStandard deviation.^cMean ± SD (*n* = 3).^dMean ± SD (*n* = 6).^eMean ± SD (*n* = 20).

Area of the patches

The diameter (*D*) of each patch was measured by a millimeter scale and the area ($\pi [D/2]^2$) was calculated and the mean area was then determined (Mukherjee et al., 2006).

Moisture content

The prepared patches were marked, weighed individually and kept in a desiccator containing activated silica at room temperature. The mass was taken time to time till it became constant (Arora & Mukherjee, 2002; Damodharan et al., 2010). Percent moisture content was determined as follows:

$$\% \text{ Moisture content} = \frac{\text{Initial mass} - \text{Final mass}}{\text{Initial mass}} \times 100$$

Moisture absorption

A previously weighed patch was exposed to 100% relative humidity (RH) in a desiccator until a constant mass for the patch was obtained (Arora & Mukherjee, 2002). The percentage of moisture uptake was calculated as follows:

$$\% \text{ Moisture absorption} = \frac{\text{Final mass} - \text{Initial mass}}{\text{Initial mass}} \times 100$$

Folding endurance

The folding endurance of patches that was determined by repeatedly folding one patch at the same place till it broke, is considered satisfactory to reveal good film properties (Khanna et al., 1997). The maximum number of times a patch can be folded at the same place without breaking gives the value of the folding endurance.

Structural integrity in simulated saliva (pH 6.8)

The structural integrity of the patches was studied in simulated saliva (Mukherjee et al., 2009). Patches were placed in separate petri dishes containing 10 mL of simulated saliva and kept in an incubator at $37 \pm 0.2^\circ\text{C}$ for 8 h (Ghosh et al., 2009). At regular intervals of every 30 min, the patches were examined for physical changes such as stickiness, color, texture and shape as depicted earlier.

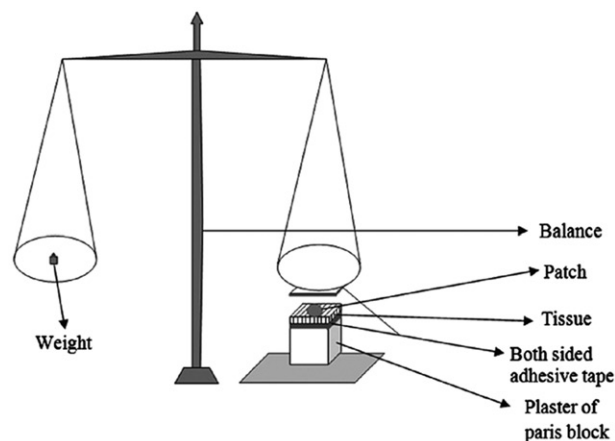


Figure 2. Bioadhesion test assembly.

Bioadhesive strength

Bioadhesive strength was measured to determine the maximum force required for detaching the applied patches from the biological membrane (Nair et al., 2013). This may vary depending on binding ability of polymer blend of a formulation with buccal mucosa. Bioadhesive strength of patches was determined using a modified method (Mukherjee et al., 2009). Fresh mucous membrane of goat was collected from a slaughter house (after taking the necessary permission from the Animal Ethics Committee, Jadavpur University, Kolkata), cleaned with distilled water and immersed in simulated saliva (at $37 \pm 0.5^\circ\text{C}$ for 2 min). The mucous membrane was fixed with a both-side adhesive tape on the top surface of a cube (each side 3 cm) made up of plaster of paris base (Figure 2). Each experimental formulation without the protective layer and backing membrane (casted separately) was attached to the mucous layer. A physical balance with two circular pans, hanged from a rod which was balanced with a fulcrum on a stand was used as a modified bioadhesion test assembly (Gupta et al., 1992). Lower surface of a pan was attached to the mucoadhesive patch by both-side adhesive tape. Weights were given on the other pan until the adhesive patch was detached from the mucous membrane. The maximum force required for complete removal of the patch from the mucous membrane was recorded (Mukherjee et al., 2009).

Surface pH study

The patches were dipped in 1 mL distilled water for two minutes at room temperature (Obaidat et al., 2011), and the pH was noted down by bringing the electrode in contact with the surface of the patch, allowing it to equilibrate for one minute (Priya et al., 2011; Chopparapu et al., 2012).

Scanning electron microscopy (SEM)

The surface morphology and distribution pattern of the drug(s) in the formulated patches were analyzed by scanning electron microscope (JEOL JSM-6100, JEOL Ltd., Tokyo, Japan) before and after *in vitro* drug release study (Mukherjee et al., 2009) by placing the samples onto stubs and sputtering platinum under vacuum before analysis.

The effect of patch on the cellular morphology of mucous membrane

Head of a goat by removing the skin was collected from the slaughter house immediately after sacrifice, after taking the permission of Animal Ethics, Committee, Jadavpur University, Kolkata, India. Experimental patches with or without drug(s) were applied to the goat mucosal membrane for 8 h. The untreated (control) and patch treated portions of the mucosal membrane were collected, washed briefly and fixed with 10% v/v formalin solution. The tissue portions were blocked in paraffin, sectioned by microtome, stained using haematoxylin-eosin solution and visualized under microscope (Carl Zeiss Pvt. Ltd., Goettingen, Germany) (Mukherjee et al., 2005).

In vitro drug release and release kinetics study

In vitro drug release from oral mucoadhesive patches was conducted using a modified method in Franz diffusion cell (Obaidat et al., 2011; Nair et al., 2013). In the receptor compartment, the backing membrane portion of the oral mucoadhesive patch was mounted with the help of cyanoacrylate and fixed by applying finger pressure for 30 s in such a way that the drug polymer matrix of the patch remained in contact with the release medium. The whole set-up was maintained at a constant temperature of $37 \pm 0.5^\circ\text{C}$ through circulating water bath. Then the release medium was constantly and continuously stirred on a magnetic stirrer by teflon coated magnetic bead at 100 rpm. The samples were withdrawn at different time intervals and an equal volume of simulated saliva was added to maintain sink condition (Obaidat et al., 2011). Absorbance of the samples was measured by UV-visible spectrophotometer at their corresponding λ_{max} values i.e., 232 nm for amoxicillin and 276 nm for diclofenac, (Bucci et al., 1998) taking simulated saliva as blank. The drug release data were plotted as cumulative percentage drug(s) release against time for different formulations (Mukherjee et al., 2009). Data obtained from *in vitro* drug release study were plotted in various kinetic models such as zero order, first order, Higuchi, Korsmeyer-Peppas, and Hixson-Crowell kinetic models. Coefficients of determination (R^2) and rate constants/release exponent for zero order (K_0), first order (K_1), Higuchi model (K_H), Korsmeyer-Peppas

model, and Hixson-Crowell model (K_{HC}) were determined (Rudra et al., 2010).

Stability study

The impact of temperature and humidity on the formulations were investigated by accelerated stability analysis. According to the International Conference on Harmonization (ICH) guidelines (ICH, 2003), the samples of formulation F3 were kept in Zone-III temperature conditions (30°C , 75% RH and 40°C , 75% RH), withdrawn at different time points (at 2nd and 3rd month) and were analyzed by FTIR-spectroscopy (ICH, 2003).

Statistical analysis

One way ANOVA followed by Tukey's multiple comparison test performed on drug release data to assess the release kinetics of the formulations; p values <0.05 were considered significant. All calculations were done using the Graph pad prism software (version 5), San Diego, CA, USA.

Results

Drug-excipients interaction study

In the present study, FTIR spectroscopy was carried out to assess the interactions, if any, between the drug(s) and the excipients, at the level of functional groups. Figure 3 provides FTIR spectra of amoxicillin trihydrate, diclofenac sodium, duro-tak[®]2516, duro-tak[®]2051, physical mixture of the drug(s) and the excipients, formulation F3, and formulation (F3) after the storage at 30°C and 40°C ; at 75% RH up to three months. Comparison of spectra suggests that there were changes in the peaks between the wave numbers 2950 cm^{-1} and 3000 cm^{-1} , 3400 cm^{-1} and 3200 cm^{-1} , 800 cm^{-1} and 850 cm^{-1} , and 900 cm^{-1} and 950 cm^{-1} . The wave numbers 2950 cm^{-1} and 3000 cm^{-1} are predominantly responsible for the strong intensity stretching vibration frequency of alkanes and 3400 cm^{-1} and 3200 cm^{-1} are the medium intensity hydrogen bond (H-bond) of $-\text{OH}$ (alcohol and phenol) (Silverstein & Webster, 1998). Wave numbers between 800 cm^{-1} and 850 cm^{-1} are the strong intensity out of plane bending vibration of aromatic hydrocarbons and those between 900 cm^{-1} and 950 cm^{-1} are the strong intensity out of plane bending vibration of alkenes. There are $-\text{OH}$ groups present in PVA, EC and tween 80. Duro-Tak[®] polymers are acrylate polymers which contain methyl acrylate, acrylic acid and ethyl acrylate. In acrylate polymers, free alkyl groups as well as $-\text{C}=\text{O}$ groups exist. Aromatic groups are present in PVA, EC and tween 80. Thus, formation of weak bonds such as weak H-bond or van der Waals force of attraction might be responsible to develop some physical interactions among the drug(s) and the excipients molecules, altering some shifts in peaks (Rudra et al., 2010). The FTIR spectrum of amoxicillin trihydrate in formulation F3 shows that characteristics peaks at 1656.55 cm^{-1} for $\text{C}=\text{O}$ stretching of amide group, 1734.66 cm^{-1} for $\text{C}=\text{O}$ stretching of β -lactam, (Mukherjee et al., 2009) whereas diclofenac sodium was characterized by the presence of NH and COO^- stretching vibrations at 3391.21 cm^{-1} and 1458.89 cm^{-1} respectively. The C-O stretching was found at 1287.25 cm^{-1}

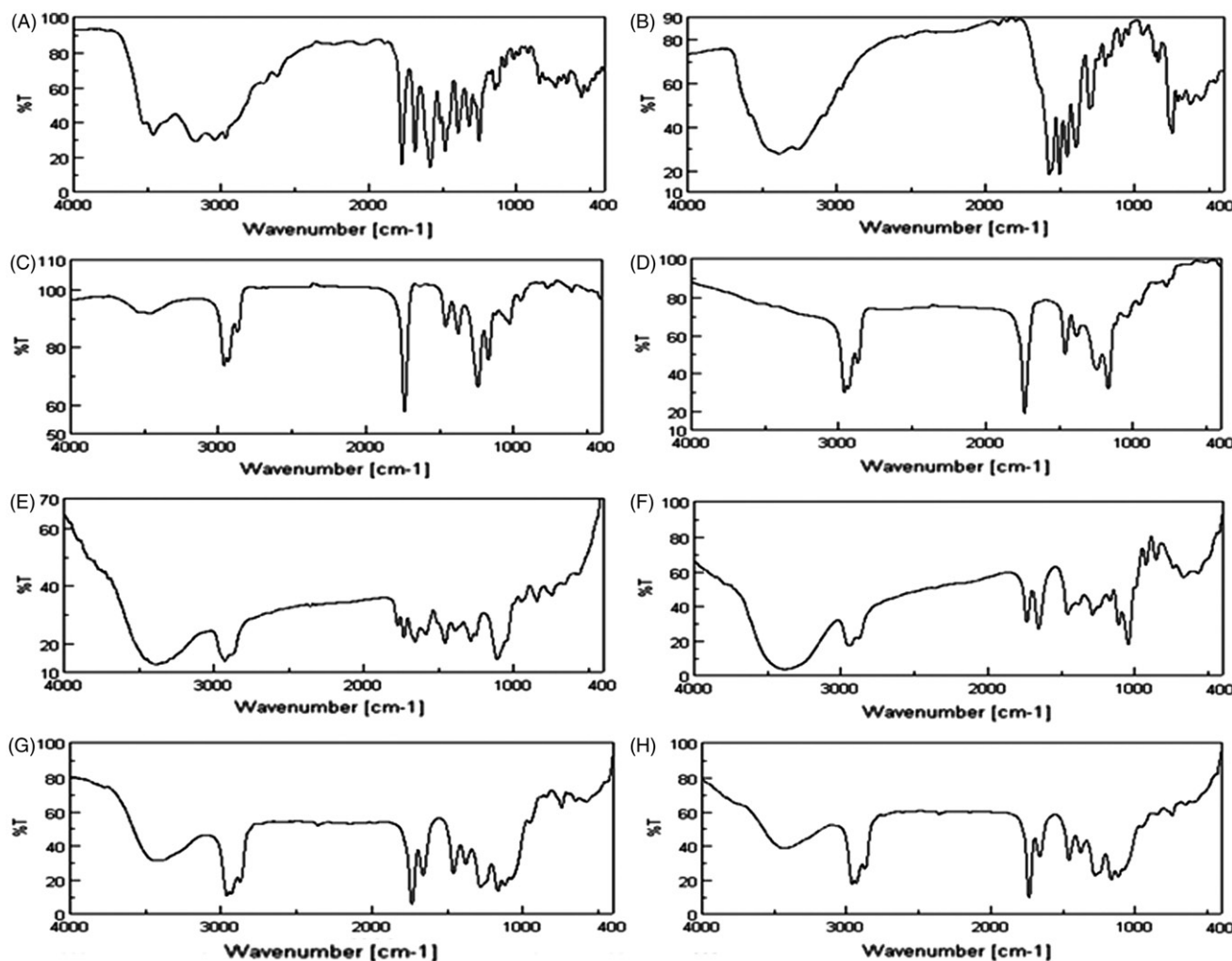


Figure 3. Fourier transform infrared (FTIR) spectra of (A) amoxicillin trihydrate, (B) diclofenac sodium, (C) duro-tak[®] 387-2516, (D) duro-tak[®] 387-2051, (E) physical mixture of drug(s) and excipients, (F) formulation F3, (G) formulation F3 at 30°C, 75% RH, (H) formulation F3 at 40°C, 75% RH.

in diclofenac sodium (Pecsok et al., 1968; Bucci et al., 1998) (Figure 3) and hence no chemical interaction between the drug molecules and the excipients exists. Physical interaction thus formed, might help to develop the polymeric matrix network and for slower drug release from the patches.

Average mass variation, thickness, diameter and area of the patches

The mean mass, thickness, area, diameter of the drug-polymer matrix is shown in Table 2. Thin patches were developed. In different formulation (F1-F3), average mass range was found from 0.39 ± 0.08 g to 0.58 ± 0.02 g. The average thickness range varied from 0.54 ± 0.03 mm to 0.59 ± 0.02 mm. The patches were circular with average diameter of 2.40 ± 0.03 cm for formulation F1; 2.36 ± 0.03 cm for formulation F2; 2.43 ± 0.03 cm for formulation F3, and had mean surface area ranging from 4.38 ± 0.12 cm² to 4.64 ± 0.14 cm².

Moisture content and moisture absorption

The average percent moisture content of the formulations F1–F3 varied between 0.79 ± 0.22 weight% and 1.18 ± 0.59 weight% and average percentage moisture absorption of those formulations were found to vary between 10.21 ± 2.07

weight% and 10.46 ± 2.31 weight%. The above mentioned data show that presence of moisture content and moisture absorption in the patches may protect the patches from dryness, brittleness and unnecessary bulkiness (Arora & Mukherjee, 2002).

Folding endurance and structural integrity of the formulations in simulated saliva

The folding endurance test was conducted for selected formulations. The values for folding endurance were found to vary from 91 ± 3.05 to 114 ± 5.29 (Table 2). The results indicate that the patches would maintain their integrity for sufficient time after being applied on the mucosal area (Priya et al., 2011). Further, structural integrity of the formulations in simulated saliva, show that the formulations maintained their texture and shape and no distortion in the presence of saliva for a long time (8 h). There was no visible swelling of the formulations in simulated saliva.

Bioadhesive strength

Table 2 represents the bioadhesive strength of the experimental dental patches containing drug(s). The bioadhesive strength of the formulations was found to vary from

Table 3. Coefficients of determination (R^2) and rate constants of drug release patterns tested on various kinetic models.

Kinetic model	Formulation 1		Formulation 2		Formulation 3	
	Amoxicillin	Diclofenac	Amoxicillin	Diclofenac	Amoxicillin	Diclofenac
Zero order	$R^{2a} = 0.910$ $K_0^c = 1.228$	$R^2 = 0.898$ $K_0 = 0.276$	$R^2 = 0.939$ $K_0 = 1.437$	$R^2 = 0.823$ $K_0 = 0.342$	$R^2 = 0.996$ $K_0 = 6.583$	$R^2 = 0.988$ $K_0 = 2.053$
First order	$R^2 = 0.919$ $K_1^d = -0.0115$	$R^2 = 0.900$ $K_1 = -0.002$	$R^2 = 0.941$ $K_1 = -0.013$	$R^2 = 0.826$ $K_1 = -0.002$	$R^2 = 0.992$ $K_1 = -0.092$	$R^2 = 0.990$ $K_1 = -0.020$
Korsmeyer-Peppas	$R^2 = 0.966$ $n^b = 0.474$	$R^2 = 0.995$ $n = 0.444$	$R^2 = 0.919$ $n = 0.540$	$R^2 = 0.972$ $n = 0.431$	$R^2 = 0.991$ $n = 0.822$	$R^2 = 0.977$ $n = 0.714$
Higuchi	$R^2 = 0.984$ $K_H^e = 3.808$	$R^2 = 0.997$ $K_H = 0.868$	$R^2 = 0.930$ $K_H = 4.263$	$R^2 = 0.977$ $K_H = 1.111$	$R^2 = 0.936$ $K_H = 19.02$	$R^2 = 0.943$ $K_H = 5.981$
Hixson-Crowell	$R^2 = 0.916$ $K_{HC}^f = -0.019$	$R^2 = 0.899$ $K_{HC} = -0.004$	$R^2 = 0.941$ $K_{HC} = -0.023$	$R^2 = 0.825$ $K_{HC} = -0.005$	$R^2 = 0.996$ $K_{HC} = -0.128$	$R^2 = 0.990$ $K_{HC} = -0.033$

^aCoefficient of determination.

^bRelease exponent.

^cZero order rate constant ($\mu\text{g mL}^{-1}\text{h}^{-1}$).

^dFirst order rate constant (h^{-1}).

^eHiguchi rate constant ($\text{h}^{-1/2}$).

^fHixson-Crowell rate constant ($\mu\text{g}^{1/3}\mu\text{m}^{-1}\text{h}^{-1}$).

$11.55 \pm 0.36 \text{ kg/mm}^2$ to $12.28 \pm 0.11 \text{ kg/mm}^2$, which was found to be good enough to remain attached to the site of application (mucosa) and simply to be taken out with little effort.

Surface pH

The surface pH was determined for the selected patches (Table 2). The pH of the formulations was found to vary from 6.09 to 6.58, which is well within the limit of normal buccal pH range (Bruschi & Freitas, 2005). Thus, the patches would not cause any irritation in the oral mucosa upon application.

Scanning electron microscopy

SEM study was carried out for the oral mucoadhesive patches before and after *in vitro* drug release study to detect the surface morphology and the drug distribution pattern of the patches (Damodharan et al., 2010). Figure 4 shows drug particles were scattered in the polymer matrix before its release. Oral mucoadhesive patches without the drug permeation enhancer (PEG 400 or tween 80) had more or less smooth surface (Figure 4A), whereas, drug particles were visible on patch surface when drug permeation enhancers were incorporated (Figure 4C and 4D). Appearance of drug particle distribution was very prominent in case of formulation with tween 80 (Figure 4D). Most of the drug particles were found to diffuse out of the formulation (F3) containing tween 80 within 8 h (Figure 4G).

The effect of patch on the cellular morphology of mucous membrane

The comparative study of buccal mucosal and submucosal tissues with and without the application of patches shows no morphological alteration in mucosal and submucosal area (Figure 5), after 8 h of administration of the patches on the buccal tissue.

In vitro drug release and release kinetics study

Figure 6 shows the release pattern of amoxicillin trihydrate and diclofenac sodium from the patches for 8 h in simulated

saliva (pH 6.8). The cumulative percentage release of amoxicillin trihydrate and diclofenac sodium from formulation F3 was about 53.55% and 17.3%, respectively over a time period of 8 h. Statistical levels of significance when assessed between the drug release data showed the variation in drug release data between any two formulations at any experimental time point was statistically significant ($p < 0.05$), except for the data between F2 versus F1. Different drug release patterns by linear kinetics were presented in Table 3. Higuchi's data of drug release was almost linear with highest coefficient of determination (R^2) values for formulation F1 and F2, suggesting the diffusion control drug release from the matrix (Basu et al., 2012; Pattnaik et al., 2012). Whereas the zero order plots had comparatively more linearity for formulation F3, which infers that the drug release occurs in sustained manner. Moreover, the formulation F3 follows Hixson-Crowell kinetics assuming the release rate is limited by the drug(s) particles dissolution rate, which is perhaps favored for incorporating tween 80 in it (Costa & Lobo, 2001).

Stability study

Formulation (F3) selected as best, based on physico-chemical characterizations and drug release pattern, was stored at 30°C and 40°C at 75% RH for 3 months. After 3 months of storage period, when the FTIR spectra of the stored formulations were compared with the freshly prepared formulation (F3), no predominant shifting of peak was detected (Figure 3F, G and H). This suggests that drug(s) did not interact with the excipients at the above mentioned temperature conditions and remained stable in the formulation.

Discussion

Investigation of interaction between drug and excipients is an important preformulation study which predominantly indicates the stability of the drug in the formulation and its release pattern (Mukherjee et al., 2008). Methods such as FTIR spectroscopy, IR spectroscopy, differential scanning calorimetry, etc. are generally used to determine drug-excipients interactions. In this study, drug-excipients interaction study was performed using FTIR spectroscopy, to determine any

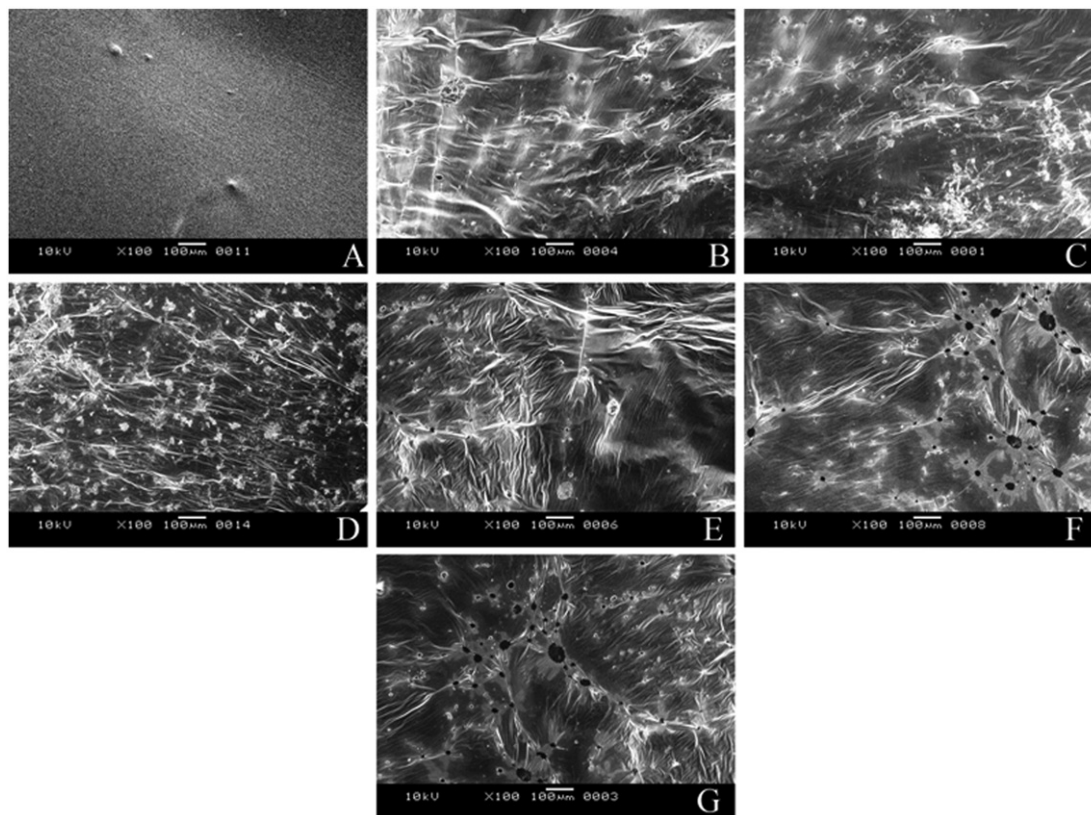


Figure 4. Scanning electron microscopic (SEM) photographs of (A) Formulation F0 (formulation without drug(s) and release enhancer), (B) Formulation F1, (C) Formulation F2, (D) Formulation F3, (E) Formulation F1 after 8 h of drug release study, (F) Formulation F2 after 8 h of release study (G) Formulation F3 after 8 h of drug release study.

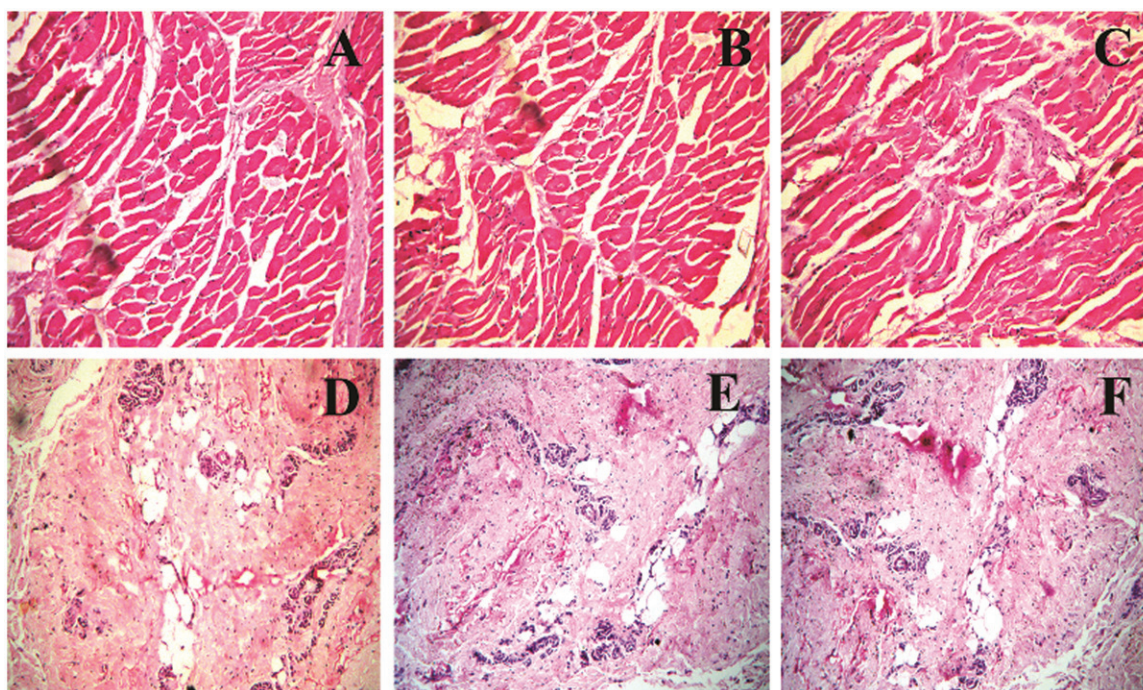


Figure 5. Morphology of goat mucosa and submucosa with or without the application of experimental patches (F3). (A) Normal (without patch) mucosa, (B) Treated (with patch without drug) mucosa, (C) Treated (with patch containing drug) mucosa, (D) Normal (without patch) submucosa, (E) Treated (with patch without drug) submucosa, (F) Treated (with patch containing drug) submucosa.

interaction between the drug(s) and the excipients. Data of drug(s)-excipients interaction study suggest that there was no chemical interaction between the drug molecules and the excipients. However, physical interactions such as

formation of weak H-bonds, van der Waals force of attraction, dipole-dipole interaction might exist, which in turn supports the formation of solid but adhesive patches with the desired tack effects, from the two liquid duro-tak polymers.

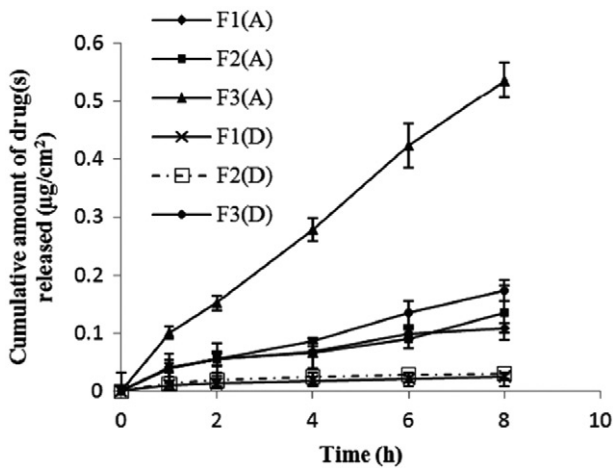


Figure 6. Cumulative amount of drug(s) released versus time (h).

Further, this could also help the slow release of drug(s) from the patches due to the modulation of drug-diffusion pathways.

Studies for various physico-chemical characterizations, including the average mass, thickness, diameter and the mean area of the patches, their moisture content, moisture-uptake capabilities, surface pH, etc. were carried out. The prepared patches were considerably thin and small in size (Morales & McConville, 2011). Low average mass of the experimental formulations suggests that the formulations were light and will not be uncomfortable to patients for their use.

The moisture content study is done to understand how much moisture is present in a formulation and moisture absorption study represents the capability of a formulation to hold maximum content of moisture when the formulation is exposed to a highly humid climate (Arora & Mukherjee, 2002). In this study, the low mean percent moisture content prevents dryness and brittleness of the formulation (Arora & Mukherjee, 2002). The moisture absorption study shows that the prepared polymeric formulations with duro-tak[®] 387-2516 and duro-tak[®] 387-2051 in 4:5 ratio (by volume) may absorb about one tenth of their weight of moisture maximally when exposed to a highly humid climate such as exposure to saliva. This suggests that upon the application of the experimental patch on the mucosa in the buccal cavity the patch will not be unnecessarily bulky due to saliva. This may cause comfort to patients for its use. Results of the folding endurance suggest that structural integrity of the formulations was maintained (Priya et al., 2011). Further, the experimental patches did not alter their physical structures or any visible decay or loss of the portion of the formulations was observed upon their exposure to simulated saliva for 8 h. The findings indicate that the patches maintained their structural integrity in simulated saliva.

Bioadhesive strength indicates the capability of a formulation to adhere to a tissue surface by forming physical bonds. The good mucoadhesive properties are generally strongly exhibited when functional groups with H-bond such as –OH, –COOH, etc., are present in mucoadhesive polymers (Smart, 2005; Baddupalli et al., 2010). Duro-tak[®] polymers used here are acrylate-vinylacetate polymers constituted

with acrylic acid, methyl acrylate, and 2-ethylhexyl acrylate (Mukherjee et al., 2006) with the presence of functional groups –OH, and –COOH to provide desired pressure-sensitive tacking effect to remain attached to the oral mucosa, tooth and gum for a long period (Baddupalli et al., 2010). Depending on the bond formation between polymers (polymer matrix) and tissue (here mucosa), bioadhesion varies (Abu-Huwajj et al., 2011). If bonds form too strongly, the patches cannot be removed easily from mucosa and if it is too weak, it will not remain attached to mucosa even for a short while. In our experiment, the obtained data of bioadhesive strength (Baddupalli et al., 2010) suggests that the formulation will remain attached to buccal mucosa for a long period, and can be removed easily by applying a little force, which, however, will not damage the tissue.

Again surface pH of the formulations was well within the range of buccal pH (Cavallari et al., 2013), indicating no pH related irritation will occur upon the application of the patches on the buccal mucosa.

The results of SEM study show that the two types of drug were scatteredly distributed in particulate form in the patches. Presence of number of holes in the patches might be due to the release of maximum amount of drug(s) from the distributed drug particles in the patches. Fissures on the patches were seen upon removal of patches from the tissues in some cases and they might be formed due to more intimate contact of the polymers to the tissues at those sites. When the patches were applied on the buccal tissue of goat for 8 h, it was observed that there was no histological alteration of mucosal and submucosal tissue architecture at the application sites of the patches and in nearby tissue areas. This suggests that the patches did not cause any undesirable effect on the buccal tissues at least when it was applied for 8 h.

Addition of release enhancers (tween 80 and PEG 400) in the oral mucoadhesive patches appreciably improved cumulative percent drug(s) release *in vitro* (ranges from 10–53% for amoxicillin trihydrate and 2–17% for diclofenac sodium) during 8 h of the drug release study. Incorporation of drug release enhancers in the formulations might enhance considerable polymer hydration (Escobar-Chávez et al., 2012) than those without drug release enhancer. Variable drug release kinetic patterns as assessed by various kinetic models show that more linearity (by assessing R^2 values) of the drug release kinetic plots was towards Higuchi and Hixson-Crowell models. Further, the data suggest that presence of release enhancers affected drug release behavior and tween 80 was found to be most effective out of the chosen drug release enhancers in the study (Siegel et al., 1981).

In the stability study, formulations were kept at 30 °C and 40 °C with 75% RH as per ICH guidelines. The formulations were taken out from the stability chambers after 2nd and 3rd month and FTIR spectra of them were determined. These spectra were compared with the FTIR spectra of freshly prepared formulations. No predominant alteration in the FTIR spectra of the stored formulations with respect to freshly prepared formulation was detected. The result indicates that no new chemical interaction took place between the drug(s) and the excipients. Hence, the formulations were stable at least up to 3 months at 30 °C and 40 °C at 75% RH (i.e. the time period of this study conducted).

Conclusions

The prepared pressure-sensitive mucoadhesive dental patches were found to release the drugs in a controlled manner for a prolonged period *in vitro* and this would be suitable to treat periodontal disease locally. They were found to possess desired mucoadhesiveness with easy administration and removal. They did not damage the buccal mucosa or submucosa morphologically upon application for a prolonged period. Among the experimental oral mucoadhesive dental patches, F3 containing duro-tak(s) at ratio of 4:5 (by volume) along with tween 80 (1% v/v) as release enhancer provided the best drug release profile over the period of 8 h. The formulations subjected for temperature dependant stability study at 30 °C and 40 °C, respectively, at 75% RH suggest that drug would remain stable in the formulations at least up to 3 months. Further study may be necessary in this direction to carry out the *in vivo* toxicity study in a suitable animal model and to establish a suitable *in vitro* and *in vivo* correlation.

Acknowledgements

The authors are thankful to Dey's Medical Stores (Manufacturing) Ltd., Kolkata, India for providing facilities to conduct stability studies.

Declaration of interest

The authors confirm that this article content has no conflicts of interest. The authors are thankful to All India Council for Technical Education, New Delhi India for sponsoring this project (Grant No: D-7/E/268/10).

References

Abu-Huwajj R, Obaidat RM, Sweidan K, Al-Hiari Y. (2011). Formulation and *in vitro* evaluation of xanthan gum or carbopol 934-based mucoadhesive patches, loaded with nicotine. *AAPS Pharm Sci Tech* 12:21–7.

Ahuja A, Ali J, Rahman S. (2006). Biodegradable periodontal intra-pocket device containing metronidazole and amoxicillin: formulation and characterization. *Pharmazie* 61:25–9.

Andrews GP, Laverty TP, Jones DS. (2009). Mucoadhesive polymeric platforms for controlled drug delivery. *Eur J Pharm Biopharm* 71: 505–18.

Arora P, Mukherjee B. (2002). Design, development, physicochemical and *in vitro* and *in vivo* evaluation of transdermal patches containing diclofenac diethylammonium salt. *J Pharm Sci* 91:2076–89.

Baddupalli B, Mohammed ZNK, Ravindar Nath A, Banji D. (2010). Mucoadhesive drug delivery system: an overview. *J Adv Pharm Tech Res* 1:381–7.

Bascones MA, Figuero RE. (2004). Periodontal diseases: microbiological considerations. *Med Oral Patol Oral Cir Bucal* 9:S75–91.

Basu S, Mukherjee B, Chowdhury SR, et al. (2012). Colloidal gold-loaded, biodegradable, polymer-based stavudine nanoparticle uptake by macrophages: an *in vitro* study. *Int J Nanomedicine* 7:6049–61.

Bruschi ML, Freitas OD. (2005). Oral bioadhesive drug delivery systems. *Drug Dev Ind Pharm* 31:293–310.

Bucci R, Magri AD, Magri AL. (1998). Determination of diclofenac salts in pharmaceutical formulations. *Fresenius J Anal Chem* 362:577–82.

Cavallari C, Fini A, Ospitali F. (2013). Mucoadhesive multiparticulate patch for the intrabuccal controlled delivery of lidocaine. *Eur J Pharm Biopharm* 83:405–14.

Chopparapu KS, Reddy PC, Doodipala N, Rao YM. (2012). Development of promethazine hydrochloride mucoadhesive patches for buccal delivery: *in vitro*, *ex vivo* and *in vivo* characterization. *Int J Pharm Sci Nanotech* 5:1697–705.

Costa P, Lobo JMS. (2001). Modeling and comparison of dissolution profiles. *Eur J Pharm Sci* 13:123–33.

Damodharan N, Roy G, Ghosh S, Mukherjee B. (2010). Skin permeation of rosiglitazone from transdermal matrix patches. *Pharm Technol* 34: 56–72.

Escobar-Chávez JJ, Rodríguez-Cruz IM, Domínguez-Delgado CL. (2012). Chemical and physical enhancers for transdermal drug delivery. In: Gallelli L, ed. *Pharmacology*. Serbia: InTech, Inc., 397–434.

Gandhi RB, Robinson JR. (1994). Oral cavity as a site for bioadhesive drug delivery. *Adv Drug Deliv Rev* 13:43–74.

Ghosh S, Roy G, Mukherjee B. (2009). Dental mold: a novel formulation to treat common dental disorders. *AAPS Pharm Sci Tech* 10:692–702.

Gupta A, Garg S, Khar RK. (1992). Measurement of bioadhesive buccal tablets: design of an *in vitro* assembly. *Indian Drugs* 30:152–5.

Gupta R, Mukherjee B. (2003). Development and *in vitro* evaluation of diltiazem hydrochloride transdermal patches based on povidone-ethylcellulose matrices. *Drug Dev Ind Pharm* 29:1–7.

Hearnden V, Sankar V, Hull K, et al. (2012). New developments and opportunities in oral mucosal drug delivery for local and systemic disease. *Adv Drug Deliv Rev* 64:16–28.

Herrera D, Alonso B, Leo'n R, et al. (2008). Antimicrobial therapy in periodontitis: the use of systemic antimicrobials against the subgingival biofilm. *J Clin Periodontol* 35:45–66.

Hoogstraate AJ, Verhoef JC, Tuk B, et al. (1996). Buccal delivery of fluorescein isothiocyanate-dextran 4400 and the peptide drug buserelin with glycodeoxycholate as an absorption enhancer in pigs. *J Control Release* 41:77–84.

International Conference on Harmonisation of Technical Requirements for Registration of Pharmaceuticals for Human Use. Stability testing of new drug substances and products Q1A (R2). Current Step 4 version dated 6 November 2003.

Khanna R, Agarwal SP, Ahuja A. (1997). Preparation and evaluation of mucoadhesive buccal films of clotrimazole for oral candida infections. *Indian J Pharm Sci* 59:299–305.

Lockhart PB, Brennan MT, Thornhill M, et al. (2009). Poor oral hygiene as a risk factor for infective endocarditis related bacteremia. *Am Dent Assoc* 140:1238–44.

Morales JO, McConville JT. (2011). Manufacture and characterization of mucoadhesive buccal films. *Eur J Pharm Biopharm* 77: 187–99.

Mukherjee B, Das S, Patra B, Layek B. (2006). Nefopam containing transdermal-matrix patches based on pressure-sensitive adhesive polymers. *Pharm Technol* 30:146–63.

Mukherjee B, Ghosh S, Das T, Doloi M. (2005). Characterization of insulin-like-growth factor II (IGF II) mRNA positive hepatic altered foci and IGF II expression in hepatocellular carcinoma during diethylnitrosamine-induced hepatocarcinogenesis in rats. *J Carcinog* 4:1–14.

Mukherjee B, Roy G, Ghosh S. (2009). Development of denticap, a matrix based sustained release formulation for treatment of toothache, dental infection and other gum problem. *Curr Drug Deliv* 6:199–207.

Mukherjee B, Santra K, Pattnaik G, Ghosh S. (2008). Preparation, characterization and *in-vitro* evaluation of sustained release protein-loaded nanoparticles based on biodegradable polymers. *Int J Nanomedicine* 3:487–96.

Nafee NA, Ismail FA, Boraie NA, Mortada LM. (2003). Design and characterization of mucoadhesive buccal patches containing cetylpyridinium. *Acta Pharm* 53:199–212.

Nafee NA, Ismail FA, Boraie NA, Mortada LM. (2004). Mucoadhesive buccal patches of miconazole nitrate: *in vitro/in vivo* performance and effect of ageing. *Drug Dev Ind Pharm* 30:985–93.

Nair AB, Kumria R, Harsha S, et al. (2013). *In vitro* techniques to evaluate buccal films. *J Control Release* 166:10–21.

Obaidat RM, Bader A, AL-Rajab W, et al. (2011). Preparation of mucoadhesive oral patches containing tetracycline hydrochloride and carvacrol for treatment of local mouth bacterial infections and candidiasis. *Sci Pharm* 79:197–212.

Özgüney IS, Karasulu HY, Kantarcı G, et al. (2006). Transdermal delivery of diclofenac sodium through rat skin from various formulations. *AAPS Pharm Sci Tech* 7:E1–7.

Paster BJ, Boches SK, Galvin JL, et al. (2001). Bacterial diversity in human subgingival plaque. *J Bacteriol* 183:3770–83.

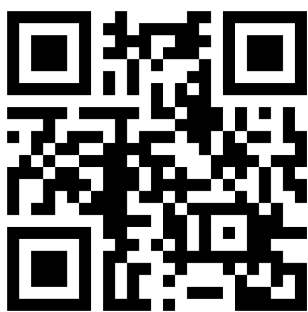
- Pattnaik G, Sinha B, Mukherjee B. (2012). Submicron-size biodegradable polymer-based didanosine particles for treating HIV at early stage: an *in vitro* study. *J Microencapsul* 29:666–76.
- Peccok RL, Shields LD, Cairns T, Mc William IG. (1968). *Modern methods of chemical analysis*. 2nd ed. New York, NY: John Wiley & Sons.
- Priya S, Mahalaxmi R, Udupa N, et al. (2011). Preparation and evaluation of buccal mucoadhesive patch of betamethasone sodium phosphate for the treatment of oral submucous fibrosis. *J Chem Pharm Res* 3:56–65.
- Puratchikody A, Prasanth VV, Mathew ST, Ashok Kumar B. (2011). Development and characterization of mucoadhesive patches of salbutamol sulfate for unidirectional buccal drug delivery. *Acta Pharm* 61:157–70.
- Rudra A, Manasa Deepa R, Ghosh MK, et al. (2010). Doxorubicin-loaded phosphatidylethanolamine conjugated nanoliposomes: *in vitro* characterization and their accumulation in liver, kidneys, and lungs in rats. *Int J Nanomedicine* 5:811–23.
- Siegel IA, Izutsu KT, Watson E. (1981). Mechanisms of non-electrolyte penetration across dog and rabbit oral mucosa *in vitro*. *Arch Oral Biol* 26:357–61.
- Silverstein RM, Webster FX. (1998). *Spectrometric Identification of Organic Compounds*. 6th ed. New York, NY: John Wiley & Sons.
- Smart JD. (2005). The basics and underlying mechanisms of mucoadhesion. *Adv Drug Deliv Rev* 57:1556–68.
- Tong DC, Rothwell BR. (2000). Antibiotic prophylaxis in dentistry: a review and practice recommendations. *JADA* 131:366–74.

Colloidal gold-loaded, biodegradable, polymer-based stavudine nanoparticle uptake by macrophages: an in vitro study

Sumit Basu^{1,2}
Biswajit Mukherjee¹
Samrat Roy Chowdhury¹
Paramita Paul¹
Rupak Choudhury³
Ajeet Kumar¹
Laboni Mondal¹
Chowdhury Mobaswar
Hossain¹
Ruma Maji¹

¹Department of Pharmaceutical Technology, Jadavpur University, Kolkata, India; ²Department of Pharmacological and Pharmaceutical Sciences, College of Pharmacy, University of Houston, Houston, TX, USA; ³Department of Biochemistry, Ballygunge Science College, Kolkata, India

→ Video abstract



Point your SmartPhone at the code above. If you have a QR code reader the video abstract will appear. Or use: <http://dx.doi.org/10.2147/IJN.S38013>

Correspondence: Biswajit Mukherjee
Department of Pharmaceutical
Technology, Jadavpur University,
Kolkata 700032, India
Tel/fax +91 33 2414 6677
Email biswajit55@yahoo.com

Objective: We describe the development, evaluation, and comparison of colloidal gold-loaded, poly(D,L-lactic-co-glycolic acid)-based nanoparticles containing anti-acquired immunodeficiency syndrome drug stavudine and uptake of these nanoparticles by macrophages in vitro.

Methods: We used the following methods in this study: drug-excipient interaction by Fourier transform infrared spectroscopy, morphology of nanoparticles by field-emission scanning electron microscopy, particle size by a particle size analyzer, and zeta potential and polydispersity index by a zetasizer. Drug loading and in vitro release were evaluated for formulations. The best formulation was incorporated with fluorescein isothiocyanate. Macrophage uptake of fluorescein isothiocyanate nanoparticles was studied in vitro.

Results: Variations in process parameters, such as speed of homogenization and amount of excipients, affected drug loading and the polydispersity index. We found that the drug was released for a prolonged period (over 63 days) from the nanoparticles, and observed cellular uptake of stavudine nanoparticles by macrophages.

Conclusion: Experimental nanoparticles represent an interesting carrier system for the transport of stavudine to macrophages, providing reduced required drug dose and improved drug delivery to macrophages over an extended period. The presence of colloidal gold in the particles decreased the drug content and resulted in comparatively faster drug release.

Keywords: stavudine, poly(D,L-lactic-co-glycolic acid), nanoparticles, colloidal gold, uptake by macrophages

Introduction

Optimization of the pharmacological action of a drug along with reduction in its toxic side effects is a prime prerequisite for an ideal drug-delivery system. Colloidal drug carriers can provide site-specific or targeted drug delivery along with optimal drug release.¹ Among these carriers, nanoparticles and liposomes have been widely investigated. Due to various technical problems, such as poor stability and low entrapment efficiency of liposomes, polymeric nanoparticles were proposed as a suitable alternative. One of the most attractive areas of research using polymeric nanoparticles is the controlled delivery of drug following parenteral, oral, pulmonary, nasal, and topical routes of administration. Polymeric nanoparticles can also be targeted to specific cells and tissues in the body by virtue of their small size and by functionalizing their surface with polymers and appropriate ligands.² Further, polymeric nanoparticles usually overcome stability issues of liposomes and can minimize the therapeutic dose and thus minimize drug-induced side effects by sustained drug release.³ A diverse range of materials has been used as drug carriers, including polymers⁴ and dendrimers,⁵ and nanomaterials

such as nanotubes,⁶ nanorods,⁷ and nanoparticles.⁸ Gold nanoparticles provide promising scaffolds for drug and gene delivery. Their unique features, such as tunable core size, monodispersity, large surface-to-volume ratio, and easy functionalization with virtually any molecule or biomolecule enable their effective targeting, transport, and tuning of delivery processes.⁹ Gold nanoparticles are the preferred delivery system because of their relatively lesser intrinsic toxicity toward the normal cell.⁹

Nanoparticles consisting of gold offer enhanced absorption and scattering, good biocompatibility, facile synthesis,⁴ and conjugation to a variety of biomolecular ligands, antibodies, and other targeting moieties,⁵ making them suitable for use in biochemical sensing and detection,^{10–12} medical diagnostics, and therapeutic applications.^{13,14}

Acquired immunodeficiency syndrome (AIDS) is a disease of the human immune system caused by the human immunodeficiency virus (HIV).⁴ This condition progressively reduces the effectiveness of the immune system and leaves the individual susceptible to opportunistic infection and tumor. It is transmitted through direct contact of a mucous membrane or the bloodstream with a bodily fluid containing HIV, such as blood, semen, vaginal fluid, pre-seminal fluid, and breast milk.⁵ There is currently no vaccine or cure for HIV or AIDS. The only known methods of prevention are based on avoiding exposure to the virus and antiretroviral treatment once affected. The antiviral therapy has unpleasant side effects, including peripheral neuropathy, acute pancreatitis, abdominal pain, diarrhea, malaise, nausea, and fatigue. AIDS patients are generally treated with nucleoside or nucleotide reverse transcriptase inhibitors that inhibit reverse transcription by blocking the reverse transcriptase enzyme responsible for conversion from single-stranded RNA to double-stranded DNA in HIV. Zidovudine, didanosine, zalcitabine, stavudine, lamivudine, and abacavir are nucleoside analogs and tenofovir and adefovir are nucleotide analogs used as reverse transcriptase inhibitors for HIV infection. These drugs have severe side effects at higher dose.

In the present study we used stavudine, which has a short half-life and poor bioavailability. Nanoparticles are used as a drug carrier for delivery of a drug to overcome the problems of short half-life, poor bioavailability, and strong side effects. In this study we developed, evaluated, and compared a poly(D,L-lactic-co-glycolic acid) (PLGA)-based nanoparticulate drug delivery system, with or without gold nanoparticles, containing stavudine. We also studied the uptake of nanoparticles by macrophages *in vitro*, since HIV

accumulates in macrophages during the early phase (first 1 to 2 years) of infection.⁶

In the present study, PLGA was used, since it is an FDA-approved biodegradable polymer capable of drug release in a sustained manner. In addition to the drug, gold nanoparticles were incorporated into the polymeric nanoparticle matrices with the following expectations: first, since a gold nanoparticle has a higher surface-to-volume ratio and gold can hold many different molecules attached physically on its surface, we wanted to see whether gold can help enhance stavudine-loading in the nanoparticle; second, gold nanoparticles and their conjugates have been reported to inhibit HIV transinfection;¹⁵ third, the presence of gold in PLGA nanoparticles can be used for imaging to localize the presence of nanoparticles in organs and tissues *in vivo*, which is the future program in the study.

Materials and methods

Materials

Stavudine was obtained from Cipla Ltd (gift sample) (Baddi, India). PLGA (85:15; molecular weight [MW] 50,000–75,000), fluorescein isothiocyanate (FITC), chloroauric acid (HAuCl₄), and trisodium citrate were purchased from Sigma-Aldrich Corporation (Bangalore, India). Polyvinyl alcohol ([PVA] MW 30,000–70,000) was obtained from SD Fine Chem Ltd (Mumbai, India). Dichloromethane (DCM) was purchased from E Merck (India) Ltd (Mumbai, India). Disodium hydrogen orthophosphate and potassium hydrogen phosphate were obtained from Process Chemical Industries (Kolkata, India). All other chemicals used were of analytic grade.

Preparation of polymeric drug-loaded nanoparticles

PVA solutions were prepared in 1.5% (1.5 g PVA in 100 mL water) and 2.5% (0.25 g of PVA in 10 mL water) concentrations. We then dissolved 250 mg PLGA in 2 mL DCM. The total amount of stavudine (Table 1) was dissolved in 0.5 mL of 2.5% PVA. The drug solution (0.5 mL) was then added drop-wise into 2 mL of the PLGA solution while homogenizing, and the mixture was homogenized (WiseTis homogenizer; Daihan Scientific Co Ltd, Seoul, South Korea) at different speeds for different formulations (Table 1) for 4 minutes. This resulted in a water-in-oil (w/o) type of emulsion. The emulsion was gradually added to 75 mL of 1.5% PVA solution and homogenized at the same speed according to the formulation for 6 minutes, which produced a water-in-oil-in-water (w/o/w) type of emulsion. The emulsion

Table 1 Composition of experimental nanoparticles with their drug loading and entrapment efficiency

Formulation code	Stavudine:PLGA (mg:mg)	Presence of colloidal gold	Speed of homogenization (rpm)	Amount recovered ^a (mg)	Drug loading ^b (%)	Entrapment efficiency ^c (%)
S1	20:250	No	15,000	165.4	5.69	76.83
S2	20:250	Yes	15,000	187.2	5.08	68.57
S3	25:250	No	16,000	150	7.93	87.23
S4	25:250	Yes	16,000	186.6	6.15	67.63
S5	0:250	No	15,000	152	NA	NA

Notes: ^aRecovery (mg) = amount of lyophilized formulation obtained (mg) out of total amount of drug and excipients used (mg); ^bDrug loading (actual) (%) = Amount of drug in nanoparticles \times 100/Amount of nanoparticles obtained; ^cDrug entrapment efficiency (%) = Drug loading (actual) (%) \times 100/Drug loading (theoretical) (%).

Abbreviations: NA, not applicable; PLGA, poly(d,l-lactic-co-glycolic acid).

was stirred at 130 rpm in a rotary vacuum evaporator (PBU-6; Superfit, Mumbai, India) with a temperature-controlled water bath (40°C) for 30 minutes for quick removal of the organic solvent (DCM). The emulsion was kept on a magnetic stirrer overnight for complete removal of the DCM. The next day, any particles that had formed were collected by centrifugation at 15,000 rpm for 1 hour. To remove free drug, polymeric particles were resuspended in water and centrifuged three times at 15,000 rpm for 30 minutes each. Particles were then freeze-dried (by prefreezing at -20°C overnight and lyophilizing at -40°C for 12 hours) in a lyophilizer (laboratory lyophilizer; IIC Industrial Corporation, Kolkata, India) and stored at 4°C. Formulations S1, S2, and S5 were prepared as described above, except that S3 and S4 were centrifuged at 16,000 rpm and no drug was added to S5.

Preparation of gold nanoparticles

Gold nanoparticles were prepared by citrate reduction of HAuCl₄ following the methods of Storhoff et al.⁷ All glass-ware were first cleaned in aqua regia (three parts HCl, one part HNO₃), rinsed with nanopure water, and dried in a hot air oven (Orion Industries, Kalka, India). An aqueous solution of HAuCl₄ (1 mM, 500 μ L) was brought to boiling while stirring continuously with a glass rod, and the entire 50 mL aliquot of 38.8 mM trisodium citrate solution was quickly added, which resulted in a color change of the solution from pale yellow to deep red. After the color change, the solution was allowed to cool and was subjected to high-speed centrifugation (3K30 Sigma Lab Centrifuge; Merrington Hall Farm, Shrewsbury, UK) at 12,800 rpm at 4°C for 20 minutes. The gold nanoparticle pellet was then resuspended in water at pH 7.0 after discarding the supernatant. The process was repeated three times to eliminate the free citrate.⁸

Preparation of gold and drug-loaded polymeric nanoparticles

PVA solutions were prepared in 1.5% (by dissolving 1.5 g PVA in 100 mL water) and 2.5% (by dissolving 0.25 g of PVA

in 10 mL water) concentrations. Colloidal gold solution (1 mL) was added to the 2.5% PVA solution. PLGA (250 mg) was dissolved in 2 mL DCM. The total amount of stavudine (Table 1) was dissolved in 0.5 mL of the 2.5% PVA-gold mixture. This drug solution (0.5 mL) was added drop-wise into 2 mL of the PLGA solution, and the mixture was homogenized at different speeds for different formulations (Table 1) for 4 minutes. The preparation method was then continued as described previously. To remove uncoated gold nanoparticles from suspension after encapsulation, the mixture was centrifuged at 6000 rpm for 1 hour. The supernatant was decanted carefully, and coated nanoparticles were separated from the supernatant by centrifugation at 15,000 rpm for 1 hour and then washed three times by centrifuging at 15,000 rpm and resuspending in water. Formulations S2 and S4 were prepared as described above, except that S4 was centrifuged at 16,000 rpm.

Nanoparticles with FITC

Stavudine-loaded nanoparticles were prepared with a fluorescent probe (FITC) to study the uptake of nanoparticles by specific cells. FITC-loaded nanoparticles were prepared essentially as described above, except that an FITC stock solution (0.4% weight [w]/volume [v] FITC in absolute ethanol) of 100 μ L was added to the polymeric phase during the preparation of the primary emulsion. The ratio of the fluorophore to nanoparticles taken was 1:80. Preparation was then continued as described above.

Evaluation and characterization of stavudine-loaded nanoparticles

Drug-excipt interactions by Fourier transform infrared spectroscopy (FTIR)

Stavudine, PLGA, PVA, gold nanoparticles, PLGA-PVA combination, stavudine-PLGA-PVA combination, and stavudine-PLGA-PVA-gold nanoparticles combination were mixed with infrared-grade potassium bromide (KBr)

and compressed into pellets by applying 5.5 t of pressure in a hydraulic press. The pellets were scanned over a wavenumber range of 4000 cm^{-1} to 400 cm^{-1} in an FTIR spectrometer (MAGNA-IR 750; Nicolet Instruments Corporation, Madison, WI).

Morphology of nanoparticles by field-emission scanning electron microscopy (FESEM)

The external morphology of nanoparticles of different formulations was analyzed by FESEM. The freeze-dried particles were spread onto metal stubs and platinum coating applied by using an ion-sputtering device. The coated particles were then examined under FESEM (JSM 6100; JEOL, Tokyo, Japan).

Determination of presence of gold in polymeric nanoparticle by energy dispersive X-ray spectroscopy (EDX)

EDX was part of the FESEM system. SEM-EDX, which uses an SEM system, helps determine the chemical composition of a specimen, and we used this to determine the presence of gold in stavudine-gold-loaded polymeric nanoparticles.

Determination of size distribution, polydispersity index (PDI), and zeta potential

Size distribution, PDI, and zeta potential were measured by a Zetasizer Nano ZS (0.6 nm to 6000 nm) with DTS software version 4.0 (Malvern Instruments Ltd, Malvern, UK). The freeze-dried formulations were suspended in double-distilled water and then poured into a glass cuvette and analyzed. For particle size measurement, dynamic light scattering is used, and the software collects and interprets data on particle size and zeta potential and calculates the average size and PDI by using the intensity, volume, and number distribution. Mean particle diameter was calculated from the measured size distributions, and the PDI was calculated based on the size range present in the suspension as determined in a Zetasizer Nano ZS (Malvern Instruments Ltd).

Drug content and entrapment efficiency study

Exactly 2 mg of each product sample was placed in separate 2 mL Eppendorf microcentrifuge tubes. A prepared solution of 5% w/v sodium dodecyl sulfate in 1 mL 0.1 M NaOH solution was added to each tube with a micropipette. The tubes were placed in an incubator shaker (Somax Incubator Shaker; Shenzhen Pango Electronic Co, Ltd, Shenzhen, China) at 120 rpm for 3 hours at 37°C. The tubes were then centrifuged for

10 minutes at 5000 rpm and the supernatant liquid collected with a micropipette. The absorbance of drug in solution was read with an ultraviolet absorption spectroscope (Beckman Instruments, Fullerton, CA) at 266 nm against a blank containing 5% w/v sodium dodecyl sulfate in 0.1 M NaOH. Drug concentrations were determined from the calibration curve. The drug-loading and drug entrapment efficiencies were calculated using the following formulae:

$$\begin{aligned} \text{Drug loading (theoretical) (\%)} \\ = \frac{\text{Amount of drug taken to prepare nanoparticles} \times 100}{\text{Amount of PLGA} + \text{drug taken}} \end{aligned} \quad (1)$$

$$\begin{aligned} \text{Drug loading (actual) (\%)} \\ = \frac{\text{Amount of drug in nanoparticles} \times 100}{\text{Amount of nanoparticles obtained}} \end{aligned} \quad (2)$$

$$\begin{aligned} \text{Drug entrapment efficiency (\%)} \\ = \frac{\text{Drug loading (actual) (\%)} \times 100}{\text{Drug loading (theoretical) (\%)}} \end{aligned} \quad (3)$$

Drug release study

To determine drug release at the different time points, 5 mg stavudine-loaded nanoparticles of different formulations were suspended in 1 mL phosphate-buffered saline ([PBS] pH 7.4) in prelabeled microcentrifuge tubes and kept in an incubator shaker (Somax Incubator Shaker) at 37°C with constant shaking at 72 rpm after brief vortexing. Each formulation was processed in triplicate, and samples were kept for specific periods of time up to 63 days. At any particular time point, only the sample for analysis was removed from the shaker, centrifuged at 15,000 rpm for 30 min at 4°C, and drug from the supernatant was analyzed at a wavelength of 266 nm with a UV-Vis spectrophotometer (Beckman Instruments). The percentage of drug release was calculated as:

$$\begin{aligned} \text{Drug release (\%)} \\ = \frac{\text{Amount of drug released}}{\text{Amount of drug loaded in 5 mg of nanoparticle}} \times 100 \end{aligned} \quad (4)$$

Drug release kinetics study

To understand the release kinetics, data obtained from in vitro drug release studies were plotted in various kinetic models: zero order as cumulative amount of drug released versus time; first order as logarithmic value of cumulative percentage of drug remained versus time; Higuchi model as cumulative percentage of drug released versus square root

of time; Korsmeyer–Peppas model as logarithmic value of cumulative percentage of drug released versus logarithmic value of time; and Hixson–Crowell model as cube root percentage drug remained versus time.¹⁶ The *in vitro* drug release data were also fitted to the Hopfenberg model.^{17,18}

In vitro cellular uptake study

Macrophages at a density of 2.5×10^5 cells/mL were suspended in serum-free Roswell Park Memorial Institute 1640 medium (Sigma-Aldrich Corporation).¹⁵ A cell suspension of 200 μ L was placed in eight-well tissue culture plates, each well of which contained 800 μ L medium. Cells were allowed to adhere for 2 hours in a CO₂ incubator with a supply of 5% CO₂ at 37°C. The medium was then removed, and the wells were washed twice with serum-free medium. The adherent macrophages were incubated with FITC–stavudine–nanoparticles (S4) at different concentrations (300 ng/mL and 500 ng/mL of medium) in 500 μ L of fresh medium. After 4 hours, wells containing macrophages were washed twice with serum-free medium, observed under confocal laser scanning microscopy (LSM MAT 510; Carl Zeiss, Jena, Germany), and photographs taken.

Intensity of the fluorescence of the individual macrophages was quantified with a defined line and color region, analyzed using Zen software (Zen Software Ltd, Manchester, UK), and fluorescence intensity histograms generated (not shown). Image software was used to correct threshold and background levels¹⁹ and to quantify the degree of fluorescence²⁰ and the quantity of nanoparticles in cells.

The quantity of gold nanoparticles within the cells was determined using the atomic emission spectroscopy of acid-digested cells.²¹ The method ensures a highly sensitive analysis, and a comparison of gold nanoparticle uptake by all exposed cells has been successfully used to quantify the uptake of the unmodified gold nanoparticle in the range of parts per billion. At 4 hours incubation time, cell aliquots were washed twice with cold PBS (pH 7.4) by centrifugation at 4000 rpm for 10 minutes at 4°C and resuspended in cold PBS. The pellet was then collected and analyzed using the method described.²¹

Results

Drug–excipient interactions provide information on the stability of the drug in formulation, the drug-release pattern from the formulation, and the lag time of drug release.¹⁰ Among the various methods available, FTIR spectroscopy provides a methodology for examining interactions between various functional groups present in drug and excipients. The FTIR spectrum of the pure drug and individual FTIR spectrum of

PLGA, PVA, PVA–PLGA, and PVA–PLGA–drug are shown in Figure 1. Comparing the results in Figure 1A with those of Figure 1B–E, it can be seen that there was minor shifting of some of the peaks between wavenumbers 3600 cm⁻¹ and 2800 cm⁻¹, 1700 cm⁻¹ and 1800 cm⁻¹, and 750 cm⁻¹ and 500 cm⁻¹. Wavenumber 3600 cm⁻¹ to 3800 cm⁻¹ is the infrared absorption frequency stretching vibration zone of strong intensity CH₃, CH₂, CH, medium intensity = CH and = CH₂, strong intensity OH (hydrogen bonded), variable intensity OH (free), medium intensity CH (aldehyde), and weak intensity NH (1° amine) and NH (2° amine).²² Wave number 1700 cm⁻¹ to 1800 cm⁻¹ is the strong intensity stretching vibration zone of C=O (saturated aldehyde), C=O (saturated ketone), cyclopentanone, and cyclobutanone.²² Wave number 750 cm⁻¹ to 500 cm⁻¹ is the bending vibration zone of weak intensity CH₂ rocking, medium intensity out of plane = CH₂, medium intensity cis -RCH=CHR, strong intensity CH deformation, strong to medium intensity CH bending and ring puckering, weak OH out of plane bending, and variable NH₂ and NH wagging.

In stavudine, CH₃, C=O, NH, N, OH are the reactive groups, whereas in PLGA, CH₃, C=O, and =O reactive groups are present. For PVA, OH and H are the predominant reactive groups. Thus, there might be some physical interactions between the functional groups of the drug and the excipients that resulted in a minor shifting of the peaks. Formation of a weak hydrogen bond, interaction due to van der Waals force, or dipole–dipole interaction among these functional groups might be responsible for these physical interactions. The presence of the characteristic peaks of the drug and the excipients suggests that there was no chemical interaction. Further, FTIR spectra of the drug with gold mixture and of the drug with gold and other excipients showed no shifting of the characteristic peaks (data not shown). Thus, FTIR spectroscopic data suggest that there was no chemical interaction between the drug and the excipients, indicating that the polymer is suitable for formulation of the anti-AIDS drug. However, a few physical interactions occurred among some functional groups of the drug and the excipients. These might have been responsible for sustained release of the drug from the formulations and might provide information on the spherical structure of the nanoparticles.

Particles were mostly in the nanoscale range with a smooth surface; however, there were some particles larger than nanosize (Figure 2). The Z-average of S1–S5 formulations were 1365 nm, 1136 nm, 211 nm, 201 nm, and 2038 nm, respectively (Table 2); polydispersity indices of the S1–S5 formulations were 0.102, 0.109, 0.424, 0.376, and 0.046, respectively. Particle size distribution (by percentage intensity) of the

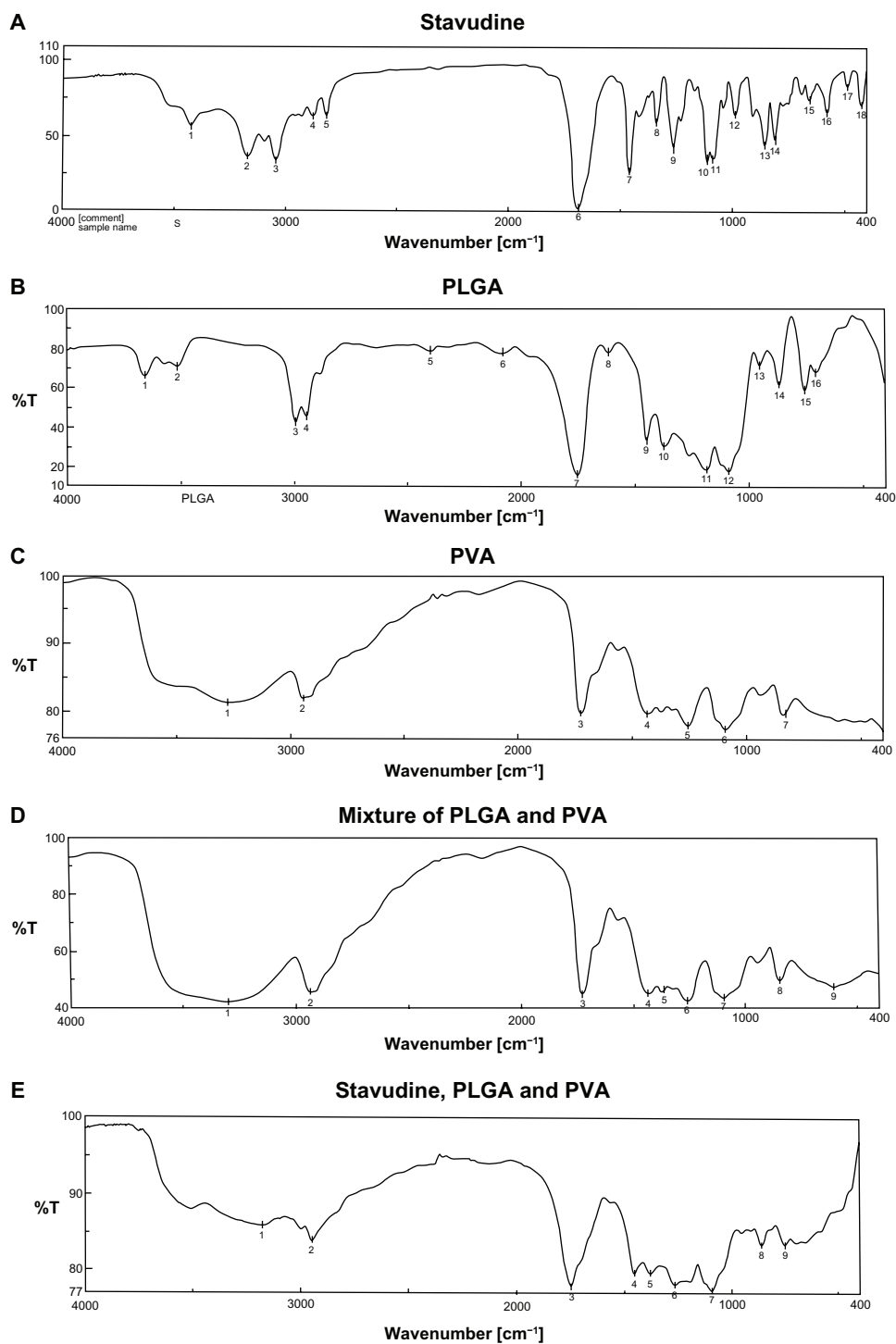


Figure 1 FTIR spectra of (A) stavudine; (B) PLGA; (C) PVA; (D) PVA and PLGA mixture; and (E) stavudine, PVA, and PLGA mixture. **Abbreviations:** FTIR, Fourier transform infrared spectroscopy; PLGA, poly(d,l-lactic-co-glycolic acid); PVA, polyvinyl alcohol.

experimental formulations are shown in Figure 3. Zeta potentials of S1–S5 were -12.6 , -8.16 , -27.8 , -19.6 , and -17 mV, respectively (Table 2). The dispersant refractive index, viscosity, and dispersant (water) dielectric constant were 1.33, 0.8872, and 78.5, respectively, at 25°C . The incorporation of gold in nanoparticles was assessed from the EDX data, which

showed the presence of gold particles in gold-encapsulated polymeric nanoparticles (Figure 4) as compared to gold nanoparticles (Figure 5) alone.

Maximum conductivity was recorded for S2 (0.034), followed by S1 (0.011) and S5 (0.012) (Table 2). However, conductivities were only slightly lower for S3 and S4.

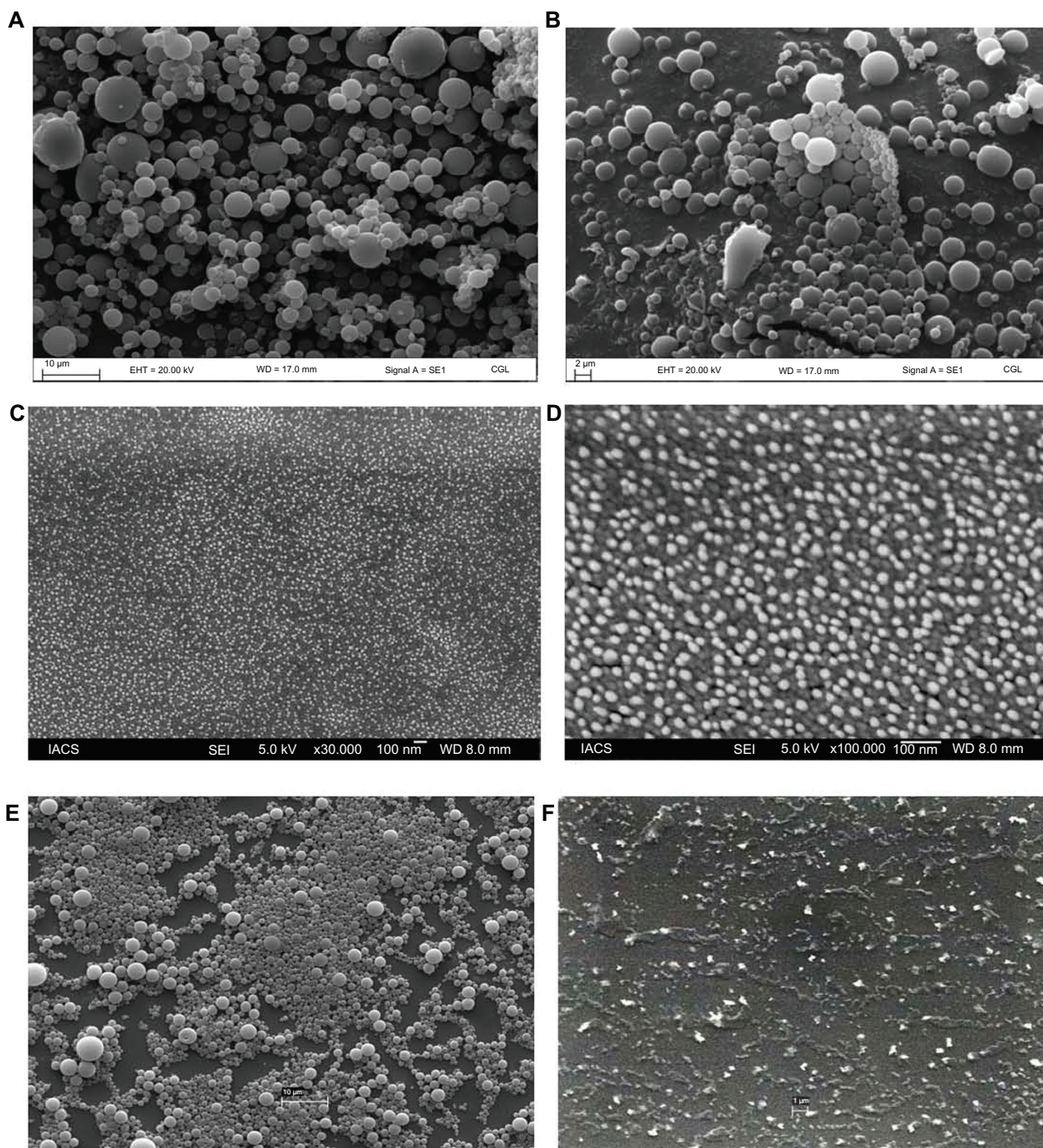


Figure 2 FESEM photographs of formulations. **(A)** Formulation S1 prepared at 15,000 rpm shows that the particles were of micrometer sizes. **(B)** Formulation S2 prepared at 15,000 rpm shows that the particles were in micron range. **(C)** Formulation S3 prepared at 16,000 rpm shows that the particles were in nanometer range. **(D)** Formulation S4 prepared at 16,000 rpm shows that the particles were in nanometer range. **(E)** Formulation S5 prepared at 15,000 rpm shows that the particles were mostly in micrometer range. **(F)** SEM photograph of the gold nanoparticles shows that the particles were in submicron range with variable sizes.

Abbreviations: FESEM, field-emission scanning electron microscopy; SEM, scanning electron microscopy.

The drug-loading values were expressed in terms of the quantity of drug entrapped in the formulations,¹¹ and the drug entrapment efficiency was associated with the percentage of drug entrapped with respect to theoretical drug loading in a particular formulation. S3 had the highest drug content and drug entrapment efficiency among the formulations S1 to S4 (Table 1).

The in vitro drug release profile of stavudine from the PLGA-based particulate drug formulations is shown in Figure 6. The cumulative amount of drug release varied between 65% and 72% of the actual drug content in the formulations for 63 days. Gold along with stavudine-loaded polymeric nanoparticles (S4) prepared at a higher homogenization

Table 2 Size distribution (Z-average [nm]), polydispersity index, zeta potential, and conductivity of experimental nanoparticulate formulations

Formulation code	Z-average (nm)	PDI	Zeta potential (mV)	Conductivity (mS/cm)
S1	1365	0.102	-12.6	0.0117
S2	1136	0.109	-8.16	0.0346
S3	211	0.424	-27.8	0.00894
S4	201	0.376	-19.6	0.00882
S5	2038	0.046	-17	0.0125

Abbreviation: PDI, polydispersity index.

speed (16,000 rpm) showed a higher percentage of drug release in 63 days compared to S3 during the same time period.

Data related to drug release as assessed by different kinetic models¹⁶ showed more linearity in R² values (Table 3) in Higuchi, Korsmeyer–Peppas, and Hopfenberg plots. This suggests anomalous diffusion of drug as well as erosion of the matrix type formulations.

Based on the size and drug-loading in gold containing PLGA nanoparticles, S4 was selected for the nanoparticle uptake study. Nanoparticle uptake by macrophages was observed in vitro after treatment of nanoparticles at two different concentrations for 4 hours (Table 4; Figure 7). As the nanoparticle concentration increased, nanoparticle uptake increased. About 34% and 45% of the nanoparticles were internalized in 4 hours at nanoparticle doses of 300 ng/mL (gold content 450 pg/0.5 × 10⁵ cells) and 500 ng/mL (gold content 867 pg/0.5 × 10⁵ cells), respectively, as assessed by fluorescence intensity.

Discussion

Stavudine-loaded PLGA nanoparticles and stavudine with colloidal gold loaded in PLGA nanoparticles were presented in this research work. PLGA nanoparticles were formulated using an emulsification solvent evaporation technique. PVA was selected as an effective stabilizer¹² and was used to stabilize the emulsion since it also helps form relatively small and uniform-sized particles.^{13,14}

FTIR spectroscopy was used for the drug–excipients interaction study to identify interactions¹⁰ at the functional group level. No chemical interaction was detected between the drug and the excipients since there was no shifting of individual characteristic peaks. However, a few physical interactions were found among some functional groups of the drug and the excipients, and these interactions might be responsible for the spherical structure of the nanoparticles and their sustained drug release.

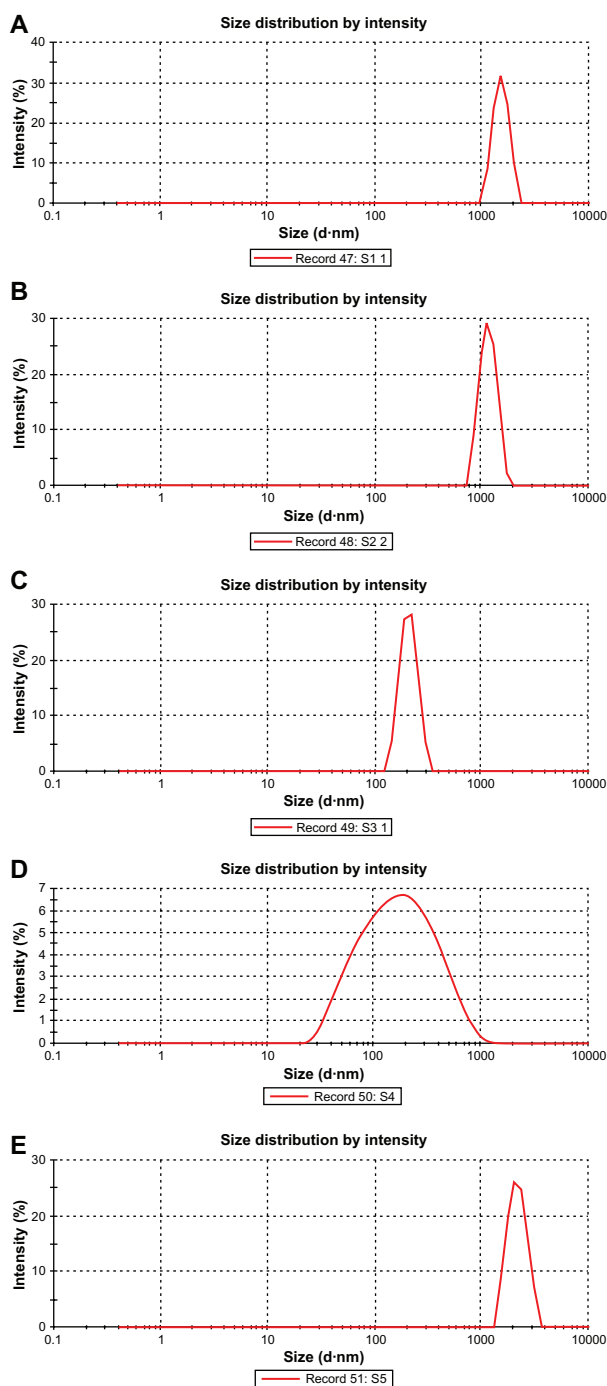


Figure 3 Size distribution of different formulations. (A) S1 (by intensity); (B) S2 (by intensity); (C) S3 (by intensity); (D) S4 (by intensity); (E) S5 (by intensity).

The experimental particles have smooth surface, and particles prepared at 15,000 rpm were larger compared to particles prepared at 16,000 rpm. The data suggest that increasing homogenization speed results in decreases to average particle diameters. Particles prepared at higher homogenizing speed were in the nanoscale range and were

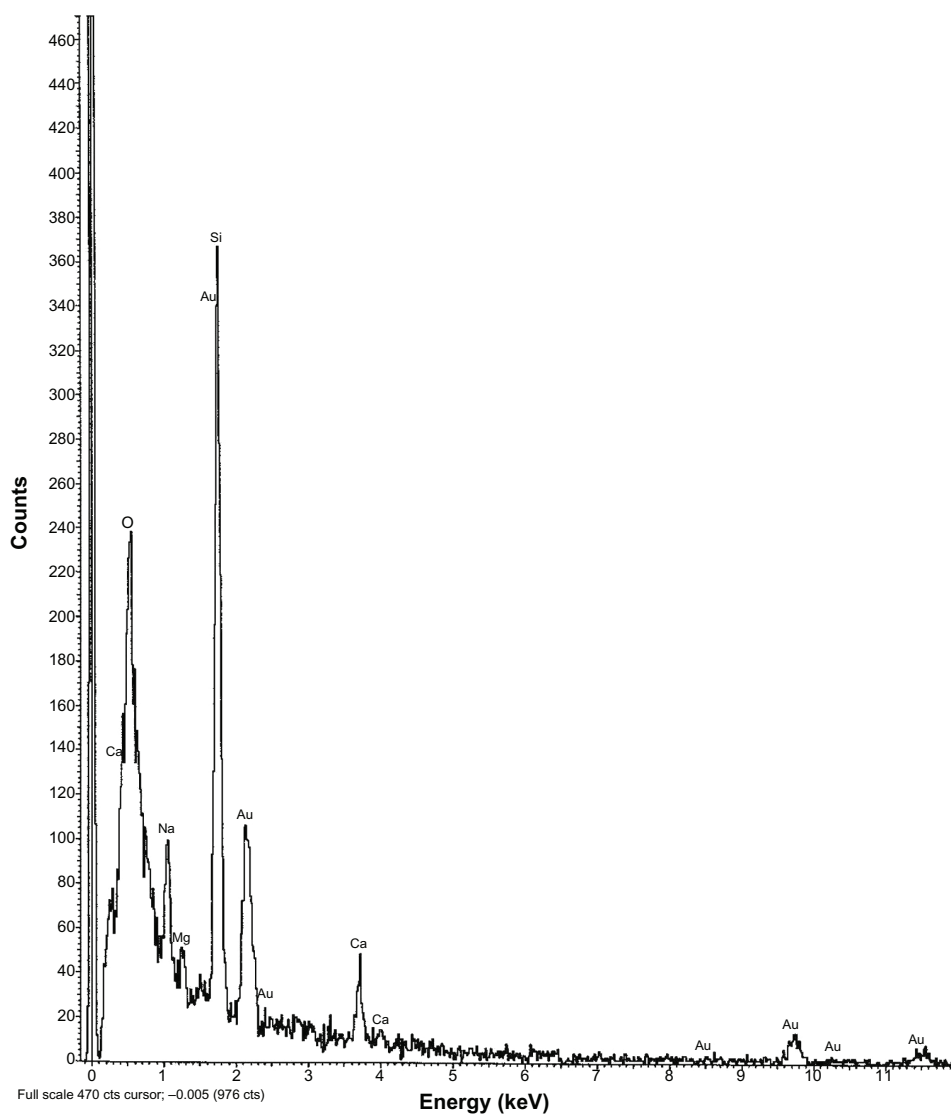


Figure 4 EDX data showing the presence of gold particles in gold-encapsulated polymeric nanoparticles.

Abbreviation: EDX, energy dispersive X-ray spectroscopy.

homogeneously distributed. Encapsulation of colloidal gold reduced the particle size even further. The incorporation of gold in the nanoparticles was confirmed by the EDX data.

An earlier study showed that polydispersity variation is present from 100 nm to as large as 20 μm .²³ In our study, polydispersity indices of the formulations varied widely. The maximum PDI value was obtained for S5. The PDI value was greater for all formulations with gold particles, suggesting that the value was enhanced due to the presence of the cationic metal.

Particles had negative zeta potentials. The resulting negative charges were caused by the dissociation of the hydrogen ion from the carboxyl group ($-\text{COOH}$) in the PLGA chain.

Addition of PVA to the formulation also conveyed a negative zeta potential to the resulting nanoparticle, further influencing both particle stability and the cellular uptake ability of the nanoparticles.^{24,25} The presence of gold particles lowered the zeta potentials of the formulation since gold is cationic.²⁶ Particles with zeta potentials greater than +30 mV and less than -30 mV are normally considered to form stable colloidal dispersion.¹⁰ If the magnitude of the zeta potential decreases, particle aggregation may occur, and this would cause a rapid precipitation of suspended nanoparticles. Our results indicate that all the formulations were unstable in terms of rapid precipitation in the colloidal state. The zeta potential values suggest that S3 had greater stability compared to the others in the dispersion state. S2 was the least stable in terms of

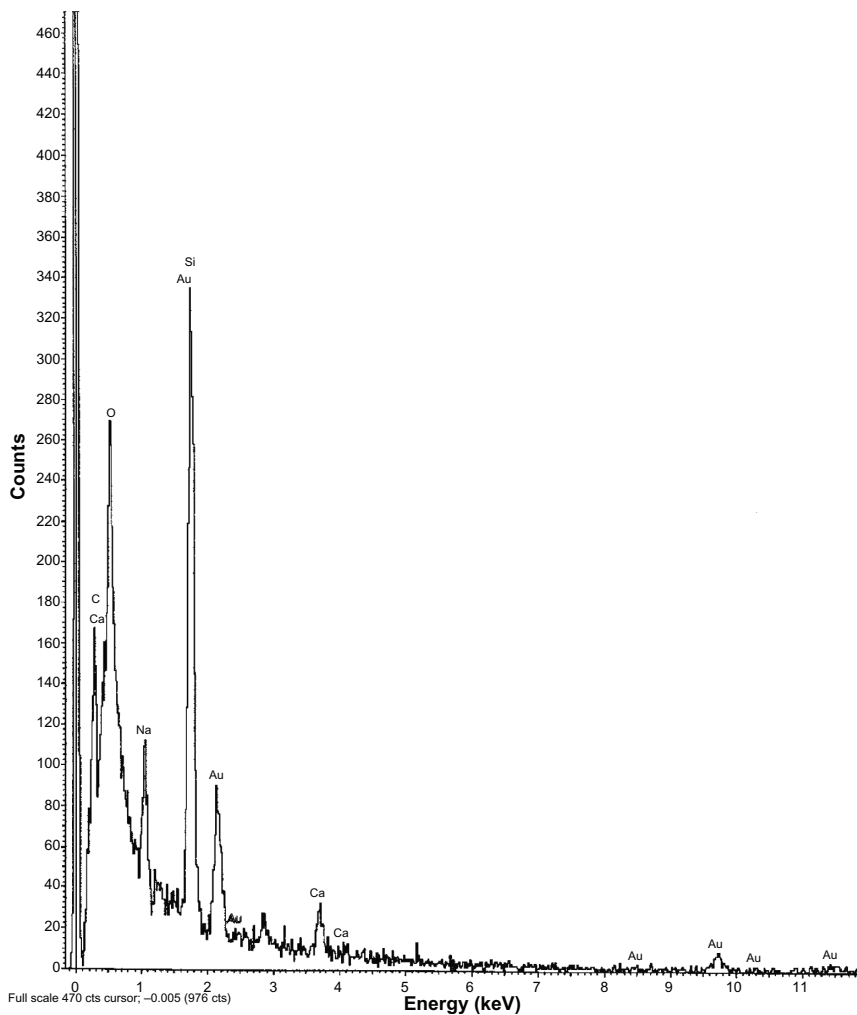


Figure 5 EDX data of colloidal gold nanoparticles alone.
 Abbreviation: EDX, energy dispersive X-ray spectroscopy.

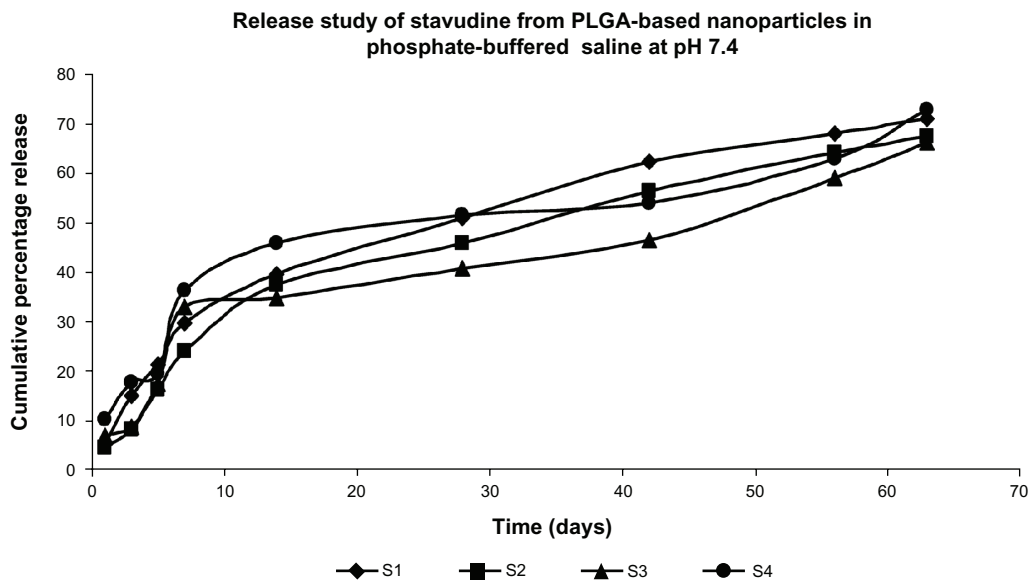


Figure 6 Release profile of didanosine from different formulations in phosphate-buffered saline (pH 7.4).
 Note: Data show means (n = 3).

Table 3 Data of drug release kinetics of various formulations

Kinetic model	Formulation S1	Formulation S2	Formulation S3	Formulation S4
Zero order	$R^2 = 0.890$ $K_0(\mu\text{g mL}^{-1} \text{h}^{-1}) = 1.0257$	$R^2 = 0.917$ $K_0(\mu\text{g mL}^{-1} \text{h}^{-1}) = 0.9542$	$R^2 = 0.886$ $K_0(\mu\text{g mL}^{-1} \text{h}^{-1}) = 0.8198$	$R^2 = 0.855$ $K_0(\mu\text{g mL}^{-1} \text{h}^{-1}) = 0.8341$
First order	$R^2 = 0.966$ $K_1(\text{h}^{-1}) = -0.0081$	$R^2 = 0.973$ $K_1(\text{h}^{-1}) = -0.0072$	$R^2 = 0.931$ $K_1(\text{h}^{-1}) = -0.0063$	$R^2 = 0.908$ $K_1(\text{h}^{-1}) = -0.0072$
Higuchi	$R^2 = 0.986$ $K_H(\text{h}^{-1/2}) = 9.2194$	$R^2 = 0.984$ $K_H(\text{h}^{-1/2}) = 8.9496$	$R^2 = 0.951$ $K_H(\text{h}^{-1/2}) = 7.8591$	$R^2 = 0.945$ $K_H(\text{h}^{-1/2}) = 8.4073$
Korsmeyer–Peppas	$R^2 = 0.825$ $n = 0.785$	$R^2 = 0.963$ $n = 0.657$	$R^2 = 0.919$ $n = 0.519$	$R^2 = 0.901$ $n = 0.453$
Hixson–Crowell	$R^2 = 0.945$ $K_{HC}(\mu\text{g}^{1/3} \text{t}^{-1}) = -0.0233$	$R^2 = 0.958$ $K_{HC}(\mu\text{g}^{1/3} \text{t}^{-1}) = -0.0212$	$R^2 = 0.918$ $K_{HC}(\mu\text{g}^{1/3} \text{t}^{-1}) = -0.0189$	$R^2 = 0.889$ $K_{HC}(\mu\text{g}^{1/3} \text{t}^{-1}) = -0.021$
Hopfenberg	$R^2 = 0.9851$ $K(\mu\text{g mg}^{-1} \mu\text{m}^{-1})\text{h}^{-1} = 0.0092$	$R^2 = 0.9679$ $K(\mu\text{g mg}^{-1} \mu\text{m}^{-1})\text{h}^{-1} = 0.0104$	$R^2 = 0.9143$ $K(\mu\text{g mg}^{-1} \mu\text{m}^{-1})\text{h}^{-1} = 0.0559$	$R^2 = 0.9199$ $K(\mu\text{g mg}^{-1} \mu\text{m}^{-1})\text{h}^{-1} = 0.1139$

forming a stable suspension, and these formulations should be stored in a lyophilized condition and reconstituted in an aqueous vehicle immediately before use.

Gold nanoparticles have a strong affinity toward sulfur of the sulfhydryl (–SH) group through covalent interaction. However, the most intriguing factor is the interaction between amine and gold nanoparticles¹⁹ as this type of interaction makes the gold nanoparticles more flexible upon attachment and release. Any electronic perturbation can tune the attachment or release of the amine-containing molecule (ie, the drug) from the gold nanoparticle surface.²⁶ In the present study drug molecules were released relatively faster from the PLGA nanoparticles containing gold. There was no physicochemical interaction detected between the drug and the gold nanoparticles, and the presence of gold in the PLGA nanoparticles reduced the size (Z-average) of the particles. Thus, the presence of gold in PLGA nanoparticles might have shortened the length of the drug diffusion pathways thereby releasing the drug relatively faster.

The drug-loading and the drug entrapment efficiencies in the formulated particles were enhanced by using an optimum amount of drug in preparatory steps²⁷ and by using the proper solvent or solvent mixture.²⁰ The drug entrapment was gradually increased with the decreasing size of nanoparticles. Our results showed that drug content was higher in drug-loaded polymeric nanoparticles without gold compared to nanoparticles with colloidal gold. No physical interaction, as assessed by FTIR, was found between drug and gold. Gold nanoparticles

allow display of a large number of carbohydrates and other similar molecules with a high density and multifunctionality by the simultaneous incorporation of different ligands in a single gold cluster in a controlled manner.²⁸ However, the lack of any distinct physicochemical interaction between the drug and the PLGA suggests that no such phenomenon took place. The presence of nanoscale-size gold particles within the polymeric nanoparticles containing drug results in less space available for the remaining drug compared to the nanoparticle containing drug without gold. Thus, the drug content was less with the polymeric nanoparticle containing gold. In addition, the presence of gold enhances the total weight of the nanoparticles, which in turn reduces the percentage of drug loading compared to the formulations without gold since the percentage of drug loading is 100 times the amount of drug present per unit quantity of nanoparticle. Thus, in spite of the presence of gold nanoparticles, which have an increased surface area to volume ratio, polymeric nanoparticles containing gold appeared to accommodate less drug molecules. In addition, drug content in the nanoparticles increased with the incorporation of more drug in the formulation. However, due to time constraints we could not determine the optimum amount of drug to achieve maximum drug loading.

In vitro drug release profiles of stavudine from PLGA nanoparticles showed that the cumulative percentage of drug release was about 70% of the drug content of the formulations in 63 days. The results support a steady and slow drug release from the experimental nanoparticles. In vitro release

Table 4 Nanoparticle (S4) uptake by macrophages

Serial no	Concentration of nanoparticles in suspension (ng/mL medium)	Effective concentration of drug (ng/mL medium)	Incubation time (hours)	Degree of nanoparticles uptake by macrophages (number of + symbols indicates the increasing degree)
1	300	17.28	4	+
2	500	28.80	4	++

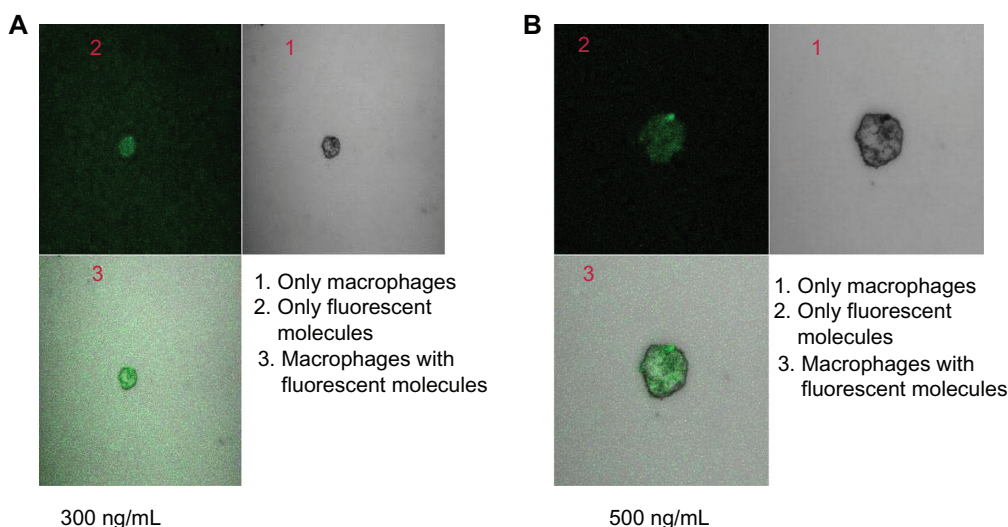


Figure 7 Confocal microscopic image of macrophages treated with (A) stavudine nanoparticles (300 ng/mL of medium) for 4 hours, and (B) stavudine nanoparticles (500 ng/mL of medium) for 4 hours.

data of stavudine from the nanoparticles were tested by the Higuchian kinetic model, which describes the release of drug from an insoluble matrix as dependent on the time based on Fickian diffusion. The release constant was calculated from the slope of the appropriate plots, and the regression coefficient was determined (Table 3). In vitro release of stavudine was best explained by Higuchi's equation as the plots showed the highest linearity followed by first-order kinetics. The corresponding plot for the Korsmeyer–Peppas equation indicated a good linearity, particularly for S3 and S4. The release exponent “n” had values in the range of 0.45 and 0.89, indicating that drug release was controlled by anomalous diffusion, ie, diffusion and erosion.^{16–18} To confirm the erosion mechanism of drug from the nanoparticles, the Hopfenberg kinetic model¹⁷ was fitted to correlate the drug release from surface-eroding polymers as long as the surface area remains constant during the degradation process. The linearity range (0.914 to 0.985) was good, suggesting that the mechanism of drug release is controlled simultaneously by diffusion and erosion.^{16–18}

Targeting of stavudine-loaded nanoparticles to macrophages has been assumed to more effectively kill HIV as the virus accumulates in macrophages.⁶ In addition, the nanoparticles were internalized by the macrophages in vitro, as assessed by FITC fluorescence intensity. Increasing the nanoparticulate concentration increased the fluorescent intensity, at least for a period of 4 hours.

Conclusion

Stavudine was released from the experimental formulations in a sustained manner over a prolonged period of time,

and this would minimize the frequency of dosing interval. A faster drug-release pattern was observed for nanoparticles containing colloidal gold compared to those without gold. The presence of colloidal gold decreased drug loading in PLGA nanoparticles. Drug release patterns appeared to follow anomalous diffusion, and macrophages, an important target group of cells in early HIV infection, were found to internalize nanoparticles (S4), suggesting that dose-related toxicity would be less. Polymer-encapsulated colloidal gold nanoparticle uptake by macrophages provides support for the use of gold nanoparticles as diagnostic and therapeutic agents, but further studies are necessary to confirm this.

Acknowledgments

We are indebted to the Department of Biotechnology, Government of India (Grant no BCIL/NER-BPMC/2012/650) and the Indian Council of Medical Research (Grant no 45/20/2011/NAN/BMS) for partially funding the research work.

Disclosure

The authors report no conflicts of interest in this work.

References

1. Kreuter J. Evaluation of nanoparticles as drug delivery systems. I. Preparation method. *Pharm Acta Helv*. 1983;58(7):196–209.
2. Wang X, Wang Y, Chen Z, Shin DM. Advances of cancer therapy by nanotechnology. *Cancer Res Tre*. 2009;41(1):1–11.
3. Soppimath KS, Aminabhavi TM, Kulkarni AR, Rudzinski WE. Biodegradable polymeric nanoparticles as drug delivery devices. *J Controlled Release*. 2001;70(1–2):1–20.
4. Sepkowitz KA. AIDS – the first 20 years. *N Engl J Med*. 2001;344(23):1764–1772.

5. Weiss RA. How does HIV cause AIDS? *Science*. 1993;260(5112):1273–1279.
6. Deneka M, Pelchen-Matthews A, Byland R, Ruiz-Mateos E, Marsh M. In macrophages, HIV-1 assembles into an intracellular plasma membrane domain containing the tetraspanins CD81, CD9, and CD53. *J Cell Biol*. 2007;177(2):329–341.
7. Storhoff JJ, Elghanian R, Mucic RC, Mirkin CA, Letsinger RL. One pot colorimetric differentiation of polynucleotides with single base imperfections using gold nanoparticle probes. *J Am Chem Soc*. 1998;120(9):1959–1964.
8. Patra HK, Banerjee S, Chaudhuri U, Lahiri P, Dasgupta AK. Cell selective response to gold nanoparticles. *Nanomedicine*. 2007;3(2):111–119.
9. Boisselier E, Astruc D. Gold nanoparticles in nanomedicine: preparations, imaging, diagnostics, therapies and toxicity. *Chem Soc Rev*. 2009;38(6):1759–1782.
10. Mukherjee B, Patra B, Layek B, Mukherjee A. Sustained release of acyclovir from nano-liposomes and nano-niosomes. *Int J Nanomedicine*. 2007;2(2):213–225.
11. Bilensoy E, Gürkaynak O, Lale Doğanand A, Atilla Hıncal A. Safety and efficacy of amphiphilic β -cyclodextrin nanoparticles for paclitaxel delivery. *Int J Pharm*. 2008;347(2):163–170.
12. Fu XD, Gao YL, Ping QN, Ren T. Preparation and in vivo evaluation of huperzine A-loaded PLGA microspheres. *Arch Pharm Res*. 2005;28(9):1092–1096.
13. Mandal TK, Bostanian LA, Graves RA, Chapman SR. Poly(D,L-lactide-co-glycolide) encapsulated poly(vinyl alcohol) hydrogel as a drug delivery system. *Pharm Res*. 2002;19(11):1713–1719.
14. Wang N, Wu XS, Li JK. A heterogeneously structured composite based on poly (lactic-co-glycolic acid) microspheres and poly (vinyl alcohol) hydrogel nanoparticles for long-term protein drug delivery. *Pharm Res*. 1999;16(9):1430–1435.
15. Arnáiz B, Martínez-Ávila O, Falcon-Perez JM, Penadés S. Cellular uptake of gold nanoparticles bearing HIV gp120 oligomannosides. *Bioconjug Chem*. 2012;23(4):814–825.
16. Pattnaik G, Sinha B, Mukherjee B, et al. Submicron-size biodegradable polymer-based didanosine particles for treating HIV at early stage: an in vitro study. *J Microencapsul*. 2012;29(7):666–676.
17. Dash S, Murthy PN, Nath L, Chowdhury P. Kinetic modeling on drug release from controlled drug delivery systems. *Acta Pol Pharm*. 2010;67(3):217–223.
18. López-Gasco P, Iglesias I, Benedí J, Lozano R, Teijón JM, Blanco MD. Paclitaxel-loaded polyester nanoparticles prepared by spray-drying technology: in vitro bioactivity evaluation. *J Microencapsul*. 2011;28(5):417–429.
19. Shan M, Klasse PJ, Banerjee K, et al. HIV-1 gp120 mannoses induce immunosuppressive responses from dendritic cells. *PLoS Pathog*. 2007;3(11):e169.
20. Falcón-Pérez JM, Nazarian R, Sabatti C, Dell' Angelica EC. Distribution and dynamics of Lamp1-containing endocytic organelles in fibroblasts deficient in BLOC-3. *J Cell Sci*. 2005;118(Pt 22):5243–5255.
21. Freese C, Gibson MI, Klok HA, Unger RE, Kirkpatrick CJ. Size- and coating-dependent uptake of polymer-coated gold nanoparticles in primary human dermal microvascular endothelial cells. *Biomacromolecules*. 2012;13(5):1533–1543.
22. Silverstein RM, Webster FX. *Spectrometric Identification of Organic Compounds*. 6th ed. New York: John Wiley & Sons; 1998:71–143.
23. Panyam J, Dali MM, Sahoo SK, et al. Polymer degradation and in vitro release of a model protein from poly (D,L-lactide-co-glycolide) nano- and microparticles. *J Control Release*. 2003;92(1–2):173–187.
24. Patil S, Sandberg A, Heckert E, Self W, Seal S. Protein adsorption and cellular uptake of cerium oxide nanoparticles as a function of zeta potential. *Biomaterials*. 2007;28(31):4600–4607.
25. Song C, Labhasetwar V, Cui X, Underwood T, Levy RJ. Arterial uptake of biodegradable nanoparticles for intravascular local drug delivery: results with an acute dog model. *J Control Release*. 1998;54(2):201–211.
26. Mocanu A, Cernica I, Tomoaia G, Bobos L-D, Horovitz O, Tomoaia-Cotisel M. Self-assembly characteristics of gold nanoparticles in the presence of cysteine. *Colloids Surf A Physicochem Eng Asp*. 2009;338(1–3):93–101.
27. Sehra S, Dhake AS. Formulation and evaluation of sustained release microspheres of poly-lactide-co-glycolide containing tamoxifen citrate. *J Microencapsul*. 2005;22(5):521–528.
28. Ojeda R, de Paz JL, Barrientos AG, Martin-Lomas M, Penadés S. Preparation of multifunctional glyconanoparticles as a platform for potential carbohydrate-based anticancer vaccines. *Carbohydr Res*. 2007;342(3–4):448–459.

International Journal of Nanomedicine

Publish your work in this journal

The International Journal of Nanomedicine is an international, peer-reviewed journal focusing on the application of nanotechnology in diagnostics, therapeutics, and drug delivery systems throughout the biomedical field. This journal is indexed on PubMed Central, MedLine, CAS, SciSearch®, Current Contents®/Clinical Medicine,

Submit your manuscript here: <http://www.dovepress.com/international-journal-of-nanomedicine-journal>

Dovepress

Journal Citation Reports/Science Edition, EMBase, Scopus and the Elsevier Bibliographic databases. The manuscript management system is completely online and includes a very quick and fair peer-review system, which is all easy to use. Visit <http://www.dovepress.com/testimonials.php> to read real quotes from published authors.

Multifunctional Systems for Combined Delivery, Biosensing and Diagnostics

Edited by

Alexandru Mihai Grumezescu

University Politehnica of Bucharest,
Bucharest, Romania



Chapter 14

Pulmonary Administration of Biodegradable Drug Nanocarriers for More Efficacious Treatment of Fungal Infections in Lungs: Insights Based on Recent Findings

Biswajit Mukherjee, Paramita Paul, Lopamudra Dutta, Samrat Chakraborty, Moumita Dhara, Laboni Mondal and Soma Sengupta

Jadavpur University, Kolkata, West Bengal, India

Chapter Outline

1	Introduction	261	7.2	Sedimentation	268
2	Lung Morphology	263	7.3	Interception	268
3	Lung Fungal Infection	263	7.4	Diffusion	268
3.1	Aspergillosis	264	7.5	Absorption	268
3.2	Fusariosis	265	8	Pulmonary Drug Delivery Devices	269
3.3	Mucormycosis	265	8.1	Nebulizer	269
3.4	Scedosporiosis	265	8.2	Compact Portable Inhaler	270
3.5	Blastomycosis	265	9	Pulmonary Formulations to Treat Lung Fungal Infection	271
3.6	Cryptococcosis	265	9.1	Liposomes	272
3.7	Coccidioidomycosis	265	9.2	Lipid Complex	272
3.8	Histoplasmosis	266	9.3	Nanoparticles	272
4	Treatment of Lung Fungal Infection	266	9.4	Nanosuspension	275
5	Clinical Status to Treat Fungal Infection by Pulmonary Route	266	9.5	Micelles	276
6	Importance of Pulmonary Route for Drug Administration	266	10	Why Pulmonary Route?	276
7	Principal Mechanisms of Respiratory Deposition	268	11	Limitations of Pulmonary Route (If Any)	276
7.1	Impaction	268	12	Conclusions	277
				References	277

1 INTRODUCTION

Ever since BC 2000, the inhalation route was exploited for the treatment of diseases. Especially Chinese and Indian people used to inhale the smoke from burned herbal preparations, such as *Ephedra sinica* or *Datura stramonium*, to treat asthma. Pedanius Dioscorides, the eminent Greek pharmacologist, botanist, and surgeon, came up with *De Materia* (first pharmacopoeia) (Andrade et al., 2013). He and Aelius Galenus (127–199/217 AD) treated their patients with sulfur vapor by inhalation route. The word *inhaler* was first coined by English physician John Mudge, in 1778 (Anderson, 2005) while

describing his invention. However, Hippocrates is recognized as the pioneer for designing the first therapeutic inhalation device. Since then, a plethora of compounds and mixtures, such as solution of picric acids, tar, iodine, have been utilized for the treatment of an array of diseases, for example, tuberculosis and other infectious diseases, by using a wide variety of methods, such as ceramic inhalers, combustible papers, burning papers, liquid atomizers, etc. During 19th and 20th centuries, asthma cigarettes became one of the popular ways to deliver drugs, but these were withdrawn in 1992 (Dessanges, 2001). According to the reports published in the literatures (Anderson, 2005; Andrade et al., 2013; Dessanges, 2001), it has been the well-known fact that antibiotic, such as penicillin, was administered by nebulization for the treatment of pulmonary infections. At the present time, inhalation devices are categorized into three different types, such as nebulizers, pressurized metered dose inhalers (pMDI), and dry powder inhalers (DPI). The inhalation route has started its journey for the treatment of diseases primarily confined into the respiratory tract. However, significant scientific and technological advances have led to a change in the paradigm and, in modern times, this route has found its potential for the treatment of a battery of local and systemic diseases, such as asthma, tuberculosis, and other bacterial infections, fungal infections, cystic fibrosis, chronic obstructive pulmonary disease, diabetes, or cancer, as well as being investigated for noninvasive vaccination (Andrade et al., 2013).

The lungs and airways, acting as principal sites of gas exchange, are exposed to a wide variety of organic, inorganic, and biological components, causing as a location for wide varieties of diseases. Therefore, the lung is very prone to an array of bacterial, fungal, and viral infections, and often it promotes systemic infections as a result. As per the mortality rate, the infections of lower respiratory tract stand on the third position globally, but they stand at the first position in developing countries, being responsible for approximately 3.5 million deaths annually (Mansour et al., 2009). This has instigated a lot of interests among the researchers around the globe to exploit the lungs for the pulmonary administration of active pharmaceutical ingredients in the form of various delivery systems. Moreover, this route offers a significant promise due to its potential advantages over peroral administrations, such as avoidance of first-pass metabolism, allowing targeted delivery to the site of action, resulting in a decrease in the side effects of the drug, high surface area responsible of local drug action, as well as systemic absorption of drugs, etc. (Yang et al., 2008a).

Among many of the existing delivery systems to become ideal carriers for pulmonary delivery, colloidal carriers (nanocarriers) have instigated a lot of interest among the researchers around the globe, due to their enormous potential as drug delivery vehicles (Andrade et al., 2013; Mansour et al., 2009; Marianecchi et al., 2011; Patton and Byron, 2007; Yang et al., 2008a). A few of them are:

1. They are very much capable of maintaining relatively uniform distribution of drugs among the alveoli.
2. They have the potential to enhance the solubility of drugs, as compared to the inherent aqueous solubility of chemical entities.
3. They provide sustained release of drugs that improves the pharmacokinetic profile of drugs, reduces dosing frequency and side effects, resulting in better therapeutic outcome and patient compliance.
4. They are biocompatible, biodegradable, as well as being able to deliver macromolecules.

Particle size solely determines the deposition of particles in different regions of lungs and, based on it, the three different mechanisms of drug deposition, namely, impaction, sedimentation, and diffusion have been proposed. In the impaction process, particles collide with the walls of the respiratory walls under the influence of the centrifugal force, and are deposited in the oropharynx region. Generally the DPI and MDI with a particle size larger than 5 μm follow this mechanism. For DPI, deposition of particles primarily depends on the inspiratory capability of patients and, if it is insufficient, dry powders deposit in the upper airways due to the mass of the particles and the inertial forces. Similarly, larger particles of MDI tend to deposit mostly in the upper respiratory tract, even under the influence of high speeds of the generated aerosols. In the case of sedimentation, the gravitational force is solely responsible, and particles with a size in the range of 1–5 μm follow this mechanism and deposit slowly in the smaller airways and bronchioles (Paranjpe and Goymann, 2014). Therefore, breathing pattern has a strong impact on the sedimentation, as it is evident that slow breathing provides sufficient duration span for sedimentation (Andrade et al., 2013; Mansour et al., 2009; Paranjpe and Goymann, 2014).

In diffusion process, Brownian motion is considered to be the major player and, due to this motion, particles move randomly, resulting in the dissolution of API in alveolar fluid upon contact with lungs surfactant, and finally deposit into deeper alveolar tissue (Yang et al., 2008a).

Nanoparticulate drug delivery systems (DDSs) deliver their therapeutic payloads through the process of sedimentation. Upon being released from the aerosol, they form aggregates that are found to have sufficient mass to sediment and deposit in the bronchiolar region.

Results obtained from many studies involving the development of nanoconstructs for pulmonary delivery, encapsulating a plethora of therapeutic payloads, are of great promise, requiring the establishment of clinical relevance in clinical trials. Apart from that, numerous other parameters, such as large-scale production, batch-to-batch reproducibility, variable lung

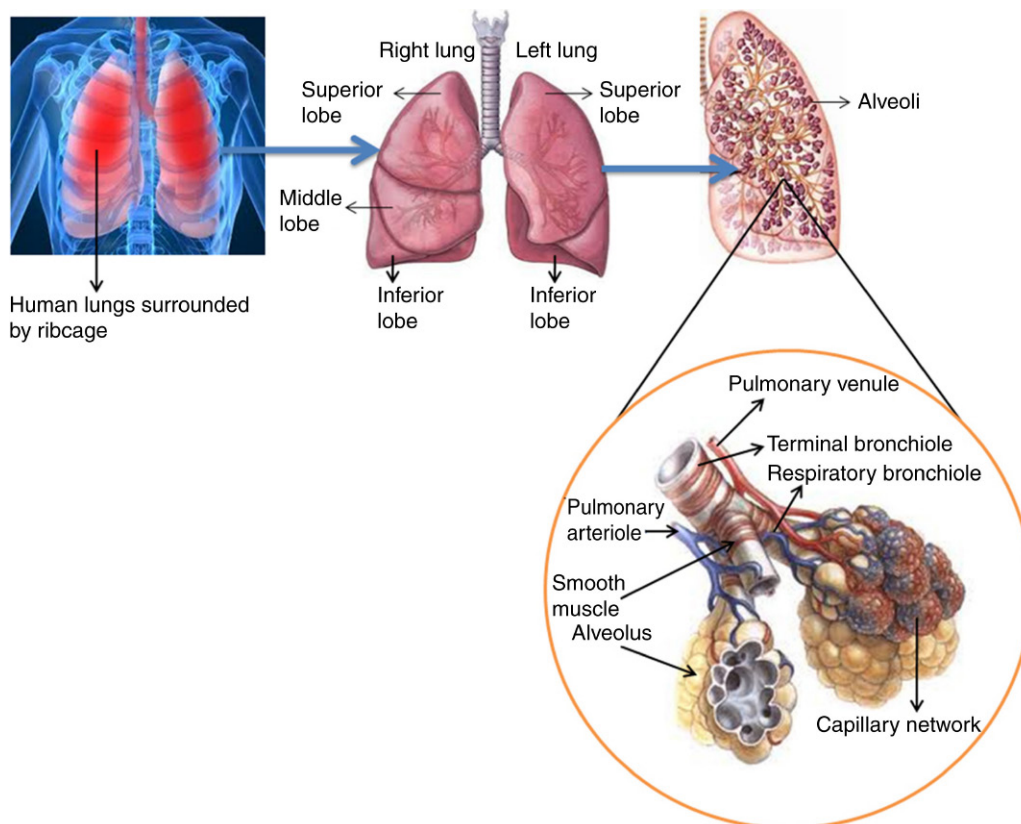


FIGURE 14.1 Diagrammatic representation of lung morphology and anatomy, showing structure of bronchioles.

deposition pattern, and cost effectiveness should be addressed properly, to ease the translation for pulmonary delivery of drug nanocarrier from laboratories to clinic.

Therefore, the focus of the present chapter is to establish the rationale and potentials of the pulmonary route for the treatment of fungal infections in lungs, for a better therapeutic management, and improved patient compliance. The chapter describes the advantages of various pulmonary delivery systems, with a special emphasis on nanocarriers.

2 LUNG MORPHOLOGY

The lungs, the gaseous exchange center of the human body, are surrounded by the chest wall, and separated by the mediastinum from the heart and other organs (positioned in the thoracic cavity) (Fig. 14.1). The left lung is constituted with two lobes, namely superior and inferior, separated by an oblique fissure, while the right lung has three lobes, that is, superior, middle, and inferior lobes, divided by oblique and horizontal fissures (Sahasrabudhe et al., 2013). The tube-like air pipe trachea acts as the passage for the air to the chest and neck; it is divided in two main branches, bronchi, each of which enters into each lung. Outside the lungs, the pleura (a balloon-like structure), the covering membrane, protects the lungs (Lai-Fook, 2004), and at the same time it produces a lubricating fluid that causes the smooth movement of lungs in the chest cavity. The main bronchi are branched into smaller bronchi that again are divided into smaller branchings known as bronchioles. The bronchi contain small glands and cartilage, while bronchioles do not contain the same. Outside the bronchi, there is a lining of cells having tiny hairs called cilia (American Lung Association, 2015). This part executes the first line of defense of lungs in fighting against bacterial or viral infection. Bronchi gradually form a tree-like branching, and become smaller. At the end part of this there is formed a grape-like structure, known as alveoli. These are small, thin air sacs that are normally surrounded by a “hair net” of capillaries. The alveolar walls are mostly constituted with type I alveolar squamous cell through which exchange of gas occurs.

3 LUNG FUNGAL INFECTION

Lungs are susceptible to fungal infections, as it is a primary passage of fungi causing deep mycosis (Panda, 2004). Several types of lung fungal infections are described further.

3.1 Aspergillosis

In recent years, aspergillus infection in lungs is very predominant. The reason may be primarily due to various factors, such as random use of corticosteroids and various immunomodulating drugs, increasing human immunodeficiency virus infection, large number of immunosuppressed patients caused by solid organs and bone marrow transplantation, etc. *Aspergillus* species are the main causative agent of aspergillosis (Thompson and Patterson, 2008). Its pathological reactions can be manifested in humans in different ways, such as allergic bronchopulmonary aspergillosis (ABPA), allergic alveolitis, aspergilloma, invasive aspergillosis, etc. (Davies and Saros, 1994; Fraser et al., 1994; Panda, 2004).

3.1.1 Allergic Bronchopulmonary Aspergillosis

ABPA, a hypersensitive reaction as aspergillus forms colonies in the bronchi, is the most common manifestation of aspergillus pulmonary disease (Greenberger, 2002). The main cause of its occurrence is due to abrupt inhalation of a large amount of aspergillus spores. Prolonged contact to aspergillus spores may exaggerate immune-mediated bronchial pathology, and often this may lead to asthma. This is generally known as ABPA. It is found that more than 20% of asthma cases exhibit ABPA (Panda, 2004).

3.1.2 Allergic Alveolitis

As described earlier, this is also caused by rapid inhalation of a huge quantity of aspergillus spores, and it is mostly manifested among the people working in moldy hay or managing compost dumps. The symptoms of allergic alveolitis, likely in form of influenza and dry cough, may appear 4–9 days later (Davies and Saros, 1994; Fraser et al., 1994; Panda, 2004).

3.1.3 Aspergillomas

Aspergillomas, also known as fungal balls, are normally found in injured or scarred lung tissue, such as bronchiectatic areas or preexisting cavities. These cavities are the very productive zone for mycelia growth, and eventually they produce a ball-like structure that maneuvers independently without entering into the blood vessel or viable tissue. Some predictive factors of this disease are growing size or number of aspergillomata, higher *Aspergillus*-specific IgG titers, immunosuppression, human immunodeficiency virus infection, lung transplantation, etc. (Addrizzo-Harris et al., 1997; Panda, 2004; Zmeili and Soubani, 2007). Aspergillomas may be the reason of hemoptysis, and this may be lethal in rare cases (Denning et al., 2003).

3.1.4 Invasive Aspergillosis

Invasive aspergillosis, the main reason of immunosuppressed patients' morbidity and death, is caused by the invasion of aspergillus fungus into viable tissue, causing tissue necrosis (Panda, 2004; Patterson et al., 2000). Mostly four types of *Aspergillus* species are liable for invasive aspergillosis, such as: *A. fumigatus*, *A. terreus*, *A. flavus*, and *A. niger*. Among all, *A. fumigatus* is the causative organism of more than 90% of such disease (Patterson et al., 2000). Examples of some invasive aspergillosis types are mentioned further.

3.1.4.1 Invasive Pulmonary Aspergillosis

One of the most prevalent forms of the invasive disease is invasive pulmonary aspergillosis (IPA). Usually after 10–14 days of hematopoietic stem cell transplantation, IPA is manifested and is normally coupled with intense granulocytopenia. Fever, pleuritic chest pain, dry cough, dyspnea, and hemoptysis are the common symptoms of IPA (Smith and Kauffman, 2012; Thompson and Patterson, 2008).

3.1.4.2 Tracheobronchial Aspergillosis

Typically tracheobronchial aspergillosis is noticeable among the patients of AIDS, or who have undergone lung transplants. Cough, fever, chest pain, and hemoptysis are few nonspecific symptoms of such aspergillosis (Thompson and Patterson, 2008).

3.1.4.3 Chronic Forms of Pulmonary Aspergillosis

Semiinvasive pulmonary aspergillosis and/or chronic necrotizing pulmonary aspergillosis are found at the lower respiratory tract, as aspergillosis spectrum. Chronic necrotizing pulmonary aspergillosis refers to chronic respiratory symptoms, cavitory lung disease, and serum precipitating antibodies to *Aspergillus* species (Hope et al., 2005; Thompson and Patterson, 2008).

3.2 Fusariosis

Out of nearly hundred species of *Fusarium*, only few of them, such as *F. solani*, *F. moniliforme*, and *F. oxysporum* are the sources of about 90% of human fungal fusariosis infection. The symptoms of fusariosis are quite similar with *Aspergillus*, such as fever, chest pain, cough, dyspnea, and pleurisy (Nucci and Anaissie, 2002; Torres and Kontoyiannis, 2011).

3.3 Mucormycosis

Mucormycosis is a fungal infection caused by Mucorales. Among three genera, such as *Rhizopus*, *Rhizomucor*, and *Mucor*, they cause 75% of mucormycosis (Kontoyiannis et al., 2010). The infection occurs in upper airways in the form of granulomatous invasion, and may gradually move forward into sinuses and/or brain tissue. A mortality rate of approximately 80% has been reported due to this infection (Panda, 2004). Mucorales species are very much susceptible to angioinvasion that may turn into tissue necrosis, and impaired immunity. Patients suffering from hematological malignancy with neutropenia, hematopoietic cell transplant recipients, diabetics, and immunocompromised hosts are vulnerable to pulmonary mucormycosis infection. The most common symptoms of mucormycosis are cough, chest pain, dyspnea, and hemoptysis (Roden et al., 2005; Smith and Kauffman, 2012).

3.4 Scedosporiosis

Scedosporium boydii complex consisting in *S. boydii*, *S. apiospermum*, and *S. aurantiacum*, and *S. prolificans* are very common fungi among *Scedosporium* species (Gilgado et al., 2009). Hematopoietic cell transplant recipients, solid organ transplant recipients, and patients suffering from hematological malignancies are prone to scedosporiosis. *S. prolificans* is able to sporulate in vivo, possibly causing greater risk of antifungal drug resistance. This phenomenon makes *S. prolificans* very unique from most other fungi (Husain et al., 2003; Rodriguez-Tudela et al., 2009).

3.5 Blastomycosis

Blastomyces dermatitidis, a dimorphic fungus, causes blastomycosis (Saccante and Woods, 2010). In case of acute pulmonary infection due to *B. dermatitidis*, patients may remain asymptomatic or may suffer from fever, dyspnea, dry cough, and mild chest pain (Smith and Kauffman, 2010). Chronic pulmonary blastomycosis may result in upper lobe cavitory lesions that may look similar to tuberculosis or histoplasmosis, or mass-like lesions. The lesions may often look like a cancerous lesion. In the infection, symptoms, such as fever, fatigue, night sweats, cough with purulent sputum and hemoptysis, weight loss, and dyspnea, may persist for weeks. The most familiar appearance of disseminated extrapulmonary blastomycosis is observed as cutaneous lesions (Smith and Kauffman, 2012). Less severe pulmonary infection by this fungus comprises mass lesions, single or multiple nodules, lobar pneumonia, and chronic fibrocavitary or fibronodular infiltrates (Limper et al., 2011).

3.6 Cryptococcosis

Cryptococcus neoformans causes cryptococcosis. However, *Cryptococcus gattii* is also responsible for cryptococcosis. *Cryptococcus* (that remains in nature in an encapsulated form) randomly produces a polysaccharide capsule while entering in the pulmonary region (Byrnes et al., 2009; Limper et al., 2011). Cryptococcosis is restricted to the lungs in immunocompetent host, and it commonly exists in patients with chronic ailments of lungs. Immunocompetent host with cryptococcosis infection may not always show symptoms. However, it may exhibit as dry cough, fever, and dyspnea that may lead to acute respiratory distress syndrome in case of immunocompromised patients (Baddley et al., 2008; Chang et al., 2006; Pappas et al., 2001).

3.7 Coccidioidomycosis

Normally two species of *Coccidioidomyces*, such as *C. immitis* and *C. posadasii*, are most commonly found. In the environment, coccidioides that are present as mold form are simply inhaled into the alveoli. These molds convert into spherules consisting of endospores in the lungs and, after maturation, these spherules split and discharge the endospores that cause coccidioidomycosis infection (Ampel, 2011; Smith and Kauffman, 2012). *Coccidioides* infections usually are asymptomatic. However, fever, dry cough, fatigue, dyspnea, and anterior chest pain may be manifested for coccidioidomycosis. For about 5%–10% of the patients, acute pneumonia complication occurs (Ampel, 2011; Anstead and Graybill, 2006). Acute

pulmonary coccidioidomycosis can be different from community-acquired pneumonia due to limited response to anti-bacterial treatment, as well as peripheral blood eosinophilia, hilar adenopathy, and existence of erythema nodosum, and erythema multiforme (Valdivia et al., 2006).

3.8 Histoplasmosis

Histoplasma capsulatum, the cause of histoplasmosis, is found as a mold in nature, and as yeast inside tissues. Inhalation of *H. capsulatum* into the alveoli causes infection into humans. Pulmonary histoplasmosis may lead to acute self-limited pneumonia that may appear in the form of dry cough, mild chest discomfort, fever, and fatigue. Often in the case of immunosuppressed patients, severe pneumonia may appear and, in some cases, it may lead to acute respiratory distress syndrome. One of the exceptional difficulties of pulmonary histoplasmosis is mediastinal fibrosis. Symptoms of this pulmonary histoplasmosis are cough, wheezing, dyspnea, and hemoptysis. But symptoms that persist for a month may vary in case of chronic cavitary pulmonary histoplasmosis. Examples of such symptoms are fever, anorexia, fatigue, weight loss, hemoptysis, and cough with purulent sputum, etc. (Kauffman, 2007; Wheat et al., 2004).

4 TREATMENT OF LUNG FUNGAL INFECTION

Voriconazole is used as first-line treatment for pulmonary aspergillosis (Herbrecht et al., 2002; Limper et al., 2011; Walsh et al., 2008). Posaconazole is also considered as an effective treatment of aspergillosis, however not approved as primary agent (Walsh et al., 2007). Echinocandins are used as second-line therapy, and/or echinocandins with voriconazole combination are applied to increase antifungal action for this purpose (Limper et al., 2011; Walsh et al., 2008).

Posaconazole and voriconazole are considered as the primary drugs for the treatment of fusariosis (Lortholary et al., 2010; Raad et al., 2006). Besides, some physicians also use lipid formulations of amphotericin B (AmB) or combination of AmB lipid formulation with voriconazole (Ho et al., 2007).

AmB is considered as the preferred drug for mucormycosis. Lipid-based formulations of AmB show better drug efficacy, as compared to the original deoxycholate formulation. Besides azole groups, posaconazole is used for step-down therapy (Lewis et al., 2010).

Voriconazole is used as a primary drug for the treatment of *S. apiospermum* and *S. prolificans* (Troke et al., 2008), and posaconazole is also considered to be effective (Torres et al., 2005).

AmB is applied to treat patients with severe blastomycosis, and it is also used for immunosuppressed patients. Once they are stable, azole is used for a few weeks. Itraconazole (ITZ) may be considered as primary agent. On the other hand, voriconazole or fluconazole can be used as second-line treatment (Chapman et al., 2008; Smith and Kauffman, 2010).

In case of cryptococcosis, AmB with flucytosine is used for a few weeks, and fluconazole is used as step-down treatment. Fluconazole is also used for a few months to treat mild to moderate cryptococcosis (Perfect et al., 2010).

AmB can be used to treat severe coccidioidomycosis, and azoles can be used to treat less severe cases (Galgiani et al., 2005). ITZ or fluconazole is used as step-down therapy for long-term treatment of coccidioidomycosis. If azoles fail as the first-line drug, posaconazole and/or voriconazole can be used in that case (Smith and Kauffman, 2012).

AmB is utilized as the preferred therapy for histoplasmosis. For mild to moderate infection, azoles are used as first-line drug and, if AmB produces a positive result as first-line therapy, azoles can be used as step-down therapy in that case. ITZ, voriconazole, and posaconazole are also preferred drugs to treat histoplasmosis (Freifeld et al., 2009; Wheat et al., 2007).

5 CLINICAL STATUS TO TREAT FUNGAL INFECTION BY PULMONARY ROUTE

Local delivery of medications to the lungs is highly desirable, especially in patients with specific pulmonary diseases, such as invasive fungal infection in the lung, cystic fibrosis, asthma, chronic pulmonary infections, or lung cancer. There are many dosage regimens available that are given orally or intravenously to treat these diseases (Table 14.1). But unfortunately till now there is no therapy available through pulmonary route, in spite of having added advantages of directly delivering the drug to the infected lungs.

6 IMPORTANCE OF PULMONARY ROUTE FOR DRUG ADMINISTRATION

The desired efficacy of a therapy mostly depends on the delivery strategy by which a drug is delivered with an optimum concentration. Above or below the maximum and minimum concentrations of a drug at its therapeutic window, it can produce moderate to severe side effects, or provide a subtherapeutic or no effect. Different DDSs already available or currently

TABLE 14.1 Drugs and Dosage Forms Used by the Routes Other Than the Pulmonary Route of Administration to Treat Lung Fungal Infection

Drug	Trade Name of the Formulation	Dosage Form and Route	Manufacturer
AmB	Amphotec	Complex; i.v.	Kadmon Pharmaceuticals, LLC
	Anolip	Lipid Complex; i.v.	Actiza Pharmaceutical
	Ampholip	Lipid Complex; i.v.	Farma glow
	Amphocil	Colloidal dispersion; i.v. infusion	Wintac Ltd.
	Abelcet	Lipid Complex; i.v.	Sigma-Tau Pharmaceuticals, Inc.
	AmBisome	Liposome; i.v. infusion	Mercury Medicare
Natamycin	Natacyn	Suspension; ophthalmic	Alcon Laboratories, Inc.
Nystatin	Nyotran	Lyophilized liposomal formulation; i.v.	Aronex Pharmaceuticals
Terconazole	Terazol 7	0.4% Cream; vaginal application	Janssen Pharmaceuticals, Inc.
Voriconazole	Vfend	Tablets; oral	Pfizer
		Suspension; oral	
		Infusion; i.v.	
ITZ	Sporanox	Solution; oral	Janssen Pharmaceuticals, Inc.
		Capsules; oral	
Tioconazole	Vagistat-1	Ointment; vaginal application	Novartis Consumer Health
Butoconazole nitrate	Gynazole 1	Cream; vaginal application	Ther-Rx and Perrigo Company
Oxiconazole nitrate	Oxistat	Cream; topical application	GlaxoWellcome
Econazole nitrate	Spectazole	Cream; topical application	Janssen Biotech, Inc.
Ketoconazole	Nizoral	2% Shampoo; application in scalp	Janssen-Cilag
	Xolegel	Gel; topical application	Aqua Pharmaceuticals
Fluconazole	Diflucan	Tablets; oral	Pfizer
		Suspension; oral	
		Infusion; i.v.	
Posaconazole	Noxafil	Suspension; oral	Merck
		Delayed-release tablets; oral	
Anidulafungin	Eraxis	Lyophilized product; i.v. infusion	Pfizer
Caspofungin acetate	Cancidas	Lyophilized product; i.v. infusion	Merck & Co., Inc.
Micafungin sodium	Mycamine	Lyophilized product; i.v.	Astellas Pharma Ltd.
Flucytosine	Ancobon	Capsules; oral	Valeant Pharmaceuticals, Inc.
Butenafine HCl	Mentax	Cream; topical application	Mylan Bertek Pharmaceuticals, Inc.
Naftifine hydrochloride	Naftin	Gel; topical application	Merz Pharmaceuticals, LLC
		Cream; topical application	
Terbinafine hydrochloride	Lamisil	Tablets; oral	Novartis
		Granules; oral	
		Gel; topical application	

AmB, Amphotericin B; ITZ, itraconazole; i.v., intravenous.

under development can be efficiently used to minimize drug degradation, prevent toxic adverse effects, and increase the bioavailability of the drugs. The developmental strategy of new formulation involves interdisciplinary approaches coordinating various branches of science and technology, for example, polymer science, pharmaceutical sciences, clinical medicine, molecular biology, etc.

Pulmonary infections caused by *Aspergillus* species are associated with significant morbidity and mortality in immunocompromised patients (Walsh et al., 2008). Although systemic drug delivery is used popularly in the treatment

of pulmonary infections, aerosolized delivery is an attractive option in the prevention of pulmonary fungal infections because the drug can act locally in a site-specific manner, with a higher local concentration, and a minimal systemic exposure.

Growing interest has given to the potential of pulmonary route as a noninvasive administration for both the systemic and local drug delivery of therapeutic agents, because of the high permeability and large area for absorption in lungs (approximately 70–140 m² in adult humans, having enormously thin mucosal membrane for absorption), and good blood supply (Groneberg et al., 2001, 2002, 2003). The alveolar epithelium of the distal lung has been shown to be a major absorption site for many of the therapeutics and various macromolecules (Sangwan et al., 2001; Scheuch and Siekmeier, 2007; Tuncer and Nevin, 2007). Further, advantages of pulmonary route of administration over peroral application are the comparatively low enzymatic activity and rapid drug absorption, with a capacity for overcoming hepatic “fast-pass metabolism.” Although for a prolonged period drugs have been administered through pulmonary route, current pulmonary drug delivery has become an attractive choice with a remarkable scientific and biomedical interest in the area of healthcare research. It has been already reported that the local respiratory disorders, such as asthma, pulmonary infection, pulmonary hypertension, and some systemic disorders (e.g., diabetes) can be well treated by pulmonary route (Gangurde et al., 2012).

7 PRINCIPAL MECHANISMS OF RESPIRATORY DEPOSITION

The respiratory deposition of inhaled drug particles in the lung is very complex, and deposition is based on many factors. Some of the influencing factors include:

- Breathing rate
- Lung volume
- Respiration volume
- Health of the subject
- Airway bifurcations leading to constant changing of hydrodynamic flow of fluid

Depending on the particle size, respiratory airflow, and structural position in the respiratory system, lung deposition occurs via one of the following principal mechanisms.

7.1 Impaction

The airways bifurcate each time, and suspended particles travel along their original path due to inertia, and impact on the airway walls.

7.2 Sedimentation

Sedimentation is the settling down of particles in the smaller airways. The rate of sedimentation is based on the low airflow rate, mainly in the small airways. Low airflow rate tends to change terminal velocity, and ultimately sedimentation occurs.

7.3 Interception

Interception occurs when a drug particle contacts on airway surface, depending on its physical size and shape.

7.4 Diffusion

Diffusion is a primary mechanism of deposition where the particles go from a region of higher concentration to a lower concentrated region, due to Brownian motion. Diffusional depositions occur mostly in the nasopharynx, and most likely in the smaller airways.

7.5 Absorption

The lung is more permeable to macromolecules, including many more therapeutic peptides and proteins than any other portal of entry into the body. Particularly, peptides that have been chemically altered to inhibit peptidase enzyme exhibit very high bioavailability by the pulmonary route. Small molecules that are highly soluble and cationic can exhibit prolonged absorption.

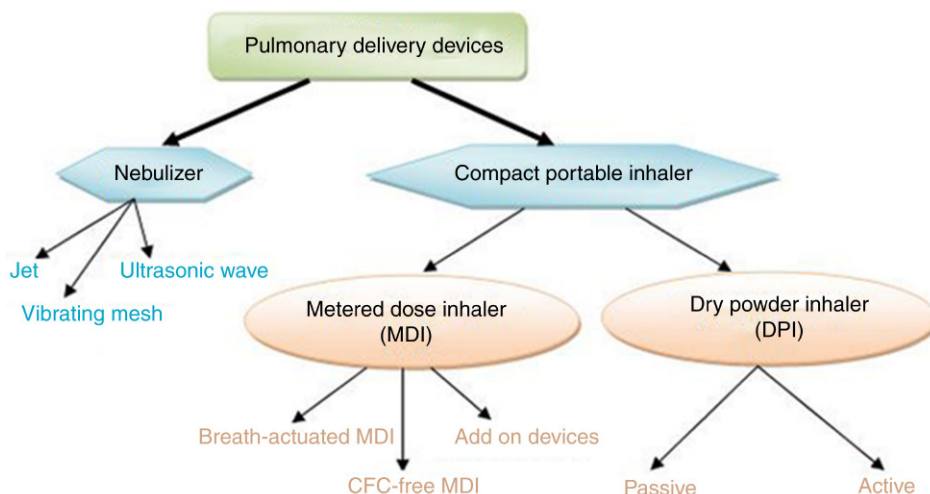


FIGURE 14.2 Evolution of pulmonary delivery devices. *CFC*, Chlorofluorocarbons; *DPI*, dry powder inhalers; *MDI*, metered dose inhalers.

8 PULMONARY DRUG DELIVERY DEVICES

The development of modern inhalation devices can be broadly divided into two categories with various varieties (Fig. 14.2):

1. Nebulizer
2. Compact portable inhaler

8.1 Nebulizer

Nebulizers have been used to treat respiratory diseases for many years. The working principle of jet nebulizer is based on Bernoulli principle by which compressed gas (air or oxygen) is passed through a narrow orifice, creating a low-pressure area at the adjacent liquid feed tube (Fig. 14.3). This evacuates the solution, with the drug being drawn up from the fluid reservoir and shattered in the gas stream through fine droplets. In an ultrasonic nebulizer, a piezoelectric crystal is used with a high vibrating frequency (usually 1–3 MHz) to generate a fountain of liquid in the mobilizing chamber.

The physical properties of pulmonary drug formulations may have an outcome based on particle size and nebulization rates. The viscosity, osmolarity, ionic strength, pH, and surface tension may also affect the nebulization of some formulations.

Constant output jet nebulizer can aerosolize most of the drug solution, and provides a large dose with very little patient coordination skill. Treatment by using a nebulizer can be time consuming, and also less effective, where there is 50% loss



FIGURE 14.3 Nebulizer and its components.

with a continuously operated nebulizer. On average, only 10% of the total dose loaded in a nebulizer is in reality deposited in the lungs (Giraud and Roche, 2002).

Recently, technically advanced novel nebulizers have been developed to reduce drug wastage and improve delivery efficacy. In a nebulizer, the aerosol output is increased by directing auxiliary air entrained at the time of inspiration by enhanced delivery designs. Adaptive aerosol delivery monitors a patient's breathing pattern in the first three breaths, and then targets the aerosol delivery into the first 50% of inhalation of each time. This commits that the aerosol is delivered to the patient during inspiration only, thereby eliminating loss during expiration that occurs with a continuous output nebulizer (Ashurst et al., 2000; Borgstrom et al., 1996).

8.2 Compact Portable Inhaler

8.2.1 Metered Dose Inhaler

It is the revolutionary invention of MDI that overcomes the problem of the hand-bulb nebulizer, and serves portability to outpatients for the first time. This inhalation device is currently the most widely used aerosol delivery device (Fig. 14.4). MDI provides a drug aerosol driven by propellants, such as chlorofluorocarbons (CFC) and hydrofluoroalkanes. MDI emits only a small portion of the drug dose to the lung. On average, only 10%–20% of the delivered dose is deposited in the lung. The high velocity and large particle size of the spray cause around 50%–80% of deposition of drug in the oropharyngeal region. Hand and mouth discoordination is another barrier in the optimal use of an MDI system.

The efficacy of an MDI device depends on a patient's breathing pattern, inspiratory flow rate (IFR), and hand and mouth coordination. Increased IFR results in a decrease in total pulmonary dose deposition and diffusion into the peripheral airway. Fast inhalations (>60 L/min) result in a less peripheral deposition, since deposition of the aerosol takes place by inertial impaction in the oropharyngeal region and the conducting airways. When aerosol is inhaled slowly, drug deposition by gravitational sedimentation in the peripheral region of the lung is improved. Peripheral drug deposition has also been shown to improve with an increase in tidal volume, and a decrease in respiratory frequency. As the inhaled volume is enhanced, aerosols are able to diffuse more into the lung peripheral region. An increased breath-holding period on completion of inhalation enables particles that penetrate the periphery to deposit in that region, instead of being exhaled during the expiratory phase. Thus, the best conditions for inhaling MDI aerosols include a starting volume equivalent to the functional residual capacity, actuation of the device at the start of inhalation, IFR of <60 L/min followed by a 10-s breathhold at the end of inspiration (Norwood et al., 1995).

8.2.2 Pressurized Metered Dose Inhalers

The pMDI is not available for all drugs or dosages, making it difficult for clinicians to prescribe the same type of device for diverse inhaled medications. This is exacerbated by the trend of many pharmaceutical companies not to release newer inhaled drugs as pMDIs. The design of the CFC-propellant pMDI requires initial and frequent priming of the device. Failure to prime the device results in the administration of a substantially lower dose than that prescribed. Unfortunately, frequent priming tends to waste drug in the atmosphere (Dalby and Suman, 2003).

8.2.3 Dry Powder Inhalers

Interest in DPIs as an effective, efficient, and environmentally friendly way of delivering drugs to the lung has accelerated in recent years. A fundamental difficulty with developing solid state aerosols or DPIs is managing both the ubiquitous and

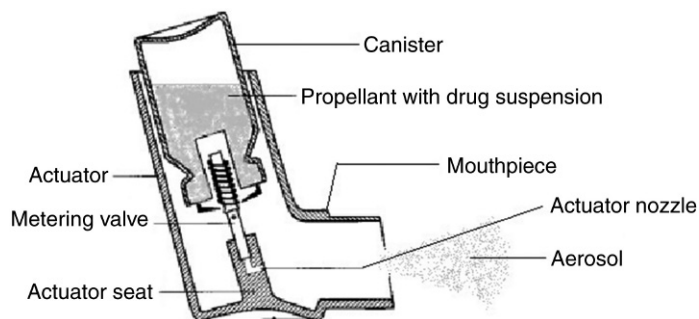


FIGURE 14.4 MDI and its components.

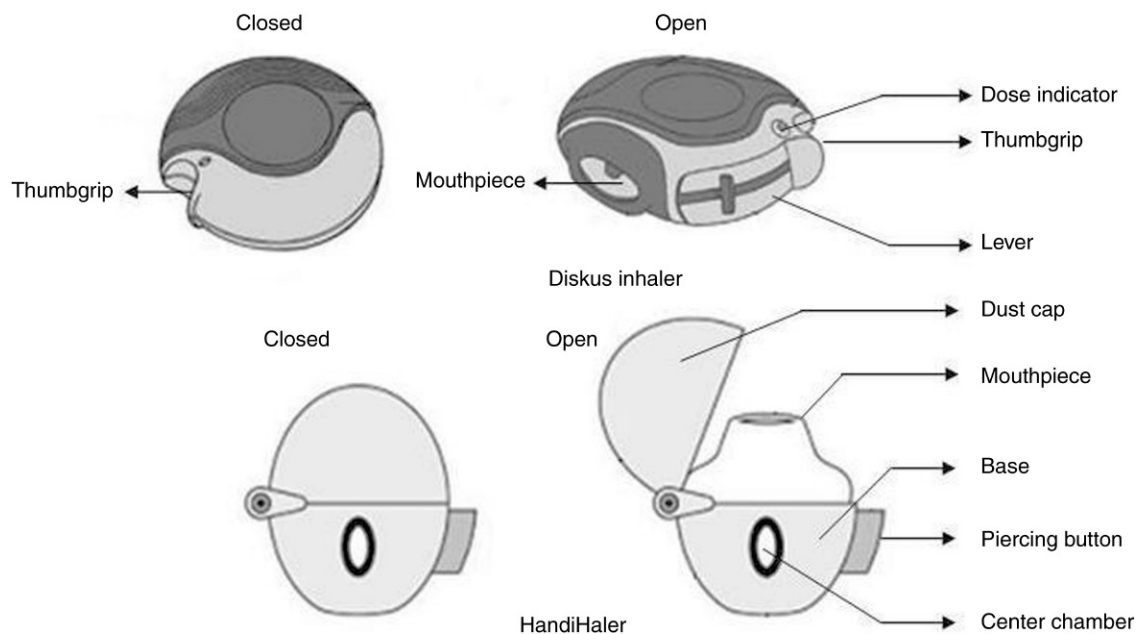


FIGURE 14.5 Schematic diagram of some currently available DPIs and their components.

the transient forces contained in powder beds. Indeed, managing such particulate forces, for example, via particle engineering techniques, is now considered central to successful DPI formulation and production (Fig. 14.5).

In consequence, much attention is currently focused on producing smart formulations, where it may be possible to achieve excellent powder flow and low cohesive forces.

Pharmaceutical scientists too frequently meet major obstacles when they engage in the world of DPI product design, because of the complications of this area resulting from the plethora of DPI device designs. There is tremendous variation in the methods used to store and meter powders, and to generate the aerosol cloud. In the case of DPI aerosol generation, there is a great deal of variation between different types of device, as well as in the fluid dynamic and electrostatic environment that the powder formulation experiences (Ashurst et al., 2000).

The drug aerosol is created in a DPI by directing air through loose powder. Most drug particles from DPIs are too large to penetrate into the lungs because of either large powder agglomerates, or the presence of large carrier particles (e.g., lactose). Thus, dispersion of the powder into fine respirable particles depends on the creation of turbulent air flow that causes the aggregates to break up into particles small enough to be carried into the lower airways, and also to separate carrier from the drug in the device chamber. Each DPI has a different airflow resistance that regulates the required inspiratory effort. The higher the resistance of the device, the more difficult it is to generate an inspiratory flow great enough to attain the maximum dose from the inhaler device. However, deposition in the lung tends to be augmented when using high-resistance inhalers (Yu and Chien, 1997). However, an efficient and robust formulation technology can provide more acceptable use of DPI products (Bogat et al., 2004).

9 PULMONARY FORMULATIONS TO TREAT LUNG FUNGAL INFECTION

Targeted drug delivery to the lungs has evolved to be one of the most widely investigated systemic or local drug delivery approaches (Le and Schiller, 2010). The evolution of novel DDSs for the treatment of pulmonary fungal infections is increasing day by day because of the recurrence of fungal infection, even after the conventional therapy occurred, due to the live spores in the lungs remaining there due to the absence of long-term drug availability at the site of infection. Pulmonary route in particular also makes it possible to deposit drugs in a more site-specific manner at high concentrations within the infected lung, thereby reducing the overall amount of drug given to patients (10%–20% of the peroral quantity), as well as increasing local drug activity while reducing systemic side effects, and avoiding first-pass metabolism.

To further exploit the other advantages presented by the lungs, as well as to overcome some challenges encountered, scientists developed interests in DDS for pulmonary administration. These systems can be broadly classified into immediate release (e.g., lactose–drug mixtures for DPI application) and controlled release systems (such as liposomes, micelles, nano- and microparticles based on polymers).

Nanodrug carriers, such as liposomes, nanoparticles (NPs), micelles, etc., have been used to improve the therapeutic index of new or established drugs by modifying drug absorption, reducing metabolism, prolonging biological half-life, or reducing cytotoxicity. Drug distribution is then controlled primarily by properties of the drug nanocarriers, and no longer by physicochemical characteristics of the drug substance only. A careful design of DDS for pulmonary route requires thorough knowledge of players, such as lung architecture, appropriate selection of the carrier materials, production process, and device for successful delivery of drug to lungs (Maji et al., 2014).

Most of the drugs are administered intravenously for the treatment of fungal infection in lung to avoid degradation in the gastrointestinal tract. Patients, however, avoid injections and i.v. treatments, because they are painful, inconvenient, and expensive. Pulmonary drug delivery offers a noninvasive alternative to injections, and can also be more efficient and effective to deliver the drug, and achieves patient compliance (Raja Kumar et al., 2014) (Table 14.2).

9.1 Liposomes

Polyene antibiotic AmB is regarded as a gold standard for the treatment of deep-seated systemic fungal infections in lung (Gulati et al., 1998; Stamm and Dismukes, 1983). Liposomal formulation of AmB was introduced in the market in the year 1990 (Katz et al., 1990) under the brand name of AmBisome (NeXstar Pharmaceuticals, San Dimas, United States), given intravenously to treat *Candida* spp., *Aspergillus* spp., *Fusarium* spp., and other fungi infections in neutropenic, visceral leishmaniasis, and methylmalonic acidemia patients (Kelsey et al., 1999; Stockler et al., 1993; Walsh et al., 2001).

To get a substantial lung tissue concentration and low systemic exposure of AmB, Fungizone (AmB desoxycholate) or AmBisome (liposomal AmB) was delivered by nebulization (Ruijgrok et al., 2000). AmBisome was found to show greater pharmacokinetics than free drug, including prolonged systemic circulation half-life, reduced plasma clearance rate, decreased renal toxicity, and most importantly, enhanced therapeutic efficacy (Walsh et al., 1998).

Aerosolized liposomal AmB was found to be more effective for the prevention of IPA in a placebo-controlled trial in patients with prolonged neutropenia (Rijnders et al., 2008).

Becker et al. (2002) concluded that efficacy of AmBisome therapy can be enhanced by the addition of Fungizone at the start of the treatment, due to the availability of the drug in the lung at start of treatment.

In another study, the surface was modified by coating with alveolar macrophage-specific ligands (O-palmitoyl mannan or OPM), and also with monoclonal antibody EBA-2 in AmB-loaded aerosolized liposomes and emulsomes (core composed of solid lipid surrounded by phospholipid bilayers), respectively for their selective presentation to lungs (alveolar macrophages) in aspergillosis infection. Further, ^{99m}Tc-labeled liposomes could be used for in vivo imaging of the infection site, as depicted by scintigraphy imaging (Vyas et al., 2009).

Systemic delivery of voriconazole for two months, followed by ITZ for one month, was ineffective; liposomal AmB was transbronchially administered directly into the pulmonary aspergilloma using a transbronchial aspiration cytology needle, resulting in the aspergilloma disappearing by seven and a half months after the first treatment (Takeda et al., 2014).

9.2 Lipid Complex

Mucormycosis have documented successful outcomes with either liposomal AmB or AmB lipid complex. Nevertheless, based on the combination of these retrospective clinical data, the historically poor success rates with AmB desoxycholate, and the animal data, show superiority of aerosolized liposomal AmB over AmB desoxycholate (Lowry et al., 2007; Spellberg et al., 2005).

9.3 Nanoparticles

ITZ has been strategically encapsulated into chitosan-based NPs using a modified ionic gelation method; drugs were fabricated as inhalable microparticles using spray-drying technique. Different ratios of chitosan:tripolyphosphate were used, and its 55% encapsulation was found at a 1:3 ratio of chitosan:tripolyphosphate. In vitro inhalation parameters, including fine particle fraction and emitted dose percentage, were measured by a twin stage impinger. The data of in vitro deposition specify that processing of NPs with mannitol and leucine could improve the aerosolization properties significantly (Jafarinejad et al., 2012).

Although AmB was investigated as desoxycholate salt, liposomal, or lipid complex form, PLGA–dimercaptosuccinic acid polymeric NPs loaded with desoxycholate AmB for sustained delivery of the drug was found to reduce the number

TABLE 14.2 Comparative Study of Pulmonary Versus Other Routes (i.v., Oral, etc.)

Drug	Spectrum/Activity	Dosage Form	Route of Administration	Conclusions	References
AmB	Aspergillosis, cryptococcosis, systemic candidiasis, histoplasmosis, blastomycosis, coccidioidomycosis, and zygomycosis	AmB deoxycholate, liposome, and lipid complex	i.v.	Less nephrotoxicity in lipid formulations	Limper et al. (2011)
	Aspergillosis	Liposomes coated with alveolar macrophage-specific ligands (OPM and OPP)	Aerosol	The ligand-anchored liposomal aerosols are very effective in rapid attainment of high drug concentration in lungs with high population of alveolar macrophages and maintain the same over prolonged period of time	Vyas et al. (2009)
	Paracoccidioidomycosis, candidiasis, aspergillosis, and cryptococcosis	NPs	i.v.	The approach was able to reduce the dosing frequency by threefold without causing renal or hepatic toxicity and avoid any increase in plasma lipid levels	Amaral et al. (2009)
Voriconazole	Invasive aspergillosis	NPs	Pulmonary	Pulmonary deposition of the NPs was studied using a customized inhalation chamber; drug was detectable in lungs until 7 and 5 days after administration, for porous and nonporous particles, respectively; porous NPs with lower MMADs showed better pulmonary deposition in deep lung regions and sustained presence in lungs than the nonporous particles	Sinha et al. (2013)
		Infusion	Aerosol	An inhaled aqueous solution of voriconazole and sulfobutyl ether- β -cyclodextrin is capable of producing high lung tissue, as well as plasma concentrations was observed following single and multiple inhaled doses in a pharmacokinetics study	Tolman et al. (2009)
ITZ	Invasive pulmonary aspergillosis caused by <i>A. fumigatus</i>	Nanostructured particles by SFL formulation	Aerosol	Aerosolized administration of SFL ITZ was effective as prophylaxis in improving survival in this murine model of IPA due to <i>A. fumigatus</i> ; the survival benefit can be explained by the ability of aerosolized SFL ITZ to limit disease progression and angioinvasion, both of which were markedly reduced, in comparison to mice that received control or ITZ oral solution by oral gavage	Alvarez et al. (2007)
	Invasive pulmonary aspergillosis	Nanostructured particles (less than 1 μ m in diameter) by EPAS and SFL	Aerosolized with the nebulizer	The prolonged survival and limited systemic exposure with aerosolized delivery of EPAS and SFL ITZ are encouraging	Hoeben et al. (2006)
	Pulmonary aspergillosis	Nanostructured particles (less than 1 μ m in diameter) by EPAS and SFL	Aerosolized with the nebulizer	An effective method of targeted delivery of ITZ to the deep lung for the treatment and prevention of acute fungal infections	McConville et al. (2006)
	Invasive pulmonary fungal infection	Chitosan-based polymeric micelles as a nanocarrier system	Nebulized	In vitro nebulization study of the ITZ-loaded formulations showed that the SA chitosan-based polymeric micelles had adequate capability as nanocarriers to deliver ITZ, and can remain their stability during nebulization	Moazeni et al. (2012)

(Continued)

TABLE 14.2 Comparative Study of Pulmonary Versus Other Routes (i.v., Oral, etc.) (cont.)

Drug	Spectrum/Activity	Dosage Form	Route of Administration	Conclusions	References
Caspofungin	Invasive aspergillosis	Caspofungin in 0.9% NaCl solutions 10 and 30 mg/mL	Aerosolized with disposable and reusable type of nebulizer	Two types of commercial nebulizing systems efficiently aerosolize the drug, the choice of which depends on whether a disposable or reusable type of jet nebulizer is most suitable for the particular patient care setting; the therapeutic potential of aerosolized caspofungin in preventing invasive aspergillosis in immunocompromised hosts warrants further evaluation in animal and human trials	Wong-Beringer et al. (2005)
Pneumocandins	<i>Candida</i> , <i>Aspergillus</i> spp, and <i>Pneumocystis carinii</i>	Solution in water for aerosol and solution in normal saline for intraperitoneal administration	Aerosol	The pneumocandins are highly active against <i>Aspergillus</i> species, and dramatic improvement in survival was found with aerosolized form	Kurtz et al. (1995)

EPAS, Evaporative precipitation into aqueous solution; MMAD, mass median aerodynamic diameter; NP, nanoparticle; OPM, O-palmitoyl mannan; OPP, O-palmitoyl pullulan; SA, stearic acid; SPL, spray-freezing into liquid.

of AmB administrations, with fewer undesirable effects and a favorable extended dosing interval required to treat mycosis intraperitoneally (Amaral et al., 2009).

Later on, AmB NPs were prepared through liquid antisolvent precipitation for oral administration. The AmB NPs exhibited 2.1 times faster dissolution rates, and 13 times equilibrium solubility, compared with the raw drug; this could be of beneficial for aerosol delivery (Zu et al., 2014).

Patients receiving oral prophylaxis of voriconazole has shown to provide a better intrapulmonary penetration into the pulmonary epithelial lining fluid in lung transplant patients (Capitano et al., 2006). Nevertheless, the suitability of an aqueous solution of voriconazole solubilized with sulfobutyl ether- β -cyclodextrin for targeted drug delivery to the lungs via nebulization has been established (Tolman et al., 2009). Another interesting study depicts that polylactide-*co*-glycolide NPs containing voriconazole made porous using an effervescent mixture for improved pulmonary delivery for sustained drug release for over 15 days. Pulmonary deposition of the particles was studied using a customized inhalation chamber (Sinha and Mukherjee, 2012) for experimental mice. Porous particles had a lower mass median aerodynamic diameter (MMAD), and the highest initial drug deposition than nonporous particles. VNPs with improved drug loading were successfully delivered to murine lungs (Sinha et al., 2013). The most recent studies involve the development of PLGA NPs containing voriconazole, radiolabeling with technetium-99m to investigate the effect on their blood clearance, biodistribution, and in vivo gamma imaging. In vivo deposition of the drug in the lobes of the mice lung, and accumulation in various major organs, has also been observed. Drug accumulation was more pronounced in the lung, in the case of administration of the NPs than that of the free drug. The free drug was found to be excreted faster than the NPs containing drug, following the inhalation route, as assessed by gamma scintigraphy study (Das et al., 2015).

Other antifungals, such as pneumocandin, have been shown to be more effective for prophylaxis against IPA in rats, when given through aerosolization, compared to parenteral treatment of the same (Kurtz et al., 1995).

The in vitro suitability of caspofungin for aerosol administration by characterizing factors that influence efficacy and airway tolerance of aerosol delivery, such as physicochemical properties, the aerodynamics of drug particles, and efficiency of nebulizing systems, etc. (Wong-Beringer et al., 2005). Aerosolization of caspofungin has been evaluated by using three different jet nebulizer and compressor systems. The ability of the drug to achieve favorable physicochemical properties for nebulization requires dilution in normal saline, and a more concentrated (30 mg/mL) solution.

ITZ DPI composed of NPs using high-pressure homogenization with tocopherol polyethylene 1000 succinate as a stabilizer has been prepared, and was embedded in carrier microparticles of mannitol and/or sodium taurocholate, by spray-drying. There followed impaction studies using a multistage liquid impactor to determine the aerodynamic performance and fine-particle fraction that is theoretically able to reach the lung (Duret et al., 2012).

A recent study shows germination of inhaled fungal spores initiates infection, causing severe pneumonia and even mortality. It has been observed that nebulized AmB-polymethacrylic acid NP prophylaxis prevents invasive aspergillosis. It was not toxic to lung epithelial cells or monocyte-derived macrophages in vitro, or in an in vivo transplant immunosuppression mouse model of life-threatening invasive aspergillosis. Three days of nebulizer based prophylaxis delivered the NP effectively to lung, and prevented both fungal growth and lung inflammation (Shirkhani et al., 2015).

Self-assembled AmB-loaded polyglutamic acid NPs were prepared and characterized, and in vitro potential against *Candida albicans* was determined. The biodegradable polyglutamic acid-based formulation of AmB showed potent antimicrobial activity similar to that of Fungizone against *C. albicans*. Interestingly, AmB-bearing PGA NPs were found to inhibit biofilm formation to a considerable extent. In summary, AmB-PGA NPs showed highly attenuated toxicity when compared with Fungizone, while retaining equivalent active antifungal properties (Zia et al., 2015)

9.4 Nanosuspension

It has been found that when nanostructured crystalline ITZ formulations were aerosolized, high lung tissue concentrations were achieved, while the systemic exposure was reduced (Hoeben et al., 2006).

Another study shows high and sustained lung tissue concentrations were achieved after inhalation of ITZ in mice, following oral and pulmonary dosing of amorphous nanoparticulate ITZ compositions, as well as the ITZ oral solution (Sporanox/Janssen) (Vaughn et al., 2006).

Administration of nanoparticulate ITZ containing polysorbate 20 as a nebulized suspension of evaporative precipitation into aqueous solution (EPAS) ITZ provided for targeted high lung concentrations in a murine model (McConville et al., 2006).

Administered as a nebulized suspension of URF, ITZ nanostructured powder agglomerates with enhanced dissolution properties, as well as high bioavailability. These engineered powders have been nebulized as dispersions to rodents to evaluate the pharmacokinetic parameters following inhalation (Yang et al., 2008b).

Nanoparticulate nystatin was found to show better in vitro and in vivo antifungal activities against *C. albicans*. A nystatin nanosuspension was prepared by wet-media milling. Immunosuppressed DBA/2 mice were orally infected with *C. albicans*, and treated with conventional nystatin suspension, nystatin nanosuspension, or saline control for 14 days. Beginning on day 3 of treatment, lower oral burdens of *C. albicans* were found in the nanosuspension group, compared with the suspension and control groups. Mouse survival was also superior in the nanosuspension group (Melkounov et al., 2013).

9.5 Micelles

There are only few reports investigating the application of inhalable polymeric micelles for delivery of antifungals for inhalation route. Water-soluble chitosan was grafted to stearic acid (SA) chains via 1-ethyl-3-(3-dimethylaminopropyl) carbodiimide mediated coupling reaction that was determined by ¹H NMR. Chitosan–SA conjugate nanomicelles of AmB of 101–248 nm was evaluated for the antifungal activity, aggregation state of the drug, nebulization efficiency, and retention of AmB in the micelles after nebulization (Gilani et al., 2011).

Another study reveals that ITZ was entrapped into the hydrophobically modified chitosan micelles (120–200 nm). The in vitro pulmonary profile of polymeric micelles was studied by an air-jet nebulizer connected to a twin stage impinger. The nebulization efficiency was up to 89%, and the fine particle fraction varied from 38% to 47%. The micelles had enough stability to remain in the encapsulation of the drug during the nebulization process (Moazeni et al., 2012).

10 WHY PULMONARY ROUTE?

In recent years, pulmonary drug delivery is an attractive route of administration of drugs due to various beneficial effects. In fact, the lungs are a competent entry point for drugs to the bloodstream due to the huge surface area for absorption (about 100 m²), the very thin absorption membrane (0.1–0.2 μm), and outstanding blood flow (5 L/min) capability that rapidly allocates molecules all over the body. Moreover, the lungs reveal fairly low local metabolic activity and, in contrast to the oral route of drug administration, pulmonary inhalation is not subjected to first-pass metabolism (Goel et al., 2013). The various advantages of pulmonary DDSs are listed here (Banker and Rhodes, 2002; Cole and Mackay, 1990; Hillery et al., 2001; Sciarra and Cutie, 1991):

1. Straight delivery of the medicament to the affected area is possible.
2. Reduced dose is required for the desired pharmacological action that results in reduced systemic side effects.
3. Quick onset of drug action.
4. Intestinal and hepatic first-pass metabolism can be avoided.
5. Much reduced hostile environment is present in the lungs than in the oral route to most drugs, including proteins and peptides.
6. While administering a dose, sterility of the product can be maintained.
7. There is better protection against drug degradation by oxygen and moisture, thus the stability is augmented for labile substances.

11 LIMITATIONS OF PULMONARY ROUTE (IF ANY)

There are not only advantages, but also some limitations of the pulmonary route of delivery. The limitations of the delivery of drugs to lungs (Sciarra and Cutie, 1991) are very important in the design of effective pulmonary DDSs. Some of them are mentioned here;

1. The oropharyngeal settlement may give local adverse effects.
2. Patients may have trouble using the delivery devices correctly.
3. Various aspects affect the reproducibility of drug delivery to the lungs, including physiological (respiratory scheme) and pharmaceutical (tool, formulation) variables. For the systemic delivery of drugs with a small therapeutic index, such deviations may be undesirable.
4. Drug absorption may be limited due to the barrier action of the mucus and the drug–mucus interactions.
5. Mucociliary clearance diminishes the retention time of drugs within the lungs that may affect the pharmacological efficacy of the slowly absorbed drugs.
6. The lungs are not an easily reachable surface for drug delivery, and complex delivery devices are required for targeted drug delivery.

12 CONCLUSIONS

Due to rapid blood turnover and fast blood flow, it is hard to maintain persistent therapeutic drug levels in lung. This causes an inability of drug molecules to kill the live fungi in totality, and the fungal spores survive. To maintain the drug concentration in lung, high dose of drug is to be given, often causing high level of toxicity in patients, and inability of the patients to continue the treatment. Fungal infection in lungs is, therefore, difficult to treat by conventional DDSs. Pulmonary drug delivery has a great potential for successful delivery of drug to the lung for effective treatment locally, and even for systemic fungal infections, resulting in a better therapeutic outcome. There are numbers of pulmonary drug delivery devices and DDSs available. Extensive research in the area is in progress. However, existing pulmonary DDSs are not effective enough, and designing the appropriate delivery strategy may explore a new avenue for pulmonary drug delivery to improve the pharmacokinetic profile of the therapeutic payloads.

REFERENCES

- Addrizzo-Harris, D.J., Harkin, T.J., McGuinness, G., Naidich, D.P., Rom, W.N., 1997. Pulmonary aspergilloma and AIDS: a comparison of HIV infected and HIV-negative individuals. *Chest* 111, 612–618.
- Alvarez, C.A., Wiederhold, N.P., McConville, J.T., Peters, J.I., Najvar, L.K., Graybill, J.R., et al., 2007. Aerosolized nanostructured itraconazole as prophylaxis against invasive pulmonary aspergillosis. *J. Infect.* 55, 68–74.
- Amaral, A.C., Bocca, A.L., Ribeiro, A.M., Nunes, J., Peixoto, D.L., Simioni, A.R., et al., 2009. Amphotericin B in poly(lactic-co-glycolic acid) (PLGA) and dimercaptosuccinic acid (DMSA) nanoparticles against paracoccidioidomycosis. *J. Antimicrob. Chemother.* 63, 526–533.
- Ampel, N.M., 2011. *Coccidioidomycosis*. In: Kauffman, C.A., Pappas, P.G., Sobel, J.D. et al., (Eds.), *Essentials of Clinical Mycology*. Springer, New York, NY, pp. 349–366.
- Anderson, P.J., 2005. History of aerosol therapy: liquid nebulization to MDIs to DPIs. *Respir. Care* 50, 1139–1150.
- Andrade, F., Diana, R., Videira, M., Ferreira, D., Sosnik, A., Sarmiento, B., 2013. Nanotechnology and pulmonary delivery to overcome resistance in infectious disease. *Adv. Drug Deliv. Rev.* 65, 1816–1827.
- American Lung Association, 2015. How lungs work. Available from: <http://www.lung.org/lung-health-and-diseases/how-lungs-work/>
- Anstead, G.M., Graybill, J.R., 2006. *Coccidioidomycosis*. *Infect. Dis. Clin. North Am.* 20, 621–643.
- Ashurst, I.I., Malton, A., Prime, D., Sumbly, B., 2000. Latest advances in the development of dry powder inhalers. *Pharm. Sci. Technol.* 3, 246–256.
- Baddley, J.W., Perfect, J.R., Oster, R.A., Larsen, R.A., Pankey, G.A., Henderson, H., et al., 2008. Pulmonary cryptococcosis in patients without HIV infection: factors associated with disseminated disease. *Eur. J. Clin. Microbiol. Infect. Dis.* 27, 937–943.
- Banker, G.S., Rhodes, T.R., 2002. *Modern Pharmaceutics* Marcel Dekker, New York, NY, (pp. 529–586).
- Becker, M.J., de Marie, S., Fens, M.H., Hop, W.C., Verbrugh, H.A., Bakker-Woudenberg, I.A., 2002. Enhanced antifungal efficacy in experimental invasive pulmonary aspergillosis by combination of AmBisome with Fungizone as assessed by several parameters of antifungal response. *J. Antimicrob. Chemother.* 49, 813–820.
- Begat, P., Morton, D.A.V., Staniforth, J.N., Price, R., 2004. The cohesive adhesive balances in dry-powder inhaler formulations II: influence on fine particle delivery characteristics. *Pharm. Res.* 21, 1826–1833.
- Borgstrom, L., Derom, E., Stahl, E., Wahlin-Boll, E., Pauwels, R., 1996. The inhalation device influences lung deposition and bronchodilating effect of terbutaline. *Am. J. Respir. Crit. Care Med.* 153, 1636–1640.
- Byrnes, III, E.J., Bildfell, R.J., Frank, S.A., Mitchell, T.G., Marr, K.A., Heitman, J., 2009. Molecular evidence that the range of the Vancouver Island outbreak of *Cryptococcus gattii* infection has expanded into the Pacific northwest in the United States. *J. Infect. Dis.* 199, 1081–1086.
- Capitano, B., Potoski, B.A., Husain, S., Zhang, S., Paterson, D.L., Studer, S.M., et al., 2006. Intrapulmonary penetration of voriconazole in patients receiving an oral prophylactic regimen. *Antimicrob. Agents Chemother.* 50, 1878–1880.
- Chang, W.C., Tzao, C., Hsu, H.H., Lee, S.C., Huang, K.L., Tung, H.J., et al., 2006. Pulmonary cryptococcosis: comparison of clinical and radiographic characteristics in immunocompetent and immunocompromised patients. *Chest* 129, 333–340.
- Chapman, S.W., Dismukes, W.E., Proia, L.A., Bradsher, R.W., Pappas, P.G., Threlkeld, M.G., et al., 2008. Clinical practice guidelines for the management of blastomycosis: 2008 update by the Infectious Diseases Society of America. *Clin. Infect. Dis.* 46, 1801–1812.
- Cole, R.B., Mackay, A.D., 1990. Concepts of pulmonary physiology. *Essentials of Respiratory Disease* Churchill Livingstone, New York, NY, pp. 49–60.
- Dalby, R., Suman, J., 2003. Inhalation therapy: technological milestones in asthma treatment. *Adv. Drug Deliv. Rev.* 55, 779–791.
- Das, P.J., Paul, P., Mukherjee, B., Mazumder, B., Mondal, L., Baishya, R., et al., 2015. Pulmonary delivery of voriconazole loaded nanoparticles providing a prolonged drug level in lungs: a promise for treating fungal infection. *Mol. Pharm.* 12, 2651–2664.
- Davies, S.F., Saros, G.A., 1994. *Fungal Infection*. In: Nadel, J.A., Murray, J.G. (Eds.), *Textbook of Respiratory Medicine*. WB Saunders Co., Philadelphia, PA, pp. 1161–1170.
- Denning, D.W., Riniotis, K., Dobrashian, R., Sambatakou, H., 2003. Chronic cavitary and fibrosing pulmonary and pleural aspergillosis: case series, proposed nomenclature change, and review. *Clin. Infect. Dis.* 37, S265–S280.
- Dessanges, J.F., 2001. A history of nebulization. *J. Aerosol Med.* 14, 65–71.
- Duret, C., Wauthoz, N., Sebti, T., Vanderbist, F., Amighi, K., 2012. New inhalation-optimized itraconazole nanoparticle-based dry powders for the treatment of invasive pulmonary aspergillosis. *Int. J. Nanomed.* 7, 5475–5489.

- Fraser, R.S., Pare, J.A.P., Eraser, R.G., Pare, P.D., 1994. Infectious diseases of lungs in synopsis of diseases of chest, second ed. WB Saunders & Co., Philadelphia, PA.
- Freifeld, A., Proia, L., Andes, D., Baddour, L.M., Blair, J., Spellberg, B., et al., 2009. Voriconazole use for endemic fungal infections. *Antimicrob. Agents Chemother.* 53, 1648–1651.
- Galgiani, J.N., Ampel, N.M., Blair, J.E., Catanzaro, A., Johnson, R.H., Stevens, D.A., et al., 2005. Coccidioidomycosis. *Clin. Infect. Dis.* 41, 1217–1223.
- Gangurde, H.H., Chordiya, M.A., Baste, N.S., Tamizharasi, S., Upasan, C.D., 2012. Approches and devices used in pulmonary drug delivery system: a review. *Asian J. Pharmaceut. Res. Health Care* 4, 11–27.
- Gilani, K., Moazeni, E., Ramezanli, T., Amini, M., Fazeli, M.R., Jamalifar, H., 2011. Development of respirable nanomicelle carriers for delivery of amphotericin B by jet nebulization. *J. Pharm. Sci.* 100, 252–259.
- Gilgado, F., Cano, J., Gené, J., Serena, C., Guarro, J., 2009. Different virulence of the species of the *Pseudallescheria boydii* complex. *Med. Mycol.* 47, 371–374.
- Giraud, V., Roche, N., 2002. Misuse of corticosteroid metered-dose inhaler is associated with decreased asthma stability. *Eur. Respir. J.* 19, 246–251.
- Goel, A., Baboota, S., Sahni, J.K., Ali, J., 2013. Exploring targeted pulmonary delivery for treatment of lung cancer. *Int. J. Pharm. Invest.* 3, 8–14.
- Greenberger, P.A., 2002. Allergic bronchopulmonary aspergillosis. *J. Allergy Clin. Immunol.* 110, 685–692.
- Groneberg, D.A., Eynott, P.R., Döring, F., Dinh, Q.T., Oates, T., Barnes, P.J., et al., 2002. Distribution and function of the peptide transporter PEPT2 in normal and cystic fibrosis human lung. *Thorax* 57, 55–60.
- Groneberg, D.A., Nickolaus, M., Spinger, J., Doring, F., Daniel, H., Fischer, A., 2001. Localization of peptide transporter PEPT2 in the lung: implications of pulmonary oligopeptide uptake. *Am. J. Pathol.* 158, 707–714.
- Groneberg, D.A., Witt, C., Wagner, U., Chung, K.F., Fischer, A., 2003. Fundamentals of pulmonary drug delivery. *Resp. Med.* 97, 382–387.
- Gulati, M., Bajad, S., Singh, S., Ferdous, A.J., Singh, M., 1998. Development of liposomal amphotericin B formulation. *J. Microencapsul.* 15, 137–151.
- Herbrecht, R., Denning, D.W., Patterson, T.F., Bennett, J.E., Greene, R.E., Oestmann, J.W., et al., 2002. Voriconazole versus amphotericin B for primary therapy of invasive aspergillosis. *N. Engl. J. Med.* 347, 408–415.
- Hillery, A.M., Lloyd, A.W., Swarbrick, J., 2001. Pulmonary drug delivery in drug delivery and targeting for pharmacists and pharmaceutical scientists. Taylor and Francis, London; New York.
- Ho, D.Y., Lee, J.D., Rosso, F., Montoya, J.G., 2007. Treating disseminated fusariosis: amphotericin B, voriconazole, or both? *Mycoses* 50, 227–231.
- Hoeben, B.J., Burgess, D.S., McConville, J.T., Najvar, L.K., Talbert, R.L., Peters, J.I., et al., 2006. In vivo efficacy of aerosolized nanostructured itraconazole formulations for prevention of invasive pulmonary aspergillosis. *Antimicrob. Agents Chemother.* 50, 1552–1554.
- Hope, W.W., Walsh, T.J., Denning, D.W., 2005. The invasive and saprophytic syndromes due to *Aspergillus* spp. *Med. Mycol.* 43, S207–S238.
- Husain, S., Alexander, B.D., Munoz, P., Avery, R.K., Houston, S., Pruet, T., et al., 2003. Opportunistic mycelial fungi in organ transplant recipients: emerging importance of non-*Aspergillus* mycelial infections. *Clin. Infect. Dis.* 37, 221–229.
- Jafarinejad, S., Gilani, K., Moazeni, E., Ghazi-Khansari, M., Najafabadi, A.R., Mohajel, N., 2012. Development of chitosan-based nanoparticles for pulmonary delivery of itraconazole as dry powder formulation. *Powder Technol.* 222, 65–70.
- Katz, N.M., Pierce, P.F., Anzeck, R.A., Visner, M.S., Canter, H.G., Foegh, M.L., 1990. Liposomal amphotericin B for treatment of pulmonary aspergillosis in a heart transplant patient. *J. Heart Transplant* 9, 14–17.
- Kauffman, C.A., 2007. Histoplasmosis: clinical and laboratory update. *Clin. Microbiol. Rev.* 20, 115–132.
- Kelsey, S.M., Goldman, J.M., McCann, S., Newland, A.C., Scarffe, J.H., Oppenheim, B.A., et al., 1999. Liposomal amphotericin (AmBisome) in the prophylaxis of fungal infections in neutropenic patients: a randomised, double-blind, placebo-controlled study. *Bone Marrow Transplant.* 23, 163–168.
- Kontoyannis, D.P., Marr, K.A., Park, B.J., Alexander, B.D., Anaissie, E.J., Walsh, T.J., et al., 2010. Prospective surveillance for invasive fungal infections in hematopoietic stem cell transplant recipients, 2001–2006: overview of the transplant-associated infection surveillance network (TRANSNET) database. *Clin. Infect. Dis.* 50, 1091–1100.
- Kurtz, M.B., Bernard, E.M., Edwards, F.F., Murrin, J.A., Dropinski, J., Douglas, C.M., et al., 1995. Aerosol and parenteral pneumocandins are effective in a rat model of pulmonary aspergillosis. *Antimicrob. Agents Chemother.* 39, 1784–1789.
- Lai-Fook, S.J., 2004. Pleural mechanics and fluid exchange. *Physiol. Rev.* 84, 385–410.
- Le, J., Schiller, D.S., 2010. Aerosolized delivery of antifungal agents. *Curr. Fungal Infect. Rep.* 4, 96–102.
- Lewis, R.E., Albert, N.D., Liao, G., Hou, J., Prince, R.A., Kontoyannis, D.P., 2010. Comparative pharmacodynamics of amphotericin B lipid complex and liposomal amphotericin B in a murine model of pulmonary mucormycosis. *Antimicrob. Agents Chemother.* 54, 1298–1304.
- Limper, A.H., Knox, K.S., Sarosi, G.A., Ampel, N.M., Bennett, J.E., et al., 2011. An official american thoracic society statement: treatment of fungal infections in adult pulmonary and critical care patients. *Am. J. Respir. Crit. Care Med.* 183, 96–128.
- Lortholary, O., Obenga, G., Biswas, P., Caillot, D., Chachaty, E., Bienvu, A.L., Antonino, C., et al., 2010. International retrospective analysis of 73 cases of invasive fusariosis treated with voriconazole. *Antimicrob. Agents Chemother.* 54, 4446–4450.
- Lowry, C.M., Marty, F.M., Vargas, S.O., Lee, J.T., Fiumara, K., Deykin, A., et al., 2007. Safety of aerosolized liposomal versus deoxycholate amphotericin B formulations for prevention of invasive fungal infections following lung transplantation: a retrospective study. *Transpl. Infect. Dis.* 9, 121–125.
- Maji, R., Dey, N.S., Satapathy, B.S., Mukherjee, B., Mondal, S., 2014. Preparation and characterization of Tamoxifen citrate loaded nanoparticles for breast cancer therapy. *Int. J. Nanomed.* 9, 3107–3118.
- Mansour, H.M., Rhee, Y.S., Wu, X., 2009. Nanomedicine in pulmonary delivery. *Int. J. Nanomed.* 4, 299–319.
- Marianecchi, C., Marzio, L.D., Rinaldi, F., Carafa, M., Alhaique, F., 2011. Pulmonary delivery: innovative approaches and perspectives. *J. Biomater. Nanobiotechnol.* 2, 567–575.
- McConville, J.T., Overhoff, K.A., Sinswat, P., Vaughn, J.M., Frei, B.L., Burgess, D.S., et al., 2006. Targeted high lung concentrations of itraconazole using nebulized dispersions in a murine model. *Pharm. Res.* 23, 901–911.

- Melkoumov, A., Goupil, M., Louhichi, F., Raymond, M., de Repentigny, L., Leclair, G., 2013. Nystatin nanosizing enhances in vitro and in vivo antifungal activity against *Candida albicans*. *J. Antimicrob. Chemother.* 68, 2099–2105.
- Moazeni, E., Gilani, K., Najafabadi, A.R., Reza Rouini, M., Mohajel, N., Amini, M., et al., 2012. Preparation and evaluation of inhalable itraconazole chitosan based polymeric micelles. *Daru* 20, 85.
- Norwood, D.L., Prime, D., Downey, B.P., Creasey, J., Sethi, S.K., Haywood, P., 1995. Analysis of polycyclic aromatic hydrocarbons in metered dose inhaler drug formulations by isotope dilution gas chromatography/mass spectrometry. *J. Pharm. Biomed. Anal.* 13, 293–304.
- Nucci, M., Anaissie, E., 2002. Cutaneous infection by *Fusarium* species in healthy and immunocompromised hosts: implications for diagnosis and management. *Clin. Infect. Dis.* 35, 909–920.
- Panda, B.N., 2004. Fungal infections of lungs: the emerging scenario. *Indian J. Tuberc.* 51, 63–69.
- Pappas, P.G., Perfect, J.R., Cloud, G.A., Larsen, R.A., Pankey, G.A., Lancaster, D.J., et al., 2001. Cryptococcosis in human immunodeficiency virus-negative patients in the era of effective azole therapy. *Clin. Infect. Dis.* 33, 690–699.
- Paranjpe, M., Goymann, C.C.M., 2014. Nanoparticle-mediated pulmonary drug delivery: a review. *Int. J. Mol. Sci.* 15, 5852–5873.
- Patterson, T.F., Kirkpatrick, W.R., White, M., Hiemenz, J.W., Wingard, J.R., Dupont, B., 2000. Invasive aspergillosis. Disease spectrum, treatment practices, and outcomes. I3 *Aspergillus* Study Group. *Medicine* 79, 250–260.
- Patton, J.S., Byron, P.R., 2007. Inhaling medicines: delivering drugs to the body through the lungs. *Nat. Rev. Drug Discov.* 6, 67–74.
- Perfect, J.R., Dismukes, W.E., Dromer, F., Goldman, D.L., Graybill, J.R., Hamill, R.J., et al., 2010. Clinical practice guidelines for the management of cryptococcal disease: 2010 update by the Infectious Diseases Society of America. *Clin. Infect. Dis.* 50, 291–322.
- Raad, I.I., Hachem, R.Y., Herbrecht, R., Graybill, J.R., Hare, R., Corcoran, G., et al., 2006. Posaconazole as salvage treatment for invasive fusariosis in patients with underlying hematologic malignancy and other conditions. *Clin. Infect. Dis.* 42, 1398–1403.
- Raja Kumar, J., Muralidharan, S., Parasuraman, S., 2014. Antifungal agents: new approach for novel delivery systems. *J. Pharm. Sci. Res.* 6, 229–235.
- Rijnders, B.J., Cornelissen, J.J., Slobbe, L., Becker, M.J., Doorduyn, J.K., Hop, W.C., et al., 2008. Aerosolized liposomal Amphotericin B for the prevention of invasive pulmonary Aspergillosis during prolonged neutropenia: a randomized, placebo-controlled trial. *Clin. Infect. Dis.* 46, 1401–1408.
- Roden, M.M., Zaoutis, T.E., Buchanan, W.L., Knudsen, T.A., Sarkisova, T.A., Schaufele, R.L., et al., 2005. Epidemiology and outcome of zygomycosis: a review of 929 reported cases. *Clin. Infect. Dis.* 41, 634–653.
- Rodriguez-Tudela, J.L., Berenguer, J., Guarro, J., Kantarcioglu, A.S., Horre, R., de Hoog, G.S., et al., 2009. Epidemiology and outcome of *Scedosporium prolificans* infection: a review of 162 cases. *Med. Mycol.* 47, 359–370.
- Ruijgrok, E.J., Vulto, A.G., Van Etten, E.W., 2000. Aerosol delivery of amphotericin B desoxycholate (Fungizone) and liposomal amphotericin B (AmBisome): aerosol characteristics and in-vivo amphotericin B deposition in rats. *J. Pharm. Pharmacol.* 52, 619–627.
- Saccante, M., Woods, G.L., 2010. Clinical and laboratory update on blastomycosis. *Clin. Microbiol. Rev.* 23, 367–381.
- Sahasrabudhe, N., Gosney, J.R., Hasleton, P., 2013. The normal lung: histology, embryology, development, aging and function. In: Hasleton, P., Flieder, D.B. (Eds.), *Spencer's Pathology of the Lung*. Cambridge University Press, Cambridge, UK, pp. 1–40.
- Sangwan, S., Agosti, J.M., Bauer, L.A., Otulana, B.A., Morishige, R.J., Cipolla, D.C., et al., 2001. Aerosolized protein delivery in asthma: gamma camera analysis of regional deposition and perfusion. *J. Aerosol. Med.* 14, 185–195.
- Scheuch, G., Siekmeier, R., 2007. Novel approaches to enhance pulmonary delivery of proteins and peptide. *J. Physiol Pharmacol.* 58, 615–625.
- Sciara, J.J., Cutie, A.J., 1991. *Pharmaceutical aerosols*, second ed. Varghese Publishing House, Bombay, India, (pp. 589–618).
- Shirkhani, K., Teo, I., Armstrong-James, D., Shaunak, S., 2015. Nebulised amphotericin B-polymethacrylic acid nanoparticles prophylaxis prevents invasive aspergillosis. *Nanomedicine* 11, 1217–1226.
- Sinha, B., Mukherjee, B., 2012. Development of an inhalation chamber and a dry powder inhaler device for administration of pulmonary medication in animal model. *Drug Dev. Ind. Pharm.* 38, 171–179.
- Sinha, B., Mukherjee, B., Pattnaik, G., 2013. Poly-lactide-co-glycolide nanoparticles containing voriconazole for pulmonary delivery: in vitro and in vivo study. *Nanomedicine* 9, 94–104.
- Smith, J.A., Kauffman, C.A., 2010. Blastomycosis. *Proc. Am. Thorac. Soc.* 7, 173–180.
- Smith, J.A., Kauffman, C.A., 2012. Pulmonary fungal infections. *Respirology* 17, 913–926.
- Spellberg, B., Edwards, Jr., J., Ibrahim, A., 2005. Novel perspectives on *Mucormycosis*: pathophysiology, presentation, and management. *Clin. Microbiol. Rev.* 18, 556–569.
- Stamm, A.M., Dismukes, W.E., 1983. Current therapy of pulmonary and disseminated fungal diseases. *Chest* 83, 911–917.
- Stockler, S., Lackner, H., Ginter, G., Schwinger, W., Plecko, B., Muller, W., 1993. Liposomal amphotericin-B (AmBisome) for treatment of cutaneous widespread candidosis in an infant with methylmalonic acidemia. *Eur. J. Pediatr.* 152, 981–983.
- Takeda, T., Itano, H., Kakehashi, R., Fukita, S., Saitoh, M., Takeda, S., 2014. Direct transbronchial administration of liposomal amphotericin B into a pulmonary aspergilloma. *Respir. Med. Case Rep.* 11, 7–11.
- Thompson, III, G.R., Patterson, T.F., 2008. Pulmonary aspergillosis. *Semin. Respir. Crit. Care Med.* 28, 103–110.
- Tolman, J.A., Nelson, N.A., Son, Y.J., Bosselmann, S., Wiederhold, N.P., Peters, J.I., et al., 2009. Characterization and pharmacokinetic analysis of aerosolized aqueous voriconazole solution. *Eur. J. Pharm. Biopharm.* 72, 199–205.
- Torres, H.A., Kontoyiannis, D.P., 2011. Hyalohyphomycoses (hyaline molds). In: Kauffman, C.A., Pappas, P.G., Sobel, J.D. et al., (Eds.), *Essentials of Clinical Mycology*. second ed. Springer, New York, NY, pp. 281–304.
- Torres, H.A., Hachem, R.Y., Chemaly, R.F., Kontoyiannis, D.P., Raad, I.I., 2005. Posaconazole: a broad spectrum triazole agent. *Lancet Infect. Dis.* 5, 775–785.
- Troke, P., Aguirrengoa, K., Arteaga, C., Ellis, D., Heath, C.H., Lutsar, I., et al., 2008. Treatment of scedosporiosis with voriconazole: clinical experience with 107 patients. *Antimicrob. Agents Chemother.* 52, 1743–1750.

- Tuncer, D.I., Nevin, C., 2007. Controlled delivery of peptides and proteins. *Curr. Pharm. Des.* 13, 99–117.
- Valdivia, L., Nix, D., Wright, M., Lindberg, E., Fagan, T., Lieberman, D., et al., 2006. Coccidioidomycosis as a common cause of community-acquired pneumonia. *Emerg. Infect. Dis.* 12, 958–962.
- Vaughn, J.M., McConville, J.T., Burgess, D., Peters, J.I., Johnston, K.P., Talbert, R.L., et al., 2006. Single dose and multiple dose studies of itraconazole nanoparticles. *Eur. J. Pharm. Biopharm.* 63, 95–102.
- Vyas, S.P., Khatri, K., Goyal, A.K., 2009. Functionalized nanocarrier(s) to image and target fungi infected immune cells. *Med. Mycol.* 47, S362–S368.
- Walsh, T.J., Anaissie, E.J., Denning, D.W., Herbrecht, R., Kontoyiannis, D.P., Marr, K.A., et al., 2008. Treatment of aspergillosis: clinical practice guidelines of the Infectious Diseases Society of America. *Clin. Infect. Dis.* 46, 327–360.
- Walsh, T.J., Goodman, J.L., Pappas, P., Bekersky, I., Buell, D.N., Roden, M., et al., 2001. Safety, tolerance, and pharmacokinetics of high-dose liposomal amphotericin B (AmBisome) in patients infected with *Aspergillus* species and other filamentous fungi: maximum tolerated dose study. *Antimicrob. Agents Chemother.* 45, 3487–3496.
- Walsh, T.J., Raad, I., Patterson, T.F., Chandrasekar, P., Donowitz, G.R., Graybill, R., et al., 2007. Treatment of invasive aspergillosis with posaconazole in patients who are refractory to or intolerant of conventional therapy: an externally controlled trial. *Clin. Infect. Dis.* 44, 2–12.
- Walsh, T.J., Yeldandi, V., McEvoy, M., Gonzalez, C., Chanock, S., Freifeld, A., et al., 1998. Safety, tolerance, and pharmacokinetics of a small unilamellar liposomal formulation of amphotericin B (AmBisome) in neutropenic patients. *Antimicrob. Agents Chemother.* 42, 2391–2398.
- Wheat, L.J., Conces, D., Allen, S.D., Blue-Hnidy, D., Loyd, J., 2004. Pulmonary histoplasmosis syndromes: recognition, diagnosis, and management. *Semin. Respir. Crit. Care Med.* 25, 129–144.
- Wheat, L.J., Freifeld, A.G., Kleiman, M.B., Baddley, J.W., McKinsey, D.S., Loyd, J.E., et al., 2007. Clinical practice guidelines for the management of patients with histoplasmosis: 2007 update by the Infectious Diseases Society of America. *Clin. Infect. Dis.* 45, 807–825.
- Wong-Beringer, A., Lambros, M.P., Beringer, P.M., Johnson, D.L., 2005. Suitability of caspofungin for aerosol delivery: physicochemical profiling and nebulizer choice. *Chest* 128, 3711–3716.
- Yang, W., Peters, J.I., Williams, 3rd, R.O., 2008a. Inhaled nanoparticles—a current review. *Int. J. Pharm.* 356, 239–247.
- Yang, W., Tam, J., Miller, D.A., Zhou, J., McConville, J.T., Johnston, K.P., et al., 2008b. High bioavailability from nebulized itraconazole nanoparticle dispersions with biocompatible stabilizers. *Int. J. Pharm.* 361, 177–188.
- Yu, J., Chien, Y.W., 1997. Pulmonary drug delivery: physiologic and mechanistic aspects. *Crit. Rev. Ther. Drug Carrier Syst.* 14, 395–453.
- Zia, Q., Khan, A.A., Swaleha, Z., Owais, M., 2015. Self-assembled amphotericin B-loaded polyglutamic acid nanoparticles: preparation, characterization and in vitro potential against *Candida albicans*. *Int. J. Nanomed.* 10, 1769–1790.
- Zmeili, O.S., Soubani, A.O., 2007. Pulmonary aspergillosis: a clinical update. *QJM* 100, 317–334.
- Zu, Y., Sun, W., Zhao, X., Wang, W., Li, Y., Ge, Y., et al., 2014. Preparation and characterization of amorphous amphotericin B nanoparticles for oral administration through liquid antisolvent precipitation. *Eur. J. Pharm. Sci.* 53, 109–117.

FURTHER READING

- Peng, H.S., Liu, X.J., Lv, G.X., Sun, B., Kong, Q.F., Zhai, D.X., et al., 2008. Voriconazole into PLGA nanoparticles: improving agglomeration and antifungal efficacy. *Int. J. Pharm.* 352, 29–35.

Current Status and Future Scope for Nanomaterials in Drug Delivery

Biswajit Mukherjee, Niladri Shekhar Dey, Ruma Maji,
Priyanka Bhowmik, Pranab Jyoti Das and
Paramita Paul

Additional information is available at the end of the chapter

<http://dx.doi.org/10.5772/58450>

1. Introduction

Nanotechnology is a revolutionary field of micro manufacturing involving physical and chemical changes to produce nano-sized materials. The word “nano” is a Latin word meaning “dwarf”. Mathematically a nanometer is equal to one thousand millionth of a meter [1]. A nanomaterial consists of aggregated as well as unbound particles. Nanotechnology in scientific terms is defined as the science which deals with processes that occur at molecular and atomic level or at nanolength size. It involves designing, synthesis and characterization of material structure by controlling the shapes and sizes at nano scale. The conversion of a particle to nano scale size changes the properties of the material such as increase in surface area, dominance of quantum effects often associated with minute sizes, higher surface area to volume ratio etc. and varies material’s magnetic, thermal and electrical property. For example, copper which is opaque at macro scale becomes transparent at nano scale. Similarly the properties of gold at nanoscale causes change in melting point from 200°C to 1068°C and colour changes from yellow to blue to violet along with the change in its catalytic property [2]. Nanoparticles are persistent in nature as well. Functional proteins may be classified as nanoparticles. Some biological system consists of nanoparticles which are devoted to locomotory function. The colours on butterfly’s wings are due to light being bounced off nanoscale layers in the structure of the wings. The red and yellow colours seen at sunset are also due to nanoparticles [3]. Super paramagnetic iron oxide less than 50 μm are used for imaging of organs. They can be even used for treating complicated brain disorder bio-imaging at nano scale size [9].

Indian craftsman and artisan used nanotechnology for designing weapons in early times. The first observation and size measurement of nanoparticle were carried out using an ultra microscope by Richard Zsigmondy in 1902. The term nanotechnology was first time used by a researcher named Norio Taniguchi in University of Tokyo in 1974. In 1980 the inventions of two atoms further advanced the field of Nanotechnology. In 1985 fullerene C_{60} was discovered by Kroto's and Smalley's research team. In 1991 carbon tubes were discovered by Saumio Iijima and by 2000 National Nanotechnology Initiative (NNI), The United States was launched which paved the way for future development in nanotechnology [2].

Nanotechnology may be considered as one of the main propellants for technological, economical change as industrial competition. Nanotechnology has integrated various disciplines including biomedicine, engineering and technology. Nanotechnology is being used for improving the existing products and to create new products. The strength can be varied accordingly with the requirements of engineering. It can be used to make the water cleaner by remediation to remove its pollutant. It has helped to clean the environment by removing pollutants and has generated cleaner and cheaper energy. It has improved the healthcare system by introducing new devices for diagnosis, monitoring, treatment of diseases and drug-delivery [1].

Nanomaterials have wide applications in pharmaceutical sciences and technology. Few other predominant areas of use of nanotechnology are in drug delivery, and as diagnostic imaging and biosensor. These devices of nanoscale size are popularly known as nanomedicine. Thus nanomedicines are sub-micron size materials ($<1\mu\text{m}$) which are used for treatment, monitoring and diagnostic purposes. In the present chapter we will discuss on the current status and future strategies of nanosize drug delivery systems.

2. Significance of nanomaterials in drug delivery

There are many reasons for which nanoscale size drug delivery systems are attractive to formulation scientists. The most important reason is that number of surface atoms or molecules to the total number of atoms or molecules increases in drug delivery systems. Thus the surface area increases. This helps to bind, adsorb and carry with other compounds such as drug, probes and proteins. The drug particles itself can be engineered to form nanoscale size materials too [4]. The nanosize device systems, sizes smaller than eukaryotic or prokaryotic cells, can eventually much more in amount reach in generally inaccessible areas such as cancer cells, inflamed tissues etc. due to their enhanced permeability and retention effect (EPR) and can impair lymphatic drainage thus that can be used for administration of genes, proteins through the peroral route of administration [5]. They can be used to target the reticuloendothelial cells, thereby facilitating passive targeting of drug to the macrophages of liver and spleen and thus enabling a natural system for treating intracellular infections [6]. The nanomaterials used for the purpose should be soluble, safe and biocompatible as well as bioavailable. They should not occlude blood vessel and less invasive and the toxicity associated with the nanomaterials for drug delivery should be

very low so that they can be used to target the specific diseased tissue in a safe concentration [7]. They need protecting drug from enzymatic and hydrolytic degradation in the gastrointestinal tract and help in bypassing the “first-pass” metabolism in the liver. They generally remain in the circulation for longer time especially those coated with hydrophilic polymers and hence suitable for enhancing the efficacy of drugs with short half-lives and can be used to monitor drug as sustained release formulation as well as for delivering DNA [8]. The dissolution rate of drug is enhanced, onset of therapeutic action is increased, and the dose is reduced. The premature loss of drug through rapid clearance and metabolism can also be prevented [6]. They also increase retention due to bio-adhesion.

Nanoscale drug delivery systems such as nanoparticles, nanoliposomes, dendrimers, fullerene, nanopores, nanotubes, nanoshells, quantum dots, nanocapsule, nanosphere, nanovaccines, nanocrystals etc. are believed to have potentials to revolutionize drug delivery systems. Further nanomaterials on chips, nano robotics, and magnetic nanoparticles attached to specific antibody, nanosize empty virus capsids and magnetic immunoassay are new dimensions of their use in drug delivery. Thus nanomaterials can be used for strategic development of new drug delivery systems and reformulating existing drugs to enhance the effectiveness, patent protection, patient-compliance, safety of drugs and decreasing the cost of health care [9].

3. Various nanoscale drug delivery systems

3.1. Nanoparticles

Nanoparticles are submicron-sized polymeric colloidal particles with therapeutic agents of interest encapsulated or dispersed within their polymeric matrix or adsorbed or conjugated onto the surface. Commonly used synthetic polymers to prepare nanoparticles for drug delivery are generally biodegradable [10]. Nanoparticles may also be composed of or transport a variety of substances such as silica, gold or other heavy metals, medicaments, quantum dots, nanocrystals, quantum rods and various contrast agents [11]. Nanoparticle systems offer major improvements in therapeutics through site specificity, their ability to escape from multi-drug resistance and the efficient delivery of an agent. They can be used for active drug targeting attaching ligand such as antibody on their surface (Figure 1).

Solid lipid nanoparticles (SLNs) refer to as lipospheres or solid lipid nanospheres, or particles and are generally solid at human physiological temperature (37°C) and have a diameter less than 1000 nm [12]. They can be formed from a range of lipids, including mono-, di- and triglycerides, fatty acids, waxes and combinations thereof. SLNs must be stabilized by surfactants to form administrable emulsions. SLNs form a strongly lipophilic matrix into which drugs can be loaded for subsequent release. SLNs have been investigated for the delivery of various cancer treatments like colon cancer, breast cancer [13].

Polymer-based nanoparticles have been extensively investigated as drug nanocarriers. The most widely researched synthetic polymers include polylactide (PLA), poly (D,L-lactide-co-

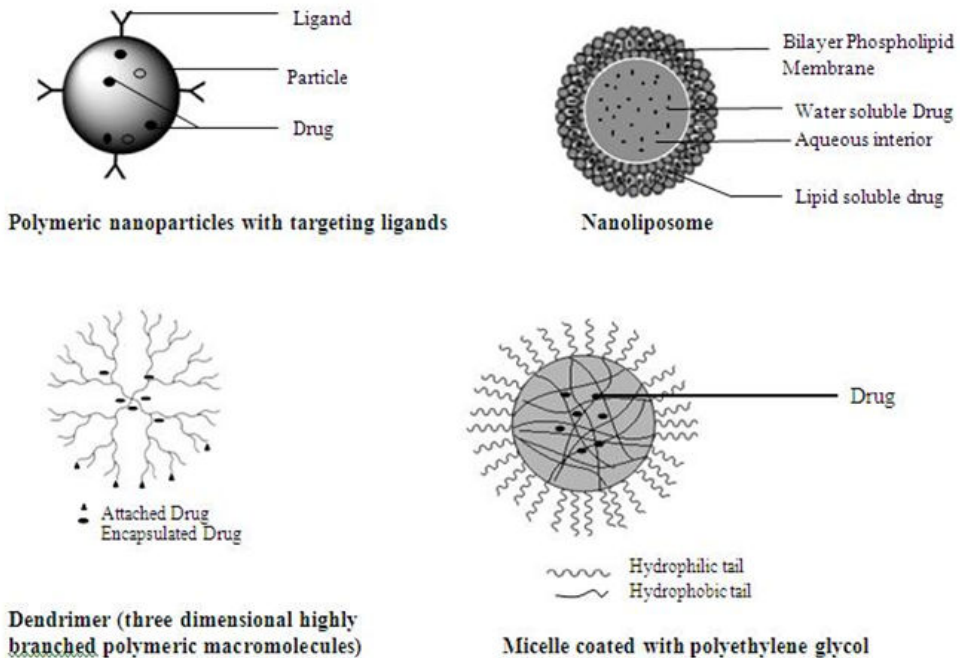


Figure 1. Different Types of Nanocarriers for drug delivery

glycolide) (PLGA) and poly ethylene glycol (PEG). All three polymers are hydrolyzed *in vivo* and are biodegradable. Other polymers based on biological polysaccharides have been extensively investigated, including chitosan, Cyclodextrin and dextrans [14].

Gold nanoparticles (NPs) consist of a core of gold atoms that can be functionalized by addition of a monolayer of moieties containing a thiol (SH) group. Gold NPs can be synthesized using NaBH_4 to reduce AuCl_4 salts in the presence of thiol containing moieties that subsequently form a monolayer around the core gold atom, depending on the stoichiometric gold/ thiol ratio [15]. Drug delivery using gold NPs has been made in DNA delivery for gene therapy and imaging [16]. PEG coated micelles containing drug are also used to deliver drug as new delivery system (Figure 1). Many other nanoparticulate synthetic, semisynthetic, natural and metals are under investigation to know their potentials as drug delivery materials.

Polymeric nanoparticles may adhere to the cell surface and release drug molecules by diffusion which may enter inside the cell to work. However the entire polymeric nanoparticles can also enter the cell by endocytosis. They bind with the cell surface receptor and formation of endosome takes place. Endosome may be lysed with the help of lysosomal enzymes and the nanoparticles release in the cytoplasm (Figure 2).

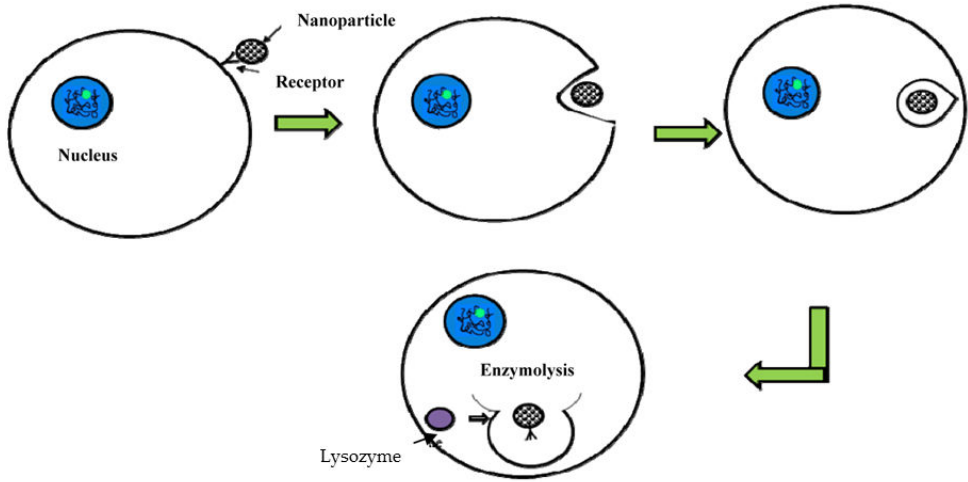


Figure 2. Endocytosis mediated cellular internalization of drug nanocarriers

3.1.1. Nanoliposomes

Nanoliposomes are the nanosize vesicles made of bilayered phospholipid membranes generally unilamellar with an aqueous interior (Figure 1) [17]. They can be used for the delivery of low molecular weight drugs, imaging agents, peptides, proteins, and nucleic acids. Different anticancer, antiviral drugs are incorporated within the liposomes [18]. Nanoliposomes can also provide slow release of an encapsulated drug, resulting in sustained exposure to the site of action and enhanced efficacy. Usually hydrophilic drugs can be loaded in aqueous compartment and lipophilic drugs are incorporated in the phospholipid layer [19]. However unlike liposome nanoliposome does not undergo rapid degradation and clearance by liver macrophages. As for the targeted drug delivery, nanoliposome plays an important role. It can be used for passive targeting or active targeting [20]. Due to the leaky vascular structure of the tumor tissue nanoliposomes get predominantly accumulated in the tumor and release the drug for a prolonged period of time in passive targeting. Active targeting is achieved by incorporating antibody, ligands etc. on the nanoliposomal surface. By active targeting liposomes directly go to the targeted organs or tissues, and release drug for a prolonged period of time, so that the normal cells are not affected and only the diseased cells are affected [21]. Targeted nanoliposomal drug delivery is more efficacious than the non-targeted drug delivery systems. C6-ceramide ligand induced nanoliposome used to treat the blood cancer directly targets the over expressed leukemic cells and decreases the high expression of survivin protein in leukemic cells [22]. The concept of long-circulating or sterically stabilized nanoliposomes is derived for novelibility of delivery systems which can circulate in the blood for a long period of time. Nanoliposomal formulations containing polyethylene glycol (PEG) alter the pharma-

cokinetic properties of various drug molecules leading to long elimination half-life [23]. Nanoliposomes are expected to bring lots of change in drug delivery in near future.

3.1.2. Dendrimers

Dendrimers are branched polymers, resembling the structure of a tree (Figure 1). Dendrimers represent three dimensional highly branched polymeric macromolecules with the diameter varying from 2.5 to 10 nm. It can be synthesized from both synthetic and natural monomers e.g. aminoacids, monosaccharides and nucleotides. Two classes of dendrimers commonly used for biomedical applications are polyamidoamines and polypropyleneimines [24]. A dendrimer is typically symmetric around the core, and when sufficiently extended it often adopts a spheroidal three-dimensional morphology in water. A central core can be recognized in their structure with at least two identical chemical functionalities. Starting from those groups, repeated units of other molecules can originate with at least one junction of branching. The repetitions of chains and branching result in a series of radially concentric layers with increased crowding [25].

The overall shapes of dendrimers range from spheres to flattened spheroids (disks) to amoeba-like structures, especially in cases where surface charges exist and give the macromolecule a "starfish"-like shape. Branching of dendrimers depends on the synthesis processes. Low molecular weight drugs can be placed into the cavities within the dendrimer molecules and are temporarily immobilized there with hydrophobic forces, hydrogen and covalent bonds [26]. The two processes for the synthesis of dendrimers are divergent and convergent methods. In the divergent method dendrimer grows outwards from a multifunctional core molecule. The core molecule reacts with monomer molecules containing one reactive and two dormant groups giving the first generation dendrimer. The convergent method is developed as a response to the weakness of the divergent synthesis. In the convergent approach, the dendrimer is constructed stepwise, starting from the end groups and progressing inwards. When the growing branched polymeric arms, called dendrons, are large enough, they are attached to a multifunctional core molecule. The convergent method is relatively easy to purify the desired product and the occurrence of defects in the final structure is minimised [27]. Due to classical polymerization dendrimers have a negligible degree of polydispersity. They are random in nature and produce molecules of various sizes. The size of dendrimers can be carefully controlled during the process of synthesis of dendrimers. Scientists are focusing on newer approaches for speeding up the synthesis process by preassembly of oligomeric branches which can be linked together to reduce the number of synthesis steps involved and also increase the dendrimer yield [28].

Dendrimers are popularly used for transfer of genetic materials in cancer therapy or other viral diseases in different organs because of their monodispersity, high density of functional groups, well-defined shape and multivalency. In gene delivery polyamidoamines (PAMAM) dendrimer is widely used. Some other types of dendrimers are peptide dendrimers, glyco-dendrimers, polypropilimine dendrimers, Polyethyleneimine (PEI) dendrimers etc.

3.1.3. Nanoshells

Nanoshells (100-200 nm) may be used for drug carrier of both imaging and therapy. Nanoshells consist of nanoparticles with a core of silica and a coating of thin metallic shell [29]. They can be targeted to a tissue by using immunological methods. Nanoshells can also be embedded in a hydrogel polymer [30]. Nanoshells are currently being investigated for prevention of micrometastasis of tumors and also for the treatment of diabetes. Nanoshells are useful for diagnostic purposes in whole blood immunoassays [31].

3.2. Fullerenes and nanotubes

Fullerenes composed of carbon in the form of a hollow sphere or ellipsoid tube. These are also known as 'bucky balls' because of their resemblance to the geodesic dome design of Buckminster Fuller. Fullerenes are being investigated for drug transport of antiviral drugs, antibiotics and anticancer agents [32]. Fullerenes have the potential to stimulate host immune response and productions of fullerene specific antibodies. Soluble derivatives of fullerenes such as C60 have shown great utility as pharmaceutical agents.

Nanotubes are nanometer scale tube like structure and they are of different types like carbon nanotube, inorganic nanotube, DNA nanotube, membrane nanotube etc. [33]. Carbon nanotubes can be made more soluble by incorporation of carboxylic or ammonium groups to their structures and can be used for the transport of peptides, nucleic acids and other drug molecules. The ability of nanotubes to transport DNA across cell membrane is used in studies involving gene therapy. DNA can be attached to the tips of nanotubes or can be incorporated within the tubes [34].

3.3. Nanopores

Nanopores (20 nm in diameter) consist of wafers with high density of pores which allow entry of oxygen, glucose and other chemicals such as insulin to pass through. Nanopores can be used as devices to protect transplanted tissues from the host immune system, at the same time, utilizing the benefit of transplantation [35]. β -Cells of pancreas can be enclosed within the nanopore device and implanted in the recipient's body. Nanopores can also be employed in DNA sequencing. Nanopores are also being developed with an ability to differentiate purines from pyrimidines [36].

3.4. Quantum dots

Quantum dots (QD) are tiny semiconductor nanocrystals type of particles generally no larger than 10 nanometers that can be made to fluoresce in different colours when stimulated by light. The biomolecule conjugation of the QD can be modulated to target various biomarkers [37]. They can be tagged with biomolecules and used as highly sensitive probes. QD can also be used for imaging of sentinel node in cancer patients for tumour staging and planning of therapy. This technology also outlines some early success in the detection and treatment of breast cancer [38]. QD may provide new insights into understanding the pathophysiology of cancer and real time imaging and screening of tumors.

Bioconjugated QD are collections of variable sizes of nanoparticles embedded in tiny beads made of polymer material. In a process called “multiplexing,” they can be finely tuned to a myriad of luminescent colors that can tag a multitude of different protein biomarkers or genetic sequences in cells or tissues [39]. The new class of quantum dot conjugate contains an amphiphilic triblock copolymer layer for *in vivo* protection and multiple PEG molecules for improved biocompatibility and circulation, making it highly stable and able to produce bright signals. Another advantage is that quantum dot probes emitting at different wavelengths can be used together for imaging and tracking multiple tumor markers simultaneously, potentially increasing the specificity and sensitivity of cancer detection [40]. Recent progress in the surface chemistry of QD has expanded their use in biological applications, reduced their cytotoxicity and rendered quantum dots a powerful tool for the investigation of distinct cellular processes, like uptake, receptor trafficking and intracellular delivery. Another application of QD is for viral diagnosis. Rapid and sensitive diagnosis of Respiratory Syncytial Virus (RSV) is important for infection control and development of antiviral drugs. Antibody-conjugated nanoparticles rapidly and sensitively detect RSV and estimate relative levels of surface protein expression. A major development is the use of dual-colour QD or fluorescence energy transfer nanobeads that can be simultaneously excited with a single light source [41]. QD linked to biological molecules, such as antibodies, have shown promise as a new tool for detecting and quantifying a wide variety of cancer-associated molecules. In the field of nanomedicine, QD can make a worthy contribution to the development of new diagnostic and delivery systems as they offer unique optical properties for highly sensitive detection and they are well defined in size and shape and can be modified with various targeting principles.

4. Applications of Nanoscale drug delivery systems

4.1. Nanotechnology for brain drug delivery

The blood brain barrier (BBB) is a structure formed by a complex system of endothelial cells, astroglia, pericytes, and perivascular mast cells, preventing the passage of most circulating cells and molecules [42]. The tightness of the BBB is attributed mainly to the vascular layer of brain capillary endothelial cells which are interconnected side-by-side by tight and adherens junctions. Among the different nanodevices, nanosize drug delivery systems between 1 and 100 nm work as a whole unit in terms of transport to cross BBB [43]. Nanosize brain drug delivery systems may promote the targeting ability of drug in brain and at the same time enhance the permeability of molecules through BBB. However crossing of BBB by the nano drug carriers will depend completely on the physicochemical and biomimetic features and does not depend on the chemical structure of drug, inside the nanoparticles [44]. Nanosize drug carriers which do not cross BBB generally can be made “stealth” coated with some polymeric materials or other chemicals to avoid the reticuloendothelial system, to display long circulation time and stability in blood, and may be functionalized to successfully cross the BBB and target brain [45].

4.2. Nanosize drug carriers in ocular drug delivery

Drug loaded nanoparticles with favourable biological properties include prolonging the residence time, decreasing toxicity and high ability of drug penetration into the deeper layers of the ocular structure and minimizing precorneal drug loss by the rapid tear fluid turnover [46]. Nanoparticles could target at cornea, retina and choroid by surficial applications and intravitreal injection. Nanocarrier based drug delivery is suitable in the case of the retina, as it has no lymph system, hence retinal neovascularisation and choroidal neovascularization have similar environments to that of solid tumors, and the EPR effect as available for solid nanoparticles in case of solid tumor may be also available for drug delivery targeted to eyes by nanoparticles [47]. Nanoparticles can deliver ocular drugs to the target sites for the treatment of various diseases such as glaucoma, corneal diseases, diabetic retinopathy etc. The uses of nanotechnology based drug delivery systems like nanosuspensions, SLNs and nanoliposomes have greater effect for ocular therapeutic efficacy [48]. Nanotechnology-based drug delivery is also very efficient in crossing membrane barriers, such as the blood retinal barrier in the eye.

4.3. Nanoparticle loaded contact lenses

Contact lenses loaded with nanoparticles can be effective for topical administration of ophthalmic drugs. Drug loaded contact lenses can also provide continuous drug release because of slow diffusion of the drug molecules through the lens matrix. The soaked contact lenses also delivered drugs only for a period of few hours for some typical drugs [49]. The duration of drug delivery from contact lenses can be significantly increased if the drug is first entrapped in nanoformulations, such as nanoliposomes, nanoparticles, or microemulsions. Such drug nanocarriers can then be dispersed throughout the contact lens material. The entrapment of drug in nanocarriers also prevents the interaction of drug with the polymerization mixture. This provides additional resistance to drug release, as the drug must first diffuse through the nanocarriers and penetrate the drug carrier surface to reach the contact lens matrix [50].

4.4. Biodistribution of nanoparticles in the retina

The ocular biodistribution of nanoparticles can provide insights into the bioavailability, cellular uptake, duration of drug action and toxicity. Factors such as particle size, composition, surface charge and mode of administration influence the biodistribution in the retinal structures and also their drainage from the ocular tissues [51]. Larger particles (2 μm) were found to remain in vitreous cavity near the trabecular meshwork from which they are discharged out from the ocular tissue within 6 days, whereas the particles 200 nm were found evenly distributed in the vitreous cavity, and the inner limiting membrane. The smaller particles ~ 50 nm crossed the retinal barriers, and was detected in the retina even after 2 months post injection [52]. The surface chemistry can also affect nanoparticle distribution. Positively charged nanoparticles can adhere to the anionic vitreous network components and aggregate within the vitreous network. The surface chemistry can also affect nanoparticle distribution. Positively charged nanoparticles can adhere to the anionic vitreous network components and aggregate

within the vitreous humor [53]. Anionic nanoparticles were found to diffuse through the vitreous humor and could even penetrate the retinal layers to be taken up by Muller Cells [54]. Vitreous humor is regarded as the barrier for non-viral ocular gene therapy because of the strong interaction of conventional cationic nature of non-viral gene vectors with the anionic vitreous humor [53]. The cationic PEI nanoparticles aggregated within vitreous humor and were prevented from distributing to the retina by the vitreal barrier. In contrast, cationic glycol chitosan (GC) nanoparticles and GC/PEI blended nanoparticles could penetrate the vitreal barrier and even reach at the inner limiting membrane because of the existence of glycol groups on nanoparticles [55].

4.5. Nanoparticles in cancer

Cancer cells are more vulnerable than normal cells to the effect of chemotherapeutic agents and the most of the anticancer drugs can cause injury to the normal cells. Optimum dose and frequency are both important factors in the persistence of cancer cells during cancer chemotherapy [56]. Now attempts are focused on efforts to kill cancer cells by more specific targeting while sparing the normal cells.

Nanoparticulate delivery systems in cancer therapies provide better penetration of therapeutic and diagnostic substances within the cancerous tissue in comparison to conventional cancer therapies [57]. Nanoparticles are constructed to take advantages of fundamental cancer morphology and modes of development such as rapid proliferation of cells, antigen expression, and leaky tumor vasculature. Nanoparticulate drug delivery systems are being developed to deliver smaller doses of chemotherapeutic agents in an effective form and control drug distribution within the body [58]. Nanocarriers can offer many advantages over free drugs in cancer chemotherapy such as they protect the drug from premature degradation, prevent drugs from prematurely interacting with the biological environment, enhance absorption of the drugs into a selected tissue (solid tumour), control the pharmacokinetic and drug tissue distribution profile and improve intracellular penetration [59].

Nanoparticulate delivery systems utilize specific targeting agents for cancer cells minimizing the uptake of the anticancer agent by normal cells and enhance the entry and retention of the agent in tumor cells (Figure 3) [60]. Nanocarriers may actively bind to the specific cancer cells by attaching targeting agents with the help of ligand molecules to the surface of the nanocarriers that bind to specific receptor antigens on the cell surface. Nanocarriers will recognize and bind to target cells through ligand receptor interactions. It is even possible to increase the drug targeting efficacy with the help of antibodies by conjugating a therapeutic agent directly to it for targeted delivery [61].

Like receptor targeting, targeting of angiogenic factors also takes advantage of properties unique to cancer cells. Anti-angiogenic treatment is the use of drugs or other substances to stop tumors from developing new blood vessels. In a study nanoparticles were formulated comprising a water-based core of Vickers microhardness sodium alginate, cellulose sulphate, and anti-angiogenic factors such as thrombospondin (TSP)-1 or TSP-517, crosslinked with dextran polyaldehyde with calcium chloride or conjugated to heparin sulphate with sodium chloride. In addition bioluminescent agent, luciferase, or contrast agent, polymeric gadolinium

was located within the polyanionic core [62] for drug targeting and detection. Similarly, many efforts are on for cancer cell targeting specifically with drug nanocarriers. Thus the drug nanocarriers are of great hope for future cancer therapy.

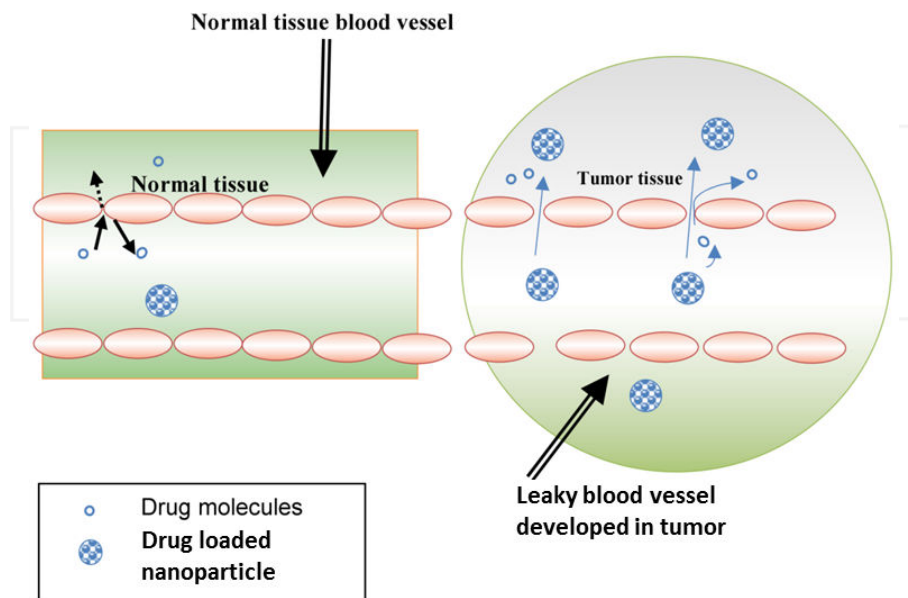


Figure 3. Schematic diagram of nanoparticle permeation and retention effect in normal and tumour tissues. Normal tissue vasculatures are lined by tight endothelial cells, hereby preventing nanoparticulate drug delivery system from escaping, whereas tumor tissue vasculatures are leaky and hyperpermeable allowing preferential accumulation of nanoparticles or nanoliposomes in the tumor interstitial space by passive targeting

4.6. Gene delivery

Transfer of genetic material in nanocarriers may be an approach for the treatment of various genetic disorders such as diabetes mellitus, cystic fibrosis, alpha 1 antitrypsin deficiency and may more. A number of systemic diseases are caused by lack of enzymes factors that are due to missing or defective genes [63]. Previously gene therapy which was used to treat genetic disorders nowadays being contemplated as carrier systems which could be implanted for combating diseases other than genetic disorder like malignant form of cancer, heart diseases and nervous diseases [64]. Nanoliposomes can be used to deliver genetic materials into cells. Nanoliposomes incorporated with PEG and galactose target liver cells effectively due to their rapid uptake by liver Kupffer cells. Gene therapy may be tried with liposomal nanocarriers for liver disorders such as Wilson's and hereditary hemochromatosis. Cationic nanoliposomes have been considered as potential non-viral human gene delivery system [65]. Another effective method for administering nanoliposomes is by using ligand receptor complex using EGF-EGFR system for targeting purpose by nanoliposomes where EGF is a small protein which

binds with receptor EGFR. Also mixing cationic lipids with plasmid DNA leads to the formation of lipoplexes where the process is driven by electrostatic interactions [66]. The negatively charged genetic material (e.g. plasmid) is not encapsulated in nanoliposomes but complexed with cationic lipids by electrostatic interactions. Plasmid liposome complexes can enter the disease cells by infusion with the plasma or endosome membrane. Allovectin-7 (gene transfer product) is composed of a plasmid containing the gene for the major histocompatibility complex antigen HLA-B7 with B2 microglobulin formulated with the cytofectin [67]. The nature of a composed lipid decides the unloading of the gene from nanoliposomes which enables control over the mode of release, doping of nanoliposomes with neutral lipids such as 1,2-Dioleoyl-sn-glycero-3-phosphoethanolamine (DOPE) which helps in endosomal membrane fusion by recognizing and destabilizing the phospholipids in a flip flop manner which paves way for the liposomes to integrate in the membrane with the dissociation of nucleic acid into the cytoplasm [64].

Viral system based gene carrier had the ability to overcome the biological barriers in the body and then access to the host nucleus replicative machinery which resulted in the exploitations of the system for drug delivery using nanotechnology [64]. The development of a non-viral method for *in vivo* gene transfer was designed where the vector was packed into compact nanoparticles by successive additions of oppositely charged polyelectrolytes including an incorporation of ligands into the DNA-polyelectrolyte shells which were mixed with Pluronic F127 gel serving as a biodegradable adhesive to keep shells in contact with the targeted vessel [68].

A novel method of gene delivery is with viruses such as adeno associated virus (AAV) which have their virulent genes removed with lentiviruses, clearly showing their efficiency [64].

8. Drug delivery with the help of empty virus capsid

The viral nanoparticles (VNPs) consist of protein core which ranges in complexity from small capsid-protein homomers to larger protein-based heteromers capable of internalizing oligonucleotides and being enveloped by lipids. Chemical modification process and genetic mutation provide the viral coat proteins with receptor binding domain that helps in cell specific targeting of VNPs [69]. Even fusion of terminal / internal proteins on the surface or inside the VNPs can be utilized for introduction of heterologous peptides, and in some cases entire proteins. VNPs can be genetically engineered by inserting amino acids for bioconjugation, peptide based affinity tags and peptides as targeting ligands for stimulation of immune response. [70].

High sequence variability due to the influence of the immune system in viral life-cycles is often seen on the surface loops of viral capsid proteins. This variability makes the loops highly susceptible to insertion of foreign sequences. VP1, the major coat protein of viruses of Polyomaviridae family, when expressed in insect cells, yeast and *Escherichia coli* self-assembles as protein cages and shows natural affinity for a cell surface glycoprotein with a terminal a 2,3-linked N-acetylneuraminic acid and attaches to a4h1-integrin receptors [71]. Virus like particle

(VLPs) constructed from the virus are used to deliver therapeutic genes to human fetal glial cells. Another technique Cell-docking involves attachment of antibodies to the surface of brain natriuretic peptide (BNPs). Coupling reaction between murine polyoma-virus and antitumor antibody B3 yielded polyoma VLPs with 30 to 40 antibody fragments bound to the surface, allowing the modified VLPs to bind to the breast carcinoma cells with high efficiencies [72].

9. A glimpse to future of nanosize drug delivery systems

Advancement of nanosize drug delivery systems establishes a new paradigm in pharmaceutical field. Convergence of science and engineering leads a new era of hope where medicines will act with increase efficacy, high bioavailability and less toxicity. Several nanoscale drug delivery systems are currently in clinical trials and few of them are already commercially available. Examples of such products are Abeicet (for fungal infection), Doxil (antineoplastic), Abraxane (metastatic breast cancer), Emend (antiemetic) etc. Despite the impressive progress in the field, very few nanoformulations have been approved by US-FDA (United States Food and Drug Administration) and even reached market in recent years. Although nanocarriers have lots of advantages because of the unique properties they have, there are many clinical, toxicological and regulatory aspects which are the matters of concern too. The biocompatibility of nanomaterials is of utmost importance because of the effect of the nanomaterials in the body ranging from cytotoxicity to hypersensitivity [8]. With the advancement of nanotechnology, the biological phenomenon such as host response to a specific nanomaterial should also be clinically transparent [9]. Therefore it is quite essential to introduce cost effective, better and safer nanobiomaterials which will provide efficient drug loading and controlled drug release of some challenging drug moieties for which there is no other suitable delivery available yet.

Nanoliposomes are well developed and presently possess the highest amount of clinical trials among other nanomaterials with some formulations currently in the market. This may be due to the fact that other materials have not been investigated for the same duration and are relatively newer in comparison. However polymer based nanomaterial, carbon nanotubes, gold nanoparticles etc. should not be overlooked because of less number of clinical trials [7].

Genexol-PM is an example which was undergone recent clinical trial. This is an amphiphilic diblock co-polymer (PEG-D, L-Lactic acid) that delivers paclitaxel. Clinical trial currently is in phase IV using Genexol-PM for recurrent breast cancer and phase III for breast cancer. Fungal infections associated with acute leukemia and for central line fungal infections, amphotericin B containing nanoliposomes are in phase IV clinical trial. ThermoDox (Doxorubicin loaded nanoliposome) is currently in phase III trials for hepatocellular carcinoma. Similarly Caelyx, a doxorubicin HCl loaded nanoliposome that is pegylated, is currently in phase IV trials for ovarian neoplasms [7]. Some recent clinical trials are shown in Table 1.

Ligand or antibody conjugated nanoformulation, bifunctional and multifunctional nanoparticles are the newer research approaches through which detection and treatment of cancerous cells can be achieved. Nanomachines are also largely in the research-and-development phase, but some primitive molecular machines have been tested. An example is nanorobot which is

capable of penetrating the various biological barriers of human body to identify the cancer cells. Thus, nanodrug delivery systems have a leading role to play in nanomedicine in near future.

Product name	Delivery material	Phase	Condition	Therapeutic Delivered	Sponsor	Clinicaltrials.gov Identifier
Genexol-PM	Amphilic diblock Copolymer forming micelle	I	Non small Cell lung cancer	Paclitaxel	Samyang Biopharmaceutical Corp	NCT01023347
Docetaxel-PNP	Polymeric nanoparticles	I	Advanced solid malignancies	Docetaxel	Samyang Biopharmaceutical Corp	NCT01103791
CYT-6091	AuNP	I	Unspecified adult solid tumor	TNF	NCI	NCT00356980
Paclitaxel poliglumex	Drug Polymer Conjugate	II	Prostate cancer	Paclitaxel	OHSU Knight Cancer Institute	NCT00459810
Kogenate FS	PEG-liposome	I	Hemophilia A	Recombinant factor VIII	Bayer	NCT00629837
Long-circulating liposomal prednisolone disodium phosphate	Liposome	II	Rheumatoid arthritis	Prednisolone	Radboud University	NCT00241982
LE-DT	Liposome	II	Pancreatic cancer	Doxetaxel	Insys Therapeutics Inc	NCT01186731
Cisplatin and Liposomal Doxorubicin	Liposome	I	Advanced cancer	Cisplatin and doxorubicin	M.D. Anderson Cancer Center	NCT00507962
Liposomal doxorubicin and bevacizumab	Liposome	II	Kaposi's sarcoma	Doxorubicin and bevacizumab	NCI	NCT00923936
AP5346	Drug polymer conjugate	Not stated	Head and neck cancer	AP5346 and oxaliplatin	University of California, San Diego	NCT00415298

Abbreviations: PEG-Polyethylene glycol, TNF-Tumor necrosis factor, NCI-National Cancer Institute, AuNP-Gold nanoparticles

Table 1. Recent Nanodrug Carriers in Clinical Trials (Source: Clinicaltrials.gov)

Nanocarriers may lead to a solution to major unsolved medical problems which will aggressively enhance quality of life.

Regulatory aspect: One of the main areas related to the safety aspects of drug-nanocarrier systems is to encourage academic organizations, industry and regulatory governmental agencies to establish convincing testing procedures on the safety aspects of the nanomaterials.

The global importance of trade for nanomaterials has established new international organizations, such as the International Council on Nanotechnology (ICON), the International Organization for Standardization (Geneva, Switzerland) etc. for sharing responsibilities in this field. In the year 1996 the NNI was established in the United States of America to coordinate governmental multi-agencies such as the Food and Drug Administration (FDA), the Department of Labor through the Occupational Safety and Health Administration (OSHA), the National Institute for Occupational Safety and Health (NIOSH), and the Environmental Protection Agency (EPA), for the development of nanoscience and technology.

10. Conclusion

Last few years several new technologies have been developed for the treatment of various diseases. The use of nanotechnology in developing nanocarriers for drug delivery is bringing lots of hope and enthusiasm in the field of drug delivery research. Nanoscale drug delivery devices present some advantages which show higher intracellular uptake than the other conventional form of drug delivery systems. Nanocarriers can be conjugated with a ligand such as antibody to favor a targeted therapeutic approach. The empty virus capsids are also being tried to use for delivering drugs as a new therapeutic strategy. Thus, nanoscale size drug delivery systems may revolutionize the entire drug therapy strategy and bring it to a new height in near future. However, toxicity concerns of the nanosize formulations should not be ignored. Full proof methods should be established to evaluate both the short-term and long-term toxicity analysis of the nanosize drug delivery systems.

Author details

Biswajit Mukherjee*, Niladri Shekhar Dey, Ruma Maji, Priyanka Bhowmik,
Pranab Jyoti Das and Paramita Paul

*Address all correspondence to: biswajit55@yahoo.com

Department of Pharmaceutical Technology, Jadavpur University, Kolkata, India

References

- [1] Ochekepe NA, Olorunfemi PO, Ngwuluka NC. Nanotechnology and drug delivery part 1: background and applications. *Trop J Pharm Res.* 2009; 8(3): 265-274.
- [2] Commission Staff Working Paper. Types and uses of nanomaterials including safety aspects accompanying the communication from the commission to the European

- Parliament, the council and the European and Economic Social Committee on the Second Regulatory Review on Nanomaterials. SWD 2012; 288 Final.
- [3] Svenson S, Prud'homme RK. Multifunctional nanoparticles for drug delivery applications. The nanotech revolution in drug delivery. Cientifica Ltd. 2007; 978-1-4614-2304-1.
 - [4] Hadjipanayis CG, Machaidze R, Kaluzova M, Wang L, Schuette AJ, Chen H, Wu X, Mao H. EGFRvIII antibody-conjugated iron oxide nanoparticles for magnetic resonance imaging- guided convection-enhanced delivery and targeted therapy of glioblastoma. *Cancer Res.* 2010; 70(15): 6303- 6312.
 - [5] Jong WHD, Borm PJA. Drug delivery and nanoparticle applications and hazards. *Int J Nanomedicine.* 2008; 3(2): 133- 149.
 - [6] Sahoo SK, Parveen S, Panda JJ. The present and future of nanotechnology in human healthcare. *Nanomed Nanotech Biol Med.* 2007; 3(1): 20-31.
 - [7] Webster DM, Sundaram P, Byrne ME. Injectable nanomaterials for drug delivery: carriers, targeting moieties, and therapeutics. *Eur J Pharm Biopharm.* 2013; 84(1): 1-20.
 - [8] Chakroborty G, Seth N, Sharma V. Nanoparticles and nanotechnology: clinical, toxicological, social, regulatory and other aspects of nanotechnology. *JDDT.* 2013; 3(4): 138-141.
 - [9] Couvreur P. Nanoparticles in drug delivery: past, present and future. *Adv Drug Delivery Rev.* 2013; 65(1): 21-23.
 - [10] Panyam J, Labhasetwar V. Biodegradable nanoparticles for drug and gene delivery to cells and tissue. *Adv Drug Delivery Rev.* 2003; 55(3):329-347.
 - [11] Praetorius NP, Mandal TK. Engineered nanoparticles in cancer therapy. *Recent Pat Drug Deliv and Formul.* 2007; 1(1): 37-51.
 - [12] Pardeike J, Hommoss A, Müller RH. Lipid nanoparticles (SLN, NLC) in cosmetic and pharmaceutical dermal products. *Int J Pharm.* 2009; 366(1-2): 170-184.
 - [13] Ogawara KI, Un K, Tanaka K, Higaki K, Kimura T. *In vivo* anti-tumor mal doxorubicin (DOX) in Dox-resistant tumor-bearing mice: involvement of cytotoxic effect on vascular endothelial cells. *J Cont Rel.* 2009; 133(1): 4-10.
 - [14] Chan JM, Zhang L, Yuet KP, Liao G, Rhee JW, Langer R, Farokhzad OC. PLGA-lecithin-PEG core-shell nanoparticles for controlled drug delivery. *Biomaterials.* 2009; 30(8): 1627-1634.
 - [15] Huang X, Jain PK, El-Sayed IH, El-Sayed MA. Gold nanoparticles: interesting optical properties and recent applications in cancer diagnostics and therapy. *Nanomedicine.* 2007; 2: 681-693.

- [16] Wei XL, Mo ZH, Li B, Wei JM. Disruption of Hep G2 cell adhesion by gold nanoparticle and paclitaxel disclosed by *in situ* QCM measurement. *Colloids Surf B Biointerfaces*. 2007; 59: 100-104.
- [17] Yousefi A, Esmaili F, Rahimian S, Atyabi F, Dinarvand R. Preparation and *in vitro* evaluation of a pegylated nano-liposomal formulation containing docetaxel. *Sci Pharm*. 2009; 77: 453-464.
- [18] Patel S, Bhirde AA, Rusling JF, Chen X, Gutkind JS, Patel V. Nano delivers big: designing molecular missiles for cancer therapeutics. *Pharmaceutics*. 2011; 3(1): 34-52.
- [19] Patel RP, Patel H, Baria AH. Formulation and evaluation of liposomes of ketokonazole. *Int J Drug Deliv Technol*. 2009; 1(1): 16-23.
- [20] Kumar A, Badde S, Kamble R, Pokharkar VB. Development and characterization of liposomal drug delivery system for nimesulide. *Int J Pharm Pharm Sci*. 2010; 2(4): 87-89.
- [21] Arab Tehrany E, Kahn CJ, Baravian C, Maherani B, Belhaj N, Wang X, Linder M. Elaboration and characterization of nanoliposome made of soya, rapeseed and salmon lecithins: application to cell culture. *Colloids Surf B Biointerfaces*. 2012; 95: 75-81.
- [22] Kumar KPS, Bhowmik D, Deb L. Recent trends in liposomes used as novel drug delivery system. *J Pharma Innovation*. 2012; 1(1): 26-34.
- [23] Dadashzadeh S, Vali AM, Rezaie M. The effect of PEG coating on *in vitro* cytotoxicity and *in vivo* disposition of topotecan loaded liposomes in rats. *Pharmaceutical Nanotechnology*. 2008; 353: 251-259.
- [24] Dhanikula RS, Hammady T, Hildgen P. On the mechanism and dynamics of uptake and permeation of polyether copolyester dendrimers across an *in vitro* blood-brain barrier model. *J Pharm Sci*. 2009; 98(10): 3748-3760.
- [25] Albertazzi L, Gherardini L, Brondi M, Sulis Sato S, Bifone A, Pizzorusso T, Ratto GM, Bardi G. *In vivo* distribution and toxicity of PAMAM dendrimers in the central nervous system depend on their surface chemistry. *Mol Pharmacol*. 2013; 10(1): 249-260.
- [26] Kannan S, Dai H, Navath RS, Balakrishnan B, Jyoti A, Janisse J, Romero R, Kannan RM. Dendrimer-based postnatal therapy for neuroinflammation and cerebral palsy in a rabbit model. *Sci Transl Med*. 2012; 4(130): 130ra46.
- [27] Klajnert B, Bryszewska M. Dendrimers: properties and applications. *Acta Bioch Pol*. 2001; 48(1): 199-208.
- [28] Huang RQ, Qu YH, Ke WL, Zhu JH, Pei YY, Jiang C. Efficient gene delivery targeted to the brain using a transferrin-conjugated polyethylene glycol-modified polyamidoamine dendrimer. *Drug Delivery Systems: Advanced Technologies Potentially Applicable in Personalised Treatment*. 2007; 21(4): 1117-1125.

- [29] Kherlopian AR, Song T, Duan Q, Neimark MA, Po MJ, Gohagan JK, Laine AF. A review of imaging techniques for systems biology. *BMC Syst Biol.* 2008; 2: 74.
- [30] Lowery AR, Gobin AM, Day ES, Halas NJ, West JL. Immunonano shells for targeted photothermal ablation of tumor cells. *Int J Nanomed.* 2006; 1(2): 149-154.
- [31] Hirsch LR, Stafford RJ, Bankson JA, Sershen SR, Rivera B, Price RE. Nanosell-mediated near-infrared thermal therapy of tumors under magnetic resonance guidance. *Proc Natl Acad Sci USA.* 2003; 100: 13549-13554.
- [32] Reilly RM. Carbon nanotubes: potential benefits and risks of nanotechnology in nuclear medicine. *J Nucl Med.* 2007; 48(7): 1039-1042.
- [33] Prato M, Kostarelos K, Bianco A. Functionalized carbon nanotubes in drug design and discovery. *Acc Chem Res.* 2008; 41(1): 60-68.
- [34] Mc Devitt MR, Chattopadhyay D, Kappel BJ, Jaggi JS, Schiffman SR, Antczak C, Njardarson JT, Brentjens R, Scheinberg DA. Tumor targeting with antibody functionalized, radiolabelled carbon nanotubes. *J Nucl Med.* 2007; 48: 1180-1189.
- [35] Freitas RA. Current status of nanomedicine and medical nanorobotics. *J Comput Theor Nanosci.* 2005; 2: 1-25.
- [36] Yadav A, Ghune M, Jain DK. Nanomedicine based drug delivery system. *JAPER.* 2011; 1(4): 201- 213.
- [37] Gangrade SM. Nanocrystals-a way for carrier free drug delivery. *Pharma Buzz.* 2011; 6: 26-31.
- [38] Gao X, Dave SR. Quantum dots for cancer molecular imaging. *Adv Exp Med Biol.* 2007; 620: 57-73.
- [39] Mulder WJM, Koole R, Brandwijk RJ, Storm G, Chin PTK, Strijkers GJ, Donega CM, Nicolay K, Griffioen AW. Quantum dots with a paramagnetic coating as a bimodal molecular imaging probe. *Nano letter.* 2006; 6: 87-90.
- [40] Jain S, Shukla K, Jain V, Saraf S. Nanoparticles: emerging carriers for delivery of bioactive agents. *Pharma Times.* 2007; 39: 30-35.
- [41] Amiot CL, Xu S, Liang S, Pan L, Zhao JX. Near-infrared fluorescent materials for sensing of biological targets. *Sensors.* 2008; 8(5): 3082-3105.
- [42] Petty MA, Lo EH. Junctional complexes of the blood brain barrier: permeability changes in neuroinflammation. *Prog Neurobiol.* 2002; 68(5): 311-323.
- [43] Rabanel JM, Aoun V, Elkin I, Mokhtar M, Hildgen P. Drug loaded nanocarriers: passive targeting and crossing of biological barriers. *Curr Med Chem.* 2012; 19(19): 3070-3102.
- [44] Youns M, Hoheisel JD, Efferth T. Therapeutic and diagnostic applications of nanoparticles. *Curr Drug Targets.* 2011; 12(3): 357-365.

- [45] Gabathuler R. Approaches to transport therapeutic drugs across the blood- brain barrier to treat brain diseases. *Neuro biology of Disease*. 2010; 37(1): 48-57.
- [46] Kesavan K, Balasubramaniam J, Kant S, Singh PN, Pandit JK. Newer approaches for optimal bioavailability of ocularly delivered drugs: review. *Curr Drug Deliv*. 2011; 8(2): 172-193.
- [47] Yasukawa T. Drug delivery systems for vitreoretinal diseases. *Prog Retin Eye Res*. 2004; 23(3): 253-281.
- [48] Behar-Cohen F. Drug delivery to target the posterior segment of the eye. *Med Sci (Paris)*. 2004; 20(6-7): 701-706.
- [49] Gulsen D, Chauhan A. Ophthalmic drug delivery through contact lenses. *Invest Ophthalmol Vis Sci*. 2004; 45(7): 2342-2347.
- [50] Gulsen D, Chauhan A. Dispersion of microemulsion drops in HEMA hydrogel: a potential ophthalmic drug delivery vehicle. *Int J Pharm*. 2005; 292(1-2): 95-117.
- [51] Amrite AC, Edelhauser HF, Singh SR, Kompella UB. Effect of circulation on the and ocular tissue distribution of 20 nm nanoparticles after periocular administration. *Mol Vis*. 2008; 14: 150-160.
- [52] Kim JH, Kim JH, Kim KW, Kim MH, Yu YS. Intravenously administered gold nanoparticles passing through the blood retinal barrier depending on the particle size, and induce no retinal toxicity. *Nanotechnology*. 2009; 20(50): 505101.
- [53] Koo H, Moon H, Han H, Na JH, Huh MS, Park JH, Kwon IC, Kim K, Kim H. The movement of self- assembled amphiphilic polymeric nanoparticles in the vitreous and retina after intravitreal injection. *Biomaterials*. 2012; 33(12): 3485-3493.
- [54] Peeters L, Sanders NN, Braeckmans K, Boussery K, Van de Voorde J, De Smedt SC, Demeester J. Vitreous: a barrier to nonviral ocular gene therapy. *Invest Ophthalmol Vis Sci*. 2005; 46(10): 3553-3561.
- [55] Kim H, Robinson SB, Csaky KG. Investigating the movement of intravitreal human serum albumin nanoparticles in the vitreous and retina. *Pharm Res*. 2009; 26(2): 329-337.
- [56] Surendiran A, Sandhiya S, Pradhan SC, Adithan C. Novel applications of nanotechnology in medicine. *Indian J Med Res*. 2009; 130: 689-701.
- [57] Malam Y, Loizidou M, Seifalian AM. Liposomes and nanoparticles: nanosized vehicles for drug delivery in cancer. *Trends Pharmacol Sci*. 2009; 30(11): 592-599.
- [58] Byrne JD, Betancourt T, Brannon-Peppas L. Active targeting schemes for nanoparticle systems in cancer therapeutics. *Adv Drug Delivery Rev*. 2008; 60: 1615-1626.
- [59] Ruoslahti E, Bhatia SN, Sailor MJ. Targeting of drugs and nanoparticles to tumors. *J Cell Biol*. 2010; 188 (6): 759-768.

- [60] Praetorius NP, Mandal TK. Engineered nanoparticles in cancer therapy. *Recent Pat Drug Deliv Formul.* 2007; 1(1): 37-51.
- [61] Peer D, Karp JM, Hong S, Farokhzad OC, Margalit R, Langer R. Nanocarriers as an emerging platform for cancer therapy. *Nature Nanotech.* 2007; 2: 751-760.
- [62] Lammers T, Hennink WE, Storm G. Tumour-targeted nanomedicines: principles and practice. *British Journal of Cancer.* 2008; 99: 392-397.
- [63] Davis PB, Cooper MJ. Vectors for airway gene delivery. *AAPS J.* 2007; 9: E11-E17.
- [64] Alex SM, Sharma CP. Nanomedicine for gene therapy. *Drug Deliv Transl Res.* 2013; 3: 437-445.
- [65] Pathak A, Vyas SP, Gupta KC. Nano-vectors for efficient liver specific gene transfer. *Int J Nanomed.* 2008; 3: 31-49.
- [66] Bunuales M, Duzgunes N, Zalba S, Garrido MJ, Ilarduya CT. Efficient gene delivery by EGF lipoplexes *in vitro* and *in vivo*. *Nanomedicine.* 2011; 6(1): 89-98.
- [67] Boettger M, Zaitsev S, Cartier R, Haberland A, Sukhorukov G, Moehwald H, Zastrow H, Schneider M. WO03087384A1 (2003).
- [68] Niu L, Xu YC, Dai Z, Tang HQ. Gene therapy for type 1 diabetes mellitus in rats by gastrointestinal administration of chitosan nanoparticles containing human insulin gene. *World J Gastroenterol.* 2008; 14: 4209-4215.
- [69] Caruso M, Belloni L, Sthandier O, Amati P, Garcia MI. Alpha4beta1 integrin acts as a cell receptor for murine polyomavirus at the level. *J Virol.* 2003; 77: 3913- 3921.
- [70] Young M, Willits D, Uchida M, Douglas T. Plant viruses as biotemplates for materials and their use in nanotechnology. *Annu Rev Phytopathol.* 2008; 46: 361-384.
- [71] Gleiter S, Lilie H. Cell-type specific targeting and gene expression using a polyoma VP1 virus-like particles. *Biol Chem.* 2003; 384(2): 247- 255.
- [72] Wang Q, Chan TR, Hilgraf R, Fokin VV, Sharpless KB, Finn MG. Bioconjugation by copper (I)-catalyzed azide-alkyne [3+2] cycloaddition. *J Am Chem Soc.* 2003; 125(11): 3192 - 3193.

6

Virus and Nanosized Viral Scaffolds as Drug Delivery Systems

MUKHERJEE BISWAJIT*, GHOSH SHAMPA, MONDAL LABONI AND PAUL PARAMITA

ABSTRACT

Well-characterized monodispersed structures with specific geometric arrangement and large surface area facilitating multivalent targeting with a high rate of production of virus in host cells encourage scientists to utilize them or their empty capsids as bionanomaterial to load drug to improve solubility, reduce toxicity and for site specific targeting. In this chapter, we focus on virus and virus-like particles (empty capsid) as drug delivery systems. The chapter highlights how viral capsids can be engineered to encapsulate / attach drug molecules into / on them. Further, methods of obtaining empty viral capsids and procedure and mechanism of drug loading in them have been described. Care has been taken to highlight drug targeting and delivery (including gene delivery) using those empty viral capsids. Although there is a reasonable progress of research in the area, a comprehensive understanding regarding their behavior in vivo may provide safe, effective and marketable products.

Key words: Bionanoparticles, Drug delivery, Targeting, Virus, Virus-like particles.

1. INTRODUCTION

Nanotechnology is a blooming phase of research, potentially with diverse and evolving applications in the areas of medicine, imaging, and material science. Bionanotechnology, an interdisciplinary area of this field, aims specifically at research and development of novel nanosized materials from

Department of Pharmaceutical Technology, Jadavpur University, Kolkata-700032

*Corresponding author E-mail: biswajit55@yahoo.com

basic biological units such as DNA and peptides (or peptidomimetics). Other natural basic elements derived from Nature's designs include the viruses and virus-like particles (VLPs), ferritins, and other self-assembled protein cages, such as heat shock protein cages and enzyme complexes.

These unique biogenic systems, formed by self-assembling through multiple noncovalent interactions, are characterized by ordered structural symmetries and sophisticated chemistry, and represent organized nanosystems with a diverse array of shapes and sizes; and yet are within the control of programmable genetic information. Nanomaterials have a large surface-to-volume ratio compared to traditional drug delivery vehicles that offers a greater capacity for drugs and/or imaging reagents. The ability to confer nanoparticles with specific ligands implicates that those diagnostic and therapeutic cargo can be delivered to specific cells/tissues. These qualities can be exploited to fine-tune the bio-nanoparticles (BNPs), with sub-molecular precision to incorporate novel functionalities for biomedical purposes, such as drug delivery, gene therapy, tumor imaging, and vaccine development. In this chapter we want to describe the scope of utilization of virus and VLPs as drug delivery systems. Additionally, the progress of research in the field will also be highlighted.

2. FROM NANO- TO BIONANO- DRUG DELIVERY SYSTEMS

So far several nanomedicine formulations have been approved for clinical use, including PEGylated liposomal doxorubicin (Doxil®/Caelyx®), albumin-bound paclitaxel (Abraxane®), nanoparticle-based contrast agents for use in magnetic resonance imaging (MRI), poly(lactic-co-glycolic acid) (PLGA) formulations for drug delivery, and virus-based vaccines (Wagner *et al.*, 2006; Lu *et al.*, 2009; Peek *et al.*, 2008). Many other additional formulations are currently undergoing clinical testing (Farrell *et al.*, 2010). However, there is a significant lag between the development of novel nanomedicine platforms and their translation into the clinic, often because encouraging *in vitro* results cannot be replicated *in vivo*, or because the materials are not biodegradable and therefore persist in the body. Researchers have therefore focused on biocompatible nanoparticle platforms, *i.e.*, delivery system chemistry of bio-nanomaterials, which are naturally biocompatible and thus promising candidates for *in vivo* use.

Several classes of nanomaterials are currently being searched on, including synthetic materials and naturally occurring bio-nanomaterials such as viral nanoparticles (VNPs). VNPs are robust, dynamic, self-assembling spatial units with symmetrical, polyvalent, and monodispersed structures and can be produced in large quantities in a short period of time, and they present programmable scaffolds. VNPs offer advantages over synthetic nanomaterials, primarily because they are biocompatible and biodegradable. VNPs derived from plant viruses and bacteriophages are